NAC-E-801

Safety Analysis of
Modified NAC-1
Spent Fuel Shipping Cask

May 16, 1980

Nuclear Assurance Corporation

24 Executive Park West
Atlanta, Georgia 30329
Telephone: (404) 325-4200
Telex: 549567

Weinbergstrasse 9
8001 Zurich, Switzerland
Telephone: (01) 47 08 44
Telex: 57275

Table of Contents

Table of Contents

Table of Contents

Table of Contents

Table of Contents

Table of Contents

List of Tables

List of Tables

List of Figures

List of Figures

List of Figures

List of Figures

List of Figures

List of Figures

List of Figures

List of Figures

1. General Information

This report presents the structural and thermal analyses of the NAC-1 spent fuel shipping cask. The analyses show the cask design meets the requirements set forth in Part 71 of Title 10, Chapter 1 of the Code of Federal Regulations.

The NAC-1 cask is designed to transport a large variety of fuel assemblies or non fuel bearing components. Salient features of the cask include a lead shield to attenuate gamma rays and an integral water filled shield to attenuate neutron emissions. The inner and outer surfaces are stainless steel so that it can be readily decontaminated following loading. The cask is normally partially filled with water during shipment or it can be drained for dry shipments.

A review of the characteristics of this cask design with respect to conformance to current licensing requirements has dictated a revised impact limiter design. This will assure that the cask can be shown by conservative analysis to survive the hypothetical accident.

The modifications to the NAC-1 cask consist of revised removable impact limiters, revised protection for the valves and altered configuration of the bottom end of the cask. The details of the cask design and all of the pertinent dimensions of the modified cask are presented in the accompanying drawings entitled "SHIPPING CASK - SPENT FUEL, NFS-4 & NAC-1" and numbered 301-211-F1 revision 0 sheets 1 thru 5 (Reference 1.1).

This report documents the structural and thermal analyses of the modified NAC-1 cask. The criticality analysis and shielding analysis are not effected by the revision to the impact limiters and remain as documented in the Safety Analysis Report for the NFS-4 and NAC-1 spent fuel shipping cask (Reference 1.2).

The structural analyses presented in Section 2. conclusively demonstrate the ability of the NAC-1 cask to endure the rigors of normal transport and the hypothetical accident without buckling or exceeding any of the stress limitations that are identified in 10CFR71 or Regulatory Guide 7.6.

Included in the analyses was a determination that deviations of the inner shell from a perfect right circular cylinder of up to 10% ovality over most of the length and up to 2% ovality at the ends are tolerable without impacting the casks capability to meet the requirements of 10CRF71 and regulatory guide 7.6. Additionally, the analyses demonstrated that there is no identifiable constraint on the bow or nonlinearity of the inner shell of the casks that would impact their capability to meet all of the requirements for licensed transport. Consequently, the drawings of the cask that are a part of the Safety Analysis Report have been modified to show a surface straightness tolerance of 0.75 inches.

A summary of the cavity measurements for all five casks is presented in Table 1-1 along with the limitations on ovality and bow that result from the analyses that are presented in this report.

Table 1-1. Measured Ovality and Bow of NAC-1 Cask Cavities

Cask	Maximum Ovality (%)	Location Inches From Bottom	Limit (%)	Maximum Ovality In First 3 Inches (%)	Limit (%)	Maximum Bow (inches)	Limit (inches)
A	1.578	126.5	10.	0.45	3.	0.450	0.75
B	0.993	144.5	10.	0.63	3.	0.110	0.75
C	1.852	120.5	10.	1.51	3.	0.160	0.75
D	0.992	120.5	10.	0.92	3.	0.124	0.75
E	1.000	36.5	10.	0.36	3.	0.115	0.75

The lower extremity of the cask cavity is the reference for the locations presented in this table. Consequently, the ovality limitations apply from 4.8 to 164.8 inches and the ovality limit of 3% applies to locations between 4.8 and 7.8 inches and 161.8 and 164.8 inches.

Refer to Figure 2.5 for definitions of ovality and bow.

1.1. Introduction

The NAC-1 spent fuel shipping cask is a universal cask capable of accommodating a broad range of fuel assemblies from either pressurized or boiling water reactors. It is designed to meet or exceed all of the requirements delineated in Part 71 of Title 10, Chapter 1 of the Code of Federal Regulations for Fissile Class III shipments of large quantities of radioactive material (Reference 1.3). The primary means of transport is by legal weight truck under sole use assignment; however, shipments by rail could be accomplished.

The analyses show that stress levels in the cask remain within acceptable limits during normal service as well as during the hypothetical accident. Additionally, the analyses demonstrate that both bow and ovality of the inner shell can be tolerated without detracting from the ability of the cask to maintain the integrity of the containment boundary during normal operation or accident conditions. Further, it is shown that no portion of the normal operation or fabrication of the casks results in stresses that are capable of causing buckling of the inner shell of the cask.

1.2. Package Description

The NAC-1 spent fuel shipping cask provides shielding to permit transport of radioactive material. The primary shield material is lead, encased within stainless steel shells where the inner shell serves as the primary containment and the outer shell provides redundant containment and also is the principal structural member of the cask. The ends of the cask are stainless steel castings that complete the shielding. The inner shell and associated valves and bolted closure are a pressure vessel that must retain its integrity during all normal transport and accident conditions. Consequently, it is designed to meet or exceed all of the requirements of the Boiler and Pressure Vessel Code that has been adopted by the American Society of Mechanical Engineers, Section III, Nuclear Vessels (Reference 1.4).

Although the cask is capable of carrying fuel or non fuel bearing components, fuel will be referred to as the cargo with the understanding that it can be either. The principal features of the cask are the containment boundary, the shielding and heat dissipation systems and the lifting and tiedown systems. The configuration of the cask as a whole is shown in Figures 1-1 and 1-2 with and without the impact limiters respectively. Each of the important systems is described in the following sections.

1.2.1. Containment Boundary

The containment boundary is the surface and seals that serve to prevent the escape of the radioactivity being transported in the cask. The primary containment boundary is the inner shell of the cask, the plug with O-rings, the drain and vent valves and the rupture disk. The primary containment is further contained by the outer shell of the cask and the end castings.

The inner shell of the cask is a right circular cylinder with internal dimensions of 13.5 inches diameter and 166.5 inches length. The shell is entirely stainless steel and is 0.3125 inches thick. The end castings are large stainless steel structures that provide structural support for the two shells and shielding for the ends of the cask. The end casting at the upper end is annular with a tapered central hole that mates with the closure plug to seal the inner containment. The lower end casting is 3 inches thick with a central section that is a frustrum of a cone which is 5 inches thick to provide additional shielding.

There are five penetrations through the containment boundary. The main penetration is the opening that permits access to the cavity for loading and unloading the fuel assemblies. This opening is closed by a stainless steel plug that is bolted to the upper end casting and sealed by double O-rings. The main section of the plug is a frustrum of a cone to avoid any openings in the shielding that could lead to radiation streaming. Three penetrations permit draining and venting of the cavity during loading and unloading operations. Each of these penetrations is sealed by a fire rated ball valve which is protected by a standoff ring, bolted cover and the impact limiters. Mechanical linkages are attached to the valve handles to assure that the valves are in the closed position prior to the installation of the covers for shipping. The remaining penetration is to provide relief in the unlikely event of overpressurization of the cavity. This penetration is sealed by a rupture disk and a relief valve. A cover is provided to keep dirt and moisture away from the relief valve. This cover is designed to rupture in the event of actuation of the relief valve.

A fourth fire rated ball valve is used to seal a penetration in the wall which is used to pressurize the region between the O-rings to assure the adequacy of the seal prior to shipment. This penetration does not directly communicate with the cask

cavity because the inner O-ring always provides a seal between the cavity and this penetration. However, this penetration will be considered as part of the containment boundary to assure that there is no possible loss of containment during shipment.

A sketch of the containment boundary is presented in Figure 1-3 where each of the penetrations is identified for clarity.

All of the valves are totally covered by the impact limiters during transport. Additionally, the valves are each protected by rings welded to the end castings that restrict penetration of any projectile that is more than four inches in diameter. These rings also protect the valve during the portion of the hypothetical accident that involves a fall onto a six inch diameter pin. Details of the valve protection rings and the covers are shown in Figure 1-4.

1.2.2. Shielding

The shielding consists of the cask wall and the neutron shield tank. The cask wall includes lead that is cast in place to attenuate gamma radiation that is emitted from the spent fuel. The 6.625 inches of lead is supplemented by two stainless steel shells which are 0.3125 and 1.25 inches thick. The ends of the cask are entirely stainless steel, 7.25 and 7.5 inches thick at the bottom and top respectively.

The thickness of the lead is reduced by 1.25 inches in the upper 25 inches of the cask wall to reduce the weight of the cask. This region is adjacent to the upper end fitting and fuel rod plenum portions of the fuel assembly and the reduced shielding remains adequate to attenuate the radiation emitted by the fuel assembly.

A stainless steel encased void region is provided at the lower end of the lead region to provide a volume that is available to accomodate any swelling of the lead due to thermal expansion or slumping of the lead during an impact. There is also a small void between the ends of the lead and the end castings which is a result of the shrinkage of the lead as it solidified after pouring.

Neutron radiation from the spent nuclear fuel is attenuated by borated water in the neutron shield tank. Water serves to reduce the energy of the neutrons so that the boron is more effective for absorbing the neutrons. The water is mixed with ethylene-glycol to form a solution that has an extremely low freezing point to avoid the volumetric expansion that accompanies the phase change. The water in the cavity during wet shipments also aids in the attenuation of neutron radiation; however, this is optional and is not required for safe shipment.

The shield tank and expansion tank are divided into four separate pairs of compartments which are independent to minimize the risk of a single failure causing complete loss of neutron shielding. Each section of the shield tank is separated from the others by radial gussets that are seal welded in place and supported by adjacent stiffeners. The stiffeners have lightening holes to reduce their weight and avoid stagnating any shield tank fluid. Each section of the shield tank is connected to a section of the expansion tank to provide volume to accomodate thermal expansion of the fluid. The openings between the shield tank and expansion tank are covered by baffels to assure that water covers the opening at all times and in all orientations. Similiarly, the expansion tank has baffels in the lower portion of each section to minimize splashing of the fluid which could either entrain air or permit the opening to the shield tank to be uncovered. Each compartment of the shield tank is protected by a rupture disk that is designed to relieve pressure that exceeds 100 psig.

A drawing of the configuration of the shield tank and the expansion tank is presented in Figure 1-5. In this figure the cask body has been removed and only the remaining portion of the shield and expansion tanks have been shown.

1.2.3. Heat Dissipation System

Heat dissipation within the NAC-1 cask is accomplished by entirely passive means. All heat released by the fuel assembly is transferred from the fuel to the cask wall by natural circulation of the water in the cavity or by a combination of conduction, convection and radiation when the shipment is dry. The heat is then conducted through the wall of the cask where copper fins at the interfaces between the lead and stainless steel walls provide a path to transfer heat across any gap that develops between the lead and the stainless steel shells due to their different rates of thermal expansion. The configuration of the copper fins and their attachment to the stainless steel walls is shown in Figure 1-6.

Natural circulation in the shield tank will transfer the heat from the cask wall to the outer surface of the shield tank where both natural circulation of the ambient air and radiation will transfer the heat to the environment.

The impact limiters are a part of the outer surface of the cask and transfer heat to the environment; however, the contact between the impact limiters and the cask body is sufficiently loose that very little heat follows this path.

1.2.4. Impact Limiters

The impact limiters are removable sacrificial members that are attached to the ends of the cask to absorb energy by crushing during impact. Balsa wood and redwood are used as the crushable materials with their grains oriented parallel to the principal side, end and corner impact directions.

The internal configuration of the impact limiters is shown in Figure 1-7. The main structure of the impact limiter is the cup that interfaces the impact limiter to the cask body. The cup also captures the redwood which is intended to protect the cask during a side impact to prevent its dislodgement during an oblique impact. The balsa wood that absorbs energy during an end impact is fabricated in three sections. The main section has its grain oriented parallel to the longitudinal axis of the cask. This section has a stepped upper surface to mate with the other sections. The second section has its grain oriented at 50° to the cask axis so that it is effective for absorbing the initial impact during an oblique impact. This section surrounds the first section in the radial direction. The final section of balsa wood has its grain oriented perpendicular to the axis of the cask and is inserted on the cask side of the first and second sections of wood. This final section is intended to provide a soft response during the initial portions of an impact to prevent excessive initial decelerations. All of the sections of balsa wood are glued together and surrounded by a stainless steel shell that includes four tubes which penetrate the end impact limiter to permit access to bolts which attach the impact limiter to the cask body. The outer shell provides no strength to the impact limiter other than providing assurance that the balsa wood and redwood remain in their respective locations to absorb the energy by crushing and not by bending.

During any accident with a side impact, the impact limiter is

designed to stop the cask before the expansion tank is impacted. This both prevents excessive deceleration forces during the impact and enhances the possibility that the neutron shield will remain effective following such an accident.

Both impact limiters are identical in their response to an impact. The impact limiter on the upper end of the cask has two additional recesses on its inside surface to accomodate the rings that protect the vent valves. Additionally, the upper impact limiter has a thicker plate over the end of the cask due to the smaller bolt circle for attachment to the cask.

1.2.5. Lifting and Tiedown Systems

The cask is lifted by means of trunnions that are attached to the cask body. There are four hollow trunnions welded to the upper end casting to permit the use of a redundant yoke or a standard two arm yoke for lifting the cask. The mating yoke has projections that engage the interior of the trunnion during lifting or rotation. Access to the lifting trunnions is possible only after the impact limiters have been removed. The configuration of the lifting trunions is shown in Figure 1-8.

Two trunnions are welded to extensions of the lower end casting which are designated as rotation trunnions. These support the cask during rotation and provide a means for attaching the cask to the transport vehicle. These trunnions are offset three inches from the cask centerline to assure that the cask will rotate in only one direction as it is lowered onto the transport vehicle.

The rotation trunnions are welded to cylindrical extensions of the lower end casting which are held in place by a pretensioned band of wire rope as shown in Figure 1-9. The trunnions penetrate the cowl that surrounds the lower extremity of the cask and are

not covered by the impact limiter during transport.

The cask is attached to the transport vehicle by fastening the rotation trunnions to cradles that are a part of the trailer. The cowl at the upper end of the cask is supported by a separate cradle.

The rotation trunnions are fastened to their cradles by caps that are bolted over the trunnions prior to transport. The attachment of the upper end of the cask to the transport vehicle employs straps that capture the cowl and hold it in its cradle. The angle of contact between the cowl and this cradle is 90 degrees. The cradle includes a rubberized pad to distribute the contact and to minimize vibration during transport.

1.2.6. Operational Features

The NAC-1 cask is designed to be easily loaded and handled at any nuclear faciltiy. The outer surfaces of the cask have been bead blasted, and the configuration of the surfaces selected to aid in decontamination. Likewise, the locations of the drain and vent valves were selected to permit rapid access for easy operation of these valves after removal of the impact limiters.

The cask does not permit the release of any of its coolant during either normal operation or hypothetical accident conditions. This reduces environmental impact of spent fuel transport and provides economic benefit. Defective fuel assemblies do not need to be encapsulated prior to shipment, eliminating time, expense and total radiation exposure.

The loaded cask, tractor and trailer weighs less than 73,280 pounds permitting unrestricted travel at night and on weekends. This improves overall shipment effeciency and cask utilization.

Since the cask is mounted on its own dedicated trailer, it is independent of the need for a rail connection to the site.

The use of wet shipments with the cavity partially filled with water eliminates the time lost while waiting for the cask cavity to dry or for helium to be flushed through the cavity.

1.2.7. Contents of Packaging

The NAC-1 cask is designed to transport any of three different combinations of fuel assemblies. A single pressurized water reactor fuel assembly or two boiling water reactor fuel assemblies can be accommodated in the corresponding basket. Additionally, four fuel assemblies from a boiling water reactor similar to the design employed for Dresden Unit 1 and the appropriate basket can be transported in the NAC-1 cask. The characteristics of the various fuel assembly types are presented in Table 1-2 (Reference 1.5).

The cargo in the NAC-1 cask can also be non fuel bearing components such as fuel assembly channels or control rods or many other possibilities. The consequences of such shipments will not be considered because fuel assemblies represent a more severe cargo by releasing more heat and radiation.

Both the basket and the water within the cavity are considered to be a part of the contents of the cask because there is the possibility that either can acquire a part of the radioactivity of the fuel assembly that is being transported. When non fuel bearing components are being transported the water and basket retain their designation as cask contents because they may contain radioactivity from previous shipments.

Table 1-2. Fuel Assembly Characteristics

Second Generation Fuel Assemblies

	PWR	BWR
Number of Assemblies	1	2
Envelope (inches)	8.6	5.44
Fuel Length (inches)	150.	144.
Enrichment (%)	3.6	3.0
Fuel Weight (kg)	480	197
Cool Time (days)	120	120

First Generation Fuel Assemblies

	Dresden 1	San Onofre	LaCrosse
Number of Assemblies	4	1	2
Envelope (inches)	4.2	7.8	5.63
Fuel Length (inches)	110.	121.	83.8
Enrichment (%)	2.5	4.1	4.0
Fuel Weight (kg)	197	-	122
Cool Time (days)	120	120	120

For individual fuel rods the maximum mass of U-235 and plutonium shall not exceed 4.0 kg. Additional fuel rods may be inserted into guide tubes provided none of the above limitations is exceeded.

continued

Irradiated Uranium Oxide as Fuel Rods

Enrichment, e (%)	Fissile Mass Limit
$e < 3$	2.0
$3 < e < 4$	1.6
$4 < e < 5$	1.5

Non Fuel Bearing Components

Solid non-fissile irradiated hardwood and neutron source components (coolant optional)

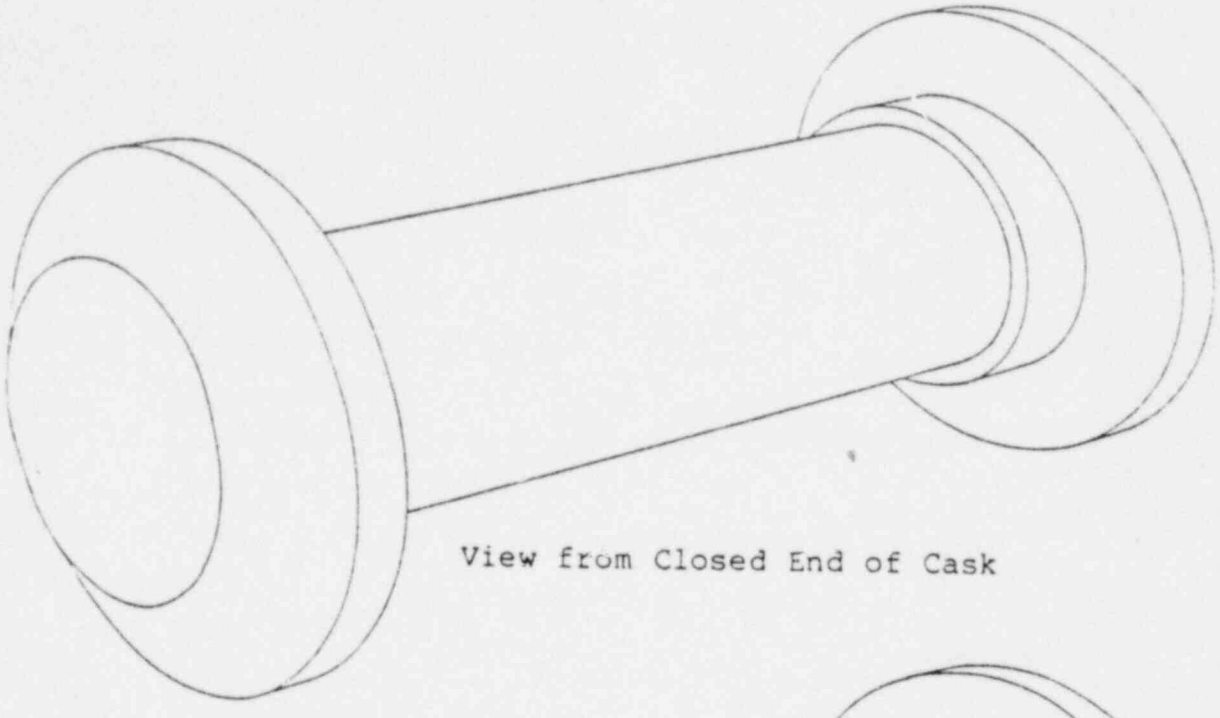

View from Closed End of Cask

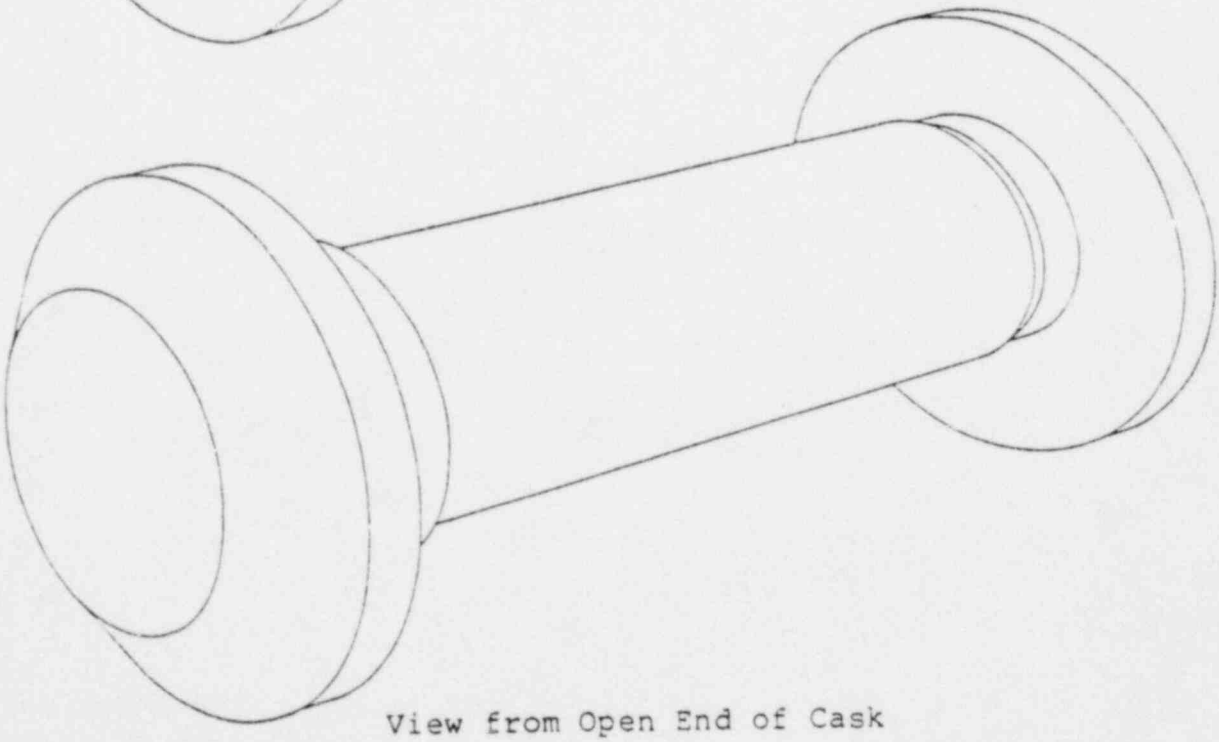

View from Open End of Cask

Figure 1-1. NAC-1 Cask External Configuration

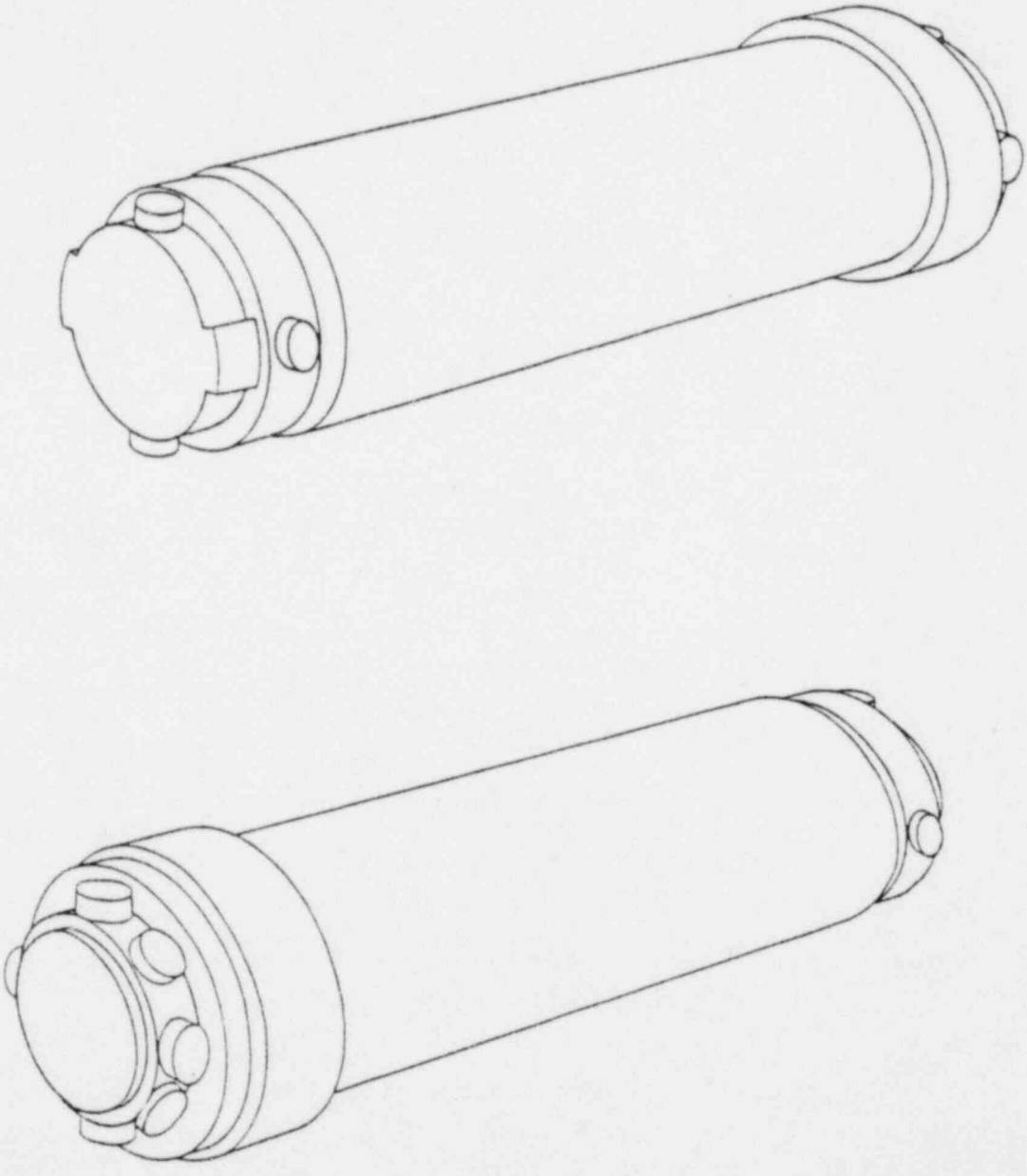

Figure 1-2. NAC-1 Cask with Impact Limiters Removed

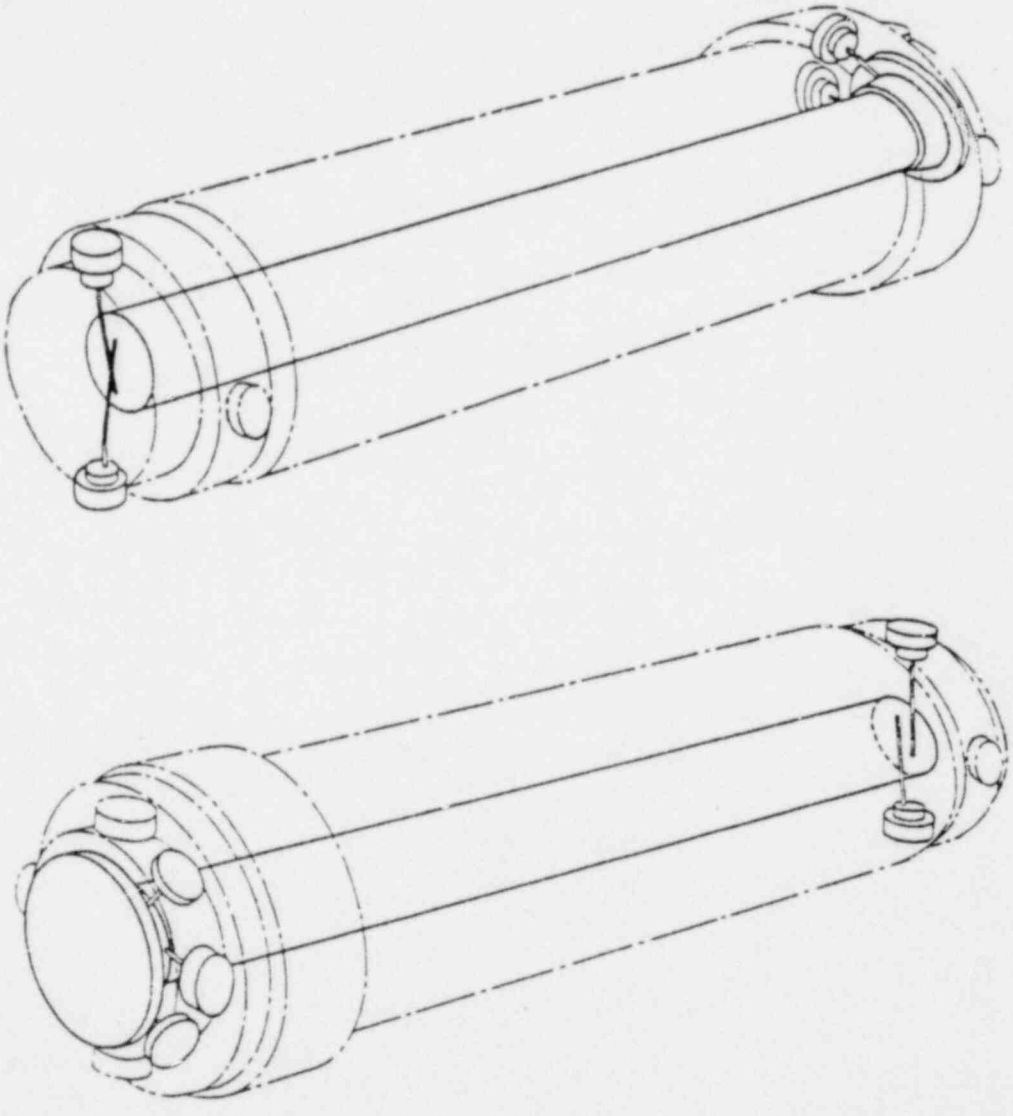

Figure 1-3. NAC-1 Cask Containment Boundary

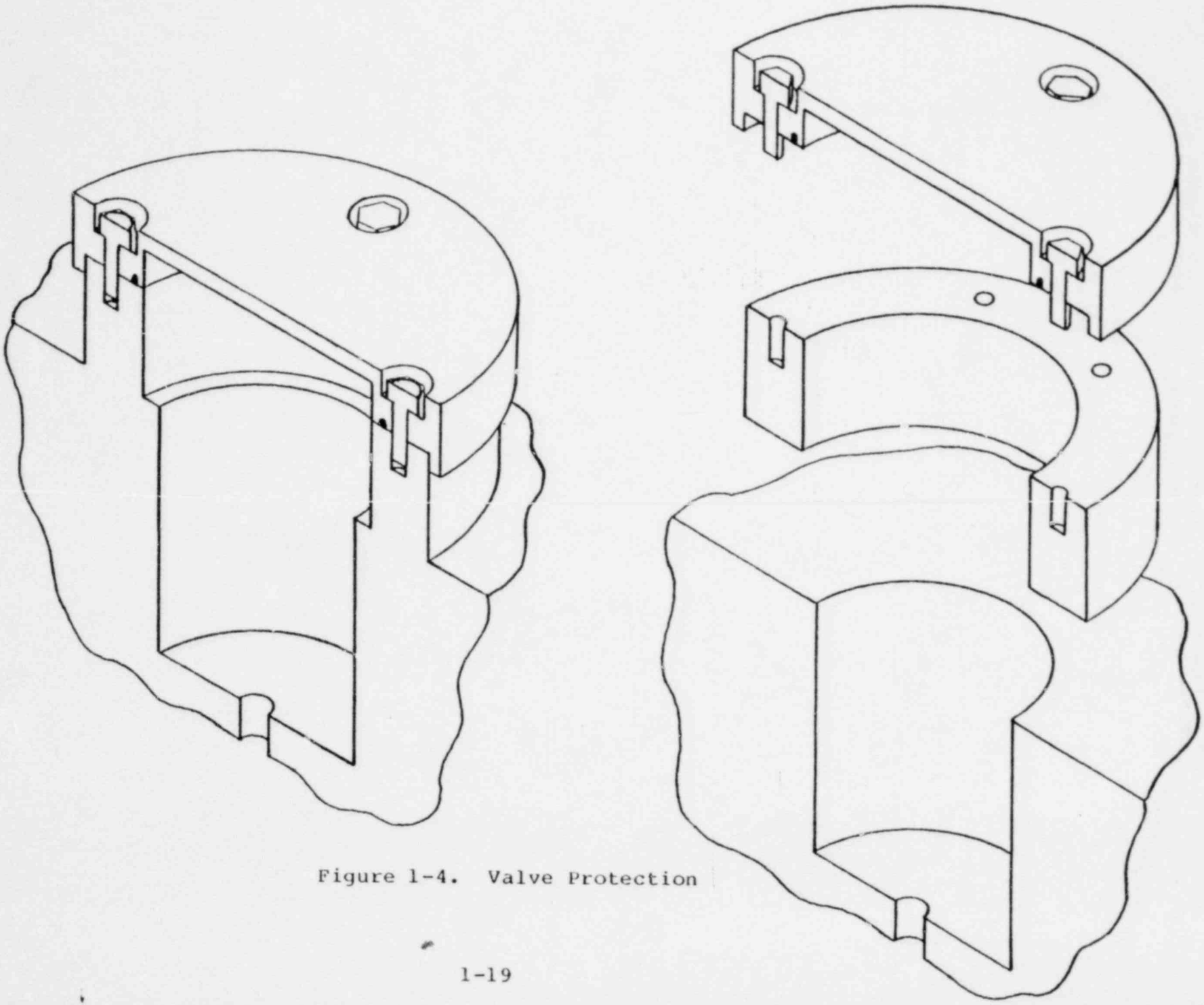

Figure 1-4. Valve Protection

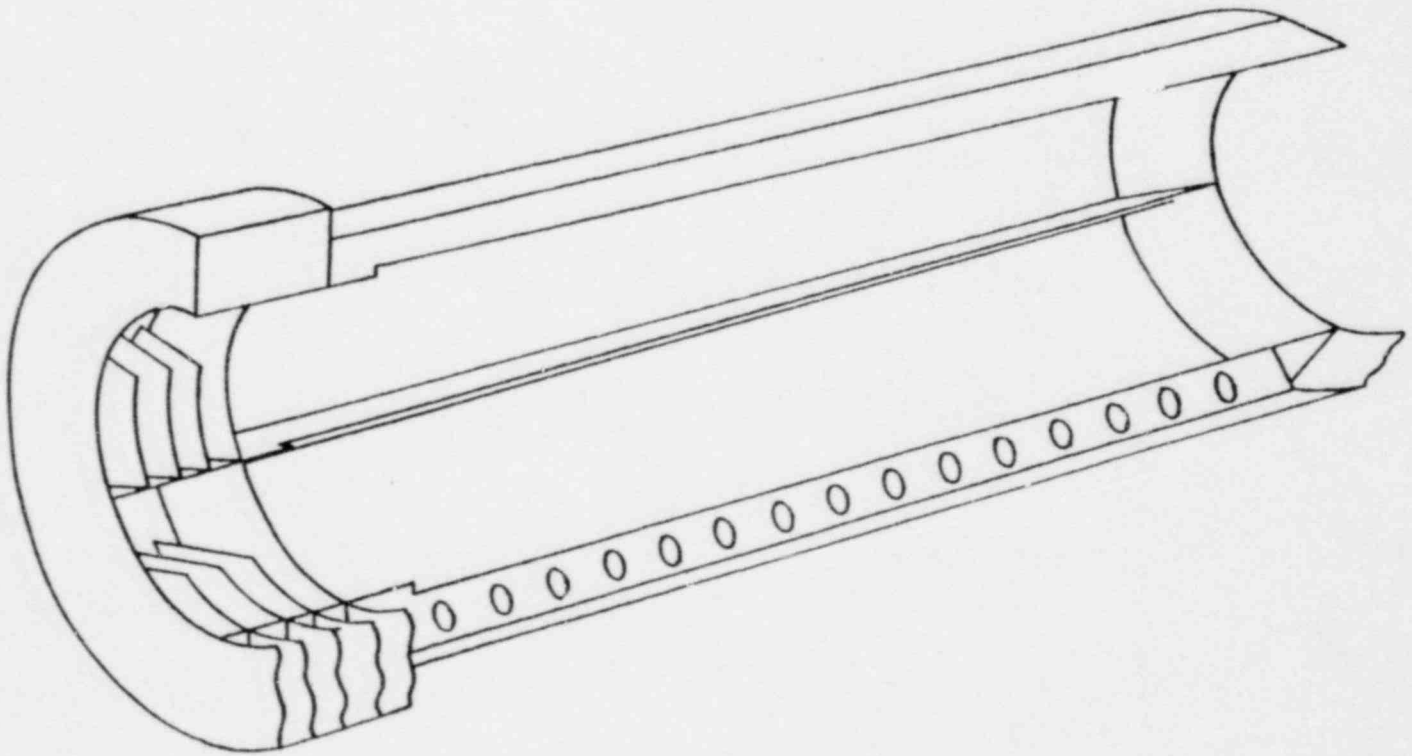

Figure 1-5. Neutron Shield Tank and Expansion Tank

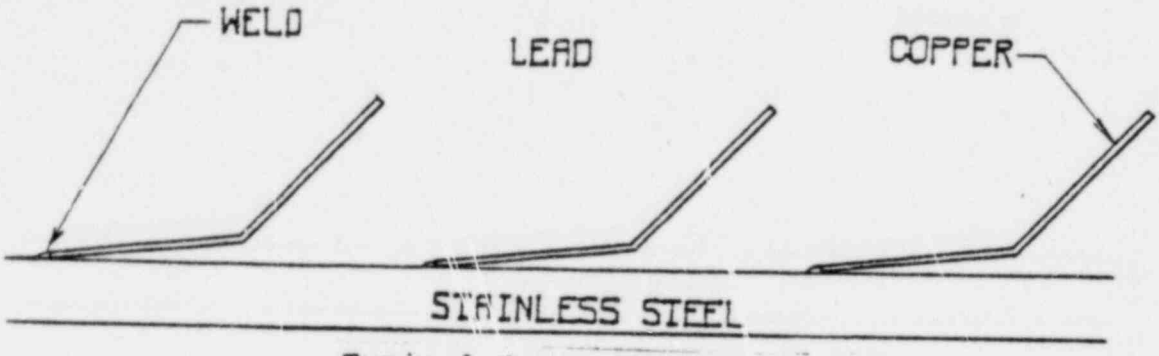

Typical Cross Section of Fin

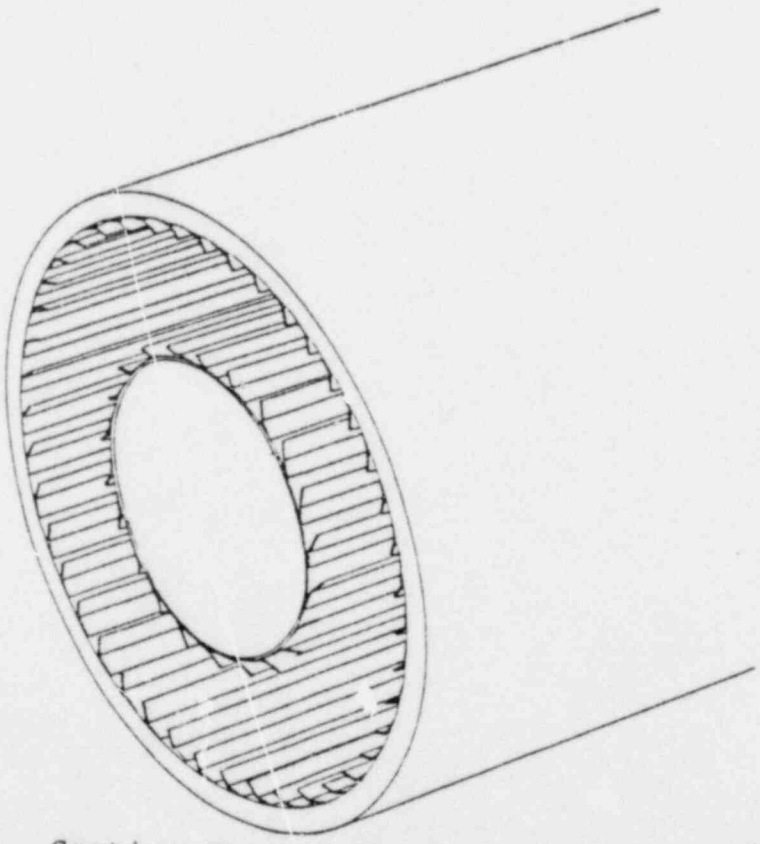

Section Through Cask Body

Figure 1-6. Copper Fins Connecting Lead and Stainless Steel

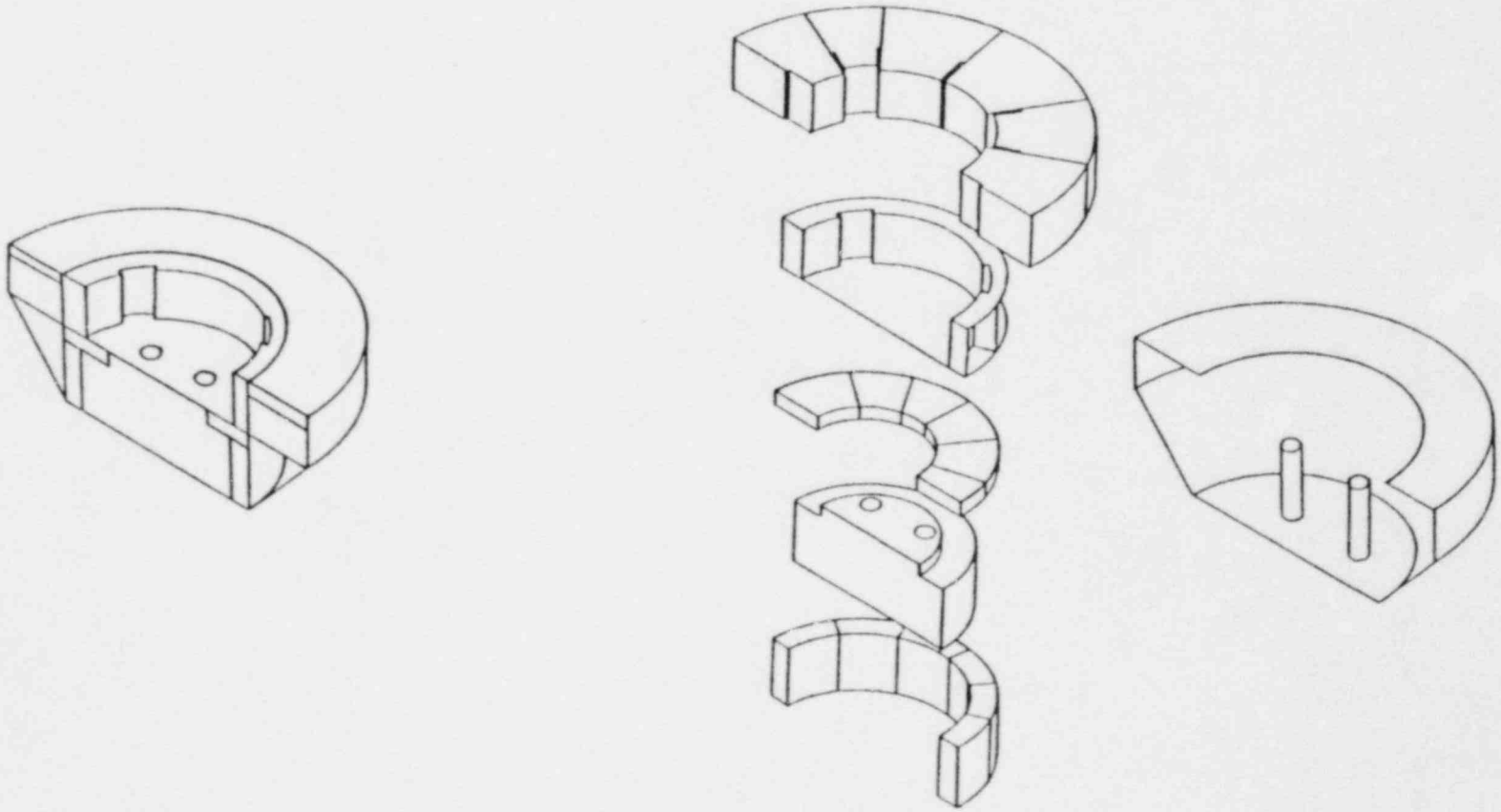

Figure 1-7. Impact Limiter Configuration

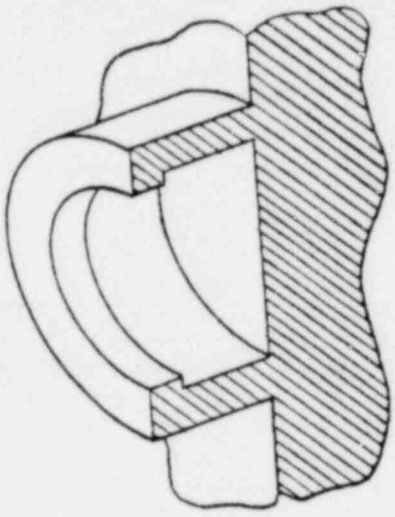

Cross Section Through Trunion

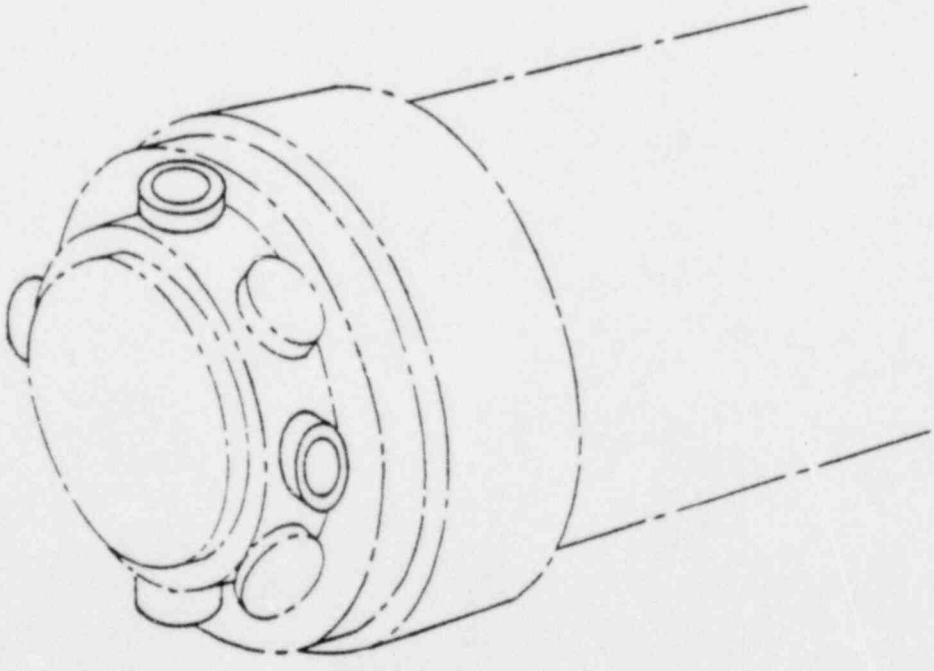

View from Open End of Cask

Figure 1-8. Lifting System

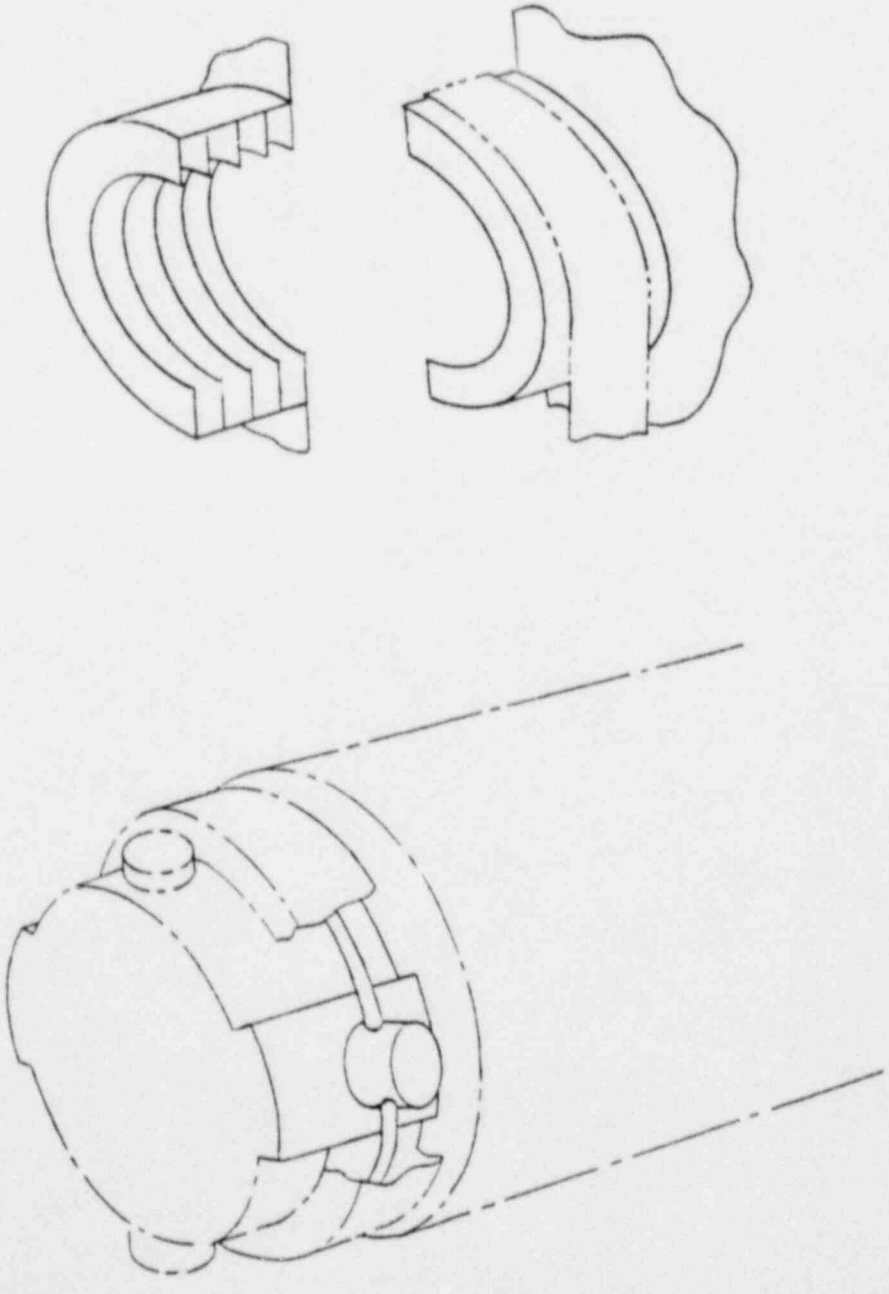

Figure 1-9. Tiedown System

1.3. Appendices to General Information

The following section contains the references that are necessary to supplement the information presented in Section 1.

1.3.1. References

1.1 Drawing 301-211-F1(Rev. 0), "SHIPPING CASK - SPENT FUEL, NFS-4 & NAC-1," April 1980.

1.2 "Safety Analysis Report for Nculear Fuel Services, Inc. Spent Fuel Shipping Cask Model No. NFS-4, Nuclear Fuel Services, Inc, U.S.N.R.C. Docket 6698, September 1972.

1.3 Part 71 of Title 10, Chapter 1 of the Code of Federal Regulations, March 2,1979.

1.4 "ASME Boiler and Pressure Vessel Code, Section III, Nuclear Vessels, "The American Society of Mechanical Enginers, New York, N.Y., 1971.

1.5 Fuel Trac, Nuclear Assurance Corporation, 1980.

2. Structural Evaluation

As required by Part 71 of Title 10, Chapter 1 of the Code of Federal Regulations (Reference 2.2), the structural analysis of the NAC-1 spent fuel shipping cask demonstrates that the package satisfies the requirements identified in Subpart C of this regulation. It is also shown that containment is not violated under any of the normal operation conditions or hypothetical accident conditions.

Analysis techniques that utilize the current state of the art for the calculation of stresses in large structures subject to both steady state and transient loadings have been used throughout this analysis. The evaluation of the structural characteristics of the containment boundary has been based upon conservative interpretation of the requirements set forth in the Boiler and Pressure Vessel Code that has been developed by the American Society of Mechanical Engineers. Every effort has been made to develop a cask design that is capable of meeting the rigors of transport while carrying nuclear fuel and this section of this report documents the results of the analyses that have been performed to provide assurance that the cask also satisfies the statutory requirements for licensing.

2.1. Structural Design

The design of the NAC-1 spent fuel shipping cask has embodied the concept of zero release of the cask contents. This is evidenced by the configuration of the seals and the protection afforded to all penetrations of the containment boundary.

2.1.1. Discussion

Satisfaction of the requirements of Part 71 of Title 10, Chapter 1 of the Code of Federal Regulations is summarized in Table 2-1 which lists all of the required analyses, the calculated primary stresses and the appropriate stress limitation or allowable stress for each analysis.

The ovality and bow of the inner shell have been considered in each of the individual analyses to conclusively prove that the inner shell does not buckle during any of the hypothetical accident conditions, normal transport conditions or during fabrication. Uncontrolled ovality of the inner shell introduces the possibility of buckling of the inner shell during the impact events that must be included in the analyses. The limitation that must be placed on the ovality of the inner shell is presented in Figure 2-1. In this figure the axial locations are measured from the end of the inner shell or the weld where the inner shell and flange on the end casting are joined. The flange on the end casting is sufficiently thicker than the inner shell that it will not experience buckling prior to the inner shell and as such is not included in Figure 2-1. The ovality of the inner shell must be less than this limit for the cask to satisfy all of the requirements set forth in 10CFR71. This restriction will be implemented by requiring the inner shell to be less than 2% oval for the first three inches at each end of the shell. The

remainder of the inner shell will be restricted to a maximum of 10% ovality. These restrictions result from the effect of ovality on the stresses during the thirty foot free falls and the one foot free falls.

Figure 2-1 does not present the ovality limitation over the full length of the inner shell because most of the limitation is off scale and does not represent a realistic limit on the configuration of the shell. Also, the limitation on the ovality is symmetric about the center of the cask so that Figure 2-1 applies to either end of the inner shell. The end impacts create the need for an ovality limit and the impact can occur on either end so the ovality limit must also be applied to either end.

The analyses do not indicate any limitation on bow of the inner shell because the thick outer shell serves to support the inner shell by the coupling at the end castings. Both shells must deform similiarly so the inner shell cannot buckle or fail in tension or compression without the outer shell also failing.

U.S. Nuclear Regulatory Commission Regulatory Guide 7.6 (Reference 2.5) imposes a second limitation on the results of these calculations, namely, the maximum range in the stress intensity is to be less than three times the design stress intensity for normal transport conditions and the maximum range in the stress intensity is to be less than the cyclic failure limit when the hypothetical accident conditions are included in the stress range. The maximum range in the stress intensity for normal transport conditions has been evaluated by preparing Figure 2-2 which identifies the axial dependence of each of the three possible combinations of stresses that form the stress intensity. Presented on this figure are all of the stresses for normal transport. The maximum stress intensity is the largest difference between the maximum and minimum stress at any point on the inner shell.

The maximum stress intensity in the inner shell during normal transport is 58,250 psi which occurrs 7.3 inches from the bottom of the cask cavity. The allowable value is three times the design stress intensity (20,000 psi) or 60,000 psi. A large fraction of the maximum range in stress intensity is due to the stresses that result from the pouring of lead into the cask wall so this range of stresses will not exist over most of the life of the cask.

The maximum range in the stress intensity for hypothetical accident conditions has been evaluated by preparing Figure 2-3 which identifies the axial dependence of each of the three possible combinations of stresses that form the stress intensity. Presented on this figure are all of the stresses for the fabrication of the cask , normal transport and hypothetical accident. The maximum stress intensity is the largest difference between the maximum and minimum stress at any axial point on the inner shell.

The maximum stress intensity in the inner shell during the hypothetical accident and including fabrication and normal transport conditions is 108,230 psi which occurrs 7.3 inches from the bottom of the cask cavity. The limiting value is the design fatigue stress for ten cycles which is 677,000 psi. A large fraction of the maximum range in stress intensity is due to the stresses that result from the pouring of lead into the cask wall and the thirty foot free fall onto the side of the cask. Consequently, this range of stress will not exist over most of the life of the cask.

The assumptions that are incorporated in each analysis and the results of the calculations are discussed in the following sections.

2.1.2. Design Criteria

The inner stainless steel shell, the bolted closure and the valves have been defined as the primary containment boundary which cannot be breached during any of the normal transport or hypothetical accident conditions. Since the cavity contents are pressurized by thermal expansion of the water, the inner shell must be considered as a pressure vessel and meet the design criteria established by the American Society of Mechanical Engineers in their Pressure Vessel Code (specifically Section III for nuclear pressure vessels). Two additional constraints were applied to the analysis of the cask. The first is the prohibition of buckling to preclude the large strains and deformations that result. The second is the restriction of the total variation of the stresses to less than the stress required for cyclic failure in ten cycles.

2.1.2.1. Stress Limitations

The sections of the ASME pressure vessel code that apply to entirely elastic analysis were utilized here to conform to the analysis methods which embody the assumption that the stainless steel components behave elastically. Such an assumption is not truly representative of the behavior of stainless steel; however, the consistent application of the analysis and stress limitations will result in valid conclusions. The use of an elastic representation of the material will result in conservatism in the results when the analysis is dominated by deformations since the elastic representation of the materials will over predict the stresses.

2.1.2.1.1. Limitations for Normal Transport

The limitations on the stresses that result from normal operation of the NAC-1 spent fuel shipping cask are based upon Section III of the American Society of Mechanical Engineers Boiler and Pressure Vessel Code (Reference 2.4). The sections that apply to the design of nuclear power plant components, specifically those portions dealing with a "design-by-analysis" approach for Class 1 components, have been used to define the stress limitations. The criteria for normal operation (Level A) have been adopted and are identified for reference in Table 2-2.

The limit on the total range of the stresses is defined by the fatigue stress that has been adopted by the ASME and is published in Appendix I of the Boiler and Pressure Vessel Code (Reference 2.4) for failure after one million cycles. The curve of the allowable stress for type 321 stainless steel is presented in Figure 2-4. This curve has been adjusted to reflect a modulus of elasticity of 27.1×10^6 that corresponds to a temperature of $300^{\circ}F$.

The interpretation of the normal operation conditions of the ASME pressure vessel code that were used were provided by the U.S. Nuclear Regulatory Commission Regulatory Guide 7.6 (Reference 2.5). This guide delineates the limitations on the stress intensity that can be employed for the analysis of spent fuel shipping casks. The specific limitations are identified in Table 2-2. The numerical values of the allowable stresses are based upon the material properties presented in Section 2.3.

2.1.2.1.2. Limitations for Accident Conditions

The limitations on the stresses in the containment boundary are based upon the faulted conditions (Level D) of the ASME pressure vessel code (Reference 2.4). Faulted conditions permit gross general deformations with some consequent loss of dimensional stability and damage. Additionally, the pressure vessel will be removed from service for inspection and repair. The limits associated with faulted conditions are permitted for combinations of conditions associated with extremely low probability postulated events whose consequences are such that the integrity and operability of the system may be impaired to the extent that conditions of public health and safety are involved.

The interpretation of the faulted conditions of the ASME pressure vessel code that were used were provided by the U.S. Nuclear Regulatory Commission Regulatory Guide 7.6 (Reference 2.5) which delineates the limitations on the stress intensity that can be employed for the analysis of spent fuel shipping casks. The specific limitations are identified in Table 2-3. The numerical values of these constraints are defined in Section 2.3

The limit on the total range of stresses is defined by the fatigue stress for failure after ten cycles. The curve of the allowable stress for type 321 stainless steel is presented in Figure 2-4. This curve has been adjusted to reflect a modulus of elasticity 27.1×10^6 that corresponds to a temperature of $300^{\circ}F$.

2.1.2.2. Buckling Limitations

There are three modes of buckling failure that are possible during normal transport or a hypothetical accident involving the NAC-1 cask. These are:

Bending
Collapse due to External Pressure
Axial Compression

Each of these modes of buckling failure must be evaluated as a function of both the initial ovality and initial bow of the cylinder. Ovality is defined as the difference between the largest and smallest diameter, expressed as a percentage of the mean diameter. Bow is defined as the difference between the centerline of the cylinder and a straight line that connects the centers of the ends of the cylinder. These definitions are illustrated in Figure 2-5.

The Knowledge Availability Systems Center of the University of Pittsburgh and Nuclear Assurance Corporation independently searched the available literature for information relative to the buckling of metal cylinders. The sources located by these two searches were thoroughly reviewed for information specifically relating to the three modes of buckling that are important to this analysis. References 2.6, 2.7, 2.8 and 2.9 provide a summary of the experimental, analytical and theoretical data in the literature.

2.1.2.2.1. Buckling During Bending

Bending a thin wall cylinder can induce a buckling type failure when the cross section is no longer capable of remaining circular. The conditions that are required to achieve buckling are dependent upon the material properties and the cross section at the point of buckling. The results of empirical and analytical predictions of the onset of buckling have been reduced to the correlation that is presented in Table 2-3. This correlation is the most conservative of the correlations that are available to represent this type of buckling.

Using this correlation the maximum bending stress in a straight circular cylinder that causes buckling is about 440,000 psi as shown in Figure 2-6. The effect of ovality of the cylinder at the point of buckling has been included in this figure by adjusting the mean radius to account for the ovality.

The impact of bowing of the cylinder has been evaluated by using the ANSYS computer program (see Appendix 2.10.1 and Reference 2.11 for a description of the ANSYS computer program) to determine the effect of bow upon the bending stress. As shown in Figure 2-7 the ANSYS model consisted of a half symmetry section of a cylinder 175 inches long that is subject to a uniform acceleration. The ends of this model were stopped to represent the bending forces experienced by the inner shell when the cask experiences a side impact. The cylinder was represented as a collection of three dimensional solid elements to allow a change in the cross section as the cylinder approached the point of buckling.

A series of four cases were run. The first case duplicated the conditions that were predicted to cause buckling by the correlation presented in Table 2-4. This case served as the reference for all further calculations. The second and third cases had varying amounts of bow introduced into the cylinder that ranged up to almost four inches deflection at the midplane of the cylinder. Each of these cases had the bending forces arranged so that the bow was in the same orientation as the bending. The final case had the bow reversed so that the initial bending served to remove the bow. The results of each of these cases is presented in Table 2-5.

The presence of the initial bow caused very little increase in the maximum tolerable bending stress even when the initial bow was almost four inches. Consequently, the presence of initial bow will not significantly reduce the stress that is required to cause the cask to buckle.

2.1.2.2.2. Collapse Type Buckling

The application of an external pressure to a cylinder can cause failure when the geometry becomes unstable and the the cross section undergoes a rapid transition to any other geometry. The initial cross section of the cylinder and the material properties are the important parameters that characterize the conditions at the onset of buckling.

The expressions that define the limiting hoop stress to assure freedom from collapse type buckling are of two forms. The first defines the limiting external pressure (p_c) for a perfect cylinder and the second introduces the effect of ovality. The expressions for the effect of ovality are based upon the assumption that the nature of the ovality is similiar to the buckled shape so that the ovality constitutes an initial portion of the process of buckling. The second major assumption is that the buckling of an oval cylinder should be limited to yielding of the extreme fibers. Plastic deformation of the cylinder is considered to be a continuation of the buckling process and its elimination will avoid any uncontrolled deformation or buckling.

The expression for collapse type buckling that is presented in Table 2-4 determines the impact of initial ovality of the cylinder when the critical pressure for a perfect cylinder is known. The three major references for buckling limits include several expressions for the critical pressure (or limiting hoop stress) for perfect cylinders. These expressions are presented in Table 2-6 along with the values of the critical pressure for the inner shell. The first and second expressions are identical; however, the regions of applicability are different. The first expression is valid for the inner shell while the second expression is slightly outside the stated range of applicability. The third expression is presented as the form that the first and second expression become when the value of θ is large. Since the

critical pressure predicted by all three expressions are very similiar, conservatism requires that the smaller be adopted in spite of the questions reguarding its validity. Consequently, all subsequent analyses were based upon an external critical pressure of 679 psi for the inner shell.

Two effects that are important to the analysis of the NAC-1 cask are the effect of end restraint upon the buckling and the effect of a hydrostatic type of pressure loading where the pressure is uniform around the circumfrence but varying along the length of the cylinder. To evaluate these effects numerically, an ANSYS model (see Appendix 2.10.1 and Reference 2.11) was developed to axisymmetrically represent one end of the inner shell of the cask including the portion of the end casting that supports the inner shell. The external pressure was varied along the length of the shell to represent the hydrostatic pressure of the lead during an end impact. The end of the flange of the end casting was rigidly fixed to represent the presence of the remainder of the end casting. The other end of the model was given symmetry boundary conditions to simulate the presence of the remainder of the inner shell. The model is shown in Figure 2-8.

The external pressure applied to the shell was increased in steps to determine the pressure at which each axial point experienced the hoop stress that is required to cause collapse of an infinitely long cylinder. The resulting pressure is the critical pressure that should be introduced into the equation in Table 2-4 to determine the effect of ovality on the limiting hoop stress. The axial position dependence of the critical pressure is presented in Figure 2-9 and the combined effect of both axial position and ovality is presented in Figure 2-10. In each of these figures the origin for measurement of the axial position is the end of the cavity.

2.1.2.2.3. Buckling due to Axial Compression

An axial force on the inner shell of the cask can result in column buckling where the shell bends rather than compresses. This is the classical type of buckling that has been studied with both theoretical and empirical investigations reported in the literature. The results of empirical and analytical predictions of the onset of buckling have been reduced to the correlation that is presented in Table 2-4. This correlation is the most conservative of the correlations that are available to represent this type of buckling.

The results of the evaluation of this correlation are presented in Figure 2-11 as a function of both ovality and bow of the cylinder. In this case the effect of both bow and ovality are relatively insignificant until the bow exceeds one inch.

The inner shell is rigidly connected to the outer shell by the end castings which can be considered to be undeformable. Consequently, the inner shell cannot buckle due to axial compression unless the outer shell also buckles because the lengths of the two shells must remain equal. The correlation described above has been evaluated for the outer shell and the results are presented in Figure 2-12.

The determination of the presence or absence of buckling was based upon the comparison of the stresses in the outer shell to the buckling limits identified in Figure 2-12. If the buckling stress has been exceeded, then the stresses in the inner shell were compared to the stress limits in Figure 2-11 to determine whether or not the inner shell has buckled. Both shells must exceed their respective buckling limits for axial buckling to occurr.

Table 2-1. Summary of Structural Analysis Results

Requirement in 10CFR71	Calculated Value psi	Limiting Value psi	Remarks
General Standards			
Lifting Devices			
Lifting Trunnions	16,226	28,600	Bearing stress on Yoke.
Lid Lifter	2,130	93,700	Shear & Tension stresses on bolts.
Tiedown Devices			
Rotation Trunnions	21,931	28,600	Bearing stress on Support Pedestal
Cowl	1,139	7,215	Pressure on Cowl Cylinder.
Standards for Type B			
Load Resistance	7,845	20,000	Bending stress in expansion tank. Table 2-14
External Pressure	25	47	Collapse pressure of impact limiter. Table 2-15
Normal Transport			
Heat	2,440	-	Hoop stress in inner shell. Figure 2-35 See Figure 2-2 for limit.
Cold	8,194	-	Axial stress in inner shell. Figure 2-36 See Figure 2-2 for limit.
Pressure	5,523	20,000	Hoop stress in shield tank. Table 2-19

continued

Vibration	2,200	26,000	Bending stress in outer shell. Table 2-21
Free Drop			
End Impact	24,800	25,000	Axial stress in inner shell with 2% ovality. Figures 2-41 and 2-45
Side Impact	10,500	25,000	Bending stress in inner shell. Figures 2-55 and 2-57
Penetration	520	831	Energy of projectile is dissipated in bending. Table 2-23
Fabrication			
Lead Pour	52,100	-	Hoop stress at first contact between lead and inner shell. Figure 2-66 See Figure 2-3 for limit
Cool Down	9,600	20,000	Hoop stress in inner shell Figure 2-67
Accident			
Free Fall			
End Impact	8,300	8,900	Hoop stress in inner shell with 2% ovality. Figure 2-79 and 2-81
Side Impact	47,000	150,000	Bending stress in inner shell. Figures 2-93 and 2-95
Corner Impact	38,200	150,000	Bending stress in inner shell. Figures 2-105 and 2-111
Oblique Impact	44,800	150,000	Bending stress in inner shell. Figures 2-110 and 2-112

continued

Puncture			
Valve	26,200	150,000	Bending stress in inner shell. Figure 2-120
Cask Body	54,000	150,000	Bending stress in inner shell. Figures 2-128 and 2-129
Thermal	35,300	-	Axial stress 35 minutes after start of fire. Figures 2-123 and 2-136 See Figure 2-2 for limit

Table 2-2. Stress Limitations for Normal Operation

Stress	Upper Bound
Primary Membrane Stress	Design Stress Intensity
Sum of Primary Membrane Stress and Primary Bending Stress	1.5 x Design Stress Intensity
Maximum Range in Stress	3 x Design Stress Intensity
Maximum Range in Stress Including Fabrication and Normal Operation	Fatigue Limit for 10^6 Cycles as Defined in Appendix I of Section III of the ASME Boiler and Pressure Vessel Code
Buckling	Not Allowed Under Any Conditions

Table 2-3. Stress Limitations for Accident Conditions

Stress	Upper Bound
Primary Membrane Stress	Lesser of 2.4 x Design Stress Intensity -or- 0.7 x Ultimate Stress
Sum of Primary Membrane Stress and Primary Bending Stress	Lesser of 3.6 x Design Stress Intensity -or- Ultimate Stress
Maximum Range in Stress Including Fabrication, Normal Operation and Accident Conditions	Fatigue Limit for 106 Cycles as Defined in Appendix I of Section III of the ASME Boiler and Pressure Vessel Code
Buckling	Not Allowed Under Any Conditions

Table 2-4. Correlations for Buckling Limits

Buckling Mode	Correlation	Reference
Bending	$\sigma = 0.36 \frac{Et}{r_m}$	Ref. 2.6, Case 42, Page 4-39.
External Pressure	$P_y^2 - \left[\frac{2\sigma_y t}{D} + \left(1 + \frac{1.5De_0}{t}\right)Pc\right]Py + \frac{2\sigma_y t}{D} Pc = 0$ $\sigma_H = \frac{Pc\,r}{t}$	Ref. 2.7, Eq.10.56, Page 308 - and - Ref. 2.9, Case 1b, Page 448.
Compression	$\sigma_a = 0.5 \left[\left\{\sigma_y + \sigma_e \left(1+ \frac{\delta_0 c}{r_G^2}\right)\right\} - \sqrt{\sigma_y + \sigma_e \left(1+ \frac{\delta_0 c}{r_G^2}\right)^2 - 4\sigma_y\sigma_e}\right]$	Ref 2.7, Eq. 3.18, Page 41.

The symbols in this Table are defined as follows:

σ_b is the bending stress to cause buckling

t is the thickness of the shell

r_m is the radius of curvature of the shell = a^2/b

E is the modulus of elasticity

a is the major radius of the elliptical cross section

b is the minor radius of the elliptical cross section

P is the collapse pressure of an elliptical shell

P_c is the collapse pressure of an perfect cylinder

σ_y is the yield stress

D_o is the outside diameter of the shell

D_i is the inside diameter of the shell

e_o is the fractional ovality of the shell

ν is Poisson's ratio

σ_e is the Euler column buckling stress

δ_o is the initial bow or displacement at the midlength

r_g is the radius of gyration = I/A

I is the moment of inertia = $\pi(D_o^4-D_i^4)/64$

A is the cross section area = $\pi\ (D_o^2-D_i^2)/4$

L is the length of the shell

K is a constant which is 0.5 for fixed end columns

Table 2-5. Results of ANSYS Calculations for Bowed Cylinders

Case	Amount of Bow inches	Force Direction	Relative Maximum Bending Stress
1	none	none	1.0
2	0.39	with bow	1.00504
3	3.88	with bow	0.94803
4	0.38	against bow	1.00504

Table 2-6. Correlations for Collapse of Perfect Cylinders

Correlation	Value	Reference
$\sigma_c = \frac{0.25E}{1-\nu^2} \left(\frac{t}{r_m}\right)^2$ or $P_c = \frac{0.25E}{1-\nu^2} \left(\frac{t}{r_m}\right)^3$ valid if $\left(\frac{L}{r_m}\right)^2 > 5 \frac{r_m}{t}$	Pc = 679 psi	2.6
$P_c = \frac{2E}{1-\nu^2} \left(\frac{t}{D}\right)^3$ valid if $\theta > 4\ D/t = 176.8$	Pc = 679 psi	2.7, Eq 10.42a Page 296
$\theta = [12(1-\nu^2)]^{0.25} \frac{L}{D}\sqrt{\frac{D}{t}}$	θ = 154.6	
$P_c = \frac{2E(t/D)}{(3+\lambda^2/2)} \left[\frac{(t/D)^2}{3(1-\nu^2)} \left\{(4+\lambda^2)^2-7\right\} + \frac{\lambda^4}{(4+\lambda^2)^2}\right]$ $\lambda = \frac{\pi D}{2L}$ valid if $\theta > D/t = 44.2$	Pc = 692 psi	2.7 Eq 10.41 Page 296

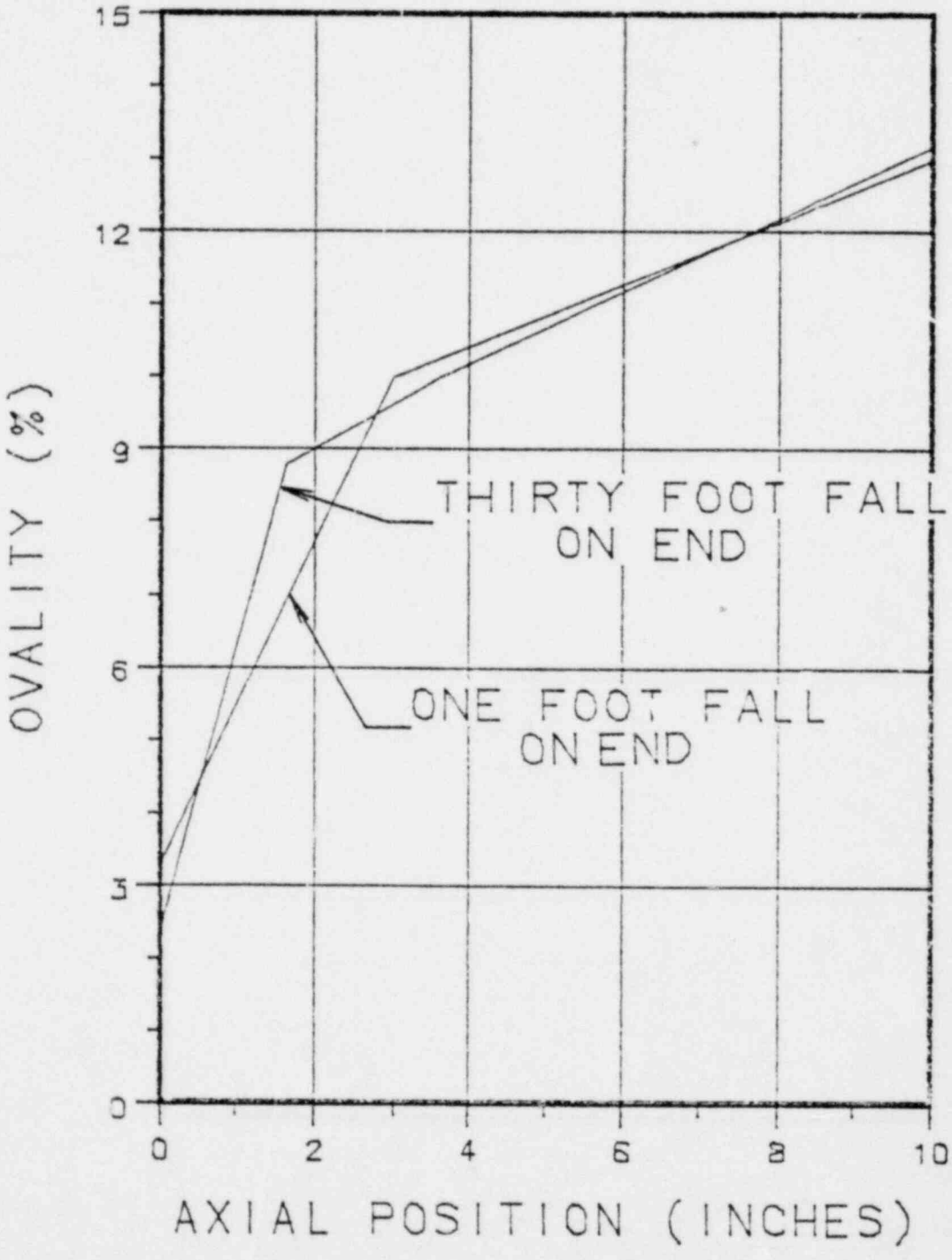

Figure 2-1. Ovality Limits for Inner Shell

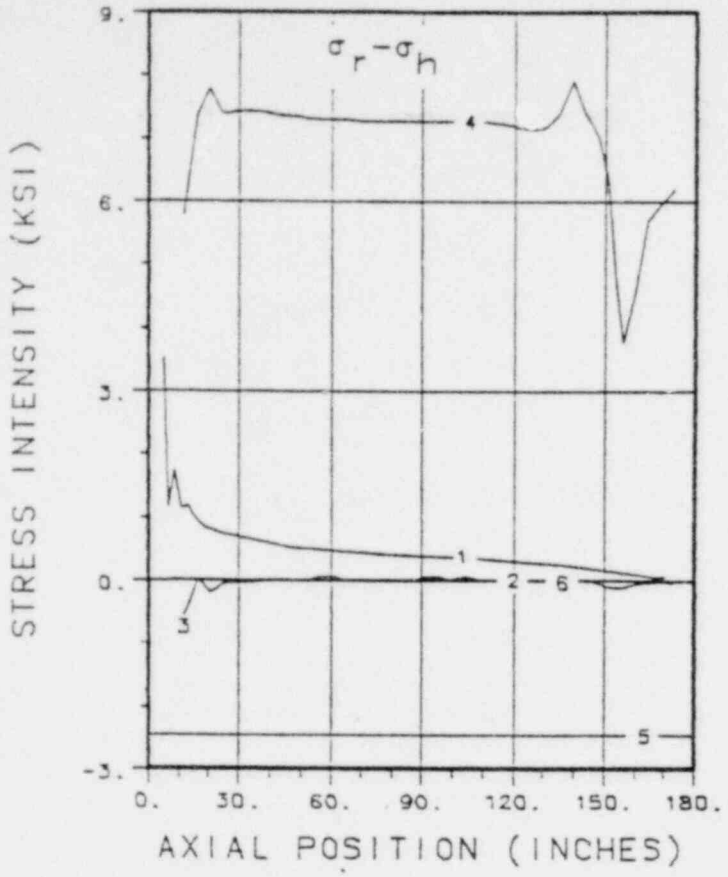

1) 1 FOOT END DROP
2) 1 FOOT SIDE DROP
3) 130 DEG AMBIENT
4) -40 DEG AMBIENT
5) PRESSURE
6) VIBRATION

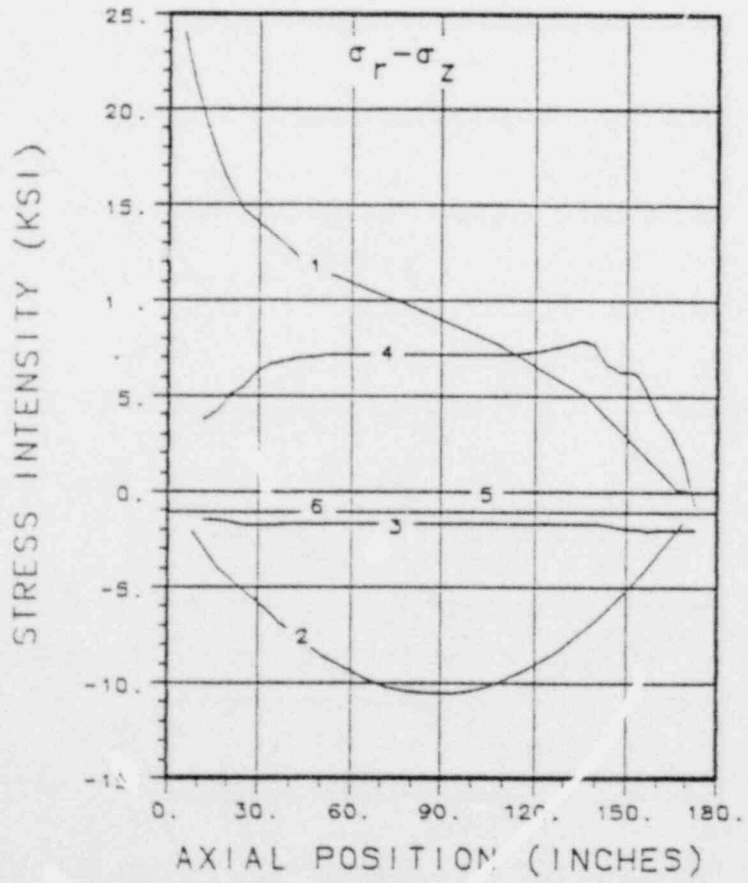

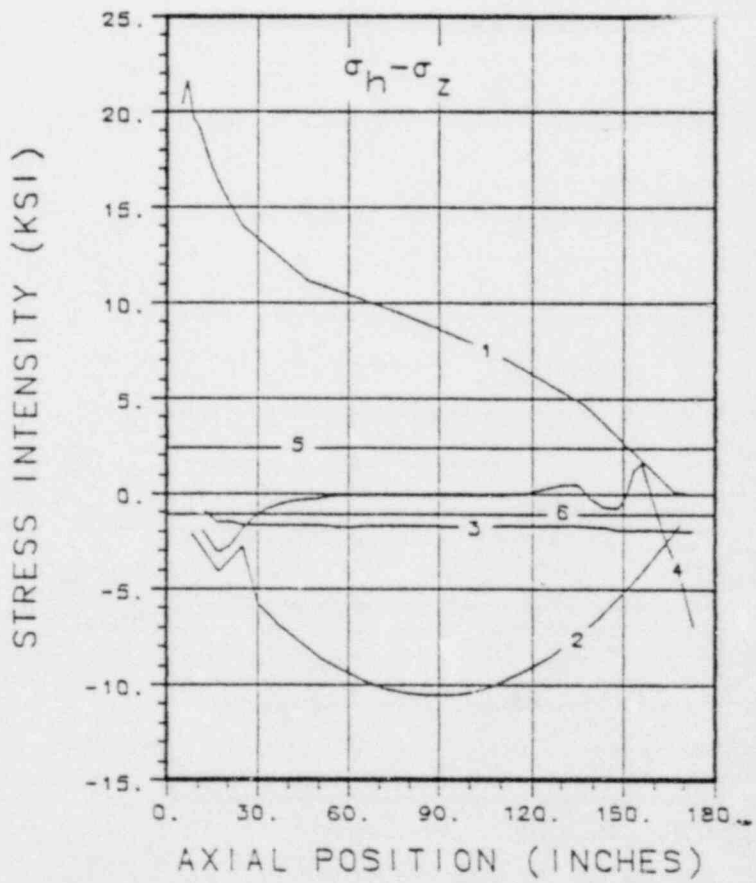

Figure 2-2. Stress Intensity During Normal Transport

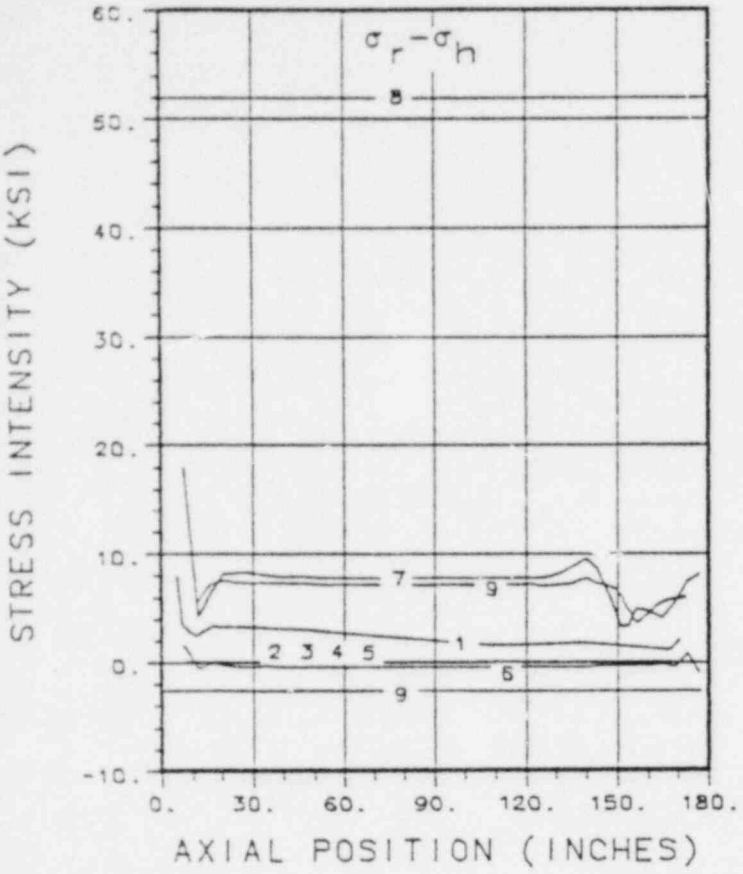

1) 30 FOOT END DROP
2) 30 FOOT SIDE DROP
3) 30 FOOT CORNER DROP
4) PIN DROP ON VALVE
5) PIN DROP AT MIDSPAN
6) 35 MINUTES INTO FIRE
7) LEAD POUR COOLDOWN
8) LEAD POUR
9) ENVELOPE OF NORMAL TRANSPORT

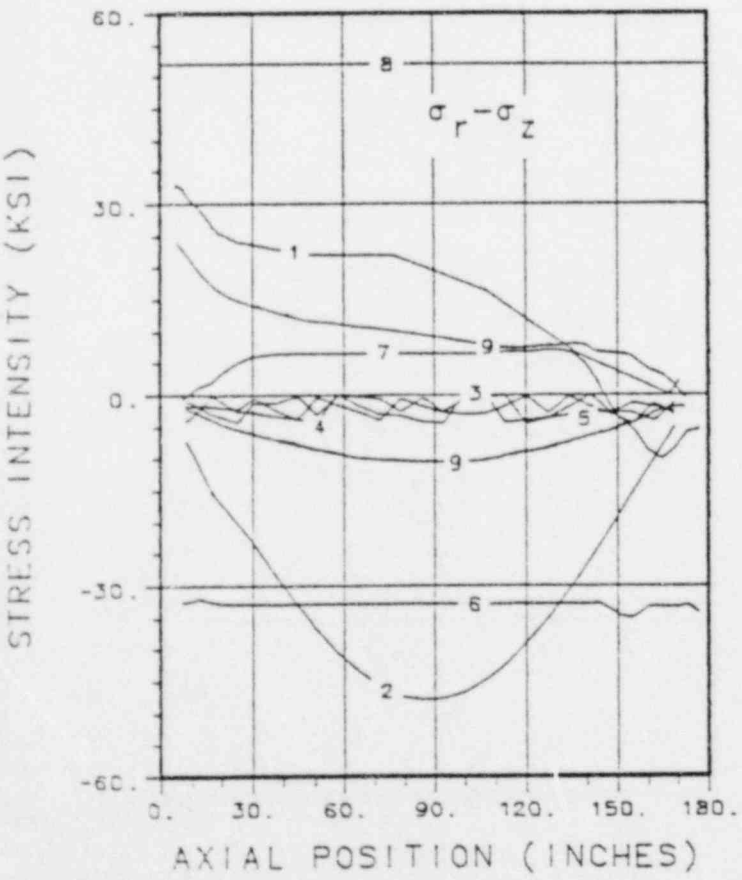

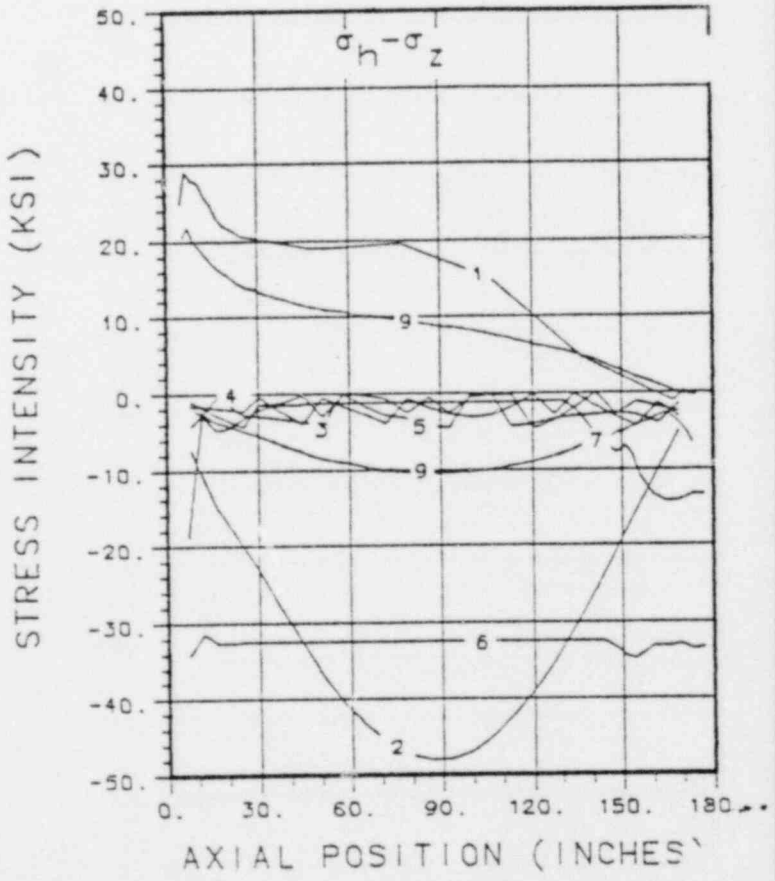

Figure 2-3. Stress Intensity During Hypothetical Accident

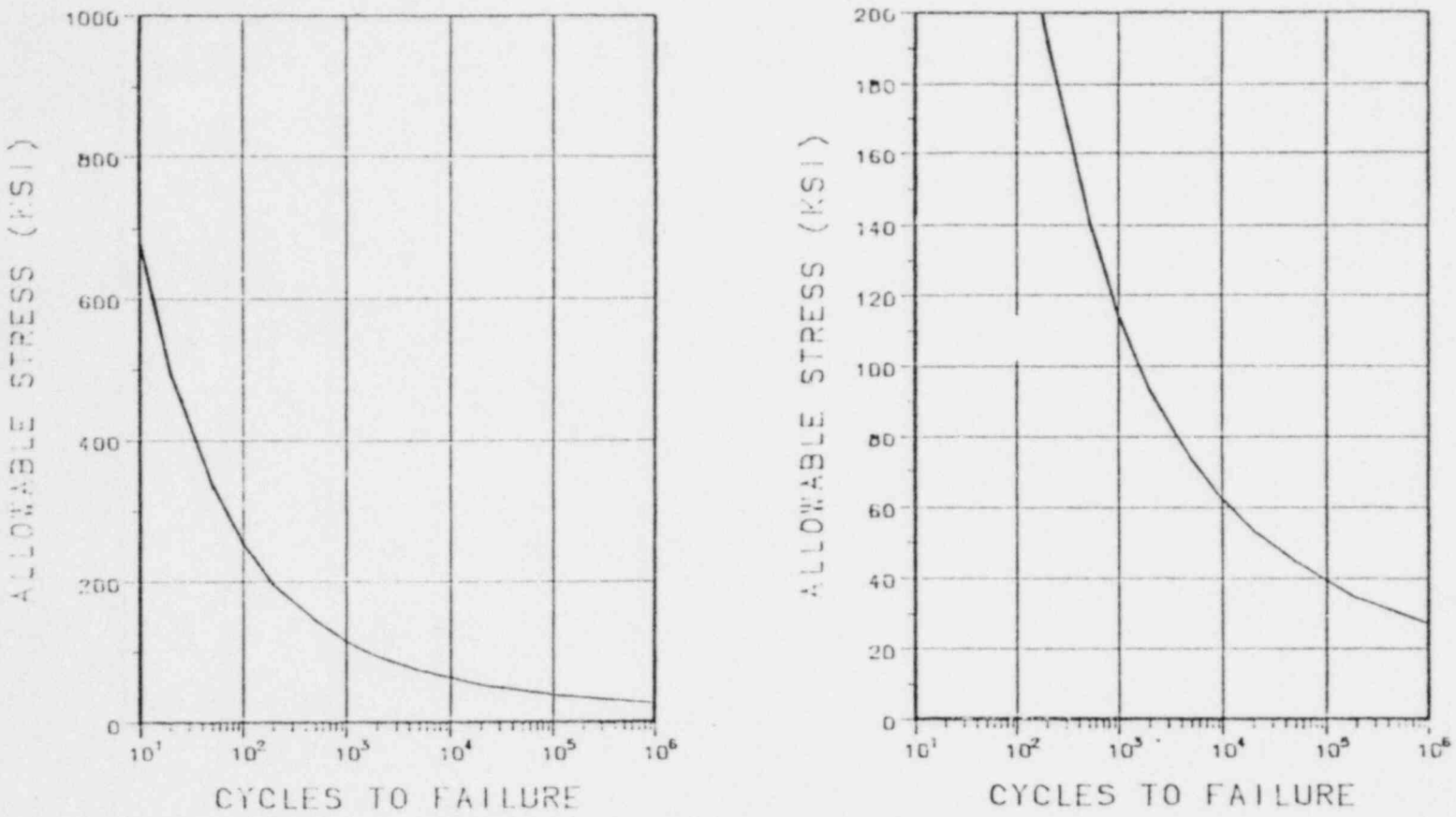

Figure 2-4. Stress Limits for Cyclic Failure

$$\text{OVALITY}(\%) = 200\,\frac{D_{MAX} - D_{MIN}}{D_{MAX} + D_{MIN}}$$

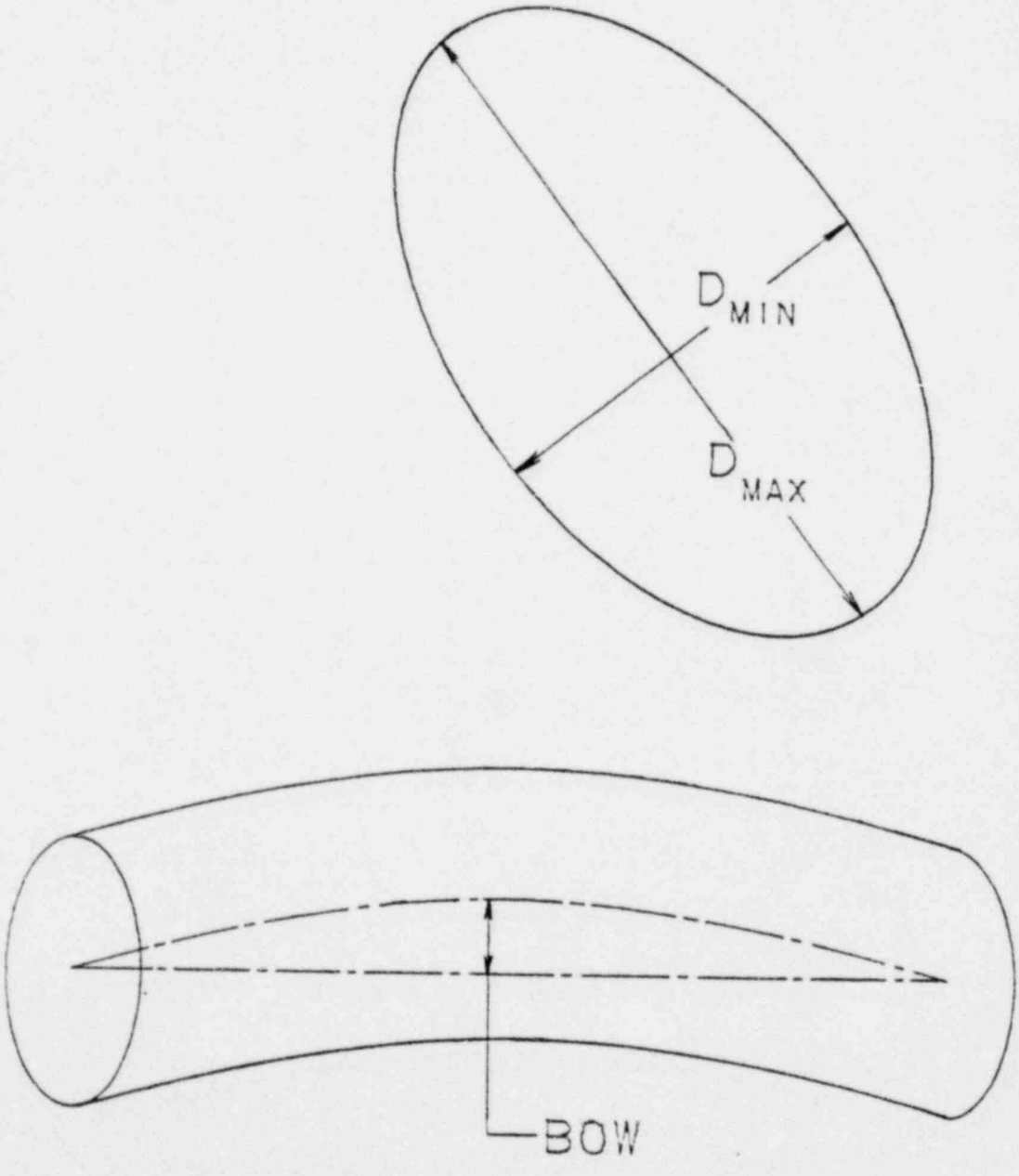

Figure 2-5. Definitions of Ovality and Bow

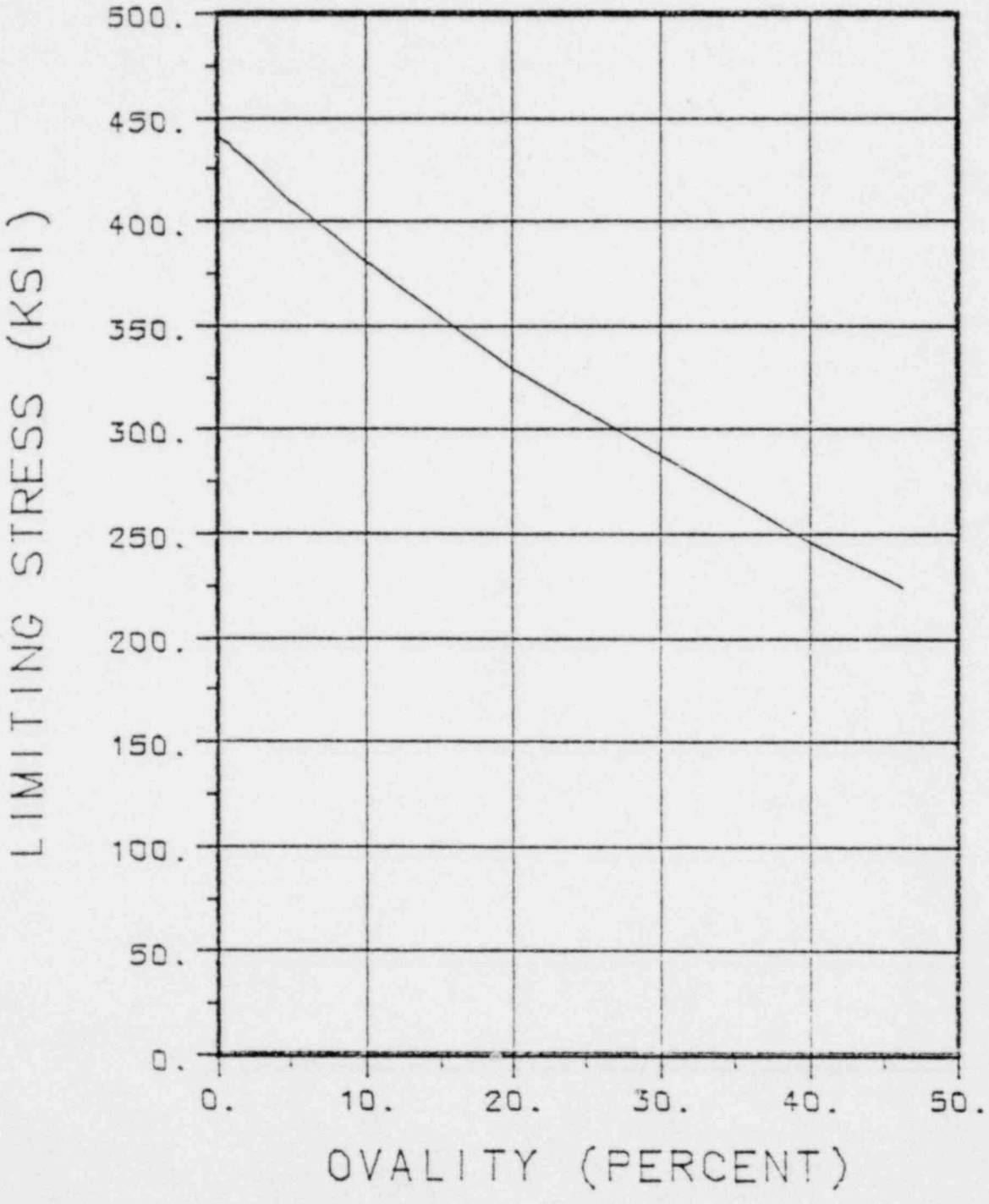

Figure 2-6. Stress Limits to Prevent Buckling in Bending

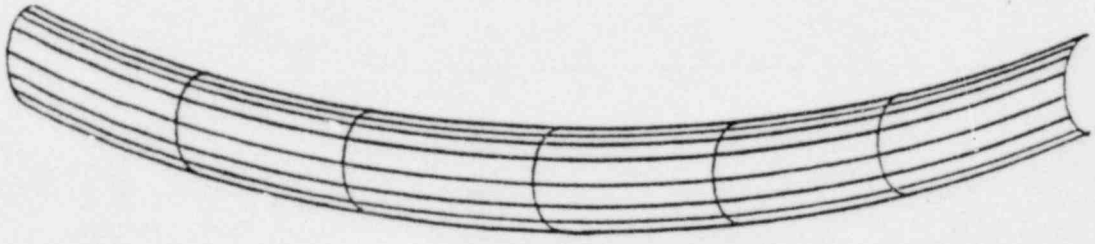

Figure 2-7. ANSYS Model of Bowed Cylinder

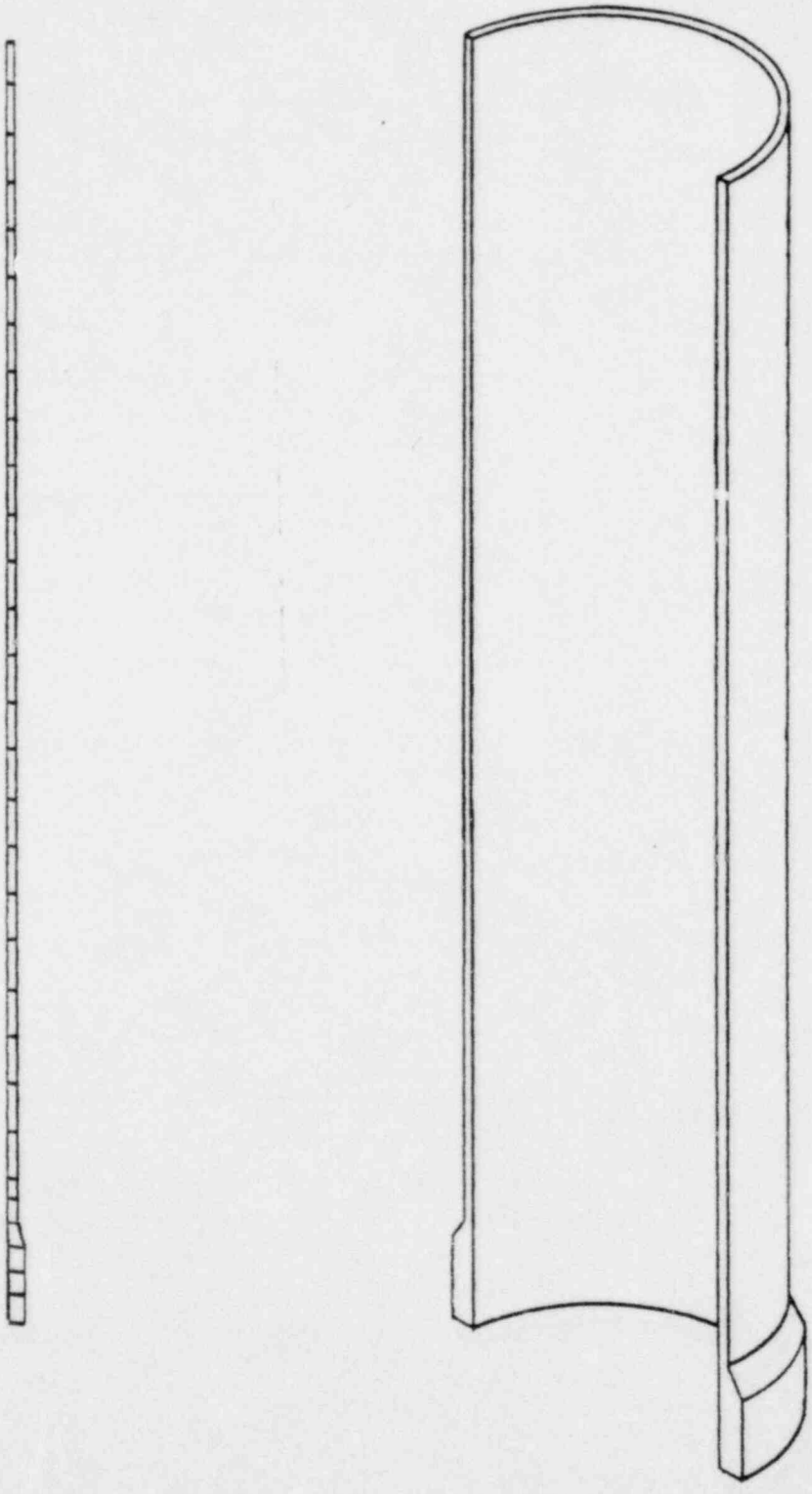

Figure 2-8. ANSYS Model of Inner Shell End Support

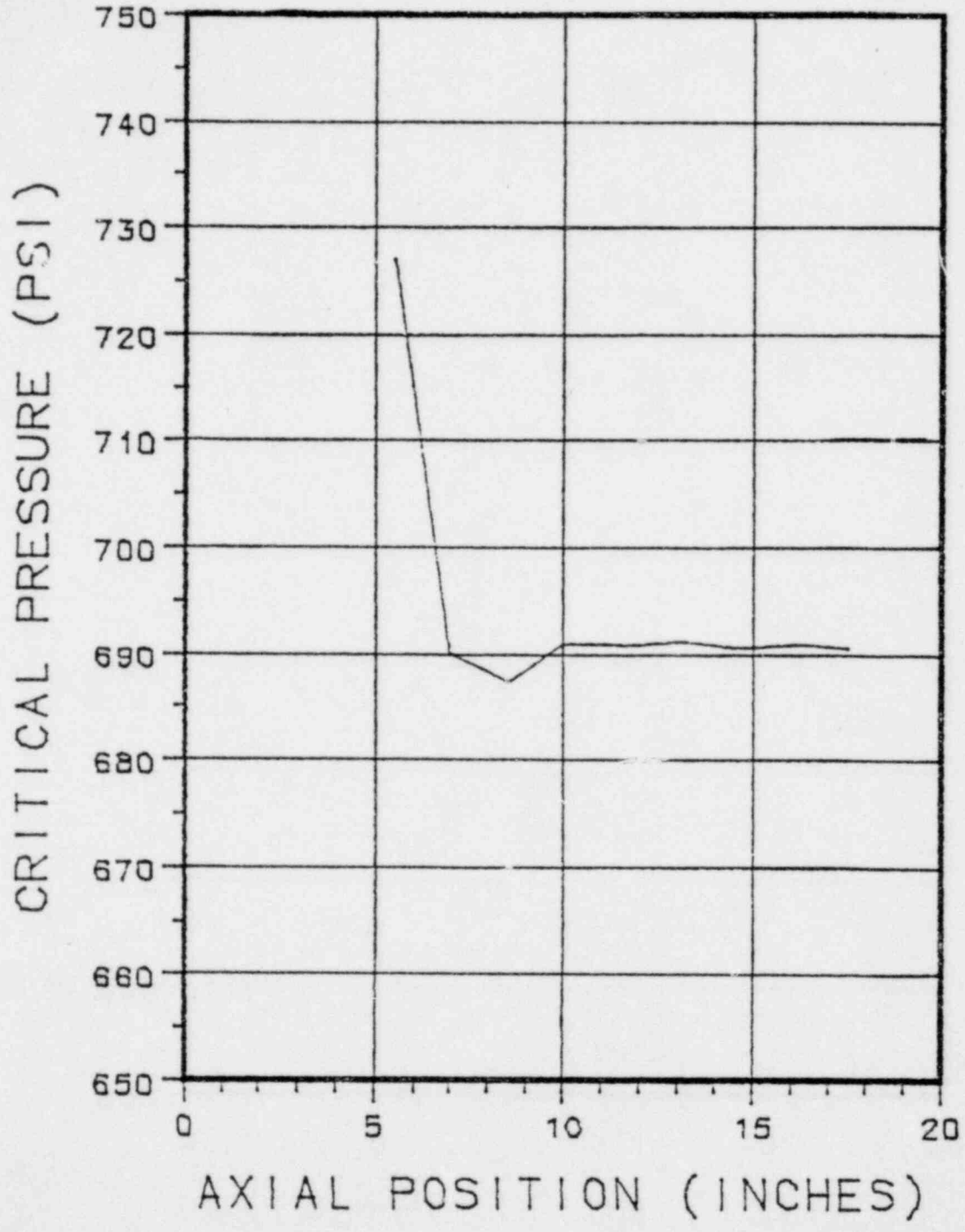

Figure 2-9. Axial Dependence of Critical Pressure

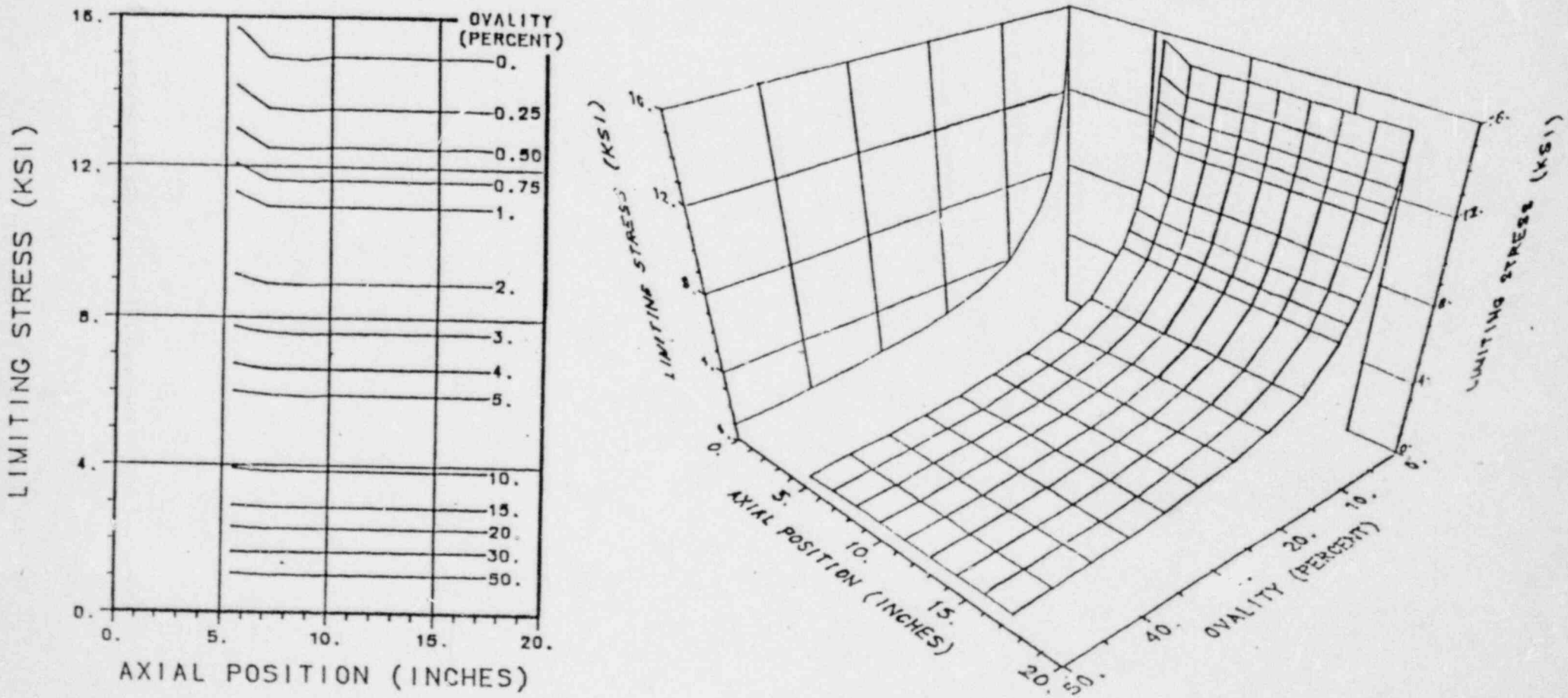

Figure 2-10. Stress Limits to Prevent Collapse by Buckling

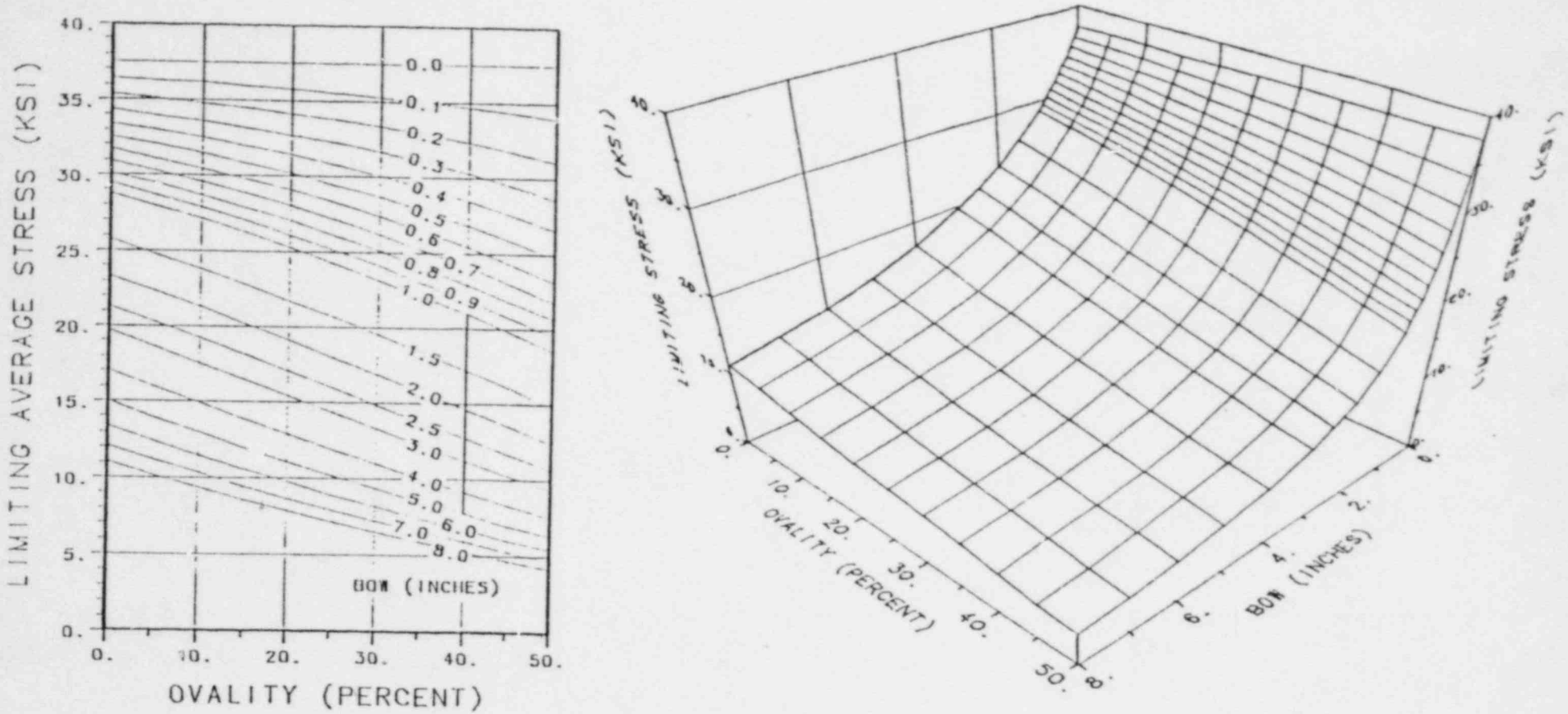

Figure 2-11. Limits to Prevent Column Buckling (Inner Shell)

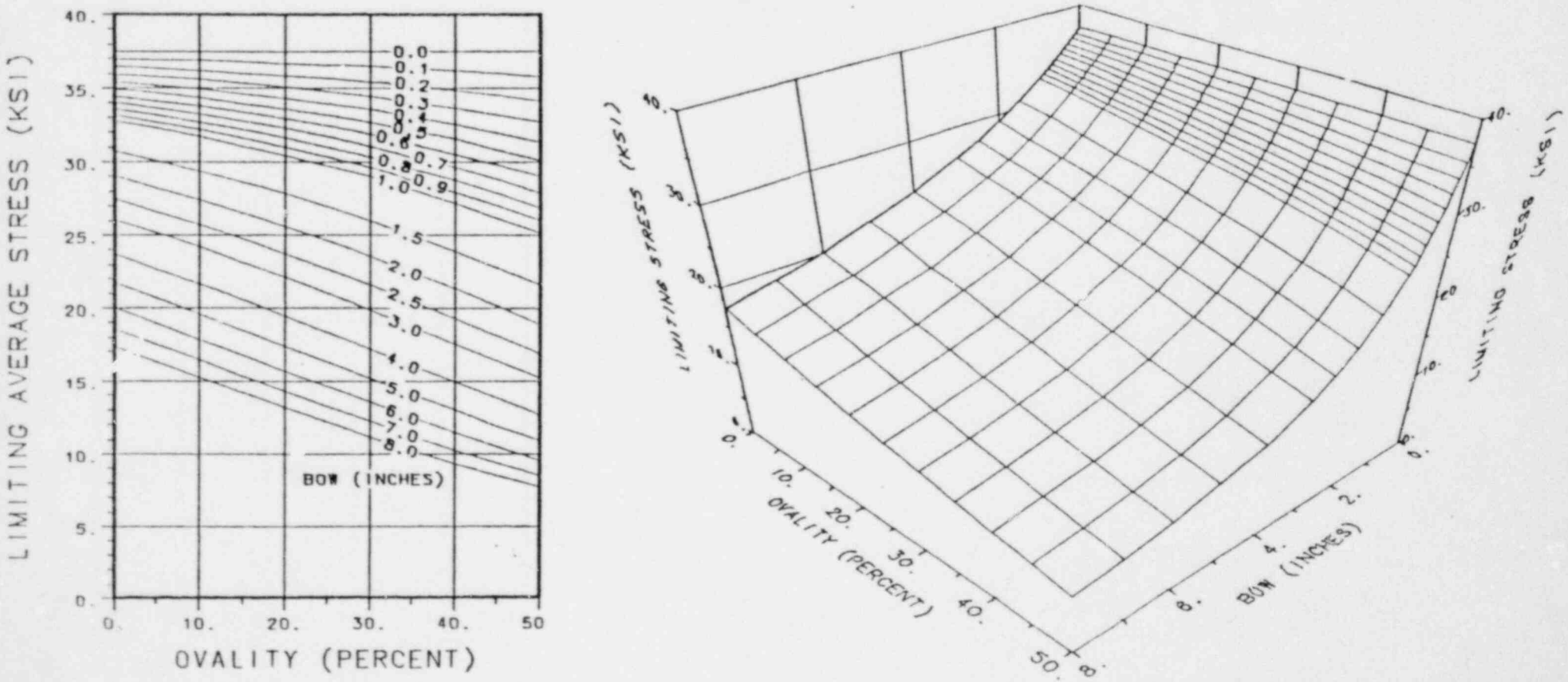

Figure 2- 2. Limits to Prevent Column Buckling (Outer Shell)

2.2. Weights and Centers of Gravity

The weights of the major components and the respective centers of gravity are presented in Table 2-7. The axial location of the center of gravity is measured from the outer surface of the bottom of the cask. The location of the centers of gravity are also presented in Figure 2-13 where the axial location of the center of gravity is indicated for each component. The center of gravity is always on the centerline of the cask because the cask is essentially symmetric about its longitudinal centerline. The fuel assembly, basket and cavity water do not have centers of gravity indicated in Table 2-7 because these are variable and are different for each separate shipment.

The weights and centers of gravity of the cask in several different configurations is presented in Table 2-8 and the location of the center of gravity is measured from the bottom of the cavity. Included in this table are the weights and centers of gravity of the cask in all possible configurations including loaded ready for shipment, loaded less impact limiters and empty. In each case the center of gravity is measured from the outer surface of the bottom of the cask. In Table 2-8 the term full refers to the presence of fuel in the basket and water in the cavity (24 gallons removed during loading). The term empty implies the absence of any fuel in the cavity of the cask; however, the basket remains in the cavity of the cask. The condition identified as "in pool" specifically identifies the weight of the cask when the lid has been removed and the cask cavity is filled with water. No credit has been taken for the bouyant effect of the water and the weight of the yoke has not been included in the tabulated weight because the yoke can be different for each facility that handles the NAC-1 cask.

The centers of gravity of the entire cask that are presented in Table 2-8 assume that the cask is horizontal and the center of

gravity of the fuel assembly corresponds to the center of the fuel within the assembly. The location of the center of gravity under other conditions must be evaluated independently.

All of the entries in Table 2-7 and 2-8 have been rounded upward to insure that all of the analyses that are dependent upon the cask weight are conservative. Where the weight of the cask is necessary in the analyses that are described in this report, the weight has been taken as 52,000 pounds which represents the upper bound of the weight of the cask under all conditions.

Table 2-7. Major Component Weights of NAC-1 Cask

Component	Weight Pounds	Axial Location of Center of Gravity Inches
Cask Body	40,500	93.6
Impact Limiters		
Upper	1,050	193.0
Lower	1,030	0.7
Lid	600	190.7
Fuel Assembly	1,550	-
Basket	1,100	-
Cavity Water	400	-
Shield Tank Fluid	2,600	91.2

Table 2-8. Weights of NAC-1 Cask

Cask Configuration	Weight Pounds	Axial Location of Center of Gravity Inches
Ready for Transport		
Full		
Wet	48,830	94.6
Dry	48,430	94.6
Empty		
Wet	47,280	94.9
Dry	46,880	95.0
Impact Limiters Removed		
Full		
Wet	46,750	94.5
Dry	46,350	94.5
Empty		
Wet	45,200	94.9
Dry	44,800	94.9
In Pool		
Full	46,350	95.0
Empty	45,100	94.9

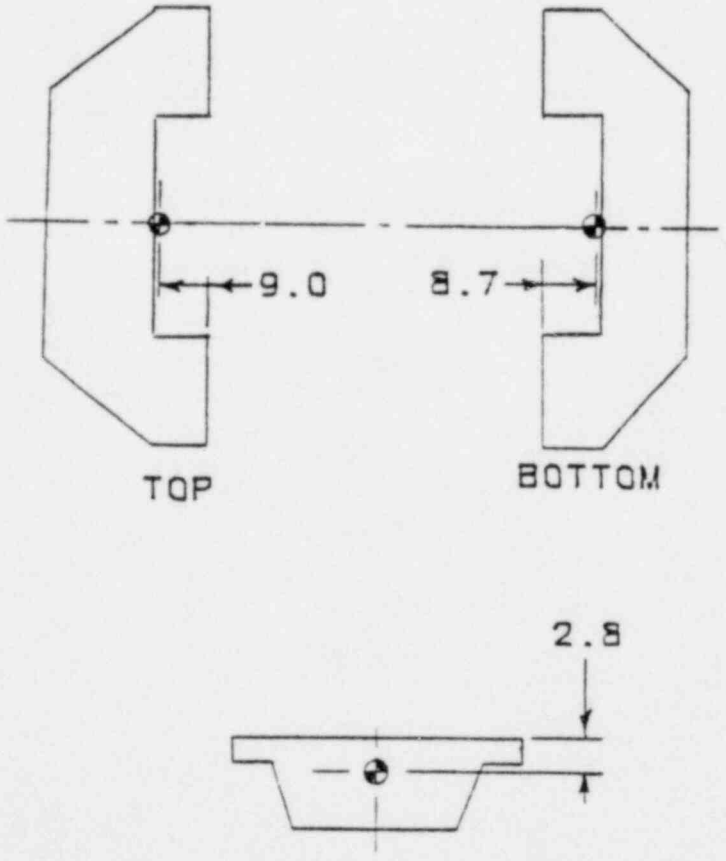

Figure 2-13. Location of Centers of Gravity of Cask Components

2.3. Mechanical Properties of Materials

Five materials are important to the structural analysis of the NAC-1 cask. Stainless steel and lead are the principal materials in the cask body while stainless steel, redwood and balsa wood are the principal materials in the impact limiters. The mechanical properties of these materials are dependent upon both the strain rate and temperature. The effects of these variables were included in the evaluation of the properties of each material of importance.

2.3.1. Stainless Steel

The analysis of the response of the NAC-1 cask during normal transport and hypothetical accident conditions requires the evaluation of minimum properties for this material. These properties were employed for the evaluation of the characteristics of the cask as well as the evaluation of the limiting stresses that define acceptable loading conditions.

The stainless steel that forms the inner and outer shells of the cask body is type 321. Type 347, 348, 304 and 316 are alternate materials for all of the stainless steel components. The properties of type 347 and 348 stainless steels are identical to the properties of type 321 stainless steel with the sole exception of the yield strength which does not decrease as rapidly as does the yield strength of type 321 as the temperature increases. Consequently, the replacement of type 321 with either type 347 or 348 results in a very slight increase in the strength of the cask components.

2.3.1.1. Static Properites

The American Society of Mechanical Engineers (Reference 2.4) has compiled a conservative set of mechanical properties of this grade of stainless steel that is applicable when the loading is static. This compilation includes temperature dependence of the material properties. The mechanical properties of type 321 stainless steel are tabulated in Table 2-9. These data represent room temperature (70°F) conditions. The temperature dependence of the properties is given in Figure 2-14. In several instances the properties had to be extrapolated to obtain values for the low temperature conditions that are encountered and the respective curves in Figure 2-14 have been dashed. Where it has become necessary to utilize data that is the result of extrapolation, the choice has been made between using the extrapolated value and the last tabulated value. The choice of the value was dictated by conservatism in each specific instance.

The coefficient of thermal expansion of stainless steel has also been tabulated in Appendix I of the ASME Boiler and Pressure Vessel Code. The quantity employed for these analyses is the mean coefficient that depicts the total expansion between two specific temperatures. The instantaneous coefficient of thermal expansion depicts the incremental change in the length and must be integrated to obtain the change in length between two temperatures. These data have been ploted as a function of temperature in Figure 2-14. The value that is presented in Table 2-9 is the mean coefficient between 70 and 625°F and does not represent the mean coefficient at 70°F.

2.3.1.2. Dynamic Properites

Dynamic loadings increase the effective strength of stainless steel because the grain structure does not have time to be reoriented during the deformation. This effect is very pronounced when the loadings are compressive as in the impact limiters during the free falls.

The strength of stainless steel has been measured and reported by several different laboratories for varying loading rates. In each series of measurements one or more samples were loaded statically to provide a consistancy check on the validity of the reported data. The data from the static measurements correlates well with the properties that are cited in reference texts for the mean properties of stainless steel. Consequently, the data that is available for the dynamic strength has to be characterized as typical of stainless steel. No data is available that can be described as representing the minimum dynamic properties of stainless steel. The effect of strain rate on the strength of stainless steel is presented in Figure 2-15. These curves have been reduced from data presented in Reference 2.12 and describe mean characteristics of stainless steel. The mean yield strength of stainless steel when subject to dynamic loading is over 50,000 psi while static loading results in a value of 37,500 psi. The effects of dynamic loading have been considered to balance the conservatism that results from the use of minimum strength properties. Thus, the dynamic strength of stainless steel that was used for the evaluation of the impact loadings is, in fact, the strength of typical specimens of stainless steel. This stress-strain curve is presented in Figure 2-16 which is based upon data presented in Reference 2.12. This data is also summarized in Table 2-10.

A true stress-true strain representation of the strength of stainless steel has been selected to assure that no errors are

introduced as a result of using tensile test data to represent compressive loadings.

2.3.2. Bolt Material

The bolts that attach the lid to the cask body are fabricated from grade A320 type L43 low alloy steel. The only properties of interest for this material are the yield strength, the design stress intensity, and the modulus of elasticity which are presented in Table 2-11 at 300 °F. The bolts are stronger at lower temperatures so considering only the high temperature properties of this material results in conservative analyses.

2.3.3. Lead

The lead that fills the central region of the cask wall is virtually pure lead which has less than 0.05% copper as an impurity (Reference 2.14). The presence of copper increases the strength of lead at temperatures above 212°F while at lower temperatures pure lead is slightly stronger than a lead-copper alloy (Reference 2.10). To assure conservatism in these analyses the properties of the lead-copper alloy was employed for high temperatures and the properties of pure lead were employed for low tempreature cases. There is no concern about the lead failing as it is totally captured in the cask wall and its shielding function requires no strength.

2.3.3.1. Static Properites

Reference 2.10 presents the strength of lead as a function of temperature for static loading. The mechanical properties of lead at room temperature have been tabulated in Table 2-12. Additionally, this data is presented in Figure 2-17 where the stress strain curve of lead is shown as a function of temperature.

The thermal expansion (contraction) of lead is important to the analysis of the stresses following the pouring of lead into the cask wall. The thermal expansion of lead is presented in Reference 2.10 as a function of temperature. This data represents the total expansion as a function of temperature. The measured data and a smoothed curve are presented in Figure 2-18.

2.3.3.2. Dynamic Properites

The plasticity of lead changes dramatically when it is loaded dynamically. Reference 2.10 describes an experimental program to determine the properties of lead at high strain rates and presents data that identifies the increase in strength as a function of strain rate. The change in the strength of lead is presented in Figure 2-19 and the stress-strain curve of lead at 325°F and a strain rate between 800 and 8000 %/sec is presented in Figure 2-20.

2.3.4. Copper

The fins that assure thermal communication between the lead and stainless steel shells are fabricated from oxygen free copper

plates. The mechanical properties of copper plate are tabulated in the Appendices to the Boiler and Pressure Vessel Code that has been published by the American Society of Mechanical Engineers. The values of the mechanical properties that were employed in this analysis are tabulated in Table 2-13. These data are appropriate only for static loading and do not apply to dynamic loadings where the effect of strain rate increases the effective strength of the copper.

2.3.5. Redwood

Redwood is employed in a sacrificial capacity to absorb impact energy by crushing. The properties of redwood have been measured and reported in references 2.15 and 2.16. These properties have been determined by forcing a circular bar into samples with their grain orientated parallel to the impact direction. A typical stress-strain curve for redwood is shown in Figure 2-21. The redwood crushes elastically and then becomes plastic where the crush strength is nearly constant. When the deformation approaches 65 to 70% of the initial length the redwood behaves as an incompressible solid. To assure conservatism in predicting the impact limiter response, the deformation to lock-up was set at 65%.

The temperature and density dependence of the crush strength of redwood have been measured at Sandia Laboratory and reported in Reference 2.16. The temperature dependence of the peak and average crush strength are presented in Figure 2-22 and the density dependence is presented in Figure 2-23. The data that are represented in these two figures have been smoothed slightly and where necessary one figure was used to adjust measured data to correspond to the conditions of the other figure. The minimum density of the redwood that is employed in the impact limiters is 21 pounds per cubic foot and the most representative temperature

of the redwood is about 70°F which result in an average crush stress of 5100 psi which has been used in all of the impact limiter evaluations.

The crush strength of any wood or fibrous material when the force is applied at an angle to the grain is given in Reference 2.17 as:

$$N = \frac{P\ Q}{P \sin^2\theta + Q \cos^2\theta}$$

where:

P is the crush strength parallel to the grain in psi,
Q is the crush strength normal to the grain in psi,
θ is the angle between the crush force and the grain in degrees.
N is the crush strength at the specified angle in psi.

Reference 2.17 also tabulates the properties of redwood and lists representative values of the average crush stress parallel and perpendicular to the grain. The ratio of these two crush strengths is 16.6%. This relationship between the crush direction and the crush strength is presented in Figure 2-24.

2.3.6. Balsa Wood

Balsa wood is also used as a sacrificial material that absorbs kinetic energy by crushing. The crush characteristics of balsa wood are similiar to the characteristics of redwood with the principal exception of the magnitude of the strength. The ratio of strength perpendicular and parallel to the grain is 7%. The deformation required to achieve lock-up has been measured at 75 to 79% of the initial length. This was treated as 75% in all of the calculations of impact limiter performance. The crushing

characteristics of balsa are presented in Figure 2-25 as a stress strain curve that is based upon measurements of the force required to push a mandrel into a confined sample of balsa wood. Figure 2-25 presents the stress-strain curve for balsa wood when the impact direction is parallel, perpendicular and at 50o to the grain. The variation in crush strength as a function of angle between the grain and crush direction is based upon the equation presented in Section 2.3.5 and the data in Figure 2-24.

When pieces of balsa wood are employed such that both crush during an impact the combined stres ,train curve is dependent upon the softer piece crushing followed by the harder piece crushing after the softer piece has reached lock-up. The combined stress-strain curve for a one inch thick piece of balsa wood on top of a 12.5 inch thick piece of balsa wood is presented in Figure 2-26. The longer piece of balsa wood has its grain oriented both parallel to the impact and at 50° to the impact in this figure. These stress-strain curves were used to define the force-deflection curves for both the side and end impact limiters.

Table 2-9. Mechanical Properties of Type 321 Stainless Steel

		Reference
Modulus of Elasticity	27.1 x 10^6 psi	Table I-6.0
Yield Strength	22,200 psi	Table I-2.2
Ultimate Strength	69,300 psi	Table I-3.2
Design Stress Intensity	20,000 psi	Table I-1.2
Strain at Yield	0.082 %	- -
Poisson's Ratio	0.275	- -
Density	497 lb/ft^3	- -
Coefficient of Thermal	9.51 x 10-6 $in/in/^oF$	

Reference refers to the specific Table in Appendix I of the ASME Boiler and Pressure Vessel Code, Section III, Division 1, 1977 Edition.

Table 2-10. Dynamic Mechanical Properties of Stainless Steel

Modulus of Elasticity	27.1 x 10^6 psi
Yield Strength	37,500 psi
Ultimate Strength	150,000 psi

Table 2-11. Mechanical Properties of Bolt Material

Modulus of Elasticity	29. x 10^6 psi
Design Stress Intensity	31,900 psi
Ultimate Strength	105,000 psi

Table 2-12. Mechanical Properties of Chemical Lead

Modulus of Elasticity	14.3 x 10^6 psi
Yield Strength	1000 psi
Ulltimate Strength	5000 psi
Strain at Yield	0.007 %
Poisson's Ratio	0.40
Density	708.5 lb/ft^3

Table 2-13. Mechanical Properties of Oxygen Free Copper

		Reference
Modulus of Elasticity	16.0×10^6 psi	Table I-6.0
Yield Strength	10,000 psi	Table I-8.4
Ultimate Strength	30,000 psi	Table I-8.4
Poisson's Ratio	0.3	- -

Reference refers to the specific Table in Appendix I of the ASME Boiler and Pressure Vessel Code, Section III, Division 1, 1977 Edition.

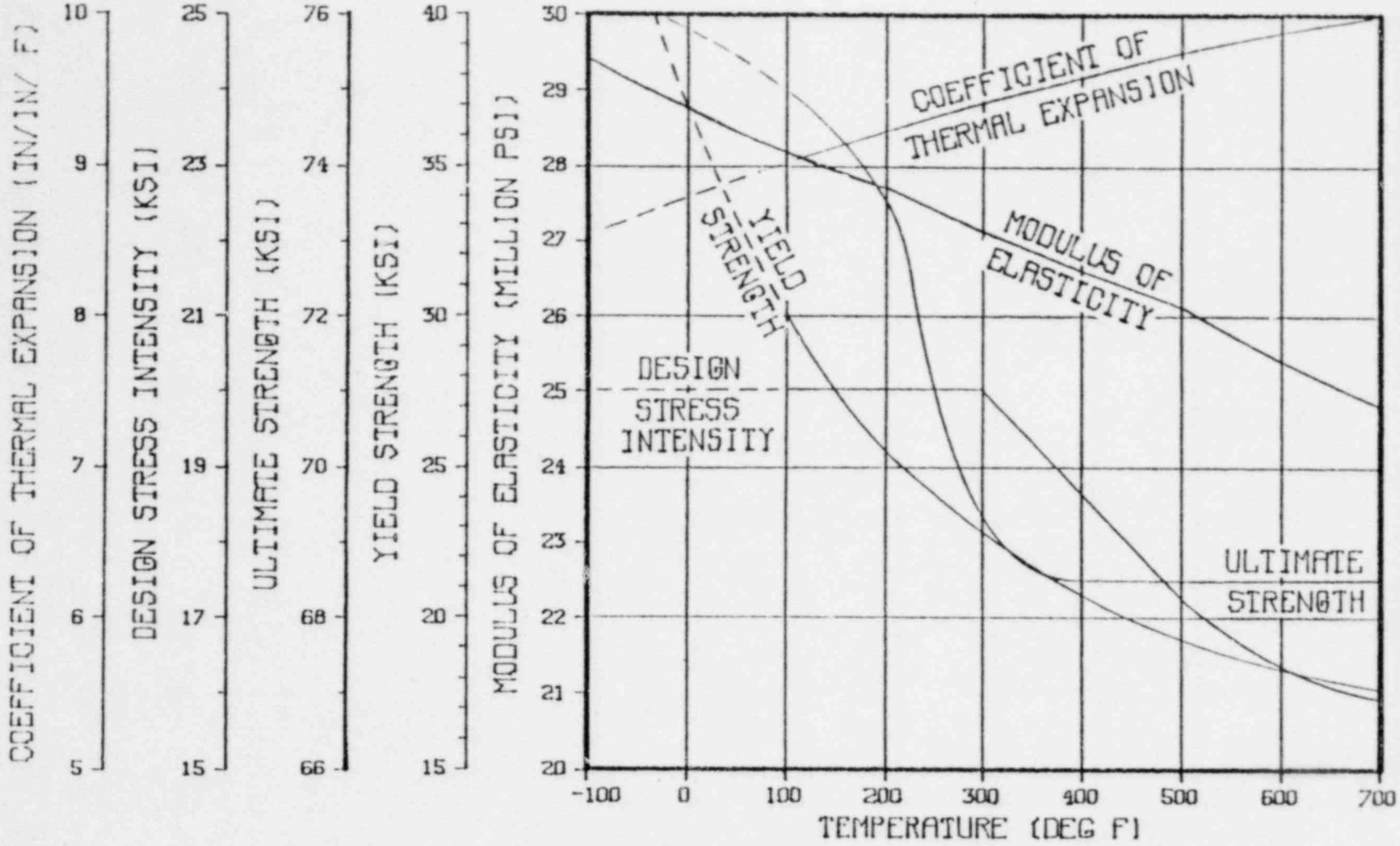

Figure 2-14. Temperature Dependence of Stainless Steel Properties

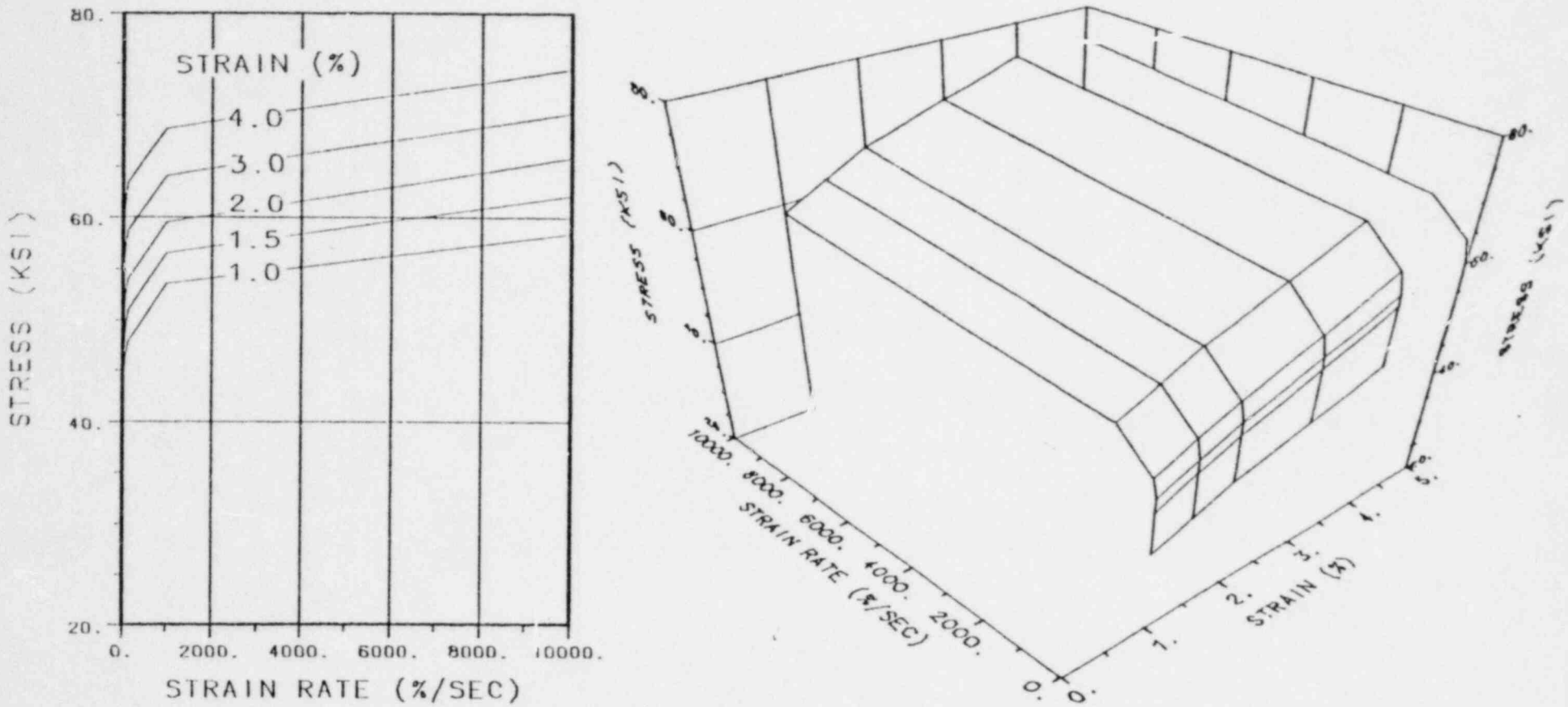

Figure 2-15. Effect of Strain Rate on Type 321 Stainless Steel

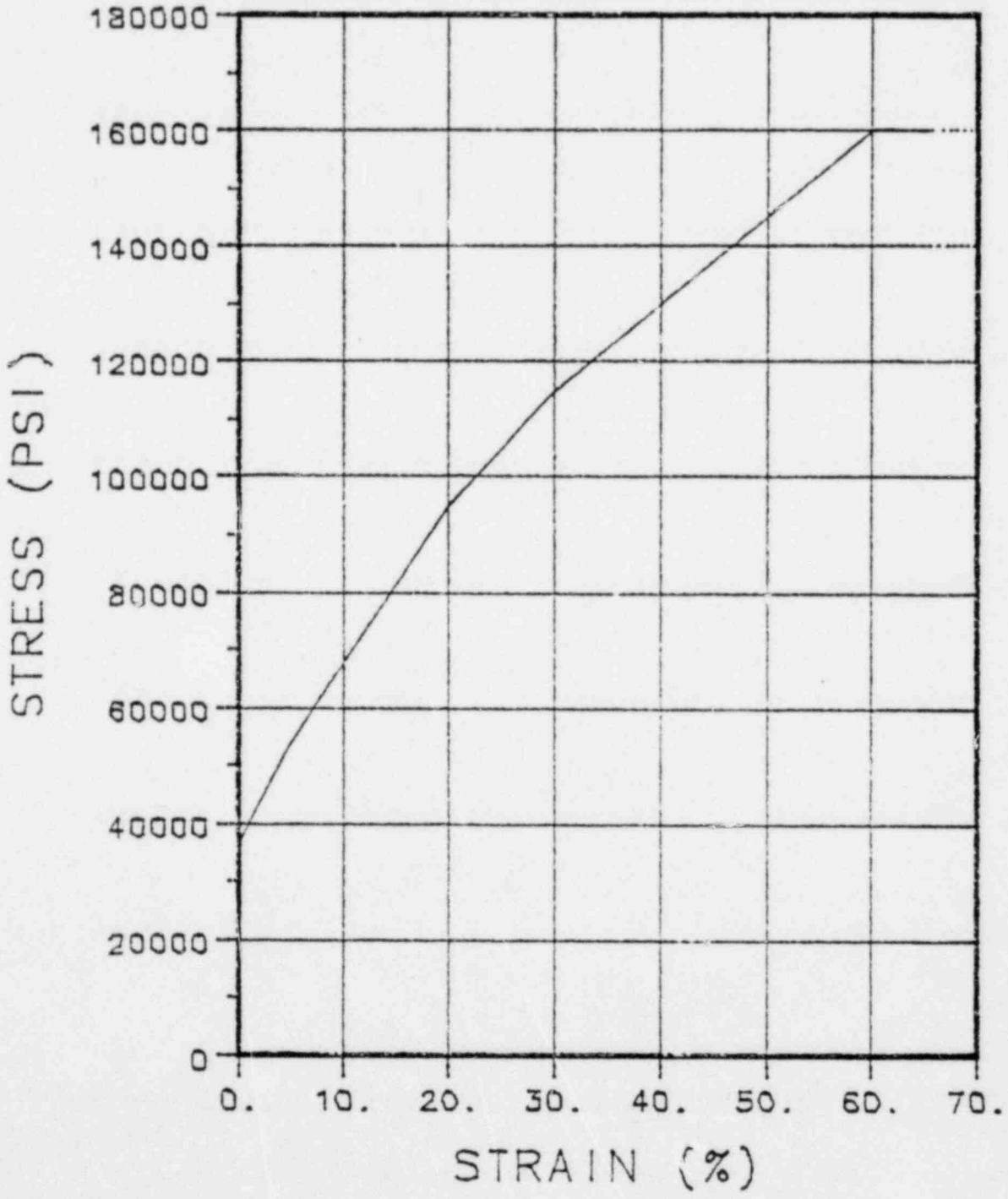

Figure 2-16. Dynamic Stress-Strain Curve for Type 321 Stainless

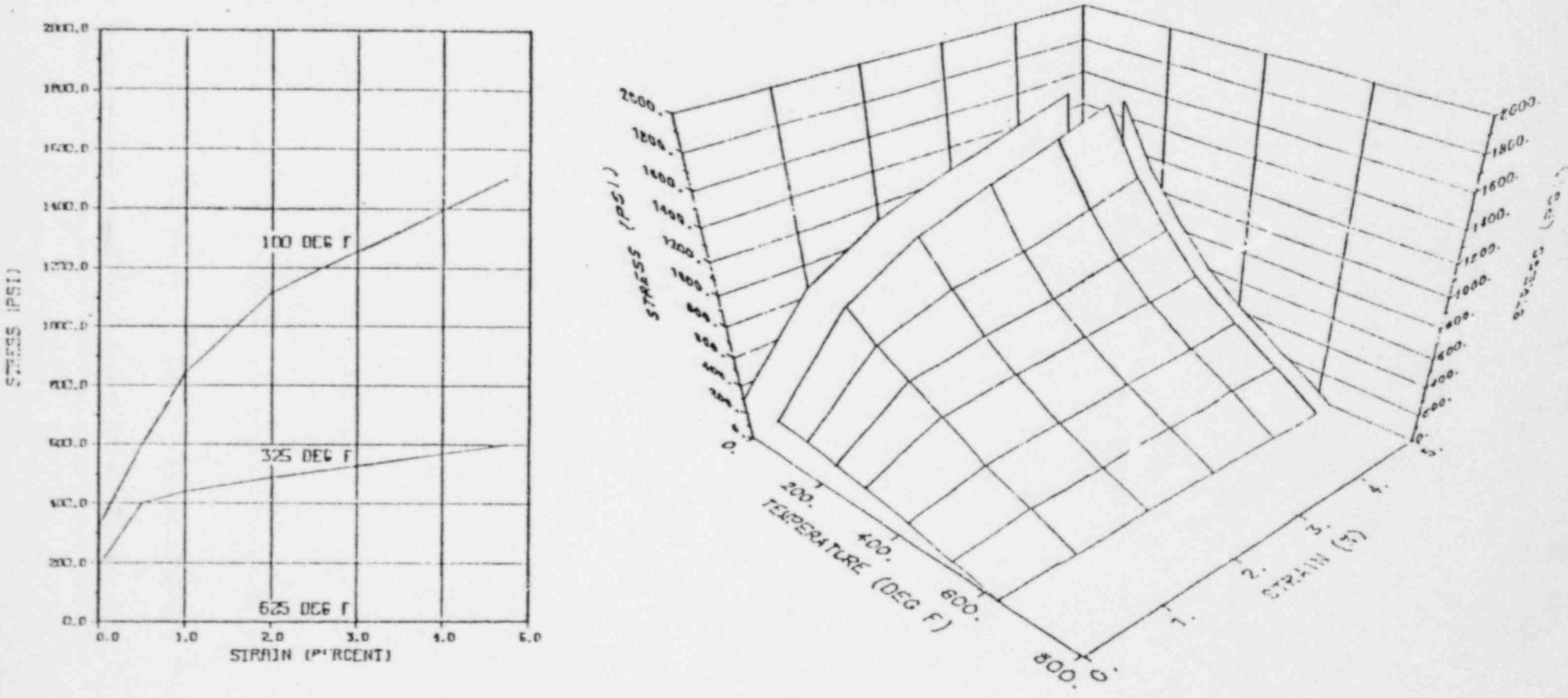

Figure 2-17. Stress-Strain Curve for Chemical Lead

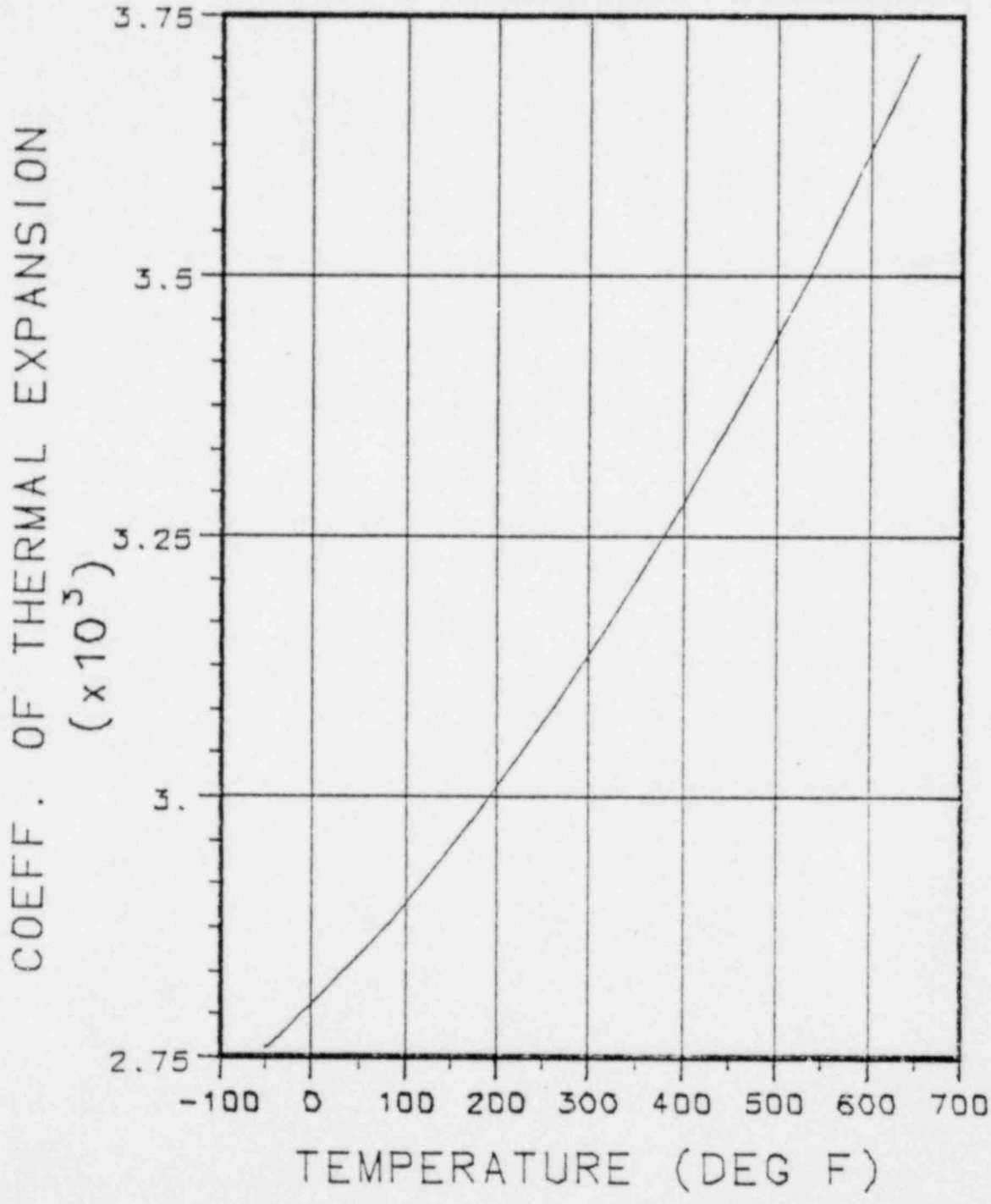

Figure 2-18. Thermal Expansion of Lead

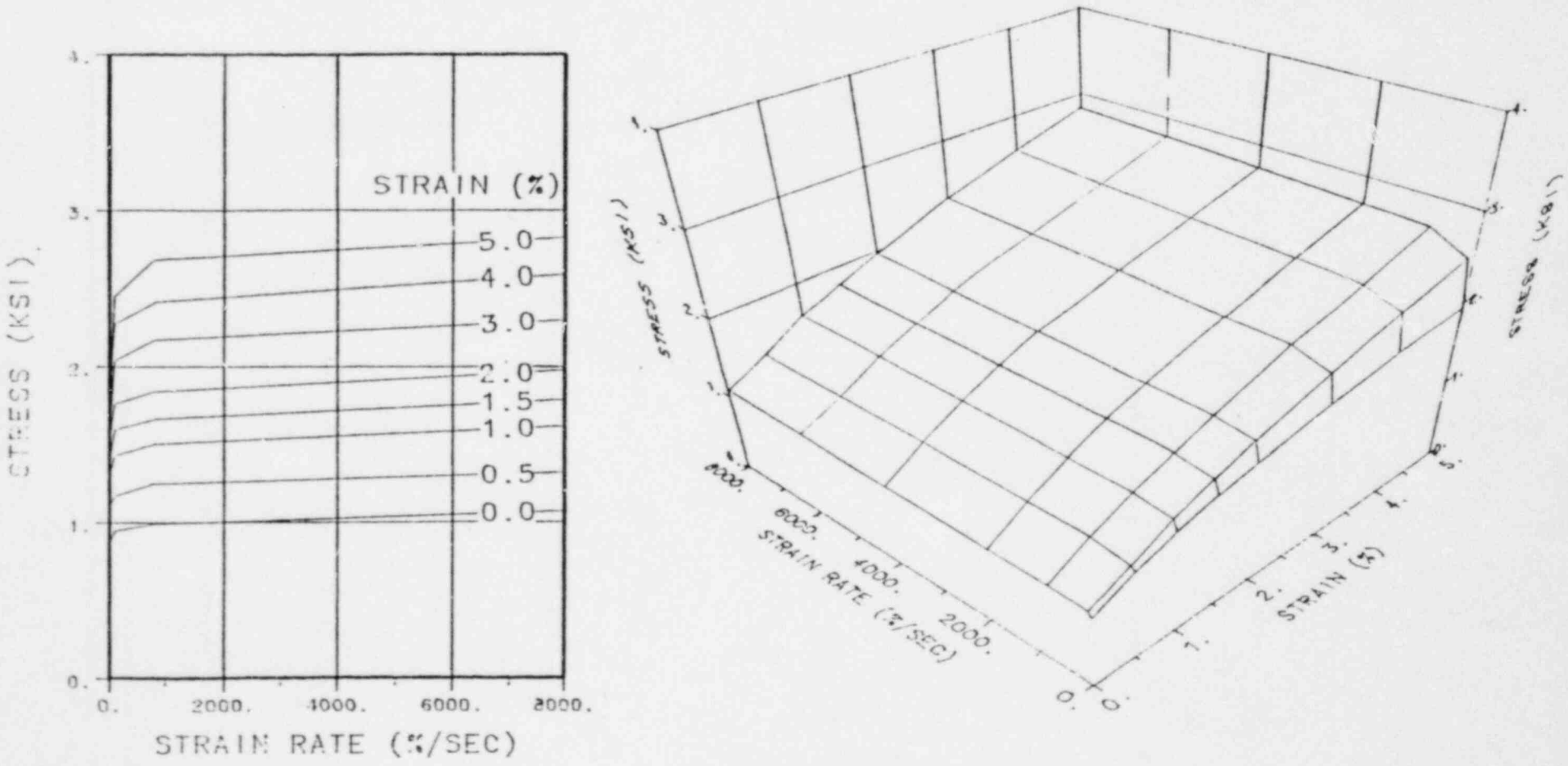

Figure 2-19. Effect of Strain Rate on Chemical Lead

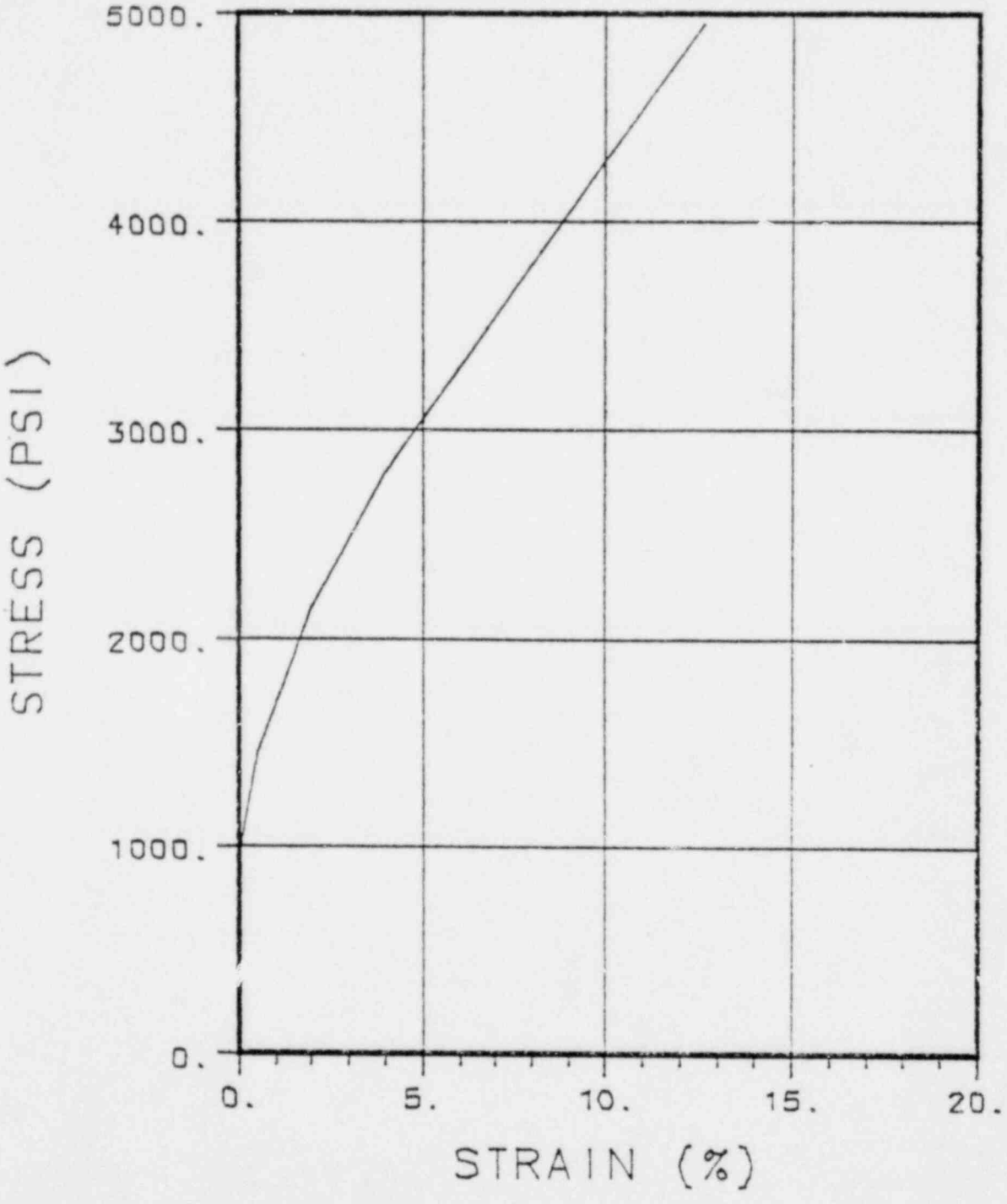

Figure 2-20. Dynamic Stress-Strain Curve for Chemical Lead

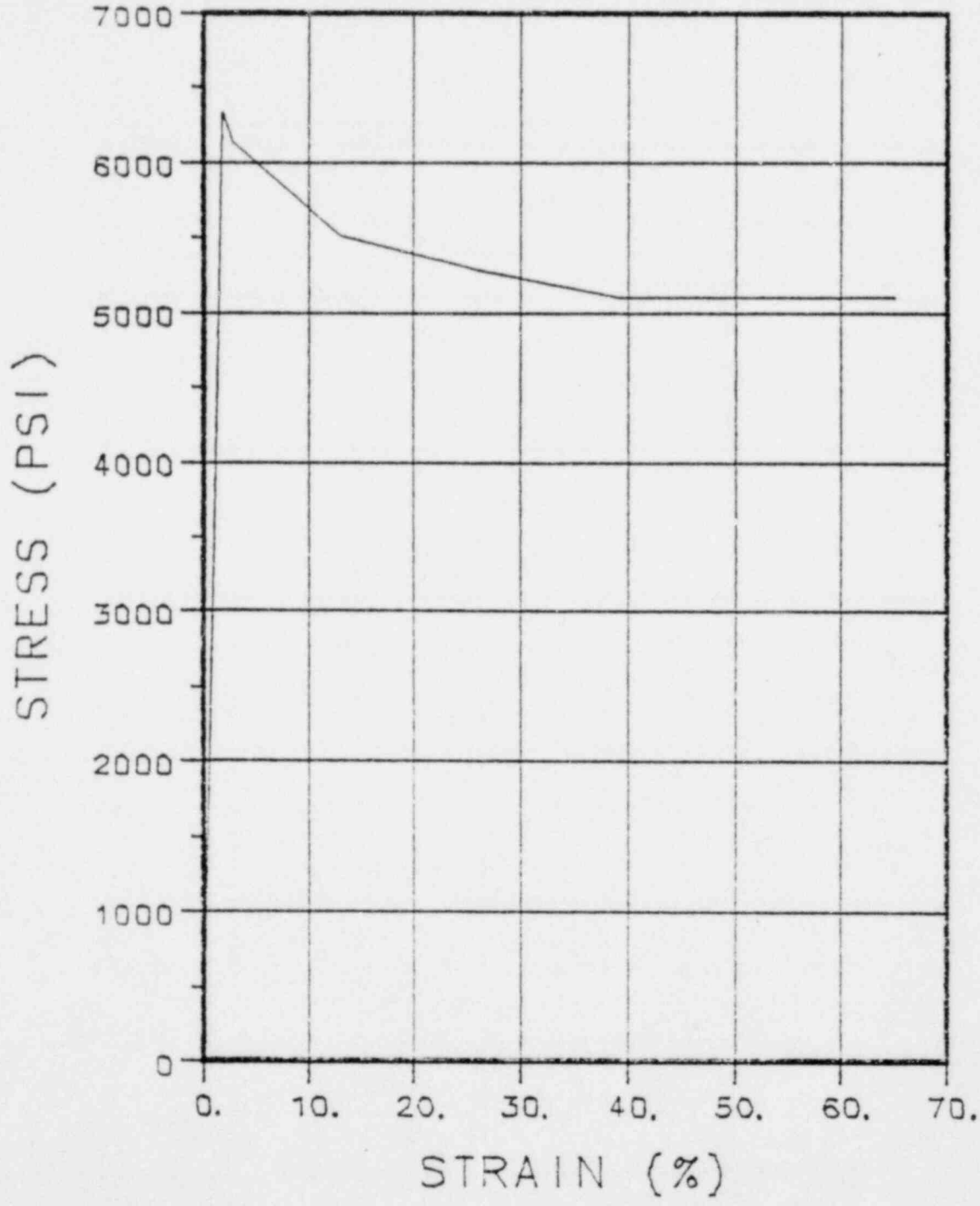

Figure 2-21. Crush Characteristics of Redwood

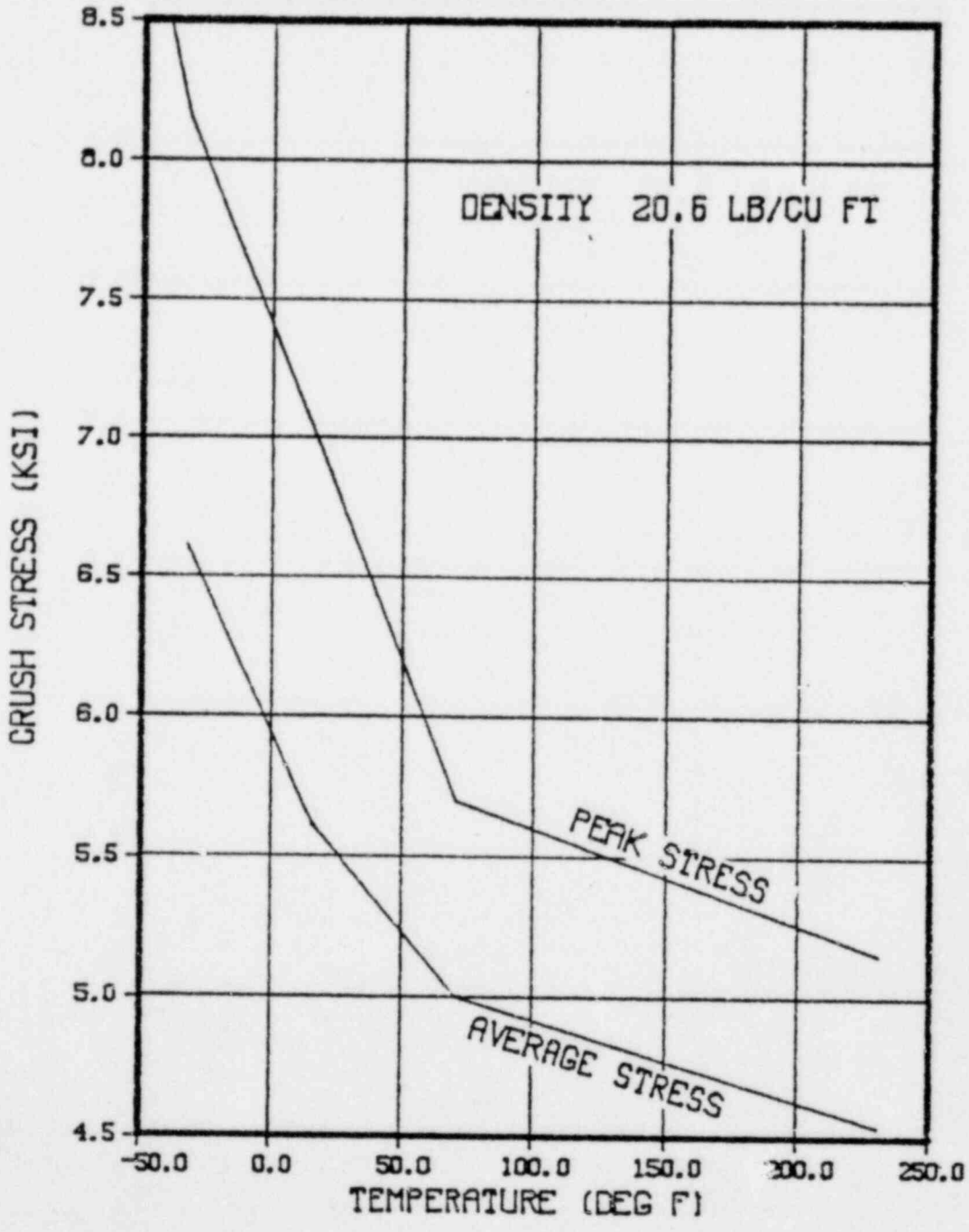

Figure 2-22. Temperature Dependence of Redwood Strength

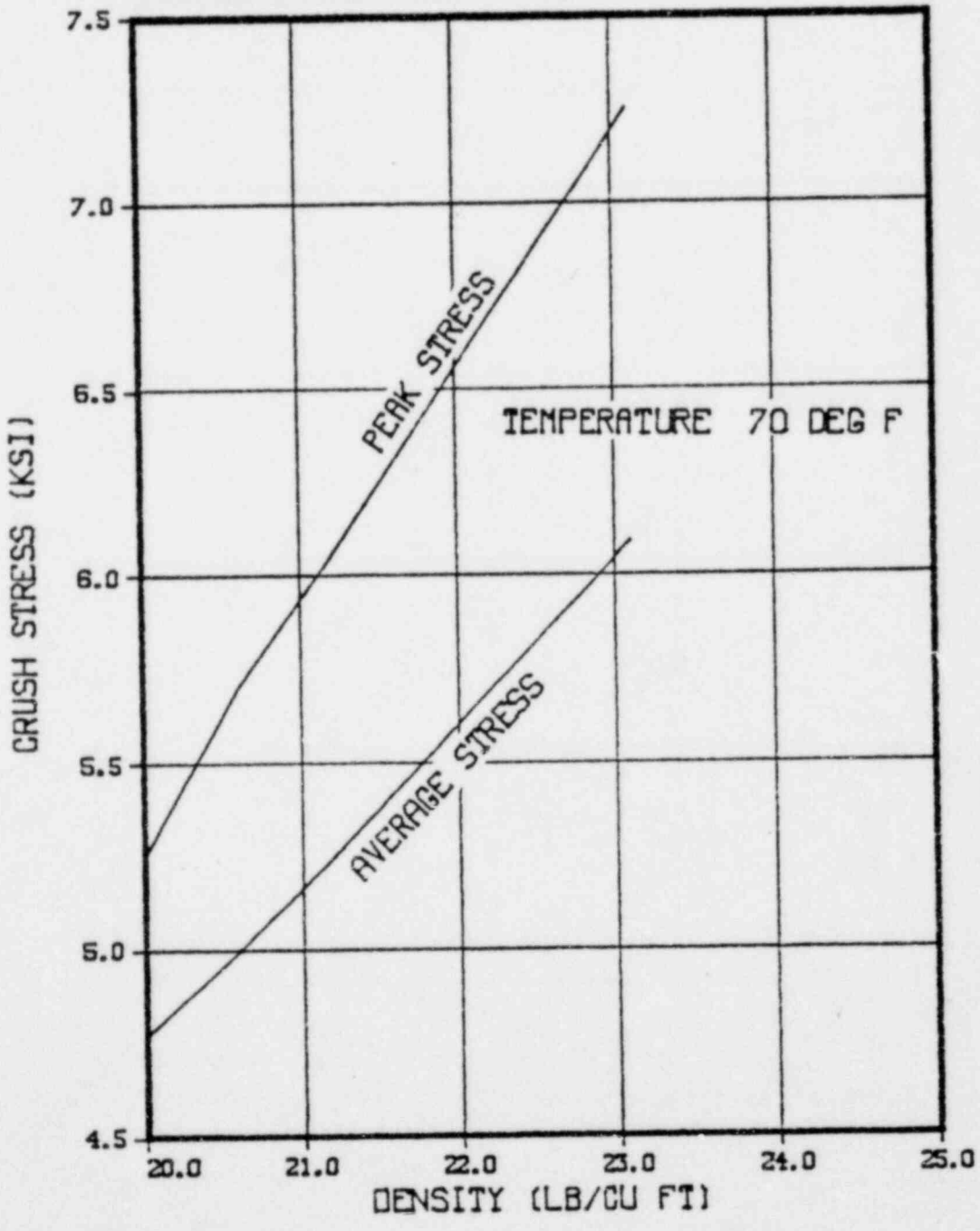

Figure 2-23. Density Dependence of Redwood Strength

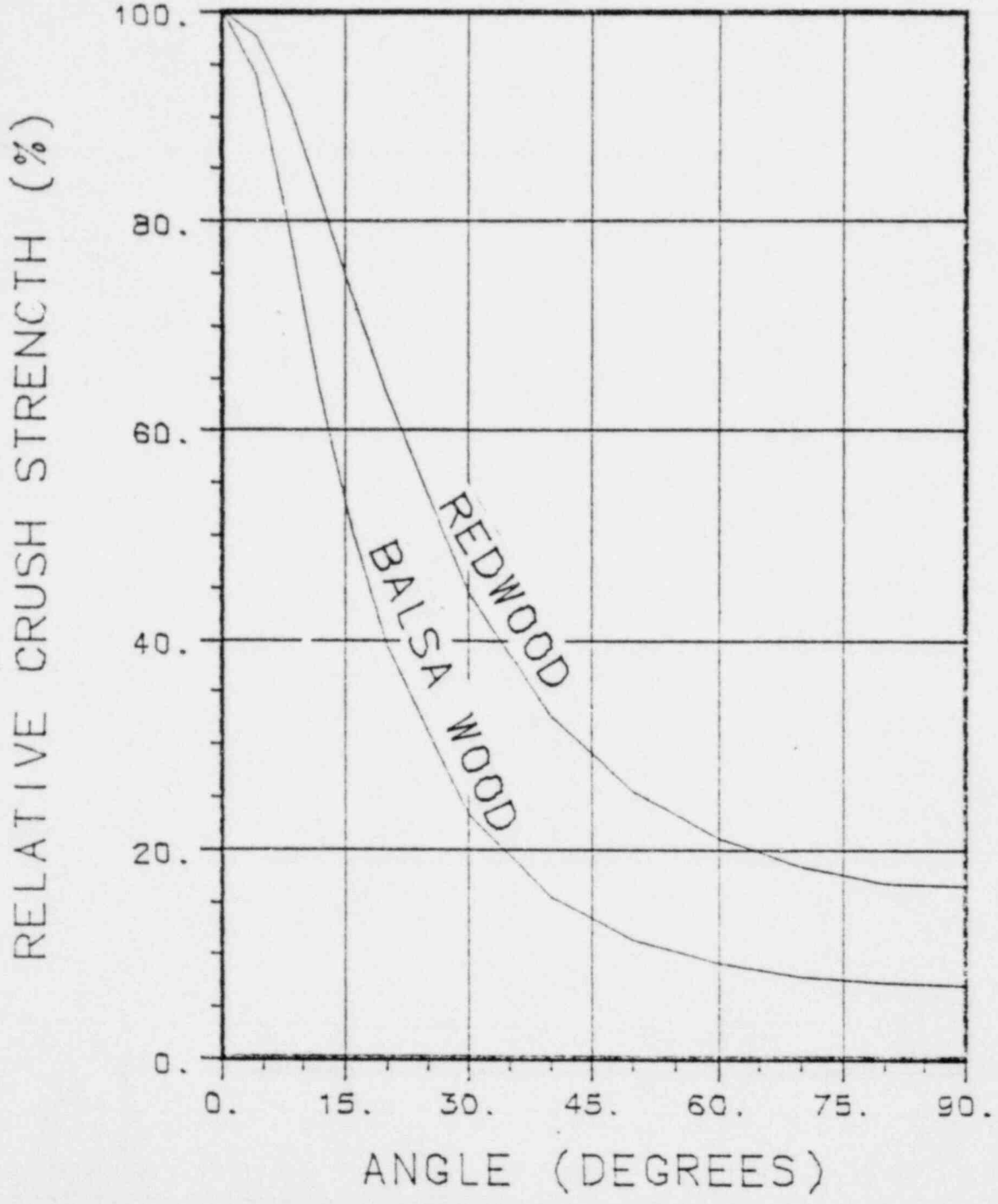

Figure 2-24. Variation of Wood Strength with Impact Angle

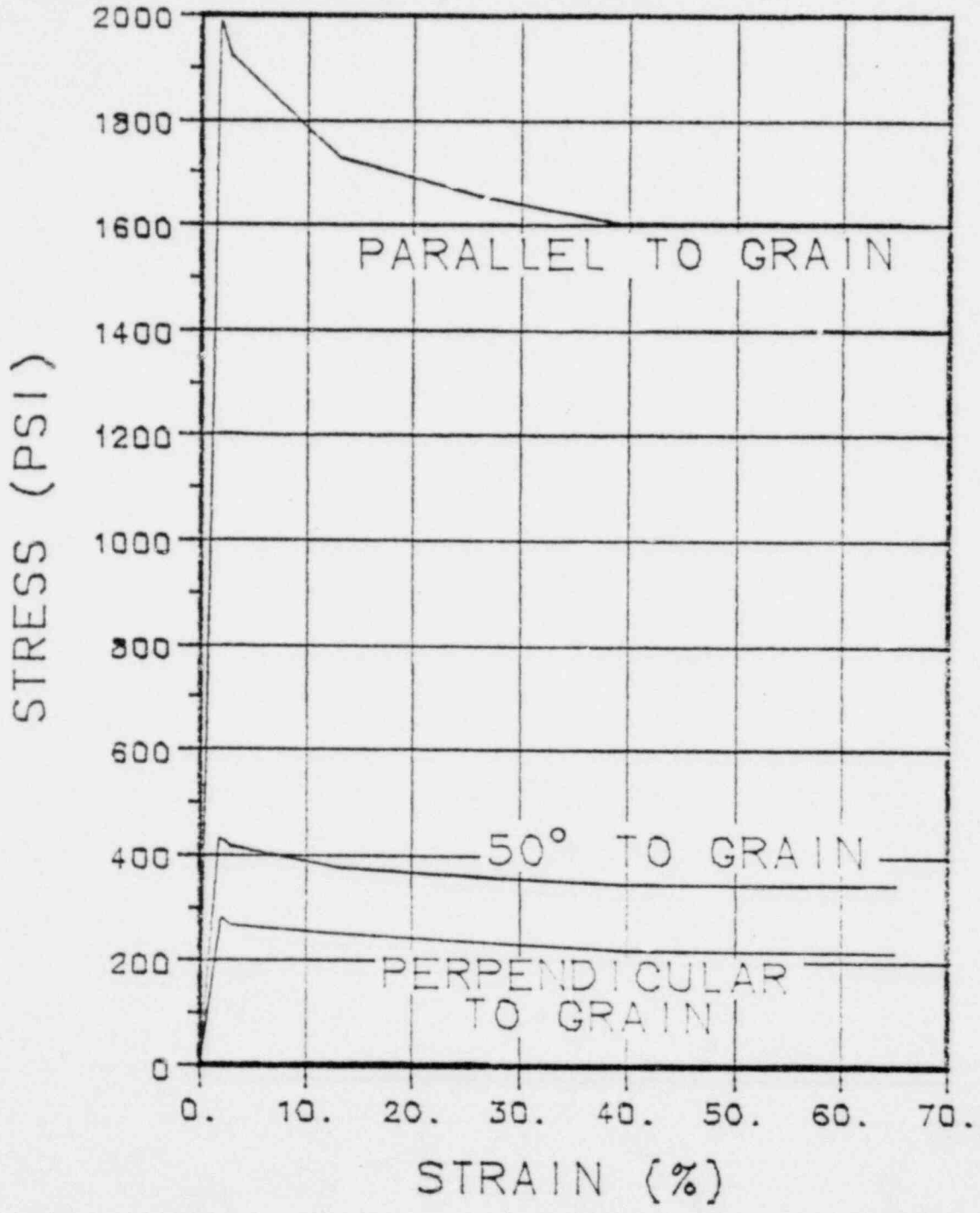

Figure 2-25. Crush Characteristics of Balsa Wood

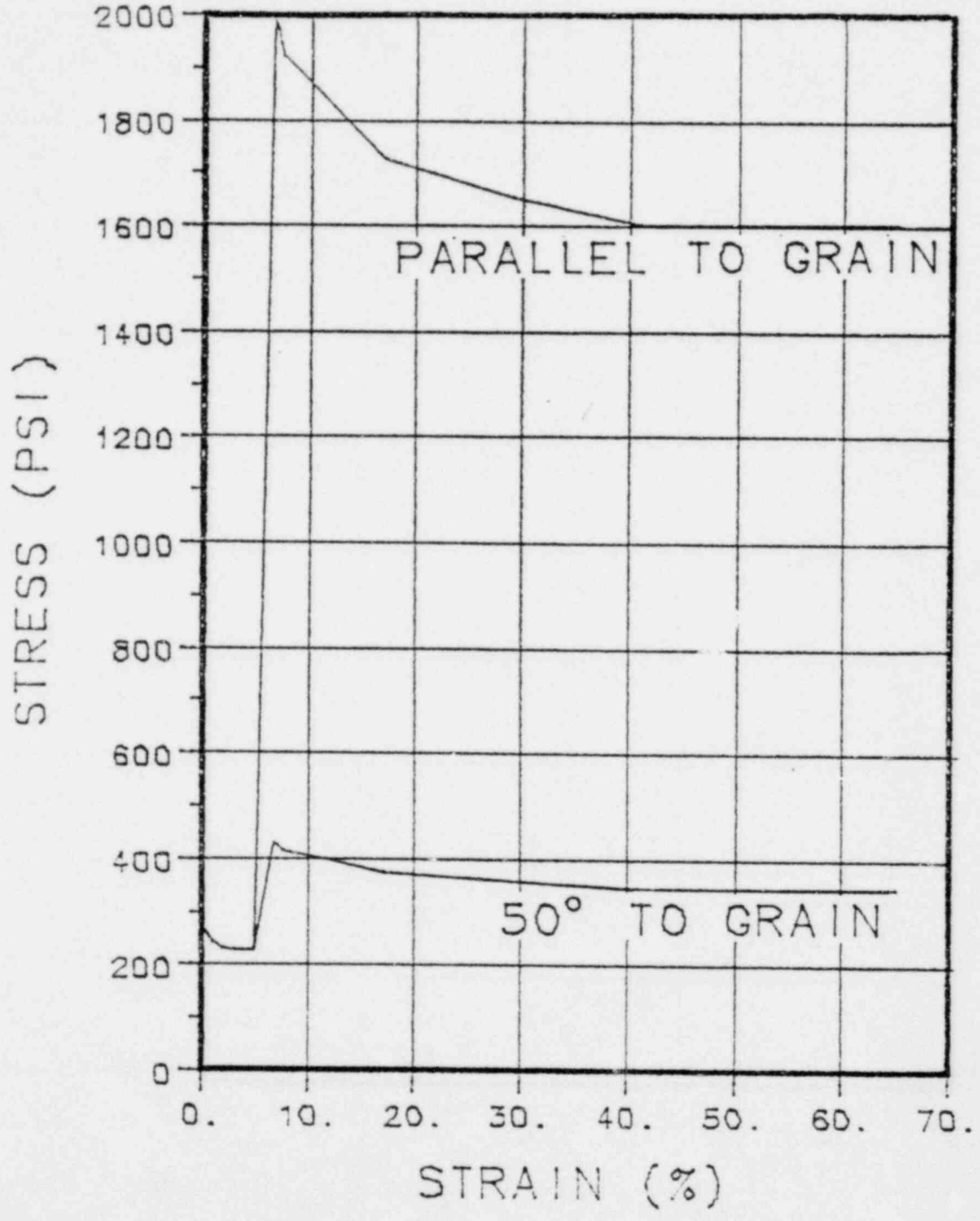

Figure 2-26. Strength of Composite Balsa Sections

2.4. General Standards for All Packages

Paragraph 71.31 of Part 71 of Title 10, Chapter 1 of the Code of Federal Regulations (Reference 2.2) establishes general standards that must be satisfied by all packages that transport radioactive material. These standards require assurance that good design practices have been employed in the design of the packaging and that the effect of the transport environment on the integrity of the package has been evaluated.

2.4.1. Chemical and Galvanic Reactions

The surfaces of the NAC-1 cask are exclusively stainless steel. The contents of the cask consist of a fuel assembly whose exterior is either zircaloy or stainless steel, the basket (stainless steel) and the water in the cavity. None of these materials experiences any chemical or galvanic reactions with the stainless steel of the cask body (Reference 2.19). Any materials that are deposited on the cask during transport (such as road salts or salt water) are washed from the surface of the cask upon reaching its destination. Consequently, there will not be sufficient time for any chemical reactions to occur.

The outer surfaces of the cask are exposed to the environment which does not normally include any materials that are corrosive to stainless steel. Consequently, no analysis is necessary to demonstrate the insensitivity of this cask to chemical or galvanic reactions.

2.4.2. Positive Closure

The principal penetration of the containment of the NAC-1 cask is sealed by the bolted closure which is held in place by six ASTM Type 320 Grade L43 bolts and is sealed by a double O-ring. At the time of closing of the cask prior to shipment a pressure test is made on the region between the O-rings to assure that a positive seal has been achieved. Any detectable leakage during this test will result in refusal of shipment and the cause of the leakage will have to be determined and repaired prior to any further shipment with that cask.

The containment is also penetrated by four holes that are sealed by ball type valves that are closed prior to shipment. The handles of the valves are configured such that the covers which provide protection for the valves cannot be installed without the valves being in the fully closed position. Leak tests have been performed on samples of these valves with essentially no detectable leakage (Reference 2.1). Consequently, the valves provide positive closure of these penetrations when the cask is prepared for transport.

The remaining penetration of the containment is closed by the rupture disk, which is positively closed by its housing, which is essentially leak proof during operation. A relief valve is installed downstream of the rupture disk which will relieve any fluid that escapes through the rupture disk and will reseat when the pressure has decayed to 200 psi or less.

2.4.3. Lifting Devices

There are two lifting devices that must be evaluated to assure that the cask will not fail while it is being lifted. These are

the trunnions and the lid lifting device.

The rotation trunnions that are welded to the lower end casting were not considered as lifting devices because they are intended only to be used as pivot points as the cask is being positioned on the transport vehicle. The rotation trunnions were analyzed as part of the tiedown system where they are shown to be able to safely carry a load of ten times the weight of the cask in the axial direction. Therefore, they do satisfy the lifting device requirement to support three times the weight of the cask.

2.4.3.1. Lifting Trunions

There are four lifting trunnions that are attached to the upper end casting. The use of a redundant yoke is permitted by the presence of four trunnions; however, the analyses were based upon the use of only two trunnions to insure conservatism during all possible operating conditions.

The yoke is designed to fit within the hollow trunnion as shown in Figure 1-8. The evaluation of the stresses within the trunnion is dependent upon the calculation of the contact area between two essentially concentric cylinders. The elastic deformation of the two cylinders is given by the following equation (Reference 2.9):

$$b = 1.6 \quad \frac{D_1 D_2}{D_1 - D_2} \quad \frac{1-\nu_1^2}{E_1} + \frac{1-\nu_2^2}{E_2}$$

where:

p is the load per length of contact (W/L)

W is 3X (the weight of the cask) (156,000 lbs)

L is the length of the contact (1.70 inches)
D_1 is the diameter of the outer surface (3.25 inches)
D_2 is the diameter of the inner surface (3.24 inches)
E_1 is the Modulus of Elasticity of the trunnion (psi)
E_2 is the Modulus of Elasticity of the yoke (psi)
V_1 is Poisson's ratio of the trunnion
V_2 is Poisson's ratio of the yoke

The trunnion is fabricated from stainless steel (see Section 2.3.1.1 for material properties) and the yoke is fabricated from high strength steel (yield stress of 50,000 psi) with the following material properties:

E_2 = 29,800,000 psi
V_2 = 0.3

These material properties are representative of 130° F which is the extreme ambient temperature in the United States. The trunnions and yoke will both be directly exposed to the environment and will experience the ambient temperature. The selection of any lower temperature will result in stronger trunnions and yoke. Introducing numerical values results in:

$$b = 1.6 \quad (45882.35) \frac{(3.25)(3.24)}{(3.25-3.24)} \quad \frac{1-.275^2}{27.1E6} + \frac{1-.3^2}{29.8E6}$$

$$= 2.828$$

The total bearing area is the product of b and the length of the contact surface (1.70 inches) which is 4.807 square inches. The bearing stress is given by (Reference 2.9):

$$\sigma br = W/2 \; / \; A = \frac{156,000}{2}/4.807 = 16,226 \text{ psi}$$

The shear stress is given by (Reference 2.9):

$$\tau_s = F \; / \; A$$

where:

τ_s is the shear stress in psi
F is the force on the trunnion or W
A is the cross section area of the trunnion or
$(D_o^2 - D_i^2)/4$
D_o is the outer diameter of the trunnion (5.25 inches)

Introducing numerical values gives:

$$\tau_s = 78,000 / (5.250-3.250)/4 = 5,842. \text{ psi}$$

The torsional shear stress is a result of the frictional forces that act at the interface between the yoke and trunnion. The torsional shear stress is given by (Reference 2.9):

$\tau_t = T\ R / J$ where:
T is the torque applied to the trunnion or (W)(R)(F)
W is 3X the weight of the cask (156,000 lbs)
F is the coefficient of friction (0.74)
R is the radius of the contact surface (1.625 inches)
J is the polar moment of inertia or $\pi (D_o^2 - D_i^2)/32$
τ_s is the torsional shear in psi

Introducing numerical values gives:

$$\tau_t = 93,795\ \ 1.625 / 63.63 = 2,395. \text{ psi}$$

The maximum torsional shear stress and the maximum vertical shear stress cannot occur simultaneously because the rotation will occur only when the cask is not vertical and once the cask is vertical all rotation will cease. However, to assure conservatism they will be added to represent the simultaneous application of vertical lifting and rotation. This gives a total shear stress of:

$$\tau_{tot} = 5,842. + 2,395. = 8,237. \text{ psi}$$

The bearing stress and shear stress are compared to the allowable stresses in both instances in Table 2-14. The stresses are substantially below the allowable stresses so the cask can be safely lifted and rotated by the yoke during any cask handling operations.

2.4.3.2. Lid Lifting Devices

After the cask has been inserted into a pool for unloading, the lid is lifted from the cask by a device that is attached to the lid at four points by bolts. The bolts are each one inch in diameter and are located on a 14 inch diameter bolt circle (the same bolt holes that are used to attach the upper end impact limiter).

The analysis of the adequacy of the bolts is based upon the lid being three times its actual weight of 700 pounds. A free body diagram of the lid while being lifted is shown in Figure 2.27. The lid lifting fixture is configured such that the crane hook is approximately 12.75 inches above the lid. To insure conservatism and to allow for any design modifications that may be necessary to accommodate the unique characteristics of the facilities utilizing this cask, the lifting point was assumed to be 7 inches above the lid. This produces the horizontal forces that are shown in Figure 2-27.

The tensile stress in each bolt is given by (Reference 2.9):

$$\sigma_t = F_v / A_b = 525. / 0.551 = 953 \text{ psi}$$

where:

F_v is the vertical component of the force on one bolt (3W/4)
A_b is the minimum cross section area of one bolt at the minor diameter
σ_t is the tensile stress in psi

The shear stress through the root area of the bolt is given by (Reference 2.9):

$$\tau_s = F_h / A_b = 525. / 0.551 = 953 \text{ psi.}$$

where:

F_h is the horizontal component of the force on one bolt (3W/4)
A_b is the minimum cross section area of one bolt at the minor diameter
τ_s is the shear stress in psi

The effective stress intensity is given by:

$$S_i=(\sigma_t^2+4T_s^2)^{1/2} = (953^2 +4(953)^2)^{1/2} = 2131 \text{ psi.}$$

where the symbols are as defined above. The effective stress is substantially below the allowable stress.

2.4.4. Tiedown Devices

The NAC-1 spent fuel shipping cask is attached to the transport vehicle during transport by straps that fasten the rotation trunnions to pedestals that are attached to the vehicle. The upper end of the cask is attached to a saddle which is also a part of the vehicle. This attachment is by means of a strap that is fastened over the cowl between the expansion tank and the impact limiter. A sketch of the cask attachment points for tiedown is presented in Figure 1-9. The pedestals and the saddle

are designed to fail during an accident so that no damage is done to the cask or the impact limiters.

The tiedown system is required to resist motion of the transport vehicle that results in simultaneous accelerations in the longitudinal, transverse and vertical directions of 10,5 and 2 g's. It has been assumed that the vertical acceleration does not include the effect of gravity so that the total vertical acceleration is 3 g's if the acceleration is downward and 1 g if the acceleration is upward.

The requirement, presented in 10CFR71, for the tiedown system is that the stresses must not exceed the yield strength of the material during normal transport conditions where the maximum accelerations are as identified above. The rotation trunnions and the cowl are stainless steel and the physical properties of this material are presented in Section 2.3.1.

2.4.4.1. Rotation Trunions

The rotation trunnions are pieces of bar stock welded to curved plates that are in turn welded to the lower end casting. The trunnions are restrained from outward motion by a wire rope that surrounds the cask and passes through the trunnions. The rotation trunnions resist vertical and transverse cask load components and the entire longitudinal cask load.

are designed to fail during an accident so that no damage is done to the cask or the impact limiters.

The tiedown system is required to resist motion of the transport vehicle that results in simultaneous accelerations in the longitudinal, transverse and vertical directions of 10,5 and 2 g's. It has been assumed that the vertical acceleration does not include the effect of gravity so that the total vertical acceleration is 3 g's if the acceleration is downward and 1 g if the acceleration is upward.

The requirement, presented in 10CFR71, for the tiedown system is that the stresses must not exceed the yield strength of the material during normal transport conditions where the maximum accelerations are as identified above. The rotation trunnions and the cowl are stainless steel and the physical properties of this material are presented in Section 2.3.1.

2.4.4.1. Rotation Trunions

The rotation trunnions are pieces of bar stock welded to curved plates that are in turn welded to the lower end casting. The trunnions are restrained from outward motion by a wire rope that surrounds the cask and passes through the trunnions. The rotation trunnions resist vertical and transverse cask load components and the entire longitudinal cask load.

2.4.4.2. Cowl

The cowl between the expansion tank and the upper end impact limiter is stainless steel with supporting circumferential gussets that provide the stiffness required to resist the tiedown system loads. The load on the cowl and gussets is a result of the strap over the cowl which fastens to the saddle on the transport vehicle. This strap is only effective for restraining vertical and/or transverse loads and does not resist any longitudinal load. The resultant of the vertical and transverse loads is assumed to be uniformly distributed over the surface of the cowl over a 180° contact arc on the strap or on a 90° contact arc on the saddle.

The pressure that is applied to the cowl by the saddle or strap is the respective load divided by the contact area. When the acceleration is upward, the strap applies the load to the cowl and when downward causesthe saddle to load the cowl.

The limitation on the stress in the cowl is the yield stress which is 25,000 psi at 300°F. However, the requirements for elastic stability (no buckling) of the cowl and gussets presents a more critical limit.

The loads, contact areas and resulting pressures are presented in Table 2-15 along with the critical pressure to avoid buckling. The critical pressure was evaluated using the methods described in Section 2.5.2 with the geometrical data and results presented in Table 2-17. Since the pressure on the cowl is less than the critical pressure, the interaction between the strap or saddle and the cowl is structurally acceptable.

The maximum compressive stress in one of the gussets is 9241 psi which is less than the limiting elastic stability compressive stress of 13,701 psi from Reference 2.9, Page 348, Case A.1.

The limitation on the stresses in the cowl is the yield stress which is 30,000 psi when the ambient temperature is 130°F. However; the requirement that the cowl not buckle when loaded presents a more severe limit.

The loads applied to the cowl have been increased by a factor of two to allow for dynamic intensification. The loads, contact areas and resulting pressures are presented in Table 2-15 along with the critical pressure to avoid buckling. The critical pressure was evaluated using the methods described in Section 2.5.2. with the geometrical data and results presented in Table 2-17. Since the pressure on the cowl is less than the critical pressure the interaction between the strap or saddle and the cowl will cause no damage.

Table 2-14. Maximum Stresses in Trunnions

Trunnion	Maximum Calculated Stress (psi)	Allowable Stress (psi)	Remarks
Lifting Trunnion	16226	28600	Bearing on yoke.
	8237	11440	Shear and torsion at base of trunnion.
Rotation Trunnion	21931	28600	Bearing on support pedestal.
	9309	11440	Shear at base of trunnion (normal transport).
	6842	11440	Shear and torsion at base of trunnion (loading or unloading).

Table 2-15. Maximum Pressures on Upper Cowl

Load Condition	Load (lbs.)	Contact Area ($in.^2$)	Maximum Pressure (psi)	Critical Pressure* (psi)
Vertical Upward & Transverse	128944	186.25	692	7215
Vertical Downward & Transverse	150030	131.70	1139	7215

*Ref. Table 2-17, Page 2-81

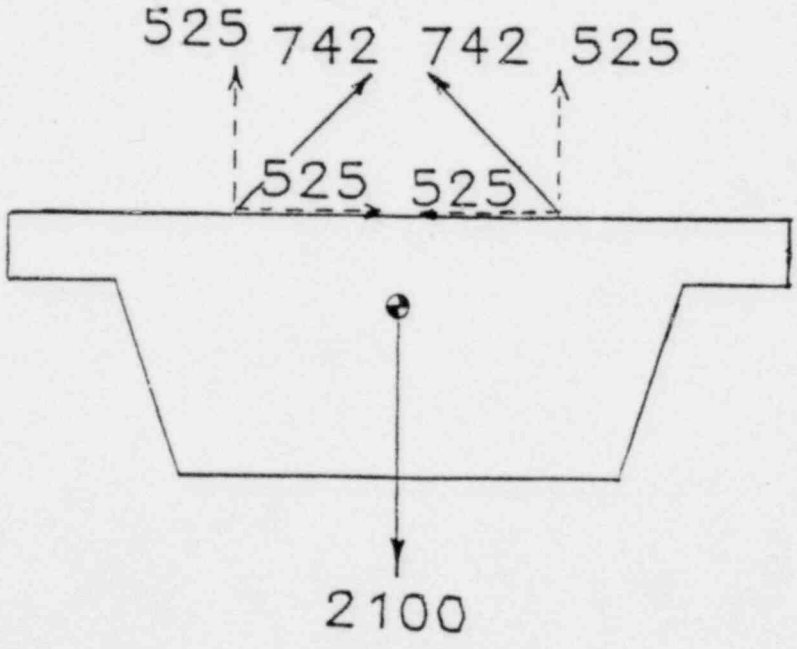

Figure 2-27. Free Body Diagram of Lid During Lifting

2.5. Standards for Type B and Large Quantity Packaging

Paragraph 71.32 of Part 71 of Title 10, Chapter 1 of the Code of Federal Regulations (Reference 2.2) requires that all transportation packages be capable of supporting five times its own weight and withstanding the effects of an external pressure of 25 psig.

2.5.1. Load Resistance

Paragraph 71.32(a) of 10CFR71 requires that all transportation packages be able to support five times its own weight when considered as a simple beam. For this analysis only the outer shell of the cask will be considered. Including either the inner shell or the outer shell of the shield tank will have little impact on the calculated stresses.

The maximum bending stress in a uniformly loaded beam simply supported at its ends is given by (Reference 2.9):

$$\sigma = M\ c\ /\ I$$

where:

M is the maximum moment or 5WL/8
c is the radius of the extreme fiber
I is the total moment of inertia or $\pi(D_o^4 - D_i^4)/64$
W is the weight of the cask (52,000 lbs)
L is the length of the cask body (193.34 inches)
D_o is the outside diameter of the shell in inches
D_i is the inside diameter of the shell in inches
σ is the maximum bending stress

The dimensions, moment of inertia and maximum bending stresses in each of the shells in the cask are presented in Table 2-16. The value of C is unique for each component. The maximum bending stresses are all less than the allowable stress of 19,600 psi as defined in Section 2.1.2. This limit is independent of temperature because the design stress intensity is independent of temperature for stainless steel.

The assumption of uniform loading on the beam is a conservative approximation because the weight of the cask is not uniformly distributed along the length of the cask. A large fraction of the weight is concentrated at the ends of the cask in the end castings and impact limiters. These components would not introduce any moment in the cask because they act on the point of support so the inclusion of these weights in the uniform loading is conservative.

The maximum stress in the outer shell of the cask occurs at the midpoint of the cask which is in the portion of the cask that has the larger outer shell. The smaller outer shell in included in Table 2.16 to demonstrate that this segment of the cask is not controlling in the stress calculation. The inner shell contributes only two percent to the resistance to bending of the cask.

2.5.2. External Pressure

Paragraph 71.32(b) of 10CFR71 requires that all transportation packages suffer no loss of containment in the event that the external pressure reaches 25 psig. There are four sections of the cask that could possibly suffer damage as a result of overpressurization. These are:

Neutron Shield Tank
Expansion Tank
Cowl Covering Cask Body
Impact Limiters

Each of these is a cylindrical shell. All are partially supported by internal gussets with the exception of the impact limiters. The principal mode of failure of these components would be by collapse type buckling of the shell. Reference 2.9 indicates that the critical pressure for collapse type buckling of a partially supported cylinder is given by the expression:

$$p = \frac{E\, t^3\, (k^2 - 1)}{12\, R^3\, (1 - \nu^2)}$$

However, if the length of the shell is short the representation of the critical pressure for buckling changes to:

$$p = 0.807\, \frac{E\, t^2}{L\, R} \left[\left(\frac{1}{(1-\nu^2)} \right)^3 \frac{t^2}{R^2} \right]^{1/4}$$

where the criteria that differentiates between short and long shells is:

$$L > 4.90\, R \sqrt{R/t} \quad \text{for long shells}$$
$$L < 4.90\, R \sqrt{R/t} \quad \text{for short shells}$$

The variables in both of these equations have the following meanings:

R is the radius to the outside of the shell in inches
t is the thickness of the shell in inches
L is the length of the shell in inches
E is the modulus of elasticity in psi
ν is Poisson's ratio
k is a constant related to the unsupported arc of the shell
α is half of the angle of the shell that is unsupported.

The relationship between k and α is given by the expression:

$$k \tan \alpha \cot k\alpha = 1$$

The second expression relates only to shells that have no partial supports so its application for this analysis is conservative because supporting gussets will inhibit collapse of the outer shell. The critical pressure for collapse of each of the outer shells of the NAC-1 cask are tabulated in Table 2-17.

Each of these critical pressures is substantially greater than the 25 psig that the cask must endure. Consequently, an overpressure of 25 psig will cause no damage to the cask and will not violate the containment of the cask. An overpressure of 47 psig will cause the outer surface of the impact limiter to collapse onto the wood. The expansion tank is internally pressurized by the expansion of the shield tank fluid so a pressure difference between the inside and outside of the expansion tank is required to cause this tank to collapse.

Table 2-16. Maximum Bending Stress in NAC-1 Cask

Component	Moment of Inertia Inches	Thickness Inches	Radius to Extreme Fiber Inches	Maximum Bending Stress psi
Inner Shell Lower End	323.	0.3125	7.0625	2797.
Outer Shell				
Upper End	8899.	1.25	13.75	4795.
Lower End	11678.	1.25	15.	5941.
Neutron Shield Tank	3854.	0.165	19.6	7763.
Expansion Tank	8798.	0.25	22.5	7845.

Table 2-17. Critical Pressures for Collapse of Cask Exterior

Component	Shell Thickness Inches	Angle Between Supports Degrees	Length Inches	Radius Inches psi	Critical Pressure psig
Impact Limiter	0.109	360.	9.00	36.000	47.
Expansion Tank	0.250	50.	16.00	22.500	354.
Shield Tank	0.165	90.	135.00	19.600	47.
Cowl					
Upper End	0.250	360.	1.25	18.625	7215.
Lower End	0.109	180.	13.00	18.625	87.

The critical pressures for the impact limiters and both cowls are based upon the expression for short tubes because their length is short compared to the criterion for differentiating between buckling of long and short tubes.

2.6. Normal Conditions of Transport

The design of the NAC-1 spent fuel shipping cask is predicated upon the ability of the cask to transport fuel with no loss of its contents nor endangerment of the environment or public health and safety. The achievement of this goal is demonstrated by analysis of the normal conditions of transport that are identified in 10CFR71, Appendix A and demonstrating that there is no loss of containment nor damage to the cask that prevents it from surviving the hypothetical accident. The following analyses demonstrate that extreme environmental conditions and minor accidents do not adversely effect the NAC-1 cask, its contents or its ability to survive a hypothetical accident.

2.6.1. Heat

Extreme environmental conditions have been analysed to demonstrate that the NAC-1 cask is not effected by an environmental temperature of either 130°F or -40°F. These two extremes represent the 99% confidence levels for the maximum and minimum temperatures in the continental United States (Reference 2.21).

2.6.1.1. Summary of Pressures and Temperatures

The cask temperatures have been calculated for two distinct cases and the results are reported in Section 3. of this report. The cases that have been considered are (Reference 2.22):

Hot Environment (130°F ambient)
- 11.5 kw decay heat
- full solar heat load
- stationary air

Cold Environment (-40°F ambient)
- 3.11 kw decay heat
- no solar heat load
- stationary air

The calculated temperatures and pressures for these two cases are summarized in Figures 2-28 and 2-29 respectively. Temperatures and pressures at key locations in the cask are also summarized in Table 2-18.

The stresses that are created in the cask wall by the elevated or depressed ambient temperature have been evaluated to provide assurance that the cask is not damaged by either extreme in the environmental conditions.

2.6.1.2. Analysis Model

The model that was employed for the evaluation of the thermal stresses was designed to combine the effects of temperature and the effects of the copper fins that connect the lead and the stainless steel shells. The copper fins are attached to the lead by either metallurgical or mechanical bonds which will bend the fins to accomodate the shrinkage or expansion of the lead. The fins will cause local stressing of the shells which will be dependent upon the temperature of the lead. Consequently, this phenomena has been incorporated into the evaluation of the thermal stresses as described in the following sections.

2.6.1.2.1. Model of Cask Body

The model for the evaluation of the thermal stresses that are induced within the cask wall consists of three axisymmetric cylinders that represent the inner and outer shells and the contained lead. The end castings are represented as solid plates that connect the cylinders. The model is shown in Figure 2-30.

The interface between the lead and the outer stainless steel shell is represented as gap and spring elements in series. These elements model the copper fins that penetrate the gap that will form between the lead and stainless steel. The spring element represents the resistance of the copper fins to the separation of the lead and stainless steel. The gap element is included to analitically allow separation of the two materials.

2.6.1.2.2. Copper Fins

The design of the NAC-1 cask utilizes copper fins that are welded to the inner and outer stainless steel shells as shown in Figure 1-6. These fins provide a means of transferring heat across any gap that will result from shrinkage of the lead during the cooling process that follows the lead pouring operation. The fins were bonded to the lead by either chemical interaction or mechanical interaction. Lead and copper readily combine to form a eutectic solution which is stronger than pure lead. The manufacturing specifications recognize this reaction and require the presence of an oxide coating on the surface of the copper fins to prevent dissolving by the molten lead. However, some reaction is possible which will leave a bond between the lead and copper fins.

A mechanical type of bonding is also probable because of the

configuration of the fins. When the lead is poured into the cavity in the cask wall some of the lead will flow into the region behind the fin and solidify to provide a mechanical type of bond that will force the fin to conform to the expansion or contraction of the lead. The continued addition of molten lead during the cooling process aids the formation of this type of bonding of the lead to the copper fins.

There is no reason to expect any bonding of the lead directly to the stainless steel shells. No special effort was expended to create a bond between the lead and stainless steel and these materials do not normally form a bond.

2.6.1.2.2.1. Model of Lead-Stainless Steel Interface

The spring constant that represents the stiffness of the copper fins was determined from an ANSYS calculation of the response of the fin to the motion of the lead. Additionally, this calculation also identifies the stresses that are induced in the stainless steel shell by the deflection of the copper fin. The ANSYS model of the fin and stainless steel is shown in Figure 2-31. Elements were closely spaced in the bend of the fin and near the joint between the fin and the stainless steel. A two inch wide segment of the inner shell was modelled to represent a symmetry section. The thinner shell was represented rather than the outer shell to insure conservatism by modeling only the weaker of the two shells. The interaction between the lead and the fin was represented as a uniform pressure along the surface of the fin where it is reasonable to expect a substantial bond between the lead and copper. The pressure loading is shown in Figure 2-32.

2.6.1.2.2.2. Interface Deformations and Stresses

The relationship between the force applied to the lead and the deflection of the copper fin was determined by varying the pressure loading on the fin and calculating the resulting deformation. The pressure was varied from 0 to 10 psi which resulted in fin deflections that varied from 0 to 0.075 inches. This spans the range of deflections that can be expected when the cask is cooled from the lead pouring conditions directly to -40°F. The maintenance of the cask at an intermediate temperature for any prolonged period of time will allow the lead to relieve the stresses by creeping.

The deformed geometry following the application of several different pressures is shown in Figure 2-33. The deformation is concentrated in the bend region of the fin and near the joint between the fin and the stainless steel. The maximum stress in both the stainless steel and the copper fins are presented in Figure 2-34. as functions of the displacement of the tip of the fin.

2.6.1.3. Differential Thermal Expansion and Stresses

The model described in section 2.6.1.2 was used to evaluate the differential expansions during the heatup from room temperature to 625°F which is the melting temperature of lead. In this portion of the calculation the lead was omitted from the model to allow the prediction of the thermal expansion of the stainless steel shells prior to the introduction of the lead. The model was revised to include the displacement of the stainless steel shells resulting from the heatup process. Consequently, the steel became stress free at the time of the lead pour. This is not representative of the true conditions; however, the calculated

stresses and strains in the stainless steel shells prior to the introduction of the lead were very small because of the uniformity of the temperature at this point in time.

The next step was to introduce lead into the model with its temperature at 625°F which implies no strength. The procedure for pouring the lead required the continual addition of molten lead during the cooldown to fill any voids that developed. Consequently, the model assumed the wall to be completely filled with lead.

Following the introduction of the lead the temperature of the model was lowered to the temperatures that correspond to an ambient of 130°F with full solar insolance. The radial, tangential (hoop) and axial stresses in the inner shell are presented in Figure 2-35 as a function of length along the cask where the origin is at the bottom of the model or 2.5 inches below the end of the cavity. The temperatures that result from an ambient of -40°F with no solar insolance and a decay heat load of 3.11 kw were also introduced into this model and the resulting stresses are presented in Figure 2-36.

The controlling forces in both of these thermal stress calculations is the shrinkage of the lead onto the inner stainless steel shell and the pulling of the copper fins away from the outer shell. The stresses are largest for the -40°F ambient conditions because this represents the largest difference in contraction between the lead and the stainless steel.

2.6.1.4. Comparison with Allowable Stresses

The thermal stresses that are presented in Figures 2-35 and 2-36 consist of two components. The first is due to the temperature gradients within the components and these stresses are classified

as secondary stresses because there is no external force producing the stresses. The second component is due to the shrinkage of the lead onto the inner shell and away from the outer shell. These stresses are primary stresses because there is an identifiable force at the surface of either stainless steel shell. For conservatism, the secondary stresses will be ignored and all of the calculated thermal stresses considered as primary stresses.

The cask cavity will be pressurized when the ambient temperature is 130°F and will have a slight vaccuum when the ambient is -40°F. This will create stresses that must be combined with the thermal stresses to completely define the stress state during normal transport.

The stresses induced by vibration are not to be combined with the thermal and cavity pressure stresses. When the cask experiences vibration, it must be in motion, invalidating the conditions of the thermal analysis. Also the stresses produced by the vibration are small and will have no substantial impact on any other operating condition.

Penetration and compression act only on the exterior of the cask and have no appreciable effect on either the inner or outer shells, so they should not be combined with the thermal and pressure stresses.

The stresses induced by the one foot free falls will tend to balance the thermal stresses so the analysis is more conservative if the thermal stresses and falls are not combined with the thermal stresses.

The stresses in the inner and outer shell due to the cavity pressure are calculated from the expressions for the stresses in a thin walled pressure vessel which are:

$$\sigma_r = (P_o - P_i) \qquad \sigma_h = (P_o - P_i)r/t$$

and

$$\sigma_z = (P_o - P_i)\, D_c^2 \,/\, (D_{i1}^2 - D_{i2}^2 + D_{o1}^2 - D_{o2}^2)$$

where:

P_o and P_i are the external and internal pressures
r is the mean radius of the shell
t is the thickness of the shell
D_c is the diameter of the cavity
D_{i1} is the outside diameter of the inner shell
D_{i2} is the inside diameter of the inner shell
D_{o1} is the outside diameter of the outer shell
D_{o2} is the inside diameter of the outer shell
σ_r is the radial stress
σ_h is the hoop stress
σ_z is the axial stress

The expression for the axial stress is based upon the condition that both shells will be loaded because the pressure is acting on the end castings which are sufficiently rigid that they will distribute the load. Introducing numerical values gives the following stresses:

σ_r = 103 psi
σ_h = 2,276 psi
σ_z = 117 psi

The limit that was identified in Table 2-2 for normal transport conditions requires the primary membrane stresses to be less than the design stress intensity. Since the thermal stresses and pressure stresses develop slowly the limits will be based upon static properties of stainless steel as described in Section 2.3.1.1. The design stress intensity is 20,000 psi for all temperatures below 300°F.

The maximum combined stresses are:

σ_r = -68 psi
σ_h = 2,720 psi
σ_z = 2,139 psi

These stresses are all substantially below the design stress intensity for stainless steel.

2.6.2. Cold

When the ambient temperature is -40°F the cavity pressure is slightly below ambient. The radial and hoop stresses will be zero in this case because the exterior shells such as the shield tank will absorb all of the stresses and not transmit the stresses to the cask body. The axial stress will be slightly compressive with a magnitude less than -17 psi.

The maximum combined thermal and pressure stresses occur when the ambient temperature is -40°F and the decay heat load is 3.11 kw. The maximum stresses are:

σ_r = -287 psi
σ_h = -8,194 psi
σ_z = -8,038 psi

These stresses are all substantially less than the design stress intensity for stainless steel.

2.6.3. Pressure

Appendix A of Part 71 of Title 10, Chapter 1 of the Code of Federal Regulations (Reference 2.2) requires that all transportation packages are to be evaluated to determine the

consequences of an external pressure that is reduced to 3.5 psia. There are four sections of the cask that could possibly suffer damage under such conditions. These are:

Neutron Shield Tank
Expansion Tank
Cowl Covering Cask Body
Impact Limiters

Since the cask is constructed while the pressure is atmospheric, the differential pressure acting on the external surfaces will be 11.5 psia. The shield tank and the expansion tank are exceptions in that they develop internal pressure as a result of normal operation.

The stress in a cylindrical shell is given by (Reference 2.9):

$$\sigma_r = (p_o - p_i) \qquad \sigma_h = (p_o - p_i)r/t \quad \text{and} \quad \sigma_z = (p_o - p_i)r/2t$$

where:

σ_r is the radial stress in psi
σ_h is the hoop stress in psi
σ_z is the axial stress in psi
p_o is the external pressure in psi
p_i is the internal pressure in psi
r is the outer radius of the shell in inches
t is the thickness of the shell in inches

The respective dimensions of the outer surfaces of the NAC-1 cask and the stresses that result from a reduced ambient pressure are presented in Table 2-19.

All of the stresses are primary membrane stresses and there is no bending stress under these conditions so the stress limitation (Table 2-2) becomes the design stress intensity. All of the stresses are substantially below the design stress intensity of

20,000 psi so no damage will result from a reduced atmospheric pressure and no loss of shielding will occur and the cask will retain its ability to withstand the rigors of the hypothetical accident.

The reduced atmospheric pressure will also induce stresses in both shells because the cavity pressure will exert a force on the end castings which will create tensile loads on both shells. The axial stress in both shells is identical and is given by the expression for stresses in a thin wall cylinder where both the inner and outer shells are restraining the forces applied to the end castings. The equation for the axial stress is:

$$\sigma_z = (p_o - p_i)\, D_c^2 \,/\, (D_{i1}^2 - D_{i2}^2 + D_{o1}^2 - D_{o2}^2)$$

where:

p_o and p_i are the external and internal pressures
D_c is the diameter of the cavity
D_{i1} is the outside diameter of the inner shell
D_{i2} is the inside diameter of the inner shell
D_{o1} is the outside diameter of the outer shell
D_{o2} is the inside diameter of the outer shell
σ_z is the axial stress

The cavity pressure is 118 psi when the ambient temperature is 130°F which gives an axial stress of 130 psi in both shells when the ambient pressure is 3.5 psi.

2.6.4. Vibration

The transport of the cask over the road on a trailer will result in vibrations being transmitted to the cask through the tiedown system. Rubber pads are incorporated in the saddle that supports the front cowl; however, the cask will still be subject to

oscillatory loads.

The peak accelerations that can be expected during truck transport have been evaluated by Sandia Laboratories and documented in Reference 2.20. The appropriate data have been reproduced in Table 2-20. The data presented in this report represent the results of measurements of the acceleration as a function of the frequency of the vibration. Actual truck shipments were instrumented to define the shock input to a 56,000 pound cargo. The reported accelerations represent the 99 percent envelopes of all of the accelerations measured in each frequency range. The largest accelerations were always associated with the lowest frequencies.

The analysis of the effect of these vibrations on the NAC-1 cask is divided into two elements. The first is the evaluation of the effects of the combined transverse and vertical acceleration and the second is the evaluation of the effect of the longitudinal acceleration. These are separated because their effect on the cask is different and the methods of analysis are different. However, the effects must be combined to determine the total stress on the cask components.

The bending stresses that are induced within the cask by either the vertical or transverse accelerations have been evaluated by considering the cask as a simply supported beam with a uniform load applied along the entire length of the cask body. The equations that describe the bending stresses and deflection of a uniformly loaded, simply supported beam are:

$$M = WL/8$$

$$\sigma_o = M\, c_o/I_o$$

$$y = 5\, M\, L^2/48\, E\, (I_i + I_o)$$

where:

W is the weight of the cask or (52,000 pounds)

L is the length of the cask body (184.5 inches)
c_o is the outer radius of the outer shell
I_i is the moment of inertia of the inner shell
I_o is the moment of inertia of the outer shell
E is the elastic modulus of the stainless steel
c_o is the bending stress in the outer shell
a is the acceleration of the cask

These equations presumed that the outer shell was absorbing all of the moment and the inner shell is ineffective for resisting bending. This is essentially true; however, the inner shell does resist some of of the moment and is subject to stresses that must be evaluated.

The end castings distribute the moment between the two shells so that the angular deflection of both shells are identical at any time. The angular deflection of the ends of the shells is proportional to M/EI so this ratio must be identical for the inner shell and the outer shell. To preserve these ratios the moments will distribute themselves in proportion to the moments of inertia or in equation form:

$$c = M_c c_c/I_c$$

or

$$M_c = c I_c/c_c$$

and

$$i = M_i c_i/I_i$$
$$o = M_o c_o/I_o$$
$$M_i = M_c I_i/(I_o + I_i)$$
$$M_o = M_c I_o/(I_o + I_i)$$

giving

$$i = M_c I_i c_i/(I_o + I_i)$$
$$o = M_c I_i c_o/(I_o + I_i)$$

or

$$i = c\ I_c\ c_i/(I_o + I_i)\ c_c$$
$$o = c\ I_c\ c_o/(I_o + I_i)\ c_c$$

where:

M_c is the moment from the calculation
M_i is the moment on the inner shell
M_o is the moment on the outer shell
I_c is the moment of inertia used in the calculation
I_i is the moment of inertia of the inner shell
I_o is the moment of inertia of the outer shell
c_c is the radius used in the calcualtion
c_i is the radius of the inner shell
c_o is the radius of the outer shell

The numerical values of the moments of inertia and the radii to the extreme fiber for the inner and outer shell are presented in Table 2-16. The results of the evaluation of these equations are presented in Table 2-21 for the vertical and transverse accelerations. A dynamic intensification factor of 2. has been applied to all of the accelerations to insure that the dynamic nature of these loads does not induce stresses that exceed the predicted values. The resulting vertical acceleration was taken as 2.04 g's to reflect the possibility that the acceleration can be downward and add to the effect of gravity. It will be assumed that both of these maximum accelerations occur simultaneously, so the cask will experience the sum of the bending stresses from the vertical and transverse accelerations. The combined stresses are indicated in Table 2-21.

The longitudinal acceleration will have two effects that must be considered which are the slumping of the lead within the cask wall and the acceleration of the water within the cask cavity. The pressure induced in the lead and the water is expressed as:

$$p = \rho a h$$

where:

p is the hydrostatic pressure
ρ is the density of the material
a is the longitudinal acceleration
h is the length of the material in the cask

The results of the evaluation of the pressures of the lead and the water are also presented in Table 2-21 where the dynamic intensification factor of 2. has been retained and both the lead and water have been assumed to exist over the entire length of the cask wall (184.5 inches for the lead and 178 inches for the water). The hydrostatic pressure of the lead is 40 psi which is equal to the axial stress in the lead at the lower extremity of the lead in the cask wall. This stress is sufficiently below the yield stress of lead that the lead will remain elastic and the inner and outer shells will be subject to a maximum hydrostatic pressure of 40 psi. The resulting hoop stress is 902 psi in the inner shell and 490 psi in the outer shell. The hydrostatic pressure of the water in the cavity is 3.6 psi which will induce a hoop stress of 76 psi in the inner shell. This hoop stress is tensile and will partially cancel the compressive hoop stress that is produced by the lead.

The final stress that is induced in the inner and outer shells by the longitudinal acceleration is a result of the force applied to the shells by the acceleration of either end casting. It is assumed that the acceleration is forward so that the lower end casting is loading the shells. The weight of the lower end casting is 1000 pounds so the force on both shells will be 540 pounds which is distributed over both shells. The cross section area of the shells is 319 square inches (306 and 13 square inches for the outer and inner respectively) resulting in a stress of 2 psi in either shell.

Combining all of the above stresses results in the following maximum stresses:

radial = 28 psi
hoop = 414 psi
axial = 1125 psi

The axial stress is the sum of the bending and axial stress. The limit on the primary membrane stresses is the design stress intensity which is 20,000 psi and the limit on the sum of the primary membrane stress and the bending stress is 1.5 times the design stress intensity which is 30,000 psi. The calculated stresses due to vibration are not close to their respective limits so the road vibration will not cause any damage to the cask.

2.6.5. Water Spray

Spraying water on the surface of the NAC-1 cask will have no effect upon the structural adequacy of the cask. All exposed surfaces of this cask are stainless steel so there are no interactions between the spray and the cask (Reference 2.19) that will degrade the capability of the materials to withstand the stresses that are imposed during either normal operation or accident conditions.

2.6.6. Free Drop

Appendix A of Part 71 of Title 10, Chapter 1 of the Code of Federal Regulations (Reference 2.2) requires that all transportation packages in excess of 30,000 pounds be evaluated to determine the consequences of a free fall through a distance of one foot onto a horizontal unyielding surface. The orientation of the cask is to be such that the maximum damage is inflicted on the cask. Since it is impossible to define the orientation of

the maximum damage prior to the analysis, the same cask orientations that are to be evaluated for the 30 foot free fall as a part of the hypothetical accident were considered. The models and representation of the impact forces that are employed in the analysis of the 30 foot free fall were employed for this analysis. These models are fully described in Section 2.7.

The analyses presented here represent an impact following steady state conditions when the ambient temperature was 130°F. Cases that represent a -40°F ambient are not presented because the strength of the stainless steel increases as the temperature decreases providing more margin between the calculated stresses and the limiting stresses. The principal concern in impact analyses for cold ambient conditions is the onset of brittle fracture which is unlikely with stainless steel.

2.6.6.1. End Impact

A free fall that results in an impact on either end of the cask will result in deformation of the impact limiter which will absorb 624,000 inch pounds of kinetic energy at the point of impact. The analysis of the one foot free fall onto the end of the cask is identical to the analysis of the 30 foot free fall that is presented in Section 2.7.1.1. The details of the model and the representation of the impact limiter will not be repeated here.

The model of the cask was used to evaluate the stresses in the cask during an end impact following a one foot free fall. At the point of impact the velocity of the cask was 96 inches per second. The portion of the end impact limiter force-displacement curve that is effective for a absorbing the energy of a one foot free fall is presented in Figure 2-37. The displacement history

of the lower end of the cask during the impact is presented in Figure 2-38. The principal phenomenon that occurs during this accident is the slumping of the lead due to the inertial loads. The displacement of the upper surface of the lead is presented in Figure 2-39 along with the displacement of the adjacent points on the inner and outer shells. The lead does slump during the impact; however, the relative displacement is small.

The lead induces compressive hoop stresses in the inner shell and tensile hoop stresses in the outer shell as well as axial stresses in both shells that are presented in Figures 2-40 to 2-43 as functions of time and axial position in the cask. The reference for axial position is the bottom of the lower end casting which is 8.0 inches below the lower end of the cavity and 12.75 inches below the lower end of the inner shell.

The calculated stresses are based upon an empty or dry cavity where there is no water and associated hydrostatic pressure on the inside of the inner shell. If water is present the hydrostatic pressure will be 277. psi which is the product of $\rho g h$ where g is the maximum deceleration of the cask (57.7 g's) and h is the height of the water (133 inches) and ρ is the density of water (62.4 lb/ft3). Additionally, if the cask has reached thermal equilibrium and the environmental temperature is 130°F, the cavity pressure will be 118 psia which is additive to the hydrostatic pressure. These two terms will reduce the hoop stresses in the inner shell by 8,730. psi; however, the consequences of the accident are more severe if the cavity is unpressurized.

The hydrostatic pressure will contribute to the axial stresses in both the inner and outer shells. The magnitude of the increase in the stress is determined from a force balance on the end castings. The internal pressure acts outward on the end casting and both shells exert a balancing force. In equation form this is expressed as:

$$p_i \ D_i^2/4 = \sigma_i A_i + \sigma_o A_o$$

where:

p_i is the internal pressure
D_i is the internal diameter
σ_i is the axial stress in the inner shell
A_i is the cross section area of the inner shell
σ_o is the axial stress in the outer shell
A_o is the cross section area of the outer shell

Introducing numerical values results in an axial stress of 133 psi in both shells. This value is negligibly small and need not be considered further in the evaluation of an end impact.

The maximum hoop stress is presented in Figure 2-44 as a function of position in both shells. This data represents the accumulation of the largest stresses at all times at each axial location. Similiarly, the maximum axial stresses in both the inner and outer shells are presented in Figure 2-45 as a function of position. An additional curve is presented for the inner shell which represents the axial stresses that will occur if the cavity has water and is pressurized to 118 psia by thermal expansion of the water.

The thermal stresses have not been included in the total stresses because the thermal stresses induce tensile hoop stresses in the lead which must be overcome by the hydrostatic forces prior to slumping of the lead. Consequently, the predicted consequences of the end drop are more severe if the cask is assumed to be in a stress free state prior to the initiation of the accident.

The limitation on the hoop and axial stresses is the lesser of the buckling stress or the ultimate stress. In this instance buckling is the more restrictive limit for both stresses and is discussed in the following section.

2.6.6.1.1. Effect of Cavity Irregularity

The analyses presented in Section 2.6.5.2. presume that the inner and outer shells are perfect cylinders. The outer shell is fully machined as the final step in its fabrication so it will be very nearly a perfect cylinder; however, the inner shell is subject to dimensional variations from a true cylinder. Consequently, it is necessary to determine the impact of dimensional variations and also to determine the variations that can be tolerated.

2.6.6.1.1.1. Collapse Buckling

The presence of ovality of either shell will increase the hoop stress because the radius in increased. The increase in the hoop stress in the inner shell is presented in Figure 2-46 as a function of the ovality. This curve has been determined from the ratio of the expressions for hoop stress in true and ovalized cylinders (Reference 2.9):

$$\frac{\sigma_{ht}}{\sigma_{ho}} = \frac{p\ r_t\ t_o}{p\ r_o\ t_i}$$

where:

p is the pressure
r is the radius of the shell
t is the thickness of the shell
σ_h is the hoop stress
t and o as subscripts refer to true and oval cylinders

The radius that is employed for elliptical cylinders is given by:

$$r = a^2 / b$$

2.6.6.1.1. Effect of Cavity Irregularity

The analyses presented in Section 2.6.5.2. presume that the inner and outer shells are perfect cylinders. The outer shell is fully machined as the final step in its fabrication so it will be very nearly a perfect cylinder; however, the inner shell is subject to dimensional variations from a true cylinder. Consequently, it is necessary to determine the impact of dimensional variations and also to determine the variations that can be tolerated.

2.6.6.1.1.1. Collapse Buckling

The presence of ovality of either shell will increase the hoop stress because the radius in increased. The increase in the hoop stress in the inner shell is presented in Figure 2-46 as a function of the ovality. This curve has been determined from the ratio of the expressions for hoop stress in true and ovalized cylinders (Reference 2.9):

$$\frac{\sigma_{ht}}{\sigma_{ho}} = \frac{p\ r_t\ t_o}{p\ r_o\ t_i}$$

where:

p is the pressure
r is the radius of the shell
t is the thickness of the shell
σ_h is the hoop stress
t and o as subscripts refer to true and oval cylinders

The radius that is employed for elliptical cylinders is given by:

$$r = a^2 / b$$

where:

a is the major radius
b is the minor radius

The factor that increases the hoop stress to account for ovality has been applied to the maximum hoop stress presented in Figure 2-42 to determine the maximum hoop stress as a function of ovality and position. The resulting maximum hoop stresses have been superimposed upon the curve of buckling stress as a function of ovality and axial position (Figure 2-10) as shown in Figure 2-47. The maximum calculated hoop stress is below the buckling limit.

There is no impact of bow of the inner shell on the collapse type buckling because collapse is a local phenomena that is independent of the straightness of the remainder of the cylinder.

2.6.6.1.1.2. Compressive Buckling

As discussed in Section 2.1.2.2.3 the inner shell cannot buckle due to axial loads unless the outer shell also buckles because both shells are coupled by the end castings and the large deformations associated with buckling cannot occur in either shell as long as the other shell remains intact. The maximum axial stresses in both shells have been presented in Figure 2-45 as a function of axial position. The axial stress that is required to cause buckling of the inner shell varies between 25,000 and 35,000 psi for both shells for ovalities in the range of 0 to 10%. Since the maximum axial stress in the outer shell is 13,200 psi the outer shell will remain intact and will support the inner shell. This is independent of the ovality of either shell because the stresses are so small. Consequently, the possibility of buckling due to axial loadings introduces no limitations on the ovality or bow of the inner shell.

2.6.6.1.1.3. Comparison to Design Stress Intensity

The hoop and axial stresses that result from a one foot free fall are primary stresses that must be less than the design stress intensity. The cask is not subject to any bending during an end impact so there will be no increase in the limit to include the presence of bending stresses.

The stresses that result from an end impact are dynamic in nature so the limitating stresses should reflect the increase in the strength of the stainless steel that is associated with dynamic application of the loads. The yield strength of stainless steel was shown to increase to at least 37,500 psi when the loading was dynamic so the design stress intensity is 25,000 psi (2/3 of yield strength) for dynamic loading.

Ovality of the inner shell will increase the hoop and axial stresses in the same manner as indicated in Sections 2.6.5.1.2.1 and 2.6.5.1.2.2. The maximum hoop and axial stresses in the inner shell have been increased to reflect ovality of the inner shell and plotted in Figures 2-47 and 2-48 as functions of axial position and ovality. Both figures also include the design stress intensity (25,000 psi) to illustrate the intersection of the limit and the calculated stress. The calculated stress intersects the limit at a few points near the center of the cask and the specific amounts of ovality that cause the calculated stress to equal the limit are presented in Figure 2-49 as a function of position.

2.6.6.2. Side Impact

A free fall of one foot with the impact on the side will result in damage to the cask that is similiar to the consequences of the

30 foot free fall that is a part of the hypothetical accident. The analysis model and analysis techniques are identical to those used in the analysis of the 30 foot free fall and reported in Section 2.7.1.2. The description of the model will not be repeated here.

The beam model of the cask was used to determine the stresses in the cask as a result of a one foot free fall where both impact limiters simultaneously make contact with the unyielding surface. The cask was given an initial velocity of 96 inches per second. The impact on the unyielding surface was represented by fixing the ends of the spars that represent the impact limiters. The force-deflection curve for the impact limiters is identical to the corresponding curve for the analysis of the 30 foot free fall. The crush characteristics of the impact limiters are defined in Section 2.7.1.2.1.2. and the portion of the force-deflection curve that is effective in a one foot fall is presented in Figure 2-50.

The principal effect of this impact is the bending of the cask due to the inertia of the center of the cask while the ends of the cask have been stopped by the impact limiters. The time histories of the ends and center of the cask are presented in Figure 2-51 and the deflection of the center of the cask relative to the lower end of the cask is presented in Figure 2-52. The calculated deformation of the entire cask is presented in Figure 2-53 which includes the vertical displacement of both ends of the cask, the center of the cask and the displacement of the center relative to either end. The stresses induced in the cask body as a result of these deformations are presented in Figure 2-54 which shows a stress wave that travels along the cask with a frequency of about 65 cycles per second.

The model of the cask body included only the outer shell because it is the principal structural member of the cask. The stresses in the inner shell must also be determined to permit comparison

to the limitations that determine the survivability of the cask during the hypothetical accident.

The end castings distribute the moment between the two shells so that the angular deflection of both shells are identical at any time during the impact. The angular deflection of the ends of the shells is proportional to M/EI so this ratio must be identical for the ANSYS model, the inner shell and the outer shell. To preserve these ratios the moments will distribute themselves in proportion to the moments of inertia or in equation form:

$$\sigma_a = M_a c_a / I_a$$

or

$$M_a = \sigma_a I_a / c_a$$

and

$$\sigma_i = M_i c_i / I_i$$
$$\sigma o = Mo\ co / Io$$
$$M_i = M_a I_i / (I_o + I_i)$$
$$M_o = M_a I_o / (I_o + I_i)$$

giving

$$\sigma_i = M_a I_i c_i / (I_o + I_i)$$
$$\sigma_o = M_a I_o c_o / (I_o + I_i)$$

or

$$\sigma_i = a I_a c_i / (I_o + I_i) c_a$$
$$\sigma_o = a I_a c_o / (I_o + I_i) c_a$$

where:

M_a is the moment from the ANSYS calculation
M_i is the moment on the inner shell
M_o is the moment on the outer shell
I_a is the moment of inertia used in the ANSYS calculation
I_i is the moment of inertia of the inner shell
I_o is the moment of inertia of the outer shell
c_a is the radius used in the ANSYS calcualtion
c_i is the radius of the inner shell
c_o is the radius of the outer shell

The moments of inertia and the radius to the outer fiber of the two shells is presented in Table 2-16. The ANSYS calculation modeled only the outer shell so the values that characterize the calculated results are those of the outer shell. Inserting numerical values gives the ratio of the bending stress in the inner shell to that calculated by ANSYS of 0.458 and the ratio of the bending stress in the outer shell to that calculated by ANSYS is 0.973. These ratios have been employed to determine the maximum stresses in the inner and outer shells that are presented in Figure 2-55. The data presented in Figure 2-55 are the results of the ANSYS calculation and do not truly represent the bending stress in either shell; although, they are very close to the stresses in the outer shell.

The limitation on the bending stress is the lesser of the buckling stress or 1.5 times the design stress intensity. The impact of ovality on the buckling is discussed in the following sections along with the comparisons of the calculated stresses to the two stress limits.

2.6.6.2.1. Effect of Cavity Irregularity

The analyses presented in Section 2.6.5.2 presume that the inner and outer shells are perfect cylinders. The outer shell is fully machined as the final step in its fabrication so it will be very nearly a perfect cylinder; however, the inner shell is subject to dimensional variations from a true cylinder. Consequently, it is necessary to determine the impact of dimensional variations and also to determine the variations that can be tolerated.

The limitations on the stresses that result from the one foot free fall are the lesser of the stresses that cause buckling of the inner or outer shell and 1.5 times the design stress intensity. Both of these limitations will be considered in the

following sections.

2.6.6.2.1.1. Bending Buckling

The only type of buckling that is possible during a side impact is buckling due to bending. The limiting stresses that assure the absence of this type of buckling were presented in Section 2.1.2.2.1 and Figure 2-6. The presence of ovality of either shell will increase the bending stress because the moment of inertia of the cross section is increased. The increase in the bending stress in the inner shell is presented in Figure 2-56 as a function of the ovality. This curve has been determined from the expression for bending stress (Reference 2.9):

$$\sigma_b = Mc/I$$

where the symbols are as defined above. The moment of inertia of an elliptical cylinder is given by:

$$I = \pi(ab^3 - ba^3)/4$$

where:

a is the major radius
b is the minor radius

The factor that increases the bending stress to account for ovality has been applied to the maximum bending stress presented in Figure 2-55 to determine the maximum bending stress as a function of ovality and position. The maximum calculated bending stress is substantially below the buckling limit.

There is no impact of bow of the inner shell on the bending type buckling because the configuration of the cross section is the controlling parameter and the presence of a bow could only serve

to change the moment arm which is a very minor correction to the conditions that could induce buckling failure.

2.6.6.2.1.2. Comparison to Design Stress Intensity

The dynamic nature of the loading during the impact that terminates a free fall necessitates the correction of the design stress intensity to reflect the increase in the strength of stainless steel when rapidly loaded. The appropriate value of the design stress intensity is 25,000 psi.

Any ovality of the inner shell will result in an increase in the hoop stress in the inner shell which is identical to the increase identified in Section 2.6.5.2.1.1. This corection has been applied to the maximum bending stress in the inner shell that was presented in Figure 2-55 and the resulting bending stress plotted as a function of axial position and ovality in Figure 2-57. This figure also includes the design stress intensity to graphically illustrate the intersection of the calculated and limiting stresses. The bending stress in the inner shell is substantially less than the design stress intensity for all reasonable amounts of ovality.

2.6.6.3. Corner Impact

The analyses of the 30 foot free fall where the impact is on a corner of the impact limiter demonstrates that the worst impact orientation at the end of a free fall is either a direct impact on an end or an impact where both impact limiters contact the ground simultaneously. This conclusion will not change when the fall is only one foot so there is no need for analysis of a free fall where impact is on the corner of the impact limiter.

2.6.7. Corner Drop

Appendix A of Part 71 of Title 10, Chapter 1 of the Code of Federal Regulations (Reference 2.2) requires that all transportation packages that are constructed primarily of wood and fiberboard and do not exceed 110 pounds in weight must be evaluated to determine the consequences of sequentially falling onto each corner of the package through a distance of one foot. Since the NAC-1 cask is primarily constructed of stainless steel and weighs approximately 50,000 pounds there is no need to analyse the consequences of such a fall.

2.6.8. Penetration

Appendix A of Part 71 of Title 10, Chapter 1 of the Code of Federal Regulations (Reference 2.2) requires that all transportation packages be able to withstand the impact of a 13 pound projectile with no adverse effects on either the ability of the cask to maintain containment or to survive a hypothetical accident. There are four locations on the cask where a projectile could potentially cause sufficient damage to impair the performance of the cask. These are:

Expansion Tank
Neutron Shield Tank
Impact Limiter
Cowl

An impact on either the neutron shield tank or the expansion tank would reduce the shielding of the cask if the outer shell of either of these two tanks were penetrated. The impact limiter is required to absorb energy during any of the free falls and damage

to these could reduce the ability of the cask to survive the hypothetical accident. Similiarly, the cowl is intended to minimize heat transfer to the cask body during a fire and damage to the cowl could preclude the ability of the cask to survive the fire accident.

2.6.8.1. Impact on Shield Tank

The configuration of the shield tank was illustrated in Figure 1-5 which showed the gussets that support the outer shell and the welded connections to the expansion tank and the conical end piece at the lower end of the cask. The consequences of an impact on the shield tank has the most potential for damage of any of the cask areas identified in the previous section because it has the largest unsupported area. The dimensions of the shield tank as well as the other portions of the cask exterior are presented in Table 2-22.

The consequences of an impact have been evaluated by considering the outer surface to be an arch with fixed edges. Equations for the stresses and displacements of an arch have been published in Reference 2.25. These equations are:

$$y_s = \frac{P r^3}{\theta E I}\left[(\pi - 2\alpha)(1 + 2\cos^2\alpha) - 8\cos\alpha + 3\sin 2\alpha\right]$$

$$H_o = P\frac{\left[\theta(1-\sin\alpha)\cos\alpha - (\pi - 2\alpha)(1+\cos 2\alpha)\right]}{\left[2(\pi-2\alpha)(\pi - 2\alpha + \sin 2\alpha) - 16\cos^2\alpha\right]}$$

$$M_o = H_o r\left[\frac{\left[2(\pi-2\alpha+2\cos\alpha)(\sin\alpha - 1) + (\pi - 2\alpha)^2\cos\alpha\right]}{\left[\theta(1-\sin\alpha)\cos\alpha - (\pi - 2\alpha)(1+\cos 2\alpha)\right]}\right]$$

$$y_n = y_s + \frac{M_o r^2}{EI}\left[1 - \sin\alpha - 0.5(\pi - 2\alpha)\cos\alpha\right]$$

$$- \frac{H_o r^3}{EI}\left[\sin\alpha + 0.75\cos 2\alpha - 0.25(\pi - 2\alpha)\sin 2\alpha - 0.75\right]$$

where:

Y_S is the displacement of the support
Y_n is the displacement of the center of the arch
H_O is the horizontal restraining force
M_O is the restraining moment

r is the radius to the inside of the arch
α is half of the difference between the arc of the arch and 180°
E is the elastic modulus
I is the moment of inertia

The definitions of these symbols are also presented in Figure 2-58.

The equations for an arch presume that the sides of the arch are free where the shield tank sides are rigidly attached to other cask components. The correction for the effect of rigidity of the sides of the arches was developed by comparing the solutions presented in Reference 2.9 for flat plates uniformly loaded with rigid support on two sides and on four sides. The expression for the stress in a uniformly loaded flat plate with fully fixed edges is:

$$\sigma_1 = - \beta_1 q b^2/t^2$$
$$\sigma_2 = \beta_2 q b^2/t^2$$
$$y = - \alpha q b^4/E t^3$$

where:
σ_1 is the stress in the long direction
σ_2 is the stress in the short direction
q is the uniformly distributed load
t is the thickness of the plate
b is the length of the short dimension of the plate
a is the length of the long dimension of the plate
β_1 and β_2 are tabulated functions of a and b

The corresponding equations for the stresses in a flat plate with two sides fixed and two sides free are:

$$\sigma_2 = - \beta q b^2/t^2$$
$$y = - \alpha q b^4/E t^3$$

wher the symbols are as defined above. The tabular functions α, β, β_1 and β_2 are presented in Figure 2-59 as a function of the ratio of the lengths of the sides (a/b). These two sets of equations have been evaluated for a variety of plate sizes to determine the correction factor that can be used to include the effect of edge fixity in the arch representation. The ratio of the displacement of the two sided plate to the displacement of the four sided plate is presented in Figure 2-60.

The expression for the displacement of an arch has been evaluated as a function of the applied load using the dimensions of the shield tank. The calculated displacement was reduced by the factor presented in Figure 2-60 to determine the equivalent displacement of an arch with all sides fixed. The resulting force-displacement curve is presented in Figure 2-61.

The final segment of this calculation is the integration of the force-displacement curve to determine the work that is done in deflecting the arch. A numerical integration technique was employed to evaluate the work which is required to cause failure of the shield tank. Failure has been defined as the bending stress in the shell reaching 69,300 psi which is the static ultimate stress. The use of a static limit was adopted to assure conservatism by ignoring the effects of strain hardening of the material during the impact. The work required to cause a bending failure is presented in Table 2-23 along with the impact energy of the projectile. The energy of the projectile is significantly less than the work required to fail the shell so there will be no penetration.

The lower end of the shield end is termi.ated with a connical section that must also be evaluated to assure that it is capable of withstanding an impact of the projectile. The methods previously described for determining the deflection of an arch were applied to an arch that is equivalent to the midsection of the connical section. The dimensions of the connical section are

presented in Table 2-22 and the work required to fail this section is presented in Table 2-23. The impact energy of the projectile is much smaller than the work required for failure so the projectile will not penetrate this portion of the shield tank. Consequently, there will be no loss of shielding and the cask will retain its ability to withstand the hypothetical accident.

2.6.8.2. Impact on Expansion Tank

The configuration of the expansion tank is shown in Figure 1-5 which identifies the location of the gussets that support the outer shell. The expansion tank is stronger than the shield tank because the outer shell is thicker and the unsupported arc is smaller. The dimensions of the two shells are compared in Table 2-22. The impact resistance of the expansion tank was evaluated with the methods identified in the previous section for the evaluation of the shield tank. The work required to cause failure of the outer shell is presented in Table 2-23 along with the impact energy of the projectile. The energy of the projectile is insufficient to penetrate the expansion tank so the cask will retain its ability to safely transport spent fuel and withstand a hypothetical accident.

2.6.8.3. Impact on Impact Limiter

The outer shell of the impact limiter is not sufficiently thick to prevent penetration of a 13 pound projectile. However, the redwood and balsa wood would stop the projectile prior to its reaching the cask body. The energy of the projectile is the product of its mass and height.

The energy absorbed by the basla wood or redwood is equal to the

energy of the projectile and is expressed as the product of the retarding force and the deformation suffered by the impact limiter. The retarding force is approximated as the product of the crush strength of the wood and the area of the projectile. In equation form this is:

$$E = F\,d = \sigma A\,d = 1600 \times 1.22\ d = 13 \times 40 = 540 \text{ in-lbs}$$

solving for the deformation d gives:

$$d = 540/(1600 \times 1.22) = 0.277 \text{ inches}$$

This estimate of the penetration is very conservative because no credit has been taken for the retarding force of the outer stainless steel shell which surrounds the impact limiter. An additional conservatism was introduced by using the crush strength of balsa wood rather than a combination of the redwood and balsa wood that is the weakest component of the impact limiter.

The maximum damage would be a 1.25 inch diameter hole 0.277 inches deep in the impact limiter. This would reduce the effective area of the impact limiter by 1.22 square inches which is inconsequential because the total area of the impact limiter that is effective for an end impact is 1590 square inches and 382 square inches for a side impact. Consequently, impact of a projectile onto either impact limiter will not impair the ability of the cask to survive the hypothetical accident.

2.6.8.4. Impact on Cowl

The impact on a cowl can be either at the upper end or the lower end of the cask. The lower cowl is thinner than the shield tank but it is stronger because the edge supports are less widely

separated. The dimensions of the two shells are compared in Table 2-22. The impact resistance of the lower cowl was evaluated with the methods identified in the previous section for the evaluation of the shield tank. The work required to cause failure of the outer shell is presented in Table 2-23 along with the impact energy of the projectile. The energy of the projectile is insufficient to penetrate the lower cowl so the cask will retain its ability to safely transport spent fuel and withstand a hypothetical accident.

The upper cowl has gussetts that are 0.125 inches thick and are 1.375 inches between centers. The gap between gussetts is 1.25 inches which is identical to the diameter of the projectile. The ability of the projectile to penetrate the cowl was not evaluated because the proximity of the gussetts to the impact point will increase the strength of this cowl beyond the strength of the other cowl. Consequently, an impact on this cowl will not impair the functional capabilities of the cask.

2.6.9. Compression

Appendix A of Part 71 of Title 10, Chapter 1 of the Code of Federal Regulations (Reference 2.2) requires that all transportation packages weighing less than 10,000 pounds be evaluated to determine the effect of a compressive loading equal to either five times the weight of the package or a pressure of two pounds per square foot, whichever is greater. Since the NAC-1 spent fuel shipping cask weighs about 50,000 pounds, this requirement does not apply to this cask.

2.6.10. Fabrication Stresses

The process of manufacturing the NAC-1 cask introduces thermal stresses into the inner and outer shells as a result of pouring molten lead into the cask wall. The thermal stresses must be evaluated to provide assurance that the manufacturing of the cask does not adversely effect the operation of the cask or its ability to survive an accident. Any residual stresses are dependent upon the strength of the lead and were relieved during the life of the cask because the lead will creep even at room temperature.

The lead pouring procedure (Reference 2.1) requires preheat to at least 550 ^{o}F by the application of flame rings around the outside of the cask. The cask is in a pit with about three-quarters of the cask underground during the entire preheating, lead pouring and cooling operations. Thus, the outer surface was exposed to an environment with a temperature of about 2000^{o}F while the inner shell was cooled by natural circulation. The temperature of the cask was monitored by three thermocouples that were attached to the inside surface of the inner shell and preheat was adequate when at least two of these thermocouples indicated 550^{o}F. During the preheating process the lead was also heated until its temperature reached at least 775^{o}F.

The lead was poured into the cask wall through two holes in the upper end casting and two additional holes were vents. The total time required for the pouring operation was about ten minutes. The cooling process consisted of two operations. The first was the sequential extinguishing of the flame rings with the lowest being the first to be extinguished and the upper flame ring the last to be extinguished. Simultaneously, molten lead was added to the cask wall an attempt to fill in any void that was created as the lead shrank during solidifaction. These two operations were intended to completelly fill the lead region of the cask wall and

2.6.10. Fabrication Stresses

The process of manufacturing the NAC-1 cask introduces thermal stresses into the inner and outer shells as a result of pouring molten lead into the cask wall. The thermal stresses must be evaluated to provide assurance that the manufacturing of the cask does not adversely effect the operation of the cask or its ability to survive an accident. Any residual stresses are dependent upon the strength of the lead and were relieved during the life of the cask because the lead will creep even at room temperature.

The lead pouring procedure (Reference 2.1) requires preheat to at least 550 ^{o}F by the application of flame rings around the outside of the cask. The cask is in a pit with about three-quarters of the cask underground during the entire preheating, lead pouring and cooling operations. Thus, the outer surface was exposed to an environment with a temperature of about 2000^{o}F while the inner shell was cooled by natural circulation. The temperature of the cask was monitored by three thermocouples that were attached to the inside surface of the inner shell and preheat was adequate when at least two of these thermocouples indicated 550^{o}F. During the preheating process the lead was also heated until its temperature reached at least 775^{o}F.

The lead was poured into the cask wall through two holes in the upper end casting and two additional holes were vents. The total time required for the pouring operation was about ten minutes. The cooling process consisted of two operations. The first was the sequential extinguishing of the flame rings with the lowest being the first to be extinguished and the upper flame ring the last to be extinguished. Simultaneously, molten lead was added to the cask wall an attempt to fill in any void that was created as the lead shrank during solidifaction. These two operations were intended to completelly fill the lead region of the cask wall and

preclude the formation of any voids.

2.6.10.1. Thermal Stresses During Lead Pouring

The process of pouring lead into the preheated cask body has been represented analytically using the HEATING-5 (Reference 2.23) computer program. The details of the thermal analysis are presented in part3 of this report that describes the thermal analysis of the modified NAC-1 cask. The results of that analysis will be summarized here for completeness.

The thermal model of the cask wall represented the inner shell as a one dimensional cylindrical shell subject to an incident heat flux on the outer surface and natural convection cooling on the inner surface. Any axial conduction of heat was neglected to assure conservatism. The process of pouring the lead into the cask wall was represented as an instantaneous change in the boundary condition on the outside of the inner shell. The heat flux boundary condition was replaced by a constant temperature boundary condition where the temperature was 775°F.

The temperature history following this representation of the introduction of the lead is shown in Figure 2-62. After about 8 seconds the temperature distribution has reached equilibrium. Any subsequent change in the temperatures of the lead was reflected in a change in the temperatures of the inner shell. However, the change in temperatures was much slower because the thermal inertia of the lead was coupled with the thermal inertia of the stainless steel shell.

The thermal stresses are governed by the following differential equations:

$$\frac{d\sigma_r}{dr} + \frac{1}{r} (\sigma_r - \sigma_\theta) = 0$$

$$\frac{dE_r}{dr} + \frac{1}{r} (E_\theta - E_r) = 0$$

$$E_r = \frac{1}{E} [\sigma_r - \nu (\sigma_Z + \sigma_\theta)] + \alpha T$$

$$E_\theta = \frac{1}{E} [\sigma_\theta - \nu(\sigma_r + \sigma_Z)] + \alpha T$$

where:

r is the radius
T is the temperature
α is the coefficient of thermal expansion
E is the modulus of elasticity
ν is Poisson's ratio

The solution of these differential equations is given by the following three integrals (Reference 2.24):

$$\sigma_r = \frac{\alpha E}{1-\nu} \frac{1}{r^2} \left(\frac{r^2 - r_0^2}{R^2 - r_0^2} \int_{r_0}^{R} Tr\,dr - \int_{r_0}^{r} Tr\,dr \right)$$

$$\sigma_\theta = \frac{\alpha E}{1-\nu} \frac{1}{r^2} \left(\frac{r^2 + r_0^2}{R^2 - r_0^2} \int_{r_0}^{R} Tr\,dr + \int_{r_0}^{r} Tr\,dr - Tr^2 \right)$$

$$\sigma_z = -\frac{\alpha E}{1-\nu} \left(T - \frac{2}{R^2 - r_0^2} \int_{r_0}^{R} Tr\,dr \right)$$

The temperature distributions presented in Figure 2-62 have been integrated numerically using trapezoidal rule and the resulting stresses are presented in Figures 2-63, 2-64 and 2-65. The history of the maximum stress is presented in Figure 2-66 and summarized in Table 2-24.

2.6.10.2. Thermal Stresses During Cooldown

The stresses that result from the cooldown portion of the lead pouring operation arise primarily from the shrinkage of the lead onto the inner stainless steel shell and the stretching of the copper fins attached to the outer stainless steel shell. The thermal stresses that arise from the temperature gradient are very small because the temperature gradients across the cask components are small.

The model for the evaluation of the thermal stresses that was described in Section 2.6.1.2. was used to determine the stresses at the conclusion of the cooldown process. The end of cooldown represents the time when the stresses will be maximum prior to the introduction of the cask into service. During the time between the conclusion of the cooldown and the initial service the lead will have an opportunity to partially relieve the stresses. This condition will not be included in the analyses to assure that the results are conservative.

The cask temperature was set to 70°F uniformly throughout the entire cask and the resulting stresses are presented in Figure 2-67.

2.6.10.3. Comparison of Thermal Stresses to Limits

The thermal stresses must be combined with the pressure stresses that are present during the lead pour to define the total stress state so that a complete comparison of the stresses to the limits is possible. The only other stress that is present during the lead pour is the hydrostatic pressure due to the liquid lead. In equation form this is expressed as:

$$p = \rho h$$

where:

p is the hydrostatic pressure
ρ is the density of lead
h is the height of the lead

The stresses in the inner shell are given by the expressions for the stresses in a thin wall cylinder which are:

$$\sigma_r = (p_o - p_i) \qquad \sigma_h = (p_o - p_i)r / 2t$$

where:

p_o and p_i are the external and internal pressures
r is the mean radius of the shell
t is the thickness of the shell
σ_r is the radial stress
σ_h is the hoop stress

There is no expression for an axial stress because the lead column is free at the ends so there can be no force applied to the ends of the cask. Introducing numerical values results in a radial stress of 85 psi and a hoop stress of 1647 psi. These values are reproduced in Table 2-24 and combined with the maximum thermal stresses to define the total stress state during the lead pour operation.

The limitation on the thermal stresses is incorporated in the comparison of the stress intensity to the limit of 3 times the design stress intensity which is discussed in Section 2.1. Since this limitation is a function of all of the conditions of normal transport it will not be repeated here.

The stresses at the conclusion of the cooldown process will be considered to be entirely primary stresses because the portion of these stresses that is not due to the shrinkage of the lead onto

the inner shell is small. The limitation on primary stresses that include no bending is the design stress intensity which is 20,000 psi for stainless steel at temperatures between 100°F and 300°F. The maximum stresses due to the cool down process are presented in Figure 2-67 and are everywhere less than 9,915 psi which is much smaller than the design stress intensity. There is no pressure or loads applied to the cask during the cool down because the cask is in fabrication and is not loaded.

Table 2-18. Extreme Temperatures During Normal Transport

Component	Temperature (deg F) (130°F ambient)	Temperature (deg F) (-40°F ambient)
cavity water	318	32
lead	301	28
valves		
relief	300	12
upper vent	290	1
lower vent	289	1
upper drain	275	-2
lower drain	271	-2
O-rings		
inner	318	32
outer	319	10
Maximum pressure	118 psia	

Table 2-19. Stresses Resulting From Reduced Atmospheric Pressure

Component	Outside Radius Inches	Thickness Inches	Internal Pressure psia	σ_r psi	σ_h psi	σ_z psi
Impact Limiter	36.	0.109	15.	- 11.5	-3798.	-1898.
Expansion Tank	22.5	0.25	50.	-46.5	-4185.	-2092.
Shield Tank	19.6	0.165	50.	-46.5	-5523.	-2761.
Cowl						
Upper	15.	0.125	15.	-11.5	-1326.	-662.
Lower	18.6	0.125	15.	-11.5	-1647.	-816.

Table 2-20. Cask Accelerations Due to Transport Vibration

Frequency Hz	Acceleration (g's) Longitudinal	Transverse	Vertical
0-5	0.27	0.10	0.52
5-10	0.14	0.07	0.27
10-20	0.19	0.19	0.37
20-40	0.10	0.07	0.19
40-80	0.10	0.10	0.37
80-120	0.07	0.10	0.37
120-180	0.07	0.10	0.52
180-240	0.05	0.10	0.52
240-350	0.07	0.14	0.52
350-500	0.05	0.07	0.37
500-700	0.05	0.02	0.10
700-1000	0.05	0.02	0.10
1000-1400	0.14	0.05	0.10
1400-1900	0.03	0.02	0.10

This data represents the 99% envelope of vibrational acceleration received by a 56,000 pound cargo during typical shipment (Reference 2.20).

Table 2-21. Stresses Due to Vibration

Direction	Acceleration	σ
Longitudinal	0.54	--
Vertical		
Upward	1.04	752
Downward	2.04	1,476
Transverse	0.38	724
Combined Vertical and Transverse	--	2,200

Table 2-22. Dimensions of Outer Surfaces

Dimension	Shield Tank	Shield Tank Cone	Expansion Tank
Outside Diameter	39.2	38.22	45.0
Thickness	0.165	0.109	0.25
Unsupported Arc	90.	90.	50.
Length	133.8	8.68	16.7
Width	30.87	38.22	15.53
a/b	4.34	3.46	1.08

	Lower Cowl	Upper Cowl
Outside Diameter	37.25	37.25
Thickness	0.109	0.25
Unsupported Arc	180.	360.
Length	13.0	1.25
Width	58.51	-
a/b	4.50	-

continued

Dimension	Impact Limiter		
	Side	End	Corner
Outside Diameter	72.	-	58.5
Thickness	0.109	0.109	0.109
Unsupported Arc	360.	-	360.
Length	9.1	-	19.0
Width	-	-	183.8
a/b	-	-	9.66

Table 2-23. Energy Absorption of Outer Surfaces

Component	Energy to Cause Failure in lbs	Projectile Energy in lbs
Shield Tank	1,460	520
Expansion Tank	831	520
Shield Tank Cone	1,375	520
Lower Cowl	910	520
Impact Limiter Corner	4,278	520

Table 2-24. Maximum Stresses During Lead Pouring

Condition	Stress		
	Radial	Hoop	Axial
Thermal Stresses During Lead Pour	482	-52,080	-52,080
Pressure Stresses	75	1648	0
Thermal Stress at End of Cooldown	384	9,063	10,206

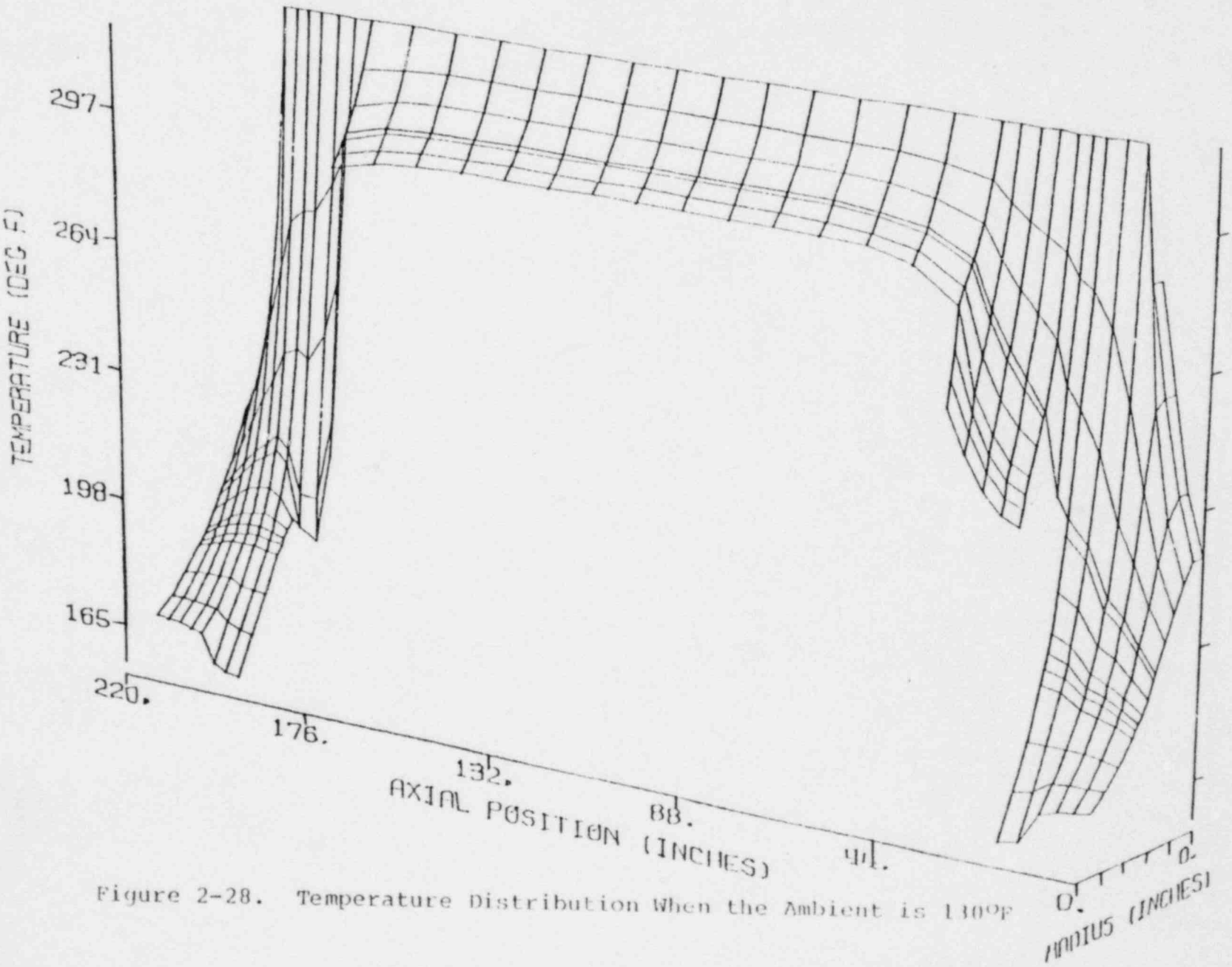

Figure 2-28. Temperature Distribution When the Ambient is 130°F

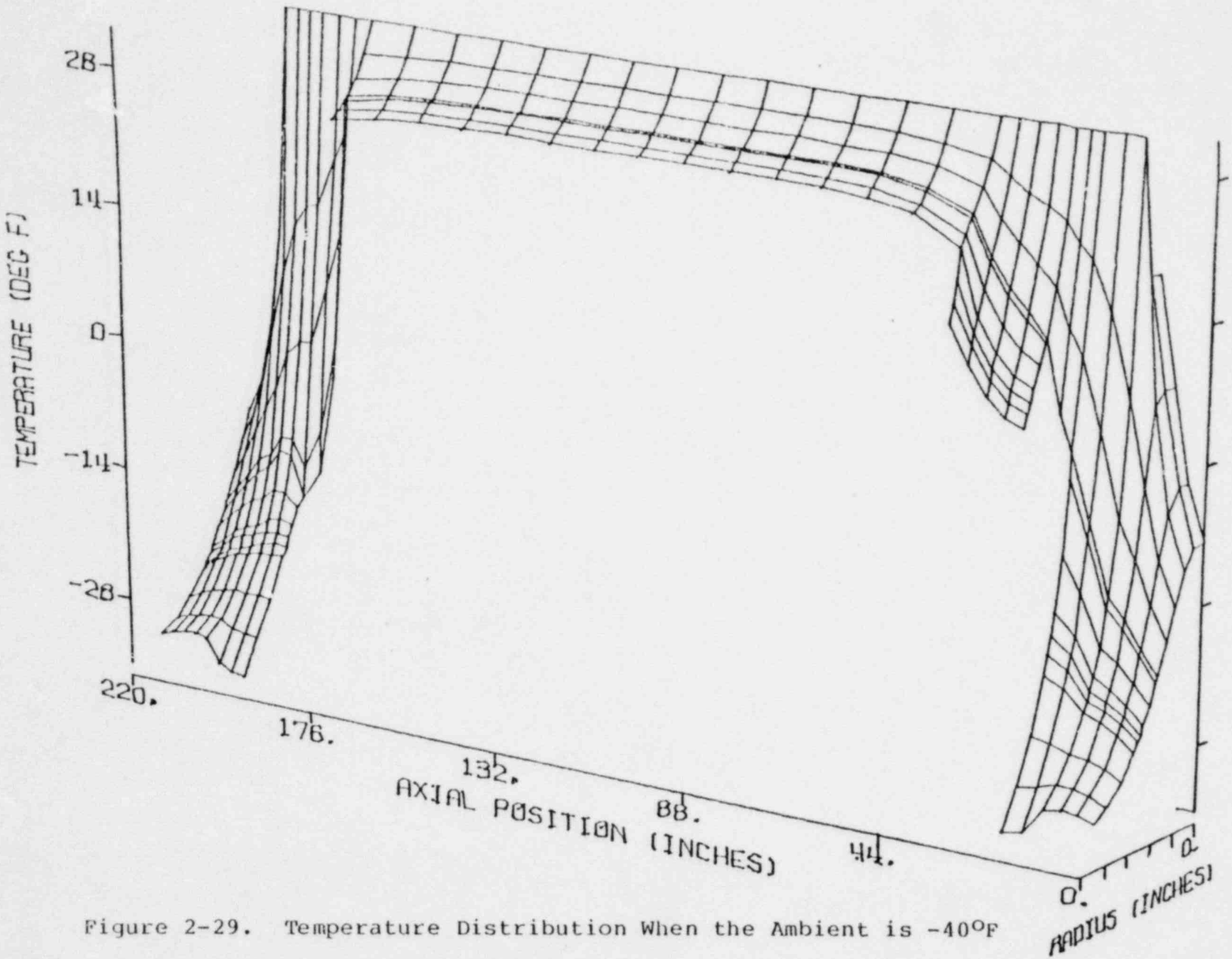

Figure 2-29. Temperature Distribution When the Ambient is -40°F

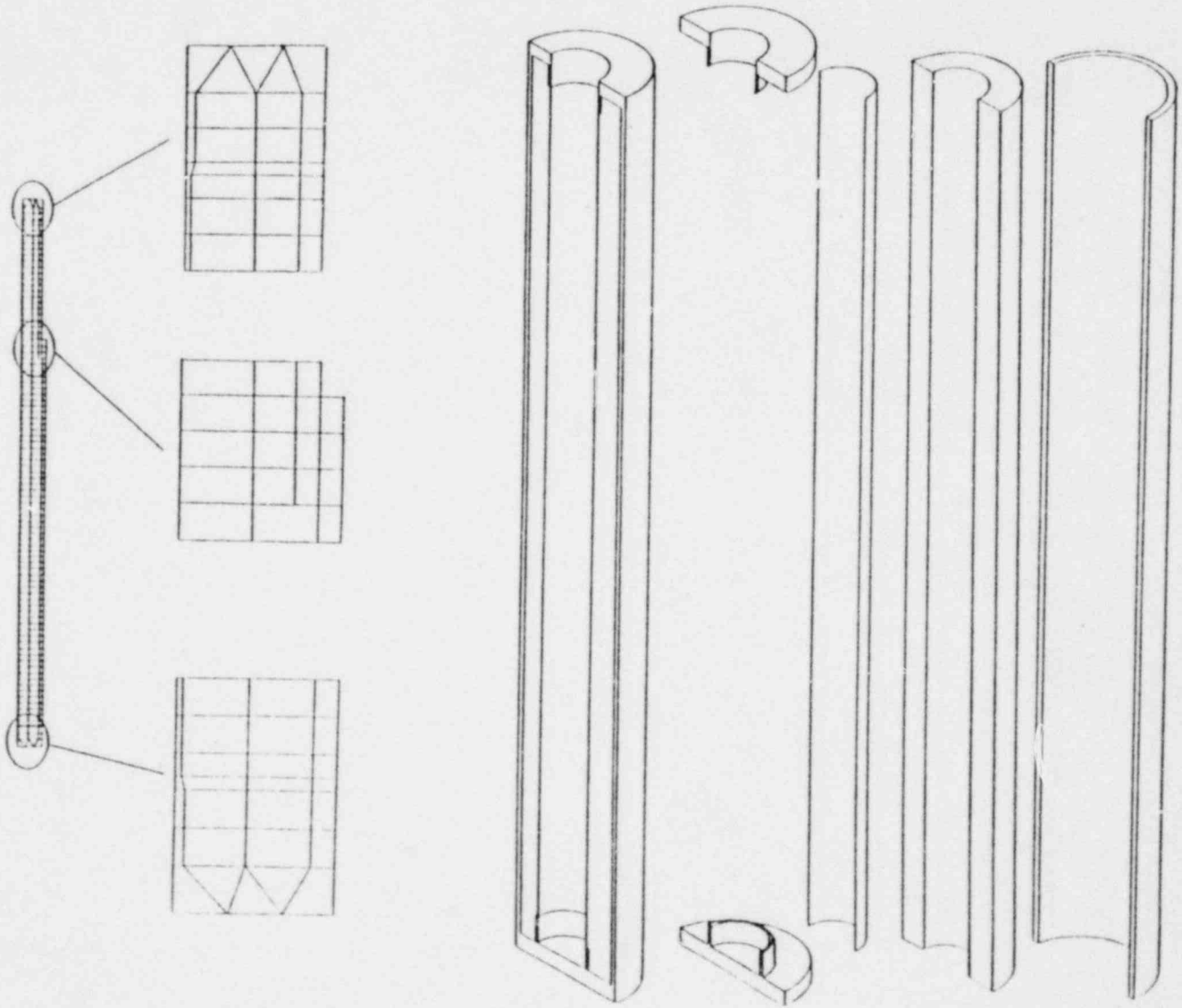

Figure 2-30. Model of Cask for Calculation of Thermal Stresses

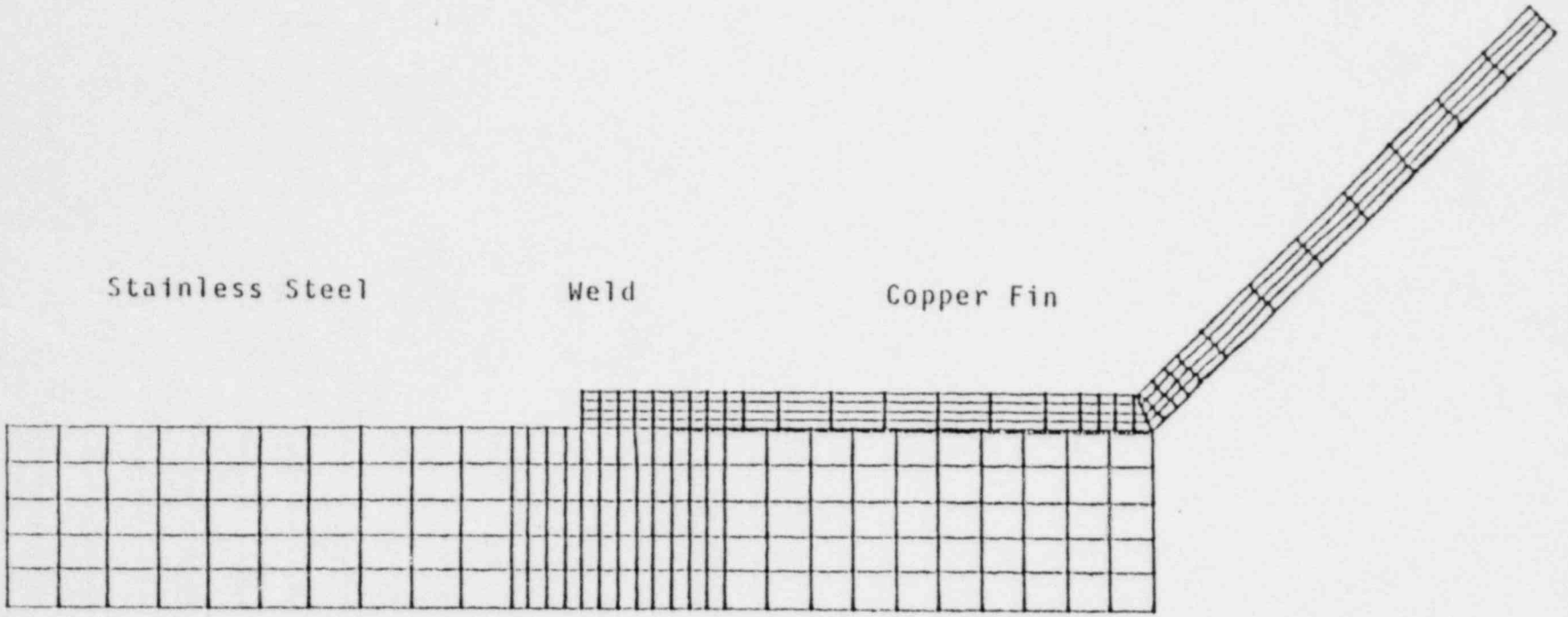

Figure 2-31. ANSYS Model of Copper Fin and Stainless Steel Shell

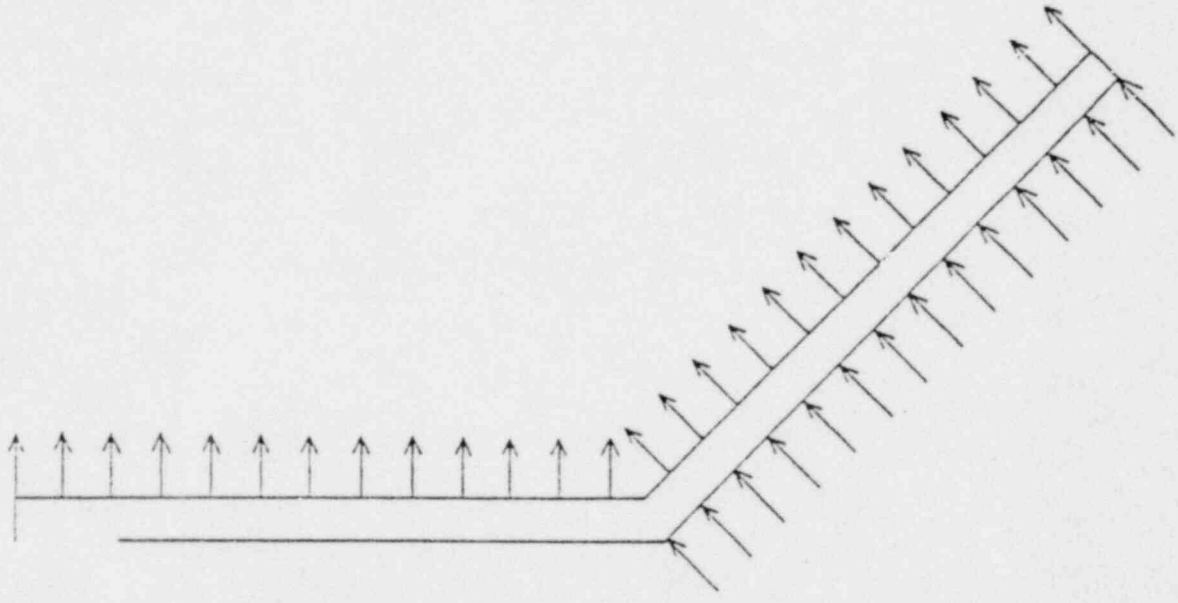

Figure 2-32. Pressure Boundary Conditions on Copper Fin

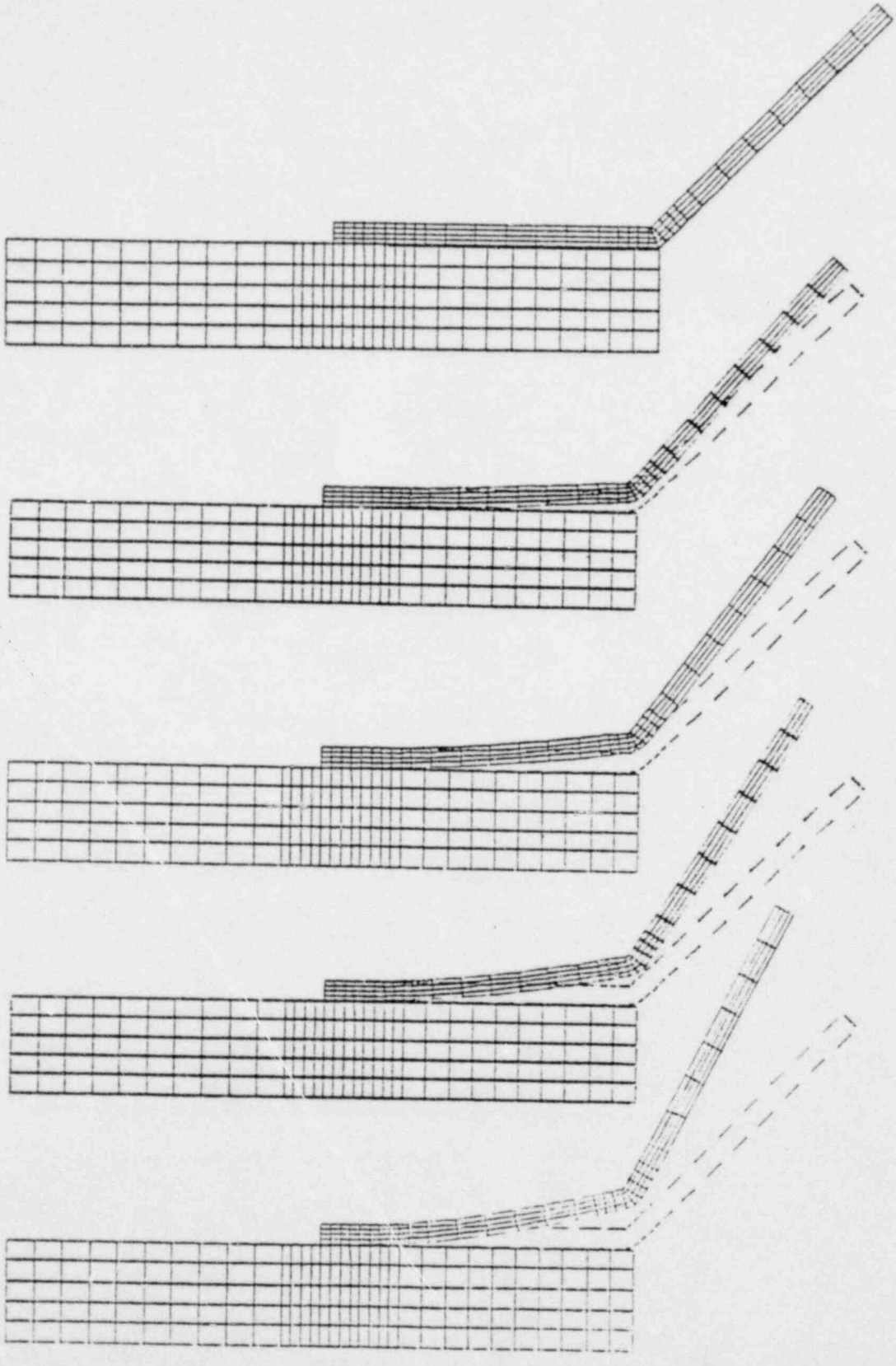

Figure 2-33. Deformed Geometry of A Copper Fin

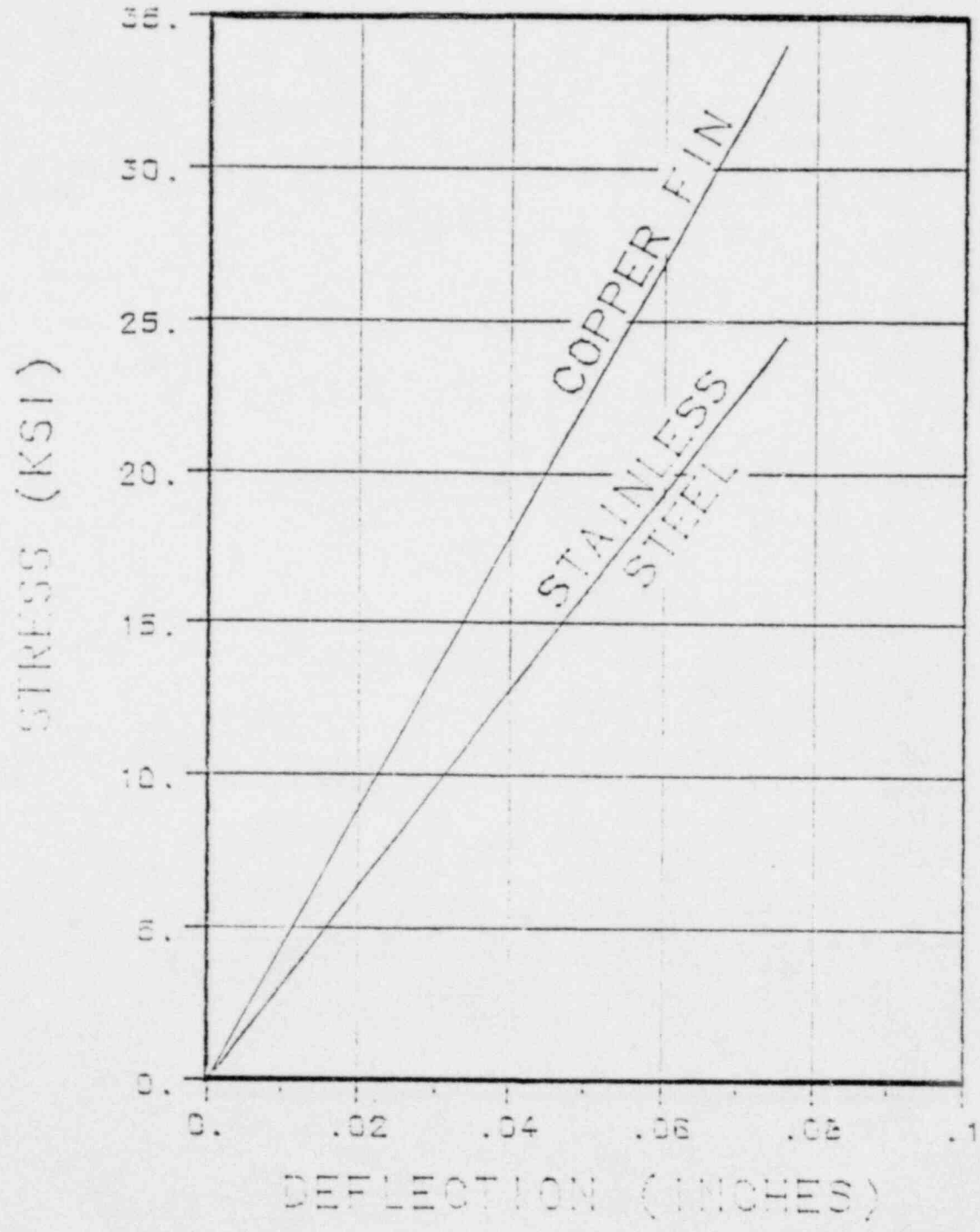

Figure 2-34. Maximum Stress as a Function of Fin Displacement

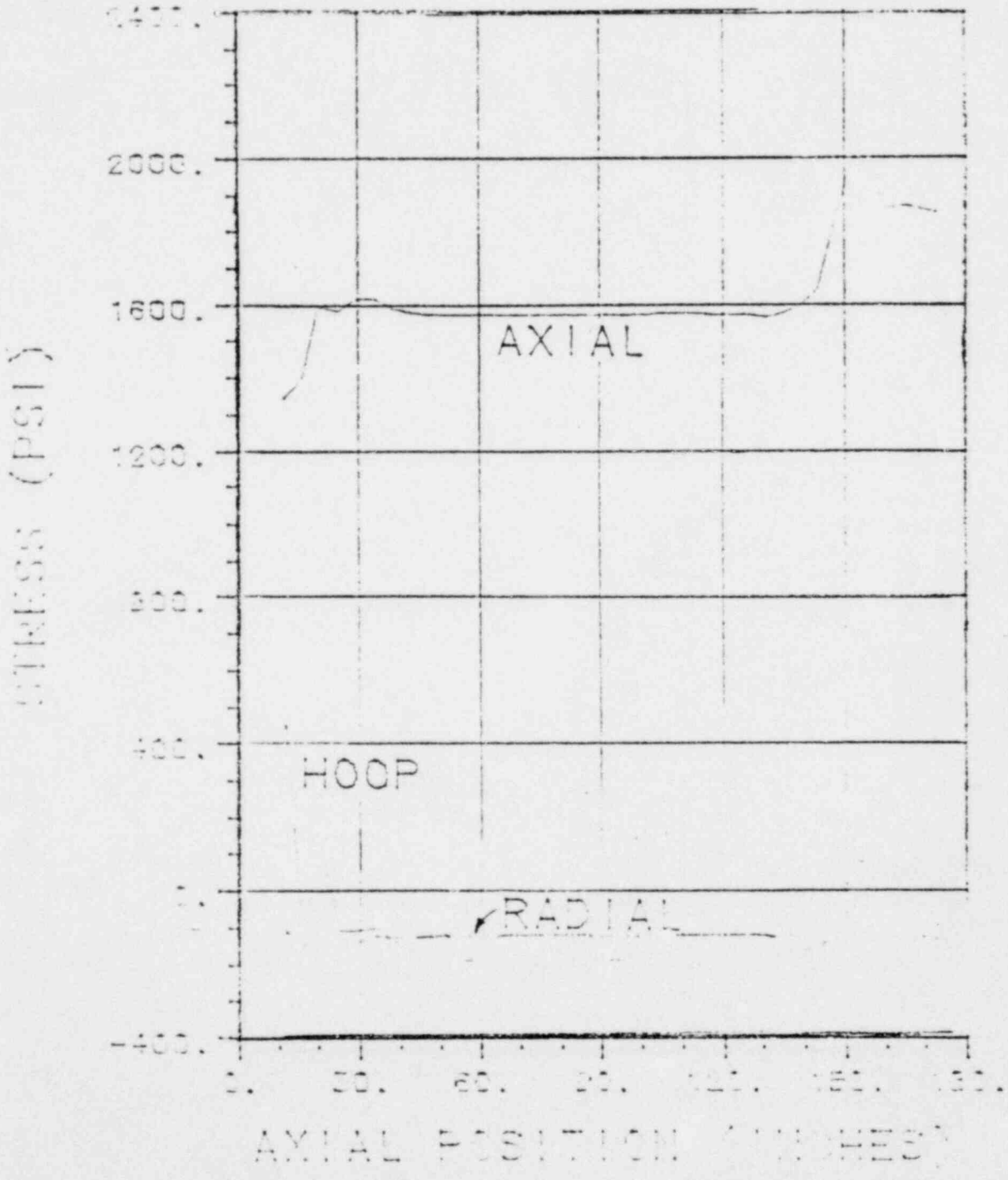

Figure 2-35. Thermal Stress Distribution when Ambient is 130°F

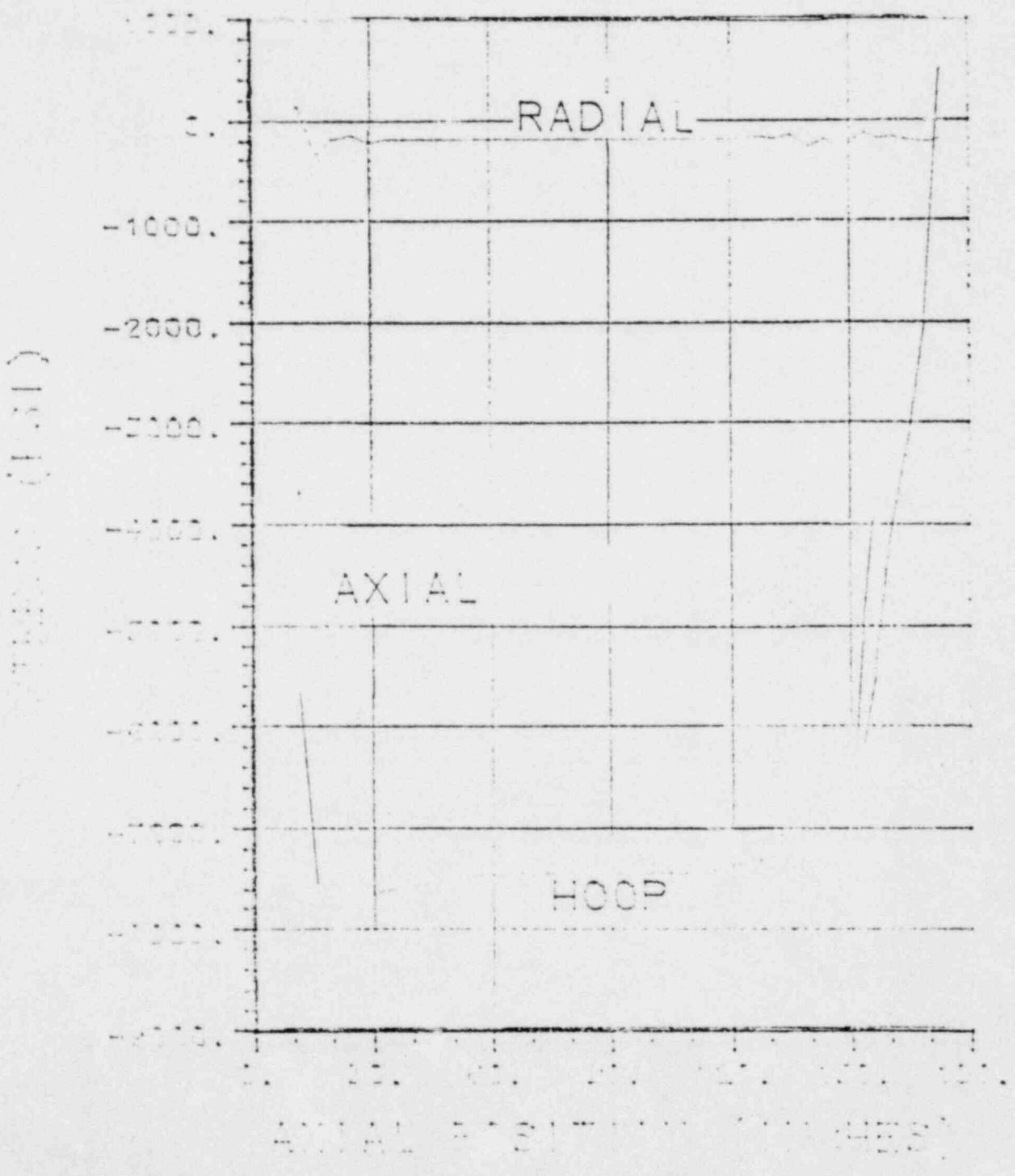

Figure 2-36. Thermal Stress Distribution when Ambient is -40°F

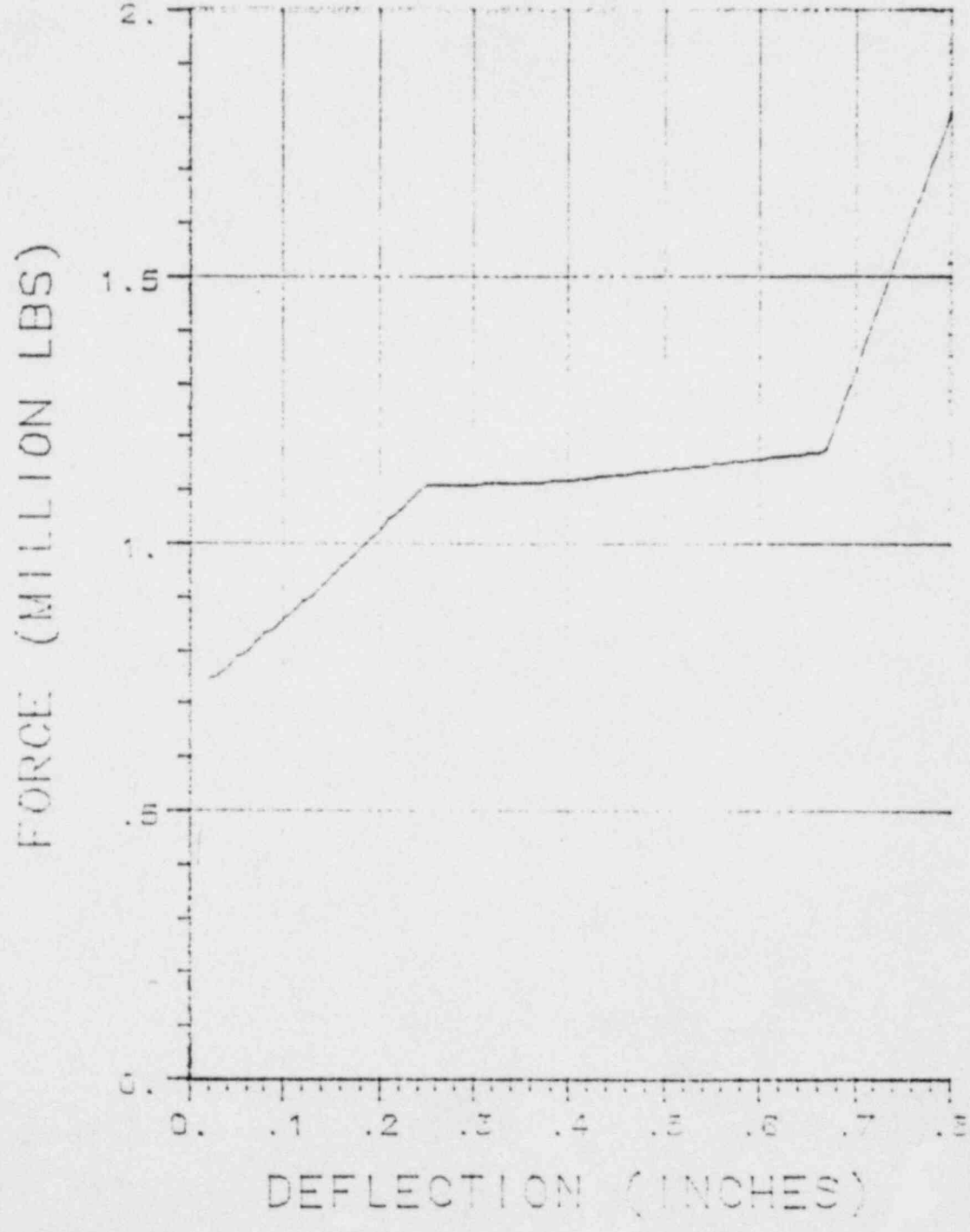

Figure 2-37. Force-Deflection Curve of End Impact Limiter

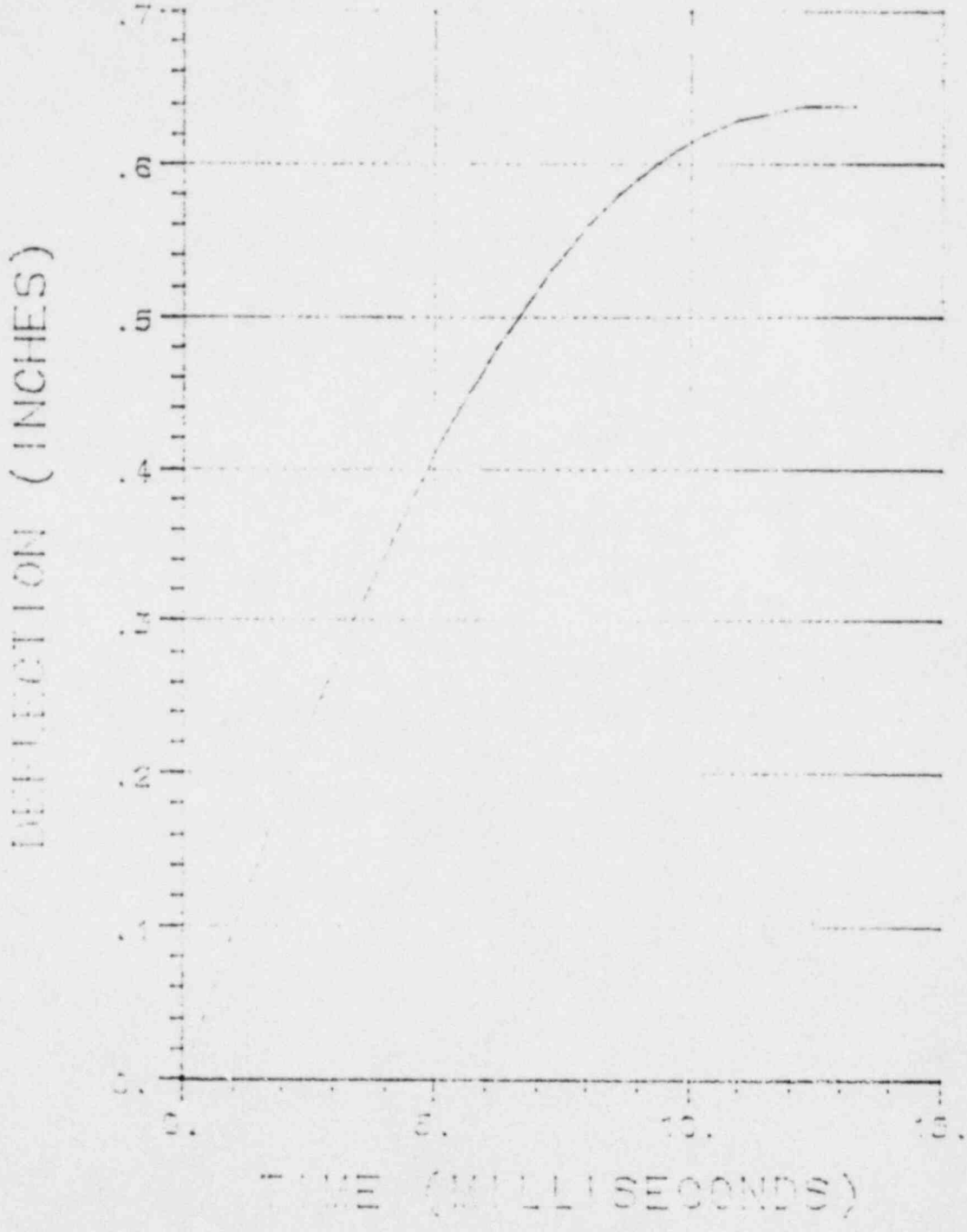

Figure 2-38. Deflection of Lower End of Cask

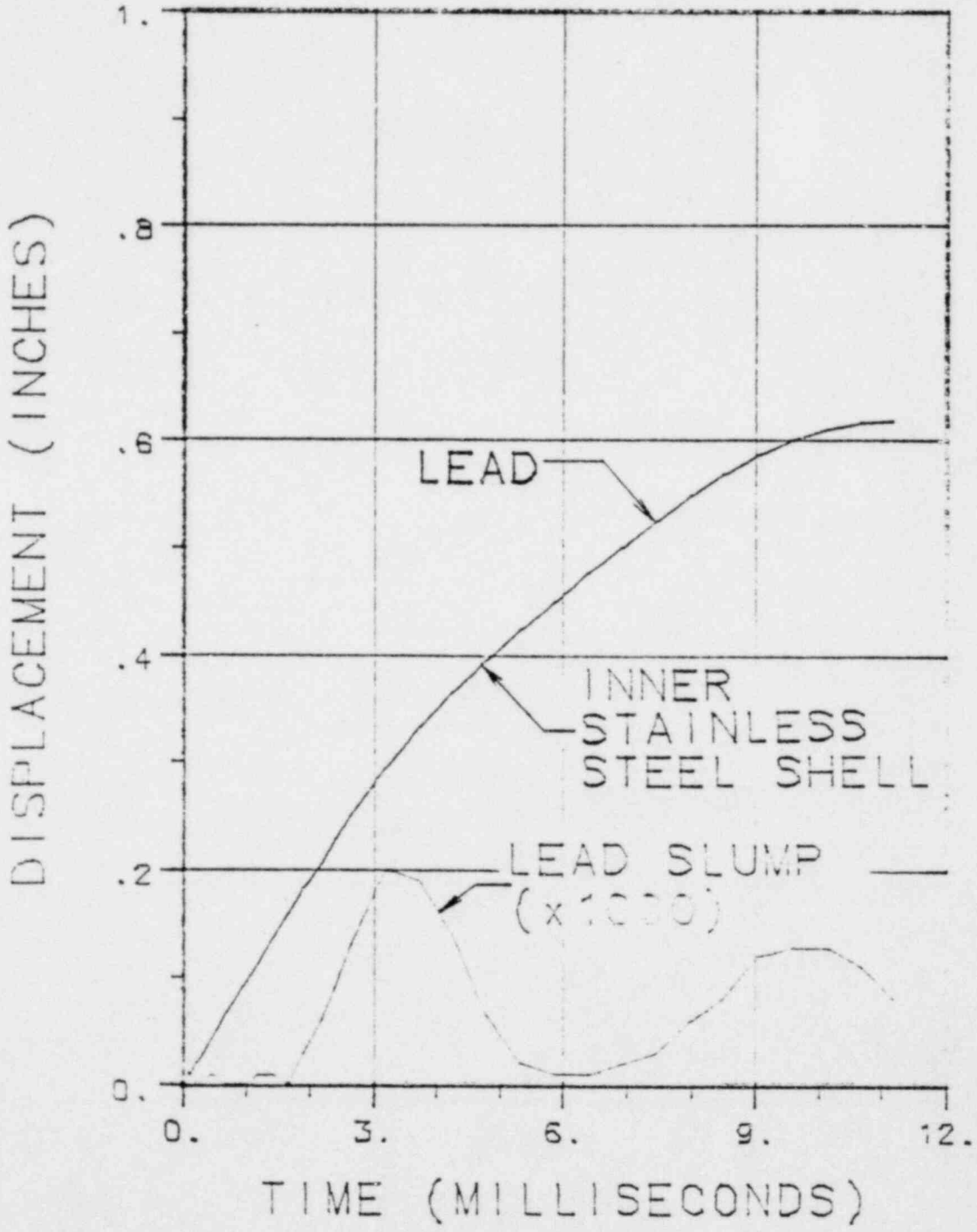

Figure 2-39. Deflection of Lead

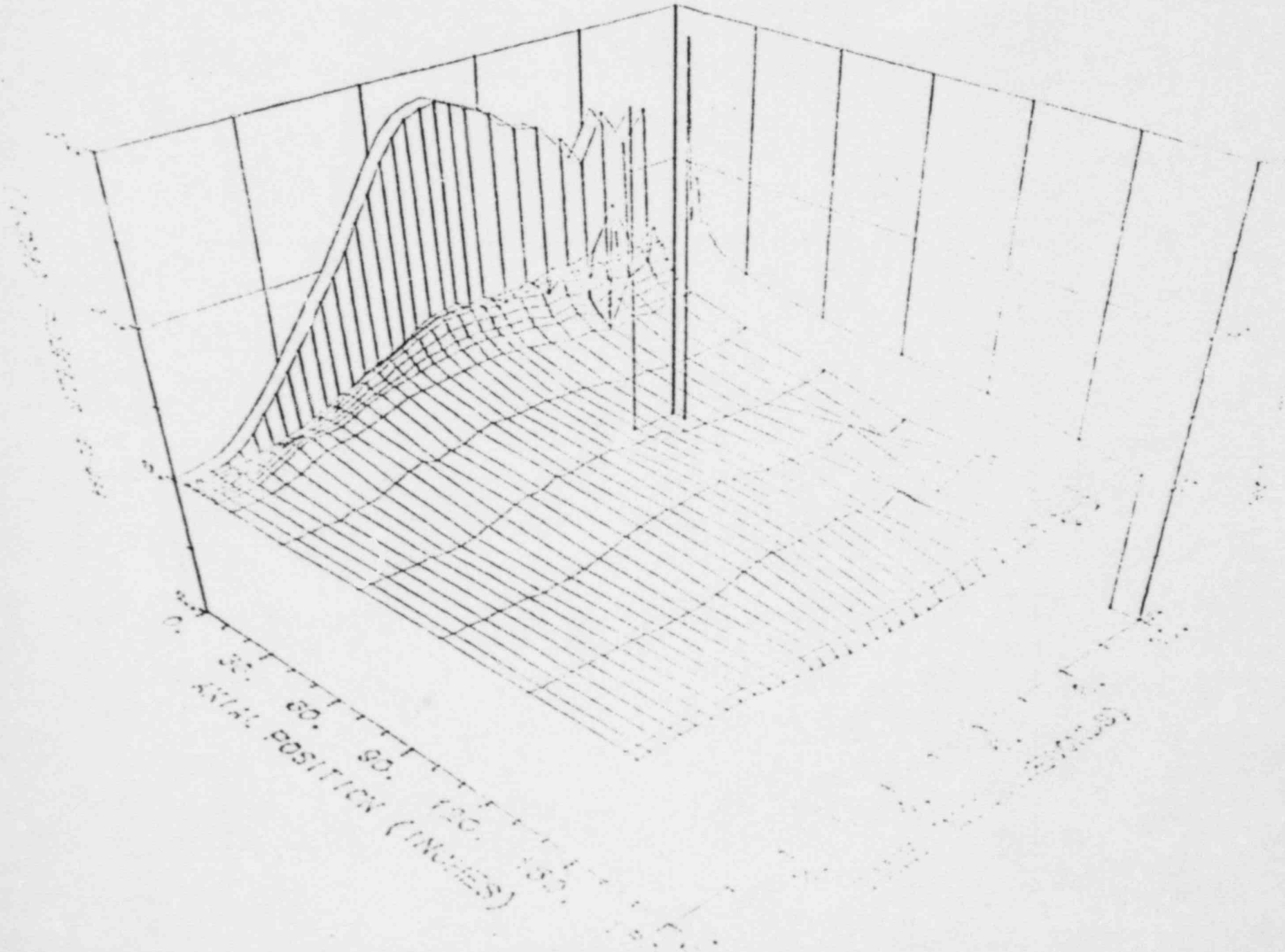

Figure 2-40. Hoop Stress in Inner Shell

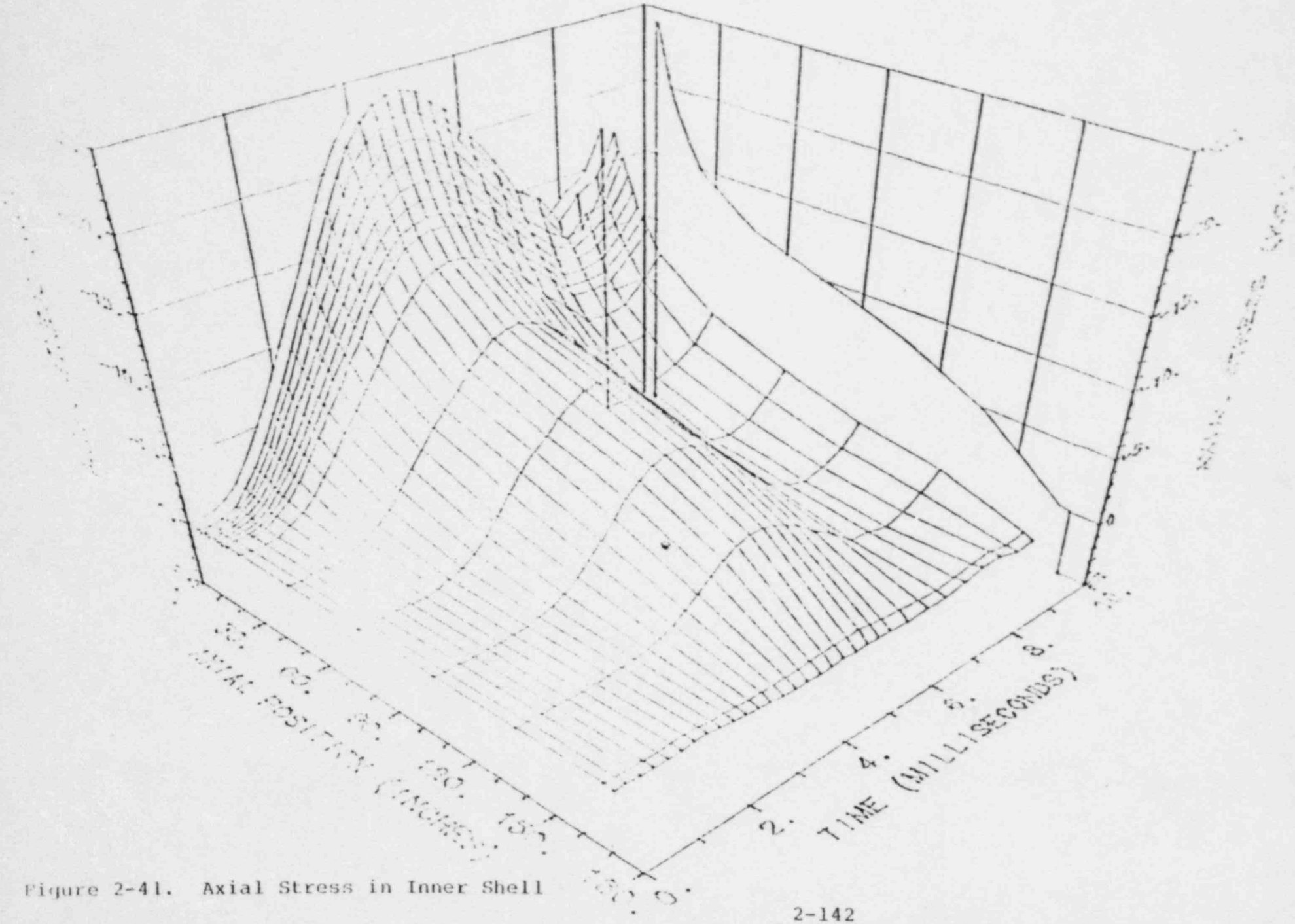

Figure 2-41. Axial Stress in Inner Shell

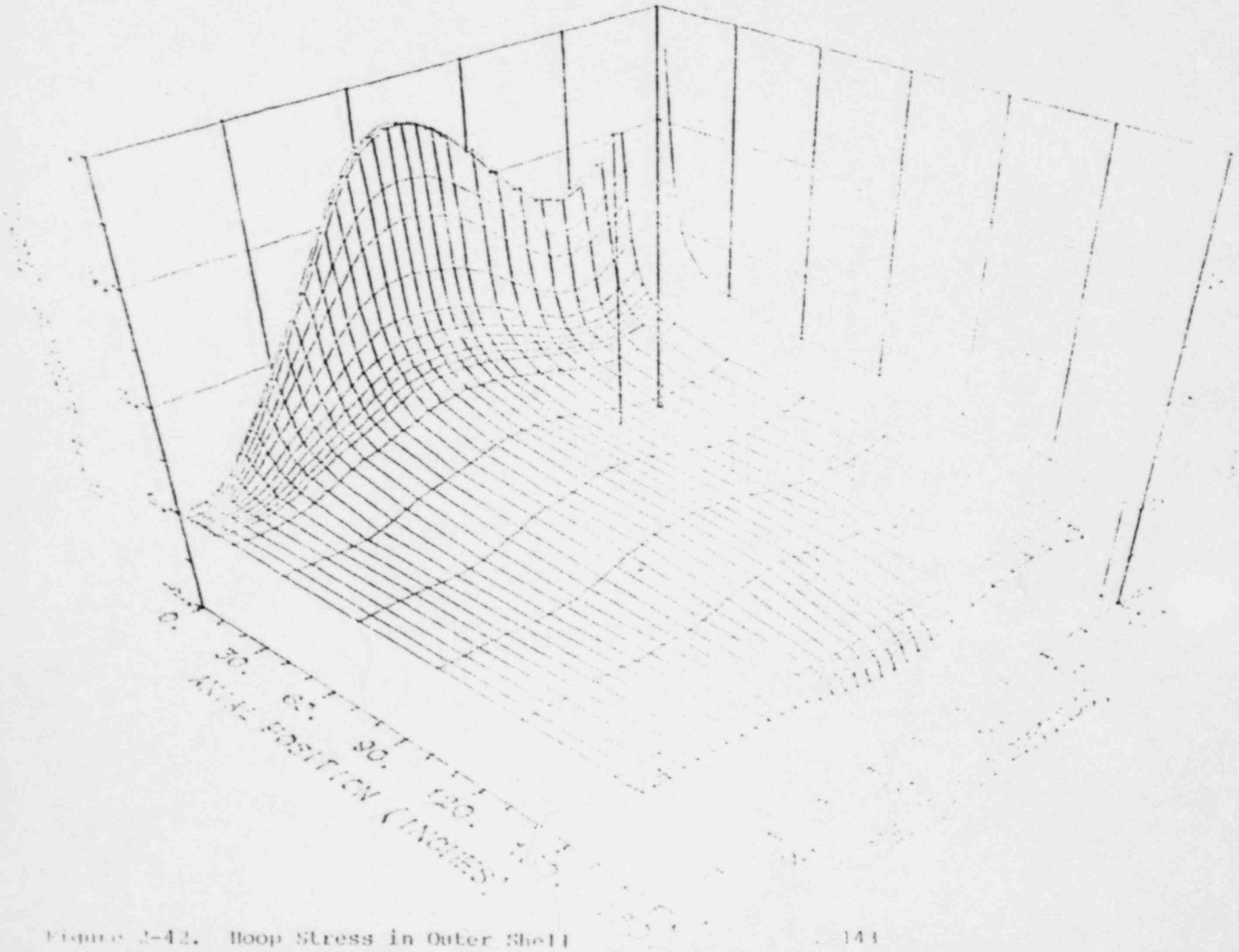

Figure 2-42. Hoop Stress in Outer Shell

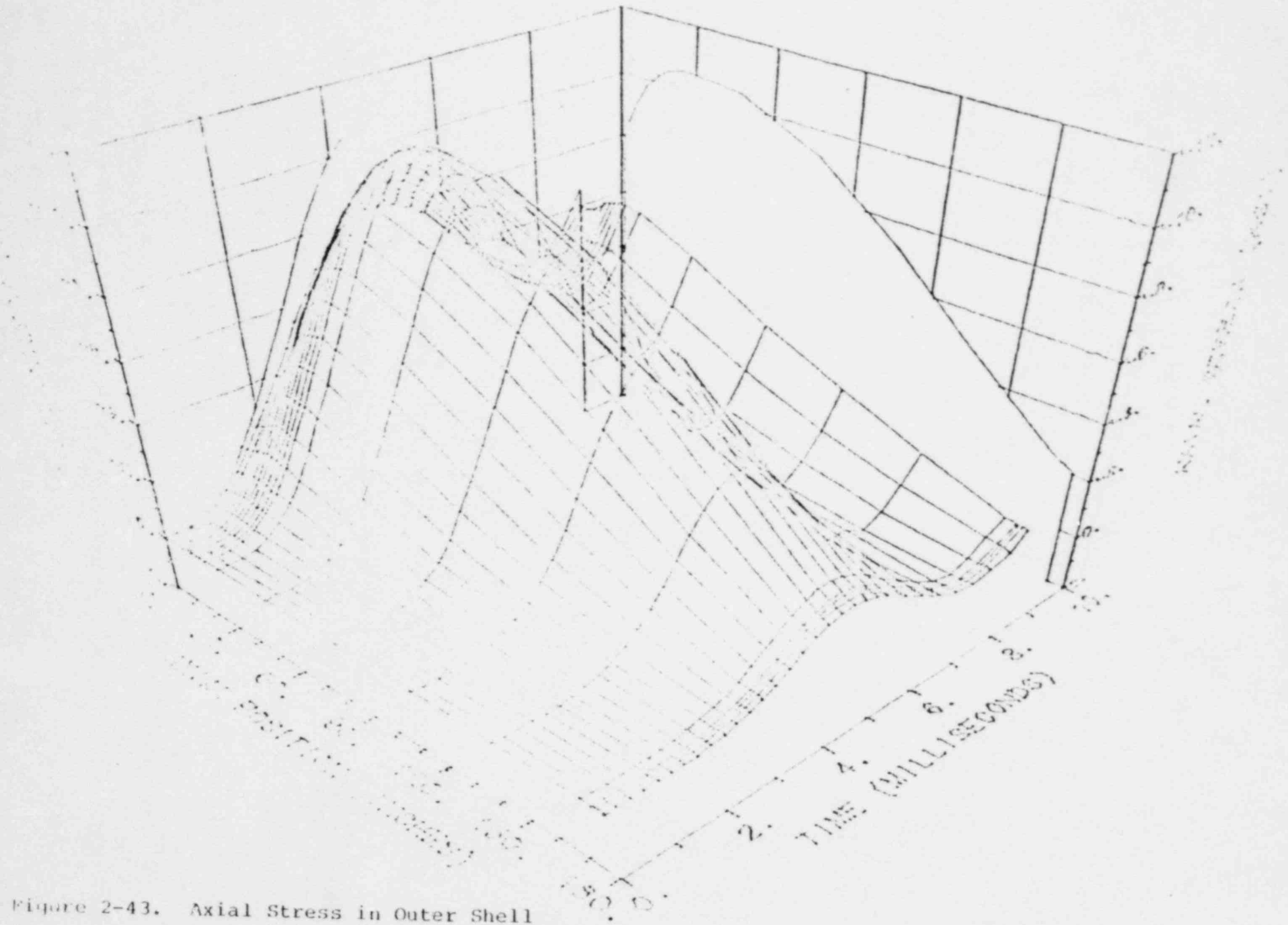

Figure 2-43. Axial Stress in Outer Shell

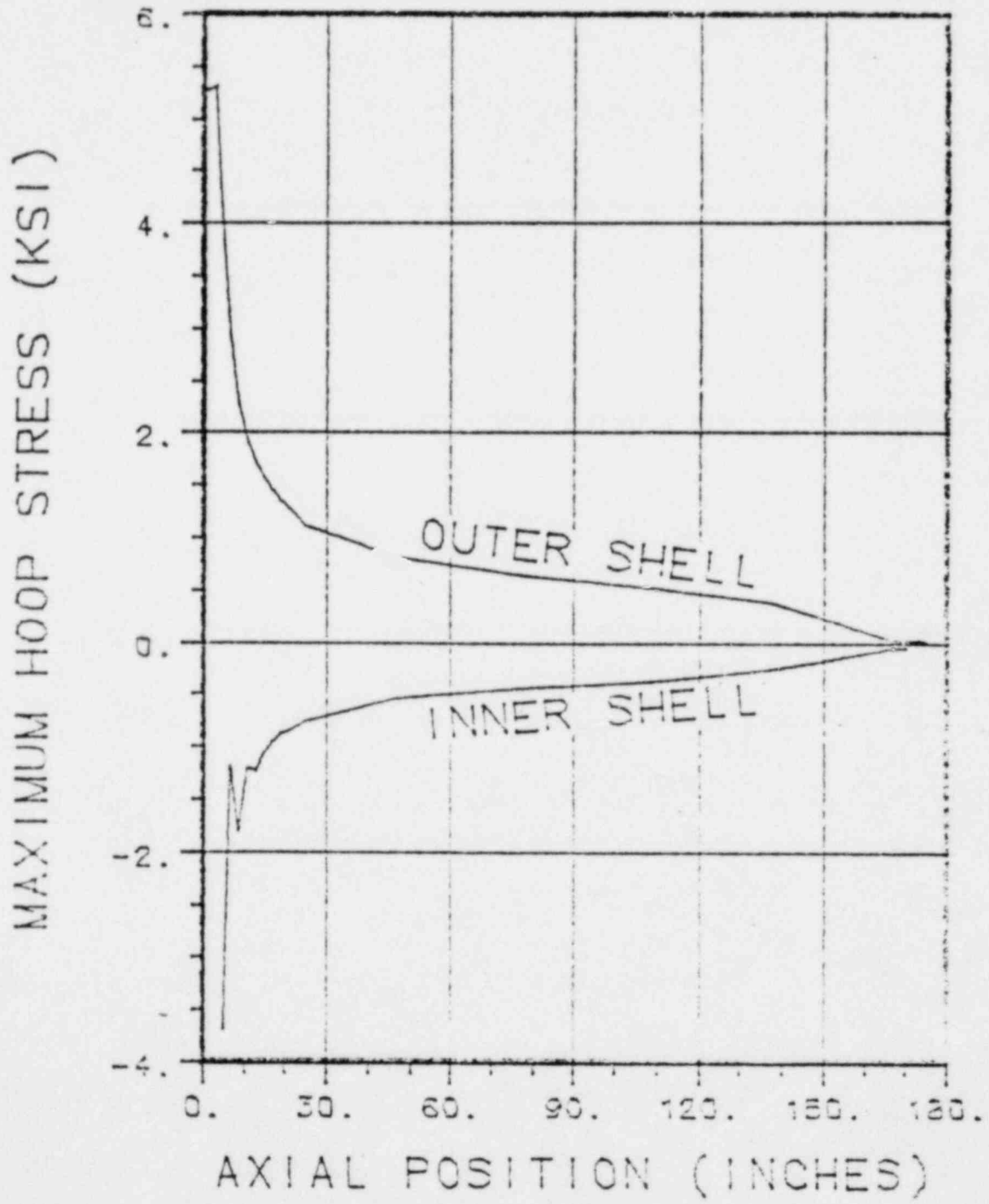

Figure 2-44. Maximum Hoop Stress in One Foot Fall on End

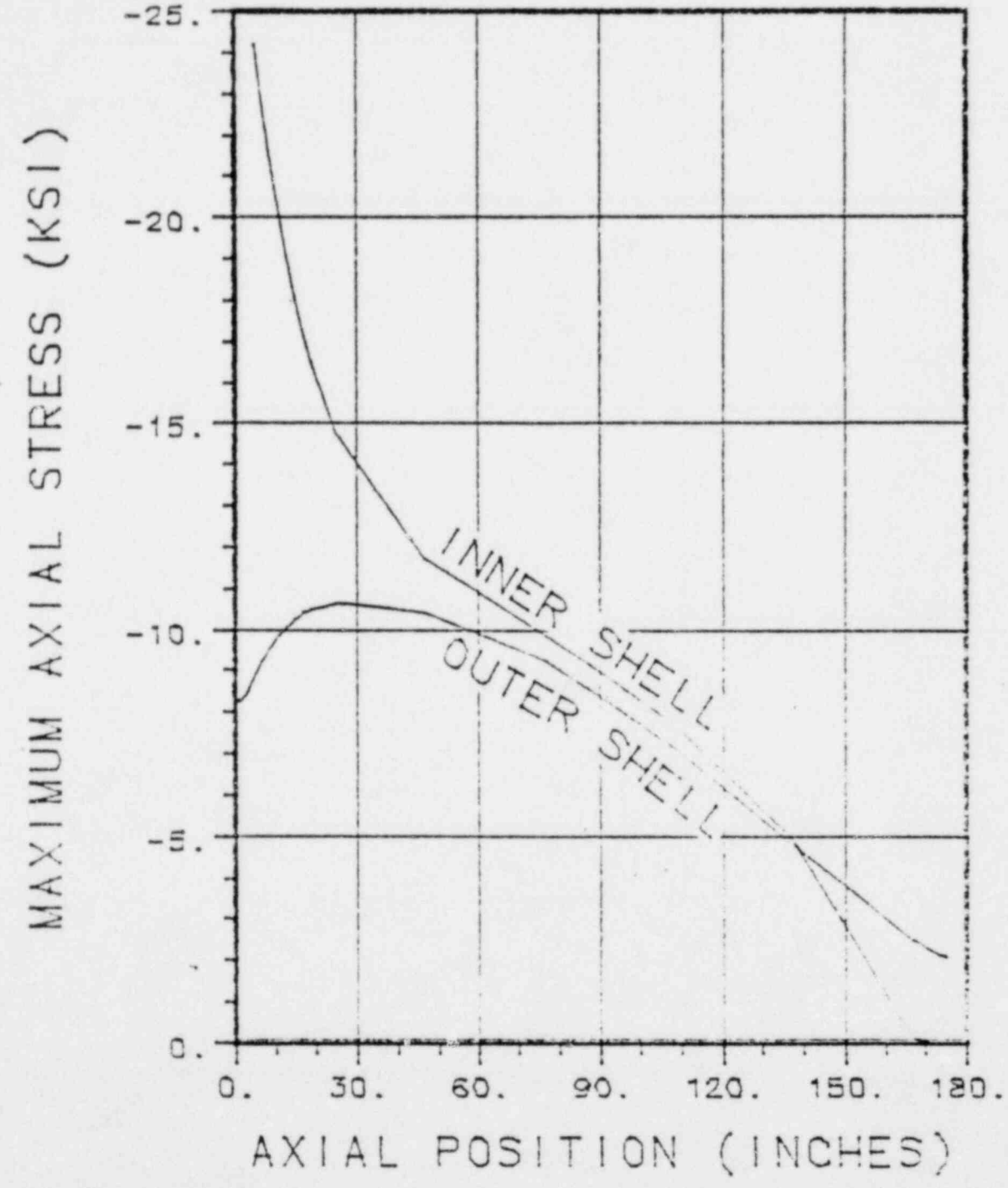

Figure 2-45. Maximum Axial Stress in One Foot Fall on End

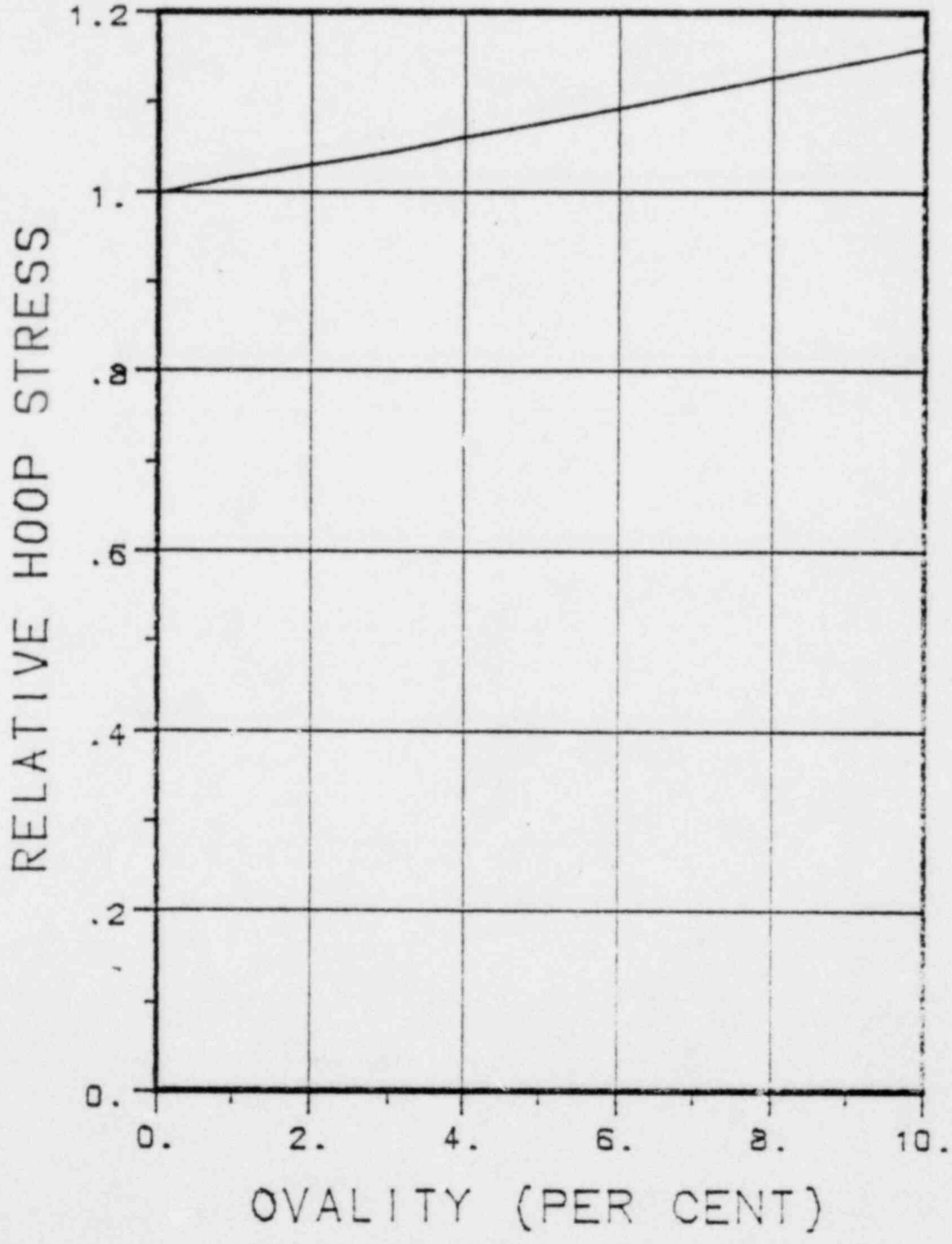

Figure 2-46. Effect of Ovality on Hoop Stress

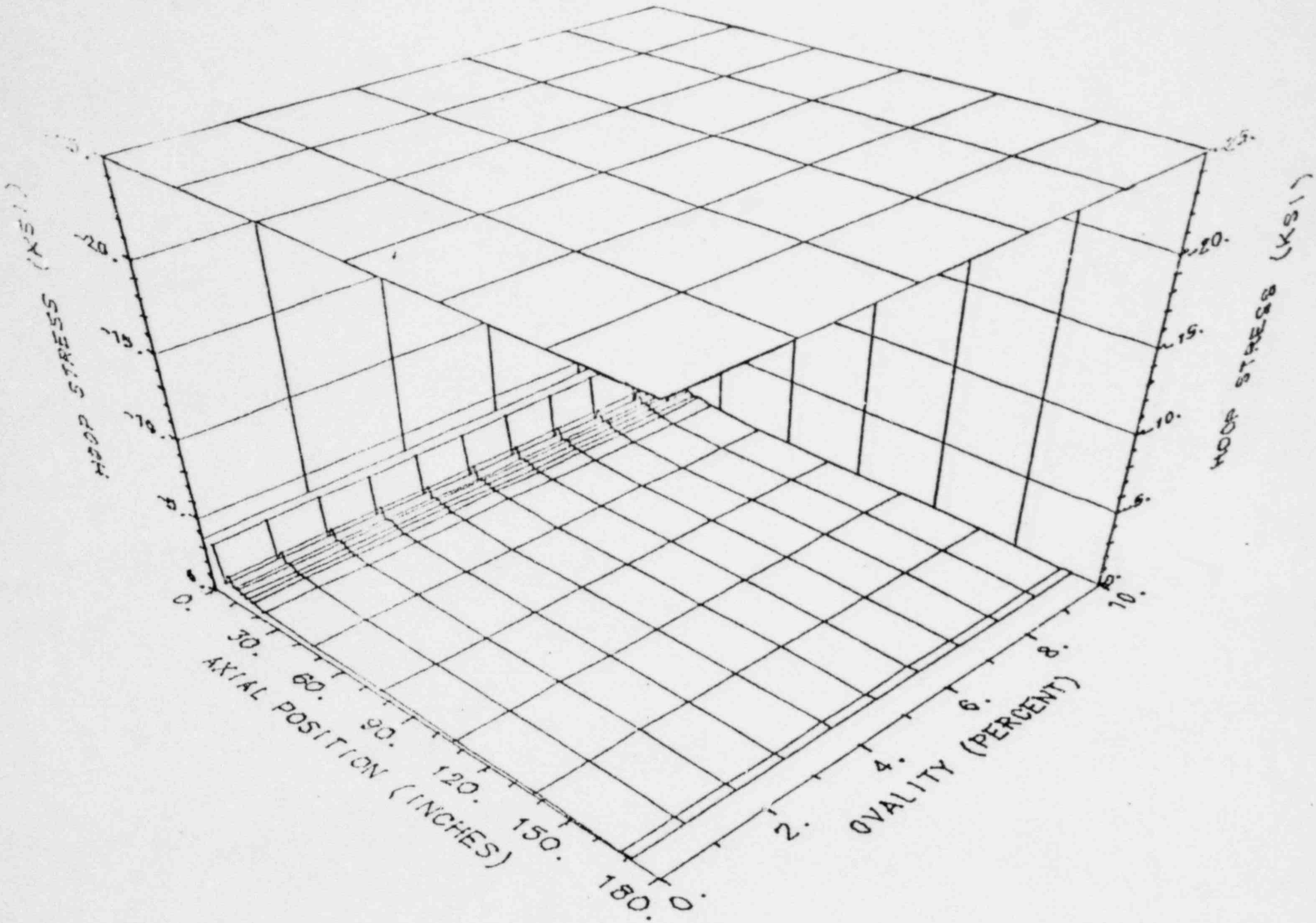

Figure 2-47. Comparison of Hoop Stress to Stress Limit

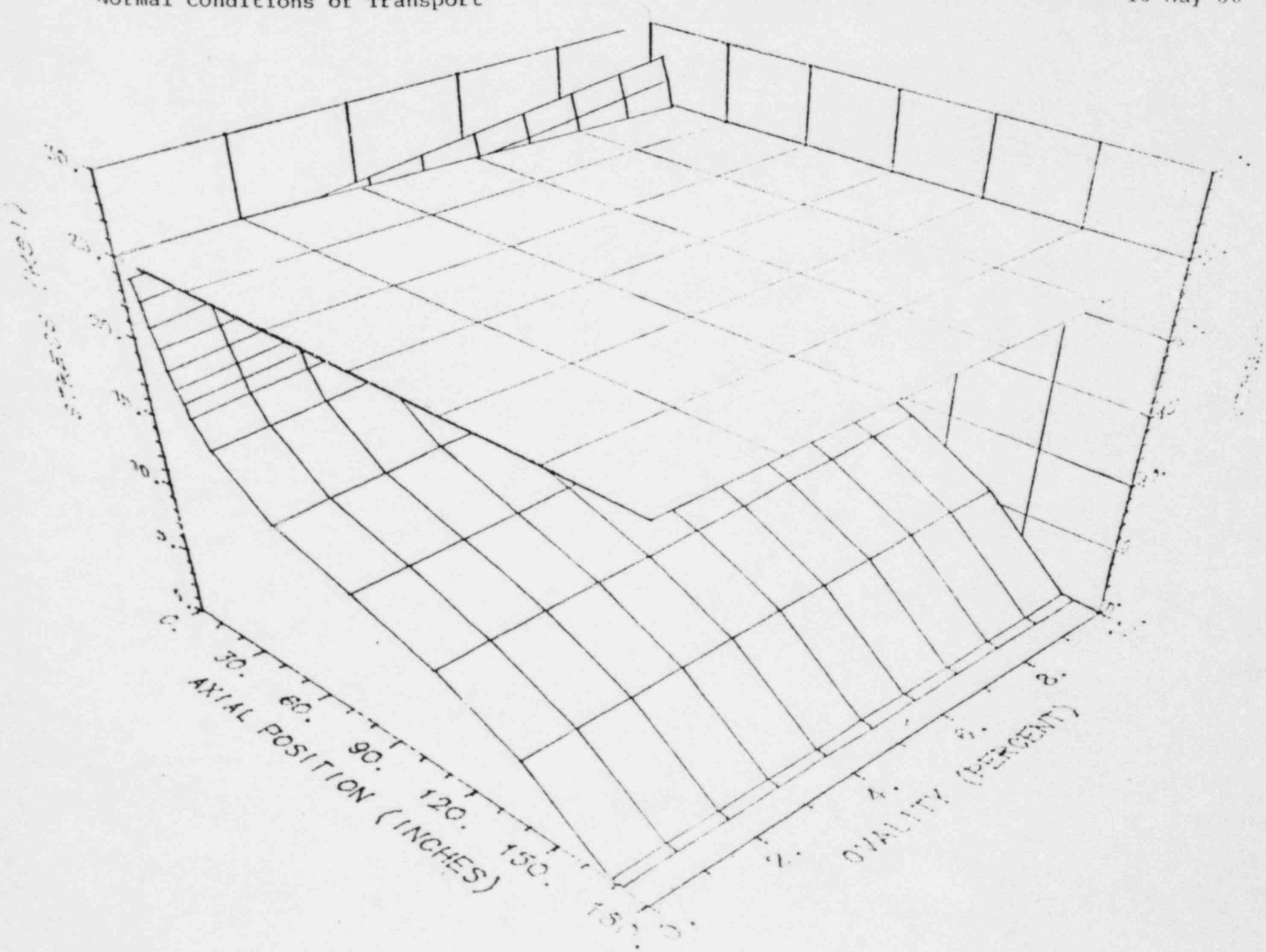

Figure 2-48. Comparison of Axial Stress to Stress Limit

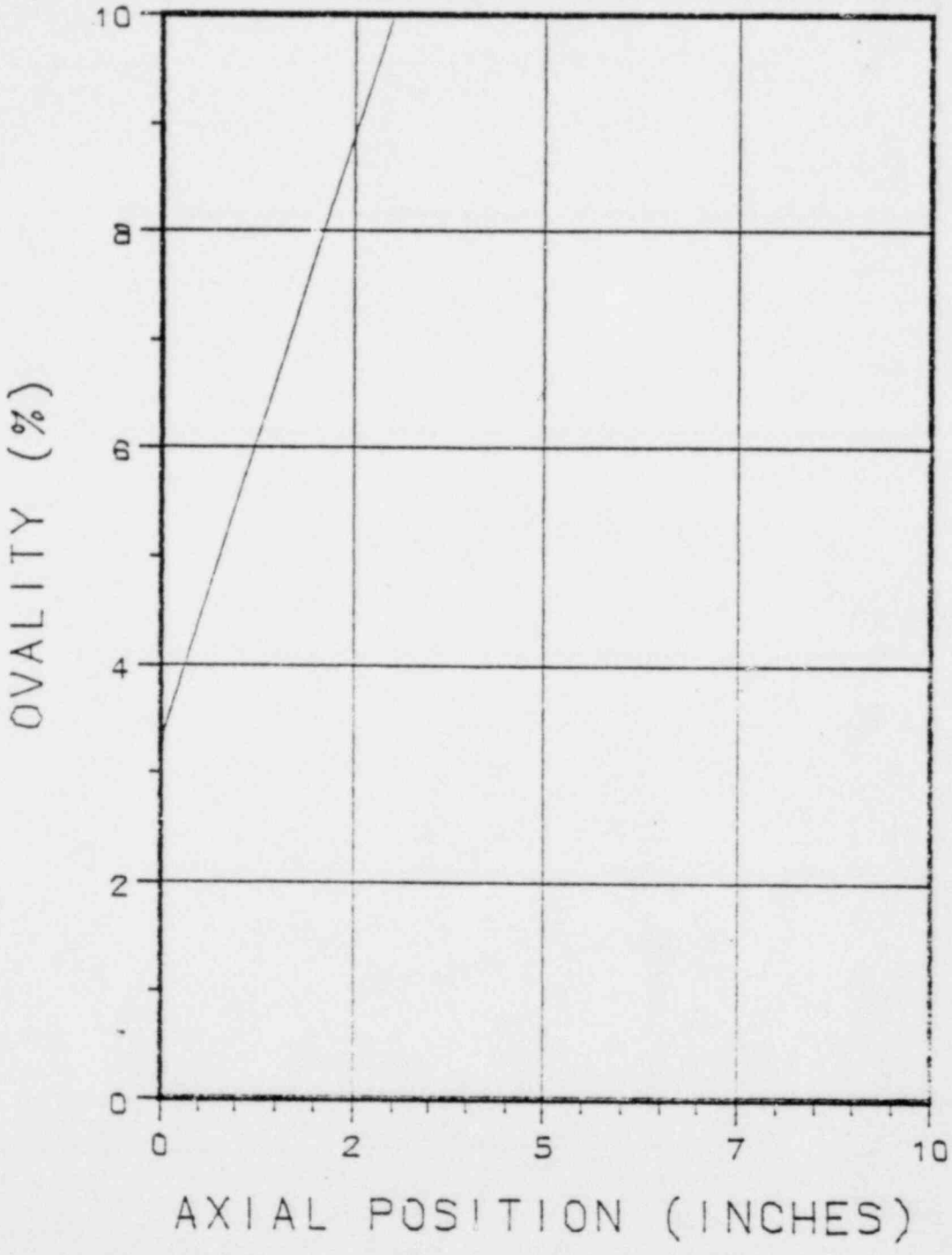

Figure 2-49. Maximum Allowable Ovality

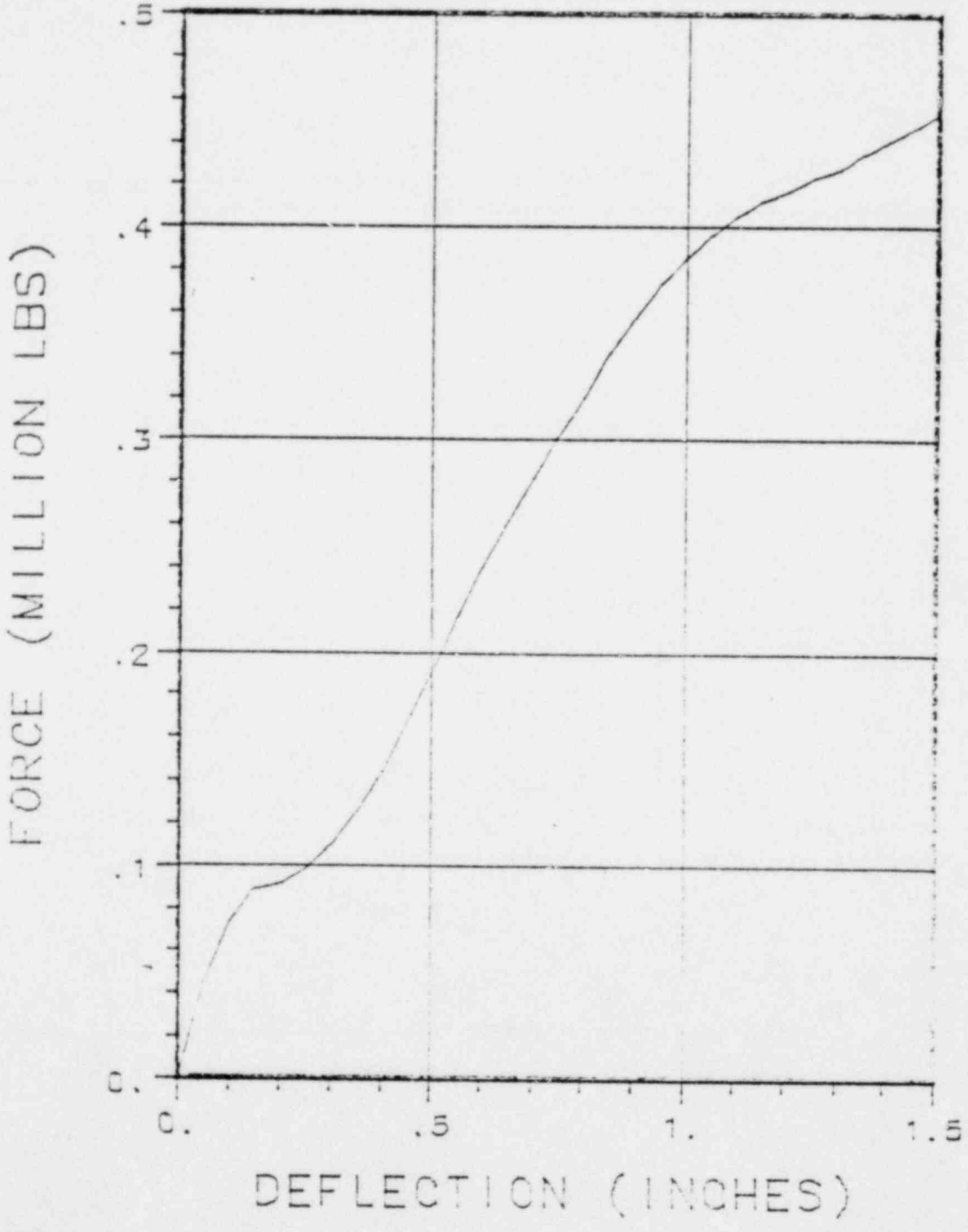

Figure 2-50. Force-Deflection Curve for Side Impact

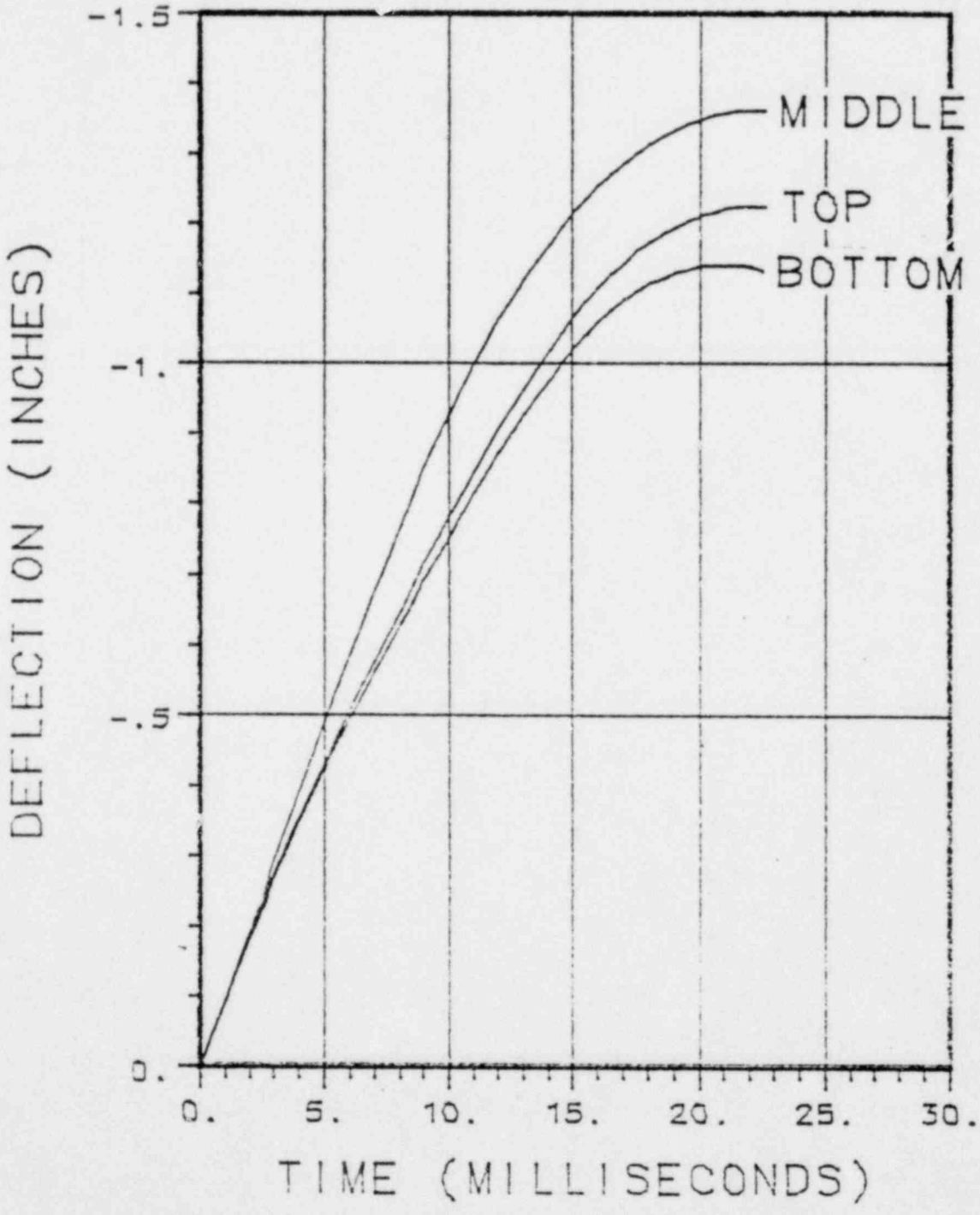

Figure 2-51. Deflection of Cask Extremities

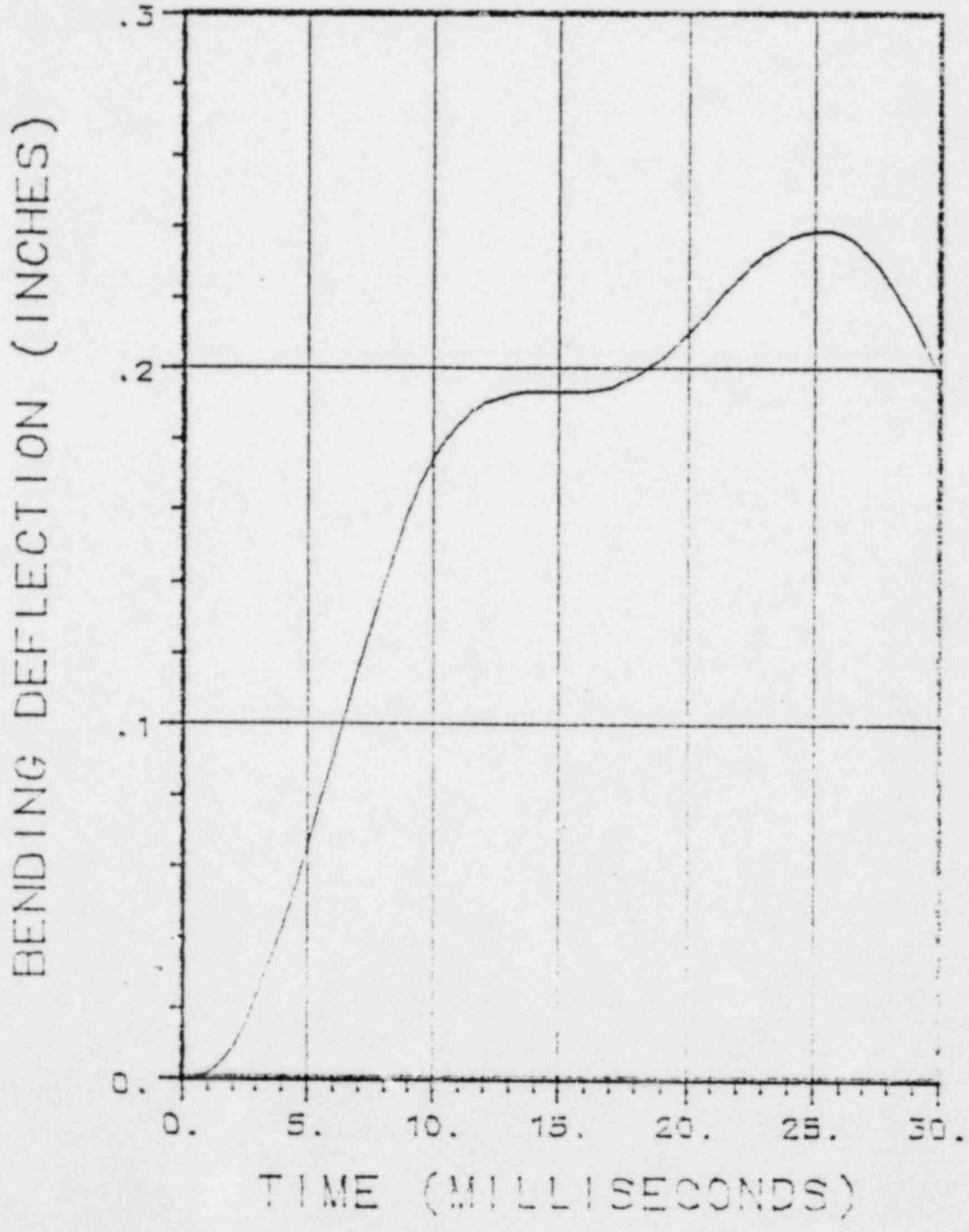

Figure 2-52. Deflection of Center of Cask

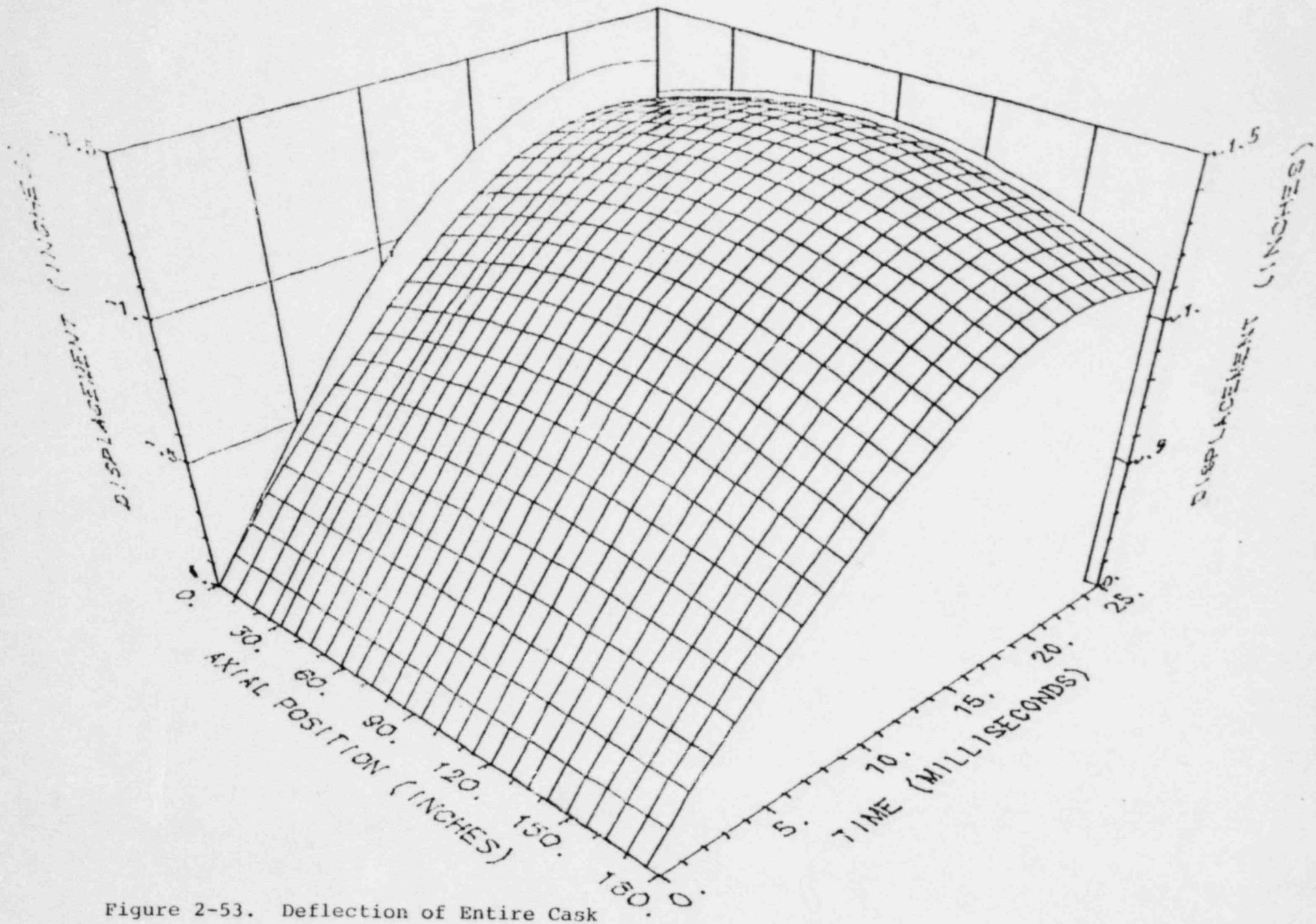

Figure 2-53. Deflection of Entire Cask

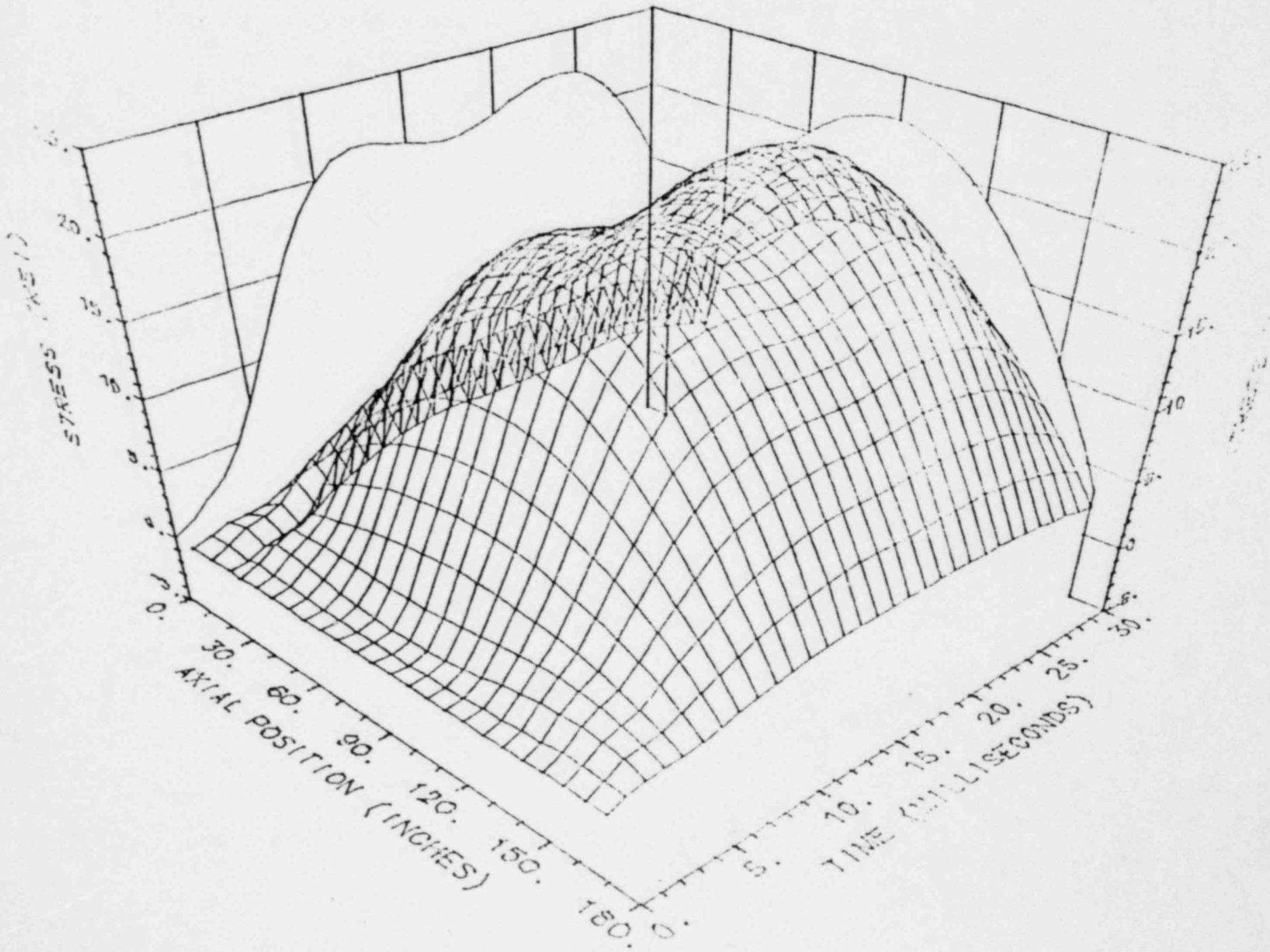

Figure 2-54. Bending Stress Distribution in Entire Cask

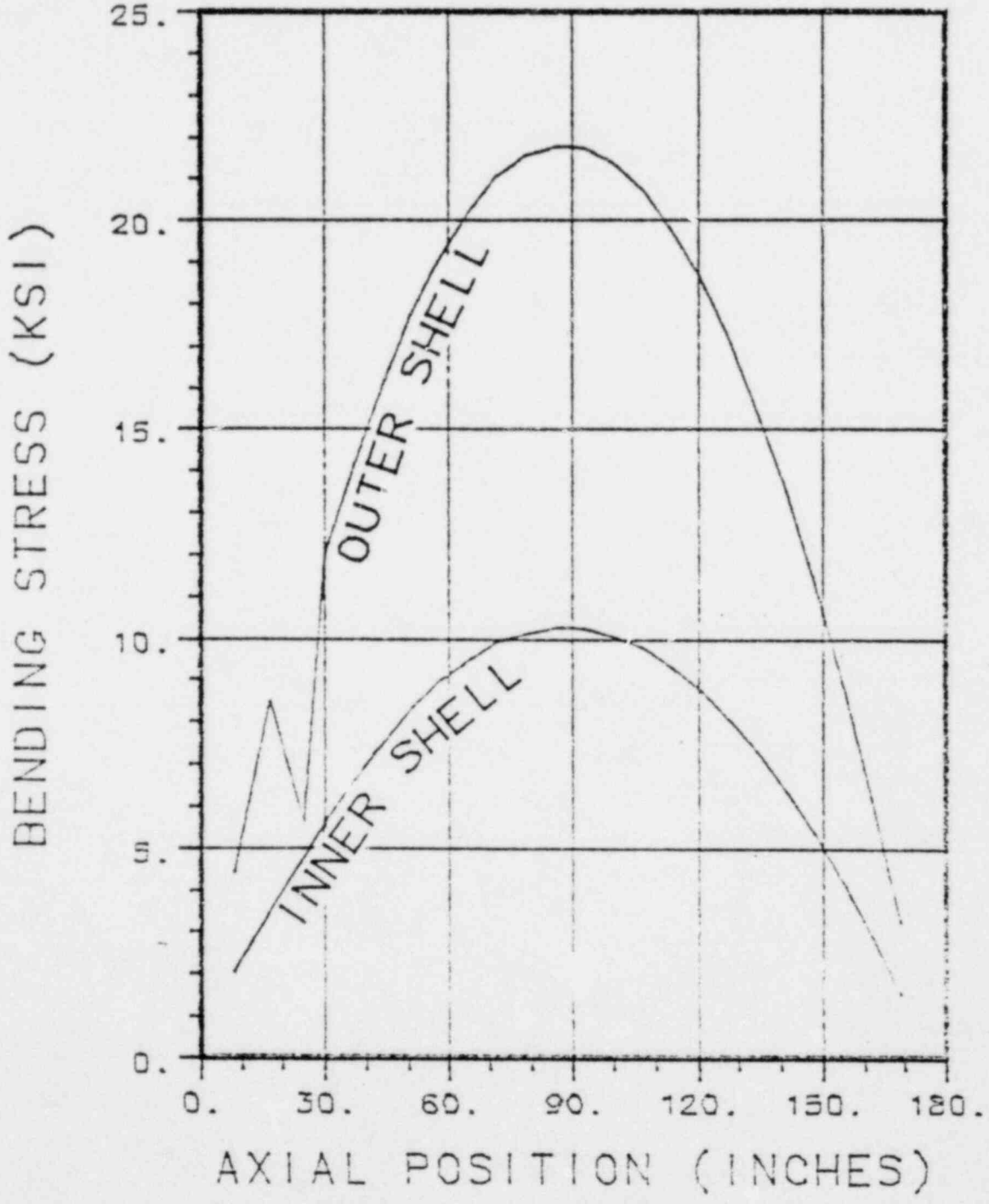

Figure 2-55. Maximum Bending Stress in Both Shells

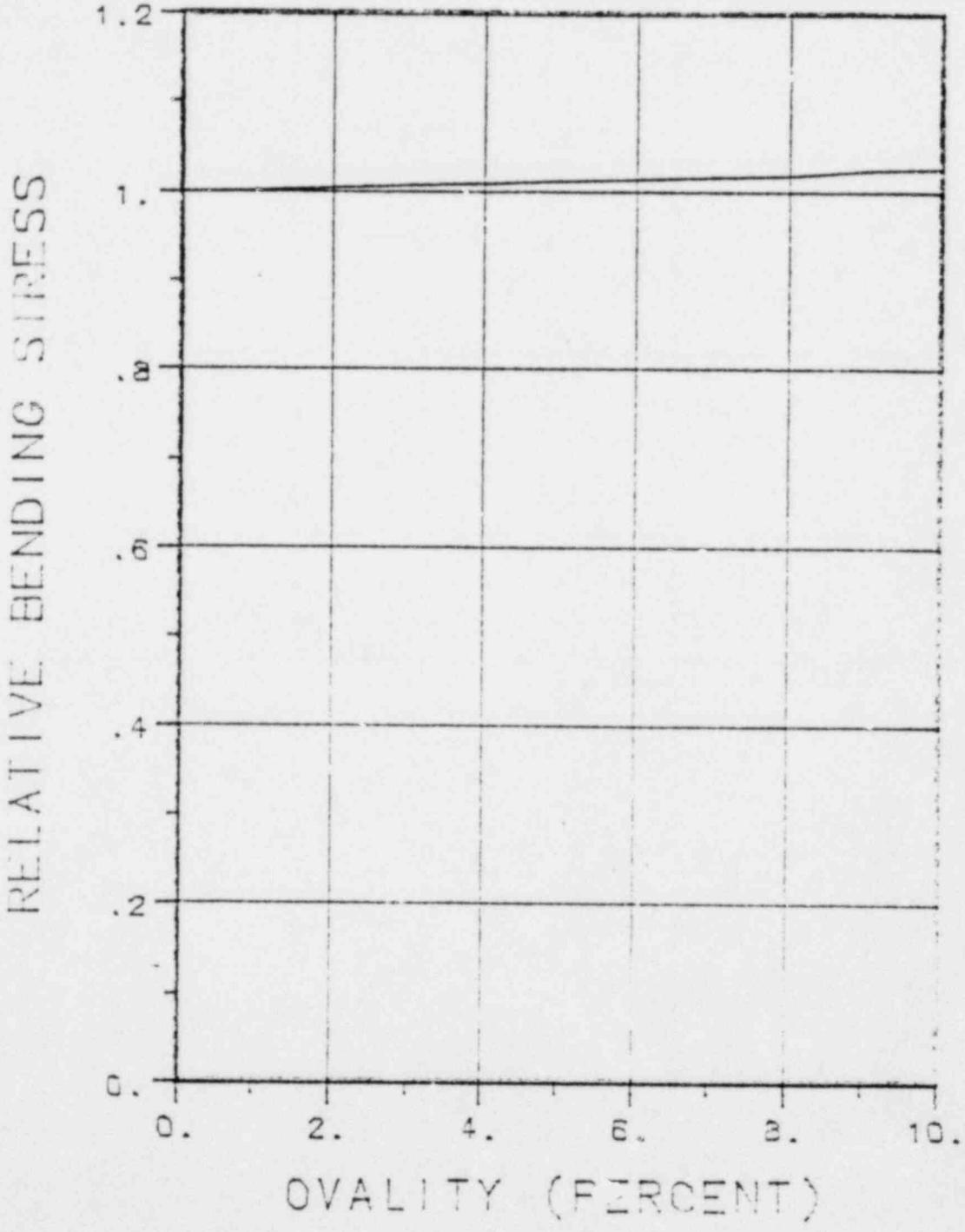

Figure 2-56. Effect of Ovality on Bending Stress

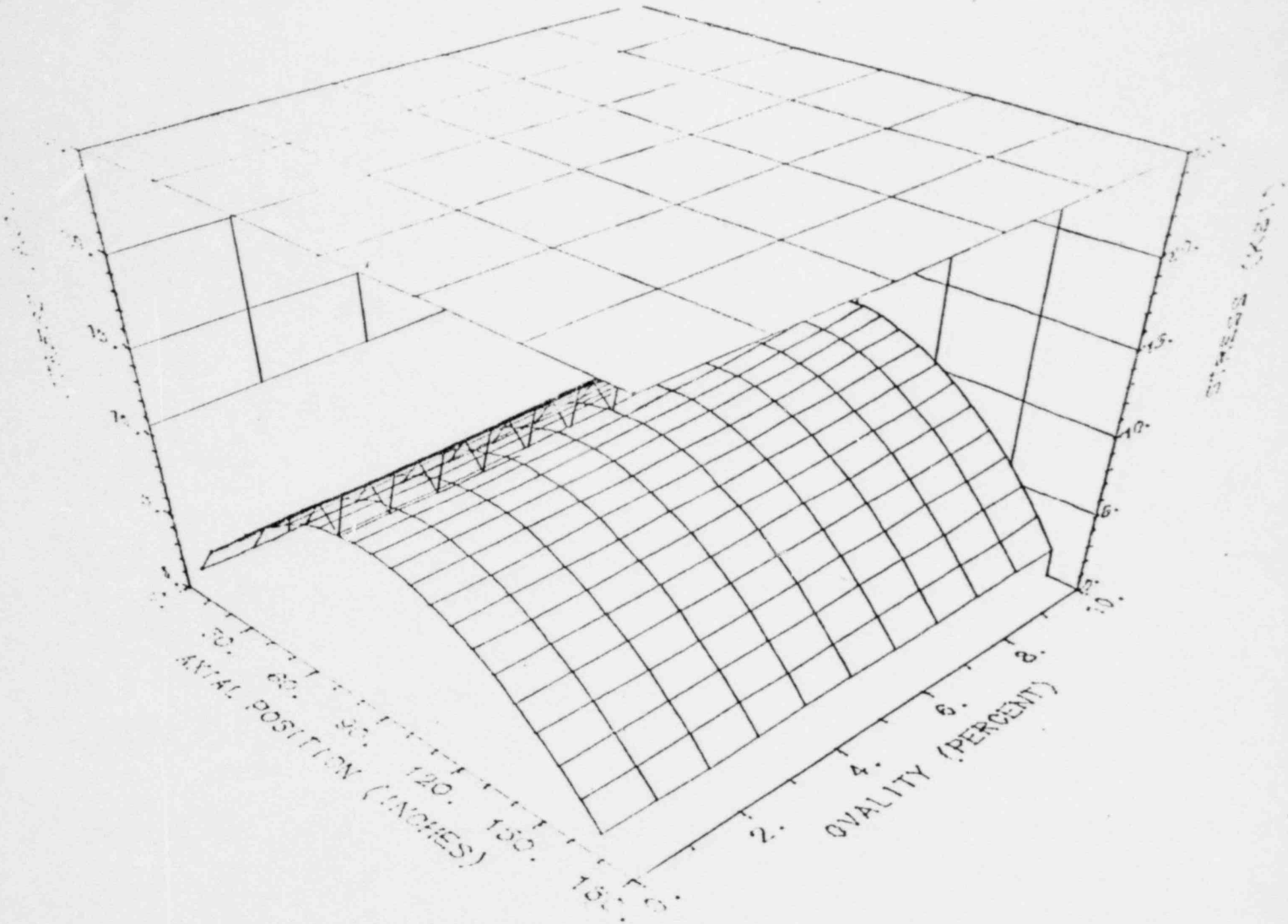

Figure 2-57. Comparison of Bending Stress to Limit

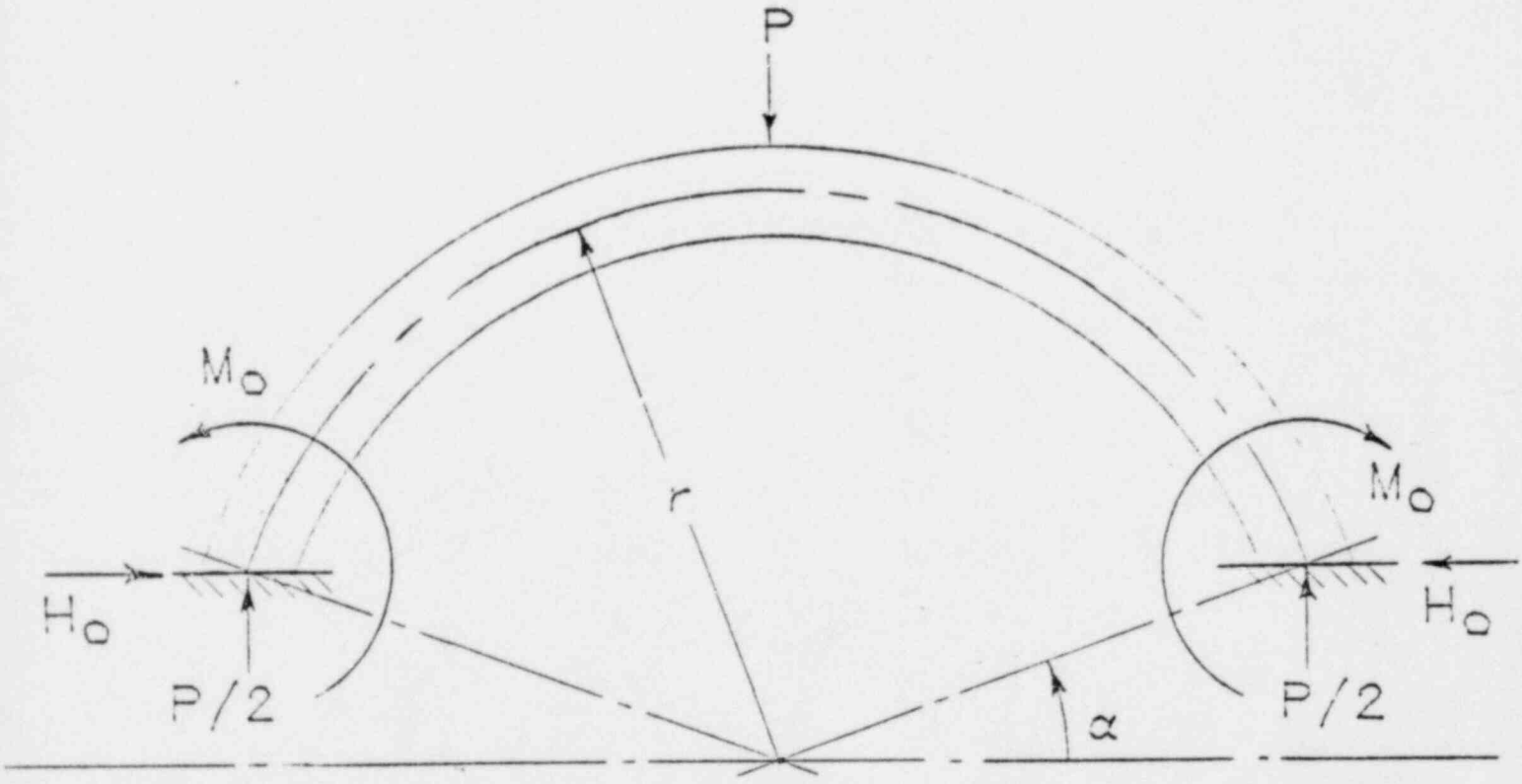

Figure 2-58. Definition of Terms for Arch

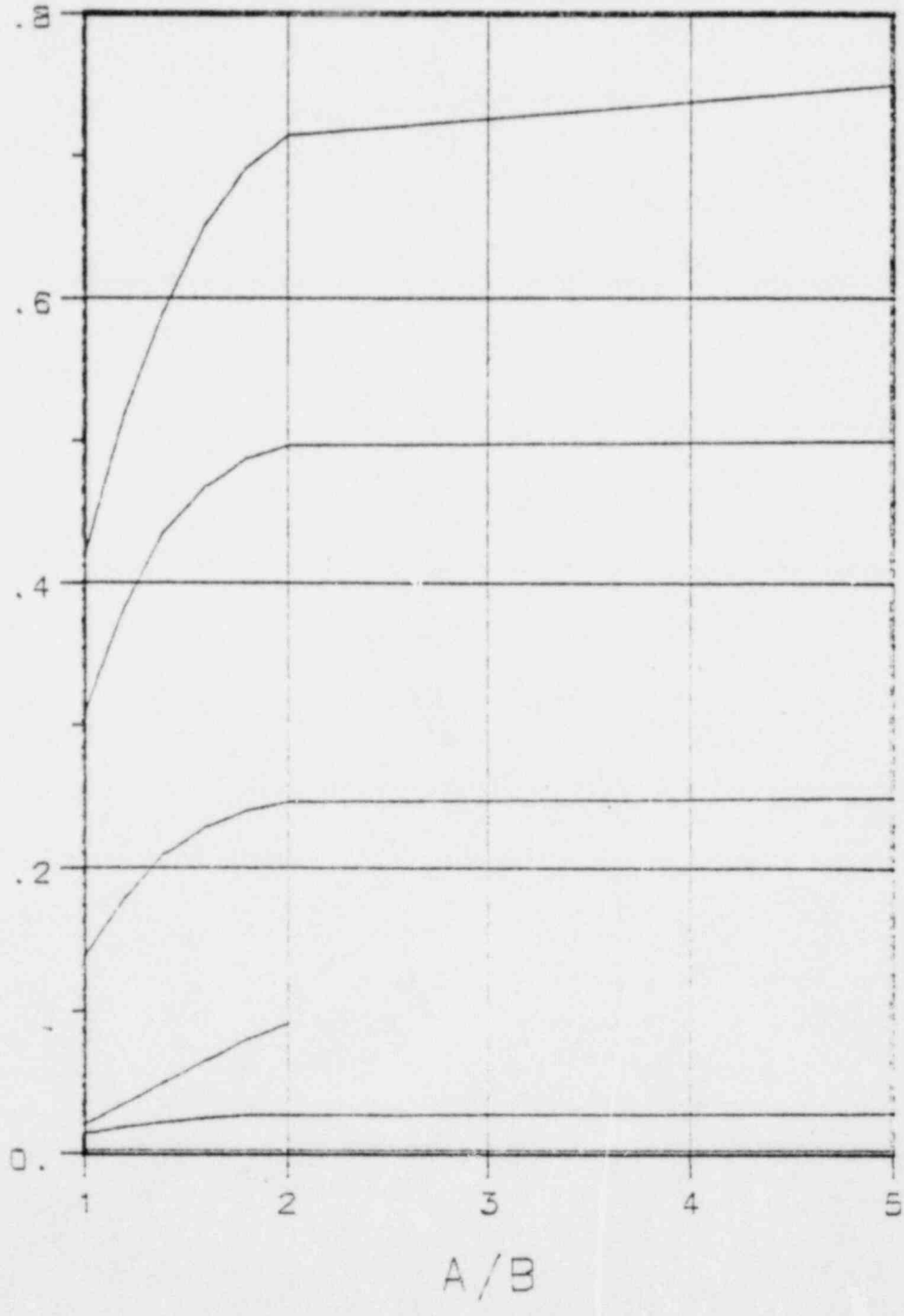

Figure 2-59. Coefficients in Solution for Plate Stresses

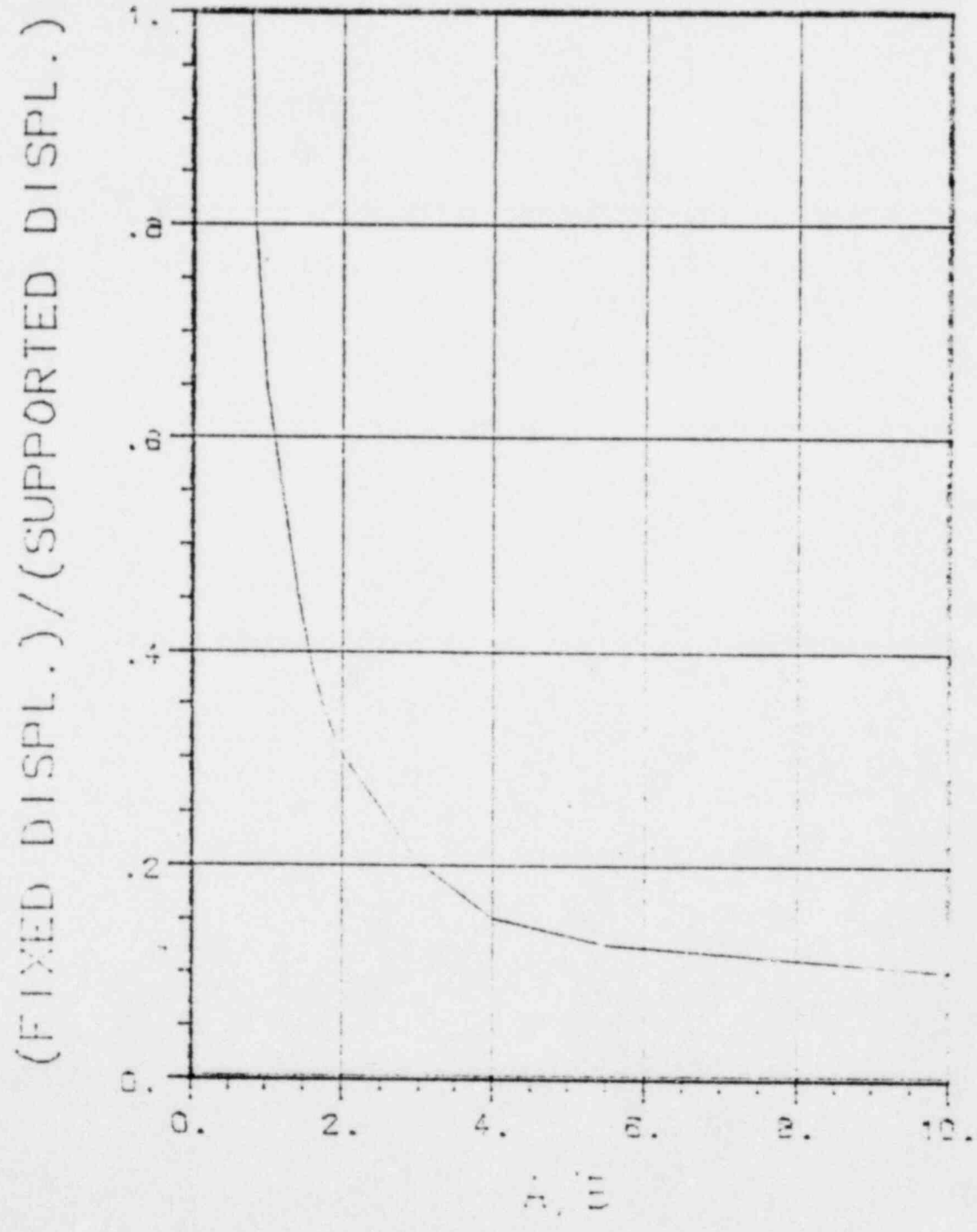

Figure 2-60. Ratio of Displacements for Flat Plates

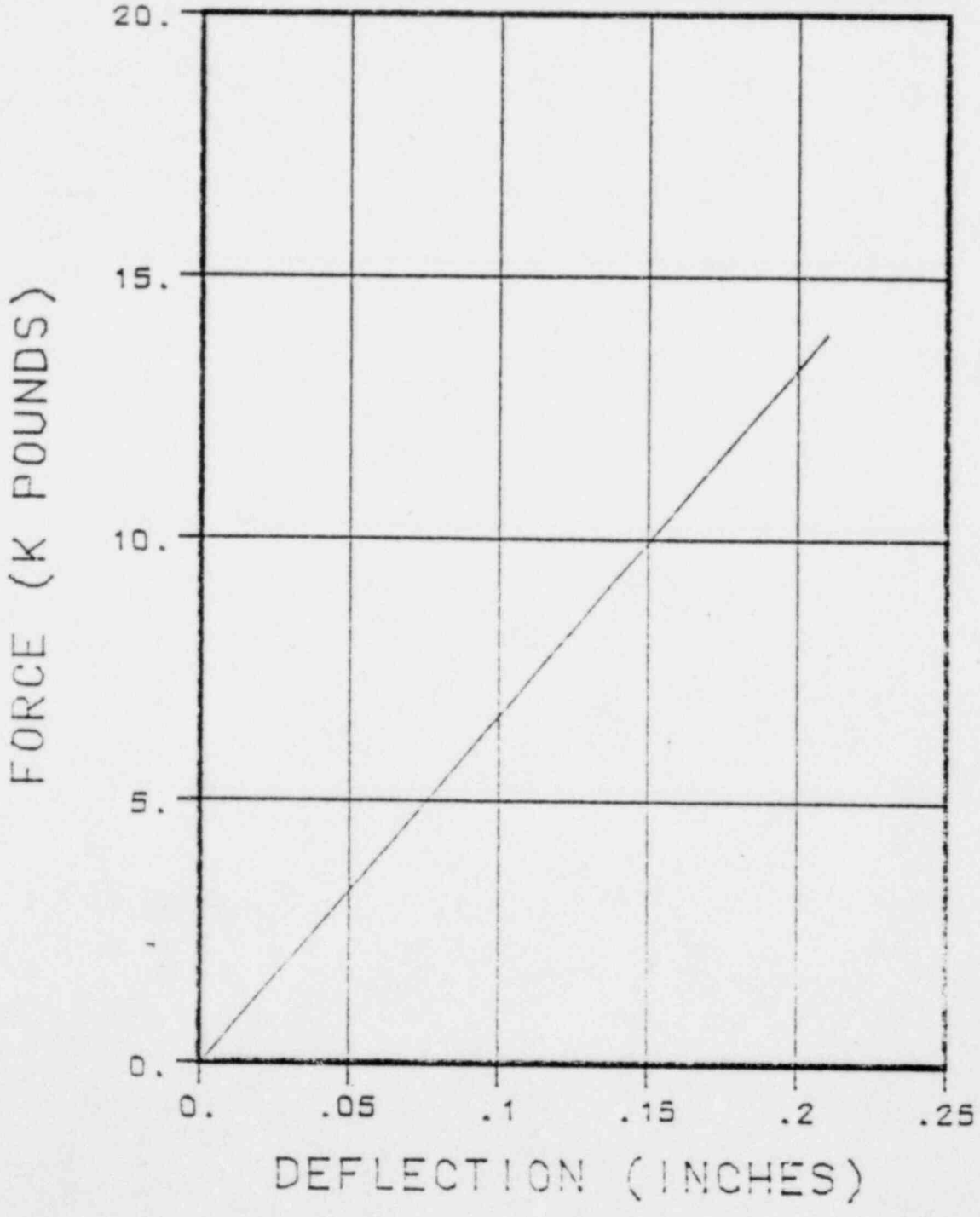

Figure 2-61. Force-Deflection Curve for Impact on Shield Tank

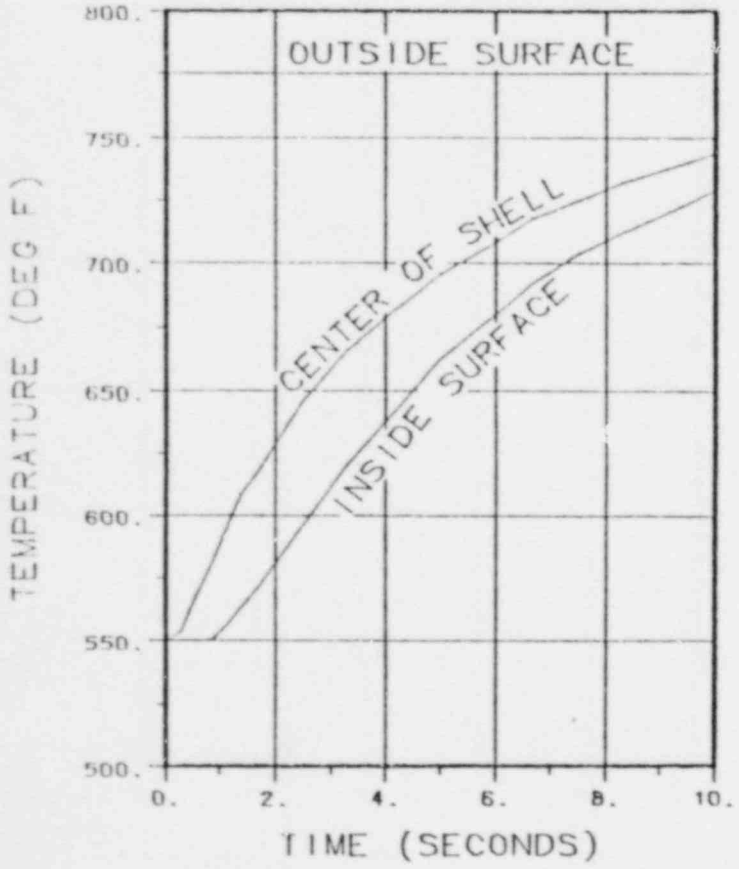

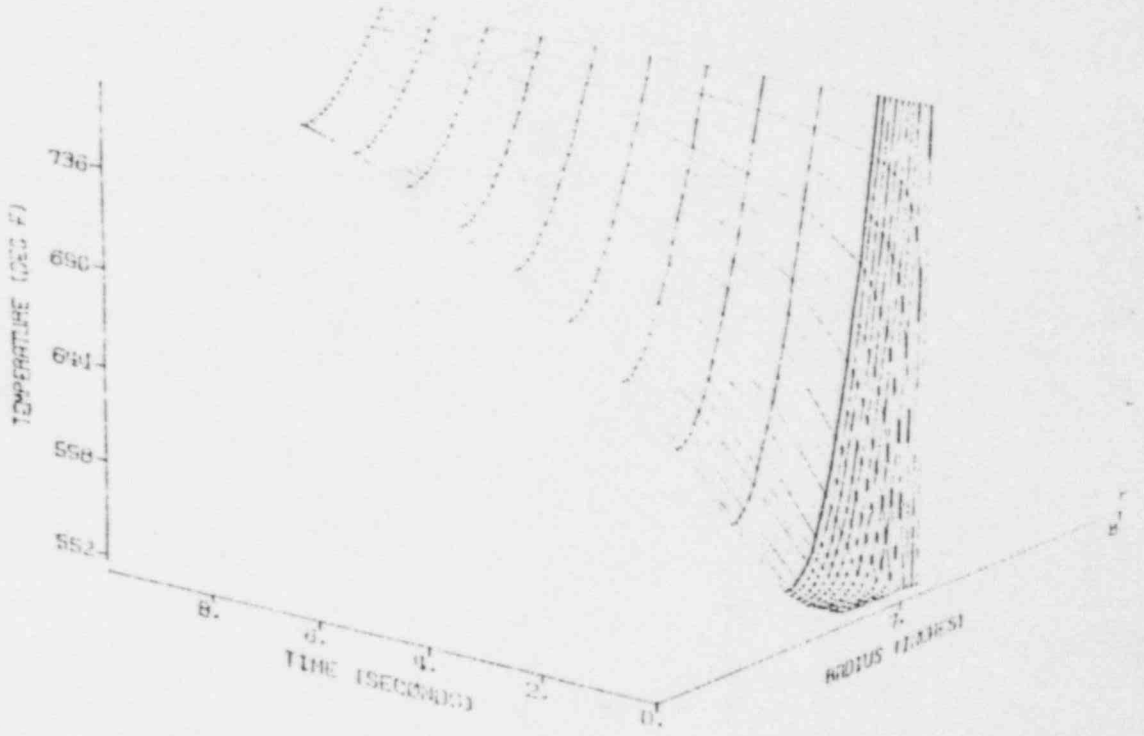

Figure 2-62. Temperature History During Lead Pour

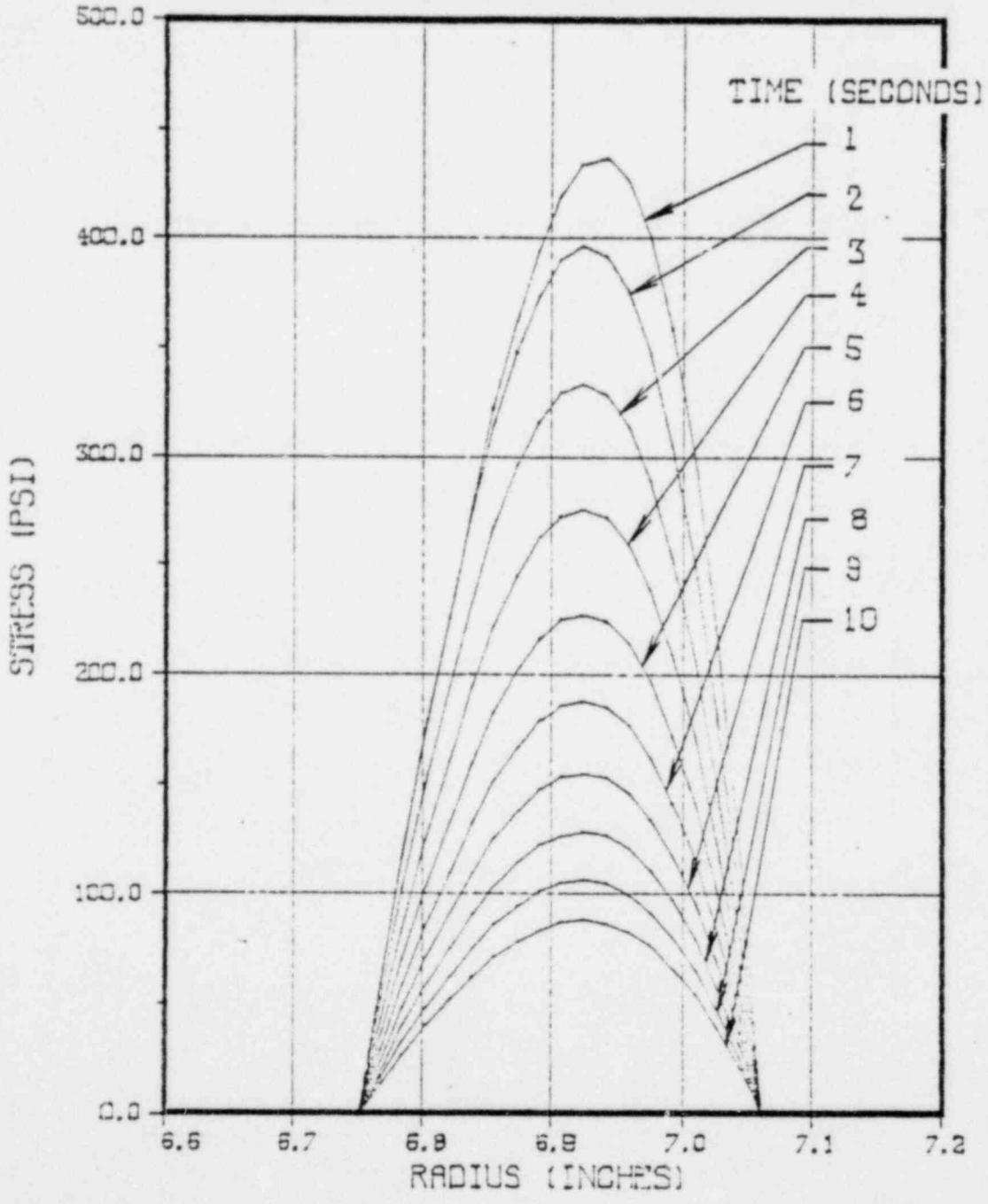

Figure 2-63. Radial Stresses During Lead Pour

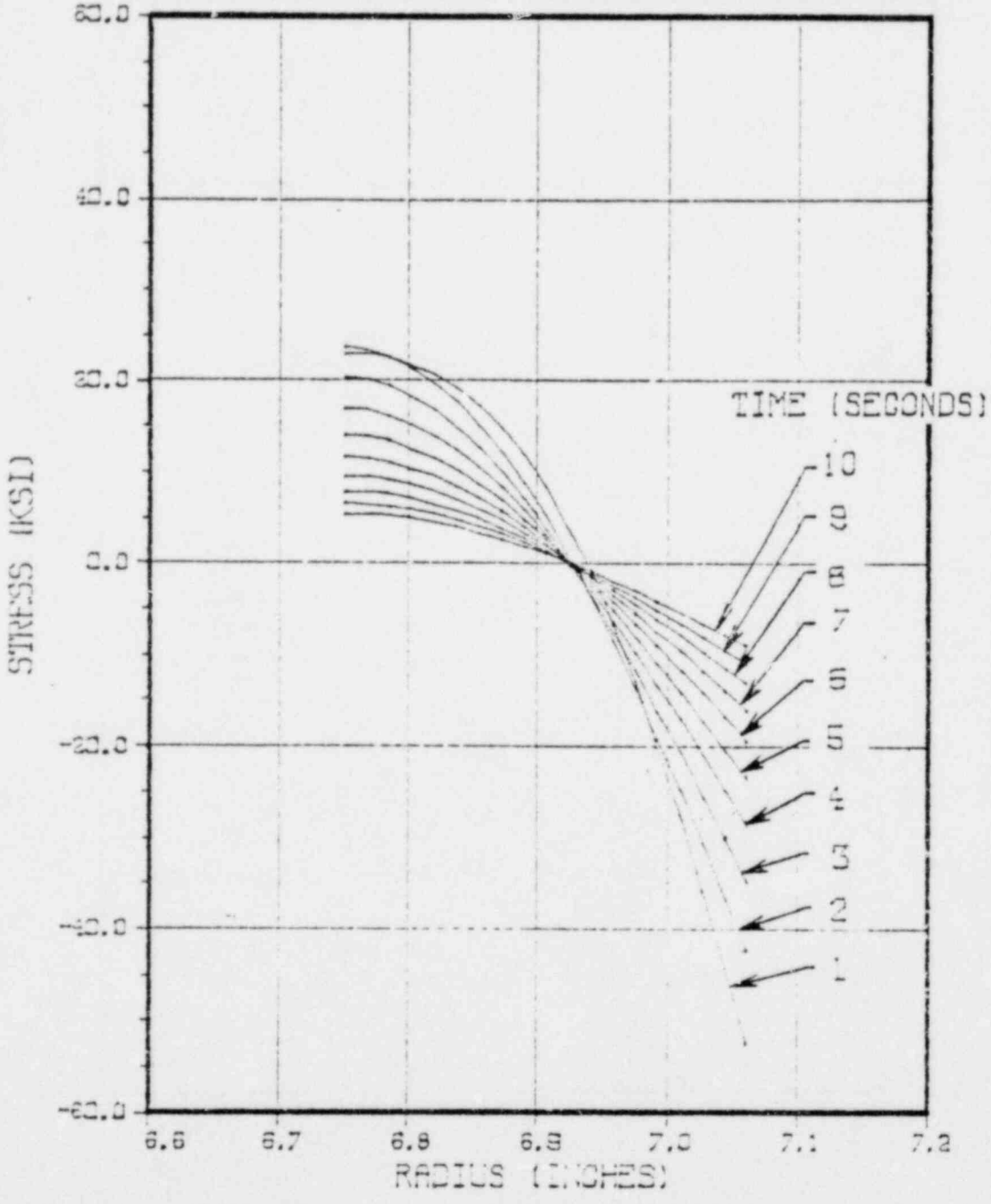

Figure 2-64. Hoop Stresses During Lead Pour

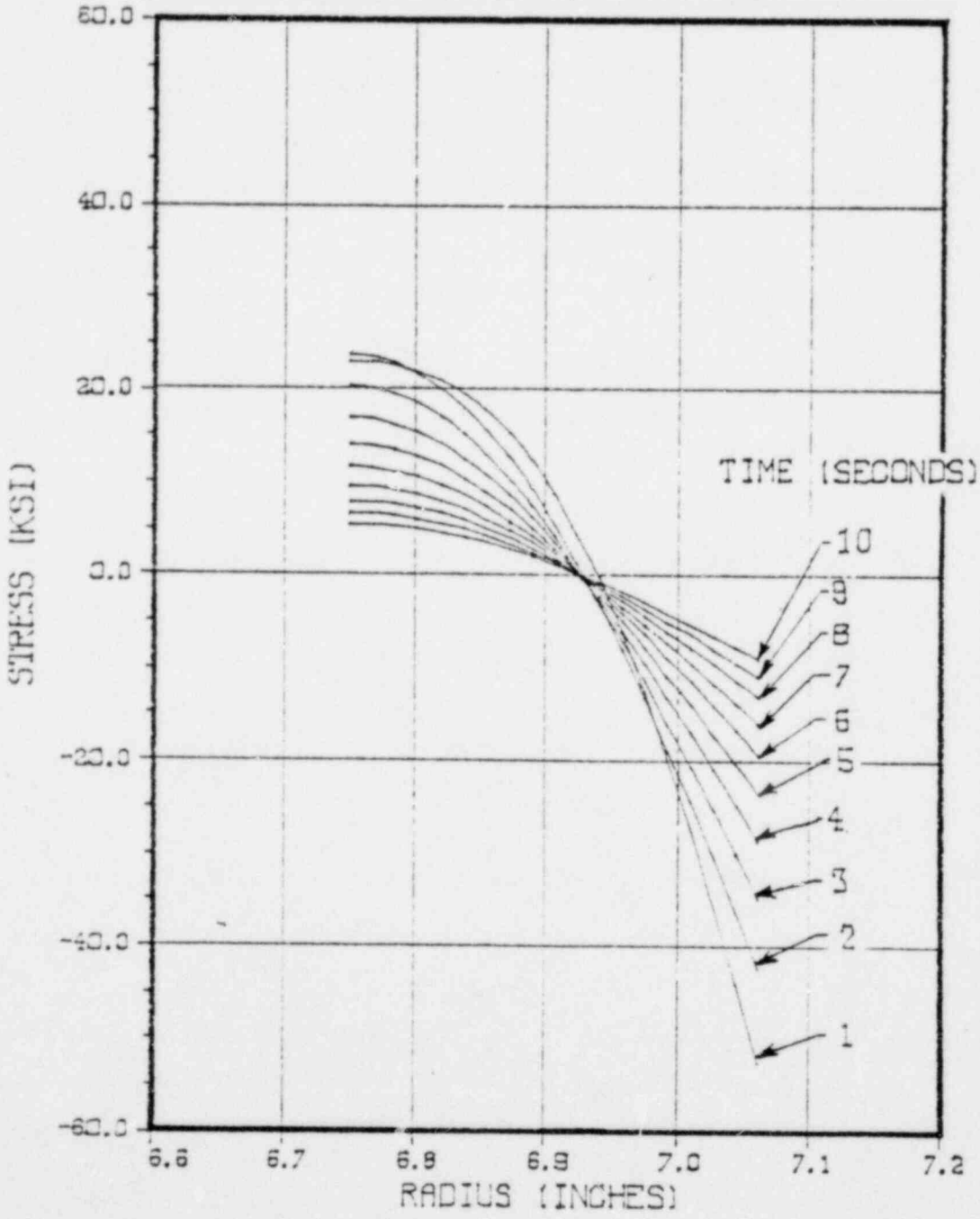

Figure 2-65. Axial Stresses During Lead Pour

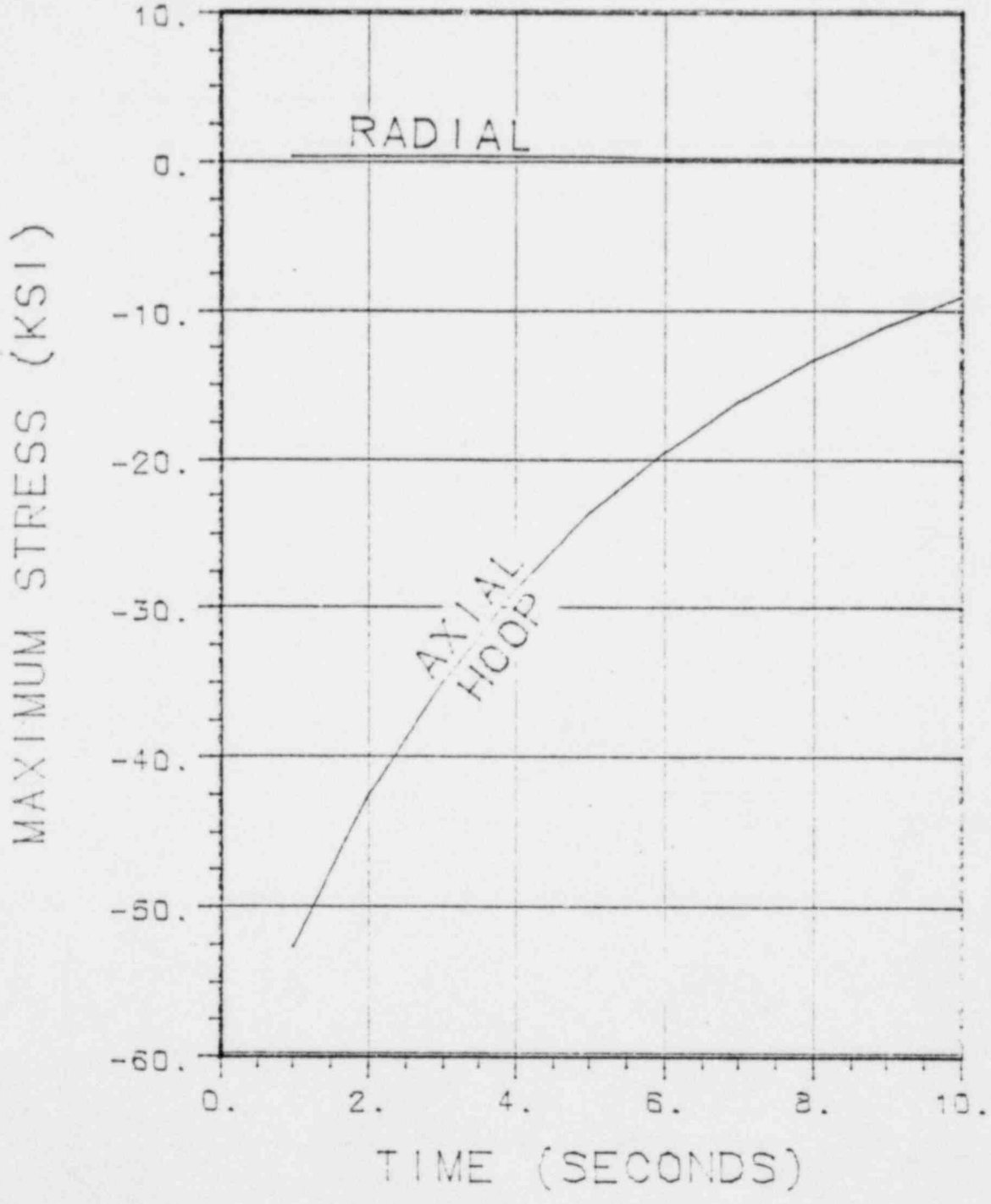

Figure 2-66. Maximum Stresses During Lead Pour

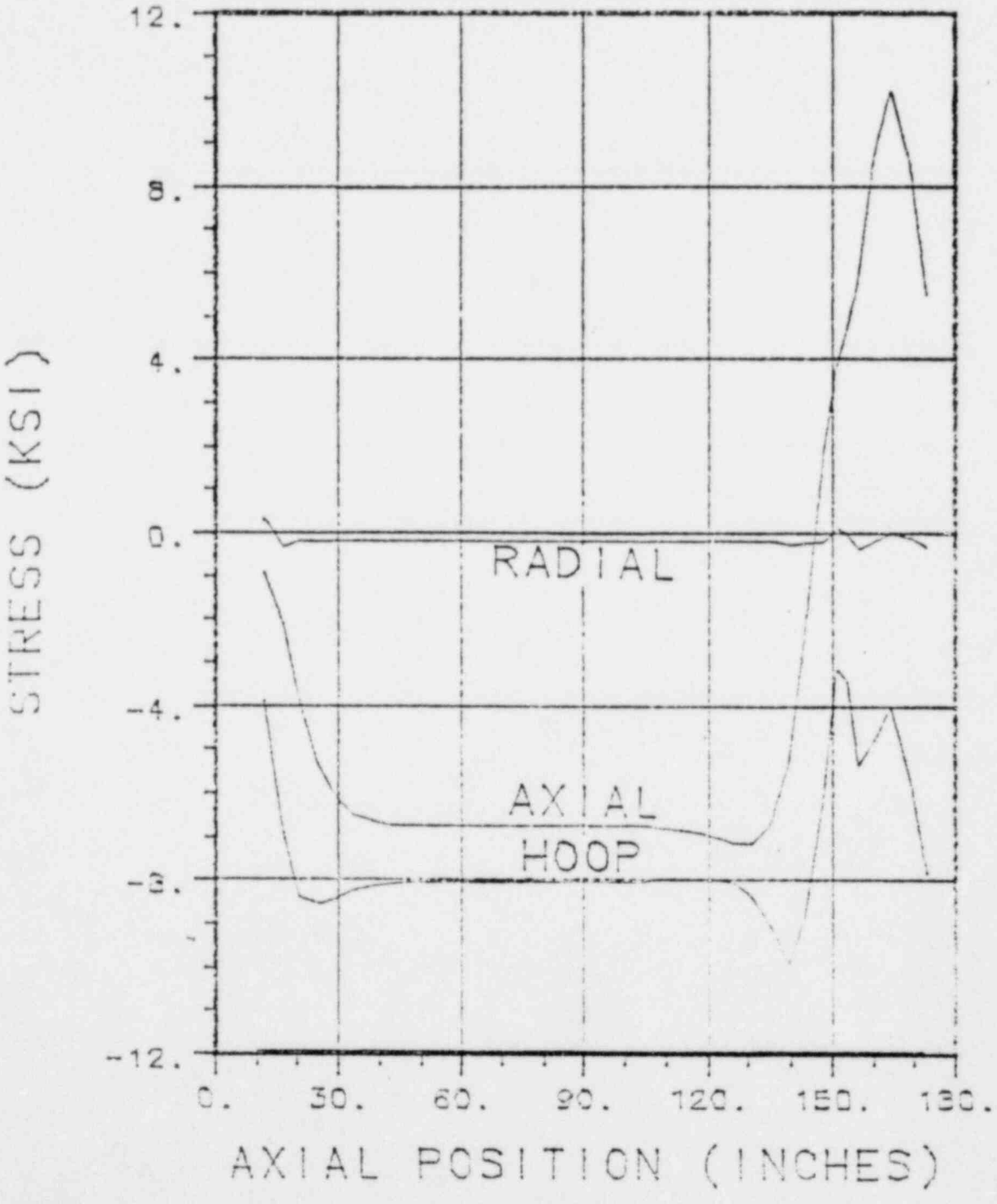

Figure 2-67. Thermal Stresses During Cooldown

2.7. Hypothetical Accident Conditions

The hypothetical accident scenario that is required to be analysed in a license application is defined in Appendix B of Part 71 of Title 10, Chapter 1 of the Code of Federal Regulations (Reference 2.2). The initiating event is a free fall through a distance of thirty feet onto a flat, horizontal unyielding surface. This is immediately followed by a free fall through a distance of forty inches with the impact on the end of a six inch diameter, mild steel pin. Following this second fall the cask is engulfed in a fire with a temperature of 1475°F for a period of thirty minutes. When the cask has completely cooled it is then immersed in a large body of water for at least eight hours.

The containment boundary must be demonstrated to remain intact during this entire accident sequence. The containment boundary includes the inner stainless steel shell, the lower end casting, the upper end casting, the bolted closure, all of the valves and the relief valve. The stresses in each of these components were determined in the following sections and compared to the criteria discussed in Section 2.1.2.1.1 to demonstrate the maintenance of the containment boundary during the hypothetical accident.

2.7.1. Free Drop

The initiating event in the hypothetical accident is a free fall through a distance of thirty feet onto a flat, horizontal unyielding surface. The impact at the conclusion of the fall is to be in the orientation that inflicts the maximum damage to the cask and particularly to the containment boundary or the inner shell of the NAC-1 cask. Since it is impossible to identify the orientation that results in the maximum damage prior to the analysis, the following sections describe the consequences of a

fall in all possible orientations.

The analyses presented here represent an impact following steady state conditions when the ambient temperature was 130°F. Cases that represent a -40°F ambient are not presented because the strength of the stainless steel increases as the temperature decreases providing more margin between the calculated stresses and the limiting stresses. The principal concern in impact analyses for cold ambient conditions is the onset of brittle fracture which is unlikely with stainless steel.

2.7.1.1. End Drop

A thirty foot free fall where the cask impacts on either end such that the center of gravity of the cask is directly over the point of impact results in deceleration forces that will tend to make the lead slump toward the impacted end. The lead motion will develope "hydrostatic like" pressures that will stress the inner and outer stainless steel shells of the cask wall. Also, axial stresses will be imparted to these same components due to the inertia of the free end of the cask.

2.7.1.1.1. Analysis Model

The model that was used to determine the response of the cask to the free fall with the impact on the end of the cask consists of two major elements which are the model of the cask body and the model of the impact limiter. These models were chosen to amplify the details of the response to the end impact.

2.7.1.1.1.1. Model of Cask Body

The model of the cask that has been employed for this analysis consists of three axisymmetric cylinders that represent the inner and outer stainless steel shells and the lead. The stainless steel shells are coupled at the impacted end by a circular plate and conical section to represent the lower end casting. The lead rests on the end casting but is not coupled to it. The configuration of this model is shown in Figure 2-68 in both an exploded view and an assembled view for clarity.

The stainless steel has been modelled as an entirely elastic material to maintain consistancy with the elastic stress limitations that were identified in Section 2.1. The lead was represented as an elastic-plastic material to incorporate the motion of the lead due to the inertial loads.

The effect of the impact limiter has been represented as a time dependent force acting on the end of the conical section of the lower end casting.

The upper ends of the inner and outer stainless steel shells were mathematically coupled such that relative motion was not permitted. This represented the effect of the upper end casting which is sufficiently rigid that the two shells will act in unison.

The lead and stainless steel are probably bonded both chemically and mechanically by the fins; however, the possibility of an incomplete bond was recognized and the model altered to reflect a more conservative representation of the interface by assuming no bond was present and including only the frictional resistance of the lead on the stainless steel. The total absence of bonding was modeled by decoupling the lead and stainless steel shells. The interface was represented by friction elements that allowed

relative motion with a restrictive force that was proportional to the normal force between the two surfaces. The coefficient of friction was taken as 0.94 (Reference 2.13) which is representative of dynamic friction between lead and carbon steel. This value was selected in the absence of any data for friction between lead and stainless steel or copper and to properly represent the friction model within ANSYS which cannot represent the transition between static and dynamic friction. The presence of a gap between the lead and stainless steel was not introduced into the model because the gap would reduce the pressure of the lead on the inner shell because there would be volume that could accomodate the initial slumping of the lead.

2.7.1.1.1.2. Impact Limiter Characteristics

The impact limiter that protects the end of the cask consists of a right circular cylinder of balsa wood with its grain oriented parallel to the centerline of the cask. This cylinder is surrounded by an annulus of balsa wood with its grain 50 degrees from the cask centerline. The central cylinder of balsa wood is penetrated by four stainless steel tubes that provide passage for the bolts that attach the impact limiter to the cask. These tubes must crush as the balsa wood is crushing. The geometry of the portion of the impact limiter that is effective during end drops is shown in Figure 1-7 where the components have been separated for clarity.

The crushing of the impact limiter during an end impact is shown schematically in Figure 2-69. The initial portion of the impact will deform the outer surface of the impact limiter. After the shock wave has traversed the thickness of the impact limiter the deformation will primarily be restricted to the inner surfaces of the impact limiter. This reversal occurrs because the deformation will restrict itself to the location of highest stress or

smallest area which is the inner surface. All of the analysis of the deformation of the impact limiter that follows is based upon the concept of crushing from the inside to the outside. The time interval for the initial exterior crushing has been estimated by using the speed of sound in air as an approximation to the speed of sound in balsa wood. At a velocity of 1100 ft/sec it will take about 1.0 milliseconds for the shock wave to travel across the 13.375 inch thickness of the balsa wood. During this time period the impact limiter will have deformed less than 0.4 inches.

The force that is transmitted to the cask body is the sum of the forces that are created by crushing the balsa wood and the stainless steel tubes. The balsa wood force is expressed as the product of the crush stress and the cross section area of the balsa wood .

The crush strength is presented in Figure 2-25 for balsa wood loaded parallel and at 50° to the grain. Figure 2-26 presents the crush strength of multiple sections of balsa wood where one section has its grain perpendicular to the crush direction. The cross section area of all regions remains constant during the entire impact.

The force imparted on the cask by the crushing stainless steel tubes is also expressed as the crush strength and the cross section area of the tubes. The crush strength of the stainless steel is identified in Figure 2-15 where the strain rate is comparable to the crushing of the impact limiter. In this case the effective area of the stainless steel tubes increases during the impact due to the Poisson's ratio effect during compression. In equation form the force transmitted to the cask is given by:

$$F_{ss} = \sigma_{ss} A_{ss}$$

where:

σ_{ss} is the crush strength of the stainless steel

A_{ss} is the area of the stainless steel

The area of the stainless steel is related to the deformation by:

$$A_{ss} = A_{iss} (1 + \nu \varepsilon)$$

where

A_{iss} is the initial area of the stainless

ν is Poisson's ratio

ε is the strain of the stainless steel

The combined force of the balsa wood and the stainless steel are presented in Figure 2-58 as a function of the displacement of the cask body.

The upper and lower impact limiters are different in that the holes that penetrate the balsa wood to permit access to the bolts are in the central core in the upper end impact limiter and they are in the annular section in the lower impact limiter. The force-deflection curves for both impact limiters have been evaluated and are compared in Figure 2-71 by showing both curves together along with the fractional difference between the two curves. The calculations of the consequences of a fall with an end impact have been calculated using the larger forces which represent an impact on the closure end of the cask. However, the integral of the force-deflection curve for the lower end impact limiter shows that both impact limiters have sufficient energy absorption capacity to stop the cask without reaching lock-up. This statement is based upon the impact limiters having endured a one foot free fall as part of the normal transport prior to the thirty foot free fall.

The force-deflection curve that was employed for the evaluation of the thirty foot free fall is presented in Figure 2-72. This curve is based upon the assumption that the cask has endured a one foot free fall prior to the thirty foot free fall.

Consequently, the initial portion of the force-deflection curve has been suppressed because it would have been consumed in the one foot fall.

2.7.1.1.2. Consequences of End Drop

The model of the cask was used to evaluate the stresses in the cask during an end impact following a 30 foot free fall. At the point of impact the velocity of the cask was 527.5 inches per second. The displacement history of the lower end of the cask during the impact is presented in Figure 2-73. The principal phenomenon that occurs during this accident is the slumping of the lead due to the inertial loads. The displacement of the upper surface of the lead is presented in Figure 2-74 along with the displacement of the adjacent points on the inner and outer shells. The lead does slump during the impact; however, the relative displacement is small.

The lead induces compressive hoop stresses in the inner shell and tensile hoop stresses in the outer shell as well as axial stresses in both shells that are presented in Figures 2-75 to 2-78 as functions of time and axial position in the cask. The reference for axial position is the bottom of the lower end casting which is 8.0 inches below the lower end of the cavity and 12.75 inches below the lower end of the inner shell.

The calculated stresses are based upon an empty, dry cavity where there is no water and associated hydrostatic pressure on the inside of the inner shell. If water is present the hydrostatic pressure will be 277. psi which is the product of ρ g h where g is the maximum deceleration of the cask (57.7 g's) and h is the height of the water (133 inches) and ρ is the density of water (62.4 lb/ft3). Additionally, if the cask has reached thermal equilibrium and the environmental temperature is 130°F,

the cavity pressure will be 118 psia which is additive to the hydrostatic pressure. These two terms will reduce the hoop stresses in the inner shell by 8,730. psi; however, the consequences of the accident are more severe if the cavity is unpressurized.

The thermal stresses have also not been included in the total stresses because the thermal stresses induce tensile hoop stresses in the lead which must be overcome by the hydrostatic forces prior to slumping of the lead. Consequently, the predicted consequences of the end drop are more severe if the cask is assumed to be in a stress free state prior to the initiation of the accident.

The hydrostatic pressure will contribute to the axial stresses in both the inner and outer shells. The magnitude of the increase in the stress is determined from a force balance on the end castings. The internal pressure acts outward on the end casting and both shells exert a balancing force. In equation form this is expressed as:

$$p_i \pi D_i^2/4 = \sigma_i A_i + \sigma_o A_o$$

where:

p_i is the internal pressure
D_i is the internal diameter
σ_i is the axial stress in the inner shell
A_i is the cross section area of the inner shell
σ_o is the axial stress in the outer shell
A_o is the cross section area of the outer shell

The elongation of both shells caused by the internal pressure must be equal since the end castings are sufficiently rigid to preclude deformation. The elongation is given by:

$$\varepsilon_i = \sigma_i/E$$

and

$$\varepsilon_o = \sigma_o / E$$

where:

ε_i is the elongation of the inner shell
ε_o is the elongation of the outer shell
E is the modulus of elasticity

Introducing numerical values as follows:

A_i = 13.560 inches^2	A_o = 112.901 inches^2
p = 118 psi	E = 27.1 x 106 psi
D_i = 13.5 inches	

results in an axial stress of 133 psi in both shells. This value is negligibly small and need not be considered further in the evaluation of an end impact.

The maximum hoop stress is presented in Figure 2-79 as a function of position in both shells. This data represents the accumulation of the largest stresses at all times at each axial location. Similiarly, the maximum axial stresses in both the inner and outer shells are presented in Figure 2-80 as a function of position. An additonal curve is presented for the inner shell which represents the axial stresses that will occur if the cavity has water and is pressurized to 118 psia by thermal expansion of the water.

The limitation on the hoop and axial stresses is the lesser of the buckling stress or the ultimate stress. In this instance buckling is the more restrictive limit for both stresses and is discussed in the following section.

2.7.1.1.3. Effect of Cavity Irregularity

The analyses presented in Section 2.7.1.1.2 presume that the inner and outer shells are perfect cylinders. The outer shell is fully machined as the final step in its fabrication so it will be very nearly a perfect cylinder; however, the inner shell is subject to dimensional variations from a true cylinder. Consequently, it is necessary to determine the impact of dimensional variations and also to determine the variations that can be tolerated.

2.7.1.1.3.1. Collapse Buckling

The presence of ovality of either shell will increase the hoop stress because the radius in increased. The increase in the hoop stress in the inner shell is presented in Figure 2-46 as a function of the ovality. This curve has been determined from the ratio of the expressions for hoop stress in true and ovalized cylinders (Reference 2.9):

$$\frac{\sigma_{ht}}{\sigma_{ho}} = \frac{p\ r_t\ t_o}{p\ r_o\ t_i}$$

where:

p is the pressure
r is the radius of the shell
t is the thickness of the shell
σ_h is the hoop stress
t and o as subscripts refer to true and oval cylinders

The radius that is employed for elliptical cylinders is given by:

$$r = a^2 / b$$

where:

a is the major radius
b is the minor radius

The factor that increases the hoop stress to account for ovality has been applied to the maximum hoop stress presented in Figure 2-79 to determine the maximum hoop stress as a function of ovality and position. The resulting maximum hoop stresses have been superimposed upon the curve of buckling stress as a function of ovality and axial position (Figure 2-10) as shown in Figure 2-81. The maximum calculated hoop stress is generally below the buckling limit; however, there are some ovalities at specific locations that could lead to buckling. The minimum allowable ovality is greater than 2% at the end of the inner shell. At positions slightly removed from the end of the shell the allowable ovality increases to over 10% because of the reduced pressure from the slumping of the lead. These limits have been reduced to a plot of maximum permissible ovality as a function of axial position in Figure 2-82. In this figure the reference for axial position is the end of the cavity to facilitate comparison with post fabrication measurements of the cavity dimensions.

There is no impact of bow of the inner shell on the collapse type buckling because collapse is a local phenomena that is independent of the straightness of the remainder of the cylinder.

2.7.1.1.3.2. Compressive Buckling

As discussed in Section 2.1.2.2.3 the inner shell cannot buckle due to axial loads unless the outer shell also buckles because both shells are coupled by the end castings and the large deformations associated with buckling cannot occurr in either

shell as long as the other shell remains intact. The maximum axial stresses in both shells have been presented in Figure 2-80 as a function of axial position. The axial stress that is required to cause buckling of the inner shell varies between 25,000 and 35,000 psi for both shells for ovalities in the range of 0 to 10%. Since the maximum axial stress in the outer shell is 13,200 psi the outer shell will remain intact and will support the inner shell. This is independent of the ovality of either shell because the stresses are so small. Consequently, the possibility of buckling due to axial loadings introduces no limitations on the ovality or bow of the inner shell.

2.7.1.2. Side Drop

The impact of the cask on its side such that both impact limiters simultaneously contact the surface subjects the cask to large bending stresses. The ends stop while the inertia of the center of the cask induces additional bending which must be dissapated by the stiffness of the cask.

2.7.1.2.1. Analysis Model

The model of the cask that was used to represent the response during a side impact consists of two major components, namely, the cask body and the impact limiters. The charcteristics of these models are described in the following two sections.

2.7.1.2.1.1. Model of Cask Body

The representation of the cask body for the analysis of the side impact following a 30 foot free fall has been restricted to a beam that has the stiffness characteristics of the outer shell. The mass per unit length represents the midsection of the cask including the contents of the cavity. Mass elements have been added at the end of the cask to represent the end castings and impact limiters. All of the masses have been multiplicatively increased to give a total cask weight of 52,000 pounds.

The impact limiters were represented as spars attached to the ends of the cask model. The spars were given stress-strain curves that duplicated the force-displacement curves of the impact limiters. The spars had no mass so they did not influence the inertial forces acting on the cask.

2.7.1.2.1.2. Impact Limiter Characteristics

The side impact limiter is an integral part of the impact limiter that is bolted to both ends of the cask. Protection during this type of impact is provided by a mixture of redwood and balsa wood that is oriented so that the grain is essentially perpendicular to the cask body. The geometry of the side impact limiter is shown in Figure 1-7 with the individual parts separated for clarity.

The crushing of the impact limiter during a side impact is shown schematically in Figure 2-83. The initial portion of the impact will deform the outer surface of the impact limiter. After the shock wave has traversed the thickness of the impact limiter the deformation can transition to the inner surface of the impact limiter. This reversal occurs because the deformation will

restrict itself to the location of highest stress or smallest area. All of the analysis of the deformation of the impact limiter that follows is based upon the concept of crushing from the outside until the crush area is equal to the crush area at the inside of the impact limiter and then the remainder of the deformation will be characterized as crushing the inside of the impact limiter. The time required for the shock wave to reach the interior has been estimated by using the speed of sound in air as an approximation to the speed of sound in redwood. At a velocity of 1100 ft/sec it will take about 1.5 milliseconds for the shock wave to travel across the 21 inch thickness of the redwood. During this time period the impact limiter will have deformed about 0.8 inches and the crush area at the outer surface of the impact limiter will be smaller than the crush area at the interface between the impact limiter and the cask body. Consequently, the impact limiter will continue to crush from the outside past the time required for the shock wave to reach the interior of the impact limiter.

The force that is transmitted to the cask body is the sum of the forces that are created by crushing the redwood, balsa wood and the stainless steel shell. The redwood and balsa wood act in parallel and their displacements or strains will be identical during the entire impact. The combined redwood and balsa wood force is expressed as the product of the crush stress and the cross section area.

The crush strength is presented in Figure 2-21 for redwood loaded parallel to the grain and the crush strength of balsa wood loaded parallel to the grain is presented in Figure 2-25. The reduction in the crush strength of the redwood and balsa wood that does not have its grain parallel to the impact direction is given by the equation in Section 2.3.5 and is evaluated in Figure 2-24.

The stainless steel shell that surrounds the wood consists of two components that are important to the crushing of the

impact limiter. The backing plate will buckle during the impact while the conical section will partially buckle to conform to deformation at the outer surface. Once the deformation has transitioned to the inner surface, the conical portion of the shell will have no further importance in the determination of the crush forces.

The force that is required to cause the backing plate to collapse has been determined with the aid of an ANSYS calculation. The model to represent this component is shown in Figure 2-84 which represents half of the plate in a full three dimensional manner. The interaction between the cask and this backing plate has been represented as a uniformly distributed force acting on the lower half of the inner surface of this plate. This force was increased and the deformations calculated to produce the required force-deflection curve. The deformations of a cross section through the center of the backing plate are shown in Figure 2-85 where each of the different loading conditions are shown displaced for clarity. The deformed geometry plots were terminated when the load reached 30,000 pounds because the plate became unstable. The plate is uncapable of supporting any larger loads. The force-deflection curve that reflects the load carrying capability of the plate is presented in Figure 2-86.

The force transmitted to the cask as a result of the crushing of the redwood and balsa wood was calculated by dividing the impact limiter into many slices parallel to the impact direction. A sketch of the segments used in the evaluation of the wood is shown in Figure 2-87. The crush strength of the wood in each slice was determined from the orientation of the grain using the equation presented in Section 2.3.5 and is evaluated in Figure 2-21. The deformation of each slice was converted into a strain to determine the crush strength of each slice from the data in Figures 2-18 and 2-22. Each slice was evaluated independently and the results combined to determine the force-deflection curve for the redwood and balsa wood.

The force-deflection curve that was employed in the evaluation of the cask stresses was selected from the data in Figure 2-77 to represent the highest forces and also included the portions of the impact limiter that had the shortest length. Further the force-deflection curve reflected the possibility of the cask having endured a one foot fall prior to the thirty foot fall. This eliminated the initial portion of the force-deflection curve and produced large forces early in the impact. The force deflection curve that was employed in the calculations is presented in Figure 2-88.

The force-deflection curve that represented the least forces that are identified in Figure 2-89 and included the longest sections of redwood was evaluated to assure its ability to stop the cask. This combination of conditions resulted in a stopping deflection of 12.1 inches which is substantially less than the 13.5 inches deflection that is required to cause the structure of the impact limiter to impact the surface or to cause the expansion tank to impact the surface. Consequently, the lesser force-deflection curve does impose lesser forces on the cask and will result in smaller stresses in the cask body.

2.7.1.2.2. Consequences of Side Drop

The model of the cask was used to determine the stresses in the cask as a result of the 30 foot free fall where both impact limiters simultaneously made contact with the unyielding surface. The cask was given an initial velocity of 527.5 inches per second. The impact on the unyielding surface was represented by fixing the ends of the spars that represent the impact limiters. The principal effect of this impact is the bending of the cask due to the inertia of the center of the cask while the ends of the cask have been stopped by the impact limiters. The time histories of the ends and center of the cask are presented in

Figure 2-90 and the deflection of the center of the cask relative to the lower end of the cask is presented in Figure 2-91. The calculated deformation of the entire cask is presented in Figure 2-92 which includes the vertical displacement of both ends of the cask, the center of the cask and the displacement of the center relative to either end. The stresses induced in the cask body as a result of these deformations are presented in Figure 2-93 which shows a stress wave that travels along the cask with a frequency of about 65 cycles per second.

The model of the cask body included only the outer shell because it is the principal structural member of the cask. The stresses in the inner shell must also be determined to permit comparison to the limitations that determine the survivability of the cask during the hypothetical accident.

The end castings distribute the moment between the two shells so that the angular deflection of both shells are identical at any time during the impact. The angular deflection of the ends of the shells is proportional to M/EI so this ratio must be identical for the ANSYS model, the inner shell and the outer shell. To preserve these ratios the moments will distribute themselves in proportion to the moments of inertia or in equation form:

$$\sigma_a = M_a c_a / I_a$$

or

$$M_a = \sigma_a I_a / c_a$$

and

$$\sigma_i = M_i c_i / I_i$$

$$\sigma_o = M_o c_o / I_o$$

$$M_i = M_a I_i / (I_o + I_i)$$

$$M_o = M_a I_o / (I_o + I_i)$$

giving

$$\sigma_i = M_a I_i c_i / (I_o + I_i)$$

$$\sigma_o = M_a I_o c_o / (I_o + I_i)$$

or

$$\sigma_i = \sigma_a I_a c_i/(I_o + I_i) c_a$$
$$\sigma_o = \sigma_a I_a c_o/(I_o + I_i) c_a$$

where:

M_a is the moment from the ANSYS calculation
M_i is the moment on the inner shell
M_o is the moment on the outer shell
I_a is the moment of inertia used in the ANSYS calculation
I_i is the moment of inertia of the inner shell
I_o is the moment of inertia of the outer shell
c_a is the radius used in the ANSYS calcualtion
c_i is the radius of the inner shell
c_o is the radius of the outer shell

The moments of inertia and the radius to the outer fiber of the two shells is presented in Table 2-15. The ANSYS calculation modeled only the outer shell so the values that characterize the calculated results are those of the outer shell. Inserting numerical values gives the ratio of the bending stress in the inner shell to that calculated by ANSYS of 0.458 and the ratio of the bending stress in the outer shell to that calculated by ANSYS is 0.973. These ratios have been employed to determine the maximum stresses in the inner and outer shells that are presented in Figure 2-94. The data presented in Figure 2-93 is the results of the ANSYS calculation and does not truly represent the bending stress in either shell; although, it is very close to the stress in the outer shell.

The limitation on the bending stress is the lesser of the buckling stress or the ultimate stress. In this instance the ultimate stress is the more restrictive limit for the stress. The impact of ovality on the buckling is discussed in the following section.

The ultimate stress for stainless steel when dynamically loaded is 150,000 psi. This value is substantially larger than the

maximum bending in the inner shell which is 46,200 psi or the maximum bending stress in the outer shell which is 98,100 psi. The strain rate at the time of the peak stress is about 0.5 in/in/sec which is well within the range of strain rates where the ultimate is 150,000 psi validating the application of this value for the limit on the primary bending stress.

2.7.1.2.3. Effect of Cavity Irregularity

The analyses presented in Section 2.7.1.2.2 presume that the inner and outer shells are perfect cylinders. The outer shell is fully machined as the final step in its fabrication so it will be very nearly a perfect cylinder; however, the inner shell is subject to dimensional variations from a true cylinder. Consequently, it is necessary to determine the impact of dimensional variations and also to determine the variations that can be tolerated.

The only type of buckling that is possible during a side impact is buckling due to bending. The limiting stresses that assure the absence of this type of buckling were presented in Section 2.1.2.2.1 and Figure 2-6. The presence of ovality of either shell will increase the bending stress because the moment of inertia of the cross section is increased. The increase in the bending stress in the inner shell is presented in Figure 2-52 as a function of the ovality. This curve has been determined from the expression for bending stress (Reference 2.9):

$$\sigma_b = Mc/I$$

where the symbols are as defined above. The moment of inertia of an elliptical cylinder is given by:

$$I = \pi(ab^3 - ba^3)/4$$

where:

a is the major radius
b is the minor radius

The factor that increases the bending stress to account for ovality has been applied to the maximum bending stress presented in Figure 2-84 to determine the maximum bending stress as a function of ovality and position. The resulting maximum bending stresses have been superimposed upon the curve of buckling stress as a function of ovality and axial position (Figure 2-6) as shown in Figure 2-95. The maximum calculated bending stress is substantially below the buckling limit.

There is no impact of bow of the inner shell on the bending type buckling because the configuration of the cross section is the controlling parameter and the presence of a bow could only serve to change the moment arm which is a very minor correction to the conditions that could induce buckling failure.

2.7.1.3. Corner and Oblique Drops

The most probable impact orientation is between an end and side impact. This possibility has been analysed by determining the consequences of a 30 foot free fall where the impact is on the corner of the impact limiter. There are two ranges of impact orientations that result in different responses to the impact. The first requires the cask to be less than 11.78° from vertical so the center of gravity is vertically over the impact area and the cask can come to rest in the impact orientation. The second range encompasses orientations where the cask is more than 11.78o from the vertical. In this range of impact orientations, there will be two impacts. The first will involve one impact limiter and the vertical motion of the cask will be arrested. The cask energy that remains will be converted into rotation and the cask

will fall such that the other impact limiter also impacts on the surface.

2.7.1.3.1. Analysis Model

The model of the cask that was employed to represent this type of impact consisted of a combination of the end and side models. Both lead slump and bending will occurr during a corner impact so the modeling must represent both phenomena. The magnitude of the bending stresses in the cask were calculated with a model that consisted of a beam representation of the outer shell of the cask using the same approach as was employed for the analysis of the side impact which was described in Section 2.7.1.2.1.1. A second model was employed to represent the effect of the lead slump which consisted of an axisymmetric representation of the cask including the lead and both inner and outer stainless steel shells. This second model was identical to the model for the representation of the end impact which was described in Section 2.7.1.1.1.1.

2.7.1.3.1.1. Model of Cask Body

The model of the cask body was identical to the model employed for the side impact with the exception of the addition of a series of beam elements at the lower end of the cask to represent the structure within the impact limiter. These beams were very stiff to prevent flexing during an impact and the spars that represent the impact limters were attached to these beams. A sketch of the elements in this model and their relationship is presented in Figure 2-96. The extreme ends of the impact limiter spars were constrained to prevent longitudinal motion but were free to translate to reproduce the effect of the crushing of the

wood in the impact limiter which will always result in forces that are normal to the side or end of the cask body.

The model of the lead slumping was adapted from the calculations performed in the analysis of the end impact in that the hoop stresses resulting from the deformation of the lead were multiplied by the cosine of the impact angle. This approach was selected to represent the reduced gravitational effect upon the lead and resultant reduction in the amount of slumping of the lead. Detailed evaluation of the lead slumping in the analysis of the end impact has shown this approach to be very conservative because a small reduction in the gravitational effect on the lead will nearly eliminate all slumping of the lead because the forces do not cause the lead to become plastic.

2.7.1.3.1.2. Impact Limiter Characteristics

The deformation of the impact limiters during a corner impact is similiar to the deformation encountered in the side and end impacts. The deformation will occur on the outside of the impact limiter until the forces are larger than the forces produced by crushing the interior of the impact limiter. At this point in the impact the deformation will occur at the interior of the impact limiter and the forces produced will be identical to the forces produced during an end and side impact. The sequence of deformations is graphically described in Figure 2-97.

The force deflection curves that have been employed in the evaluation of the corner impact are identical to the force-deflection curves employed in the side and end impacts and presented in Figures 2-78 and 2-60 respectively. The presence of the balsa wood with its grain at 50° to the cask axis presents a stiff member that will leave the deformation to rapidly transition to the interior of the impact limiter and permit the

use of the side and end impact limter representations unaltered. The application of the force-deflection curves in the modeling of the cask body permits each to be effective at retarding the component of motion that is causing the cask to crush that impact limiter.

The energy that is dissipated in the initial impact was calculated by numerically integrating the force-deflection curves for the end and side impact limiters including the relative motion of the cask into both impact limiters. The moments that acted on the cask were also evaluated by considering the impact limiter to be imparting forces to the structure of the impact limiter at the extremities of the gussetted backing plate (45 inch O.D. and 9 inches from the end of the cask body). At the conclusion of the initial impact the cask entered a second free fall region where all of the motion was rotational. During this period the only forces acting on the cask were the support at the impacted end which prevented linear motion and gravity which accelerated the cask until the second impact limiter made contact with the unyielding surface. The velocity at the beginning and end of the free rotation period are presented in Figure 2-98 as a function of the angle of the cask away from vertical at the time of the intital impact. The time required for the free rotation is presented in Figure 2-99 as a function of the initial orientation of the cask. The kinetic energy associated with the beginning and conclusion of the free rotation period are presented in Figure 2-100 which decisively identifies 90o as the worst orientation of the cask at the point of initial impact. The stiffness of the end impact causes more energy to be absorbed during the intital impact so the worst corner impact becomes that orientation where the end impact limiter has the least effect.

2.7.1.3.2. Consequences of Corner and Oblique Drops

Two different impact angles have been evaluated. The first is the result of the cask being at 11.78° from the vertical at the time of impact. The center of gravity is directly over the initial impact point when the cask is in this orientation and it is possible for the cask to remain in this orientation following the conclusion of the impact. The second case represents the worst impact orientation where the center of gravity is not over the impact area and the cask will have to endure a second impact following rotation to a horizontal position.

The characteristic of both of these impacts that makes them very different from the other impacts that have been evaluated is the fact that both the side and end impact limiters absorb energy in these impacts. The beam model described in Section 2.7.1.3.1. was used to determine the bending stresses in the cask during an impact where the cask was 11.78° from the vertical. As in the side impact the parameter that governs the response of the cask is the deflection of the ends and center of the cask during the impact. The time histories of the deflections of the ends and center of the cask are presented in Figure 2-101. The cask deformations and resulting bending stresses are presented in Figures 2-103 and 2-104 respectively. As was discussed in Section 2.7.1.2.2. these bending stresses represent only the outer shell of the cask and the bending stresses in the inner shell are only 45.8% of the stresses presented in Figure 2-104. The maximum bending stresses in the inner and outer shells are presented in Figure 2-105.

The maximum hoop stress in this impact will be 97.9% of the hoop stresses in the end impact resulting in larger margins between the calculated stresses and the stresses required to cause collapse buckling of the inner shell.

As was demonstrated in Section 2.7.1.3.1.2. the oblique drop that will impart the most energy into the cask is an impact where the cask orientation is as close to horizontal as is possible. To provide assurance that an oblique impact will not cause dynamic overstressing of the cask wall, one oblique impact was evaluated where the impact angle was such that the second impact limiter traveled 7.5 inches after the first impact limiter had made contact with the unyielding surface. This particular case was selected because the second impact will occurr at about the time the stress wave reaches the end of the cask and the possibility of reinforcement of the wave is the largest.

As is the side and corner impacts the parameter that governs the response of the cask is the deflection of the ends and center of the cask which are presented in Figure 2-106 and the relative deflection of the center with respect to the lower end is presented in Figure 2-107. The deflection of the entire cask body is presented in Figure 2-108 and the resulting bending stresses are presented in Figure 2-109 as a function of both axial position and time.

In this case as well as the side and corner impacts the stresses in the inner shell are 45.8% of the calculated stresses and the stresses in the outer shell are 97.8% of the calculated stresses. These correction factors have been used to determine the maximum stresses in the inner and outer shells which are presented in Figure 2-110.

In both the corner and oblique impacts the maximum bending stress is less than the maximum bending stress in the side impact and the maximum hoop and axial stress is less than the corresponding stress during an end impact. The limitation on the hoop, axial and bending stresses is the lesser of the buckling stress or the ultimate stress. In this instance buckling is the more restrictive limit for the axial and hoop stresses and the ultimate stress is the more restrictive limit for the bending

stresses. The impact of ovality of the buckling stress is discussed in the following section.

The ultimate stress for dynamically loaded stainless steel is 150,000 psi based upon the data presented in Section 2.3.1.2. This limit is substantially larger than the maximum bending stress in the corner impact which is 25,200 psi and the maximum bending stress in the oblique impact where the maximum bending stress in the inner shell is 43,100 psi and 91,500 psi in the outer shell. The margin between the hoop and axial stresses and the stresses required to cause buckling is larger than the corresponding margin in the end impact so there will be no possibility of failure of the containment boundary by buckling.

2.7.1.3.3. Effect of Cavity Irregularity

The analyses presented in the previous section presume that both shells are perfect cylinders. The outer shell is very nearly a perfect cylinder; however, the inner shell is subject to dimensional variations which could enhance the possibility of buckling. Consequently, it is necessary to determine the impact of dimensional variations and the maximum allowable variations.

The effect of ovality of the inner shell has been identified in Section 2.7.1.2.3. and applies to this analysis as well. The factor that increases the maximum bending stress to account for ovality of the inner shell is presented in Figure 2-84 and it has been applied to the maximum bending stress in the inner shell that is presented in Figure 2-105 to determine the maximum bending stress as a function of position and ovality that is presented in Figure 2-111. Superimposed upon this figure is the bending buckling limit that was determined in Section 2.1.2.2.1 and presented in Figure 2-3. The two surfaces do not intersect and are not close so there will be no possibility of buckling of

the cask due to bending.

The margin between the hoop stresses and the stresses required to cause collapse type buckling are larger in this corner drop than the margin identified in the end impact so there is no possibility of this type of buckling. An important element in this conclusion is that the location where collapse type buckling and bending type buckling are most likely to occur are very different. This eliminates any possibility of interaction of the two types of buckling failure.

2.7.1.4. Summary of Results

The NAC-1 cask is fully capable of withstanding the rigors of a thirty foot free fall without loss of its ability to maintain its containment boundary. The analyses of the fall when the impact is on an end shows that the stresses induced in the cask wall are all below the stresses that are required to cause buckling provided that the inner shell is less than 2% oval at its extremity and less than 10% oval over the remainder of the length of the shell. A fall where the impact is on the side of the cask produces stresses that are below the limiting ultimate stress. When the impact is on a corner of the impact limiter the stresses induced in the cask have been shown to be less than the stresses in either the end or side impacts. This is true when the impact orientation is such that the cask remains stationary after impact or freely rotates to a second impact because the center of gravity was not vertically over the impact area.

2.7.2. Puncture

The accident scenario that is delineated in Appendix B of Part 71 of Title 10, Chapter 1 of the Code of Federal Regulations (Reference 2.2) requires that all transportation packages be proven to suffer no loss of containment as a result of a free fall through forty inches onto the end of a mild steel pin. The orientation of the cask at the time of impact is to be such that the worst damage is inflicted on the cask. There are three locations where the impact could possibly violate the containment. These are:

Direct Impact on a Valve
Direct Impact on the Relief Valve
Impact on Midspan of the Cask Body

An impact at any other point will have much less severe consequences and need not be considered. Each of these three points of impact are considered in the following sections.

2.7.2.1. Impact on a Valve

There are three valves that are connected to the cavity of the cask by holes drilled in the end castings. These valves are recessed in both end castings and further protected by rings welded to the end casting. Each valve is covered to prevent contamination during shipping or handling.

The analysis of the impact of the cask on a pin consists of two phases. The first is the evaluation of the valve protection ring to provide assurance that the impact does not damage the valve and cause a loss of containment. The second is the evaluation of the bending of the cask body as a result of the impact on one end

of the cask. The failure criteria are different for these two portions of the analysis. There is no limit on the stresses in the first portion of the analysis other than the elimination of a component whenever the stresses reach the ultimate stress and fracture is predicted. The object of the analysis in this instance is to prove that there is no impact on the valve body or its appendages which could cause damage to the internal seals within the valve. The limitations on the second part of the analysis are identical to the limitations for the 30 foot free fall where the stresses cannot exceed the ultimate stress or produce buckling.

2.7.2.1.1. Analysis Model

A portion of the end casting that surrounds the valve and the protective ring have been modelled as axisymmetric cylinders. The model included the inner shell of the impact limiter and the cover that protects the valve during shipment. A graphic representation of the model is shown in Figure 2-113.

The impacting pin was represented as a rigid body with a relative velocity between the pin and the cask body of 175.7 inches per second. This corresponds to a free fall through a distance of forty inches with no credit taken for air resistance.

The second model that is required to determinethe response of the cask to the impact on a pin is a beam representation of the outer shell that is identical to the model employed for the analysis of the side impact following a thirty foot free fall which is described in Section 2.7.1.2.1. One mass-less spar was replaced by a condition where the displacement history of the cask end was specified while the other end of the cask retained its spar to represent the response of the impact limiter.

2.7.2.1.2. Stresses and Deformations

The deformations that result from the impact of the cask onto the pin were determined with the axisymmetric model described in the previous section. The resulting deformations at selected points in time are presented in Figure 2-114. In each of these figures the deformed geometry is reproduced as calculated.

The maximum penetration of the pin into the combined cover and protecting ring is 0.5 inches which is less than the 0.6 inch minimum clearance between the end of the quick disconnect fitting that is attached to each valve. The calculated deformations indicate that the bolted cover will remain symmetrically located over the protecting ring and will not deform into the cavity that is provided for the valve. Consequently, the pin does not impact on the valve or any of its appendages and no part of the protective material is forced into the valve so there is no reason to expect any loss of sealing capability of the valve.

The impact of the cask on the unyielding surface following the impact on the pin was evaluated by determining the displacement-time history of the impacted end of the cask from the previous calcualtions of the deformation of the valve. This data is presented in graphical form in Figure 2-115 and was used as input to the beam model of the cask to describe the motion of one end of the cask. The other end of the cask was allowed to impact on an unyielding surface when the deformation of the valve protecting ring was complete.

As in the remainder of the side and corner impacts deflections of the ends and center of the cask are important fc. determining the response of the entire cask. The time histories of the deflections of the ends and center are presented in Figure 2-116. The deflections of the entire cask are presented in Figure 2-118 and the resulting bending stresses are presented in Figure

2-119. Since these stresses are substantially lower than the stresses calculated for the oblique impact following a thirty foot free fall there is no need to evaluate the stresses in the respective shells and compare these stresses to the ultimate stress and the stresses that will cause buckling in bending.

2.7.2.2. Impact on Relief Valve

The impact of the pin on the relief valve rather than a drain or vent valve is a less severe accident. The impact of the pin will not impact on the relief valve or the check valve attached to the relief valve because the valves are totally recessed within the end casting. Consequently, there is more metal to retard the penetration of the pin and limit the intrusion of the pin prior to impact on the valve.

The second portion of the analysis that evaluates the stresses in the cask body as a result of the impact on the pin is unchanged because the relief valve and the vent valves are identically located along the cask (at different angles relative to the trunnions).

2.7.2.3. Impact on Cask Body

The impact of the cask body onto a six inch diameter pin will cause the cask to bend without the aid of an impact limiter because the impact can occurr at any location along the cask body. The bending will be maximized if the impact is at the midpoint of the cask so that the cask motion will be totally arrested by the impact and all of the energy transformed into deformation of the cask or bending of the body. An impact at any other position along the cask body will allow a portion of the

cask energy to be transformed into rotation with the resultant reduction of the damage to the cask.

The analysis of the impact of the cask on a pin consists of two phases. The first is the evaluation of the outer and inner shells with the lead to provide assurance that the impact does not damage the cask wall and cause a loss of containment. The second is the evaluation of the bending of the cask body as a result of the impact on the cask. The failure criteria are different for these two portions of the analysis. There is no limit on the stresses in the outer shell because this shell is expected to be damaged. However, the inner shell must not experience stresses that exceed the ultimate stress as a result of either the direct impact or the bending that follows.

2.7.2.3.1. Analysis Model

The model of the cask body consisted of a unit depth representation of the cross section of the cask near the midpoint of the cask. The outer shell and the lead were modeled as elastic-plastic materials while the inner shell was modeled as an elastic material to conform to the stress limitations identified in Section 2.1. A graphic representation of the model is presented in Figure 2-121.

The impacting pin was represented as a rigid body with a width of six inches and a unit depth to correspond to the remainder of the model. This representation of the geometry is very conservative because no credit is taken for the strength of the material that is adjacent to the impact point. Inclusion of this material would have required a three-dimensional model and would have reduced the predicted deformation of the outer shell.

The relative velocity between the pin and the cask body was 175.7

inches per second which corresponds to a free fall through a distance of forty inches with no credit taken for air resistance.

The second model that is required to determine the response of the cask to the impact on a pin is a beam representation of the outer shell that is identical to the model employed for the analysis of the side impact following a thirty foot free fall which is described in Section 2.7.1.2.1.

2.7.2.3.2. Stresses and Deformations

The deformations that result from the impact of the cask onto the pin were determined with the two dimensional model described in the previous section. The resulting deformations and stress contours at selected points in time are presented in Figure 2-122. In each of these figures the deformed geometry is not to scale because the deformations have been enlarged for clarity. The maximum plotted deformation is the same in each of the figures.

The deformation of the center of the cask body was used as input to the beam model of the cask to describe the motion of the center of the cask. The deflection history of the center of the cask is presented in Figure 2-123.

As in the remainder of the side and corner impacts the deflections of the ends and center of the cask are important for determining the response of the entire cask. The time histories of the deflections of the ends and center are presented in Figure 2-124. The deflections of the entire cask are presented in Figure 2-126 and the resulting bending stresses are presented in Figure 2-127.

In this case as well as the side and corner impacts the stresses

in the inner shell are 45.8% of the calculated stresses and the stresses in the outer shell are 97.8% of the calculated stresses. These correction factors have been used to determine the maximum stresses in the inner and outer shells which are presented in Figure 2-128.

The limitation on the hoop and bending stresses is the lesser of the buckling stress or the ultimate stress. In this instance the ultimate stress is the more restrictive limit for the bending stresses. The impact of ovality of the buckling stress is discussed in the following section.

The ultimate stress for dynamically loaded stainless steel is 150,000 psi based upon the data presented in Section 2.3.1.2. This limit is substantially larger than the maximum bending stress in this impact where the maximum bending stress in the inner shell is 43,100 psi and 91,500 psi in the outer shell.

2.7.2.3.3. Effect of Cavity Irregularity

The analyses presented in the previous section presume that both shells are perfect cylinders. The outer shell is very nearly a perfect cylinder; however, the inner shell is subject to dimensional variations which could enhance the possibility of buckling. Consequently, it is necessary to determine the impact of dimensional variations and the maximum allowable variations.

The effect of ovality of the inner shell has been identified in Section 2.7.1.2.1. and applies to this analysis as well. The factor that increases the maximum bending stress to account for ovality of the inner shell is presented in Figure 2-84 and it has been applied to the maximum bending stress in the inner shell that is presented in Figure 2-128 to determine the maximum bending stress as a function of position and ovality that is

presented in Figure 2-129. Superimposed upon this figure is the bending buckling limit that was determined in Section 2.1.2.2.1 and presented in Figure 2-6. The two surfaces do not intersect and are not close so there will be no possibility of buckling of the cask due to bending.

2.7.3. Thermal

The accident scenario that is delineated in Appendix B of Part 71 of Title 10, Chapter 1 of the Code of Federal Regulations (Reference 2.2) requires that all transportation packages be proven to suffer no loss of containment as a result of exposure to a fire of one half hour duration with no artificial cooling to be applied until at least three hours after the termination of the fire. The elevated temperatures will create thermal stresses as a result of the thermal expansion.

2.7.3.1. Summary of Pressures and Temperatures

The cask temperatures have been calculated when the cask is exposed to a one-half hour fire with the surface blackened by the fire to produce an emissivity of 0.8. Prior to the start of the fire, the cask was assumed to have equilibrated while the ambient temperature was 130° F, in direct sunlight with the cask stationary. The results of this analysis is reported in Section 3.5 of this report.

The calculated temperature distributions are summarized in Figures 2-130 and in Table 2-25. The stresses induced by the fire must be evaluated to assure that no loss of containment will result from the fire.

2.7.3.2. Differential Thermal Expansion and Stresses

The model for the calculation of the thermal stresses during the fire portion of the hypothetical accident is identical to the model employed for the analysis of the thermal stresses resulting from either of the extreme environmental conditions. The details of the model are described in Section2.6.1.2 and will not be repeated here.

The analysis of the consequences of the fire was based upon the assumption that the impact limiters were intact because that provided the largest surface area for heat to be transferred from the fire to the cask body.

The stresses that result from the temperature distributions during the fire at five specific times are presented in Figure 2-131 to 2-134. The time dependence of the radial, hoop and axial stresses are summarized in Figures 2-135 to 2-137 respectively. The major consequence of the fire is to relieve the thermal stresses in the cask that remain following the contraction of the lead following the lead pouring operation during manufacture.

2.7.3.3. Comparison with Allowable Stresses

The thermal stresses that are produced by the fire are considered to be primary stresses because they primarily result from the interaction of adjacent components, namely the lead and the inner shell. The portion of the thermal stresses that are the result of only the temperature gradients within the components are secondary stresses because they are both self limiting and not opposed by any external forces acting on the component involved. The stresses that arise from the thermal gradients are small compared to the stresses due to the contraction of the lead onto

the inner shell; consequently, all of the thermal stresses will be considered as primary stresses.

The thermal stresses are additive to the stresses that are present in the cask at the time of the fire. The sequence of events in the hypothetical fire dictates that the impact accidents have concluded so the only stresses that are present at the time of the fire are the result of the pressure in the cavity. At the conclusion of the fire the cavity pressure is 824 psia. The stresses in the inner and outer shell as a result of this pressure are calculated based on the expressions for the stresses in a thin walled pressure vessel which are:

$$\sigma_r = (P_o - P_i) \qquad h = (P_o - P_i)r / 2t$$

and

$$\sigma_z = (P_o - P_i)\, D_c^2 / (D_{i1}^2 - D_{i2}^2 + D_{o1}^2 - D_{o2}^2)$$

where:

P_o and P_i are the external and internal pressures
r is the mean radius of the shell
t is the thickness of the shell
D_c is the diameter of the cavity
D_{i1} is the outside diameter of the inner shell
D_{i2} is the inside diameter of the inner shell
D_{o1} is the outside diameter of the outer shell
D_{o2} is the inside diameter of the outer shell
σ_r is the radial stress
σ_h is the hoop stress
σ_z is the axial stress

The expression for the axial stress is based upon the condition that both shells will be loaded because the pressure is acting on the end castings which are sufficiently rigid that they will distribute the load.

The maximum thermal stresses occur 5 minutes after the

conclusion of the fire when the cavity pressure is 178 psi. Introducing this pressure gives the following stresses:

σ_r = 824 psi
σ_h = 18,210 psi
σ_z = 928 psi

These stresses are additive to the thermal stresses that are presented in Figures 2-124 giving the following total stresses:

σ_r = 1,072 psi
σ_h = 19,043 psi
σ_z = 36,006 psi

After four hours the cavity pressure reaches its maximum value of 824 psi and the maximum thermal hoop stress is 4,800 psi. When combined with the stress due to the cavity pressure the total hoop stress is 23,000 psi which is also below the limiting stress. The time and position dependent stresses presented in Figures 2-135, 2-136 and 2-137 demonstrate that these two conditions represent the worst possible combinations of pressure and thermal stresses and they are all well below the limiting stress.

The limit that was identified in Table 2-3 for accident conditions requires the primary membrane stresses to be less than the lesser of 2.4 times the design stress intensity or 0.7 times the ultimate stress. Since the thermal stresses and pressure stresses develope slowly the limits are based upon static properties of stainless steel as described in Section 2.3.1.1. The design stress intensity is 17,200 psi and the ultimate stress is 68,500 psi at 500°F. Consequently, the limiting stress is 41,280 psi and the maximum primary membrane stress is substantially below this limit.

2.7.4. Water Immersion

The submersion of the NAC-1 cask into a large body of water will have no effect upon the structural behavior of the cask because the stainless steel and water do not interact in a manner that will reduce the strength of the stainless steel (Reference 2.19).

2.7.5. Summary of Damage

The damage that is done to the NAC-1 cask during the hypothetical accident is minimal and does not diminish its ability to maintain the containment boundary. The thirty foot fall or the fall onto the pin will cause the failure of the shield tank and resultant loss of the neutron shielding however, the gamma shielding and the cavity water will remain intact to provide a portion of the shielding. The fall onto the pin will plastically deform the portion of the cask but the deformation will be highly localized and the remainder of the cask will suffer bending which will not result in any failure of the stainless steel shells.

The calculated stresses including the maximum stress intensities are summarized in Section 2.1, Table 2-1 and Figure 2-2. The stress levels are all within the allowable stresses for pressure vessels so there will be no loss of containment during the entire hypothetical accident.

Table 2-25. Maximum Temperatures During Fire Accident

Component	Temperature After Fire (deg F)	Temperature 3 hours after fire (deg F)	Maximum Temperature (deg F)
cavity water	352	514	514
lead	452	462	510
valves			
relief	336	502	505
upper vent	345	491	495
lower vent	344	489	493
upper drain	316	466	486
lower drain	312	460	480
O-rings			
inner	352	509	509
outer	387	514	514
Maximum internal pressure		824 psia	

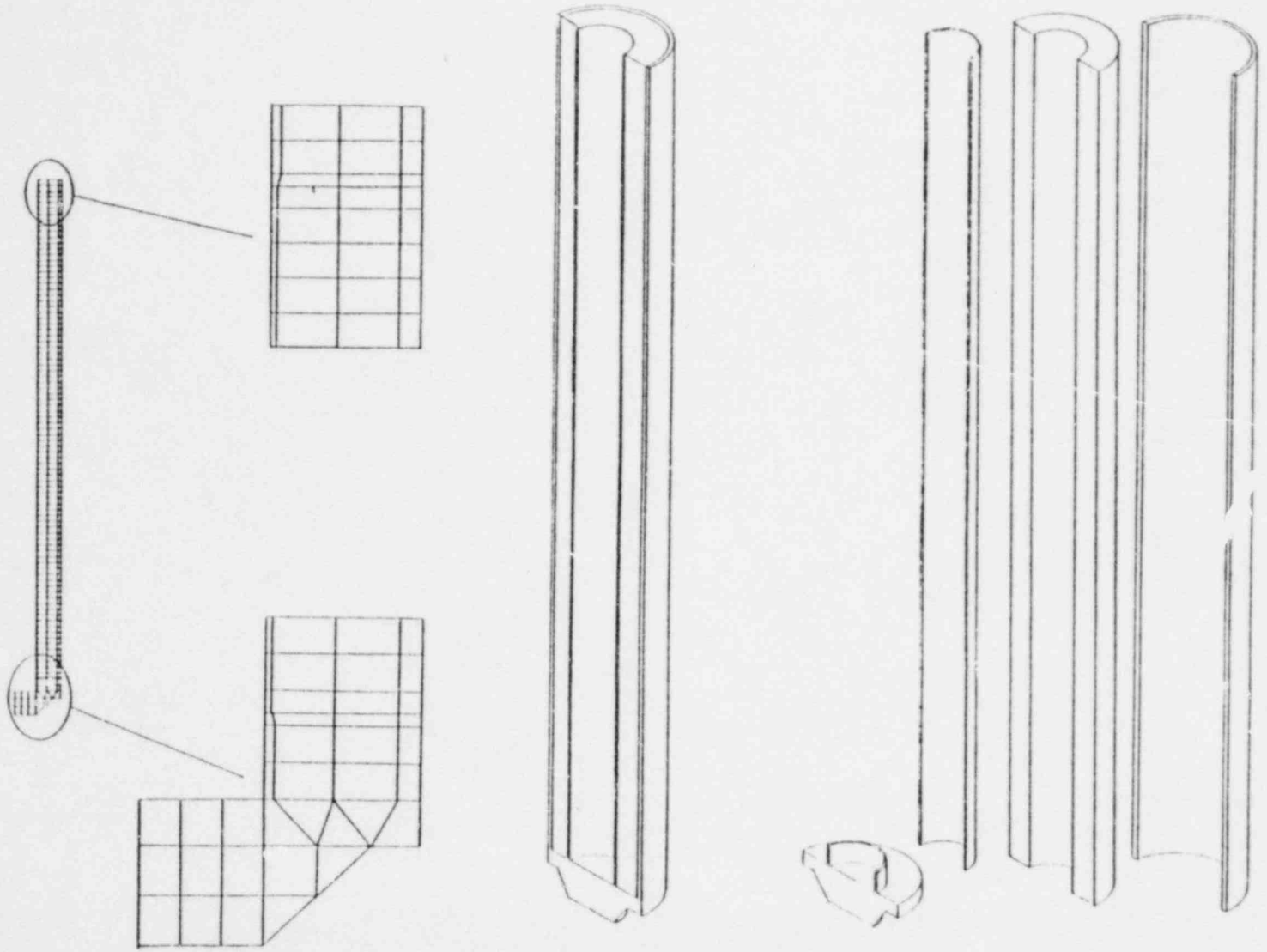

Figure 2-68. ANSYS Model for End Drop

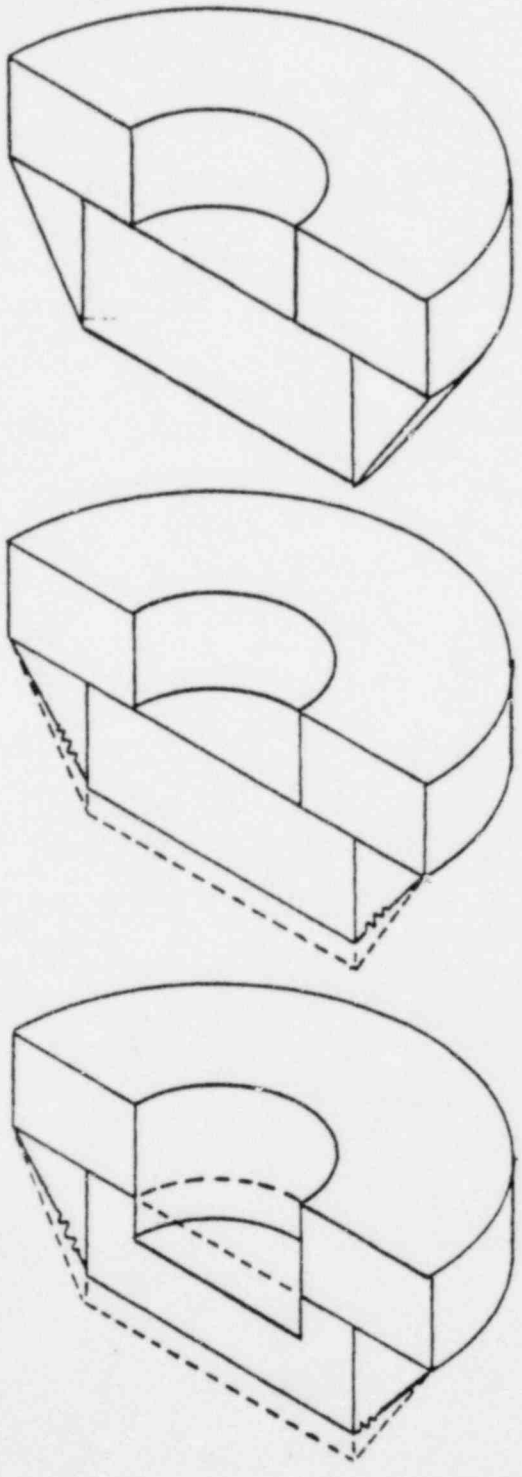

Figure 2-69. Crush Dynamics During End Drop

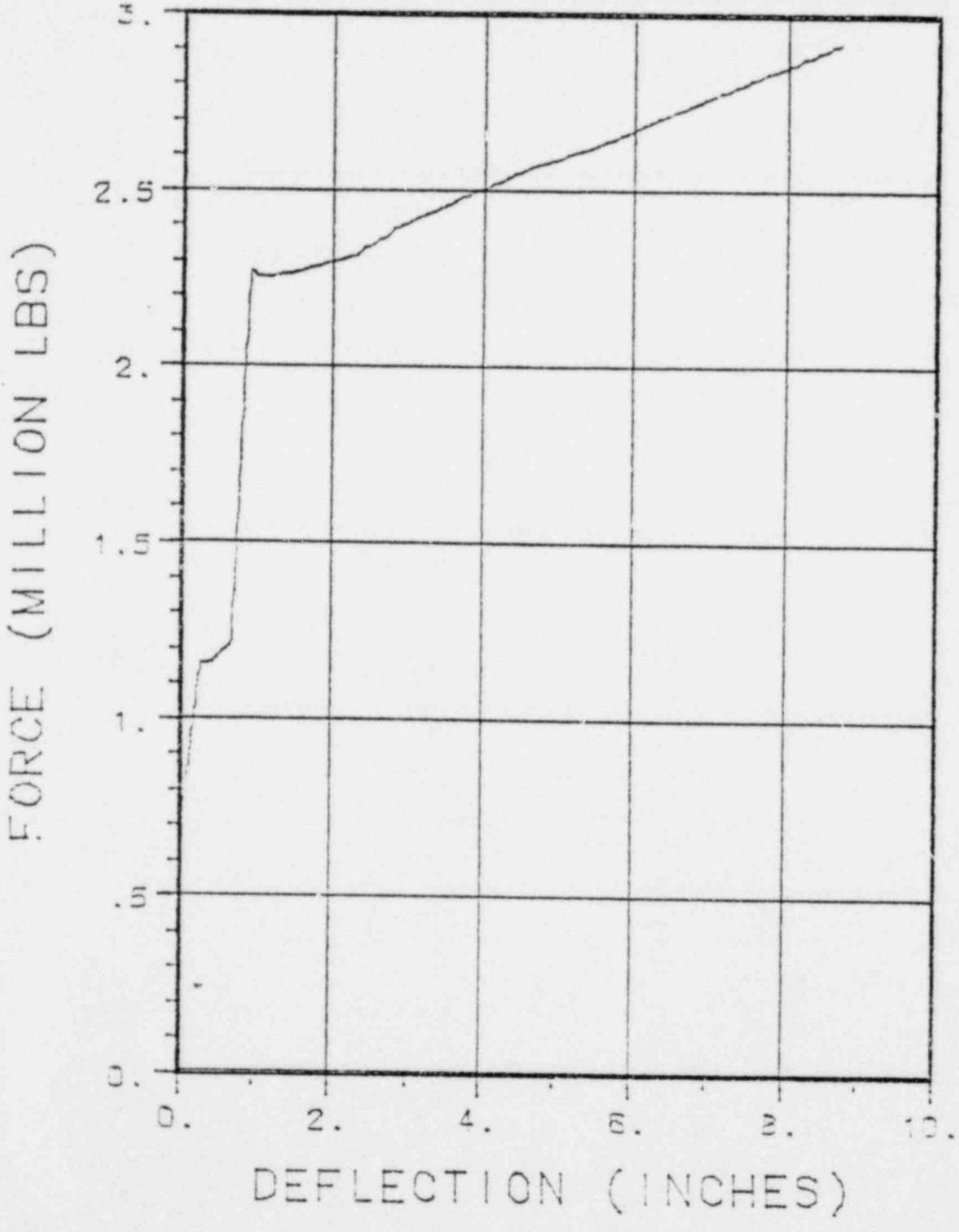

Figure 2-70. Force-Deflection Curve for End Impact Limiter

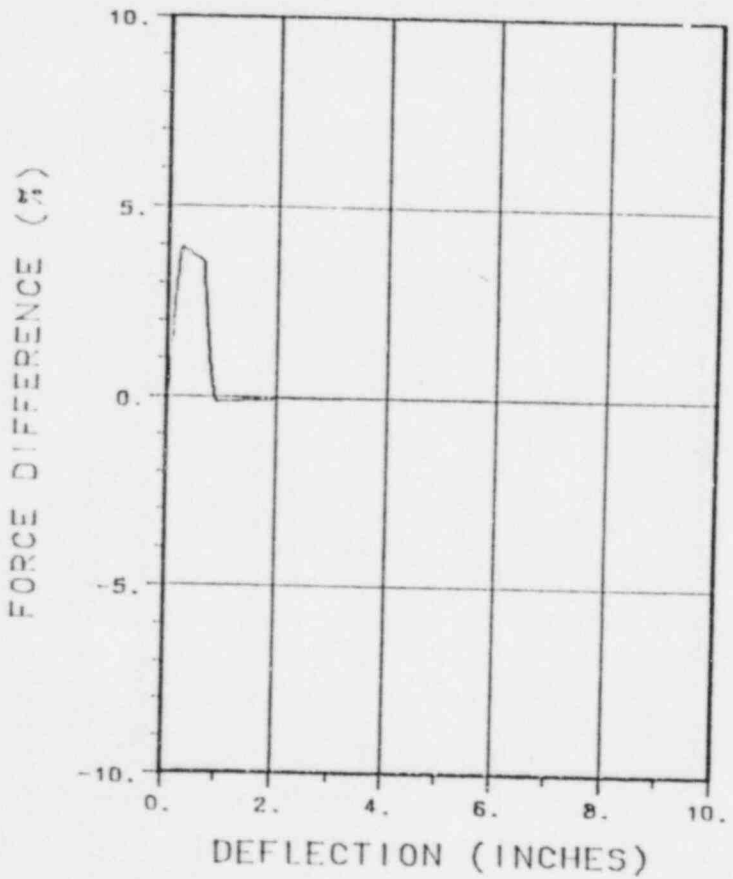

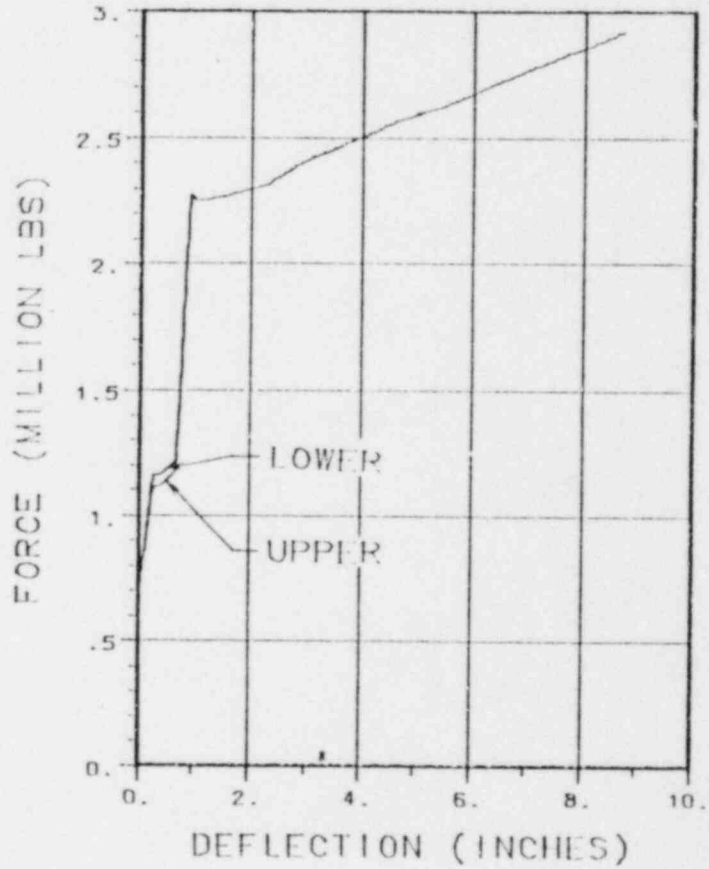

Figure 2-71. Comparison of Upper and Lower Impact Limiters

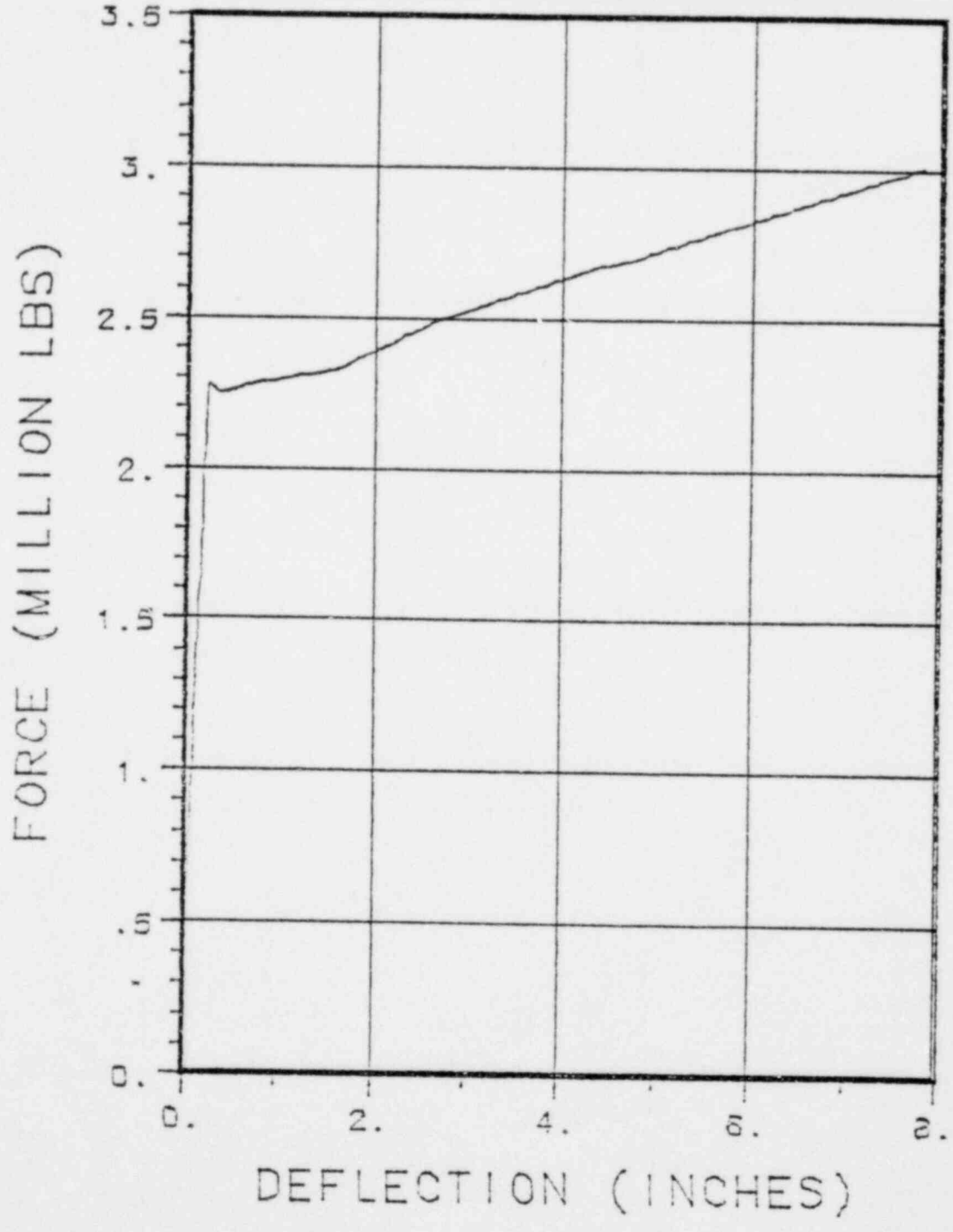

Figure 2-72. Force-Deflection Curve for Deformed Impact Limiter

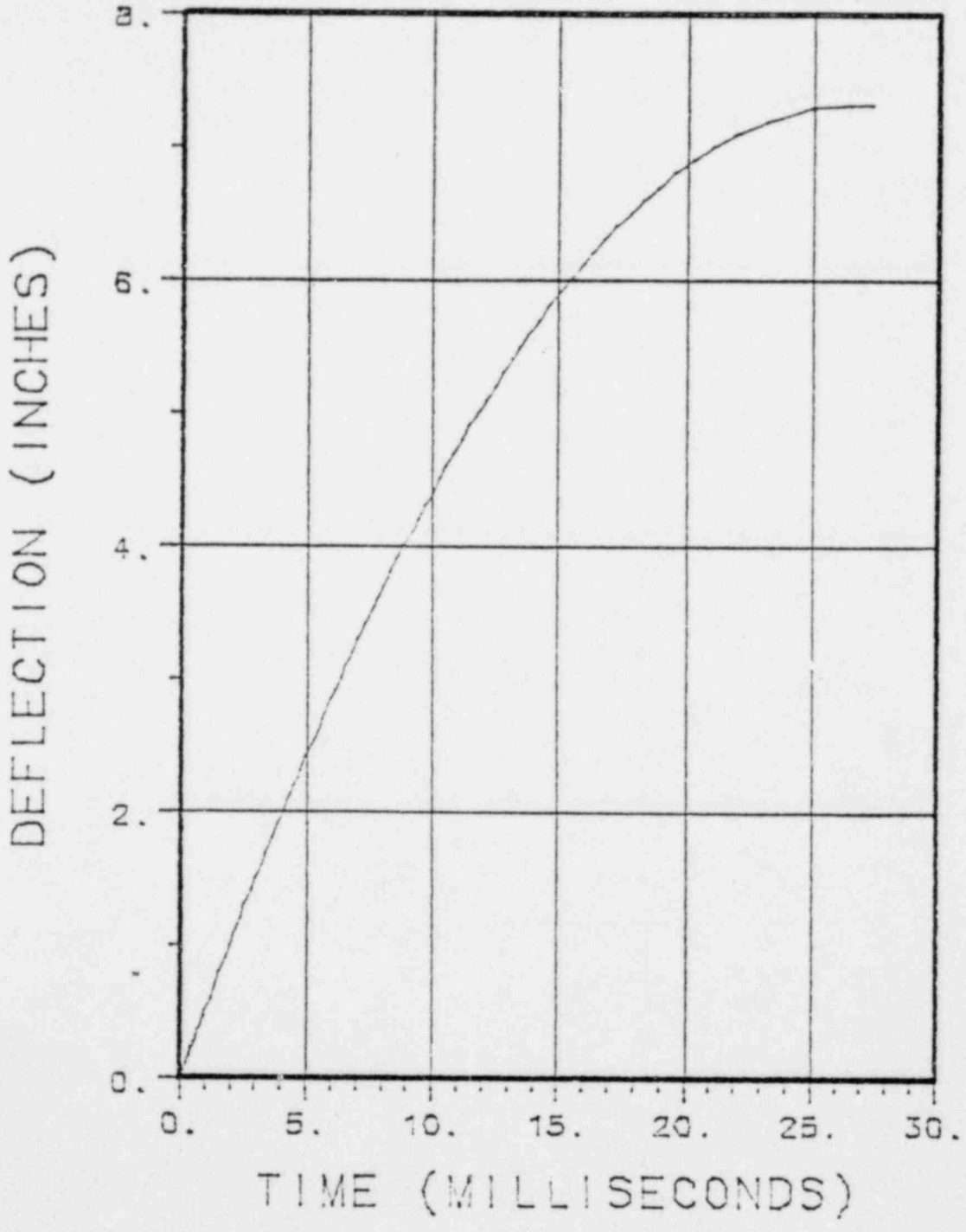

Figure 2-73. Deflection of Lower End of Cask

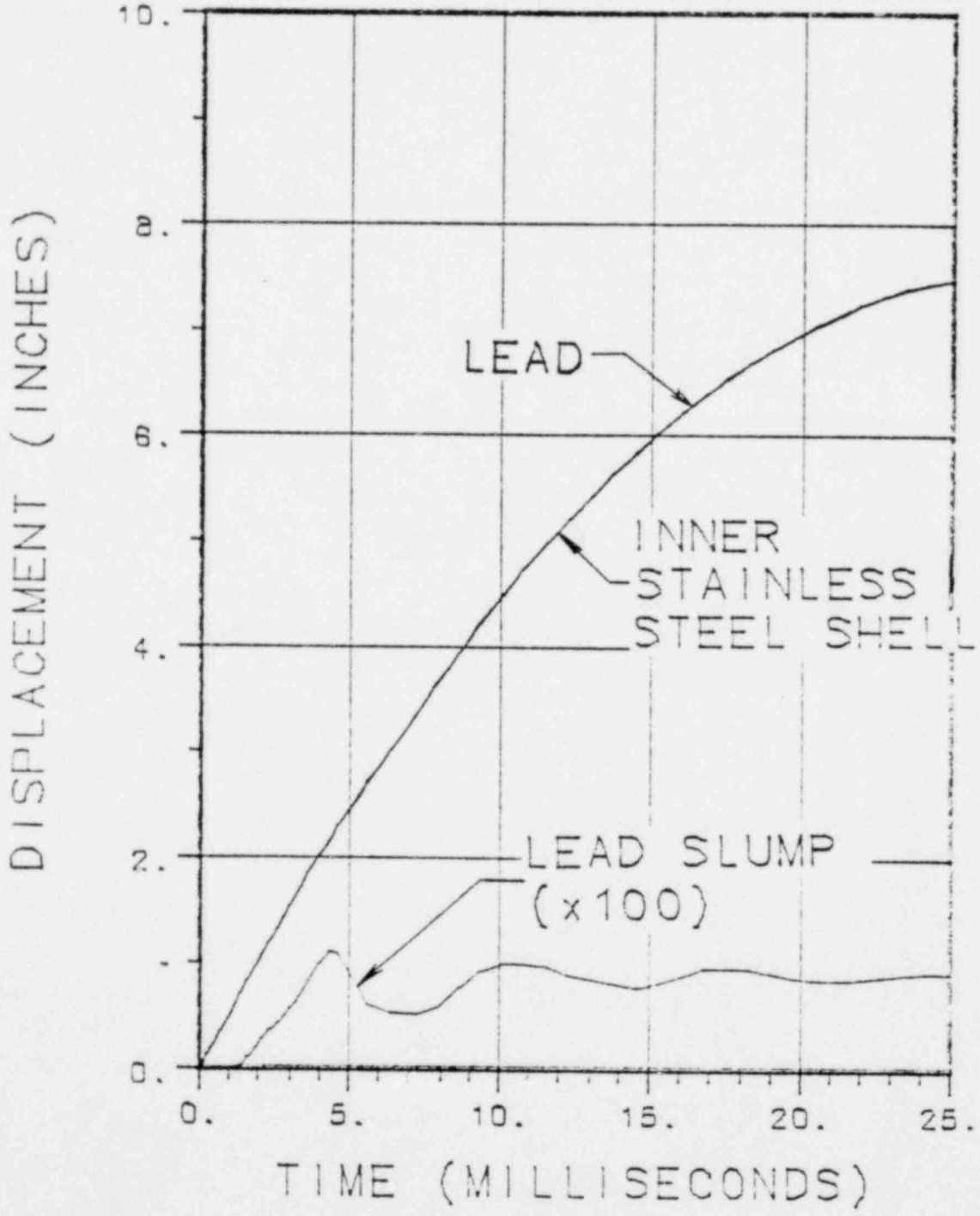

Figure 2-74. Deflection of Lead

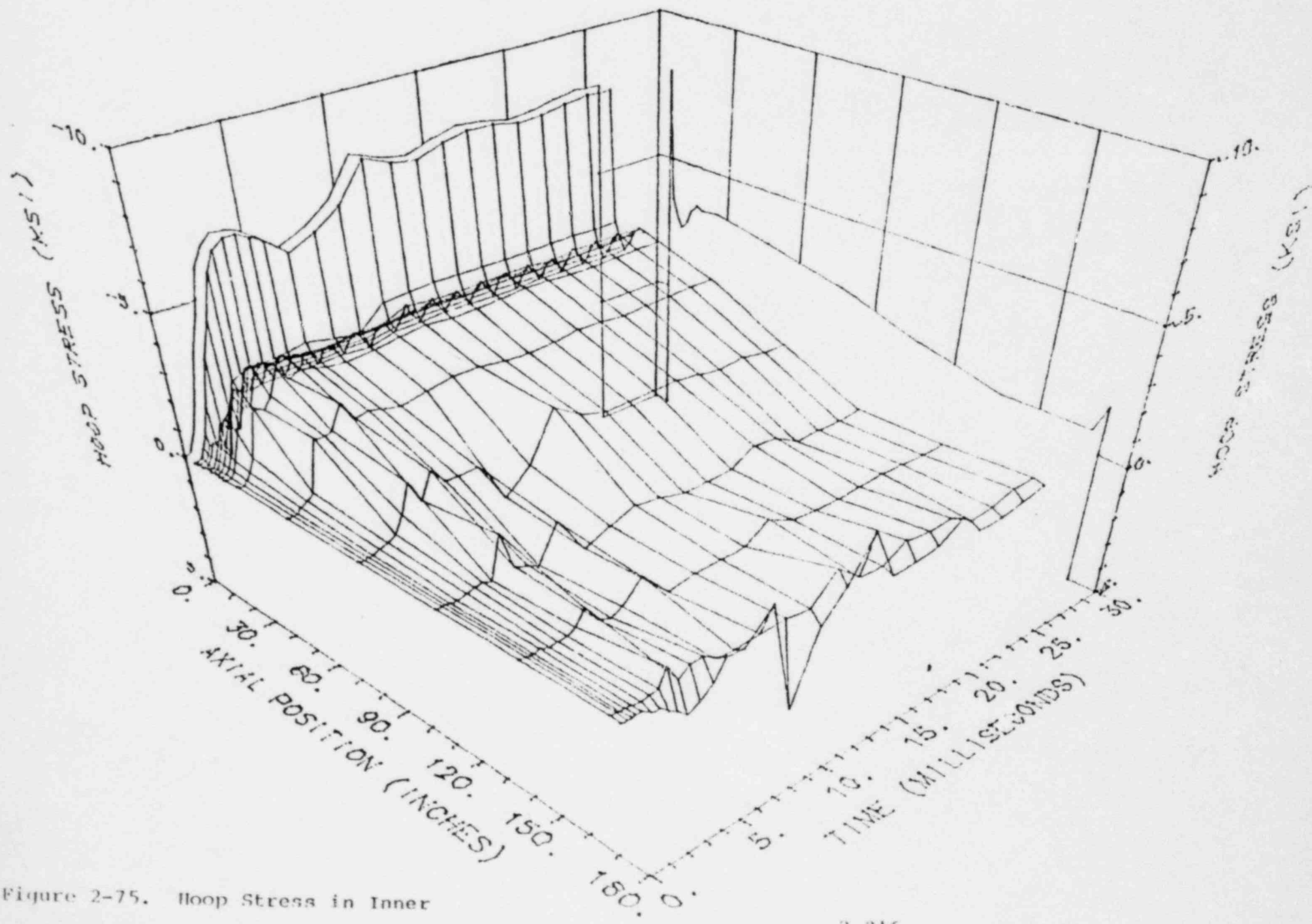

Figure 2-75. Hoop Stress in Inner Shell During End Impact

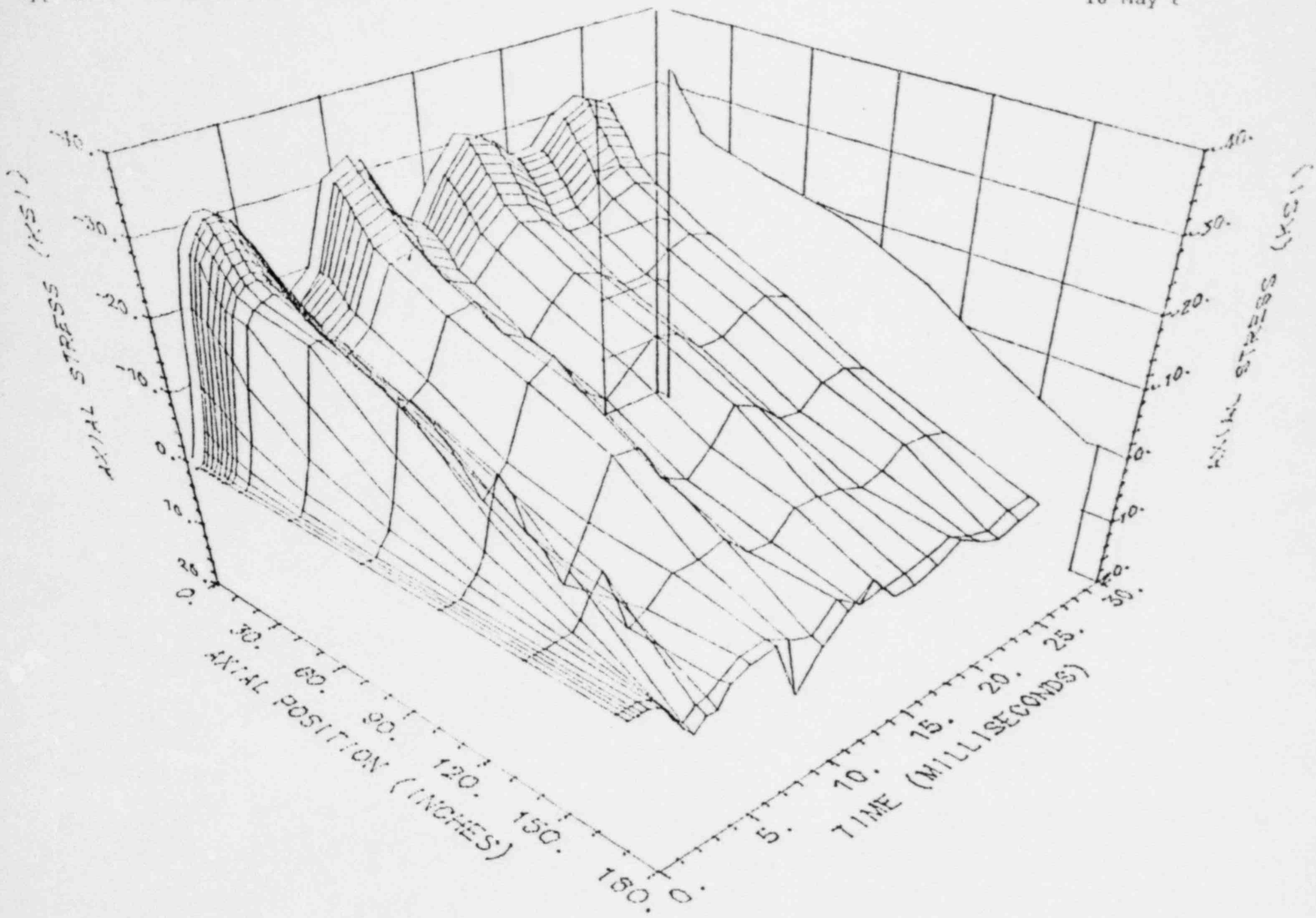

Figure 2-76. Axial Stress in Inner Shell During End Impact

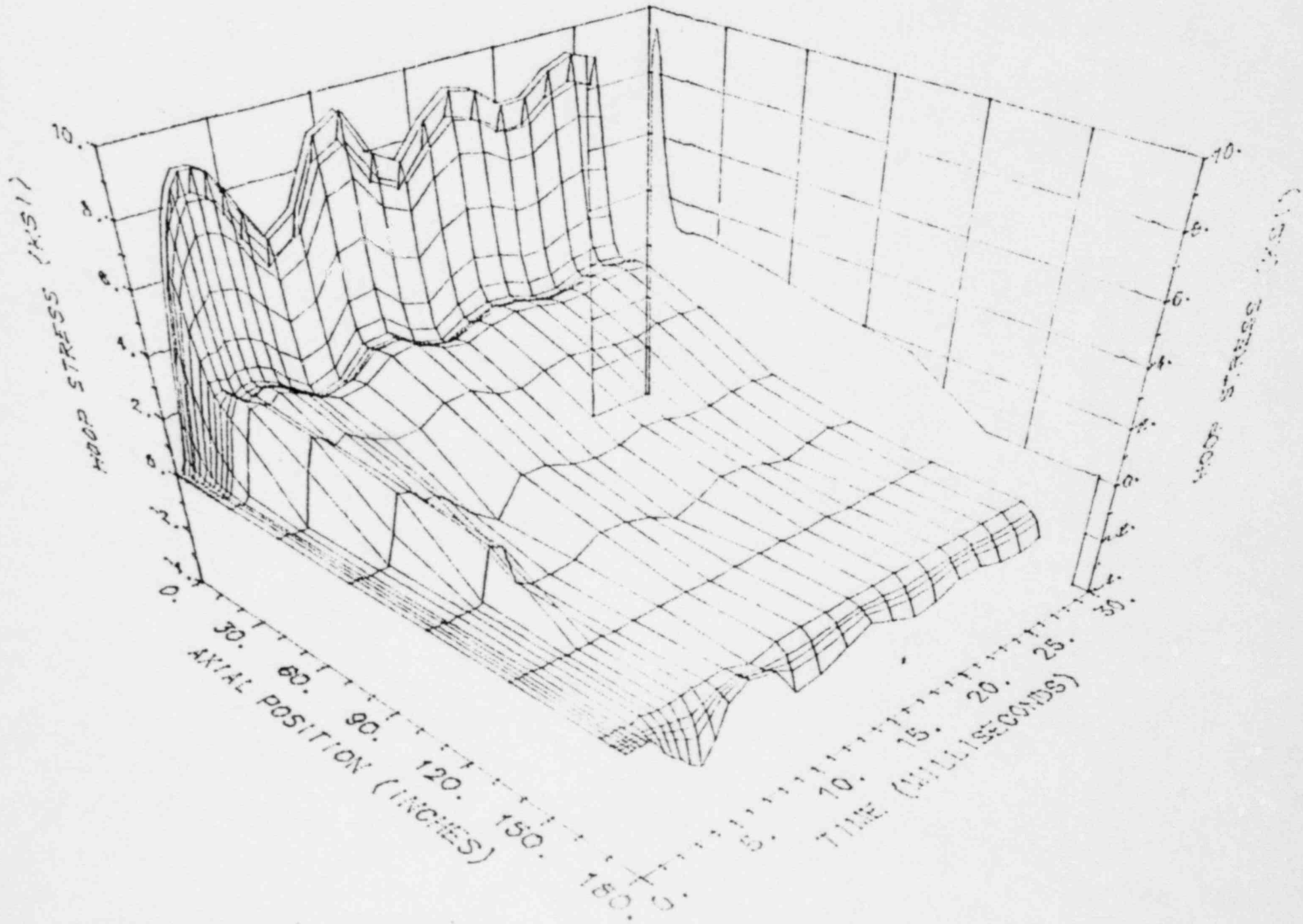

Figure 2-77. Hoop Stress in Outer Shell During End Impact

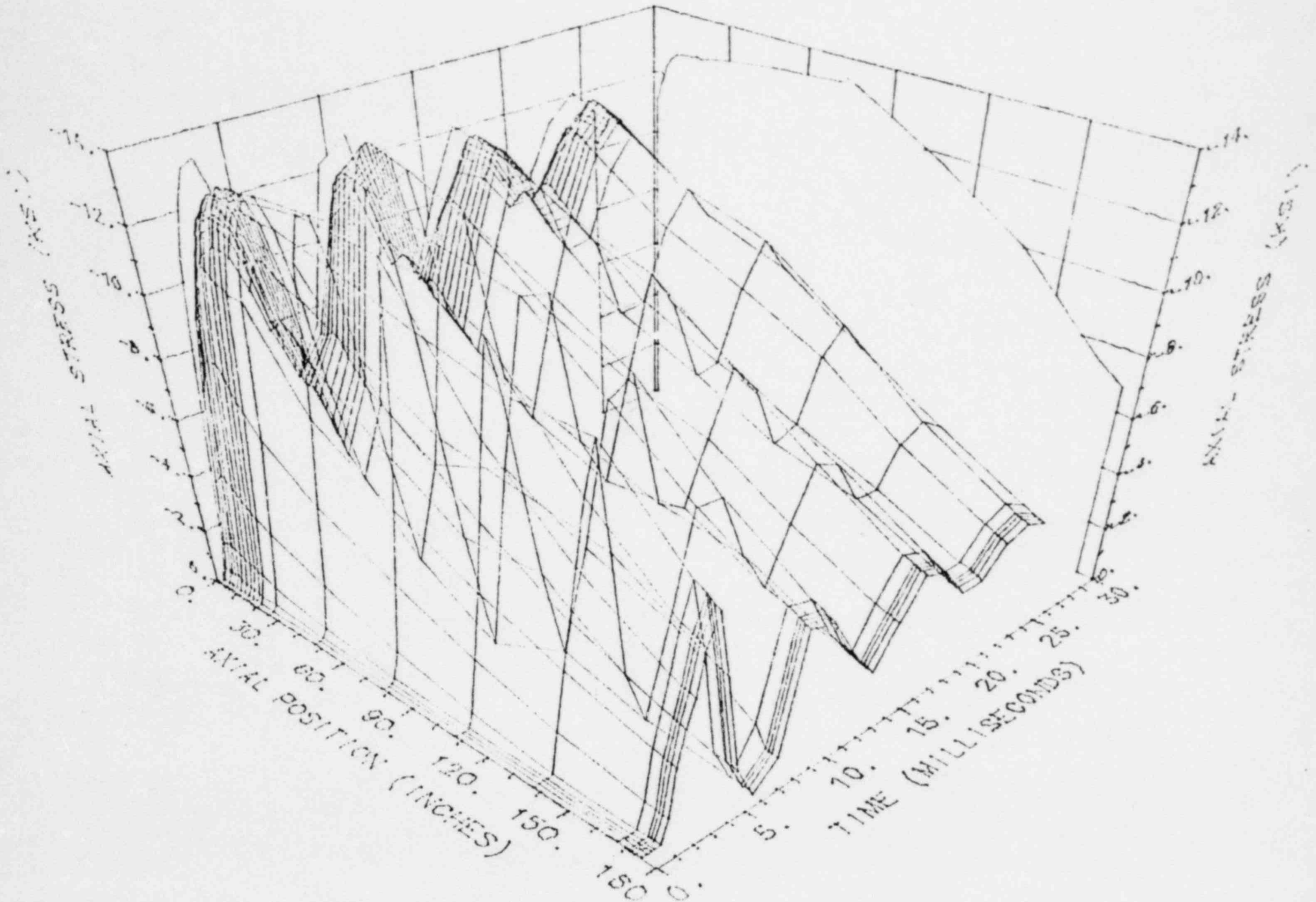

Figure 2-78. Axial Stress in Outer Shell During End Impact

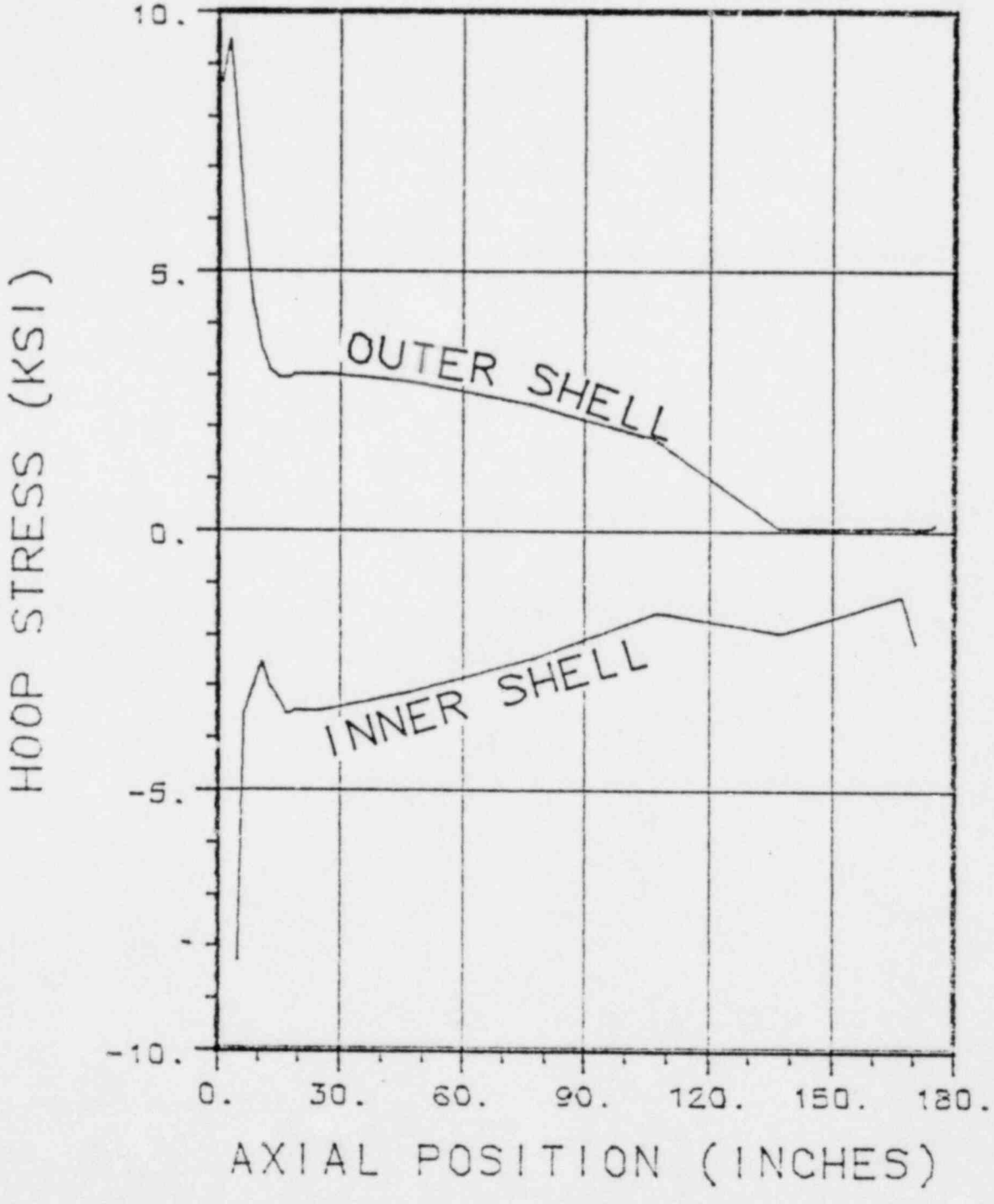

Figure 2-79. Maximum Hoop Stress During End Impact

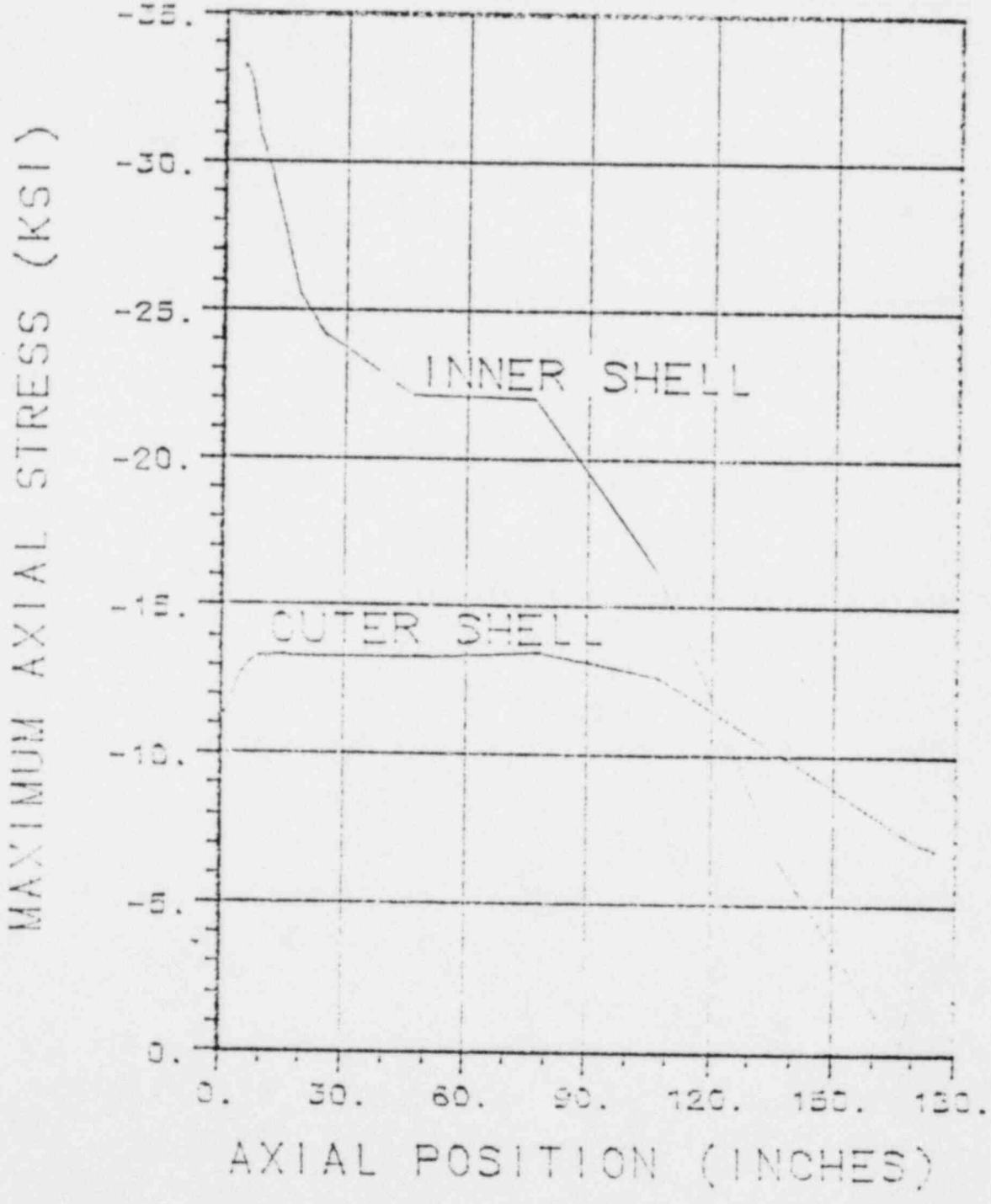

Figure 2-80. Maximum Axial Stress During End Impact

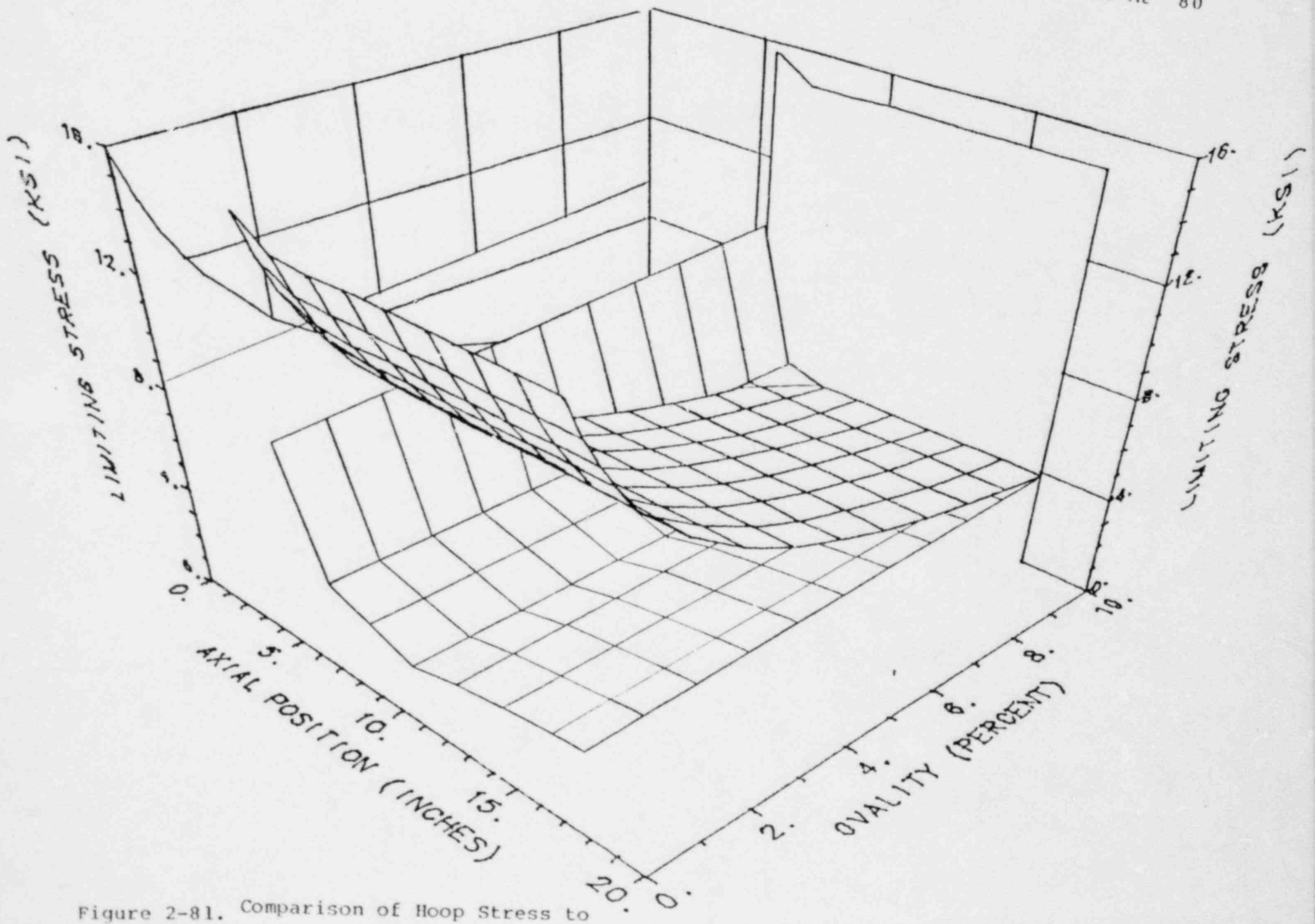

Figure 2-81. Comparison of Hoop Stress to Buckling Limit

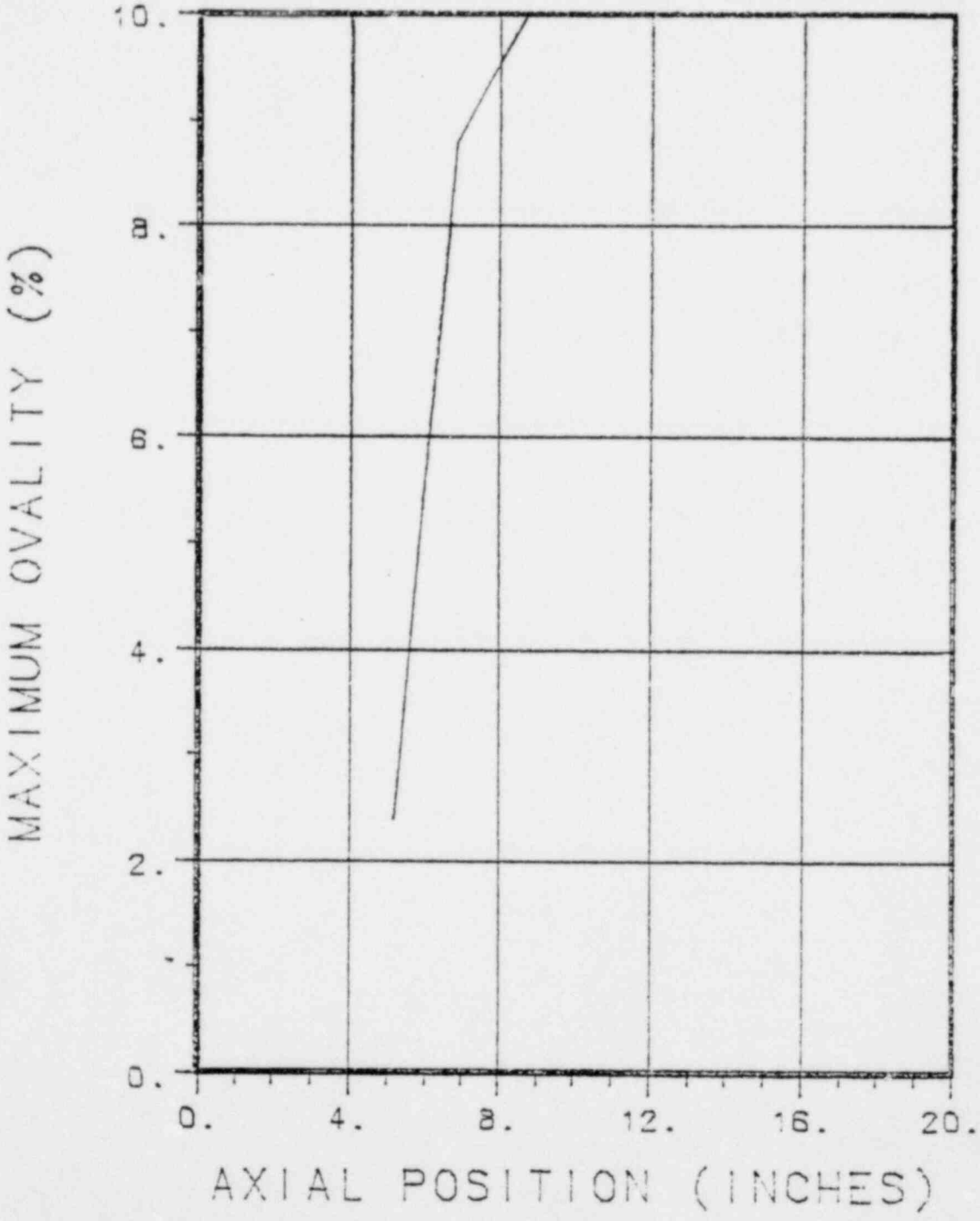

Figure 2-82. Maximum Ovality

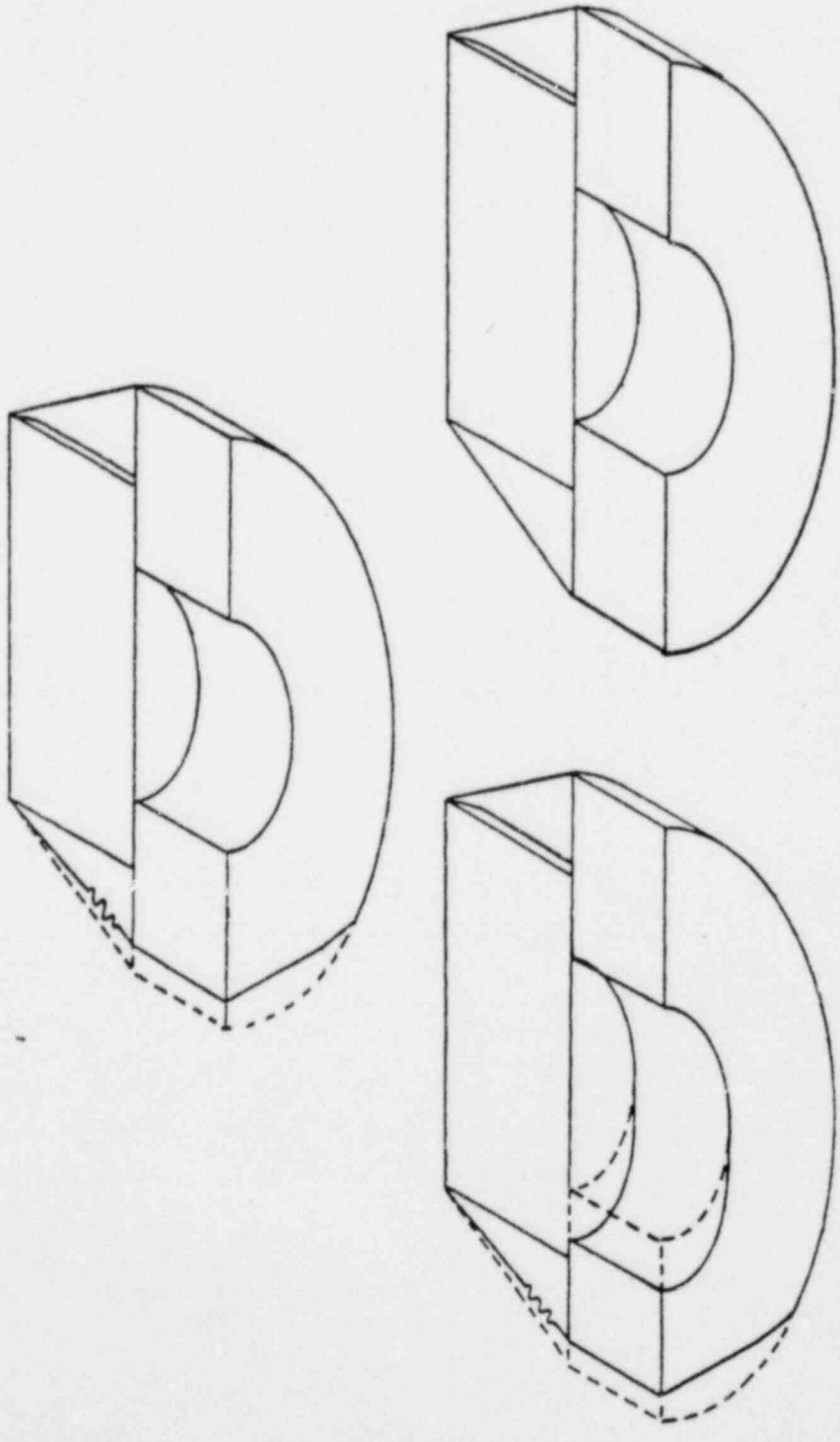

Figure 2-83. Crush Dynamics During Side Impact

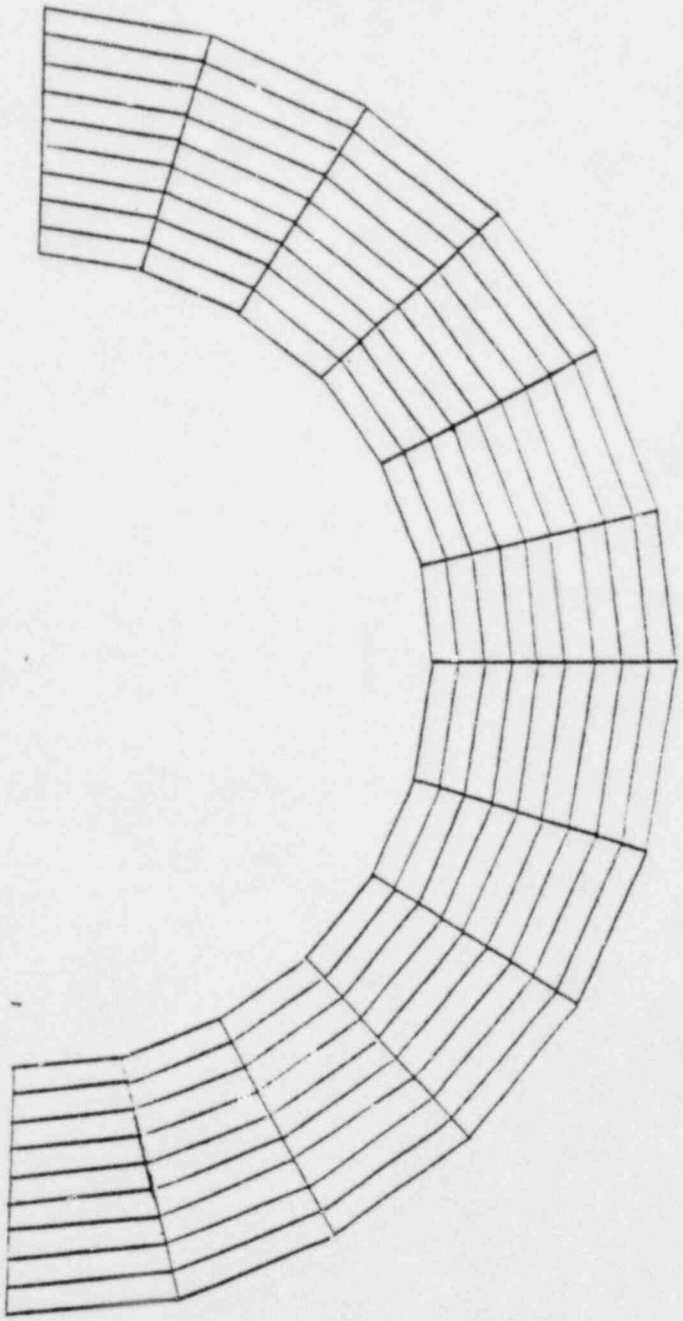

Figure 2-84. ANSYS Model of Backing Plate

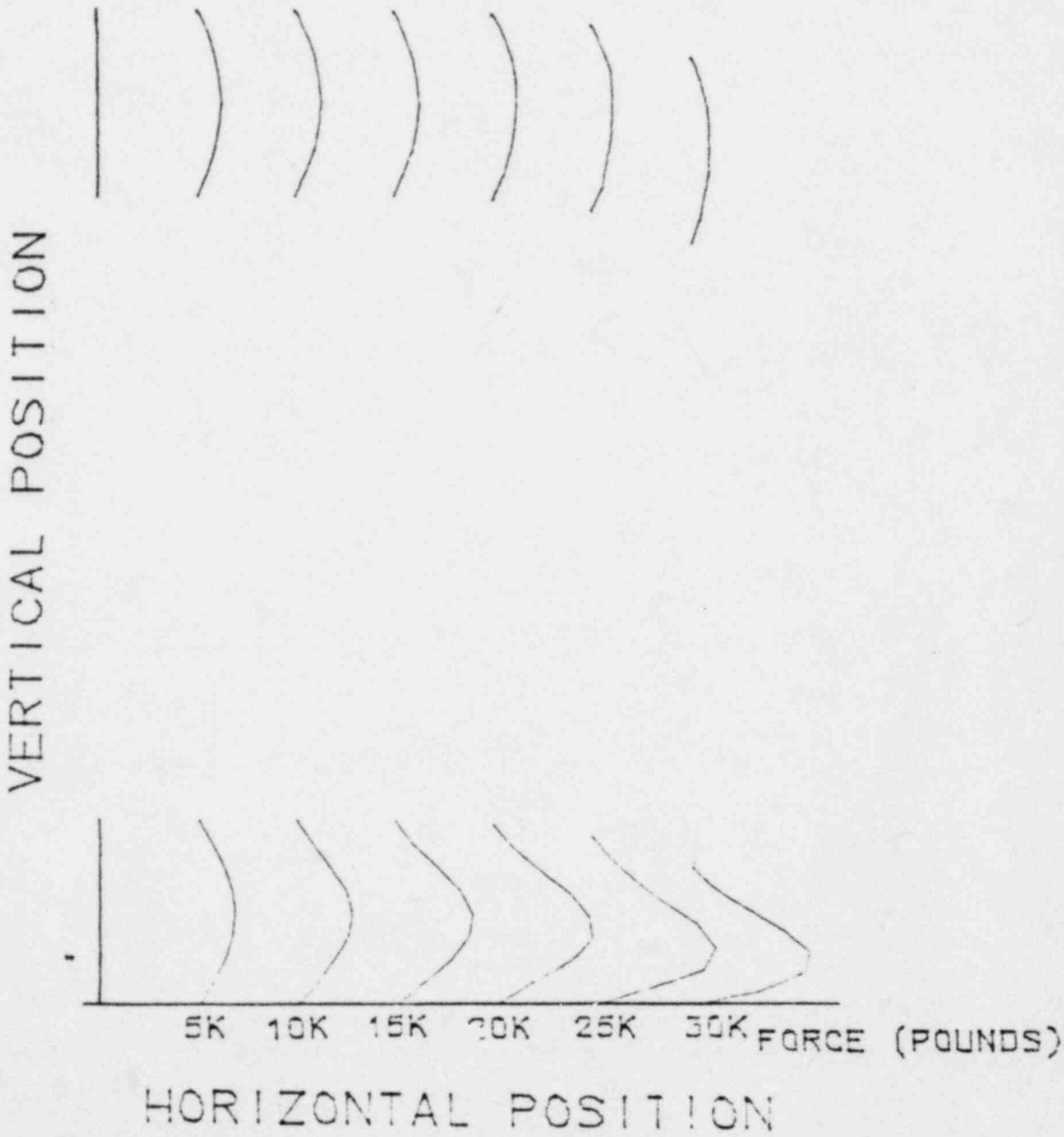

Figure 2-85. Deflection of Backing Plate During Impact

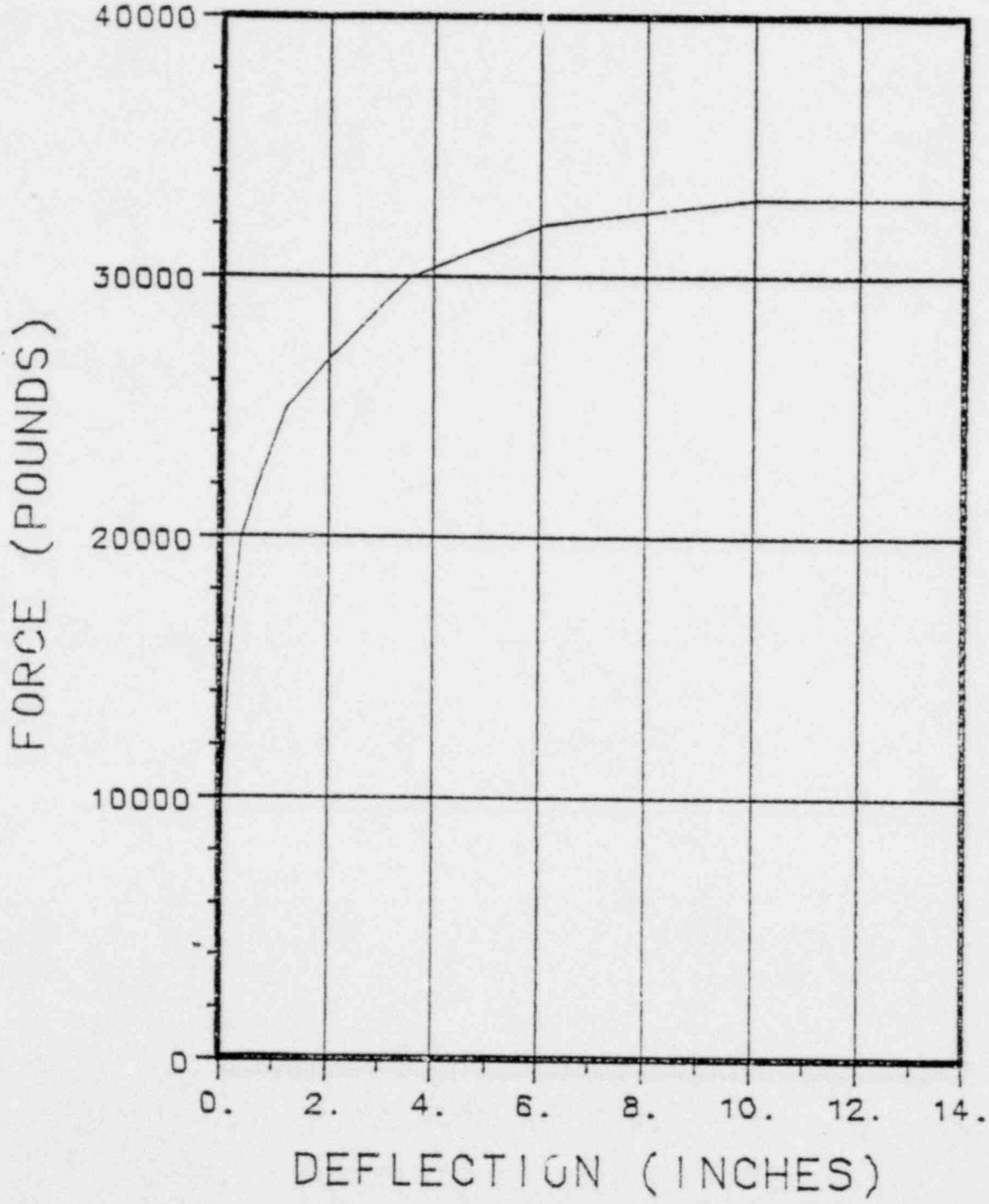

Figure 2-86. Force-Deflection Curve for Backing Plate

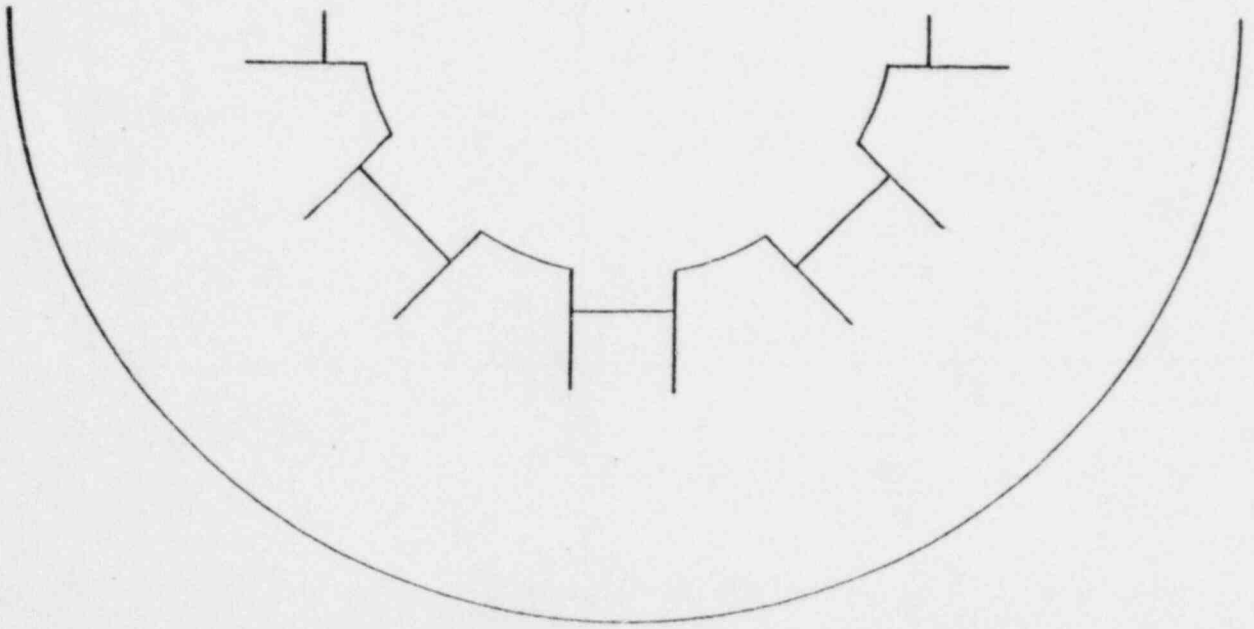

Figure 2-87. Wood Geometry

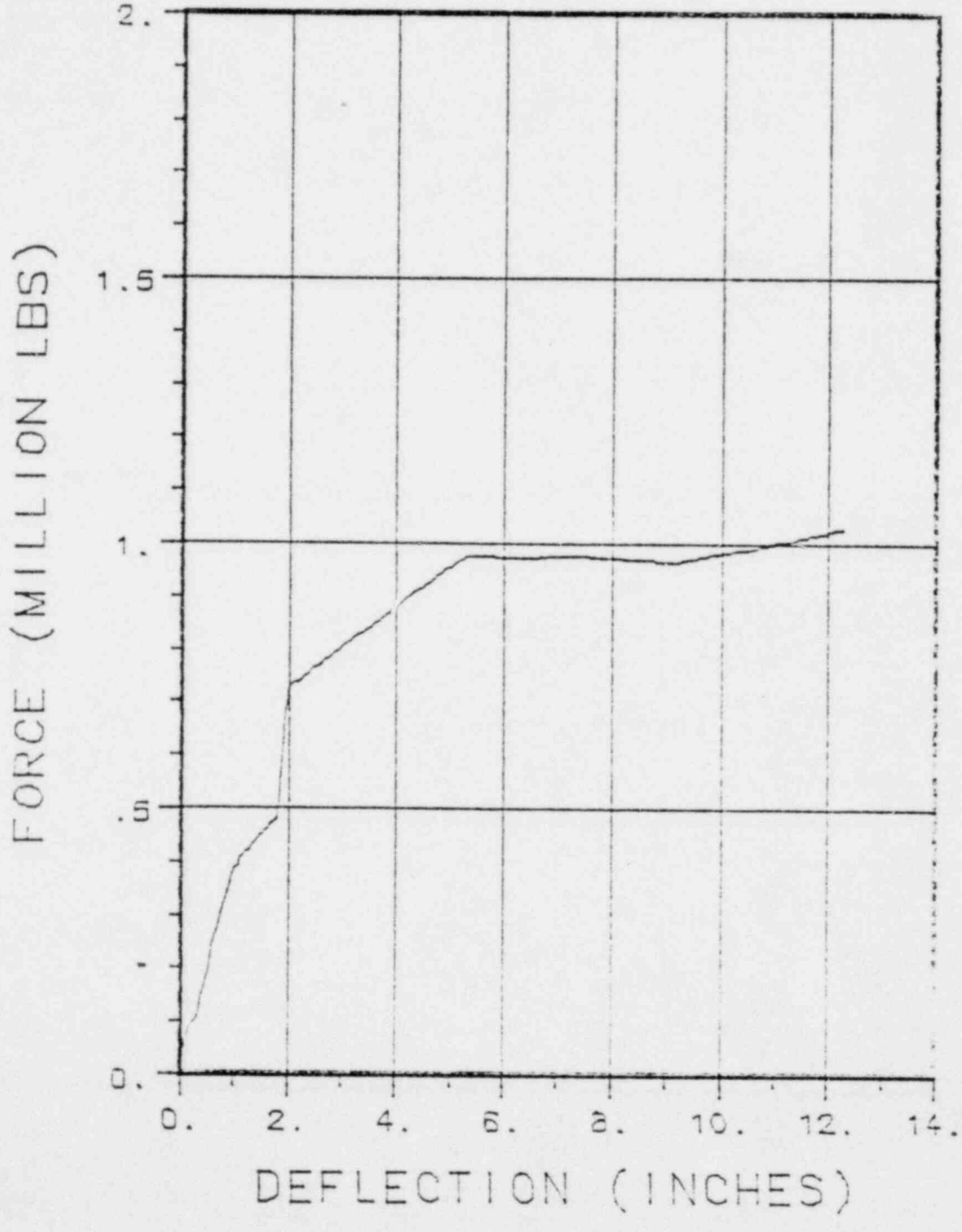

Figure 2-88. Force-Deflection Curve for Side Impact Limter

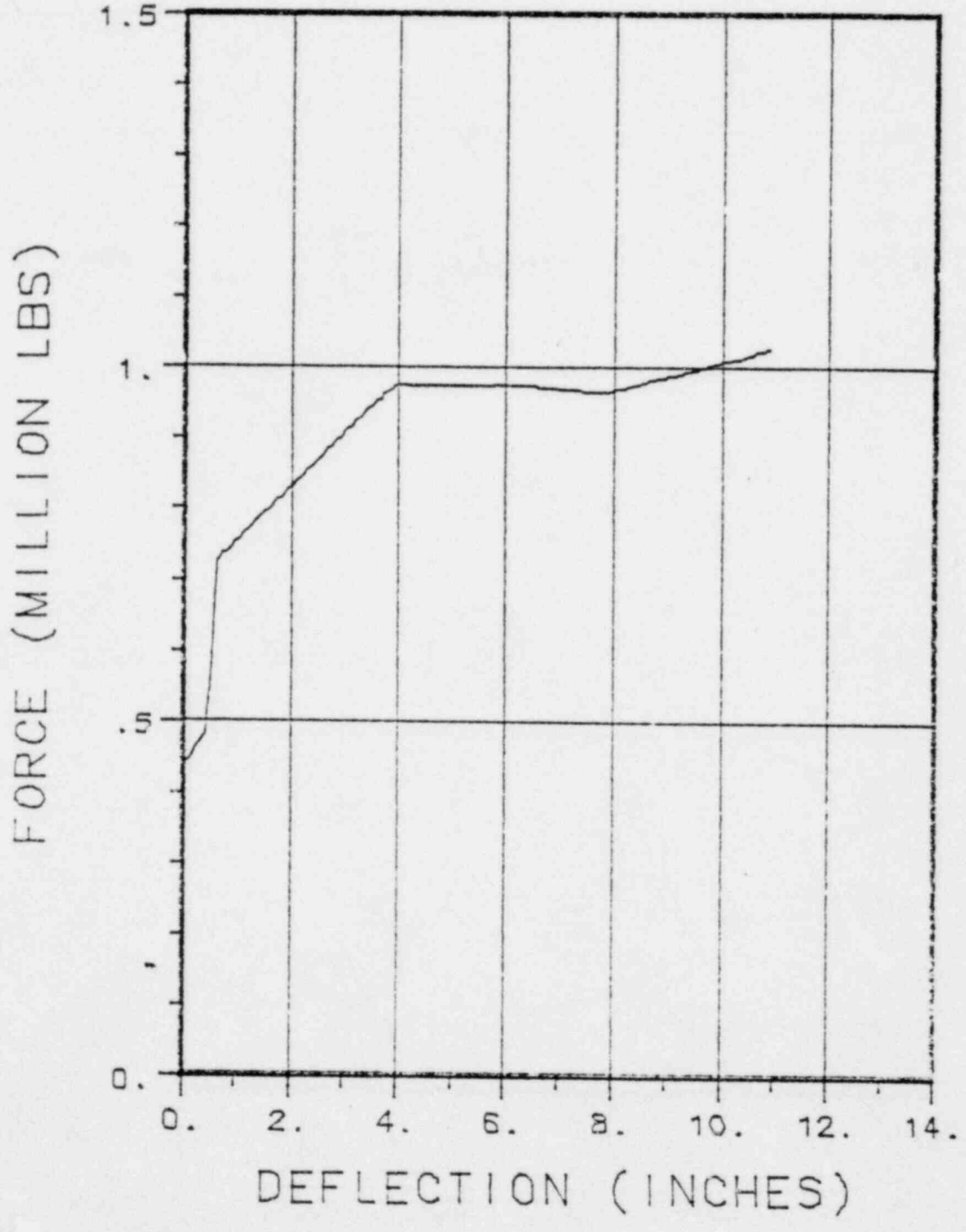

Figure 2-89. Force-Deflection Curve for Deformed Impact Limiter

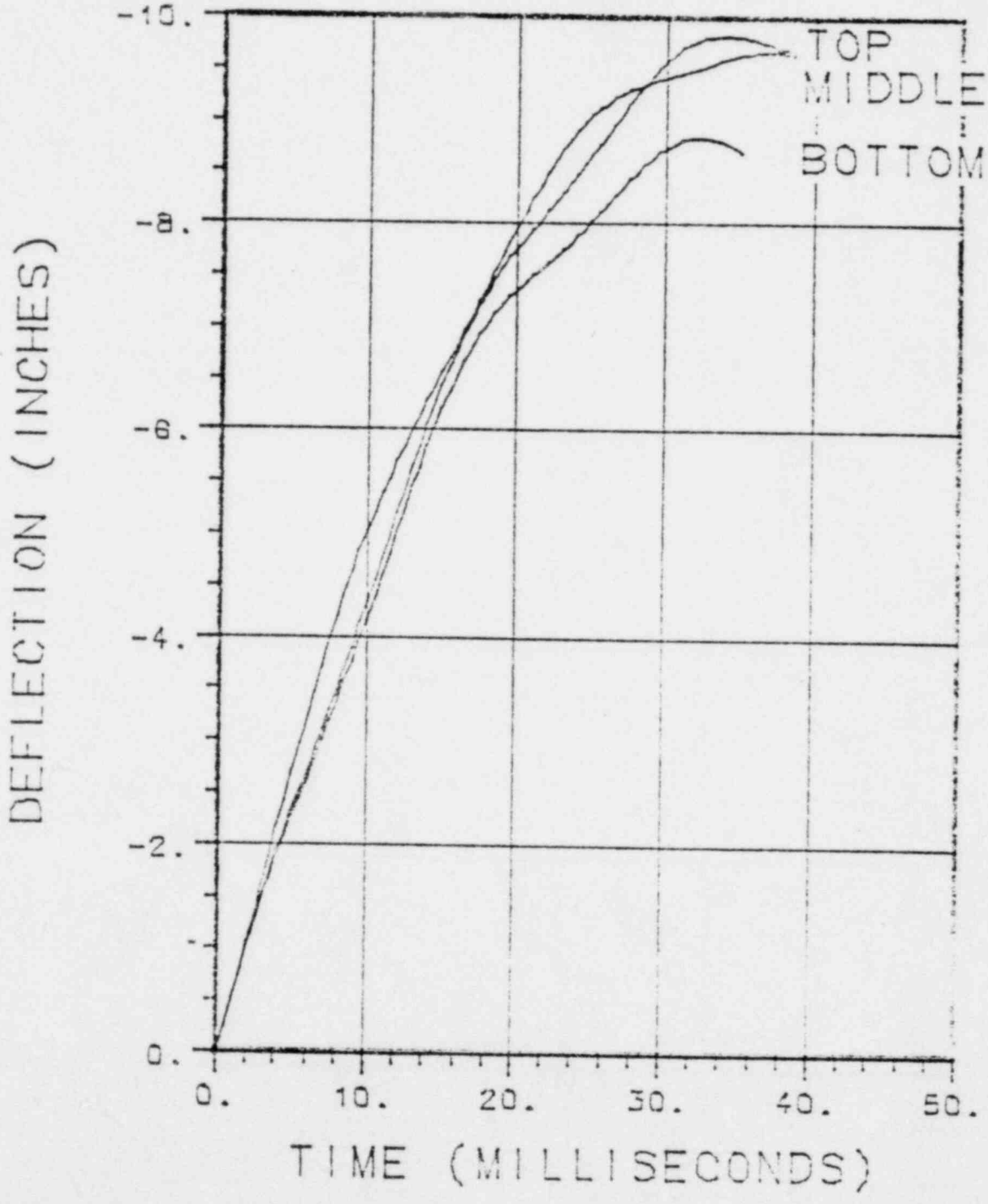

Figure 2-90. Deflection of Ends of Cask During Side Impact

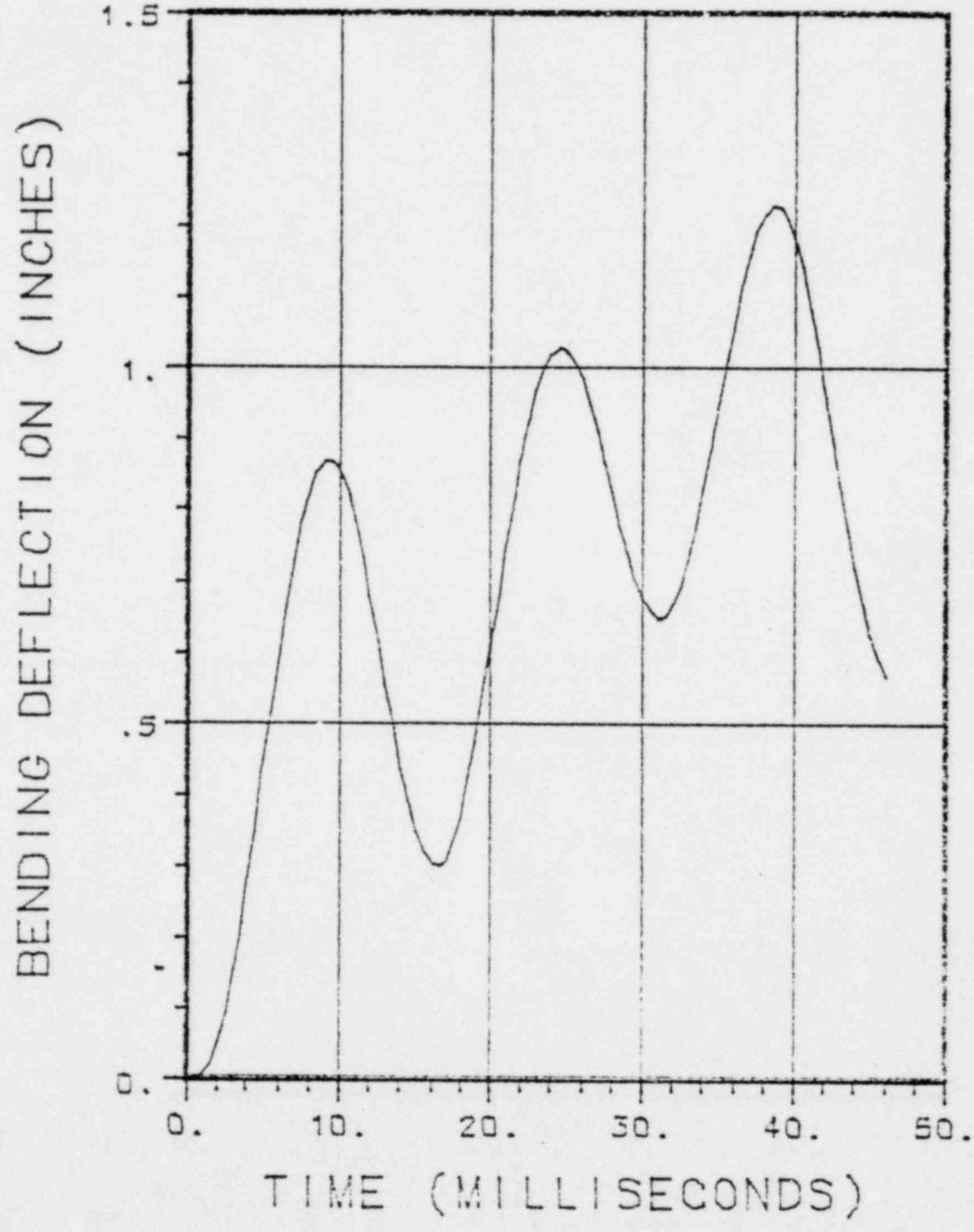

Figure 2-91. Deflection of Center During Side Impact

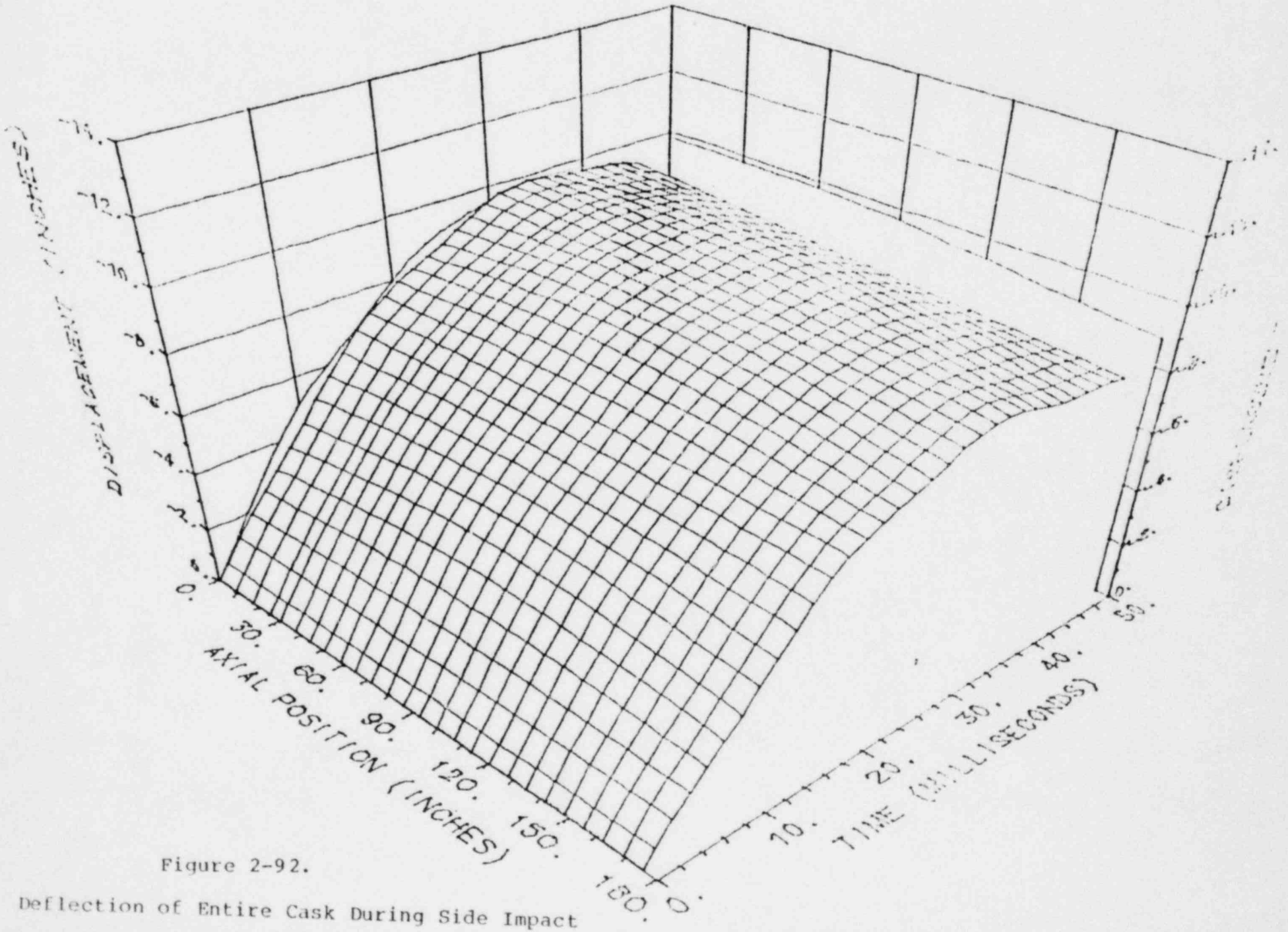

Figure 2-92.

Deflection of Entire Cask During Side Impact

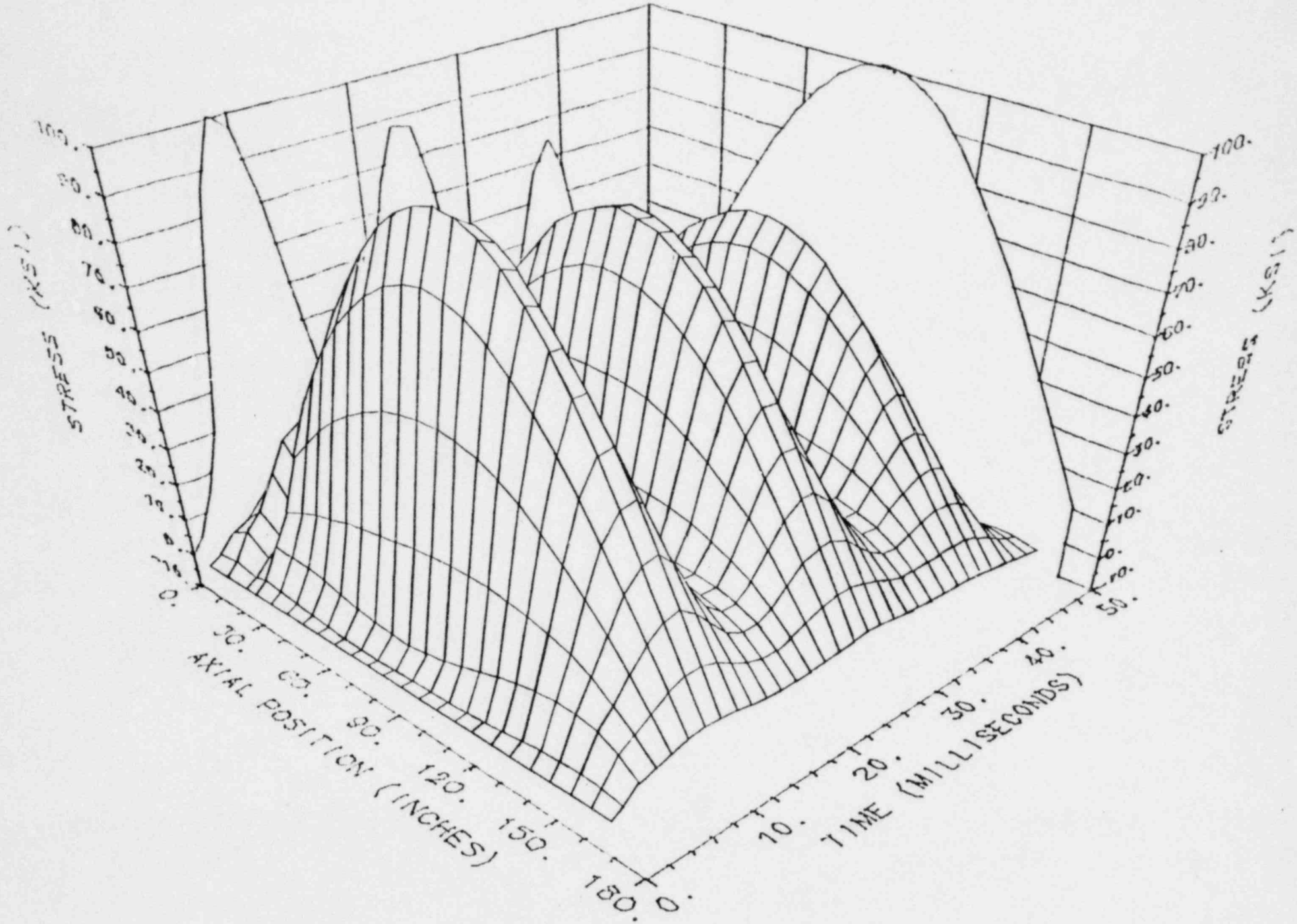

F ure 2-93. Bending Stress in Entire Cask

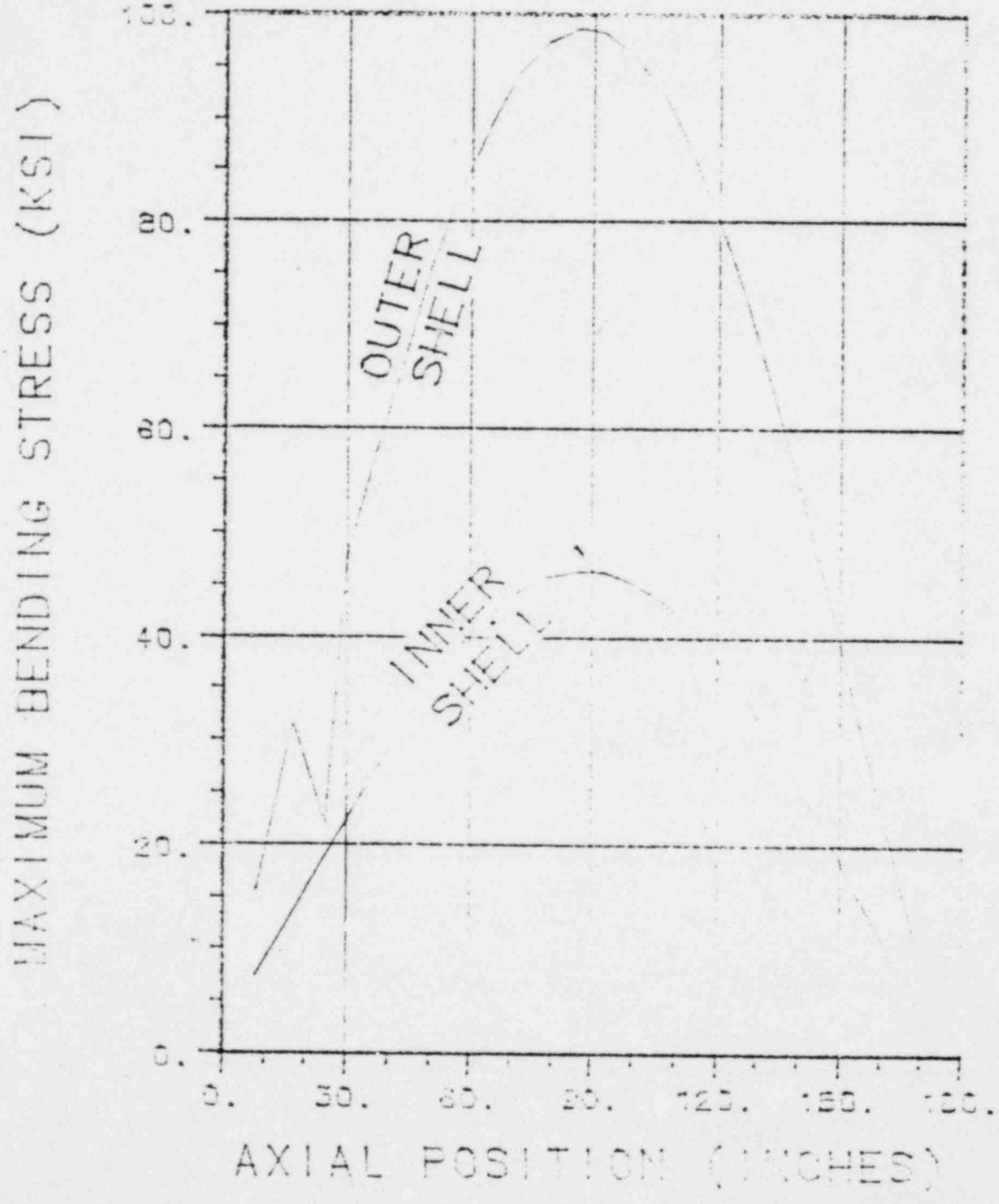

Figure 2-94. Maximum Bending Stress During Side Impact

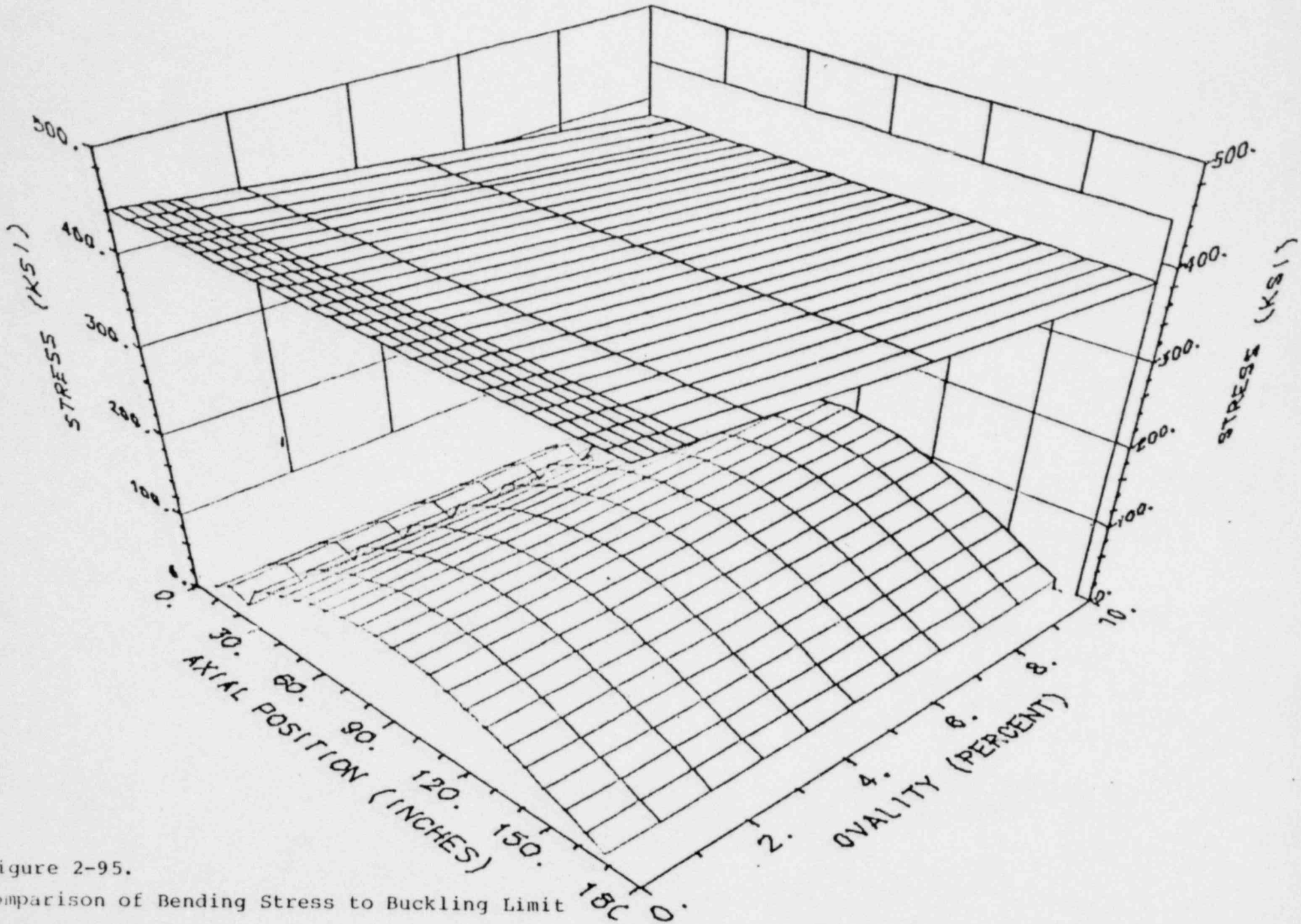

Figure 2-95.
Comparison of Bending Stress to Buckling Limit

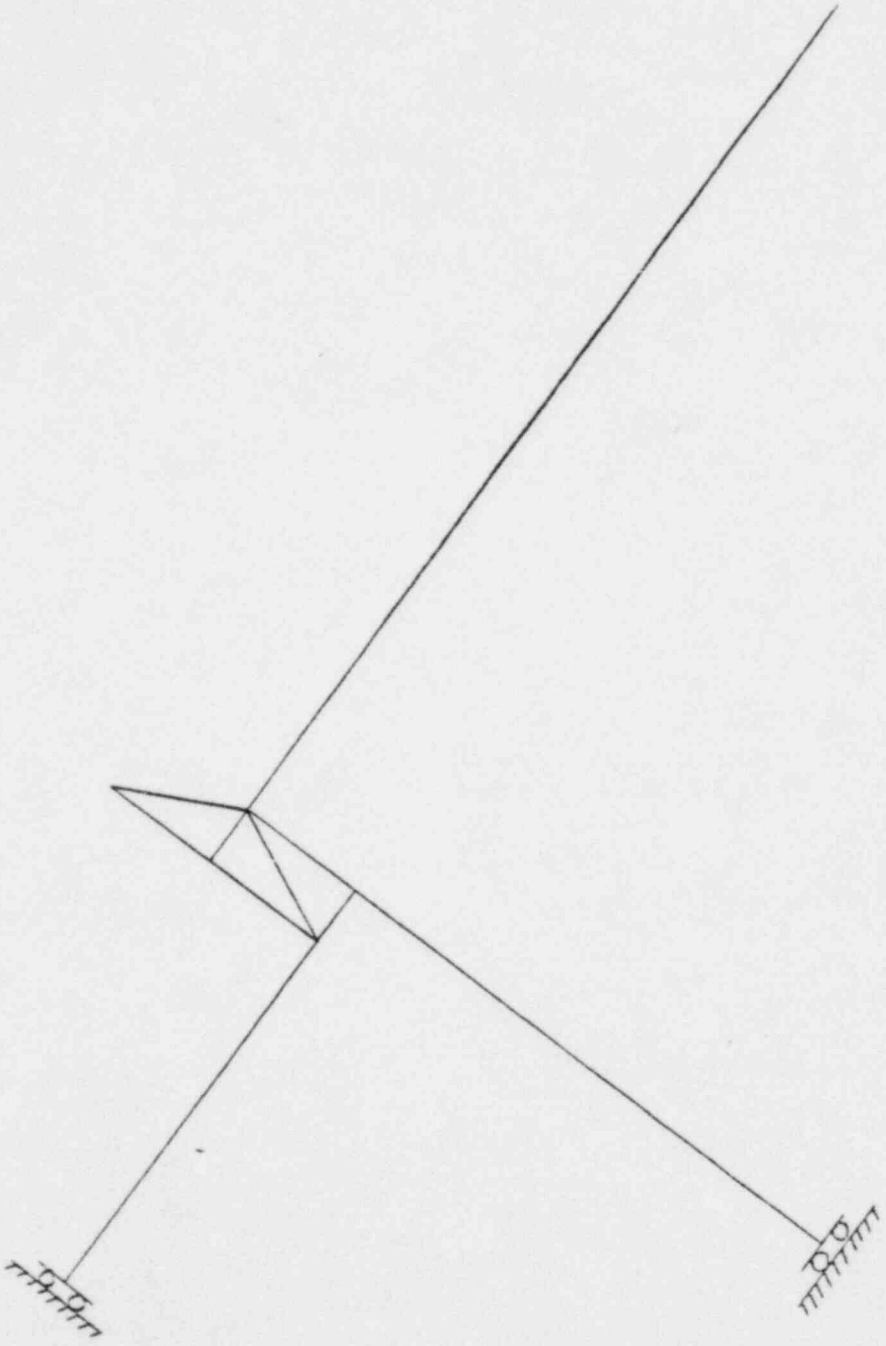

Figure 2-96. ANSYS Model for Corner Impacts

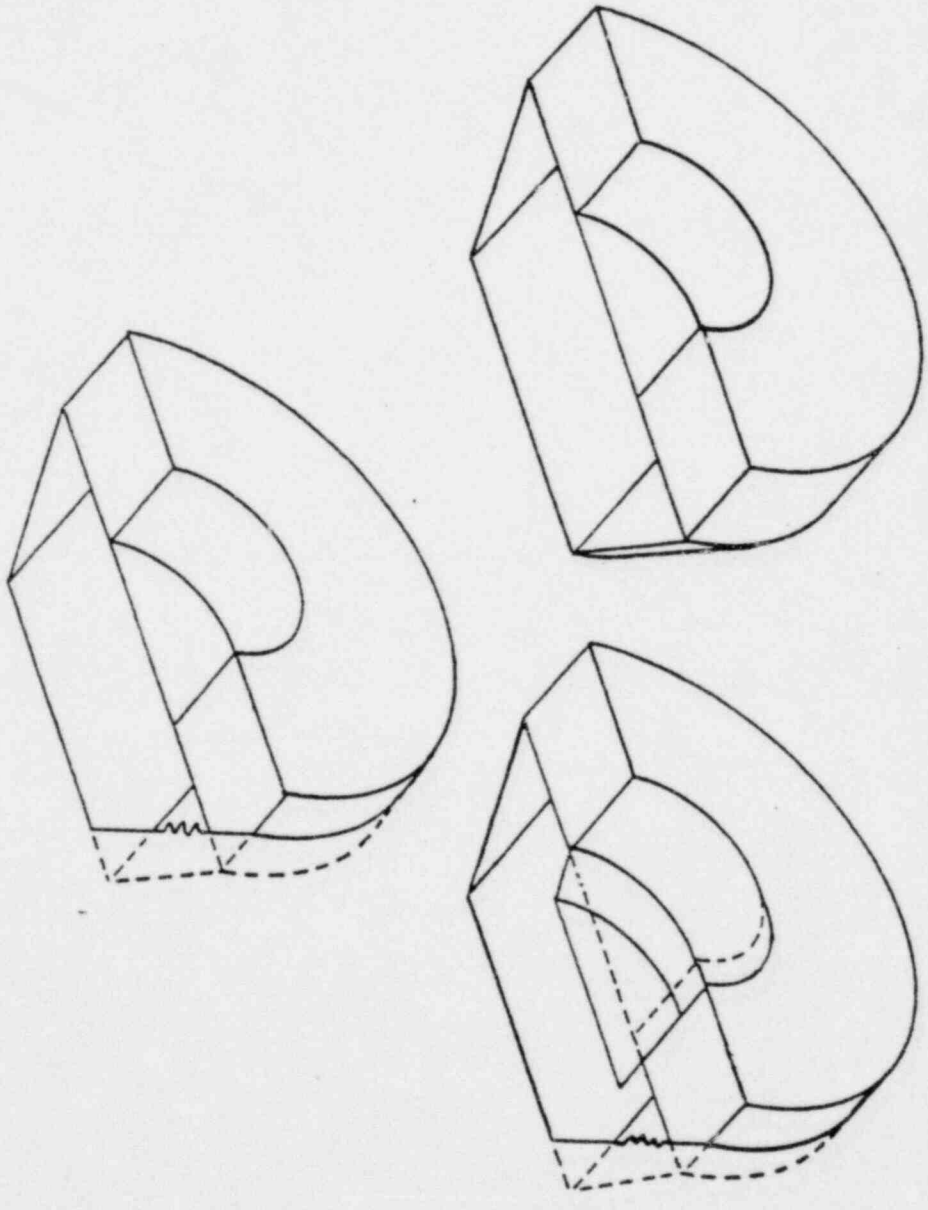

Figure 2-97. Crush Dynamics During Corner Impact

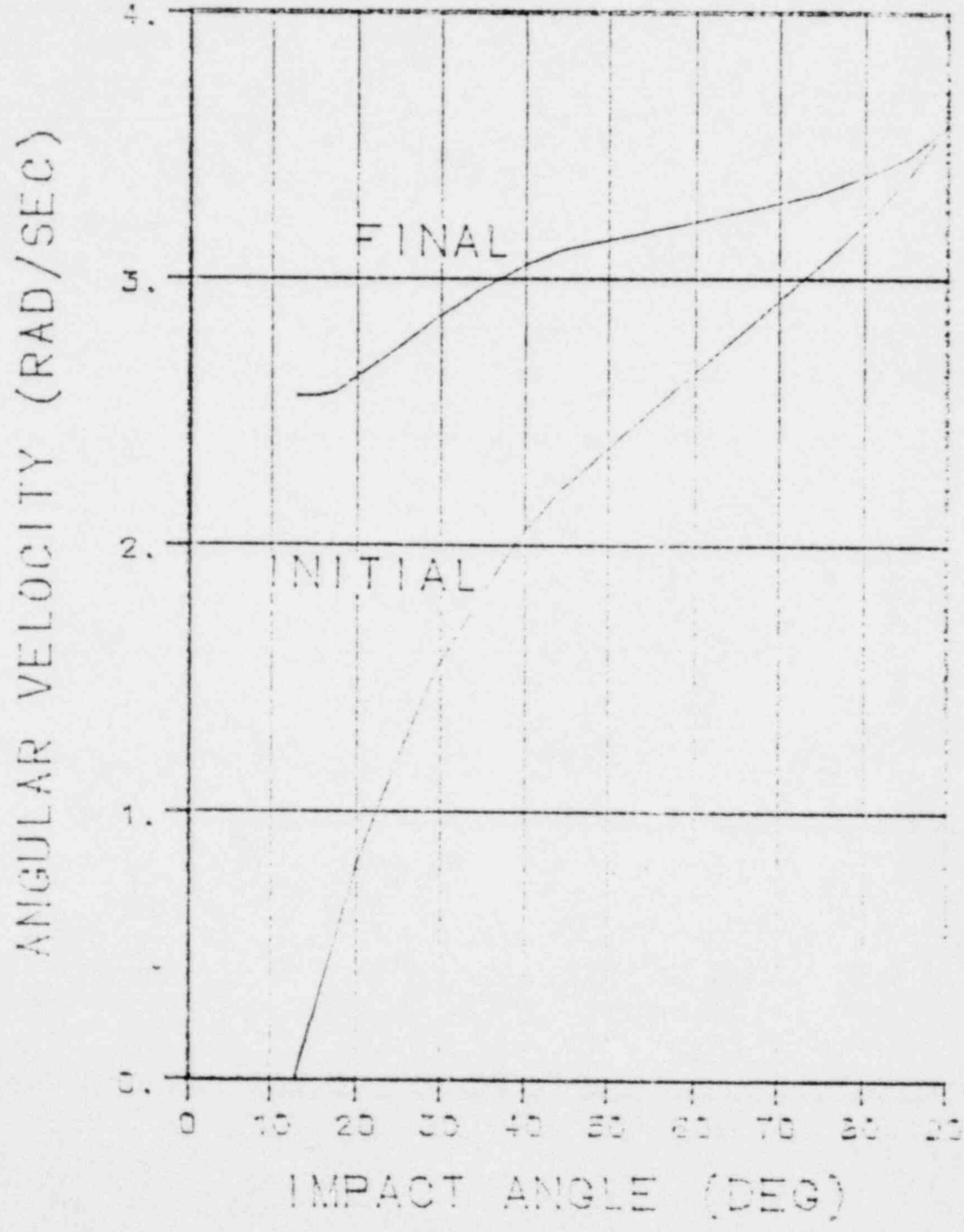

Figure 2-98. Rotation Velocity During Free Rotation

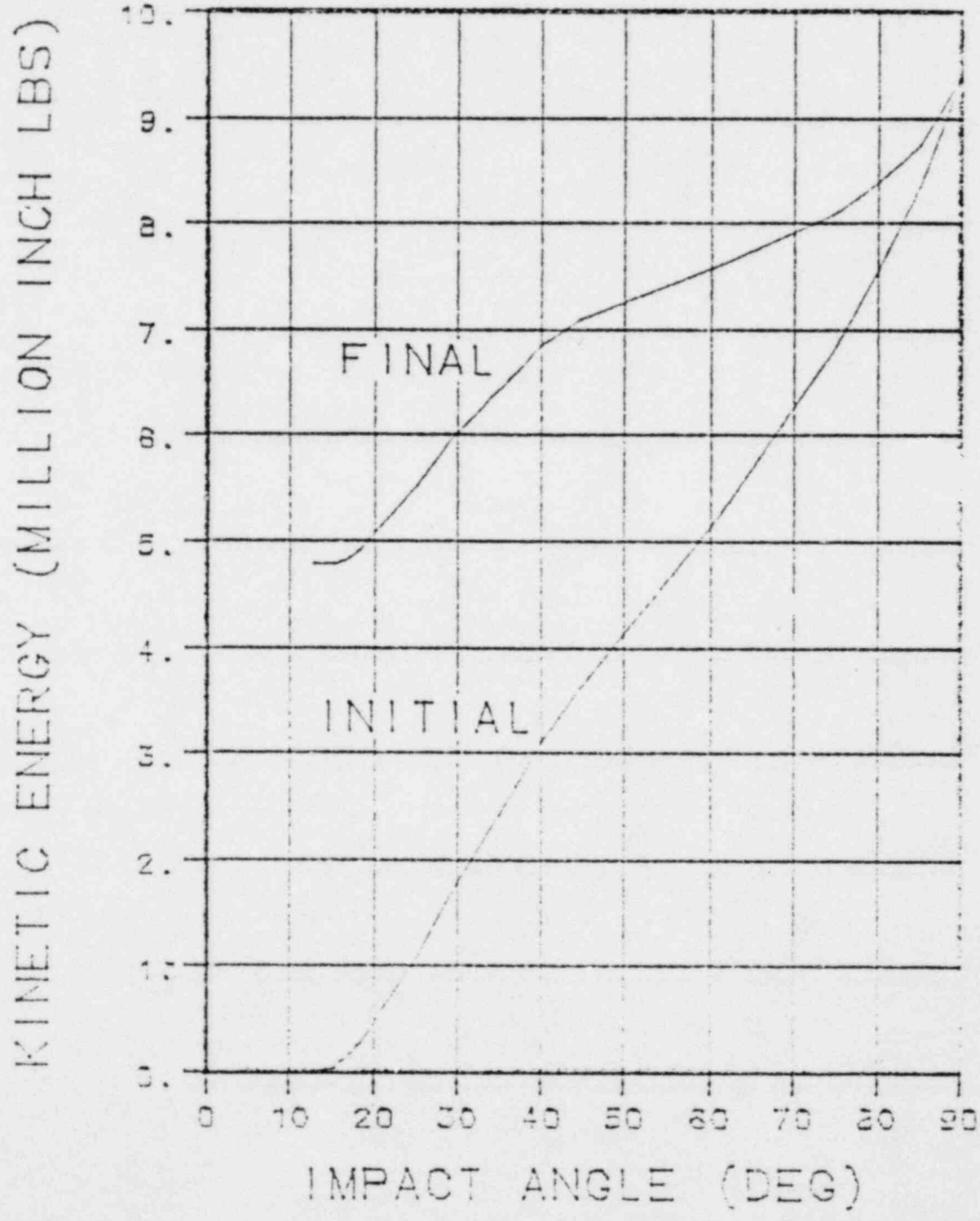

Figure 2-99. Rotation Kinetic Energy During Free Rotation

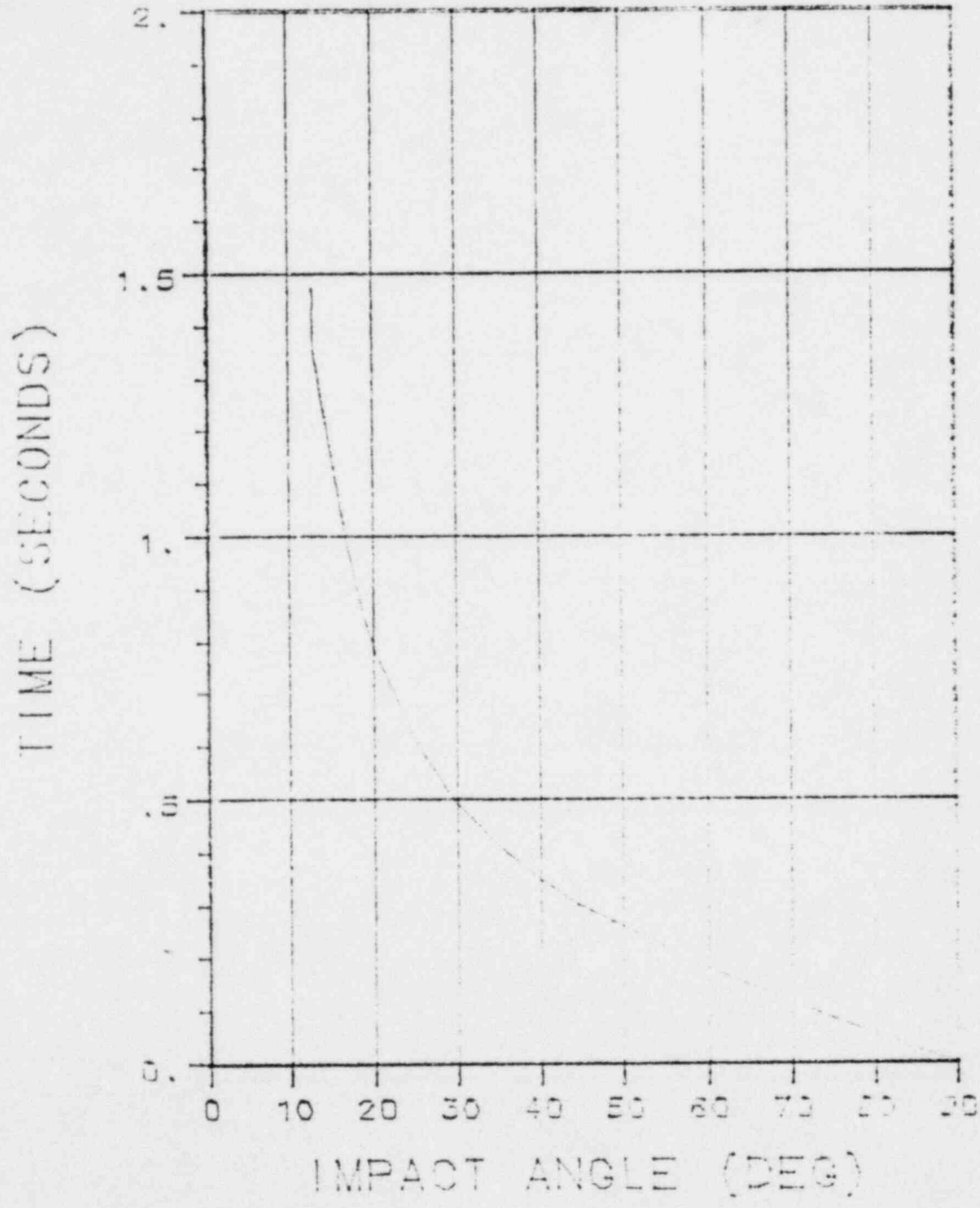

Figure 2-100. Rotation Time During Free Rotation

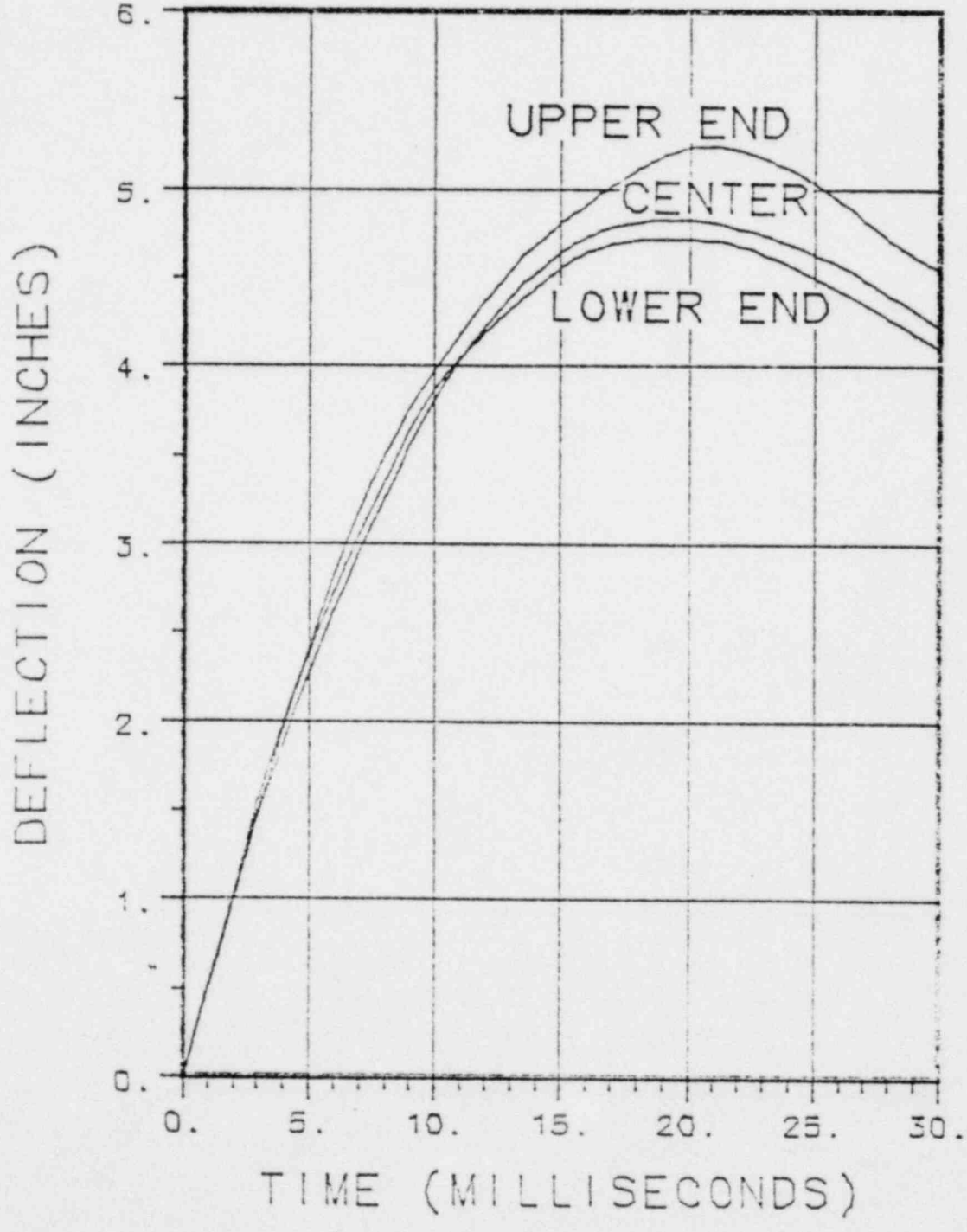

Figure 2-101. Deflection of Cask Ends During Corner Impact

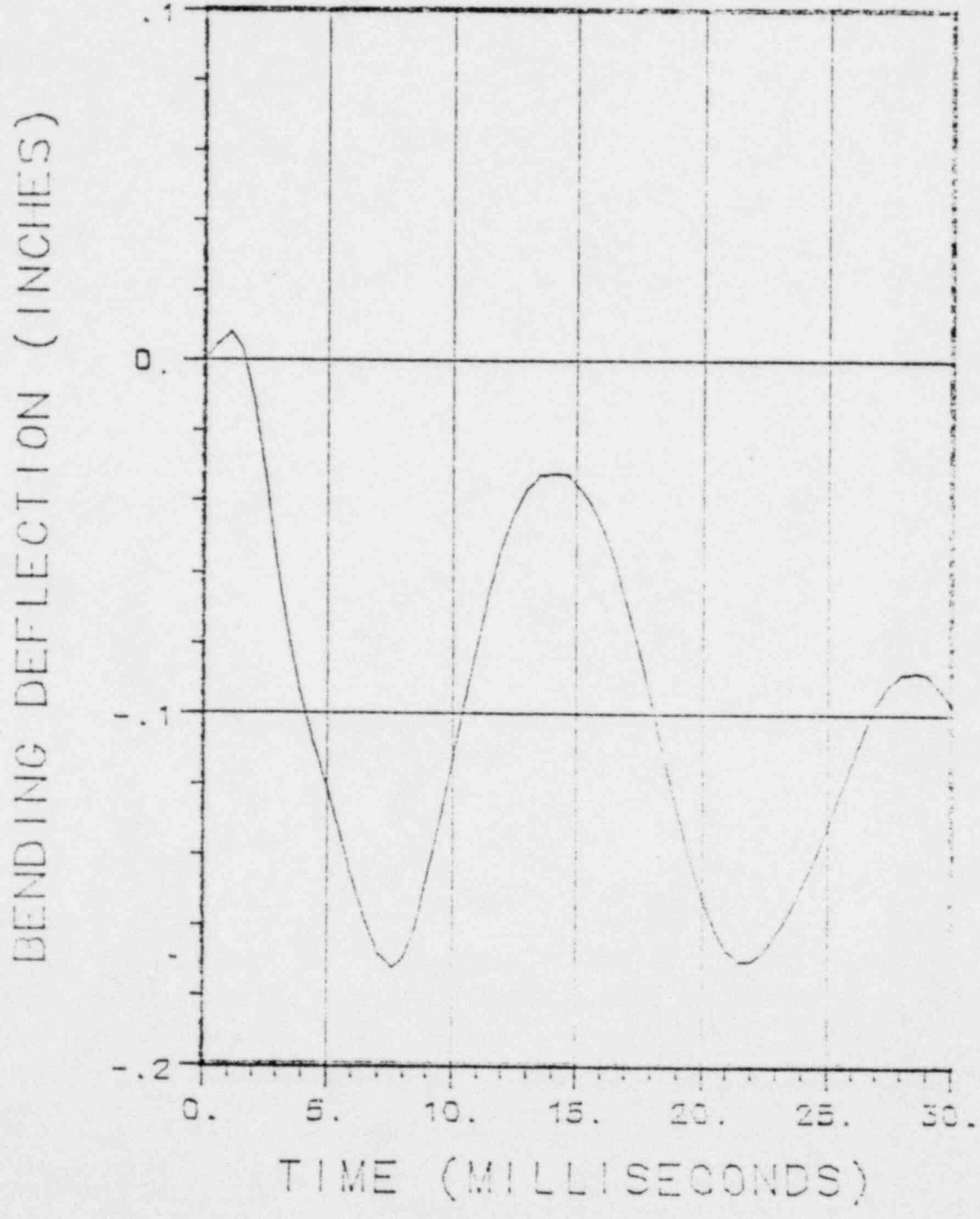

Figure 2-102. Deflection of Cask Center During Corner Impact

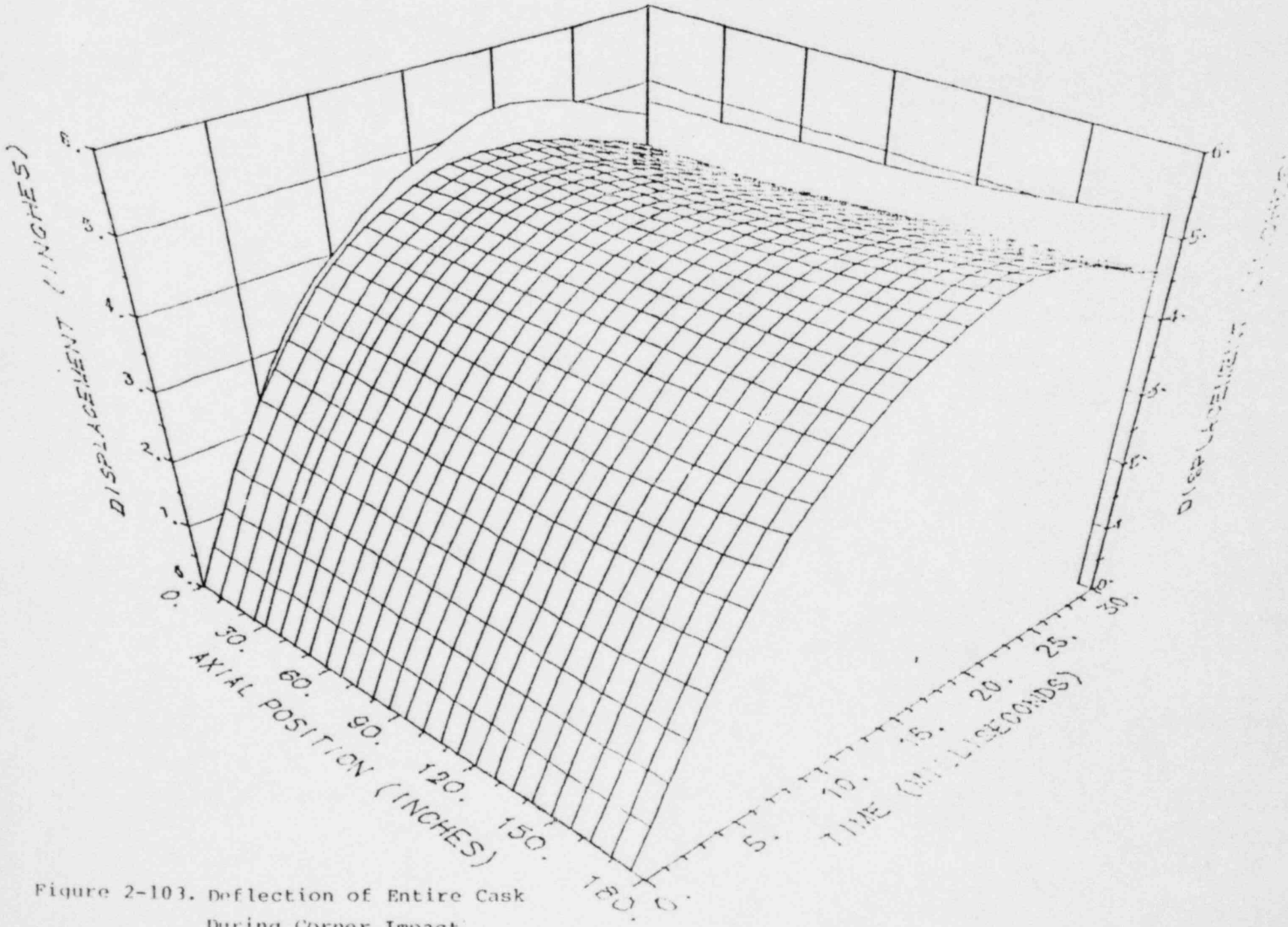

Figure 2-103. Deflection of Entire Cask During Corner Impact

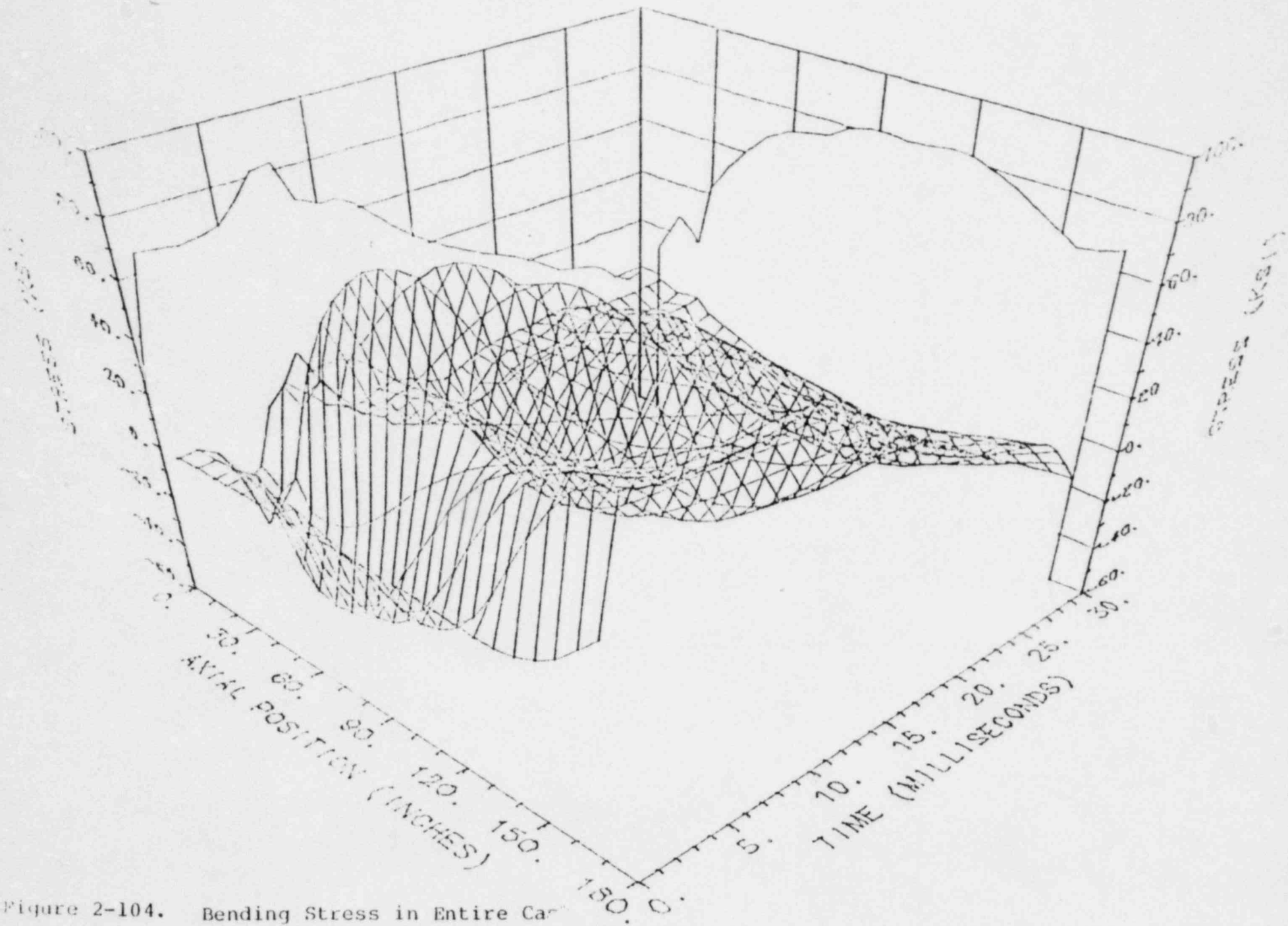

Figure 2-104. Bending Stress in Entire Ca[illegible] During Corner Impact

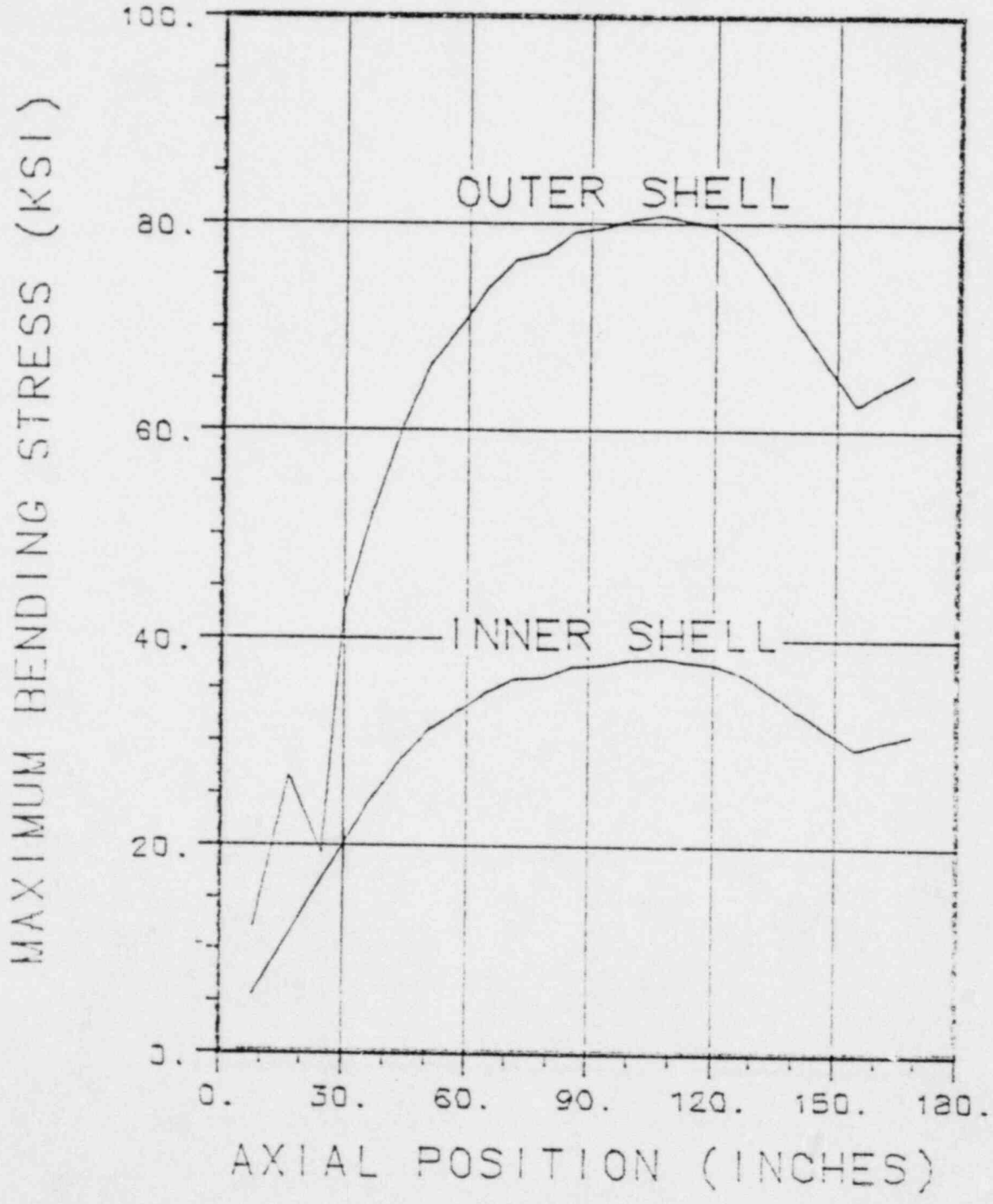

Figure 2-105. Maximum Bending Stress During Corner Impact

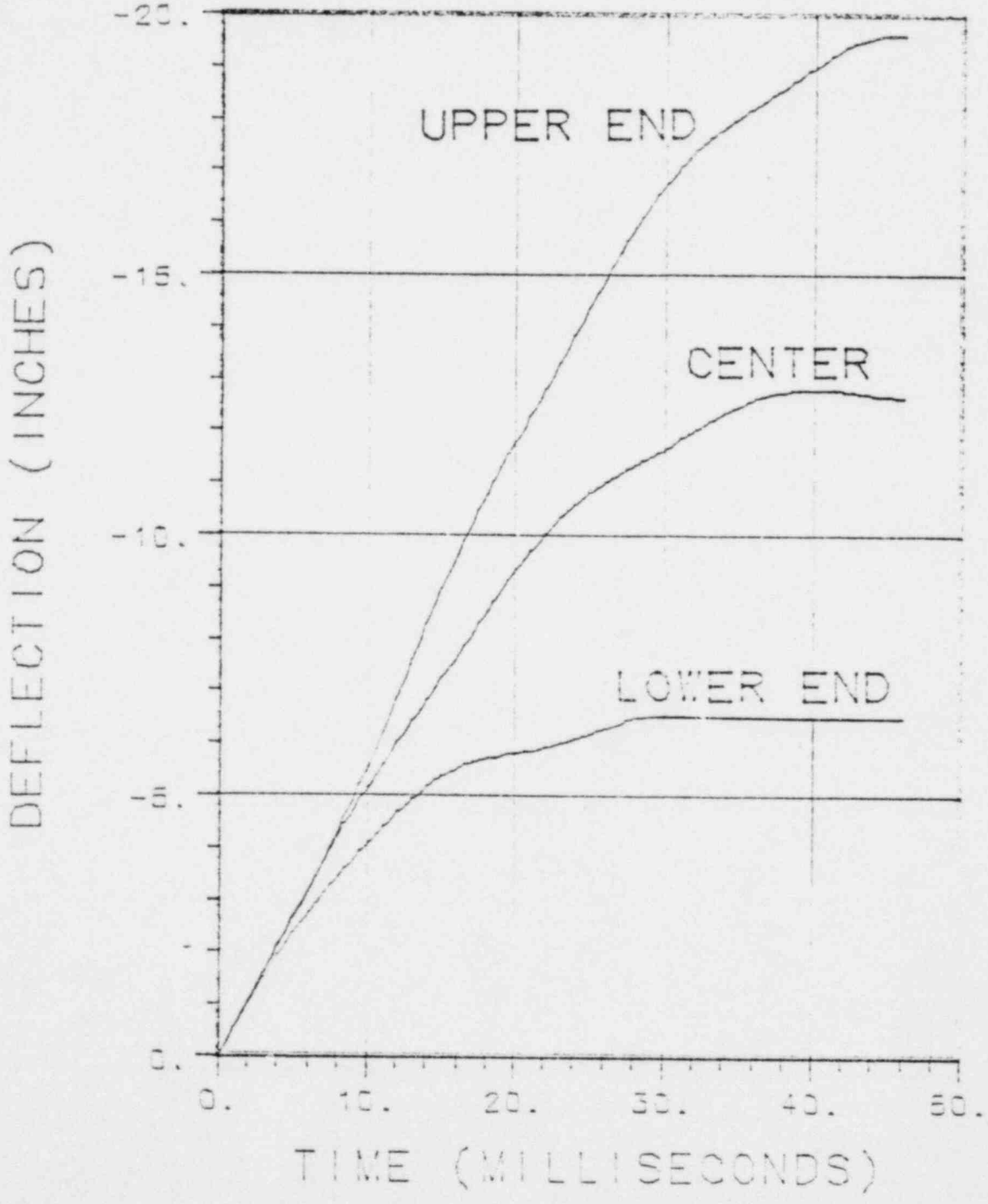

Figure 2-106. Deflection of Cask Ends During Oblique Impact

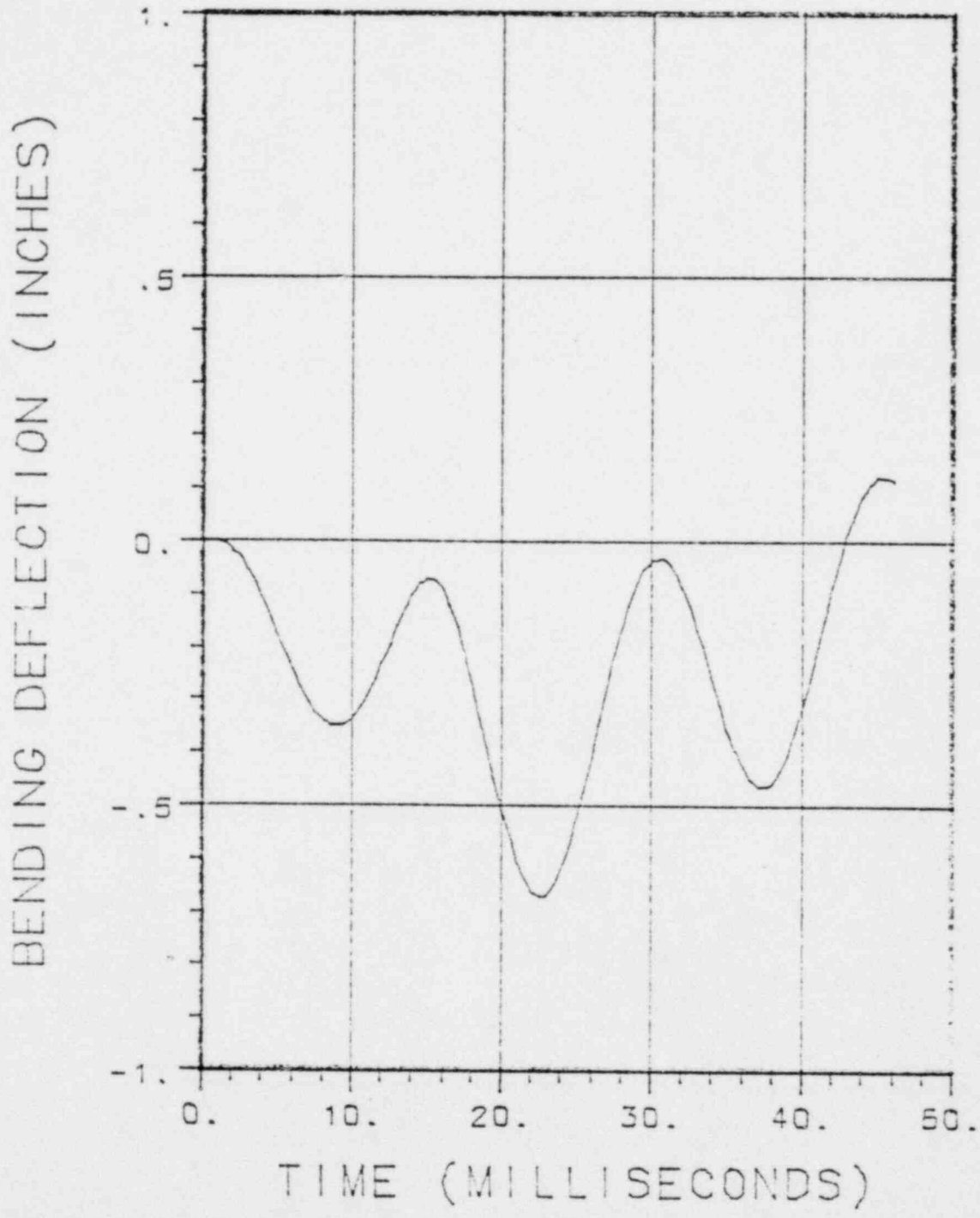

Figure 2-107. Deflection of Cask Center During Oblique Impact

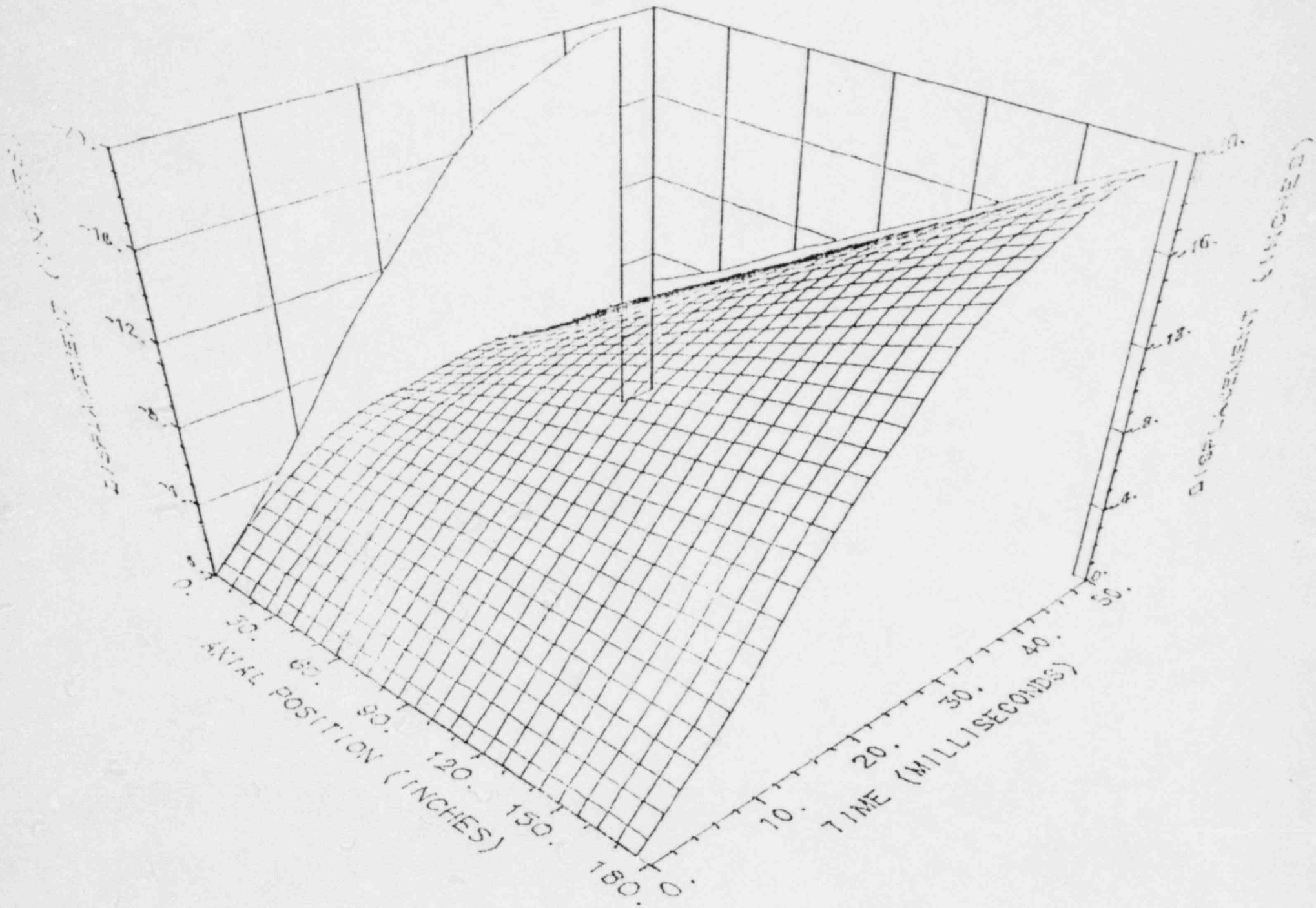

Figure 2-108. Deflection of Entire Cask During Oblique Impact

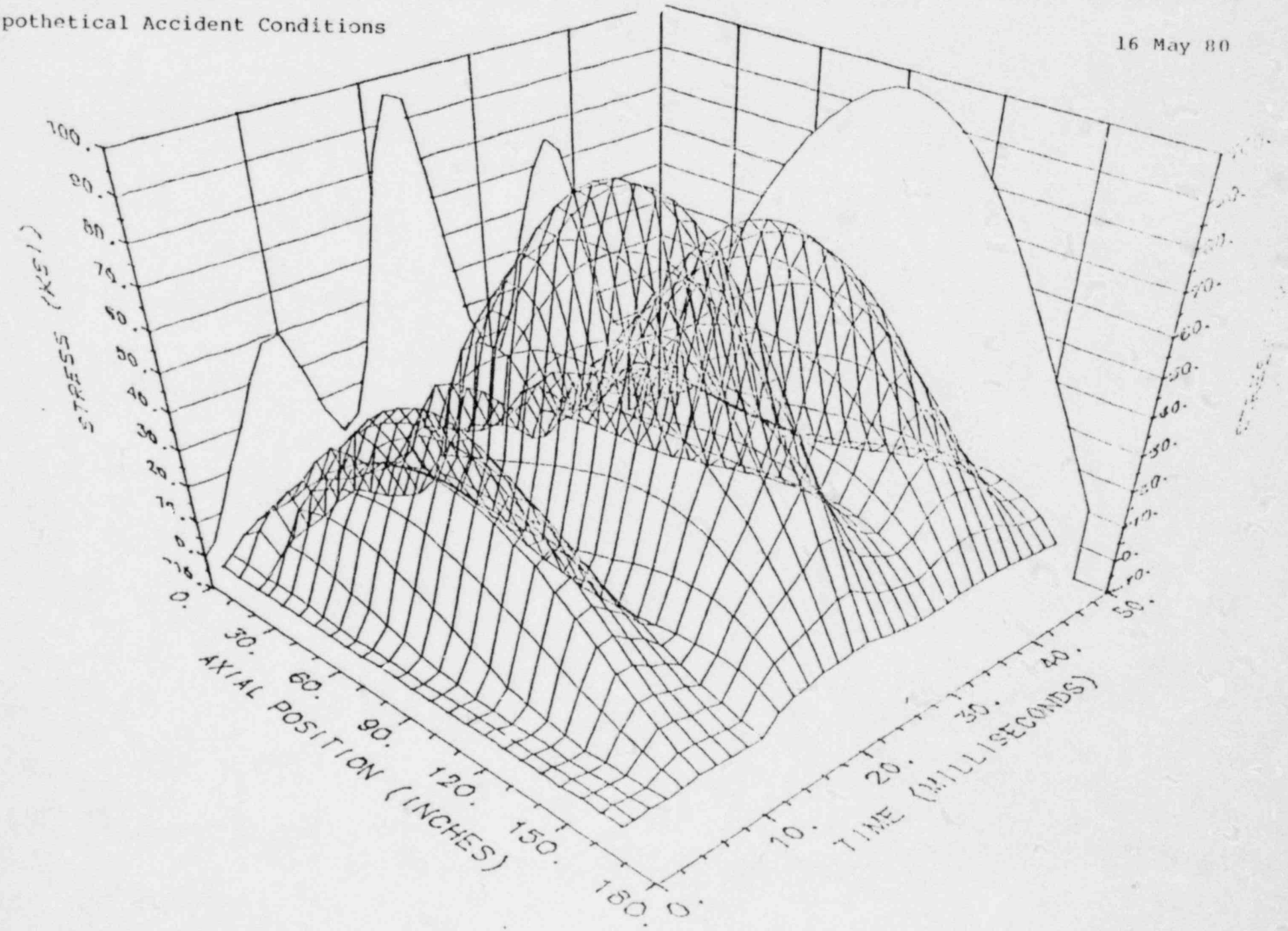

Figure 2-109. Bending Stress in Entire Cask During Oblique Impact

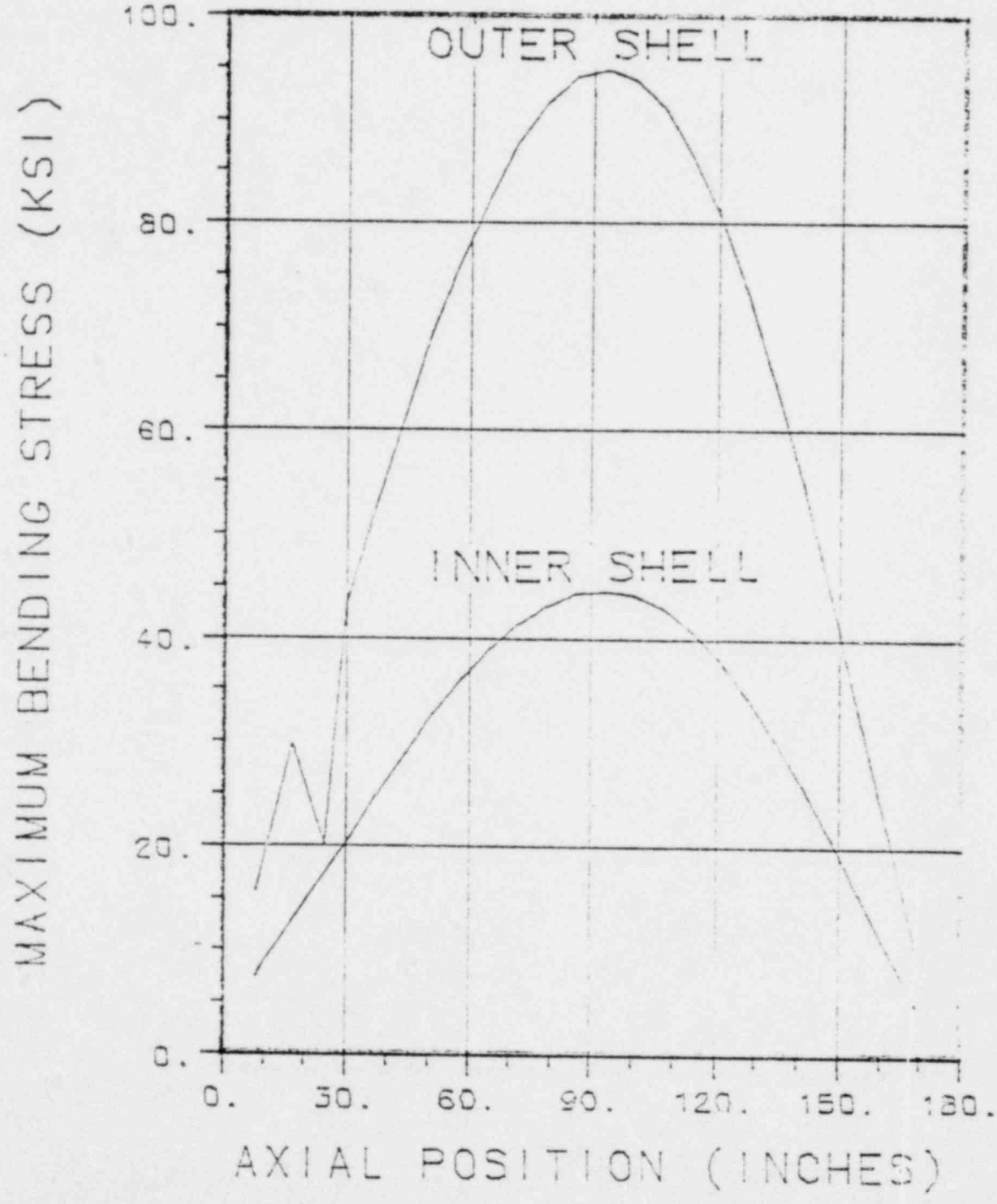

Figure 2-110. Maximum Bending Stress During Oblique Impact

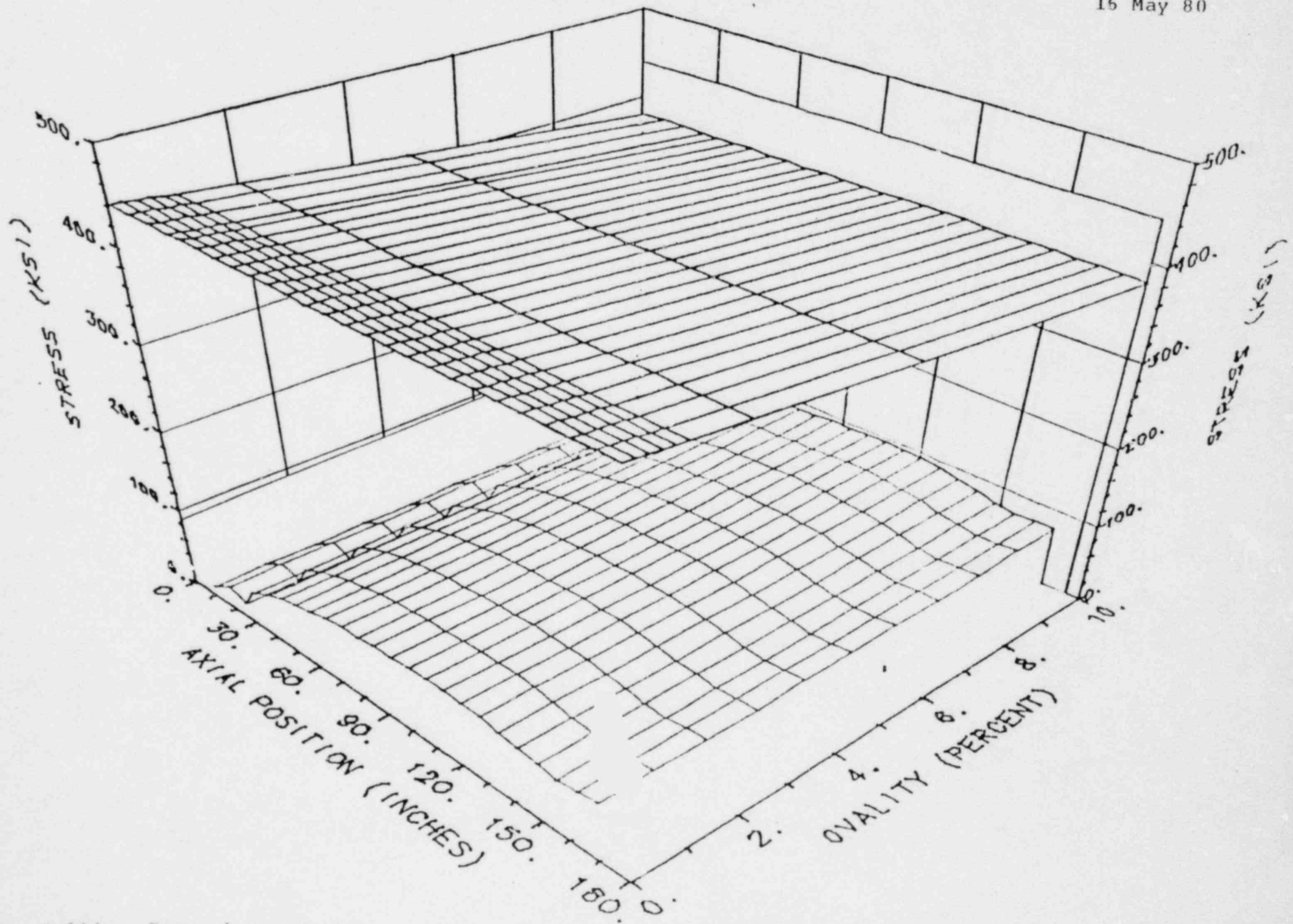

Figure 2-111. Comparison of Stress to Buckling Limit for Corner

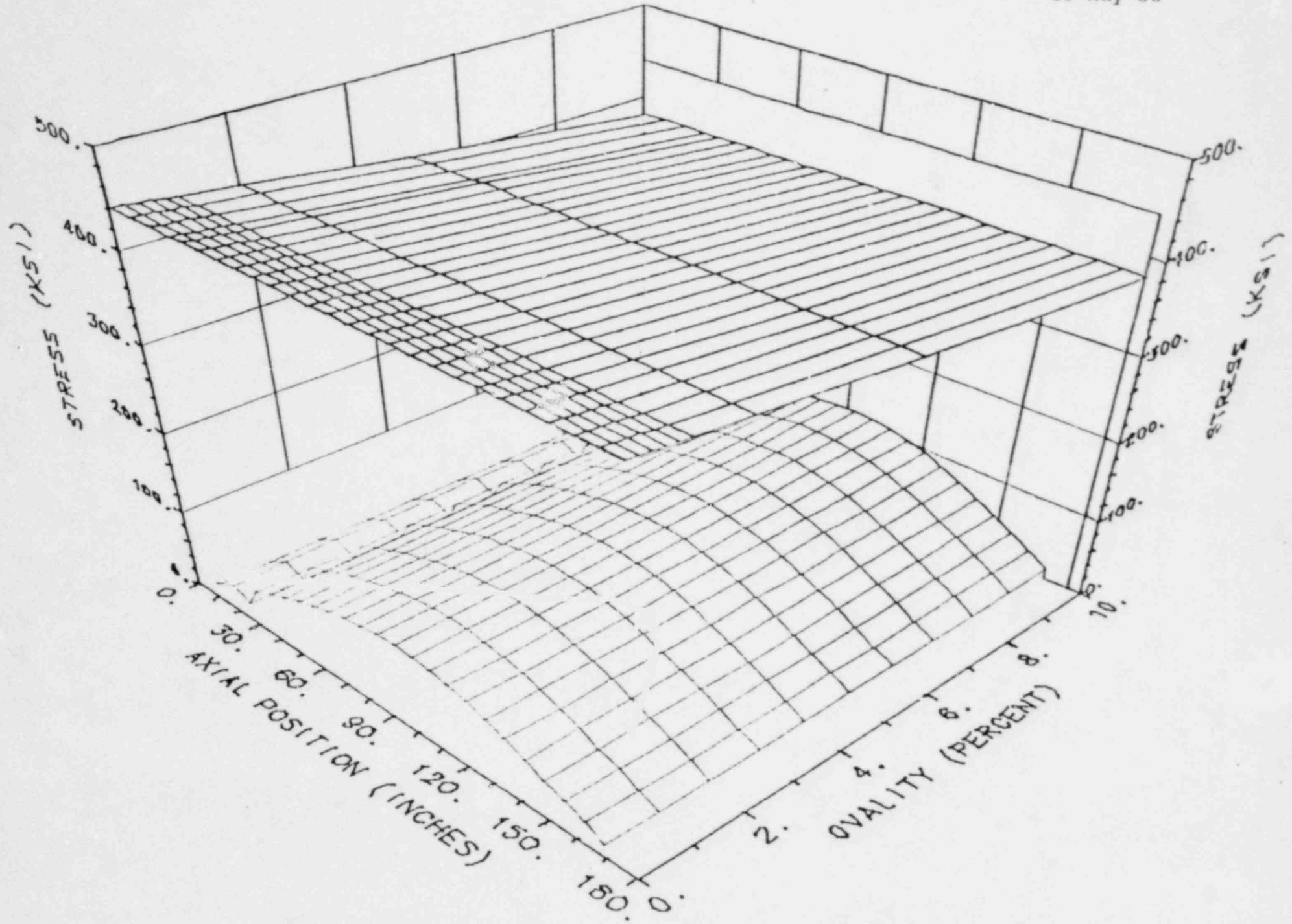

Figure 2-112. Comparison of Stress to Buckling Limit for Oblique

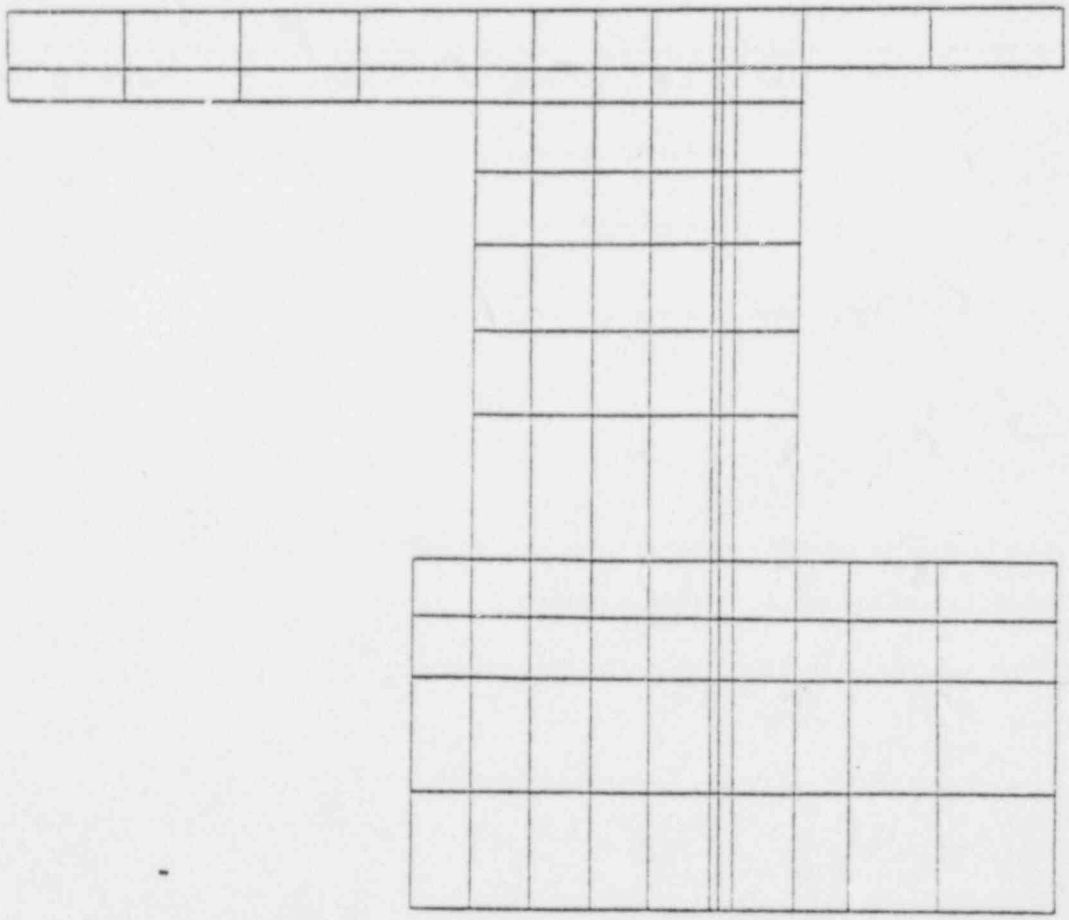

Figure 2-113. ANSYS Model of Valve Protection Ring

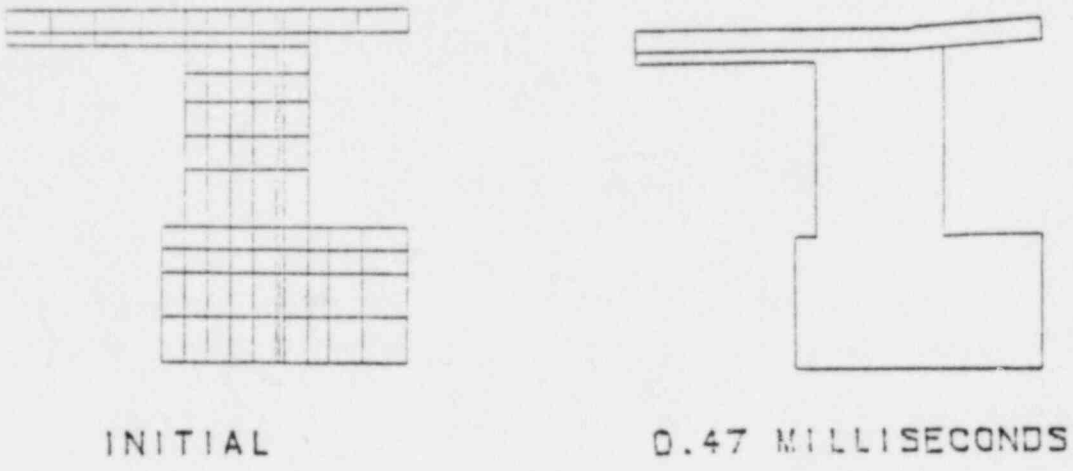

Figure 2-114. Deformed Geometry of Valve Protection Ring

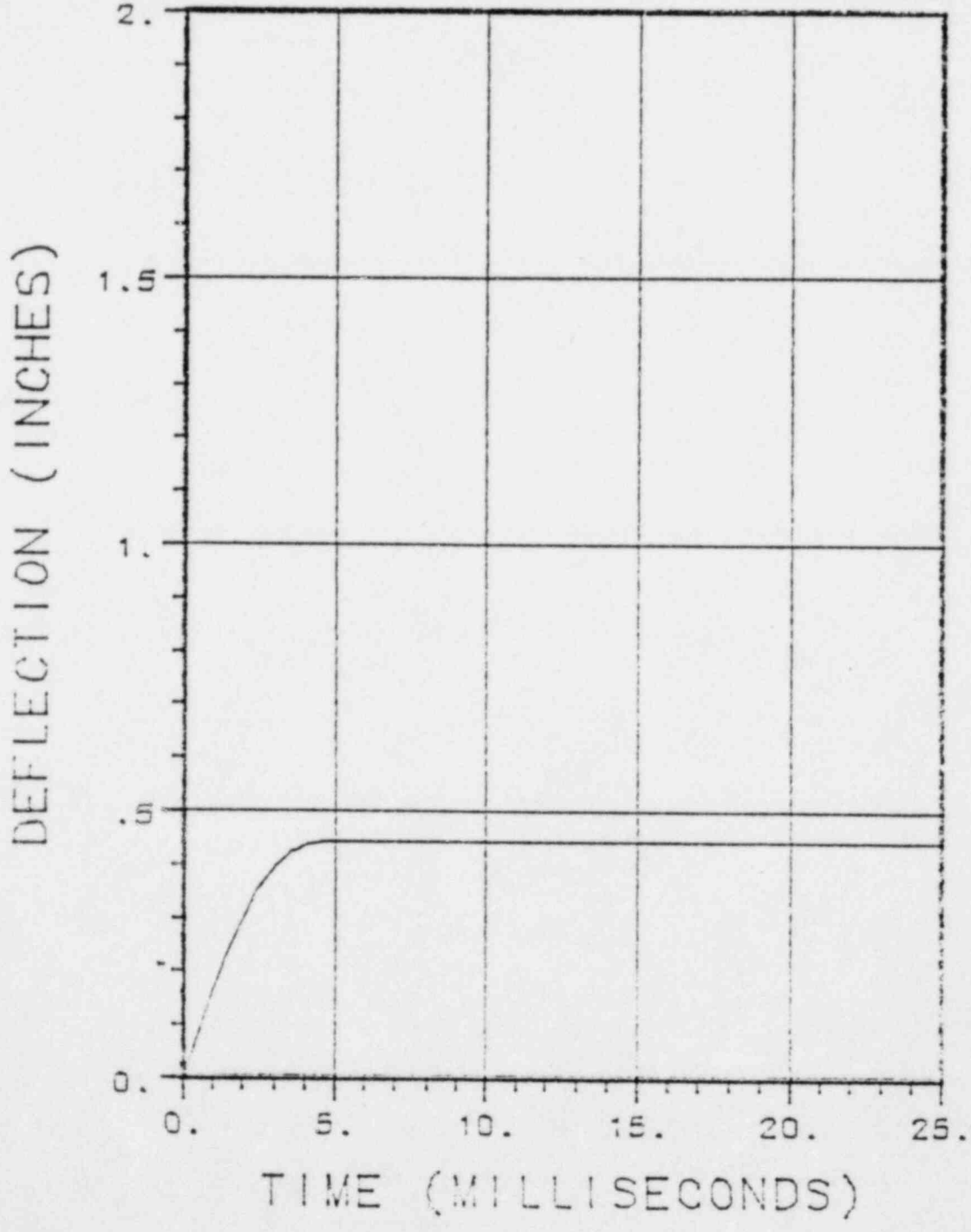

Figure 2-115. Deflection of Cask During Impact on Valve

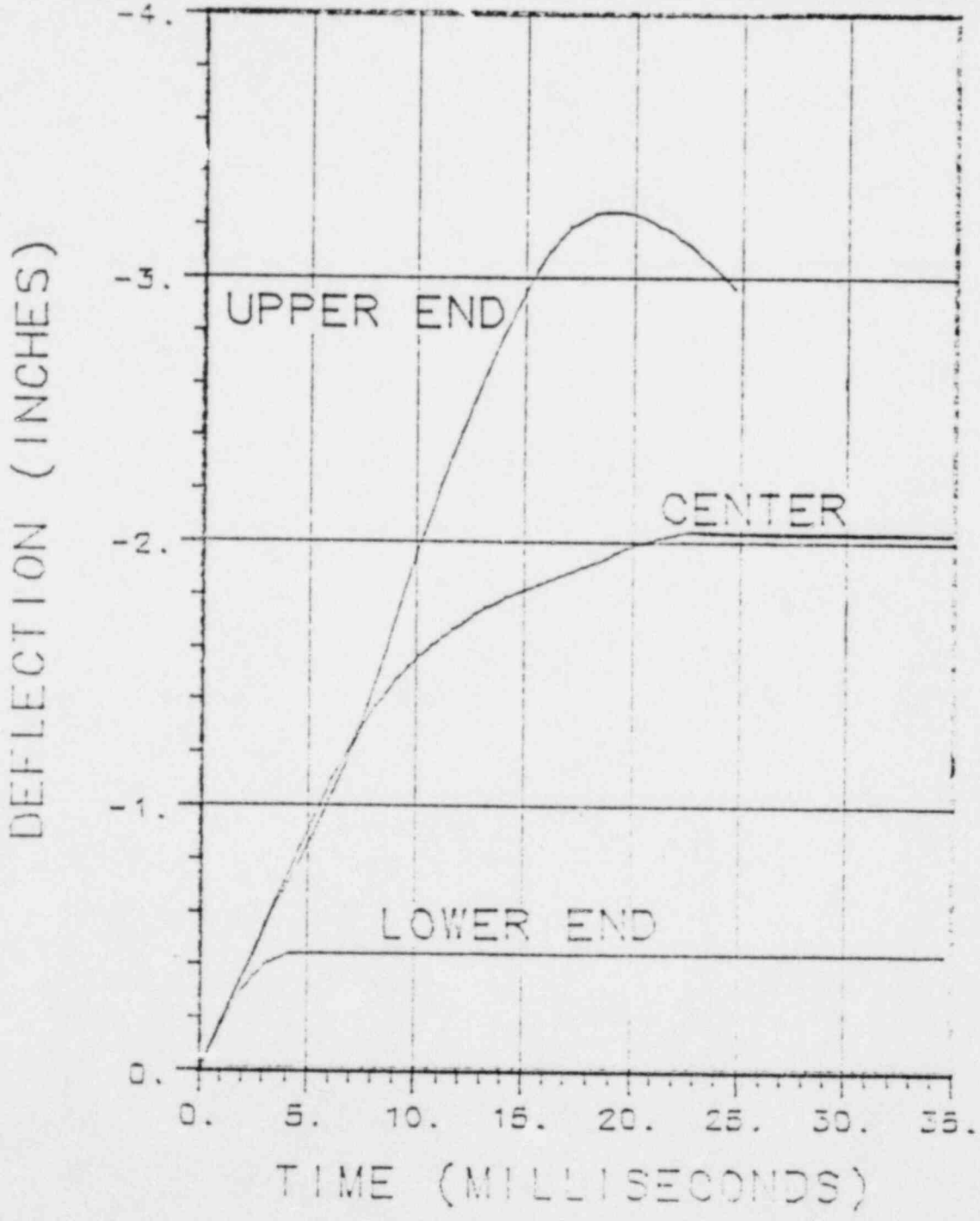

Figure 2-116. Deflection of Cask Ends During Impact on Valve

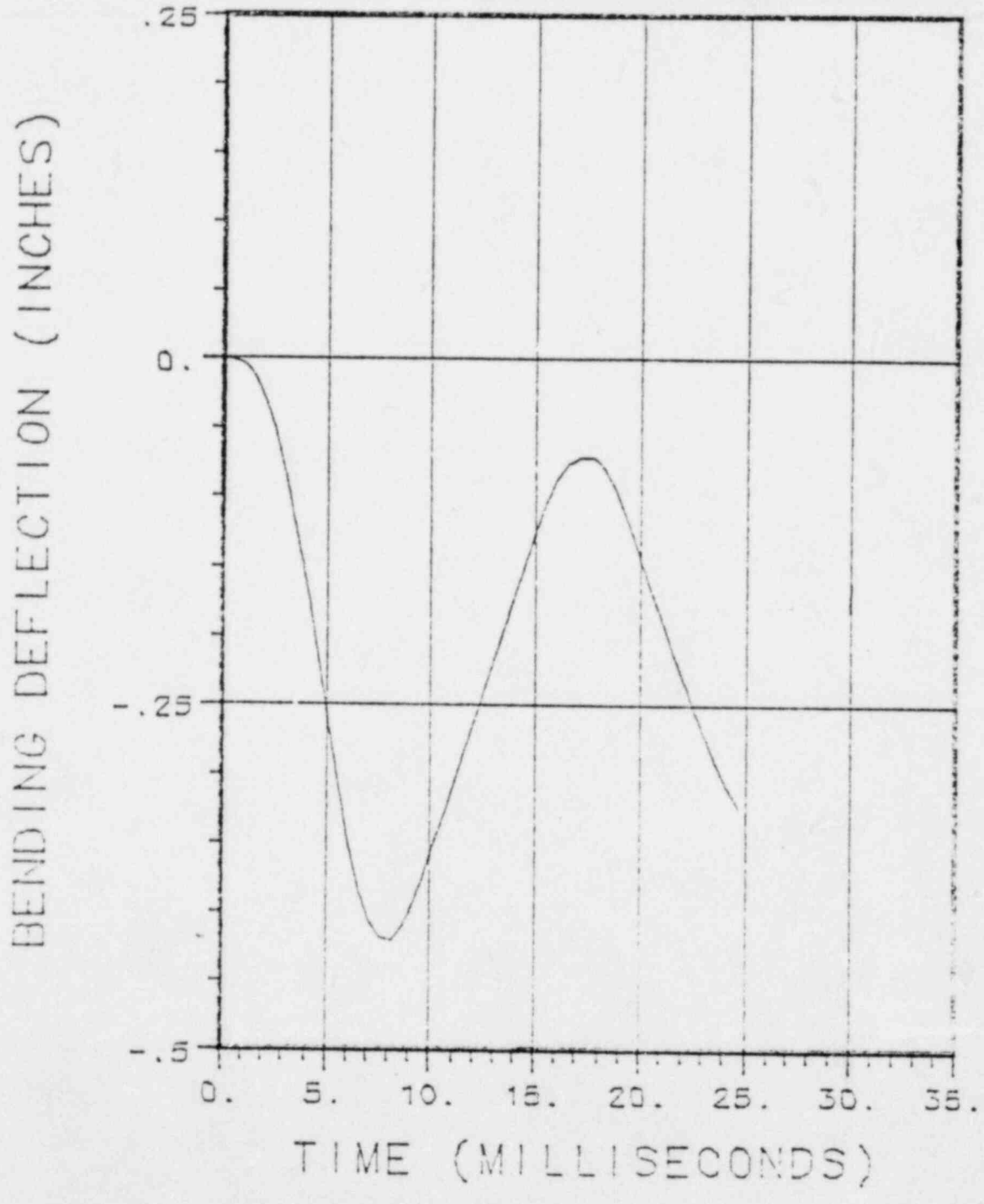

Figure 2-117. Deflection of Cask Center During Impact on Valve

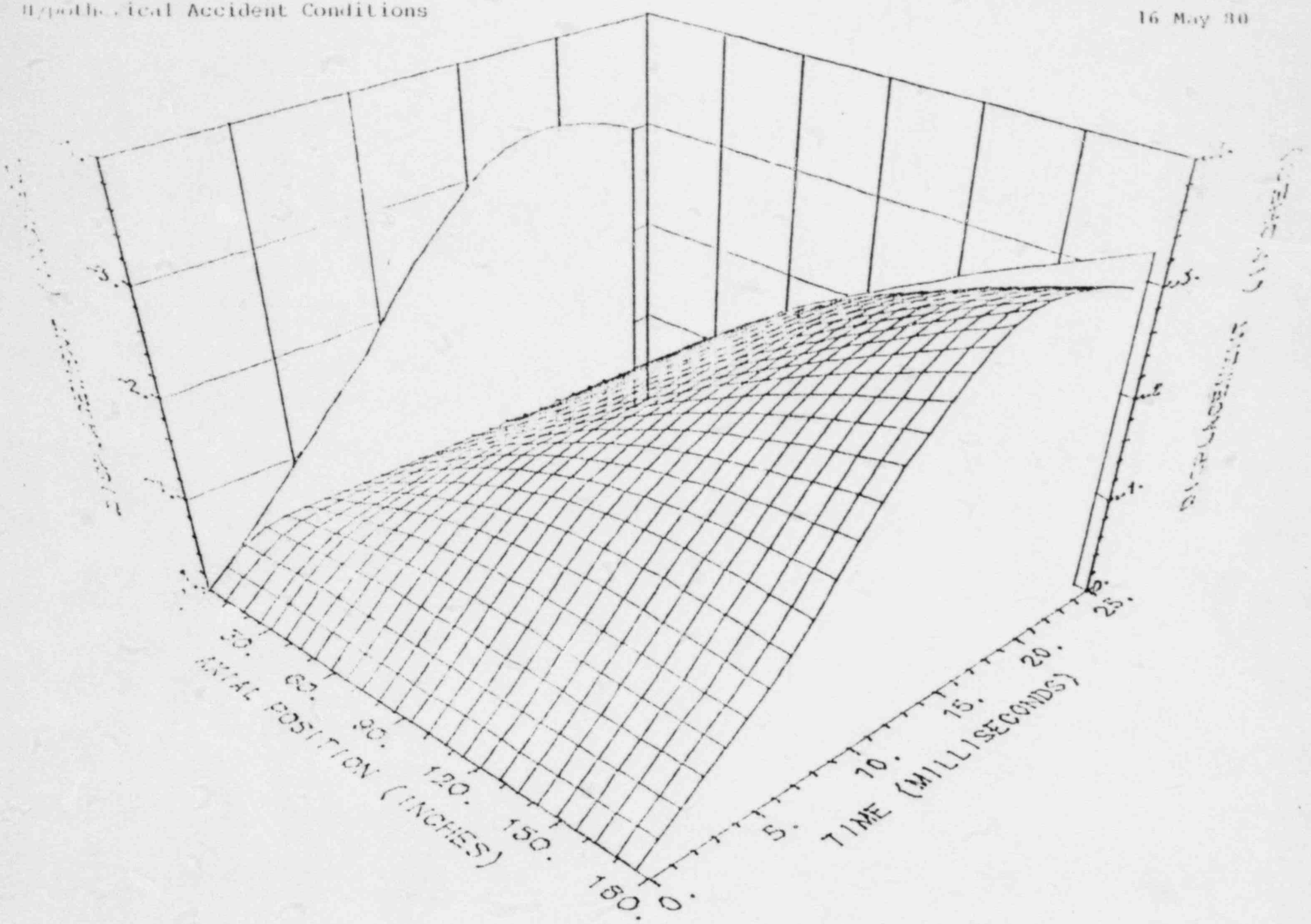

Figure 2-118. Deflection of Entire Cask During Impact on Valve

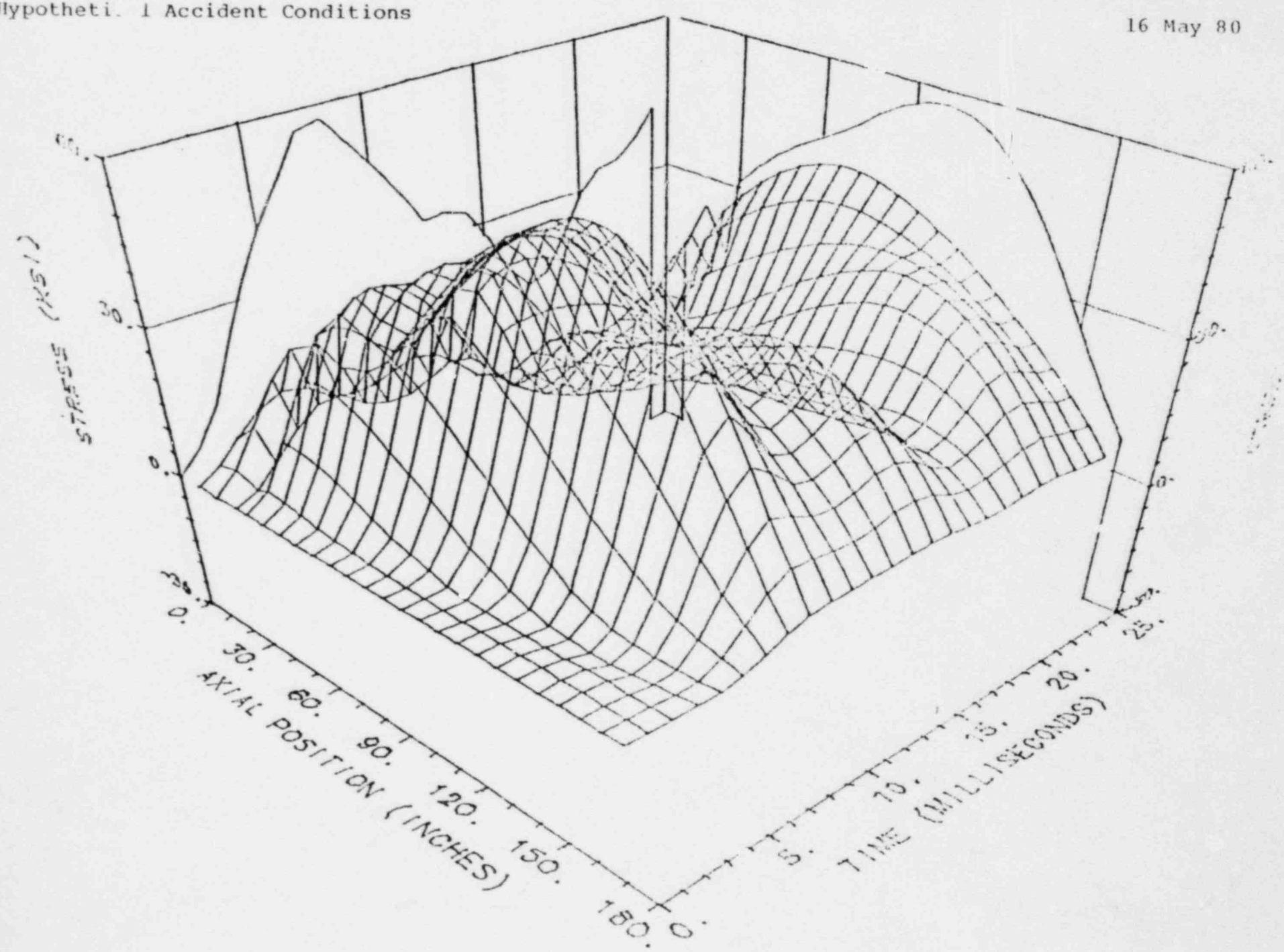

Figure 2-119. Bending Stress in Entire Cask During Impact on Valve

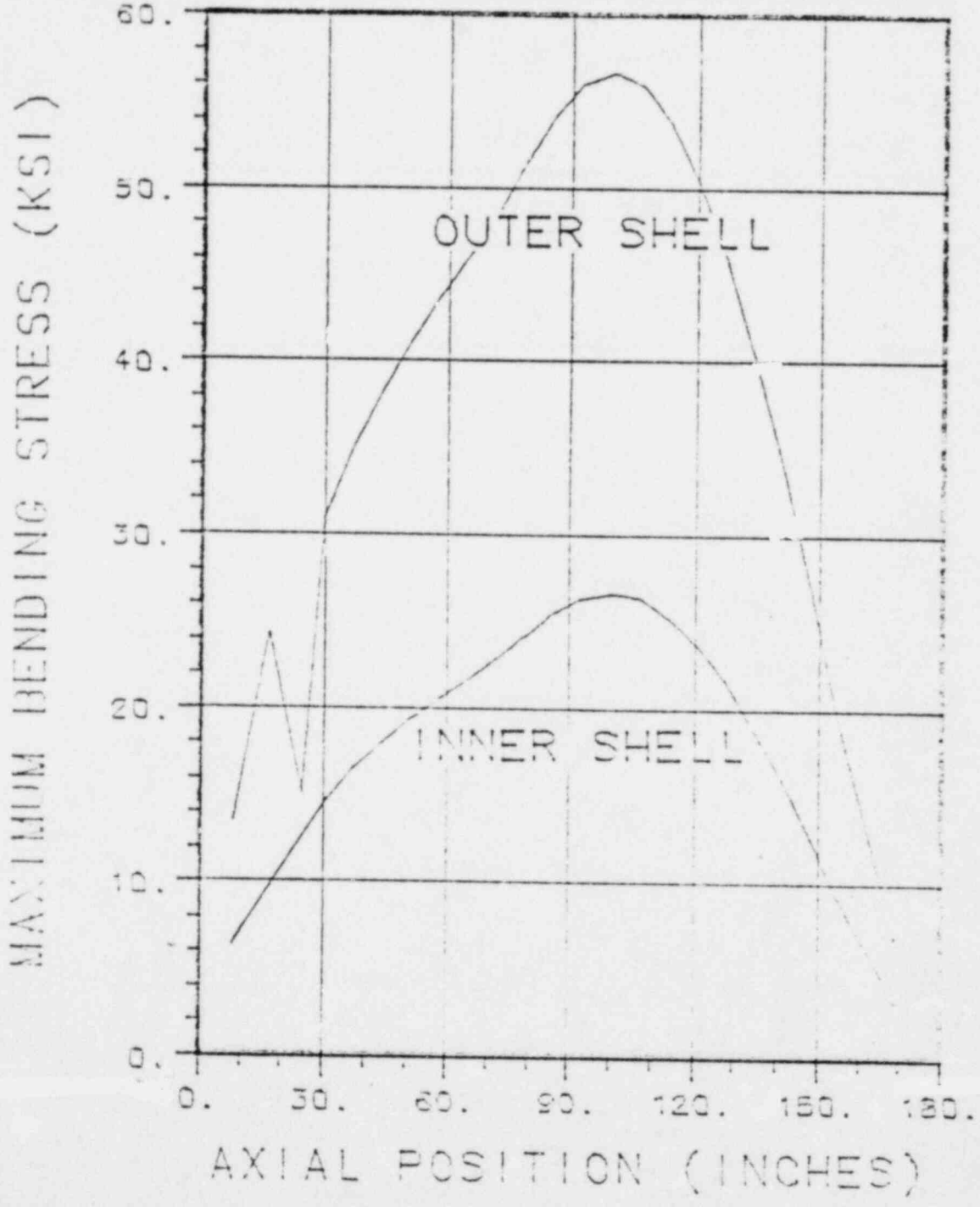

Figure 2-120. Maximum Stress During Impact on Valve

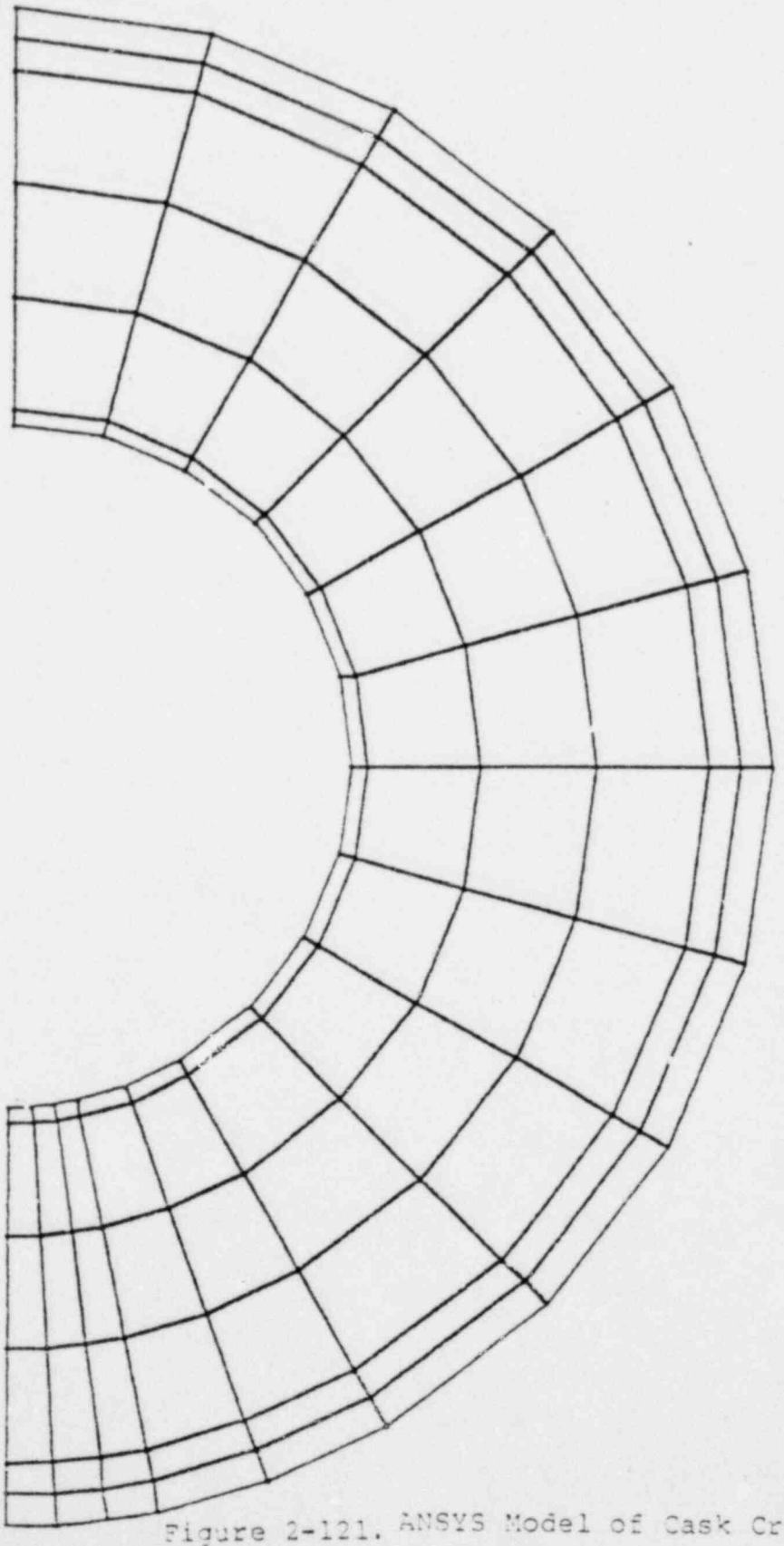

Figure 2-121. ANSYS Model of Cask Cross Section

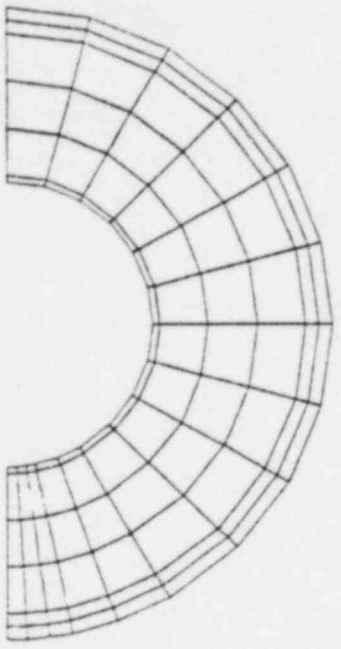

INITIAL

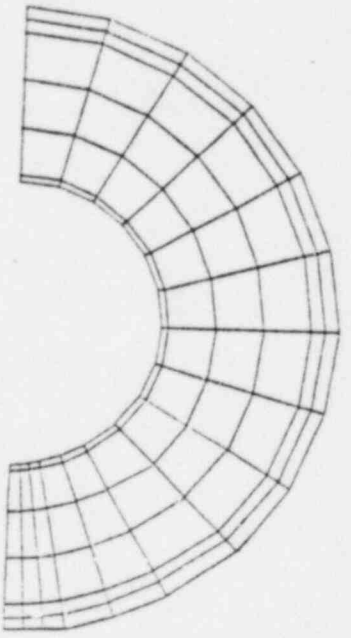

1.325 MILLISECONDS

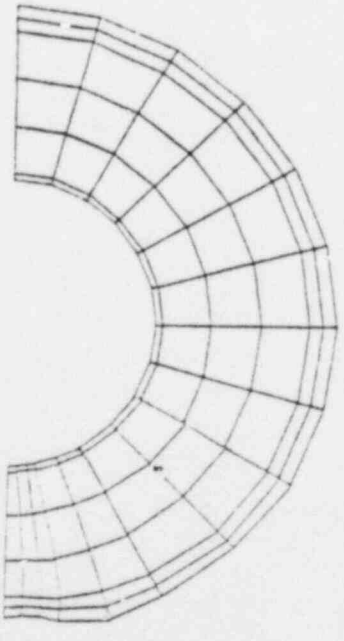

9.0 MILLISECONDS

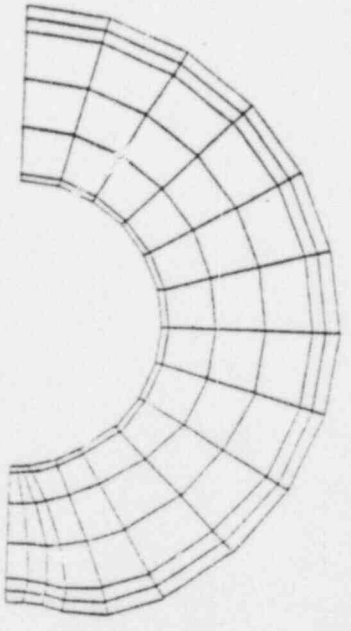

15.45 MILLISECONDS

Figure 2-122. Deformed Geometry of Cask Cross Section

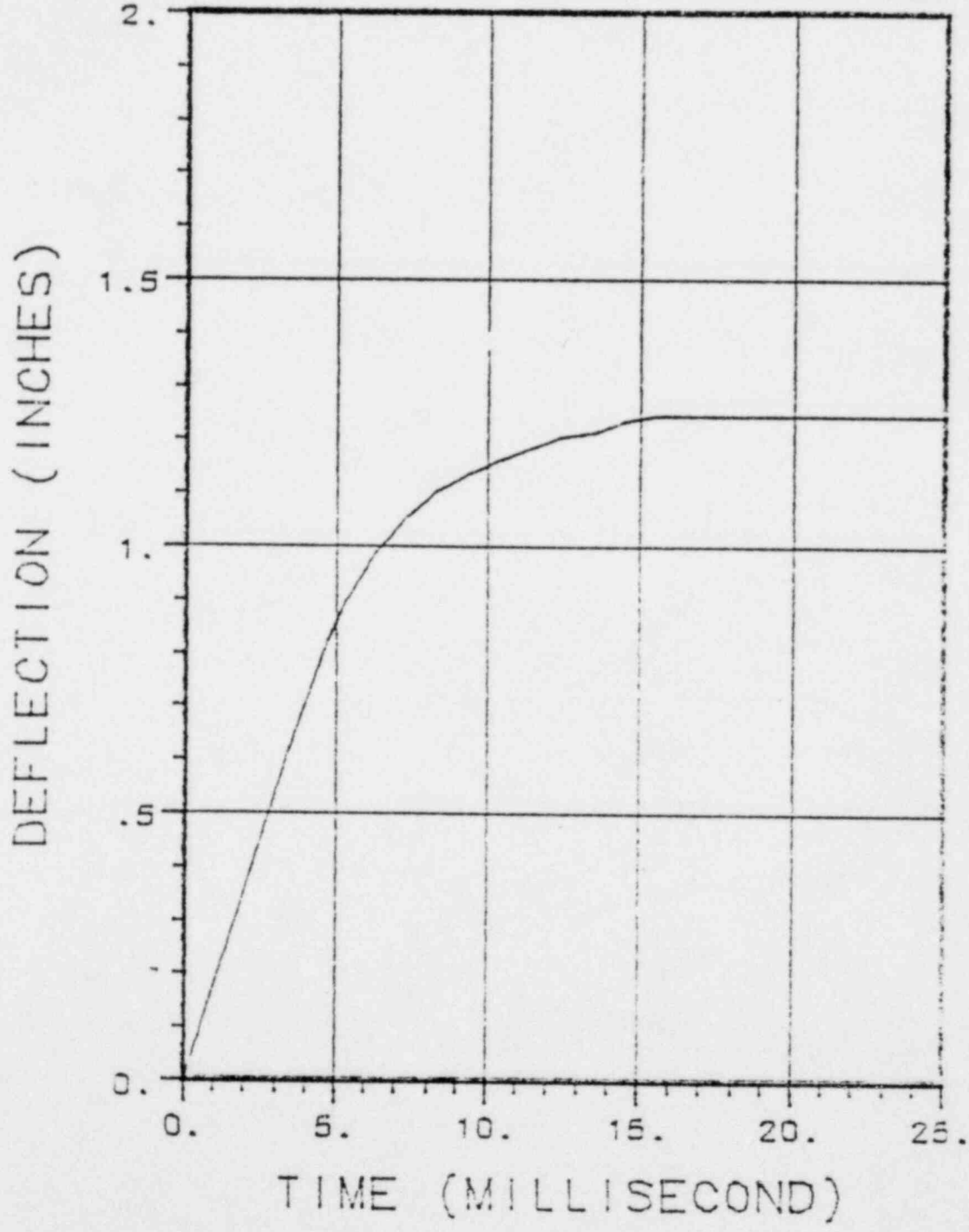

Figure 2-123. Deflection of Cask Center During Impact on Pin

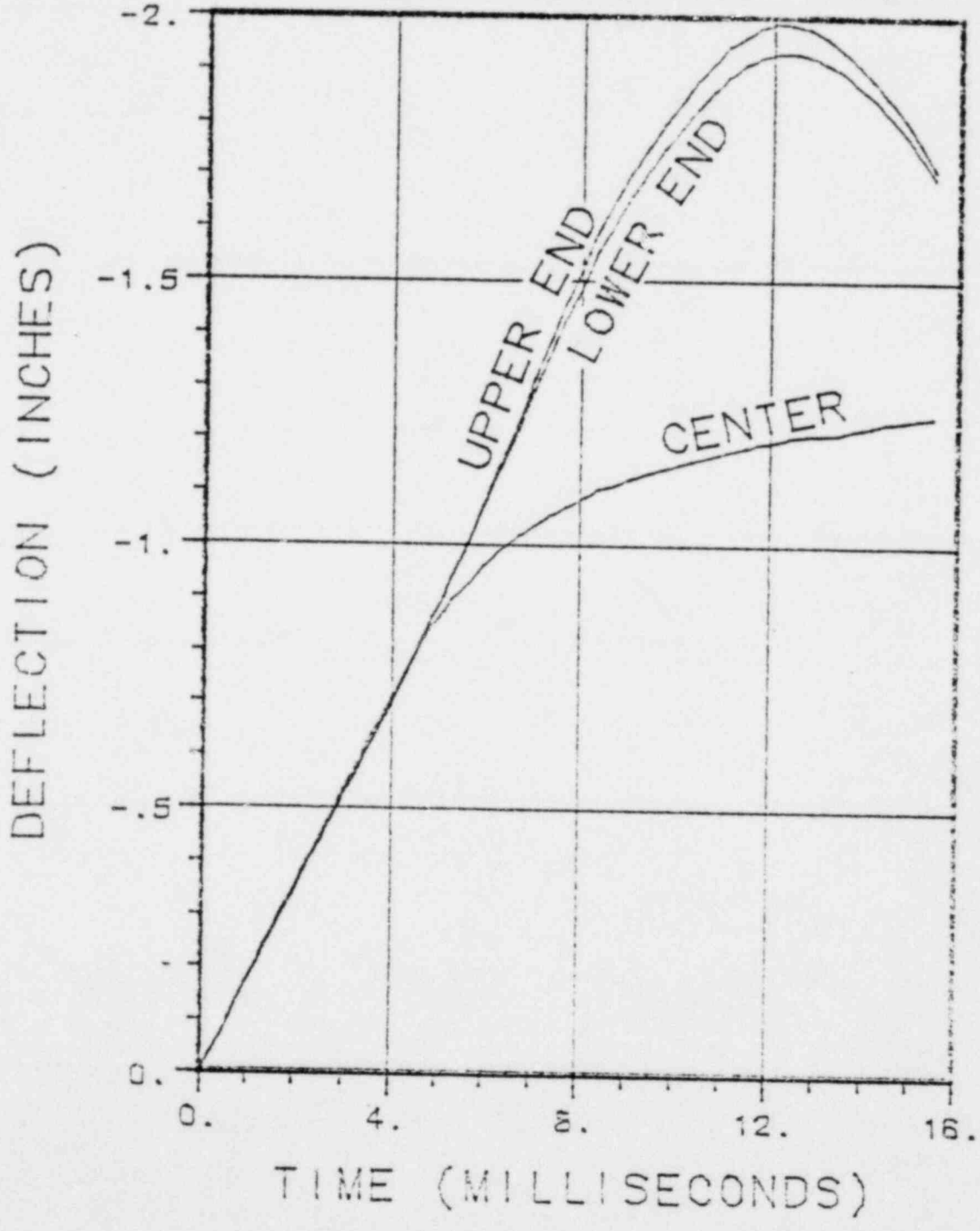

Figure 2-124. Deflection of Cask Ends During Impact at Midspan

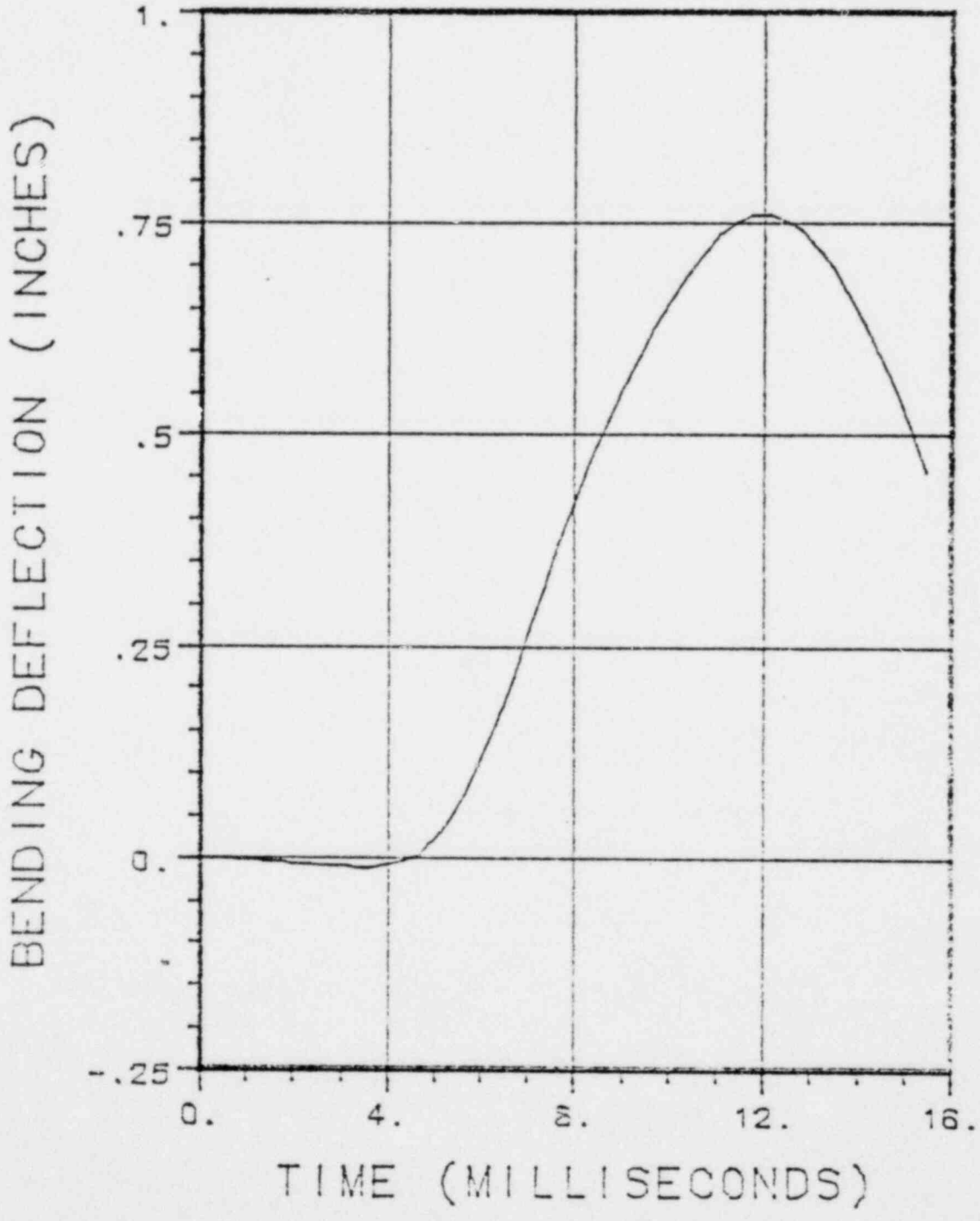

Figure 2-125. Deflection of Cask Ends with Respect to Center

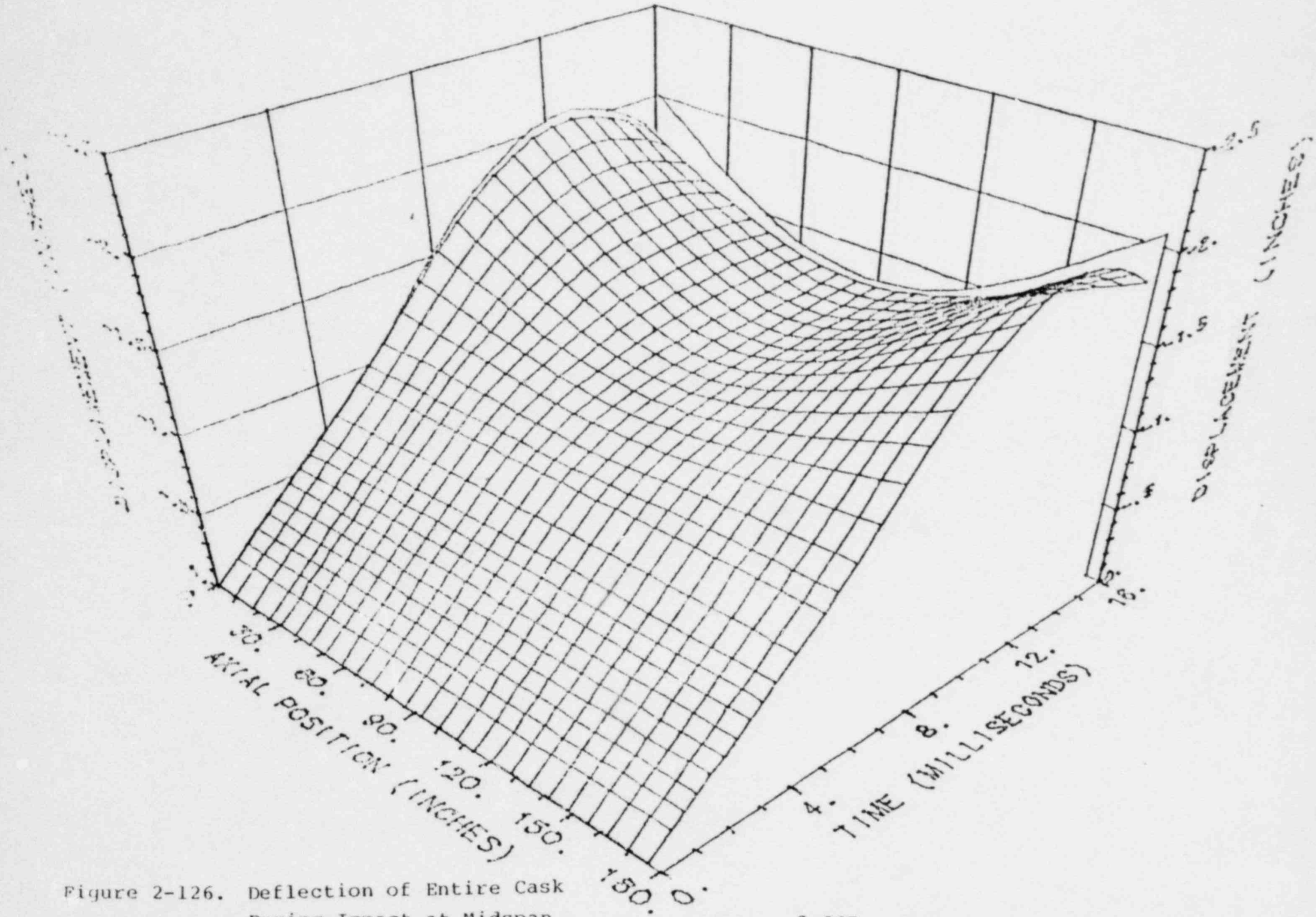

Figure 2-126. Deflection of Entire Cask During Impact at Midspan

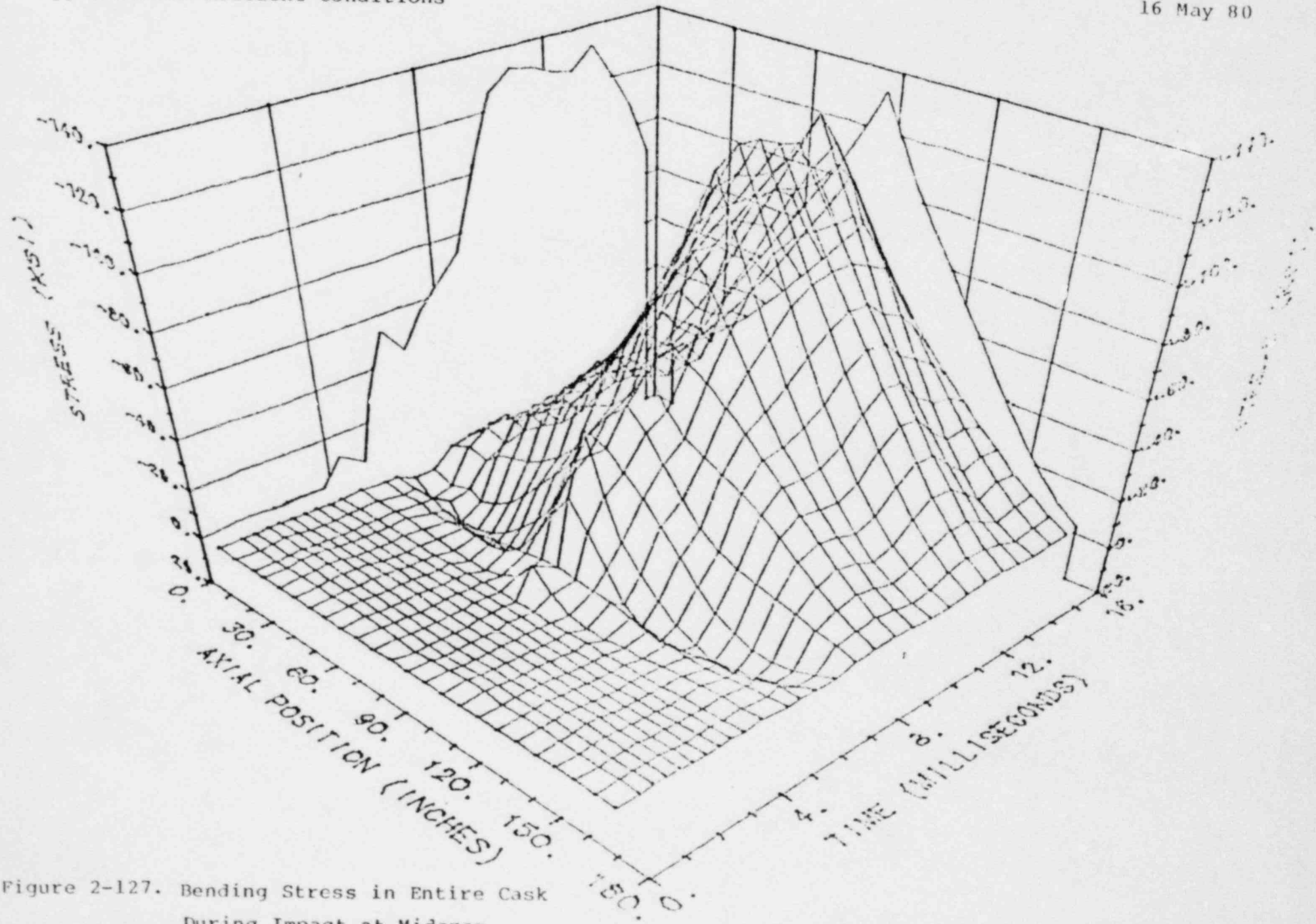

Figure 2-127. Bending Stress in Entire Cask During Impact at Midspan

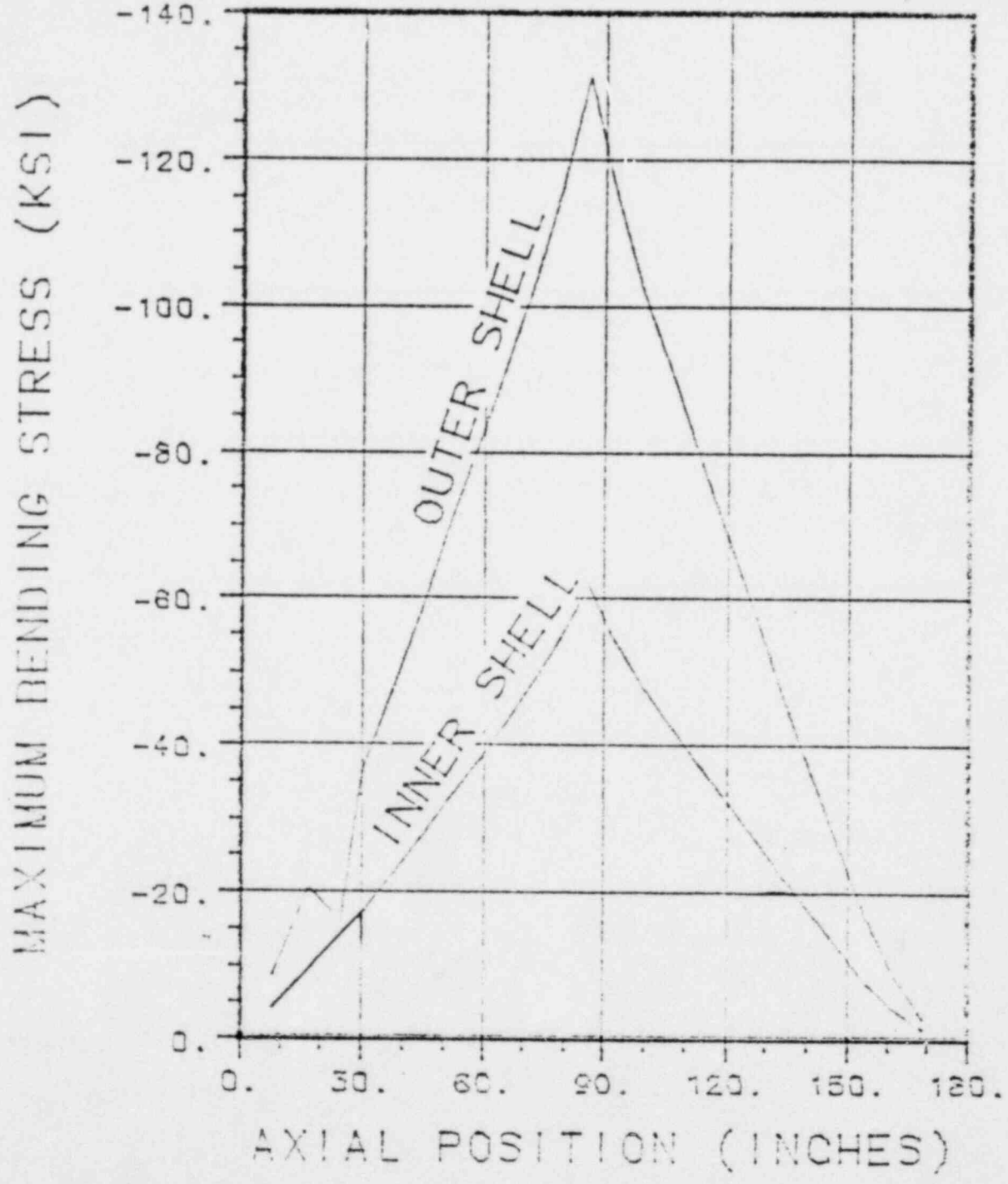

Figure 2-128. Maximum Stress During Impact at Midspan

Hypothetical Accident Conditions

16 May 80

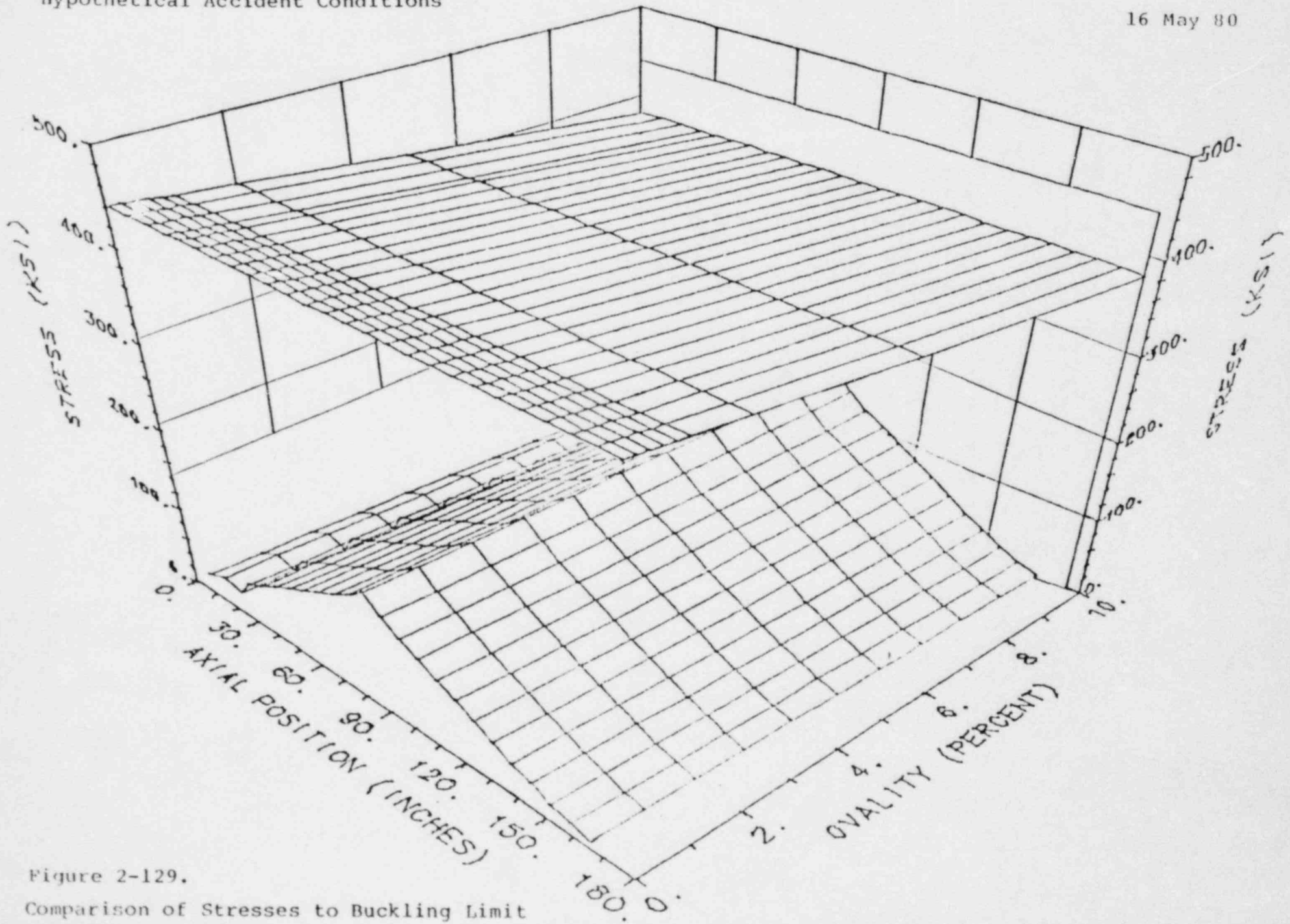

Figure 2-129.

Comparison of Stresses to Buckling Limit

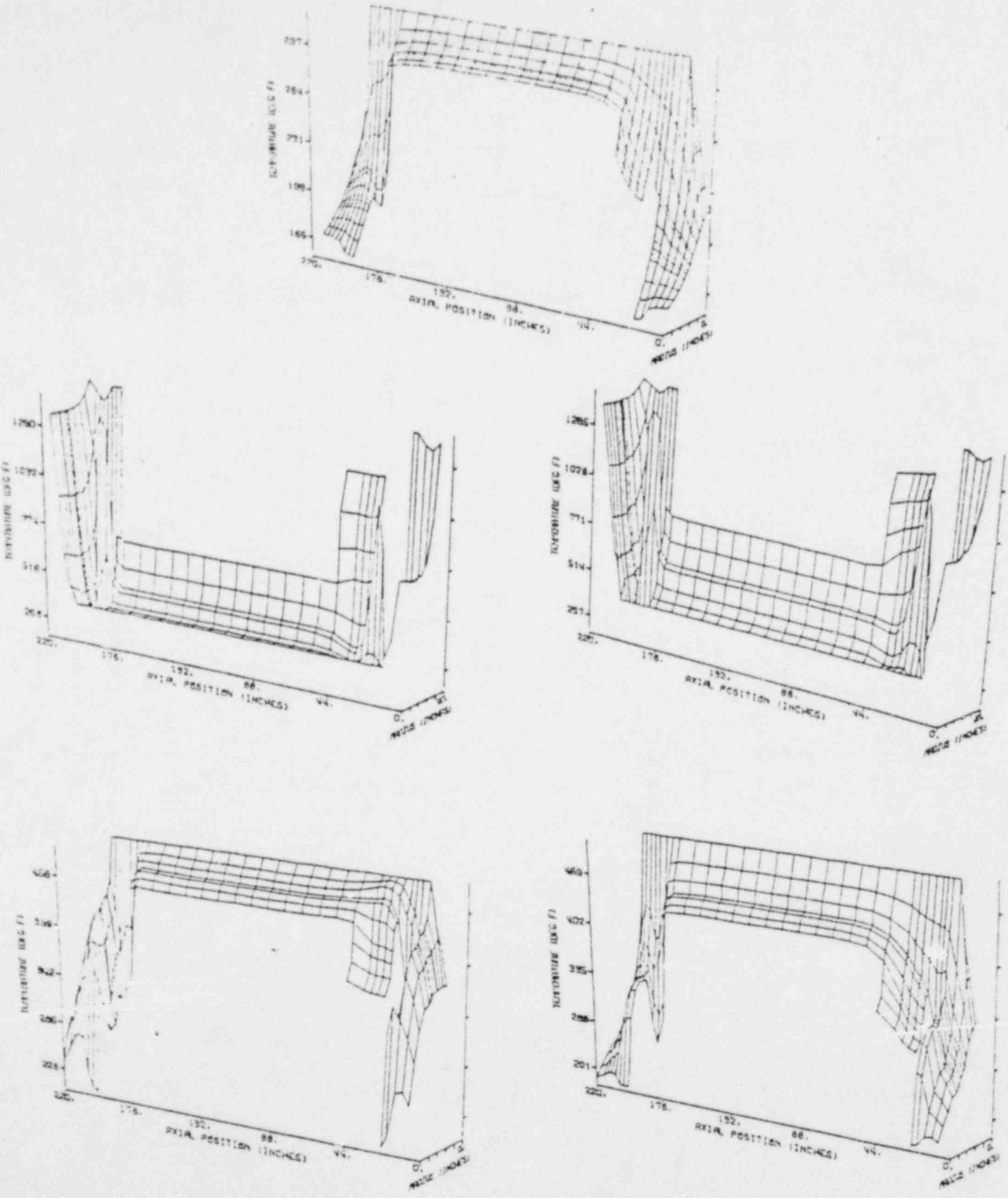

Figure 2-130. Temperature Profiles During Fire

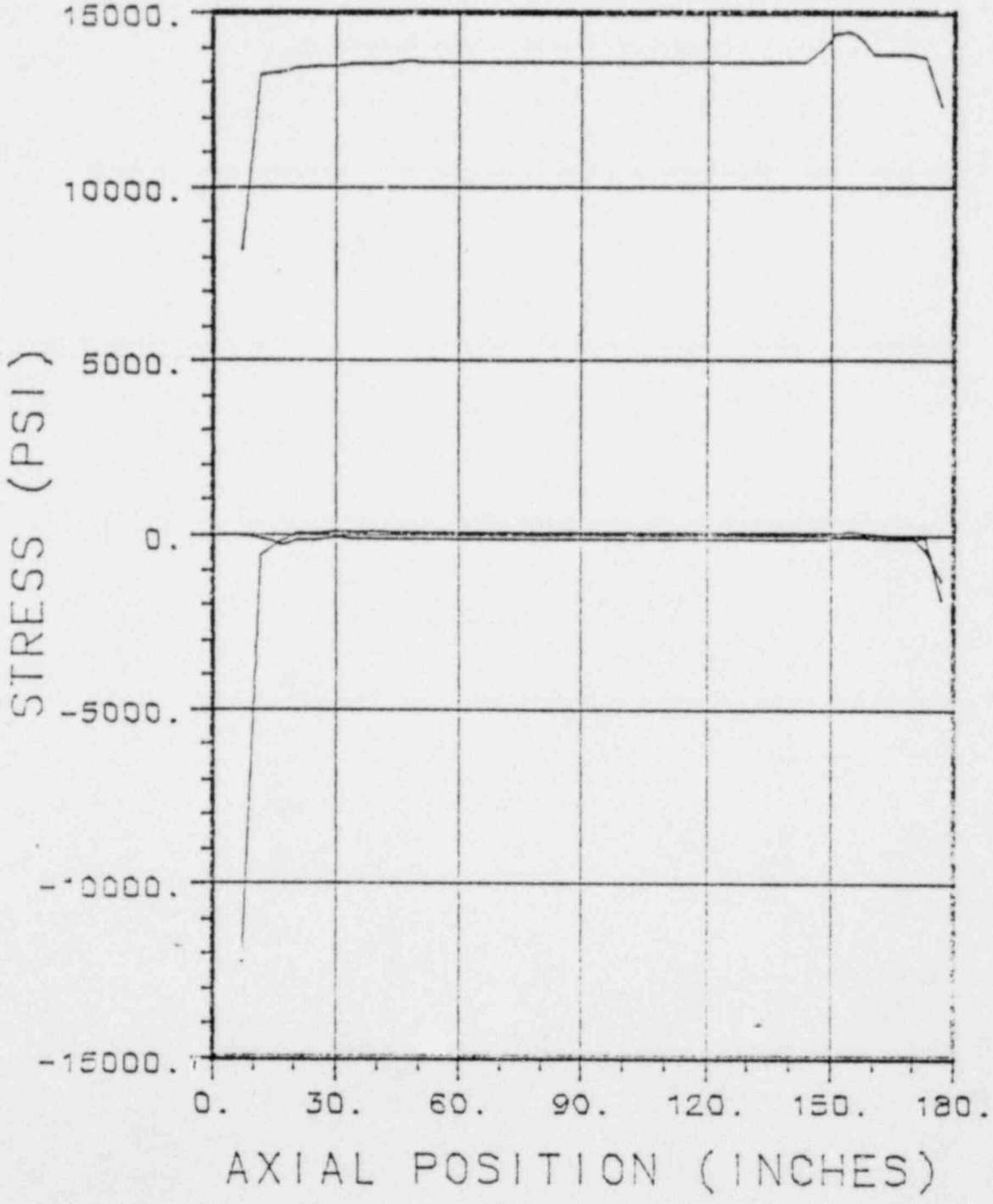

Figure 2-131. Thermal Stresses After 15 Minutes of Fire

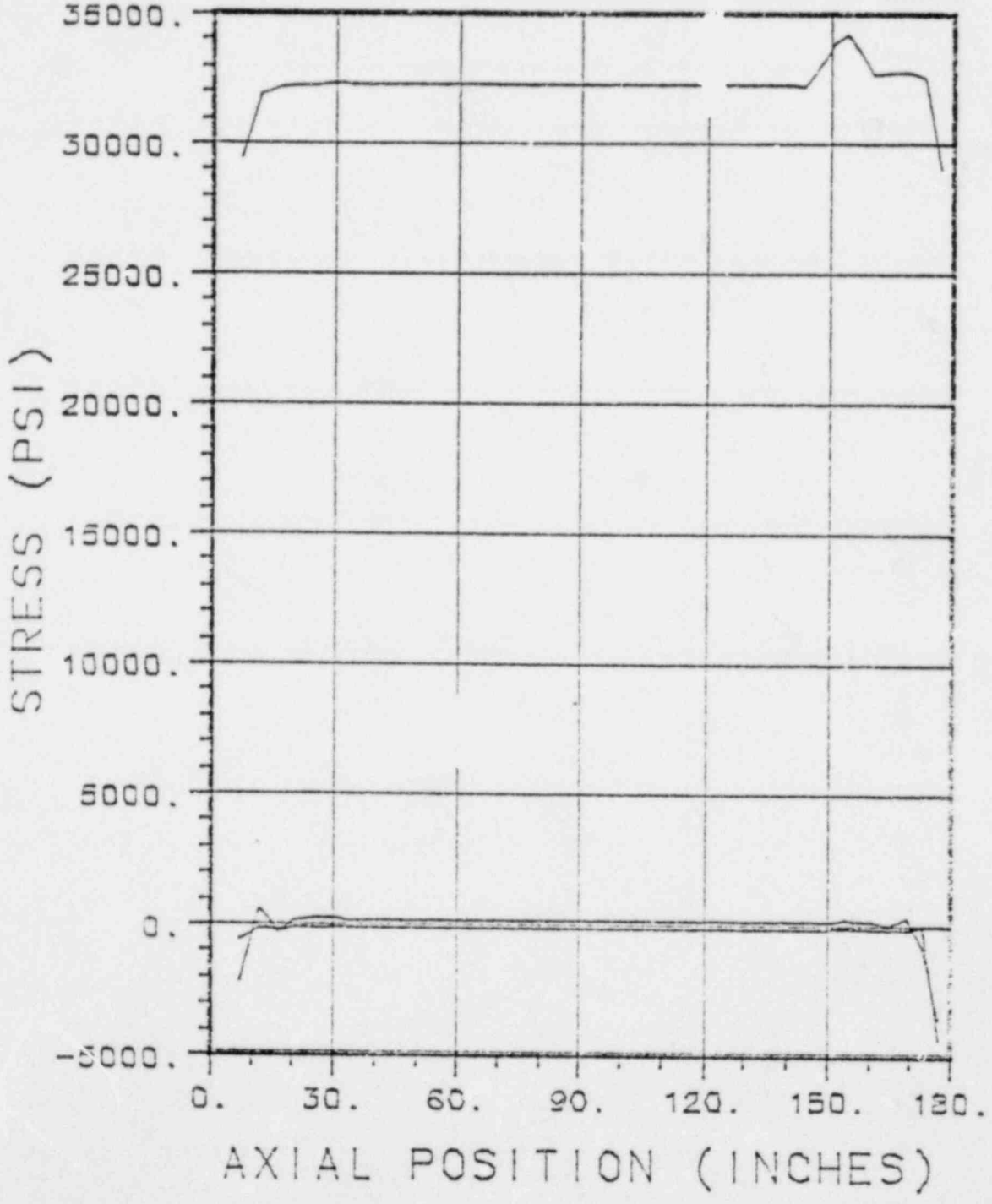

Figure 2-132. Thermal Stresses After 30 Minutes of Fire

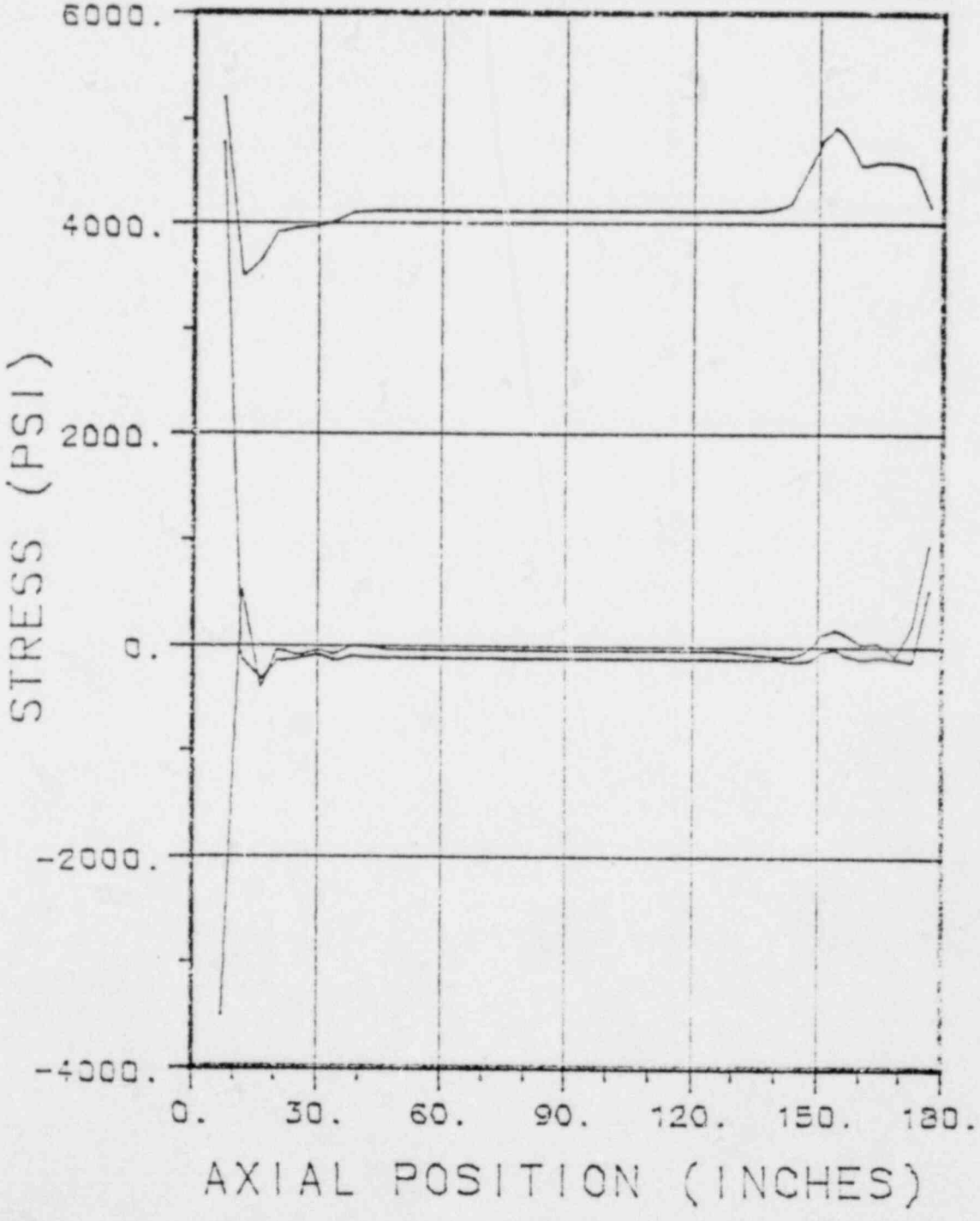

Figure 2-133. Thermal Stresses 2 Hours After Start of Fire

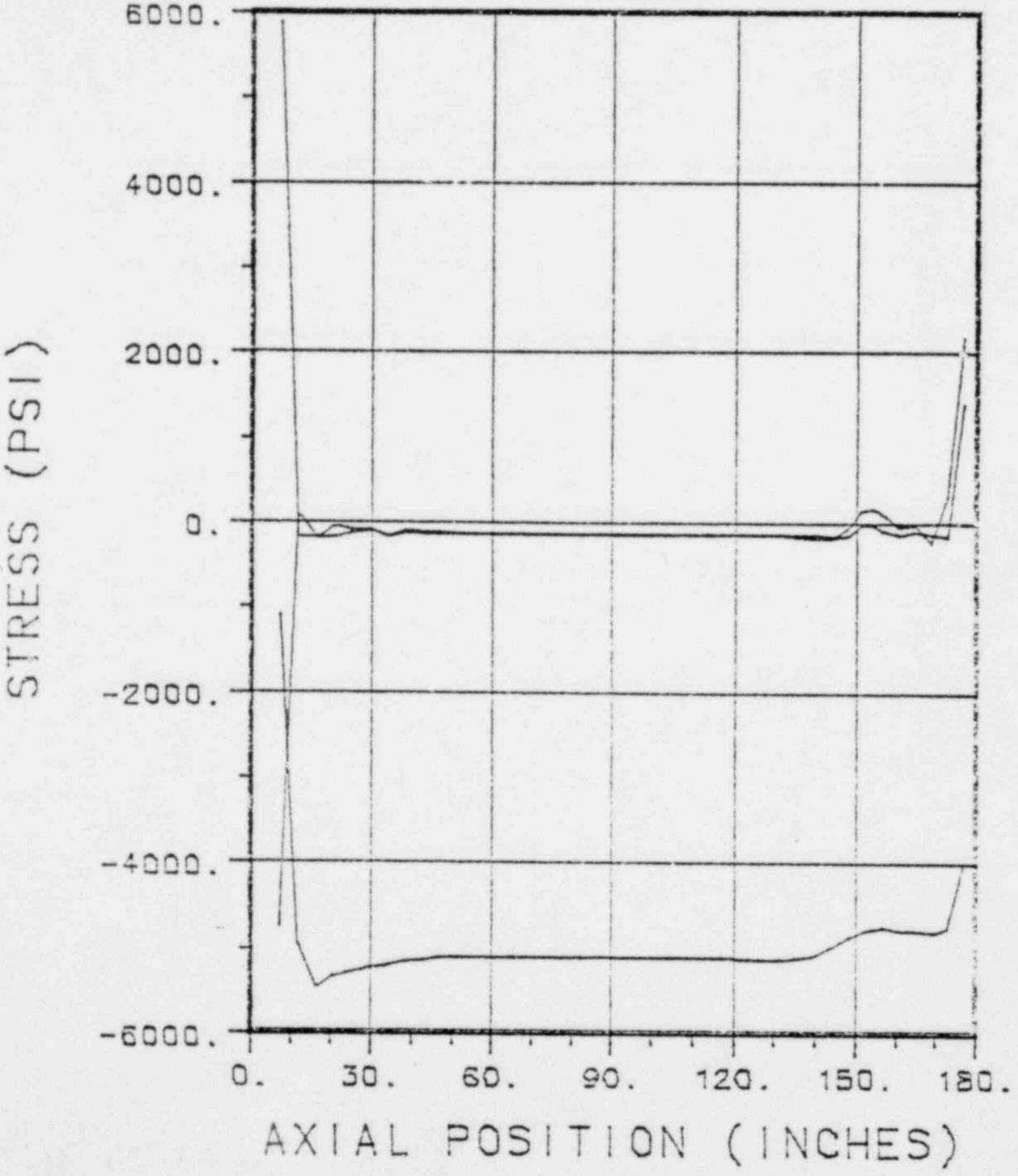

Figure 2-134. Thermal Stresses 4 Hours After Start of Fire

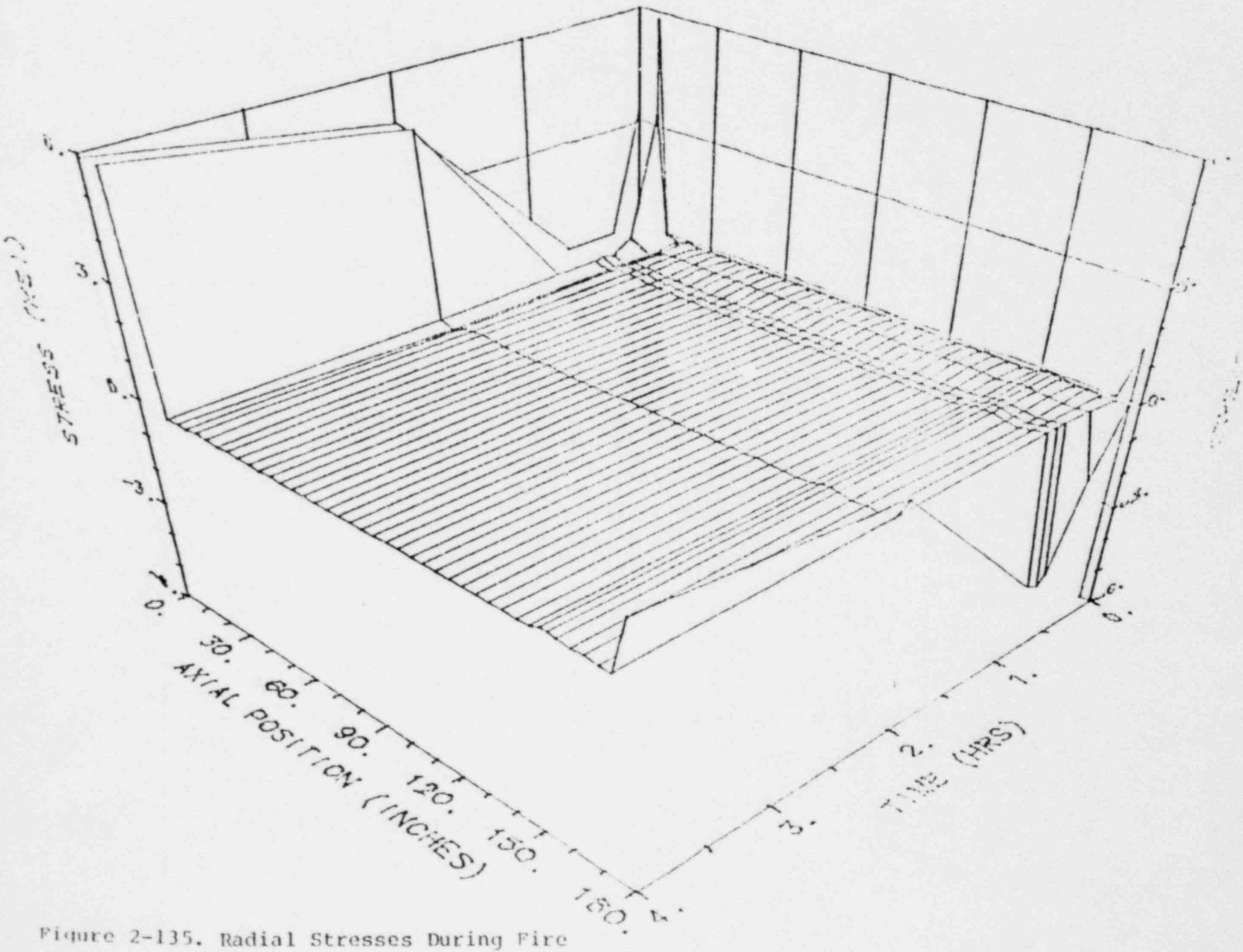

Figure 2-135. Radial Stresses During Fire

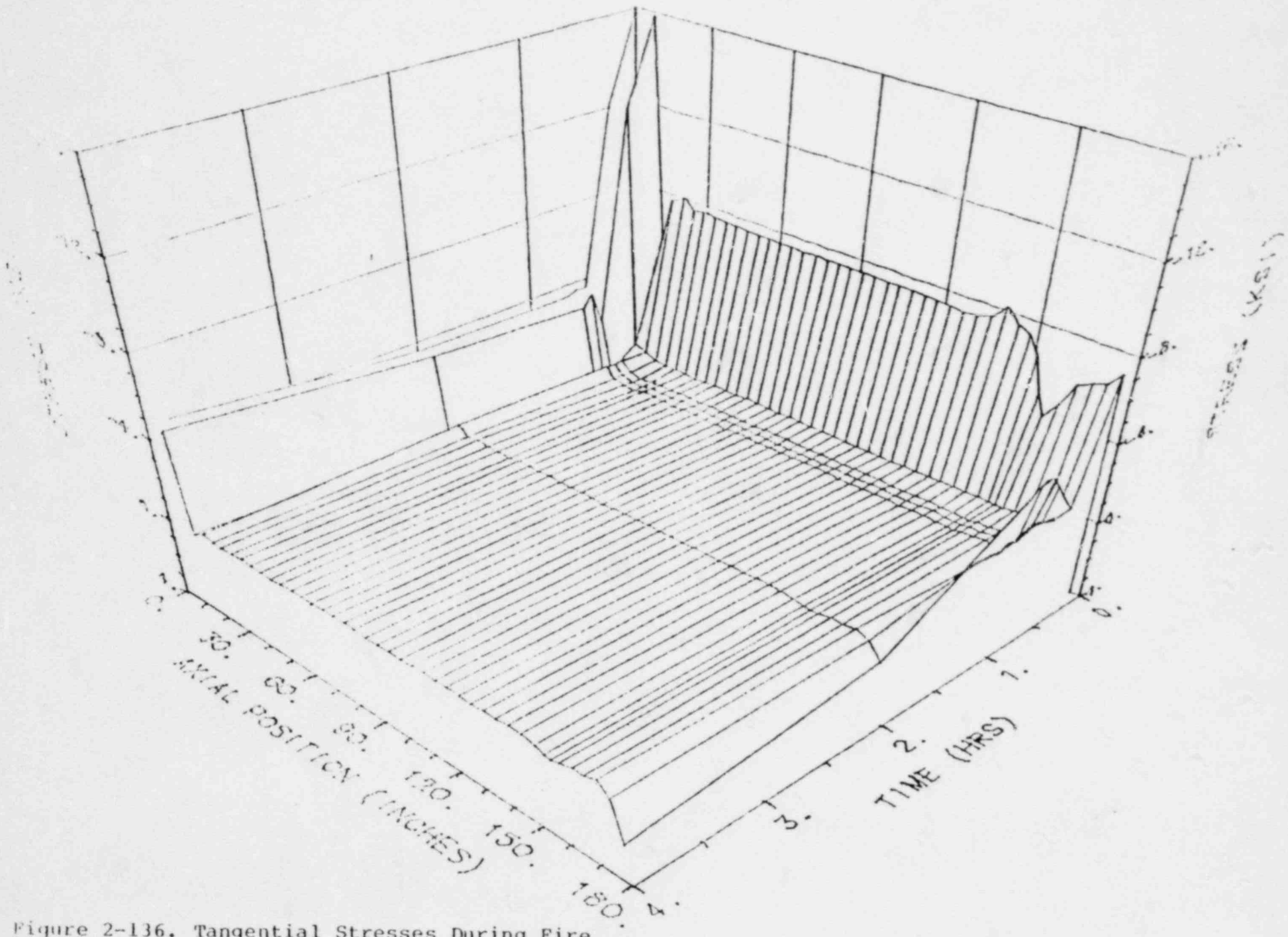

Figure 2-136. Tangential Stresses During Fire

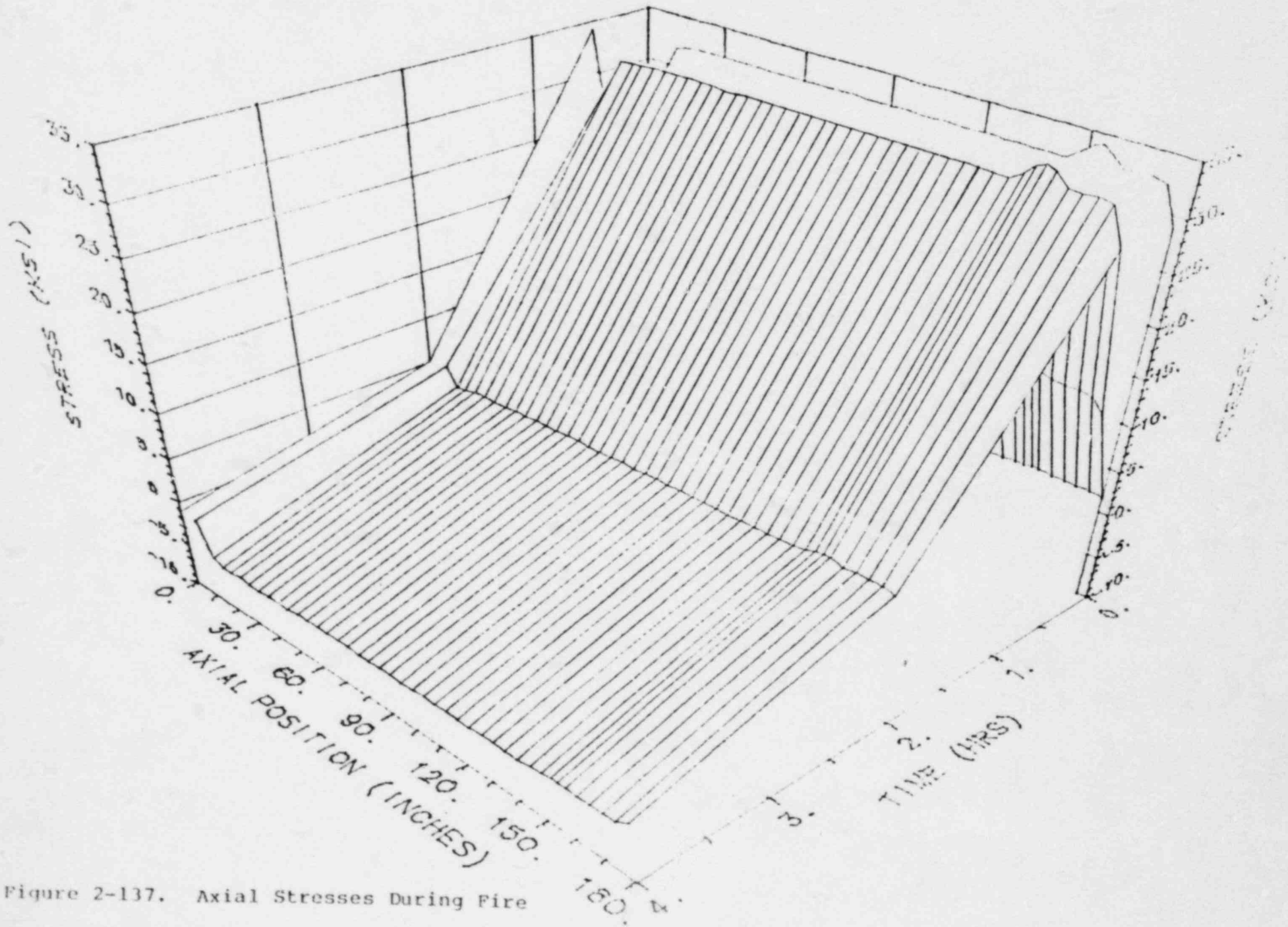

Figure 2-137. Axial Stresses During Fire

2.8. Special Form

Special form is defined in Part 71 of Title 10, Chapter 1 of the Code of Federal Regulations (Reference 2.2) to include all those types of fuel that could be expected to survive modest impacts without loss of containment of their radioactivity. Since the spent nuclear fuel to be transported in the NAC-1 cask is zircalloy clad which has been irradiated to the point where the clad could be considered to be brittle, no credit was taken for special form.

2.9. Fuel Rods

The analysis of the structural characteristics of the fuel rods is required only if the cladding is required to maintain containment of the fission products during normal transport and accident conditions. Since the NAC-1 cask is designed as a zero release cask, there is no need to require any containment of the fission products other than the cask itself. Consequently, no analysis of the fuel rods is required.

2.10. Appendices to Structural Analysis

The following sections contain material that is intended to supplement the information presented in the previous sections.

2.10.1. ANSYS Program Description (Reference 2.11)

All of the computer aided analysis of the NAC-1 cask that is reported here utilized the ANSYS computer program. ANSYS is a large scale computer program for the solution of several classes of engineering problems including problems with static and dynamic loads and elastic, plastic or creep stresses with large or small deflections.

The matrix displacement method of solution, based upon finite element idealization, is employed throughout the program. The library of finite elements available numbers more than forty. This variety of elements gives ANSYS program the capability of analyzing two- and three-dimensional structures by representing the components as either planes or solids with or without symmetry conditions.

Loading on the structure may be forces, displacements, pressures or response spectra. Loading may be arbitrary time functions for linear and nonlinear dynamic analyses. The ANSYS program uses the wave front (or "frontal") direct solution method for the system of simultaneous linear equations developed by the matrix displacement method, and gives high accuracy results in a minimum of computer time. The program has the capability of solving for the stress distributions in large structures. There is no "band width" limitation in the problem definition; however, there is a "wave front" restriction. The magnitude of the "wave front" restriction depends upon the amount of core storage available for

a given problem. The wave front limitation is restrictive only for the analysis of large three dimensional structures or when ANSYS is used on a small computer.

The input format for the ANSYS program has been designed to make problem definition as easy as possible. Options for multiple coordinate systems using either cartesian, cylindrical or spherical coordinates are available, as well as multiple region generation capabilities to minimize the input data for repeated regions. Sophisticated geometry generation capabilities are included for two-dimensional plane and axisymmetric structures and for intersecting three-dimensional sheet and solid structures.

Revision 3, Update 37 of ANSYS was utilized for this analysis of the NAC-1 cask. This version was installed and operated on the CYBER 176 computer owned and operated by United Computing Systems,Inc. in Dallas Texas. This version of ANSYS was installed and is maintained by Swanson Analysis Systems,Inc. They also maintain the necessary program benchmarking and documentation of the results of the benchmark calculations (Reference 2.25).

2.10.2. References

2.1 "Safety Analysis Report for Nculear Fuel Services, Inc. Spent Fuel Shipping Cask Model No. NFS-4, Nuclear Fuel Services, Inc, U.S.N.R.C. Docket 6698, September 1972.

2.2 Part 71 of Title 10, Chapter 1 of the Code of Federal Regulations, March 2,1979.

2.4 "ASME Boiler and Pressure Vessel Code, Section III, Nuclear Vessels," The American Society of Mechanical Enginers, New York, N.y., 1971.

2.5 "Design Criteria for the Structural Analysis of Shipping Cask Containment Vessels," Regulatory Guide 7.6 Revision 1, U.S. Nuclear Regulatory Commission, Office of Standards Development, March 1978.

2.6 Gerard, Bruce and Herbert Becker, Handbook of Structural Stability, Part III - Buckling of Curved Plates and Shells, NACA Technical Note 3783, August 1957.

2.7 Johnston, Bruce G.,ed., Guide to Stability Design Criteria for Metal Structures, John Wiley and Sons, 3rd Edition, 1976.

2.8 Handbook of Structural Stability, edited by Column Research Committee of Japan, 1971.

2.9 Roark,Raymond J., Formulas for Stress and Strain, McGraw-Hill Book Company, New York,N.Y., Fourth Edition, 1965.

2.10 Rack, Henry J. and Gerald A. Knorovksy, "An Assessment of Stress-Strain Data Suitable for Finite Element Elastic-Plastic Analysis of Shipping Containers," NUREG/CR-0481, SAND77-1872, Sandia Laboratories, September 1978.

2.11 DeSalvo, Gabriel J., "ANSYS Engineering Analysis System Verification Manual," Swanson Analysis Systems, Inc, June 1, 1976

2.12 Robinson,R.A., W.J.Zielenbach, and A.A.Lawrence, "A Survey of Strain Rate Effects for some Common Structural Materials Used in Radioactive Material Packaging and Transportation Systems," BMI-1954, UC-71, Battelle Columbus Laboratories, Columbus, Ohio, August 1976.

2.13 Hanford Engineering Development Laboratory," Nuclear Systems Materials Handbook, Richland, Washington, 1978.

2.14 Four Letters from Richard H. Perry of the Edward Lead Co. to Excelco Developments, Inc. dated:

September 3, 1974 (unit 1) September 3, 1974 (unit 3)
September 3, 1974 (unit 2) October 31, 1974 (unit 4)

2.15 "Standard Specifications for Grades of California Redwood Lumber," Redwood Inspection Service, San Francisco, California 1978.

2.16 Von Riessemann, Walter A. and Tommy R. Guess, "The Effects of Temperature on the Energy Absorbing Characteristics of Redwood," NUREG/CR-0332, SAND 77-1589, Sandia Laboratories, Albuquerque, New Mexico, June 1978.

2.17 Baumeister, Theodore and Lionel S. Marks, "Standard Handbook for Mechanical Engineers," Mc-Graw Hill Book Company, New York, Seventh Edition, December 1966.

2.18 Hill, T.K. and W.W. Joseph, "Energy-Absorbing Characteristics of Materials, SLA-74-0159, Sandia Laboratories Albuquerque, New Mexico, 1974

2.19 Perry, Robert H. and Cecil H. Chilton, Chemical Engineer's Handbook, McGraw-Hill Book Company, New York, N.Y., Fifth Edition, 1973.

2.20 Magnuson, Clifford F., "Shock and Vibration Environment For A Large Shipping Container During Truck Transport (Part II),"

NUREG/CR-0128, SAND 78-0337, Sandia Laboratories, Albuquerque, New Mexico, February 13,1978.

2.21 Temperature Extremes

2.22 "Load Combinations For The Structural Analysis of Shipping Casks," Regulatory Guide 7.8, U.S. Nuclear Regulatory Commission, Office of Standards Development, May 1977.

2.23 Turner, W.D., D.C. Elrod and I.I. Siman-Tov, "HEATING-5 An IBM 360 Heat Conduction Program," ORNL/CSD/TM-15, Union Carbide Corporation, Nuclear Division, Oak Ridge National Laboratory, Oak Ridge, Tennessee.

2.24 D'Isa, Frank A., Mechanics of Metals, Addison-Wesley Publishing Company,Inc., Reading, Massachusetts, 1968.

2.25 DeSalvo, Gabriel J. and John A Swanson, "ANSYS Engineering Analysis System User's Manual," Swanson Analysis Systems, Inc., July 1,1979.

2.10.3. Sample Input for ANSYS

The following pages present typical input for ANSYS calculations of the following sections of the cask:

30 Foot Fall on End
30 Foot Fall on Side
30 Foot Fall on Corner
Evaluation of Thermal Stresses

These tabulations of the input data do not include the control cards that were employed at the time of execution because they are not essential to the accurate execution of these calculations.

Table 2-20. ANSYS Input for 30 Foot Fall on End

```
THIRTY FOOT FALL END DROP (NAC-1)
TOM THOMPSON
 ,4,,1,1,1,2,,,,6,,,,,,1,,1
70.,70.,,,,,,,,1,1
1,42,,,1
2,42,,,1
3,42,,,1
4,21,,,4
5,12,,,1,,,2
6,42,,,1
7,1
-1
-90.,1.E14,.00001
-90.,1.E14,.00001
0.75
100.
0.0,1.E14,.00001
4.694

-2,,,,,,,,,,,,90,1,4
2,1,101,102,,,,,1,1
202,201,301,302,,,,,2,2,,,2,100,1
601,602,502,501,,,,,3,3
101,201,,,,,,,4,5,1,,91
401,501,,,,,,,4,5,2,,91
711,,,,,,,,,4,6
101,201,,,,,,,4,5,5
501,401,,,,,,,4,5,5
691,,,,,,,,,4,3
701,301,,,,,,,4,5,5
692,695,696,693,,,,,5,6
693,696,697,694,,,,,5,6
694,697,698,1,,,,,5,6
```

```
1,698,699,101,,,,,5,6
101,699,701,701,,,,,5,6
701,699,700,700,,,,,5,6
701,700,501,501,,,,,5,6
501,700,702,601,,,,,5,6
695,703,704,696,,,,,5,6
696,704,705,697,,,,,5,6
697,705,706,698,,,,,5,6
698,706,707,699,,,,,5,6
699,707,700,700,,,,,5,6
703,708,709,704,,,,,5,6
704,709,710,705,,,,,5,6
705,710,711,706,,,,,5,6
706,711,707,707,,,,,5,6
712,711,,,,,,,6,7,4
-1
100,-2,3,2,0.5
1,,,,6.75
3,,1,,6.75,4.05
100,-2,85,2,0.3125
4,,,,6.75,4.75
5,,,,6.75,6.0
87,,1,,6.75,170.000
88,,,,6.75,171.255
100,-2,3,2,0.5
89,,,,6.75,171.955
91,,1,,6.75,175.875
100,-2,91,2,3.34375
301,,,,10.40625
303,,1,,10.40625,4.05
304,,,,10.40625,4.75
305,,,,10.40625,6.0
387,,1,,10.40625,170.000
388,,,,10.40625,171.255
389,,,,10.40625,171.955
391,,1,,10.40625,175.875
```

```
100,-2,91,2,1.25
501,,,,13.75
503,,1,,13.75,4.05
504,,,,13.75,4.75
505,,,,13.75,6.0
587,,1,,13.75,170.000
588,,,,13.75,171.255
589,,,,13.75,171.955
591,,1,,13.75,175.875
201,,,,7.25
203,,1,,7.25,4.05
204,,,,7.0625,4.75
205,,,,7.0625,6.0
287,,1,,7.0625,170.000
288,,,,7.0625,171.255
289,,,,7.25,171.955
291,,1,,7.25,175.875
692,,,,0.,0.
693,,,,2.25,0.
694,,,,4.5,0.
695,,,,0.,-2.5
696,,,,2.25,-2.5
697,,,,4.5,-2.5
698,,,,6.75,-2.5
699,,,,9.5625,-2.5
700,,,,12.375,-2.5
701,,,,10.406,0.
702,,,,15.,-2.5
703,,,,0.,-5.25
704,,,,2.25,-5.25
705,,,,4.5,-5.25
706,,,,6.75,-5.25
707,,,,9.5625,-5.25
708,,,,0.,-8.0
709,,,,2.25,-8.0
710,,,,4.5,-8.0
```

```
711,,,,6.75,-8.0
712,,,,6.75,-108.0
-1
91,191,291,391,491,591,691,-1
END
EX,1 ,27.1E6
ALPX,1,,0.
NUXY,1,,.275
DENS,1,,.000740
EX,2,,1.4E6
ALPX,2,,0.
NUXY,2,,.4
DENS,2,,.00106
EX,3,,27.1E6
ALPX,3,,0.
NUXY,3,,.275
DENS,3,,.000740
MU,4,,.95
EX,5,,27.1E6
ALPX,5,,0.
NUXY,5,,.275
DENS,5,,.000740
EX,6,,30.E8
ALPX,6,,O.
NUXY,6,,.275
DENS,6,,1.647E-5
END
2


0.,.0007,.005,.02,.04,.08
50.,1000.,1450.,2150.,2800.,3800.
100.,1000.,1450.,2150.,2800.,3800.
200.,1000.,1450.,2150.,2800.,3800.
300.,1000.,1450.,2150.,2800.,3800.
400.,1000.,1450.,2150.,2800.,3800.
```

```
-1
UY,1,,4,91,191,591,691
UY,1,,4,708,709,710,711
END
1,,,2,.0002
,,,,,,,,,,1,,1
708,,UX,,,711,1
692,,UX
695,,UX
703,,UX
712,,UX
91,,UX,,,691,100
695,,UY,-.1054,,702,1
712,,UY,-.1054
91,,UY,-.1054
END
712,FY
END
-1
-1,,1,2,.0004
,,,,,,,,,,1,,1
695,-,UY,,,702,1
91,-,UY
712,,UY,-.2108
END
712,FY
END
-1
-1,,4,1,.000838
,,,,,,,,1,1,1,,1
712,-,UY
-1
712,FY,.362401E6
END
-1
-1,,2,1,.001049
```

```
,,,,,,,,1,1,1,,1
-1
712,FY,.357113E6
END
-1
-1,,10,2,.003370
,,,,,,,,1,1,1,,1
-1
712,FY,.369356E6
END
-1
-1,,8,2,.005997
,,,,,,,,1,1,1,,1
-1
712,FY,.397488E6
END
-1
-1,,28,4,.026780
,,,,,,,,1,1,1,,1
-1
712,FY,.471177E6
END
-1
END
FINISH
```

Table 2-21. ANSYS Input for 30 Foot Fall on Side

```
THIRTY FOOT FALL - SIDE DROP
RASCHREIBER
   0  4     1 1 2      0 5            1    1
300.0          300.0
  1 23       1
  2 21  4
  3  1
-1
27.5         1.25
30.0         2.5
30.0         1.25
8.778
2.35
100.0
-1
   101       1                                    4      3      6
     1                                            0      2      4
     1       2                                    1      1      1
     2       3                                    1      1      1
     3       4                                    1      1      1
     4       5                                    2      1      2
     5       6                                    3      1      3     21
    26                                            0      2      5
   102      26                                    4      3      6
-1
     1        0.0
     4   1    25.0
     5         30.0
    26   1    175.626
   101         0.0          -100.0
   102         175.626      -100.0
-1
EX      1     27.1E6
```

```
ALPX    1     0.0
DENS    1     0.00572
EX      2     27.1E6
ALPX    2     0.0
DENS    2     0.00390
EX      3     27.1E6
ALPX    3     0.0
DENS    3     0.00638
EX      4     .749E6
ALPX    4     0.0
NUXY    4     .275
DENS    4     0.0
END
     4

0.0          0.0035     0.0065     0.0400     0.0800     0.1090
70.0         4775.15    7257.38    9762.91    9762.91    10295.1
400.0        4775.15    7257.38    9762.91    9762.91    10295.1

-1
  1      1  10.0005

      1 UY    -0.26356                  26     1
    101 UY    -0.26356                 102     1
      1 UX
    101 UX                             102     1
-1
-1
-1
 -1      1  10.001

     1-UY                              26     1
   101 UY    -0.52712                 102     1
```

```
     1 UX
   101 UX                                  102      1
-1
-1
-1
   0    92  10.047
                                                  1   1   1                1
END
FINISH
```

Table 2-22. ANSYS Input for 30 Foot Fall on Corner

```
CENTER OF GRAVITY CORNER DROP
RASCHREIBER
  00  4  1 1 1 2     0 5           1   1
300.0          300.0
  1 23      1
  2 21  4
  3 23      1
  4 23      2
  5 23      1
  6 1
-1
27.5        1.25
30.0        2.5
30.0        1.25
8.778
2.35
45.0
100.0       3.0
400.0       5.00000
100.0
-1
     1                                    0     2     4
     1      2                             1     1     1
     2      3                             1     1     1
     3      4                             1     1     1
     4      5                             2     1     2
     5      6                             3     1     3    21
    26                                    0     2     5
    26     27                             4     4     6
    26     28                             4     3     8
    26     29                             4     3     8
    26     32                             4     5     8
    27     28                             4     5     7
```

```
    27    29                                    4    5    7
    33    30                                    6    6    9
    33    31                                    5    6    9
    28    32                                    4    4    6
-1
     1      0.0
     4   1   25.0
     5      30.0
    26   1   175.626
    27      186.125
    28      186.125      22.5
    29      186.125      -22.5
    30      186.125      122.5
    31      286.125      22.5
    32      175.626      22.5
    33      186.125      22.5
    34      175.626      22.5
-1
EX      1    27.1E6
ALPX    1
DENS    1    0.00572
EX      2    27.1E6
ALPX    2
DENS    2    0.00390
EX      3    27.1E6
ALPX    3
DENS    3    0.00638
EX      4    27.1E8
ALPX    4
DENS    4
EX      5    9.9E6
ALPX    5
DENS    5
EX      6    1.364E6
ALPX    6
DENS    6
```

```
END
     5

0.0          0.0023       0.0780
70.0         22770.3      30066.0
400.0        22770.3      30066.0

     6

0.0          0.0035       0.0065       0.0400       0.0800       0.1090
70.0         4775.15      7257.38      9762.91      9762.91      10295.1
400.0        4775.15      7257.38      9762.91      9762.91      10295.1

-1
UX   1       2     28     33
UY   1       2     28     33
UX   1       2     32     34
UY   1       2     32     34
-1
  1      1   1 .0002

     1 UX    0.10318                    29     1
     1 UY    0.02152                    29     1
    30 UY    0.02152
    31 UY    0.02152
    30 UX    0.10318
    31 UX    0.10318
    30 ROTZ
    31 ROTZ
    32 UY    0.02152
```

```
    32 UX   0.10318
-1
-1
-1
 -1     1  1 .0004

     1-UX                                29     1
     1-UY                                29     1
    30 UY   0.20636
    31 UY   0.20636
    30 UX   0.04304
    31 UX   0.04304
    30 ROTZ
    31 ROTZ
    32-UY
    32-UX
-1
-1
-1
  0   60  4 0.0304
                                          1  1  1              1
END
FINISH
```

Table 2-23. ANSYS Input for Thermal Stress Evaluation

```
THERMAL STRESSES - 70 DEG BASE CASE
RASCHREIBER
  00  0  1 1 1   1     5                0
625.0        625.0
  1 42 01
  2 42 01
  3 12     1
  4 14 1
  5 42 01
  6 42 01
-1
-90.0      27.99E8   0.0        1.0
0.0        27.99E8   0.0        1.0
13897.84
13897.84
11784.74
7975.47
13076.60
13076.60
-1
/INPUT14
-1
/INPUT15
-1
EX      1    27.99E6
NUXY    1    0.275
ALPX    1    9.51E-6
DENS    1    0
MU      2    0.95
EX      3    2.357E6
NUXY    3    0.4
ALPX    3   2
            6
```

```
-279.6      14.2E-6     -99.6       15.3E-6     67.8        16.1E-6
260.4       17.0E-6     440.4       18.5E-6     620.4       20.4E-6
DENS   3    0
END
     3


0.0         0.00014     0.005       0.010       0.020       0.0475
100.0       330.0       600.0       850.0       1120.0      1500.0
325.0       200.0       400.0       440.0       490.0       600.0
625.0       0.00014     0.005       0.010       0.020       0.0475

-1
UX   2 10  2   367   368
UY   2 10  2   367   368
-1
  1  0  1  1
                                                  1  1  1              1
     1 UX   0.0                                   UY
    11 UX   0.0
-1
-1
-1
 -1  2-10  1
                                                  1  1  1              1
-1
-1
-1
     1      70.0                      470     1
-1
END
FINISH
     1          0.000000    0.000000    0.000000    0.000000    0.000000
     2          3.393000    0.000000    0.000000    0.000000    0.000000
     3          6.785000    0.000000    0.000000    0.000000    0.000000
     4          7.285000    0.000000    0.000000    0.000000    0.000000
```

5	10.580000	0.000000	0.000000	0.000000	0.000000
6	10.580000	2.518000	0.000000	0.000000	0.000000
8	13.830000	0.000000	0.000000	0.000000	0.000000
9	15.080000	0.000000	0.000000	0.000000	0.000000
11	0.000000	2.518000	0.000000	0.000000	0.000000
12	3.393000	2.518000	0.000000	0.000000	0.000000
13	6.785000	2.518000	0.000000	0.000000	0.000000
14	7.285000	2.518000	0.000000	0.000000	0.000000
15	7.285000	2.518000	0.000000	0.000000	0.000000
16	10.580000	2.518000	0.000000	0.000000	0.000000
17	13.830000	2.518000	0.000000	0.000000	0.000000
18	13.830000	2.518000	0.000000	0.000000	0.000000
19	15.080000	2.518000	0.000000	0.000000	0.000000
21	6.785000	6.283000	0.000000	0.000000	0.000000
22	7.258000	6.283000	0.000000	0.000000	0.000000
23	7.258000	6.283000	0.000000	0.000000	0.000000
24	10.580000	6.283000	0.000000	0.000000	0.000000
25	13.830000	6.283000	0.000000	0.000000	0.000000
28	13.830000	6.283000	0.000000	0.000000	0.000000
29	15.080000	6.283000	0.000000	0.000000	0.000000
31	6.785000	7.288000	0.000000	0.000000	0.000000
32	7.097500	7.288000	0.000000	0.000000	0.000000
33	7.097500	7.288000	0.000000	0.000000	0.000000
34	10.580000	7.288000	0.000000	0.000000	0.000000
35	13.830000	7.288000	0.000000	0.000000	0.000000
38	13.830000	7.288000	0.000000	0.000000	0.000000
39	15.080000	7.288000	0.000000	0.000000	0.000000
41	6.785000	11.688000	0.000000	0.000000	0.000000
42	7.097500	11.688000	0.000000	0.000000	0.000000
43	7.097500	11.688000	0.000000	0.000000	0.000000
44	10.580000	11.688000	0.000000	0.000000	0.000000
45	13.830000	11.688000	0.000000	0.000000	0.000000
48	13.830000	11.688000	0.000000	0.000000	0.000000
49	15.080000	11.688000	0.000000	0.000000	0.000000
51	6.785000	16.088000	0.000000	0.000000	0.000000
52	7.097500	16.088000	0.000000	0.000000	0.000000

53	7.097500	16.088000	0.000000	0.000000	0.000000
54	10.580000	16.088000	0.000000	0.000000	0.000000
55	13.830000	16.088000	0.000000	0.000000	0.000000
58	13.830000	16.088000	0.000000	0.000000	0.000000
59	15.080000	16.088000	0.000000	0.000000	0.000000
61	6.785000	20.488000	0.000000	0.000000	0.000000
62	7.097500	20.488000	0.000000	0.000000	0.000000
63	7.097500	20.488000	0.000000	0.000000	0.000000
64	10.580000	20.488000	0.000000	0.000000	0.000000
65	13.830000	20.488000	0.000000	0.000000	0.000000
68	13.830000	20.488000	0.000000	0.000000	0.000000
69	15.080000	20.488000	0.000000	0.000000	0.000000
71	6.785000	24.888000	0.000000	0.000000	0.000000
72	7.097500	24.888000	0.000000	0.000000	0.000000
73	7.097500	24.888000	0.000000	0.000000	0.000000
74	10.580000	24.888000	0.000000	0.000000	0.000000
75	13.830000	24.888000	0.000000	0.000000	0.000000
78	13.830000	24.888000	0.000000	0.000000	0.000000
79	15.080000	24.888000	0.000000	0.000000	0.000000
81	6.785000	29.288000	0.000000	0.000000	0.000000
82	7.097500	29.288000	0.000000	0.000000	0.000000
83	7.097500	29.288000	0.000000	0.000000	0.000000
84	10.580000	29.288000	0.000000	0.000000	0.000000
85	13.830000	29.288000	0.000000	0.000000	0.000000
88	13.830000	29.288000	0.000000	0.000000	0.000000
89	15.080000	29.288000	0.000000	0.000000	0.000000
91	6.785000	33.688000	0.000000	0.000000	0.000000
92	7.097500	33.688000	0.000000	0.000000	0.000000
93	7.097500	33.688000	0.000000	0.000000	0.000000
94	10.580000	33.688000	0.000000	0.000000	0.000000
95	13.830000	33.688000	0.000000	0.000000	0.000000
98	13.830000	33.688000	0.000000	0.000000	0.000000
99	15.080000	33.688000	0.000000	0.000000	0.000000
101	6.785000	38.088000	0.000000	0.000000	0.000000
102	7.097500	38.088000	0.000000	0.000000	0.000000
103	7.097500	38.088000	0.000000	0.000000	0.000000

104	10.580000	38.088000	0.000000	0.000000	0.000000
105	13.830000	38.088000	0.000000	0.000000	0.000000
108	13.830000	38.088000	0.000000	0.000000	0.000000
109	15.080000	38.088000	0.000000	0.000000	0.000000
111	6.785000	42.488000	0.000000	0.000000	0.000000
112	7.097500	42.488000	0.000000	0.000000	0.000000
113	7.097500	42.488000	0.000000	0.000000	0.000000
114	10.580000	42.488000	0.000000	0.000000	0.000000
115	13.830000	42.488000	0.000000	0.000000	0.000000
118	13.830000	42.488000	0.000000	0.000000	0.000000
119	15.080000	42.488000	0.000000	0.000000	0.000000
121	6.785000	46.888000	0.000000	0.000000	0.000000
122	7.097500	46.888000	0.000000	0.000000	0.000000
123	7.097500	46.888000	0.000000	0.000000	0.000000
124	10.580000	46.888000	0.000000	0.000000	0.000000
125	13.830000	46.888000	0.000000	0.000000	0.000000
128	13.830000	46.888000	0.000000	0.000000	0.000000
129	15.080000	46.888000	0.000000	0.000000	0.000000
131	6.785000	51.288000	0.000000	0.000000	0.000000
132	7.097500	51.288000	0.000000	0.000000	0.000000
133	7.097500	51.288000	0.000000	0.000000	0.000000
134	10.580000	51.288000	0.000000	0.000000	0.000000
135	13.830000	51.288000	0.000000	0.000000	0.000000
138	13.830000	51.288000	0.000000	0.000000	0.000000
139	15.080000	51.288000	0.000000	0.000000	0.000000
141	6.785000	55.688000	0.000000	0.000000	0.000000
142	7.097500	55.688000	0.000000	0.000000	0.000000
143	7.097500	55.688000	0.000000	0.000000	0.000000
144	10.580000	55.688000	0.000000	0.000000	0.000000
145	13.830000	55.688000	0.000000	0.000000	0.000000
148	13.830000	55.688000	0.000000	0.000000	0.000000
149	15.080000	55.688000	0.000000	0.000000	0.000000
151	6.785000	60.088000	0.000000	0.000000	0.000000
152	7.097500	60.088000	0.000000	0.000000	0.000000
153	7.097500	60.088000	0.000000	0.000000	0.000000
154	10.580000	60.088000	0.000000	0.000000	0.000000

155	13.830000	60.088000	0.000000	0.000000	0.000000
158	13.830000	60.088000	0.000000	0.000000	0.000000
159	15.080000	60.088000	0.000000	0.000000	0.000000
161	6.785000	64.488000	0.000000	0.000000	0.000000
162	7.097500	64.488000	0.000000	0.000000	0.000000
163	7.097500	64.488000	0.000000	0.000000	0.000000
164	10.580000	64.488000	0.000000	0.000000	0.000000
165	13.830000	64.488000	0.000000	0.000000	0.000000
168	13.830000	64.488000	0.000000	0.000000	0.000000
169	15.080000	64.488000	0.000000	0.000000	0.000000
171	6.785000	68.888000	0.000000	0.000000	0.000000
172	7.097500	68.888000	0.000000	0.000000	0.000000
173	7.097500	68.888000	0.000000	0.000000	0.000000
174	10.580000	68.888000	0.000000	0.000000	0.000000
175	13.830000	68.888000	0.000000	0.000000	0.000000
178	13.830000	68.888000	0.000000	0.000000	0.000000
179	15.080000	68.888000	0.000000	0.000000	0.000000
181	6.785000	73.288000	0.000000	0.000000	0.000000
182	7.097500	73.288000	0.000000	0.000000	0.000000
183	7.097500	73.288000	0.000000	0.000000	0.000000
184	10.580000	73.288000	0.000000	0.000000	0.000000
185	13.830000	73.288000	0.000000	0.000000	0.000000
188	13.830000	73.288000	0.000000	0.000000	0.000000
189	15.080000	73.288000	0.000000	0.000000	0.000000
191	6.785000	77.688000	0.000000	0.000000	0.000000
192	7.097500	77.688000	0.000000	0.000000	0.000000
193	7.097500	77.688000	0.000000	0.000000	0.000000
194	10.580000	77.688000	0.000000	0.000000	0.000000
195	13.830000	77.688000	0.000000	0.000000	0.000000
198	13.830000	77.688000	0.000000	0.000000	0.000000
199	15.080000	77.688000	0.000000	0.000000	0.000000
201	6.785000	82.088000	0.000000	0.000000	0.000000
202	7.097500	82.088000	0.000000	0.000000	0.000000
203	7.097500	82.088000	0.000000	0.000000	0.000000
204	10.580000	82.088000	0.000000	0.000000	0.000000
205	13.830000	82.088000	0.000000	0.000000	0.000000

208	13.830000	82.088000	0.000000	0.000000	0.000000
209	15.080000	82.088000	0.000000	0.000000	0.000000
211	6.785000	86.488000	0.000000	0.000000	0.000000
212	7.097500	86.488000	0.000000	0.000000	0.000000
213	7.097500	86.488000	0.000000	0.000000	0.000000
214	10.580000	86.488000	0.000000	0.000000	0.000000
215	13.830000	86.488000	0.000000	0.000000	0.000000
218	13.830000	86.488000	0.000000	0.000000	0.000000
219	15.080000	86.488000	0.000000	0.000000	0.000000
221	6.785000	90.888000	0.000000	0.000000	0.000000
222	7.097500	90.888000	0.000000	0.000000	0.000000
223	7.097500	90.888000	0.000000	0.000000	0.000000
224	10.580000	90.888000	0.000000	0.000000	0.000000
225	13.830000	90.888000	0.000000	0.000000	0.000000
228	13.830000	90.888000	0.000000	0.000000	0.000000
229	15.080000	90.888000	0.000000	0.000000	0.000000
231	6.785000	95.288000	0.000000	0.000000	0.000000
232	7.097500	95.288000	0.000000	0.000000	0.000000
233	7.097500	95.288000	0.000000	0.000000	0.000000
234	10.580000	95.288000	0.000000	0.000000	0.000000
235	13.830000	95.288000	0.000000	0.000000	0.000000
238	13.830000	95.288000	0.000000	0.000000	0.000000
239	15.080000	95.288000	0.000000	0.000000	0.000000
241	6.785000	99.688000	0.000000	0.000000	0.000000
242	7.097500	99.688000	0.000000	0.000000	0.000000
243	7.097500	99.688000	0.000000	0.000000	0.000000
244	10.580000	99.688000	0.000000	0.000000	0.000000
245	13.830000	99.688000	0.000000	0.000000	0.000000
248	13.830000	99.688000	0.000000	0.000000	0.000000
249	15.080000	99.688000	0.000000	0.000000	0.000000
251	6.785000	104.088000	0.000000	0.000000	0.000000
252	7.097500	104.088000	0.000000	0.000000	0.000000
253	7.097500	104.088000	0.000000	0.000000	0.000000
254	10.580000	104.088000	0.000000	0.000000	0.000000
255	13.830000	104.088000	0.000000	0.000000	0.000000
258	13.830000	104.088000	0.000000	0.000000	0.000000

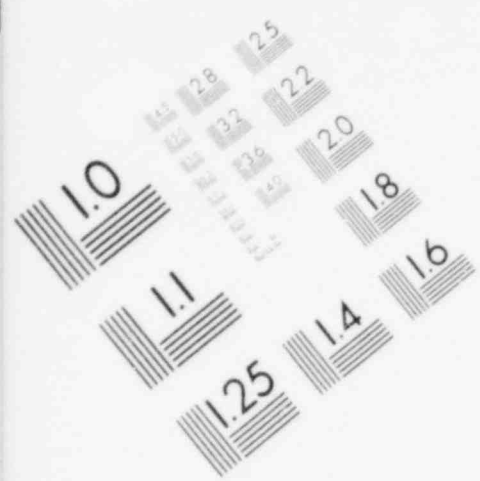

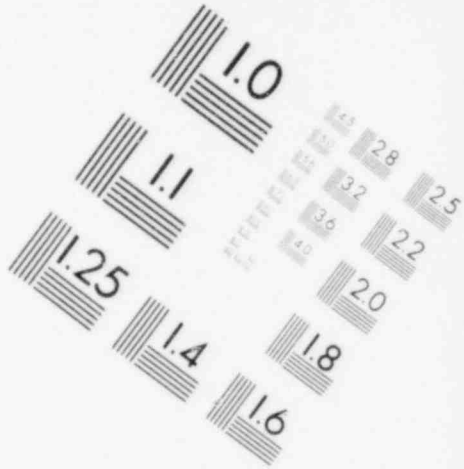

IMAGE EVALUATION
TEST TARGET (MT-3)

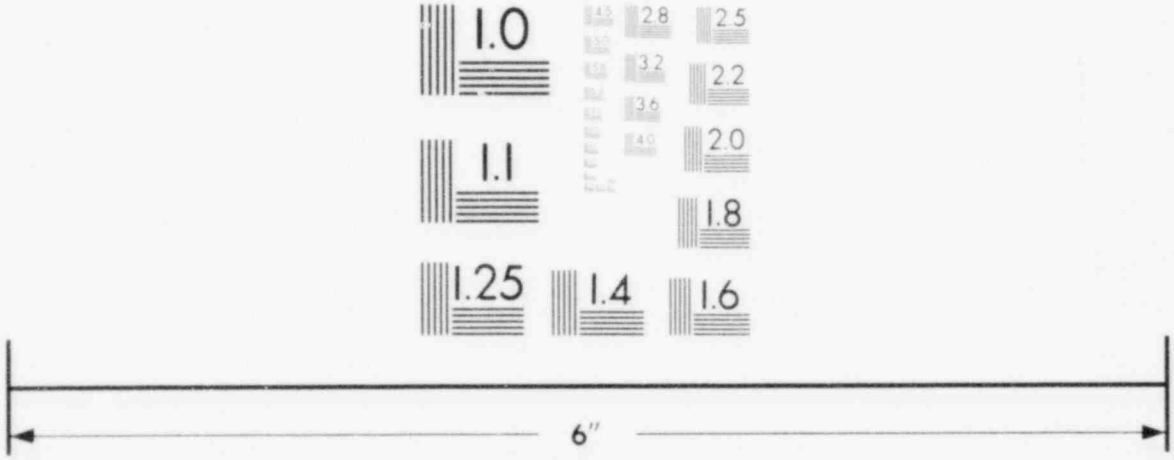

MICROCOPY RESOLUTION TEST CHART

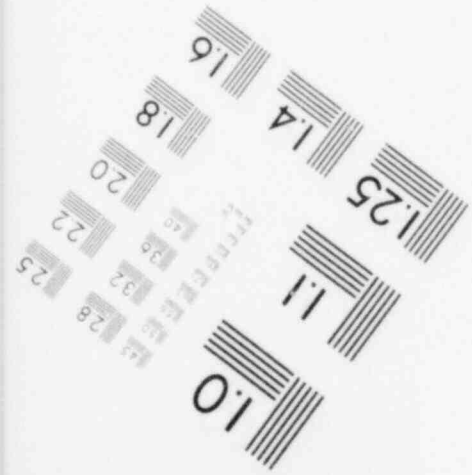

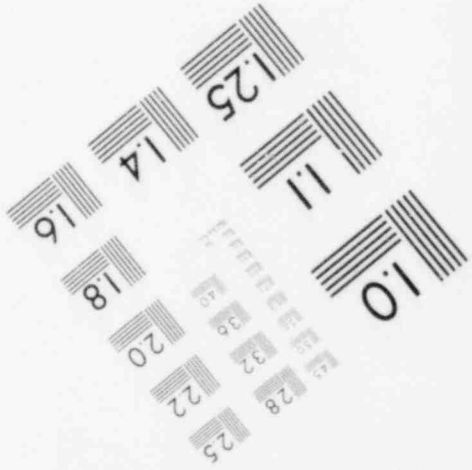

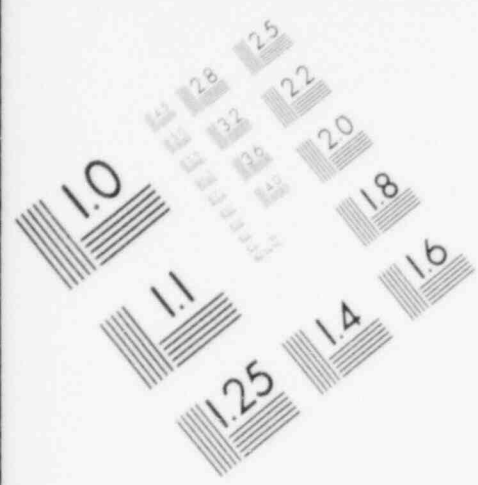

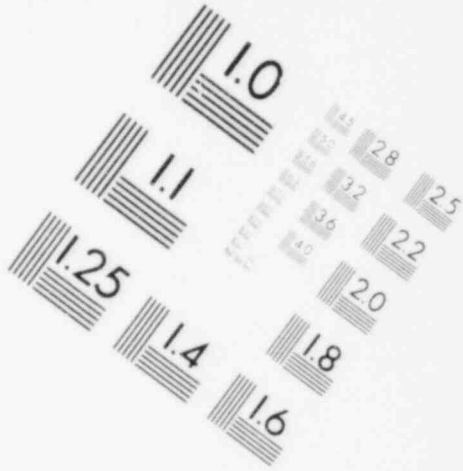

IMAGE EVALUATION
TEST TARGET (MT-3)

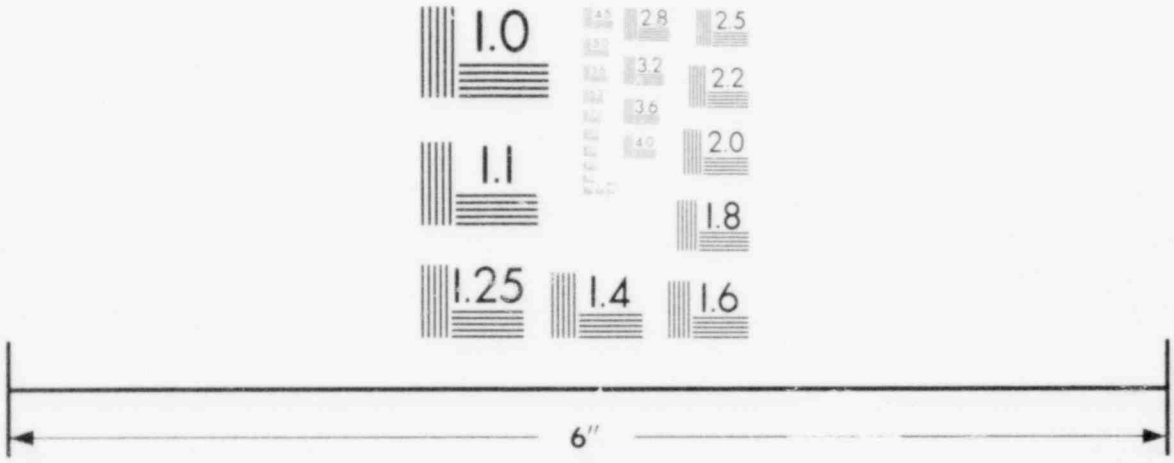

MICROCOPY RESOLUTION TEST CHART

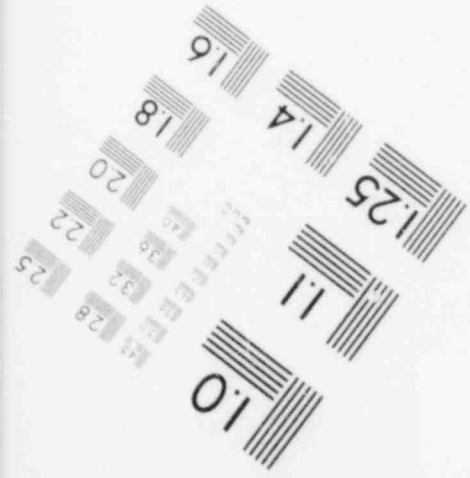

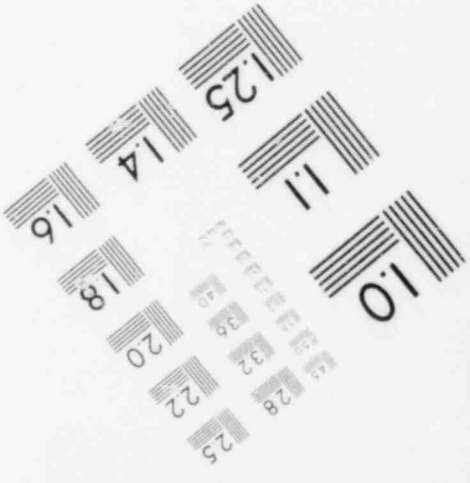

259	15.080000	104.088000	0.000000	0.000000	0.000000
261	6.785000	108.488000	0.000000	0.000000	0.000000
262	7.097500	108.488000	0.000000	0.000000	0.000000
263	7.097500	108.488000	0.000000	0.000000	0.000000
264	10.580000	108.488000	0.000000	0.000000	0.000000
265	13.830000	108.488000	0.000000	0.000000	0.000000
268	13.830000	108.488000	0.000000	0.000000	0.000000
269	15.080000	108.488000	0.000000	0.000000	0.000000
271	6.785000	112.888000	0.000000	0.000000	0.000000
272	7.097500	112.888000	0.000000	0.000000	0.000000
273	7.097500	112.888000	0.000000	0.000000	0.000000
274	10.580000	112.888000	0.000000	0.000000	0.000000
275	13.830000	112.888000	0.000000	0.000000	0.000000
278	13.830000	112.888000	0.000000	0.000000	0.000000
279	15.080000	112.888000	0.000000	0.000000	0.000000
281	6.785000	117.288000	0.000000	0.000000	0.000000
282	7.097500	117.288000	0.000000	0.000000	0.000000
283	7.097500	117.288000	0.000000	0.000000	0.000000
284	10.580000	117.288000	0.000000	0.000000	0.000000
285	13.830000	117.288000	0.000000	0.000000	0.000000
288	13.830000	117.288000	0.000000	0.000000	0.000000
289	15.080000	117.288000	0.000000	0.000000	0.000000
291	6.785000	121.688000	0.000000	0.000000	0.000000
292	7.097500	121.688000	0.000000	0.000000	0.000000
293	7.097500	121.688000	0.000000	0.000000	0.000000
294	10.580000	121.688000	0.000000	0.000000	0.000000
295	13.830000	121.688000	0.000000	0.000000	0.000000
298	13.830000	121.688000	0.000000	0.000000	0.000000
299	15.080000	121.688000	0.000000	0.000000	0.000000
301	6.785000	126.088000	0.000000	0.000000	0.000000
302	7.097500	126.088000	0.000000	0.000000	0.000000
303	7.097500	126.088000	0.000000	0.000000	0.000000
304	10.580000	126.088000	0.000000	0.000000	0.000000
305	13.830000	126.088000	0.000000	0.000000	0.000000
308	13.830000	126.088000	0.000000	0.000000	0.000000
309	15.080000	126.088000	0.000000	0.000000	0.000000

311	6.785000	130.488000	0.000000	0.000000	0.000000
312	7.097500	130.488000	0.000000	0.000000	0.000000
313	7.097500	130.488000	0.000000	0.000000	0.000000
314	10.580000	130.488000	0.000000	0.000000	0.000000
315	13.830000	130.488000	0.000000	0.000000	0.000000
318	13.830000	130.488000	0.000000	0.000000	0.000000
319	15.080000	130.488000	0.000000	0.000000	0.000000
321	6.785000	134.888000	0.000000	0.000000	0.000000
322	7.097500	134.888000	0.000000	0.000000	0.000000
323	7.097500	134.888000	0.000000	0.000000	0.000000
324	10.580000	134.888000	0.000000	0.000000	0.000000
325	13.830000	134.888000	0.000000	0.000000	0.000000
328	13.830000	134.888000	0.000000	0.000000	0.000000
329	15.080000	134.888000	0.000000	0.000000	0.000000
331	6.785000	139.288000	0.000000	0.000000	0.000000
332	7.097500	139.288000	0.000000	0.000000	0.000000
333	7.097500	139.288000	0.000000	0.000000	0.000000
334	10.580000	139.288000	0.000000	0.000000	0.000000
335	13.830000	139.288000	0.000000	0.000000	0.000000
338	13.830000	139.288000	0.000000	0.000000	0.000000
339	15.080000	139.288000	0.000000	0.000000	0.000000
341	6.785000	143.688000	0.000000	0.000000	0.000000
342	7.097500	143.688000	0.000000	0.000000	0.000000
343	7.097500	143.688000	0.000000	0.000000	0.000000
344	10.580000	143.688000	0.000000	0.000000	0.000000
345	13.830000	143.688000	0.000000	0.000000	0.000000
348	13.830000	143.688000	0.000000	0.000000	0.000000
349	15.080000	143.688000	0.000000	0.000000	0.000000
351	6.785000	148.088000	0.000000	0.000000	0.000000
352	7.097500	148.088000	0.000000	0.000000	0.000000
353	7.097500	148.088000	0.000000	0.000000	0.000000
354	10.580000	148.088000	0.000000	0.000000	0.000000
355	13.830000	148.088000	0.000000	0.000000	0.000000
358	13.830000	148.088000	0.000000	0.000000	0.000000
359	15.080000	148.088000	0.000000	0.000000	0.000000
361	6.785000	151.150000	0.000000	0.000000	0.000000

362	7.097500	151.150000	0.000000	0.000000	0.000000
363	7.097500	151.150000	0.000000	0.000000	0.000000
364	10.580000	151.150000	0.000000	0.000000	0.000000
365	12.580000	151.150000	0.000000	0.000000	0.000000
366	12.580000	151.150000	0.000000	0.000000	0.000000
367	13.830000	151.150000	0.000000	0.000000	0.000000
368	13.830000	151.150000	0.000000	0.000000	0.000000
369	15.080000	151.150000	0.000000	0.000000	0.000000
371	6.785000	153.675000	0.000000	0.000000	0.000000
372	7.097500	153.675000	0.000000	0.000000	0.000000
373	7.097500	153.675000	0.000000	0.000000	0.000000
374	10.580000	153.675000	0.000000	0.000000	0.000000
375	12.580000	153.675000	0.000000	0.000000	0.000000
376	12.580000	153.675000	0.000000	0.000000	0.000000
377	13.830000	153.675000	0.000000	0.000000	0.000000
378	13.830000	153.675000	0.000000	0.000000	0.000000
379	15.080000	153.675000	0.000000	0.000000	0.000000
381	6.785000	156.200000	0.000000	0.000000	0.000000
382	7.097500	156.200000	0.000000	0.000000	0.000000
383	7.097500	156.200000	0.000000	0.000000	0.000000
384	10.580000	156.200000	0.000000	0.000000	0.000000
385	12.580000	156.200000	0.000000	0.000000	0.000000
386	12.580000	156.200000	0.000000	0.000000	0.000000
387	13.830000	156.200000	0.000000	0.000000	0.000000
388	13.830000	156.200000	0.000000	0.000000	0.000000
389	15.080000	156.200000	0.000000	0.000000	0.000000
391	6.785000	160.346000	0.000000	0.000000	0.000000
392	7.097500	160.346000	0.000000	0.000000	0.000000
393	7.097500	160.346000	0.000000	0.000000	0.000000
394	10.580000	160.346000	0.000000	0.000000	0.000000
395	12.580000	160.346000	0.000000	0.000000	0.000000
396	12.580000	160.346000	0.000000	0.000000	0.000000
397	13.830000	160.346000	0.000000	0.000000	0.000000
401	6.785000	164.492000	0.000000	0.000000	0.000000
402	7.097500	164.492000	0.000000	0.000000	0.000000
403	7.097500	164.492000	0.000000	0.000000	0.000000

404	10.580000	164.492000	0.000000	0.000000	0.000000
405	12.580000	164.492000	0.000000	0.000000	0.000000
406	12.580000	164.492000	0.000000	0.000000	0.000000
407	13.830000	164.492000	0.000000	0.000000	0.000000
411	6.785000	168.638000	0.000000	0.000000	0.000000
412	7.097500	168.638000	0.000000	0.000000	0.000000
413	7.097500	168.638000	0.000000	0.000000	0.000000
414	10.580000	168.638000	0.000000	0.000000	0.000000
415	12.580000	168.638000	0.000000	0.000000	0.000000
416	12.580000	168.638000	0.000000	0.000000	0.000000
417	13.830000	168.638000	0.000000	0.000000	0.000000
421	6.785000	172.784000	0.000000	0.000000	0.000000
422	7.097500	172.784000	0.000000	0.000000	0.000000
423	7.097500	172.784000	0.000000	0.000000	0.000000
424	10.580000	172.784000	0.000000	0.000000	0.000000
425	12.580000	172.784000	0.000000	0.000000	0.000000
426	12.580000	172.784000	0.000000	0.000000	0.000000
427	13.830000	172.784000	0.000000	0.000000	0.000000
431	6.785000	176.930000	0.000000	0.000000	0.000000
432	7.0975	176.93			
433	7.0975	176.93			
434	10.580000	176.930000	0.000000	0.000000	0.000000
435	12.580000	176.930000	0.000000	0.000000	0.000000
436	12.580000	176.930000	0.000000	0.000000	0.000000
437	13.830000	176.930000	0.000000	0.000000	0.000000
441	6.785000	177.930000	0.000000	0.000000	0.000000
442	7.285000	177.930000	0.000000	0.000000	0.000000
443	7.285000	177.930000	0.000000	0.000000	0.000000
444	10.580000	177.930000	0.000000	0.000000	0.000000
445	12.580000	177.930000	0.000000	0.000000	0.000000
446	12.580000	177.930000	0.000000	0.000000	0.000000
447	13.830000	177.930000	0.000000	0.000000	0.000000
451	6.785000	181.330000	0.000000	0.000000	0.000000
452	7.285000	181.330000	0.000000	0.000000	0.000000
453	7.285000	181.330000	0.000000	0.000000	0.000000
454	10.580000	181.330000	0.000000	0.000000	0.000000

455	12.580000	181.330000	0.000000	0.000000	0.000000
456	12.580000	181.330000	0.000000	0.000000	0.000000
457	13.830000	181.330000	0.000000	0.000000	0.000000
461	6.785000	183.590000	0.000000	0.000000	0.000000
462	7.285000	183.590000	0.000000	0.000000	0.000000
464	10.580000	183.590000	0.000000	0.000000	0.000000
465	12.580000	183.590000	0.000000	0.000000	0.000000
466	12.580000	183.590000	0.000000	0.000000	0.000000
467	13.830000	183.590000	0.000000	0.000000	0.000000
468	10.580000	181.330000	0.000000	0.000000	0.000000
469	13.83	151.15			
470	12.58	151.15			

/INPUT 18

1	2	12	11	0	0	0	0	1	1	1 0
2	3	13	12	0	0	0	0	1	1	1 0
3	4	14	13	0	0	0	0	1	1	1 0
4	5	6	14	0	0	0	0	1	1	1 0
5	8	18	6	0	0	0	0	1	1	1 0
8	9	19	18	0	0	0	0	1	1	1 0
13	14	22	21	0	0	0	0	1	2	1 0
22	23	0	0	0	0	0	0	2	3	1 0
14	15	0	0	0	0	0	0	2	3	1 0
14	15							2	3	2
15	16	24	23	0	0	0	0	3	5	1 0
6	16							2	3	2
16	17	25	24	0	0	0	0	3	5	1 0
17	18	0	0	0	0	0	0	2	3	1 0
17	18							2	3	2
25	28	0	0	0	0	0	0	2	3	1 0
18	19	29	28	0	0	0	0	1	6	1 0
21	22	32	31	0	0	0	0	1	2	1 0
32	33	0	0	0	0	0	0	2	3	1 0

23	24	34	33	0	0	0	0	3	5	3 0
24	25	35	34	0	0	0	0	3	5	3 0
35	38	0	0	0	0	0	0	2	3	1 0
35	38	0	0	0	0	0	0	1	4	3 0
28	29	39	38	0	0	0	0	1	6	1 0
31	32	42	41	0	0	0	0	1	2	1 0
42	43	0	0	0	0	0	0	2	3	1 0
42	43	0	0	0	0	0	0	1	4	4 0
33	34	44	43	0	0	0	0	3	5	3 0
34	35	45	44	0	0	0	0	3	5	3 0
45	48	0	0	0	0	0	0	2	3	1 0
45	48	0	0	0	0	0	0	1	4	4 0
38	39	49	48	0	0	0	0	1	6	1 0
41	42	52	51	0	0	0	0	1	2	1 0
52	53	0	0	0	0	0	0	2	3	1 0
52	53	0	0	0	0	0	0	1	4	4 0
43	44	54	53	0	0	0	0	3	5	3 0
44	45	55	54	0	0	0	0	3	5	3 0
55	58	0	0	0	0	0	0	2	3	1 0
55	58	0	0	0	0	0	0	1	4	4 0
48	49	59	58	0	0	0	0	1	6	1 0
51	52	62	61	0	0	0	0	1	2	1 0
62	63	0	0	0	0	0	0	2	3	1 0
62	63	0	0	0	0	0	0	1	4	4 0
53	54	64	63	0	0	0	0	3	5	3 0
54	55	65	64	0	0	0	0	3	5	3 0
65	68	0	0	0	0	0	0	2	3	1 0
65	68	0	0	0	0	0	0	1	4	4 0
58	59	69	68	0	0	0	0	1	6	1 0
61	62	72	71	0	0	0	0	1	2	1 0
72	73	0	0	0	0	0	0	2	3	1 0
72	73	0	0	0	0	0	0	1	4	4 0
63	64	74	73	0	0	0	0	3	5	3 0
64	65	75	74	0	0	0	0	3	5	3 0
75	78	0	0	0	0	0	0	2	3	1 0
75	78	0	0	0	0	0	0	1	4	4 0

68	69	79	78	0	0	0	0	1	6	1 0
71	72	82	81	0	0	0	0	1	2	1 0
82	83	0	0	0	0	0	0	2	3	1 0
82	83	0	0	0	0	0	0	1	4	4 0
73	74	84	83	0	0	0	0	3	5	3 0
74	75	85	84	0	0	0	0	3	5	3 0
85	88	0	0	0	0	0	0	2	3	1 0
85	88	0	0	0	0	0	0	1	4	4 0
78	79	89	88	0	0	0	0	1	6	1 0
81	82	92	91	0	0	0	0	1	2	1 0
92	93	0	0	0	0	0	0	2	3	1 0
92	93	0	0	0	0	0	0	1	4	4 0
83	84	94	93	0	0	0	0	3	5	3 0
84	85	95	94	0	0	0	0	3	5	3 0
95	98	0	0	0	0	0	0	2	3	1 0
95	98	0	0	0	0	0	0	1	4	4 0
88	89	99	98	0	0	0	0	1	6	1 0
91	92	102	101	0	0	0	0	1	2	1 0
102	103	0	0	0	0	0	0	2	3	1 0
102	103	0	0	0	0	0	0	1	4	4 0
93	94	104	103	0	0	0	0	3	5	3 0
94	95	105	104	0	0	0	0	3	5	3 0
105	108	0	0	0	0	0	0	2	3	1 0
105	108	0	0	0	0	0	0	1	4	4 0
98	99	109	108	0	0	0	0	1	6	1 0
101	102	112	111	0	0	0	0	1	2	1 0
112	113	0	0	0	0	0	0	2	3	1 0
112	113	0	0	0	0	0	0	1	4	4 0
103	104	114	113	0	0	0	0	3	5	3 0
104	105	115	114	0	0	0	0	3	5	3 0
115	118	0	0	0	0	0	0	2	3	1 0
115	118	0	0	0	0	0	0	1	4	4 0
108	109	119	118	0	0	0	0	1	6	1 0
111	112	122	121	0	0	0	0	1	2	1 0
122	123	0	0	0	0	0	0	2	3	1 0
122	123	0	0	0	0	0	0	1	4	4 0

113	114	124	123	0	0	0	0	3	5	3 0
114	115	125	124	0	0	0	0	3	5	3 0
125	128	0	0	0	0	0	0	2	3	1 0
125	128	0	0	0	0	0	0	1	4	4 0
118	119	129	128	0	0	0	0	1	6	1 0
121	122	132	131	0	0	0	0	1	2	1 0
132	133	0	0	0	0	0	0	2	3	1 0
132	133	0	0	0	0	0	0	1	4	4 0
123	124	134	133	0	0	0	0	3	5	3 0
124	125	135	134	0	0	0	0	3	5	3 0
135	138	0	0	0	0	0	0	2	3	1 0
135	138	0	0	0	0	0	0	1	4	4 0
128	129	139	138	0	0	0	0	1	6	1 0
131	132	142	141	0	0	0	0	1	2	1 0
142	143	0	0	0	0	0	0	2	3	1 0
142	143	0	0	0	0	0	0	1	4	4 0
133	134	144	143	0	0	0	0	3	5	3 0
134	135	145	144	0	0	0	0	3	5	3 0
145	148	0	0	0	0	0	0	2	3	1 0
145	148	0	0	0	0	0	0	1	4	4 0
138	139	149	148	0	0	0	0	1	6	1 0
141	142	152	151	0	0	0	0	1	2	1 0
152	153	0	0	0	0	0	0	2	3	1 0
152	153	0	0	0	0	0	0	1	4	4 0
143	144	154	153	0	0	0	0	3	5	3 0
144	145	155	154	0	0	0	0	3	5	3 0
155	158	0	0	0	0	0	0	2	3	1 0
155	158	0	0	0	0	0	0	1	4	4 0
148	149	159	158	0	0	0	0	1	6	1 0
151	152	162	161	0	0	0	0	1	2	1 0
162	163	0	0	0	0	0	0	2	3	1 0
162	163	0	0	0	0	0	0	1	4	4 0
153	154	164	163	0	0	0	0	3	5	3 0
154	155	165	164	0	0	0	0	3	5	3 0
165	168	0	0	0	0	0	0	2	3	1 0
165	168	0	0	0	0	0	0	1	4	4 0

158	159	169	168	0	0	0	0	1	6	1 0
161	162	172	171	0	0	0	0	1	2	1 0
172	173	0	0	0	0	0	0	2	3	1 0
172	173	0	0	0	0	0	0	1	4	4 0
163	164	174	173	0	0	0	0	3	5	3 0
164	165	175	174	0	0	0	0	3	5	3 0
175	178	0	0	0	0	0	0	2	3	1 0
175	178	0	0	0	0	0	0	1	4	4 0
168	169	179	178	0	0	0	0	1	6	1 0
171	172	182	181	0	0	0	0	1	2	1 0
182	183	0	0	0	0	0	0	2	3	1 0
182	183	0	0	0	0	0	0	1	4	4 0
173	174	184	183	0	0	0	0	3	5	3 0
174	175	185	184	0	0	0	0	3	5	3 0
185	188	0	0	0	0	0	0	2	3	1 0
185	188	0	0	0	0	0	0	1	4	4 0
178	179	189	188	0	0	0	0	1	6	1 0
181	182	192	191	0	0	0	0	1	2	1 0
192	193	0	0	0	0	0	0	2	3	1 0
192	193	0	0	0	0	0	0	1	4	4 0
183	184	194	193	0	0	0	0	3	5	3 0
184	185	195	194	0	0	0	0	3	5	3 0
195	198	0	0	0	0	0	0	2	3	1 0
195	198	0	0	0	0	0	0	1	4	4 0
188	189	199	198	0	0	0	0	1	6	1 0
191	192	202	201	0	0	0	0	1	2	1 0
202	203	0	0	0	0	0	0	2	3	1 0
202	203	0	0	0	0	0	0	1	4	4 0
193	194	204	203	0	0	0	0	3	5	3 0
194	195	205	204	0	0	0	0	3	5	3 0
205	208	0	0	0	0	0	0	2	3	1 0
205	208	0	0	0	0	0	0	1	4	4 0
198	199	209	208	0	0	0	0	1	6	1 0
201	202	212	211	0	0	0	0	1	2	1 0
212	213	0	0	0	0	0	0	2	3	1 0
212	213	0	0	0	0	0	0	1	4	4 0

203	204	214	213	0	0	0	0	3	5	3 0
204	205	215	214	0	0	0	0	3	5	3 0
215	218	0	0	0	0	0	0	2	3	1 0
215	218	0	0	0	0	0	0	1	4	4 0
208	209	219	218	0	0	0	0	1	6	1 0
211	212	222	221	0	0	0	0	1	2	1 0
222	223	0	0	0	0	0	0	2	3	1 0
222	223	0	0	0	0	0	0	1	4	4 0
213	214	224	223	0	0	0	0	3	5	3 0
214	215	225	224	0	0	0	0	3	5	3 0
225	228	0	0	0	0	0	0	2	3	1 0
225	228	0	0	0	0	0	0	1	4	4 0
218	219	229	228	0	0	0	0	1	6	1 0
221	222	232	231	0	0	0	0	1	2	1 0
232	233	0	0	0	0	0	0	2	3	1 0
232	233	0	0	0	0	0	0	1	4	4 0
223	224	234	233	0	0	0	0	3	5	3 0
224	225	235	234	0	0	0	0	3	5	3 0
235	238	0	0	0	0	0	0	2	3	1 0
235	238	0	0	0	0	0	0	1	4	4 0
228	229	239	238	0	0	0	0	1	6	1 0
231	232	242	241	0	0	0	0	1	2	1 0
242	243	0	0	0	0	0	0	2	3	1 0
242	243	0	0	0	0	0	0	1	4	4 0
233	234	244	243	0	0	0	0	3	5	3 0
234	235	245	244	0	0	0	0	3	5	3 0
245	248	0	0	0	0	0	0	2	3	1 0
245	248	0	0	0	0	0	0	1	4	4 0
238	239	249	248	0	0	0	0	1	6	1 0
241	242	252	251	0	0	0	0	1	2	1 0
252	253	0	0	0	0	0	0	2	3	1 0
252	253	0	0	0	0	0	0	1	4	4 0
243	244	254	253	0	0	0	0	3	5	3 0
244	245	255	254	0	0	0	0	3	5	3 0
255	258	0	0	0	0	0	0	2	3	1 0
255	258	0	0	0	0	0	0	1	4	4 0

248	249	259	258	0	0	0	0	1	6	1 0
251	252	262	261	0	0	0	0	1	2	1 0
262	263	0	0	0	0	0	0	2	3	1 0
262	263	0	0	0	0	0	0	1	4	4 0
253	254	264	263	0	0	0	0	3	5	3 0
254	255	265	264	0	0	0	0	3	5	3 0
265	268	0	0	0	0	0	0	2	3	1 0
265	268	0	0	0	0	0	0	1	4	4 0
258	259	269	268	0	0	0	0	1	6	1 0
261	262	272	271	0	0	0	0	1	2	1 0
272	273	0	0	0	0	0	0	2	3	1 0
272	273	0	0	0	0	0	0	1	4	4 0
263	264	274	273	0	0	0	0	3	5	3 0
264	265	275	274	0	0	0	0	3	5	3 0
275	278	0	0	0	0	0	0	2	3	1 0
275	278	0	0	0	0	0	0	1	4	4 0
268	269	279	278	0	0	0	0	1	6	1 0
271	272	282	281	0	0	0	0	1	2	1 0
282	283	0	0	0	0	0	0	2	3	1 0
282	283	0	0	0	0	0	0	1	4	4 0
273	274	284	283	0	0	0	0	3	5	3 0
274	275	285	284	0	0	0	0	3	5	3 0
285	288	0	0	0	0	0	0	2	3	1 0
285	288	0	0	0	0	0	0	1	4	4 0
278	279	289	288	0	0	0	0	1	6	1 0
281	282	292	291	0	0	0	0	1	2	1 0
292	293	0	0	0	0	0	0	2	3	1 0
292	293	0	0	0	0	0	0	1	4	4 0
283	284	294	293	0	0	0	0	3	5	3 0
284	285	295	294	0	0	0	0	3	5	3 0
295	298	0	0	0	0	0	0	2	3	1 0
295	298	0	0	0	0	0	0	1	4	4 0
288	289	299	298	0	0	0	0	1	6	1 0
291	292	302	301	0	0	0	0	1	2	1 0
302	303	0	0	0	0	0	0	2	3	1 0
302	303	0	0	0	0	0	0	1	4	4 0

293	294	304	303	0	0	0	0	3	5	3 0
294	295	305	304	0	0	0	0	3	5	3 0
305	308	0	0	0	0	0	0	2	3	1 0
305	308	0	0	0	0	0	0	1	4	4 0
298	299	309	308	0	0	0	0	1	6	1 0
301	302	312	311	0	0	0	0	1	2	1 0
312	313	0	0	0	0	0	0	2	3	1 0
312	313	0	0	0	0	0	0	1	4	4 0
303	304	314	313	0	0	0	0	3	5	3 0
304	305	315	314	0	0	0	0	3	5	3 0
315	318	0	0	0	0	0	0	2	3	1 0
315	318	0	0	0	0	0	0	1	4	4 0
308	309	319	318	0	0	0	0	1	6	1 0
311	312	322	321	0	0	0	0	1	2	1 0
322	323	0	0	0	0	0	0	2	3	1 0
322	323	0	0	0	0	0	0	1	4	4 0
313	314	324	323	0	0	0	0	3	5	3 0
314	315	325	324	0	0	0	0	3	5	3 0
325	328	0	0	0	0	0	0	2	3	1 0
325	328	0	0	0	0	0	0	1	4	4 0
318	319	329	328	0	0	0	0	1	6	1 0
321	322	332	331	0	0	0	0	1	2	1 0
332	333	0	0	0	0	0	0	2	3	1 0
332	333	0	0	0	0	0	0	1	4	4 0
323	324	334	333	0	0	0	0	3	5	3 0
324	325	335	334	0	0	0	0	3	5	3 0
335	338	0	0	0	0	0	0	2	3	1 0
335	338	0	0	0	0	0	0	1	4	4 0
328	329	339	338	0	0	0	0	1	6	1 0
331	332	342	341	0	0	0	0	1	2	1 0
342	343	0	0	0	0	0	0	2	3	1 0
342	343	0	0	0	0	0	0	1	4	4 0
333	334	344	343	0	0	0	0	3	5	3 0
334	335	345	344	0	0	0	0	3	5	3 0
345	348	0	0	0	0	0	0	2	3	1 0
345	348	0	0	0	0	0	0	1	4	4 0

338	339	349	348	0	0	0	0	1	6	1 0
341	342	352	351	0	0	0	0	1	2	1 0
352	353	0	0	0	0	0	0	2	3	1 0
352	353	0	0	0	0	0	0	1	4	5 0
343	344	354	353	0	0	0	0	3	5	3 0
344	345	355	354	0	0	0	0	3	5	3 0
355	358	0	0	0	0	0	0	2	3	1 0
355	358	0	0	0	0	0	0	1	4	5 0
348	349	359	358	0	0	0	0	1	6	1 0
351	352	362	361	0	0	0	0	1	2	1 0
362	363	0	0	0	0	0	0	2	3	1 0
362	363	0	0	0	0	0	0	1	4	6 0
353	354	364	363					3	5	1
354	355	365	364	0	0	0	0	3	5	1 0
365	355	367	367	0	0	0	0	3	5	1 0
367	368							2	3	1
367	368							2	3	2
365	470							2	3	1
365	470							2	3	2
358	359	369	368	0	0	0	0	1	6	1 0
361	362	372	371	0	0	0	0	1	2	1 0
372	373	0	0	0	0	0	0	2	3	1 0
372	373	0	0	0	0	0	0	1	4	6 0
363	364	374	373	0	0	0	0	3	5	1 0
364	365	375	374	0	0	0	0	3	5	1 0
375	376	0	0	0	0	0	0	2	3	1 0
375	376	0	0	0	0	0	0	1	4	6 0
470	469	377	376	0	0	0	0	1	6	1 0
368	369	379	378	0	0	0	0	1	6	1 0
371	372	382	381	0	0	0	0	1	2	1 0
382	383	0	0	0	0	0	0	2	3	1 0
382	383	0	0	0	0	0	0	1	4	6 0
373	374	384	383	0	0	0	0	3	5	1 0
374	375	385	384	0	0	0	0	3	5	1 0
385	386	0	0	0	0	0	0	2	3	1 0
385	386	0	0	0	0	0	0	1	4	6 0

376	377	387	386	0	0	0	0	1	6	1 0
378	379	389	388					1	6	1
381	382	392	391	0	0	0	0	1	2	1 0
392	393	0	0	0	0	0	0	2	3	1 0
392	393	0	0	0	0	0	0	1	4	7 0
383	384	394	393	0	0	0	0	3	5	1 0
384	385	395	394	0	0	0	0	3	5	1 0
395	396	0	0	0	0	0	0	2	3	1 0
395	396	0	0	0	0	0	0	1	4	7 0
386	387	397	396	0	0	0	0	1	6	1 0
391	392	402	401	0	0	0	0	1	2	1 0
402	403	0	0	0	0	0	0	2	3	1 0
402	403	0	0	0	0	0	0	1	4	7 0
393	394	404	403	0	0	0	0	3	5	1 0
394	395	405	404	0	0	0	0	3	5	1 0
405	406	0	0	0	0	0	0	2	3	1 0
405	406	0	0	0	0	0	0	1	4	7 0
396	397	407	406	0	0	0	0	1	6	1 0
401	402	412	411	0	0	0	0	1	2	1 0
412	413	0	0	0	0	0	0	2	3	1 0
412	413	0	0	0	0	0	0	1	4	7 0
403	404	414	413	0	0	0	0	3	5	1 0
404	405	415	414	0	0	0	0	3	5	1 0
415	416	0	0	0	0	0	0	2	3	1 0
415	416	0	0	0	0	0	0	1	4	7 0
406	407	417	416	0	0	0	0	1	6	1 0
411	412	422	421	0	0	0	0	1	2	1 0
422	423	0	0	0	0	0	0	2	3	1 0
422	423	0	0	0	0	0	0	1	4	7 0
413	414	424	423	0	0	0	0	3	5	1 0
414	415	425	424	0	0	0	0	3	5	1 0
425	426	0	0	0	0	0	0	2	3	1 0
425	426	0	0	0	0	0	0	1	4	7 0
416	417	427	426	0	0	0	0	1	6	1 0
421	422	432	431	0	0	0	0	1	2	1 0
432	433	0	0	0	0	0	0	2	3	1 0

423	424	434	433	0	0	0	0	3	5	1 0
424	425	435	434	0	0	0	0	3	5	1 0
435	436	0	0	0	0	0	0	2	3	1 0
435	436	0	0	0	0	0	0	1	4	8 0
426	427	437	436	0	0	0	0	1	6	1 0
431	432	442	441	0	0	0	0	1	2	1 0
442	443	0	0	0	0	0	0	2	3	1 0
433	434	444	443	0	0	0	0	3	5	1 0
434	435	445	444	0	0	0	0	3	5	1 0
445	446	0	0	0	0	0	0	2	3	1 0
436	437	447	446	0	0	0	0	1	6	1 0
441	442	452	451	0	0	0	0	1	2	1 0
452	453	0	0	0	0	0	0	2	3	1 0
452	453							2	3	2
443	444	454	453	0	0	0	0	3	5	1 0
454	468							2	3	2
444	445	455	454	0	0	0	0	3	5	1 0
455	456							2	3	2
455	456	0	0	0	0	0	0	2	3	1 0
446	447	457	456	0	0	0	0	1	6	1 0
451	452	462	461	0	0	0	0	1	1	1 0
452	468	464	462	0	0	0	0	1	1	1 0
468	456	466	464	0	0	0	0	1	1	1 0
456	457	467	466	0	0	0	0	1	1	1 0

/INPUT 18

3. Thermal Evaluation

The safe transport of spent nuclear fuel requires that the heat generated by radioactive decay within the fuel assemblies be transferred to the environment. The NAC-1 spent fuel shipping cask has been designed to provide assurance that the fuel assemblies are adequately cooled during all phases of normal operation as well as during a hypothetical accident that involves a fire. This chapter presents the thermal analyses which demonstrate the adequacy of the cask to withstand normal operating conditions as well as survive the hypothetical accident scenario.

3.1. Discussion

The NAC-1 spent fuel shipping cask is a right circular cylindrical sandwich of stainless steel and lead that transports a stainless steel basket with one pressurized water reactor fuel assembly. Additional baskets are available to transport either two or four fuel assemblies from boiling water reactors or non fuel bearing components. The outside of the cask is surrounded by a neutron shield tank or impact limiters as shown in Figure 1-1. There are no features of this design that incorporate any mechanical aids for cooling the cask.

The characteristics of the fuel assembly or assemblies to be transported in the NAC-1 cask are summarized in Table 1-1. The data that are relevant to the thermal analysis are the volumes of the fuel assembly and the energy being emitted from the fuel assembly.

The temperature in the cask during steady state as well as transient conditions was calculated with a quasi-three-dimensional model. The cask was divided into seven sections which were coupled by the common bulk water temperature in the cavity and the ambient temperature surrounding the cask. The maximum decay heat load was assumed to be 11.5 kilowatts. Cask temperatures for normal transport conditions with a 130°F ambient temperature are summarized in Table 3-1.

When the ambient conditions are conducive to freezing of the cavity coolant, precautions must be taken to assure that freezing does not occur. The decay heat load that is necessary to prevent freezing is 3.11 kW when the ambient temperature is -40°F. The cask temperatures under these conditions are also presented in Table 3-1. Should the decay heat be less than 3.11 kW, and sub freezing temperatures anticipated during shipment, the cavity should be drained and the fuel shipped dry.

The hypothetical fire accident is assumed to be initiated following steady state operation when the ambient temperature is 130°F. The duration of the fire is one half hour; however, no external cooling is assumed to be available until three hours later. The cask temperature at the conclusion of the fire and at three hours after the fire are presented in Table 3-2. The maximum temperature at each location of importance and the time at which the maximum temperature occurs is also presented in Table 3-2.

All of the temperatures in Tables 3-1 and 3-2 are within the allowable ranges of the components of the cask. The fire does not cause the cavity pressure to exceed 900 psig, resulting in an adequate safety margin to the relief pressure setting of the rupture disk which is 1100 psig.

Table 3-1. Summary of Cask Temperatures During Normal Transport

Component	Temperature (deg F) (130 F ambient)	Temperature (deg F) (-40 F ambient)
cavity water	318	32
lead	301	28
valves		
relief	300	12
upper vent	290	1
lower vent	289	1
upper drain	275	-2
lower drain	271	-2
O-rings		
inner	318	32
outer	319	10
Maximum pressure	118 psia	

Table 3-2. Summary of Cask Temperatures During Hypothetical Fire Accident

Component	Temperature After Fire (deg F)	Temperature 3 hours after fire (deg F)	Maximum Temperature (deg F)
cavity water	352	514	514
lead	452	462	510
valves			
relief	336	502	505
upper vent	345	491	495
lower vent	344	489	493
upper drain	316	466	486
lower drain	312	460	480
O-rings			
inner	352	509	509
outer	387	514	514

Maximum internal pressure 824 psia

3.2. Thermal Properties of Materials

To perform the thermal analysis of the NAC-1 spent fuel shipping cask, the physical properties of several materials and fluids must be known. The properties which are of importance to this analysis are presented in the following sections. Where the properties are plotted as a function of temperature, the curves are constructed of straight line segments to duplicate the linear interpolation which is employed by HEATING-5 (see appendix) to determine the properties at temperatures between tabulated values.

The property values have been extracted from three main sources. The appendicies to the ASME Boiler and Pressure Vessel Code for pressure vessels (Reference 3.1) was the preferred source. When this source did not have the necessary data, the tables of thermal properties that were prepared to supplement the TRUMP computer program (Reference 3.2) or tabular data extracted from other references (3.3 - 3.6) were utilized. The lowest values for the thermal conductivity are utilized in the analyses to introduce conservativeness into the results.

3.2.1. Thermal Properties of Solids

There are four solid materials that are utilized in the NAC-1 spent fuel shipping cask. They are:

- type 321 stainless steel
- high purity lead
- oxygen free copper
- fiberglass woven cloth

In addition to these materials the fuel assembly that is being

transported also contains uranium dioxide and Zircaloy-2 or -4.

The thermal conductivity and specific heat of stainless steel (Type 321) are presented as functions of temperature in Figures 3-1 and 3-2, respectively. The thermal conductivity data were taken from Reference 3.1 and the values for the specific heat were extracted from Reference 3.2. The density of stainless steel was treated as a temperature independent property with a value of 0.286 pounds per cubic inch (Reference 3.1).

The thermal conductivity and specific heat of lead are presented in Figures 3-3 and 3-4 as temperature dependent funtions. Both of these sets of data have been taken from Reference 3.2. The density was assumed to be constant with a value of 0.410 pounds per cubic inch (Reference 3.2).

Copper forms the heat transfer fins that thermally connect the lead to the stainless steel shells. The thermal conductivity and specific heat of copper are presented in Figures 3-5 and 3-6, respectively. The density was considered to be a temperature independent property with a value of 0.323 pounds per cubic inch (Reference 3.2).

The fuel assembly being transported is situated in the cask cavity and therefore must be considered in the evaluation of the heat capacity of the cavity contents. The specific heat of uranium dioxide and Zircaloy are presented as temperature dependent functions in Figure 3-7. These data have been extracted from MATPRO (Reference 3.7) which is a collection of fuel assembly material properties. The heat capacities were evaluated for conditions representing end of life following complete burnup in a reactor.

The thermal conductivity and specific heat of the fiberglass woven cloth were assumed to be constant over the temperature range used in this analysis (-40°F to 1475°F) with values of

0.00833 BTU/hr-in-^{o}F and 0.25 BTU/lb-^{o}F, respectively (Reference 3.3).

3.2.2. Thermal Properties of Liquids

There are two liquids in the NAC-1 cask which are important to heat transfer through the cask. These are the water in the cask cavity and the solution of water, ethylene glycol, and potassium tetraborate that fills the neutron shield tank. Both liquids transfer heat by natural convection and both are integral parts of the total heat capacity of the cask.

The heat transfer from the fuel assembly to the cask wall is accomplished by natural convection in the water. The heat transfer coefficient that represents natural circulation around a horizontal cylinder in air or water has been measured and predicted analytically. The results are presented in many references (3.3 - 3.4) on heat transfer and fluid flow. A plot of the dimensionless representation of the heat transfer coefficient is presented in Figure 3-8 where the Nusselt number is represented as a function of the product of the Grashof and Prandtl numbers. The data have been fitted to the following expression where the product of the Grashof and Prandtl numbers is between E^{-8} and E^{-11}:

$$Nu = 0.13\ (Gr \times Pr)^{1/3}$$

where: $Nu = hD/k$

$$Gr = \frac{g\beta D^3 \Delta T}{\nu^2}$$

$$Pr = \frac{\rho C_p \mu}{k}$$

h is the surface heat transfer coefficient

in BTU/hr-in-^{o}F

D is the diameter of the cylinder in inches

k is the thermal conductivity in BTU/hr-in-^{o}F

g is the gravitational constant in in/sec^2

β is the volumetric expansion coefficient in 1/^{o}F

ΔT is the temperature difference between the surface and the ambient

ν is the kinematic viscosity in ft^2/hr

Cp is the specific heat in BTU/lb-^{o}F

ρ is the density in lb/cubic foot

When the expansions for the dimensionless numbers are introduced into this correlation, it takes on the following form:

$$h = C\ (\Delta T)^{1/3}$$

where: $$C = 0.13\ k\ (\ g\beta/\nu^2 \cdot Pr\ )^{1/3}$$

The cylindrical diameter that appears in the Grashof and Nusselt numbers is dependent upon the geometry of the heat transfer surface. However, because the exponent of the Grashof number is 1/3, the diameter is self-cancelling and is not a parameter in the final expression. Consequently, the form and constants for representing natural circulation of air may be applied to surfaces without alteration. Should the form of the correlation change, this conclusion will no longer be valid and the coefficients will be dependent upon the geometry of the heat transfer surfaces.

The values of the term $g\beta/\nu^2$ and the Prandtl number for water are presented in Figure 3-9 as a function of the film temperature. This temperature is defined as the arithmetic average of the surface and bulk fluid temperatures and is employed to include the variation of the fluid properties within the moving fluid. The term $g\beta/\nu^2$ is identified as the Grashof number when the cylinder dimension is one foot and the

temperature difference is one degree Fahrenheit. A tabular presentation of the properties of water is presented in Table 3-3. The heat transfer coefficient that describes natural circulation heat transfer in water is presented as a temperature dependent function in Figure 3-10. The data in this figure are based upon a temperature difference between the heated surface and bulk fluid temperatures of $1^{o}F$. Thus, the heat transfer coefficient is the product of the value in Figure 3-10 and the cube root of the temperature difference.

The text in Reference 3.3 that accompanies Figure 3-10 indicates that the above correlation is only valid when the Prandtl number is close to unity. Evaluation of the analytically derived expressions for laminar flow matches the expressions presented in this figure when the Prandtl number is set to unity. However, the data presented in this figure is based on room temperature measurements as well as measurements at higher temperatures. Consequently, the expression "Prandtl number near unity" can be interpreted as including the range $\sim$0.5 to $\sim$2.0. When the water temperature is below $70^{o}F$ this correlation should not be used.

Natural circulation of the solution of ethylene glycol and water in the neutron shield tank differs completely from the natural circulation of the water in the cask cavity. The shield tank is divided into four individual tanks by gusset plates that are seal welded to the cask body and the shield tank. The flow patterns that result from natural circulation in these tanks are represented in Figure 3-11. The upper shield tank has flow patterns that are characterized by intermixed upward and downward flowing columns of water which is similar to the flow pattern for natural convection between horizontal plates. The geometry of the lower tank will restrict upward movement such that all flow is along the surface. As the flow reaches the bounding gusset plate, it is able to move only toward the shield tank outer wall where it cools and flows downward along the wall completing the circuit.

The representation of the heat transfer in the upper shield tank is that of an internal thermal resistance across a gap. The thermal resistance is based on a correlation for natural convection between horizontal plates which is given as:

$$h = .069 \frac{k}{\delta} (Gr)^{1/3} (Pr)^{0.407}$$

The terms are as defined previously and δ is the spacing between plates $(R_o - R_i)$.

The representation of the heat transfer in the lower shield tank is based upon the analytical development of the relationship that describes natural circulation adjacent to a flat vertical plate (Reference 3.4). These expressions are:

$$h = \frac{0.902 (Pr)^{1/2} (\frac{Gr}{4})^{1/4}}{(0.861+Pr)^{1/4}} \cdot \frac{k}{D} \quad \text{laminar flow}$$

$$h = \frac{0.0246 (Gr)^{2/5} (Pr)^{7/15}}{[1+0.494 (Pr)^{2/3}]^{2/5}} \cdot \frac{k}{D} \quad \text{turbulent flow}$$

The use of these expressions is based upon the anticipated flow pattern which is quite similar to the flow pattern adjacent to a vertical plate. The length that appears in the Grashof number and in these expressions will be taken as the diameter to properly relate the circular flow path to the curved surface in diverting the flow.

The transition between laminar and turbulent flow is very difficult to define because it is expressed as a range of the product of Prandtl and Grashof numbers. To be more specific, the transition was defined for this analysis as the point where the two correlations gave equal values for the heat transfer coefficient. This is within the range of values that defines the transition and also avoids and numerical instabilities that would result from a discontinuity in the values of h.

The Grashof and Prandtl numbers of a 30% water and 70% ethylene glycol solution are presented in Figure 3-12. These data are taken from Reference 3.5. Utilizing these data to evaluate the heat transfer coefficient for the upper and lower shield tanks, the heat transfer coefficient is expressed as:

$$h=C(\Delta T)^{1/3}$$

The data in Figures 3-13 and 3-14 for the upper and lower shield tanks, respectively, are obtained using the above equation. Only the coefficient C is presented in these figures because that is the form of the input utilized within HEATING-5. The ethylene glycol solution must not freeze. Therefore, any mixture of ethylene glycol and water which freezes at a temperature below $-40^{o}F$ is unacceptable. Figure 3-15 is a graph of the freezing point of a ethylene glycol solution (weight per cent) as a point of an ethylene glycol solution (weight per cent) as a The solution in the shield tank is nominally 70% ethylene glycol by

weight, but it can range from a low of 53% to a high of 84% by weight without the occurence of freezing.

3.2.3. Thermal Properties of Gases

The only gas that is important to the heat transfer within the NAC-1 spent fuel shipping cask is air. Air surrounds the cask and serves to transport heat from the cask to the environment. This gas is also trapped within the cask where it transports heat in parallel to the stainless steel gusset plates. In both instances natural circulation is the principal mode of heat transfer since conduction of heat through air is negligible.

The correlation that represents the results of experimental measurements of the heat transfer coefficient for natural convection of air around the outside of a long cylindrical body is given by:

$$Nu = 0.13\ (Gr \times Pr)^{1/3}$$

This expression is identical to that given in the previous section for natural circulation of water because it represents experiments using either air or water as the heat transfer medium. This correlation is also valid for vertical plates as well as cylinders because the empirical foundation includes both geometries. Additionally, the dimension of the heated or cooled surface in the Nusselt and Grashof numbers is self-cancelling so this correlation is independent of the size of the surfaces transferring heat.

The Grashof and Prandtl numbers for air are presented as a function of temperature in Figure 3-16. In addition a tabular

representation of the important thermal properties of air are presented in Table 3-4. The Grashof number presented in Figure 3-16 is based upon a temperature difference of $1^{o}F$ and a dimension of one foot so the term plotted is indicative of the value of the ratio $g\beta/\nu^2$.

The heat transfer coefficient is expressed as the product of a coefficient times the cube root of the temperature difference or:

$$h = C(\Delta T)^{1/3}$$

where: $$C = 0.13\ k\ (\ g\beta/\nu^2 \cdot Pr\ )^{1/3}$$

The value of the coefficient C is plotted as a function of temperature in Figure 3.17.

The conduction of heat through stationary air is a necessary part of the evaluation of the performance of the fins that form the interface between the lead and the stainless steel. The thermal conductivity of stationary air is plotted in Figure 3.18 as a function of temperature.

The natural circulation of ambient air around the outside of the cask will be restricted at the bottom of the cask because of the presence of the trailer. The floor of the trailer is perforated to permit some flow of air to the lowest regions of the cask; however, this flow will be more restricted than the flow which reaches the middle and upper portions of the cask surface. To conservatively model this phenomenon, the cask surface that was 25 degrees on either side of the centerline at the bottom of the cask was represented as transferring heat to the environment at a comparable rate to two flat horizontal plates. The correlation selected is representative of heat transfer from a heated upper plate to a cooled lower plate which is a conservative

representation of the geometry and simultaneously ignores the presence of any free flow of air to this region. In equation form this correlation is given by:

$$h=0.000833\ (\Delta T/L)^{1/4}$$

where: h is the heat transfer coefficient in BTU/hr-in^2-^{o}F

ΔT is the temperature difference between the heated and cooled plates in ^{o}F

L is the distance between the plates in feet

The difference between the plates has been taken as one foot to approximate the spacing between the cask and trailer and the curvature of the cask. The heat transfer coefficient thus becomes:

$$h = 0.000833\ (\Delta T)^{1/4}$$

This was employed with no dependence of the coefficient upon the temperature of the heated surface.

A summary of the correlations which have been utilized to represent natural circulation of the various fluids within the NAC-1 cask is presented in Table 3-5. This table summarizes the application of each correlation in the analysis of the cask. Equally as important as the summary of the equation form of the correlations is the comparison of the values of the heat transfer coefficients that are presented in Figure 3-19. In each case the temperature of the medium receiving the heat was constant at 100^{o}F in evaluating the heat transfer coefficients. A temperature of 100^{o}F for the receiving surface is unrealistic for this application of the heat transfer coefficients in water; however, this temperature was selected to provide a uniform basis for

comparison of all the natural circulation heat transfer coefficients.

3.2.4. Radiation

Heat transfer by radiation is a small but important part of the heat rejection to the environment during normal transport and a major heat transfer mechanism during the thermal accident. The heat transfer between two bodies is expressed as:

$$q/A = F \varepsilon \sigma (T^4 - T_o^4)$$

where q/A is the heat flux in BTU/hr-in^2
F is the geometric view factor
ε is the emissivity
T is the surface temperature in ^oR
T_o is the ambient temperature in ^oR
σ is the Stefan-Boltzman constant, .1189 x 10-10 BTU/hr-in^2-$^oR4$

The geometric view factor represents the fraction of radiation leaving the surface that can reach the receiving surface. The instances of radiation heat transport in this analysis involve heat transfer from the cask surface to the environment or heat transfer within an enclosed region within the cask. Since all of the heat leaving a surface will reach the receiving surface in both situations, the view factor is taken as unity for all applications of radiation heat transport.

The surface emissivity represents the imperfection of the surfaces in absorbing or emitting radiant energy. For heat transfer between two surfaces, the effective emissivity is given by:

$$\varepsilon = \frac{1}{\frac{1}{\varepsilon_1} + \frac{1}{\varepsilon_2} + 1}$$

The emissivity of the environment is taken as unity to reflect the fact that all of the heat radiated from the cask is absorbed by the environment. In this instance the effective emissivity becomes equal to ε_1 or the emissivity of the cask surface.

The emissivity of the stainless steel outer surface of the cask is presented in many references (3.3 - 3.4) with values ranging from 0.1 to 0.2. The value of 0.15 will be used to approximate conditions when the cask is new and the surface is clean and bright. During the life of the cask, the surface will become dull with a surface film that will increase the emissivity. Such changes will increase the ability of the cask to reject heat to the environment.

During and after the fire accident, the emissivity of the stainless steel has been increased to 0.8 to reflect the blackening of the surface by a coat of carbon or ash during the fire. In this case the emissivity of the environment was taken as 0.9.

The insolation has been assumed to be constant at the average values which represent the mean of the energy deposited during the twelve hours of sunlight per day. The specific values employed are:

Curved Surfaces	0.85 BTU/hr-in^2
Vertical Surfaces	0.43 BTU/hr-in^2

The insolation on a curved surface is applied only to the horizontal component of the surface area.

3.2.5. Cavity Contents

An important characteristic of the cavity contents is the height of the water in the cask. The orientation of the fuel assembly and basket within the cavity during horizontal transport is shown in Figures 3-20, 3-21, and 3-22. The orientation of the basket is fixed by locators within the cavity and the orientation of the cask is fixed by trunnion position and the offset of the lower trunnions that ensures loading onto the truck in only one orientation.

The water volume in the cavity has been calculated by dividing the cask cavity into four different regions representing the different sections of the basket and fuel assembly. The configuration of the three baskets and the respective fuel assemblies are shown in Figures 3-20, 3-21, and 3-22. The resulting volumes are presented in Figure 3-23. The fuel assembly has been assumed to be resting on the basket and the volume displaced by the fuel rods has been represented precisely. Removing twenty four gallons will result in a water height 1.8 inches above the center of gravity when a single PWR fuel assembly is being transported and 2.3 or 2.4 inches above the center for either two or four BWR fuel assemblies, respectively. The lower height was used throughout the analysis to force the heat through the smaller contact area between the water and cask resulting in conservatively higher temperatures.

TABLE 3.3 THERMAL PROPERTIES OF WATER

T (F)	ρ (lb_m/cu ft)	Cp (Btu/lb_m F)	k (Btu/hr ft F)	Pr	$\frac{g\beta}{\nu^2}$ (1/F cu ft)
100	62.0	0.998	0.364	4.52	118×10^6
150	61.2	1.00	0.384	2.74	440.0
200	60.1	1.00	0.394	1.88	1.11×10^9
250	58.8	1.01	0.396	1.45	2.14
300	57.3	1.03	0.395	1.18	4.00
350	55.6	1.05	0.391	1.02	6.24
400	53.6	1.08	0.381	0.927	8.95
450	51.6	1.12	0.367	0.876	12.10
500	49.0	1.19	0.349	0.87	15.30
550	45.9	1.31	0.325	0.93	17.80
600	42.4	1.51	0.292	1.09	20.60

TABLE 3.4 THERMAL PROPERTIES OF DRY AIR[3.4]

T (F)	ρ (lb_m/cu ft)	Cp (Btu/lb_m F)	k (Btu/hr ft F)	Pr	$\frac{g\beta}{\nu^2}$ (1/F cu ft)
0	0.086	0.239	0.0133	0.73	4.2×10^6
32	0.081	0.240	0.0140	0.72	3.16×10^6
100	0.071	0.240	0.0154	0.72	1.76×10^6
200	0.060	0.241	0.0174	0.72	0.850×10^6
300	0.052	0.243	0.0193	0.71	0.444×10^6
400	0.046	0.245	0.0212	0.689	0.258×10^6
500	0.0412	0.247	0.0231	0.683	0.159×10^6
600	0.0373	0.250	0.0250	0.685	0.106×10^6

TABLE 3.5

SUMMARY OF NATURAL CONVECTION HEAT TRANSFER COEFFICIENT CORRELATIONS

Description	Correlation	Range of Applicability	Location in Cask Analysis
Natural circulation around cylinder in infinite body of fluid	$h = 0.13 \frac{k}{D} (Gr \cdot Pr)^{1/3}$	$10^9 \leq Gr \cdot Pr) \leq 10^{12}$ $Pr \simeq 1$	1. Cavity water to cask wall 2. Shield tank surface to ambient air
Natural circulation around cylinder in infinite body of fluid	$h = \frac{0.902(Pr)^{1/2}(Gr/4)^{1/4}}{(0.861 + Pr)1/4} \frac{k}{D}$	$T < 215^{o}F$	1. Lower shield tank
	$h = \frac{0.0246(Gr)^{2/5}(Pr)^{7/15}}{[1 + 0.494(Pr)^{2/3}]^{2/5}} \frac{k}{D}$	$T > 215^{o}F$	
Natural circulation between flat parallel plates (bottom heated, top cooled)	$h = 0.069 \frac{k}{\delta} (Gr)^{1/3}(Pr)^{0.407}$ $(\delta = R_{outer} - R_{inner})$		1. Upper shield tank
Natural circulation between flat parallel (top heated, bottom cooled)	$h = 0.000833(\Delta T/L)^{1/4}$ (L is spacing between plates - taken as 1 foot)		1. Shield tank surface to ambient air at bottom of cask

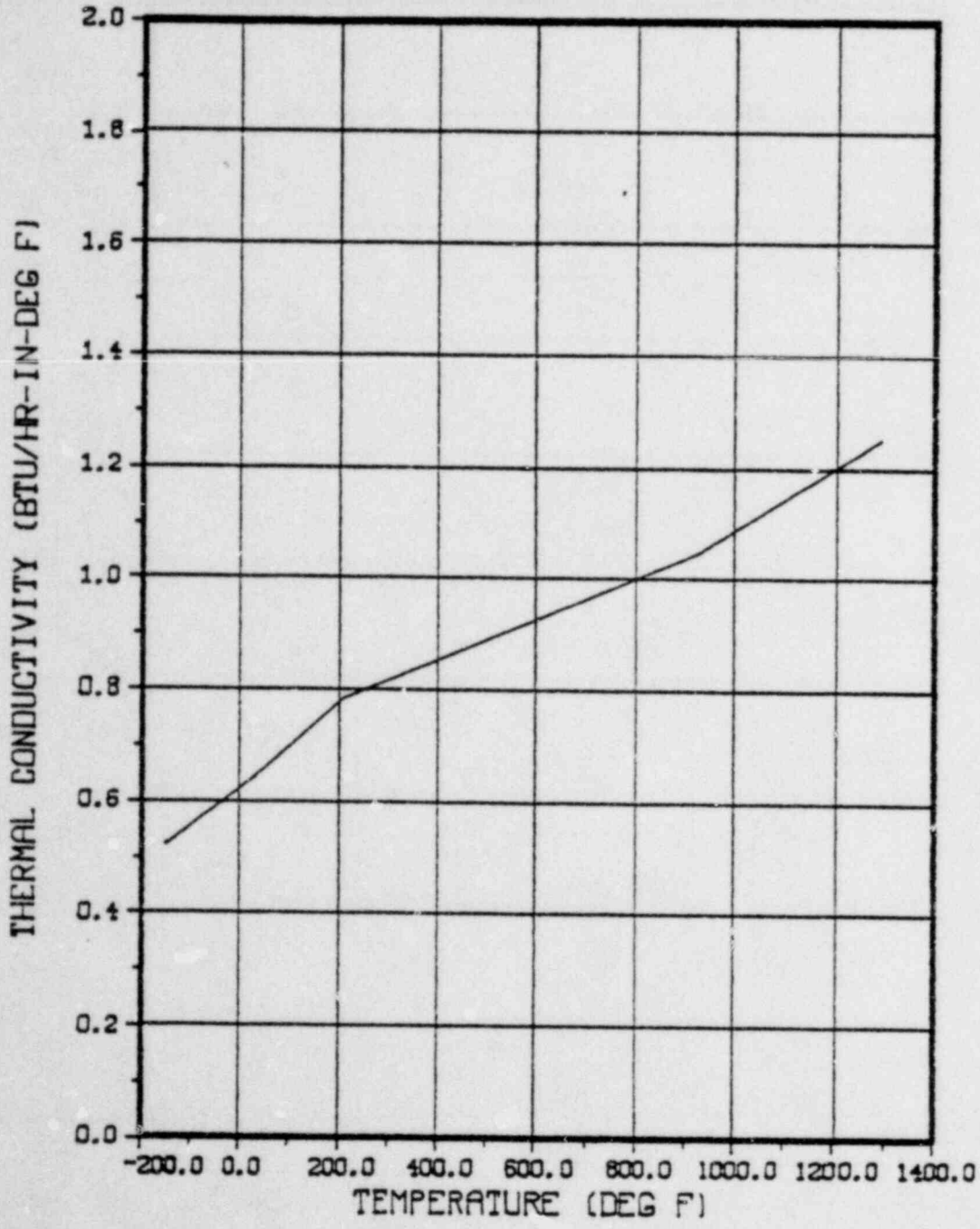

Figure 3-1. Thermal Conductivity of Type 321 Stainless Steel

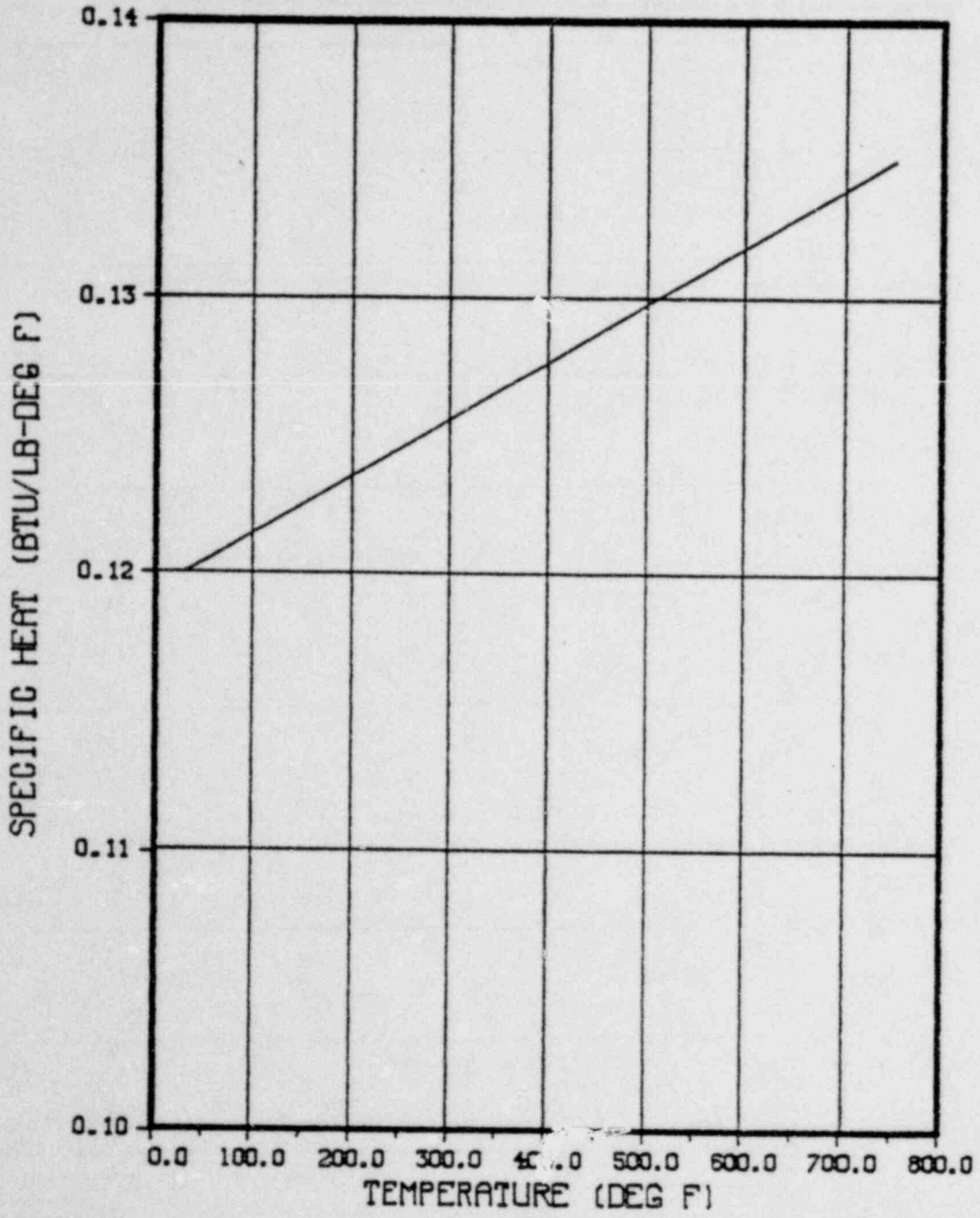

Figure 3-2. Specific Heat of Type 321 Stainless Steel

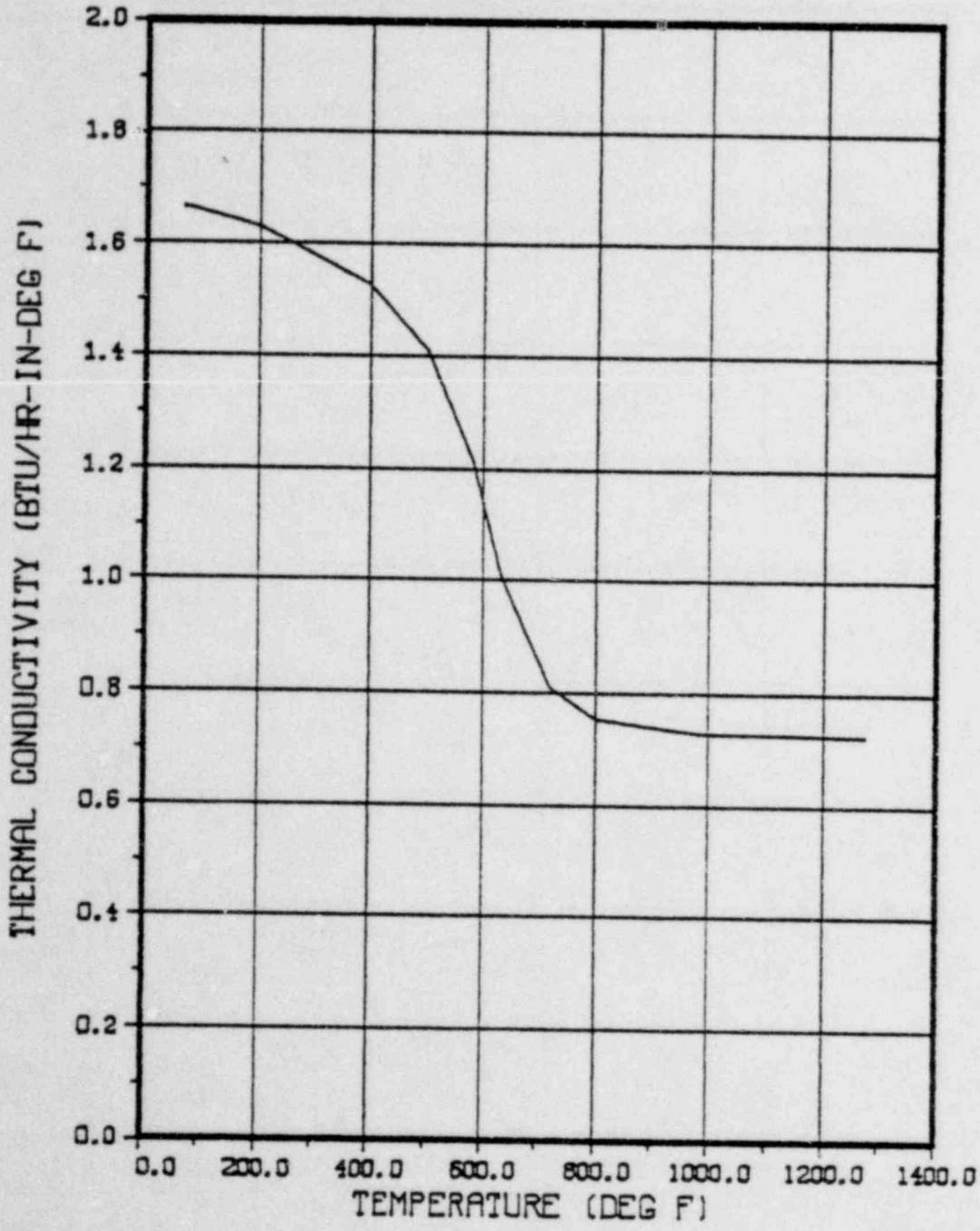

Figure 3-3. Thermal Conductivity of Lead

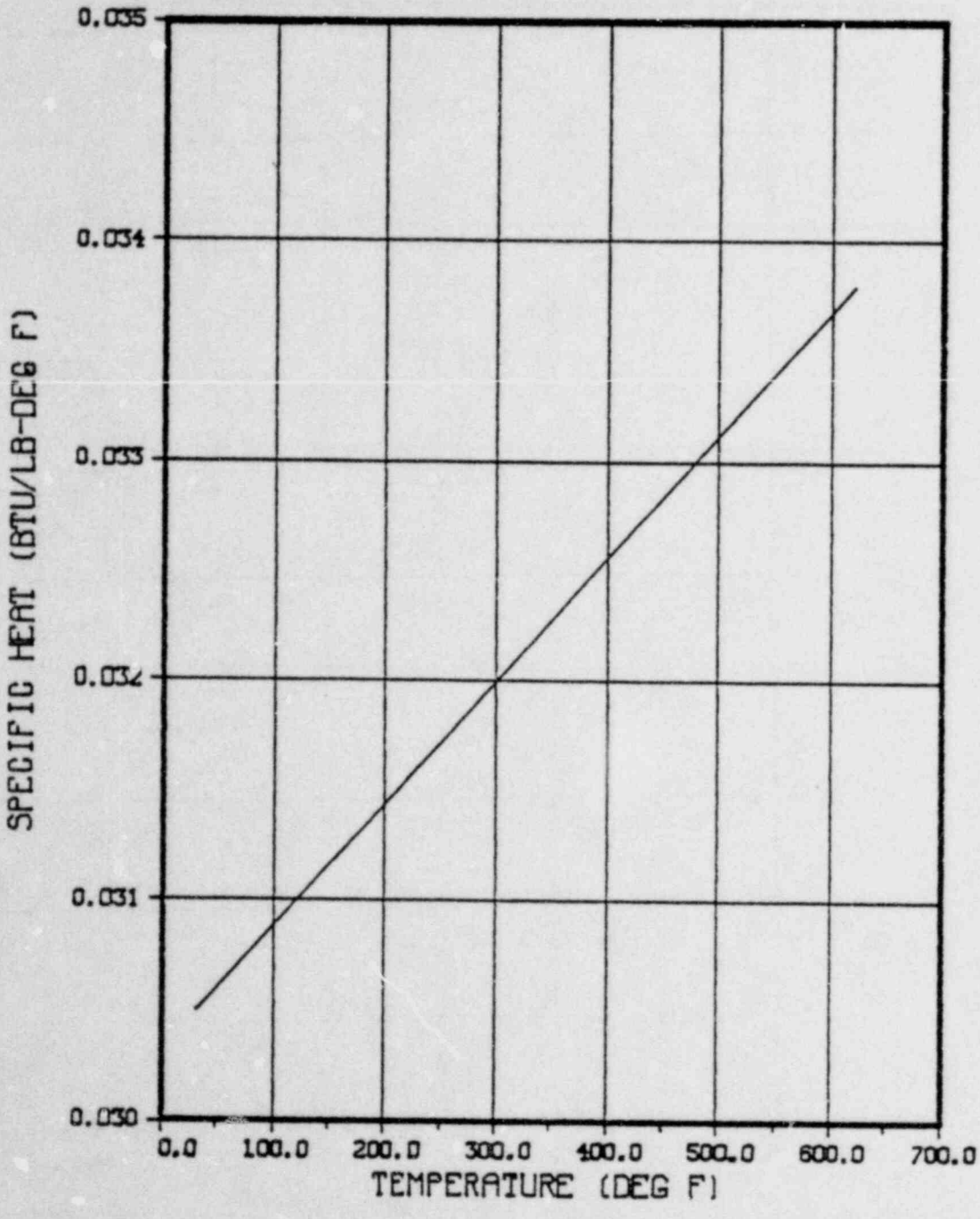

Figure 3-4. Specific Heat of Lead

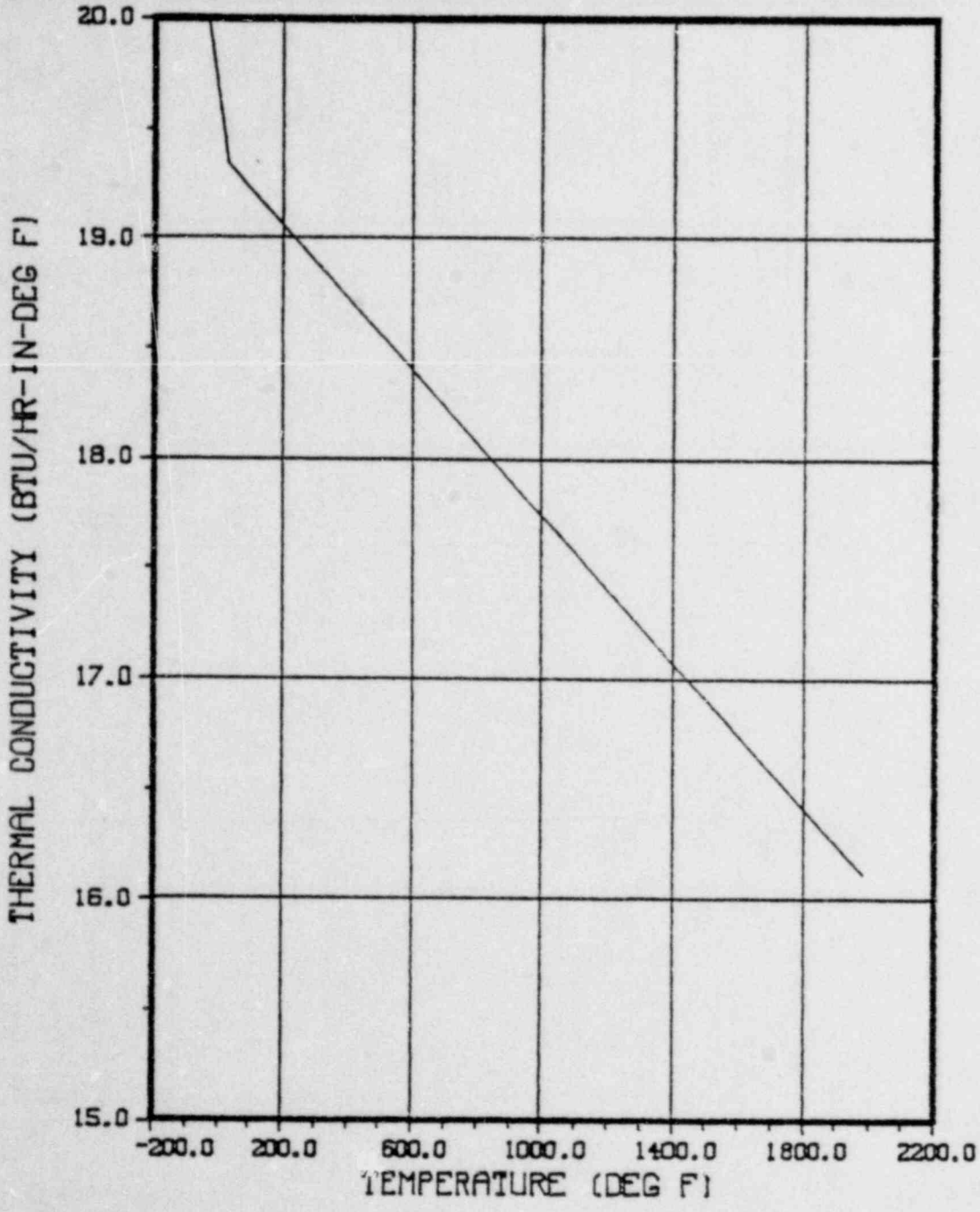

Figure 3-5. Thermal Conductivity of Copper

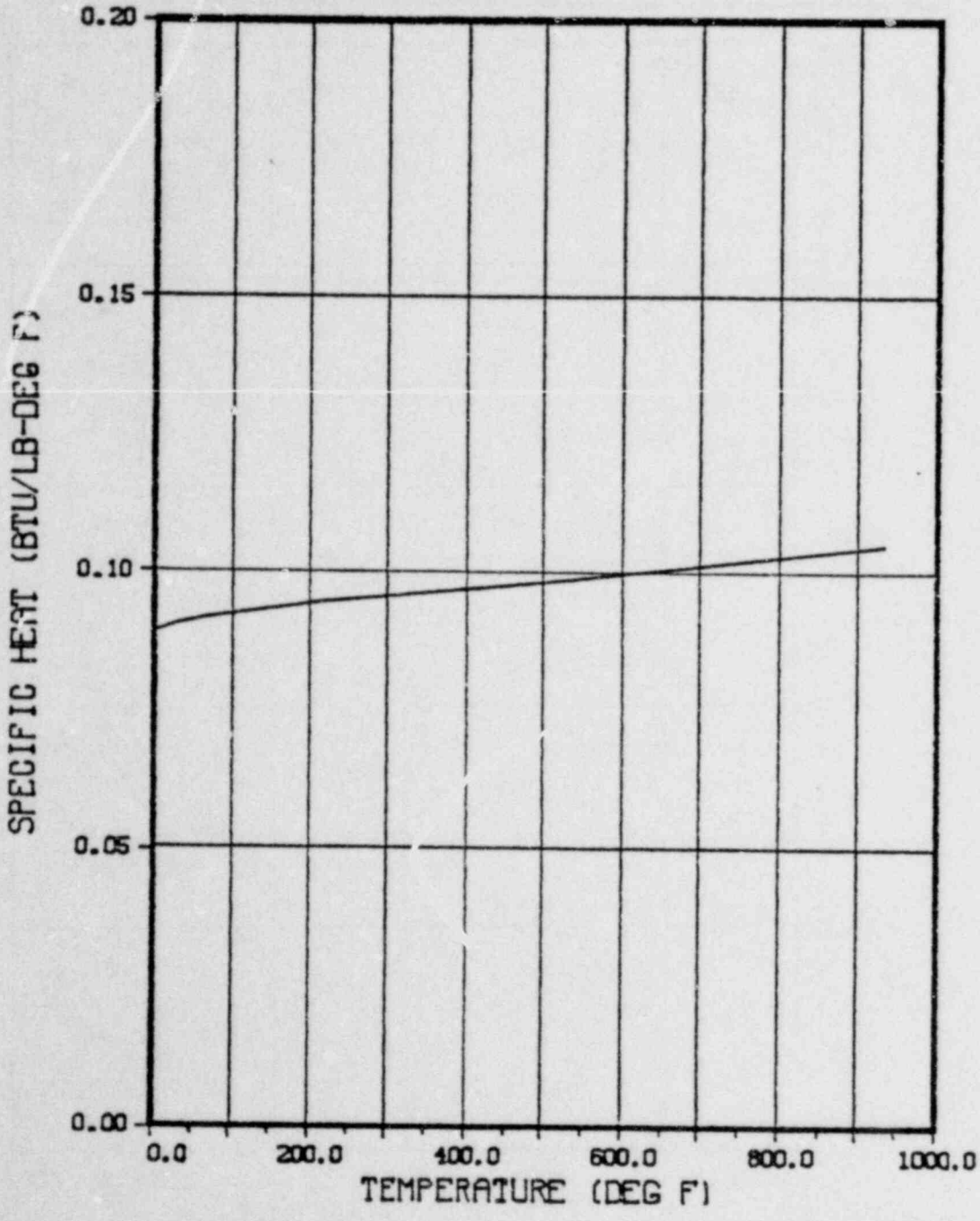

Figure 3-6. Specific Heat of Copper

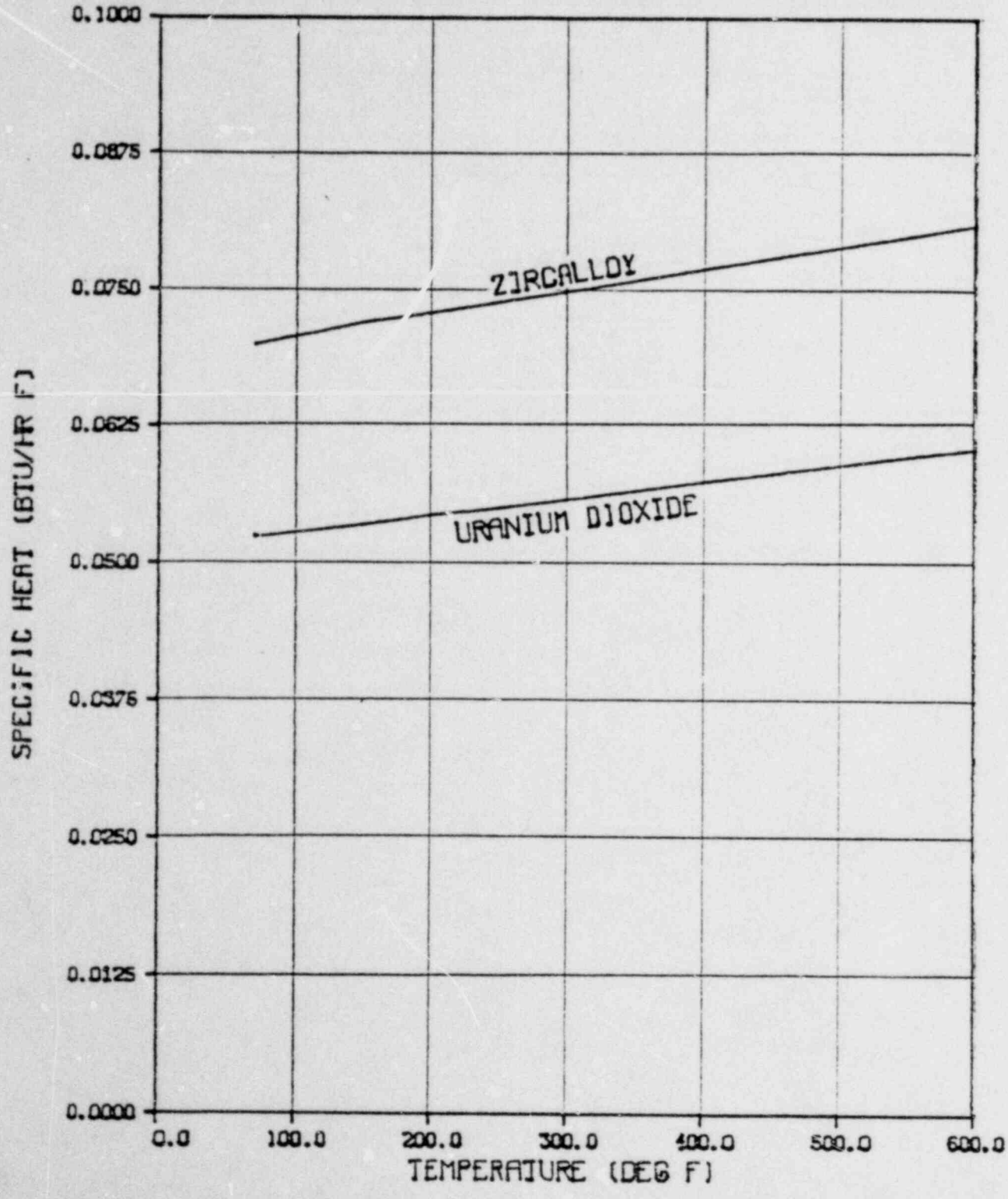

Figure 3-7. Specific Heat of Zircalloy and Uranium Dioxide

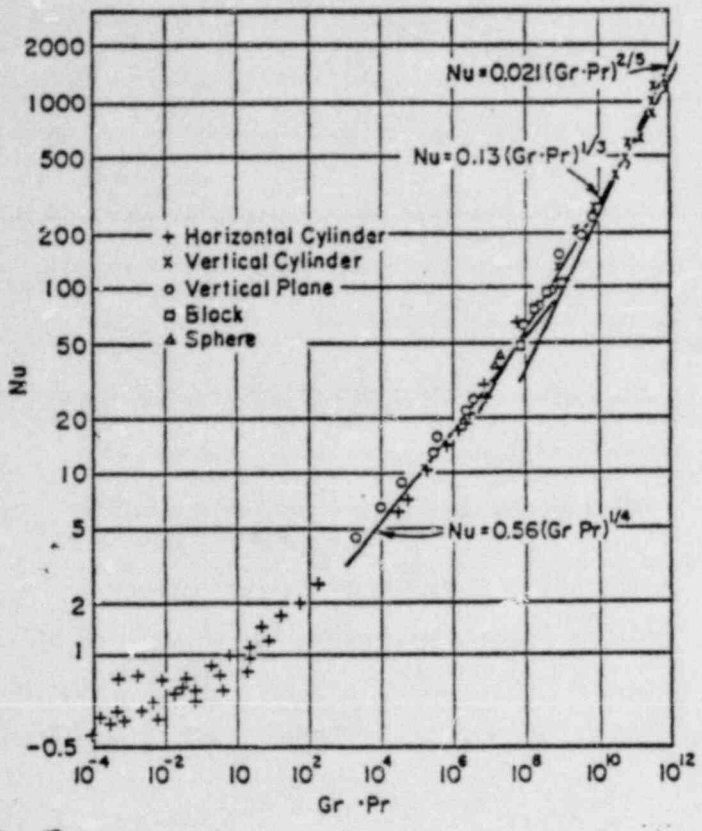

Figure 3-8. Empirical Data Representing Natural Circulation of Air and Water

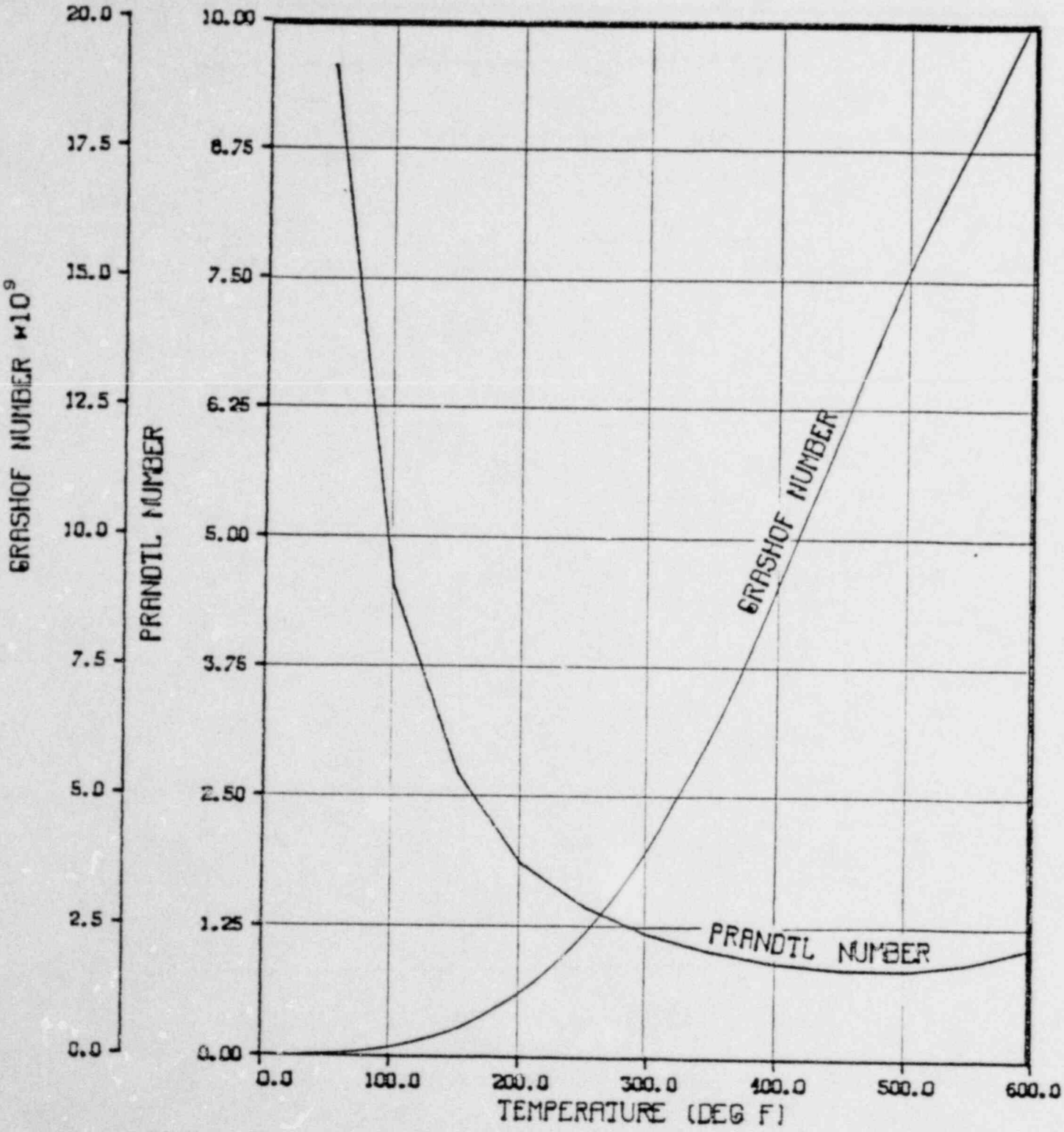

Figure 3-9. Grashof and Prandtl Numbers of Water

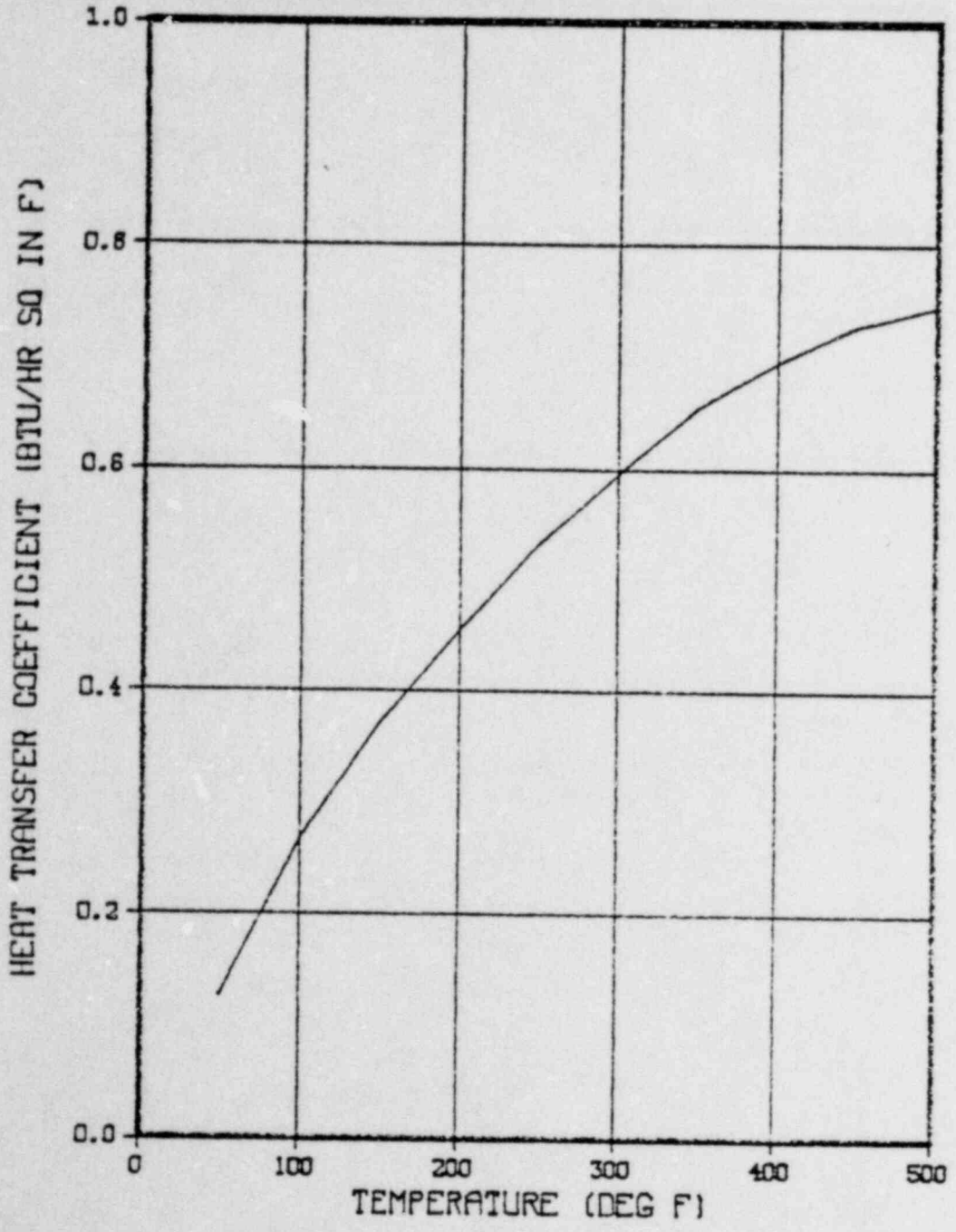

Figure 3-10. Heat Transfer Coefficient Representing Natural Circulation in Water

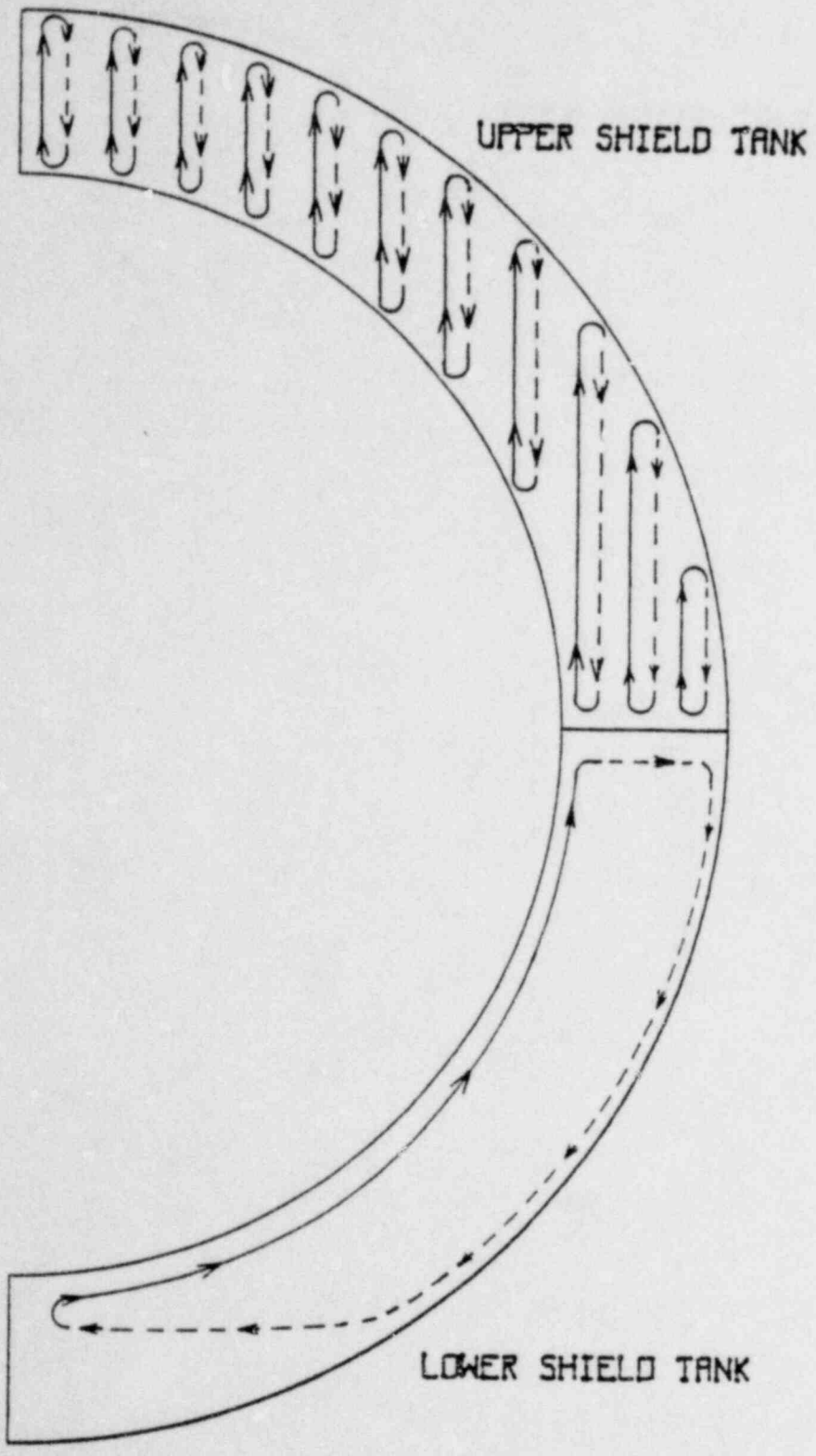

Figure 3-11. Natural Circulation Flow Patterns in Shield Tank

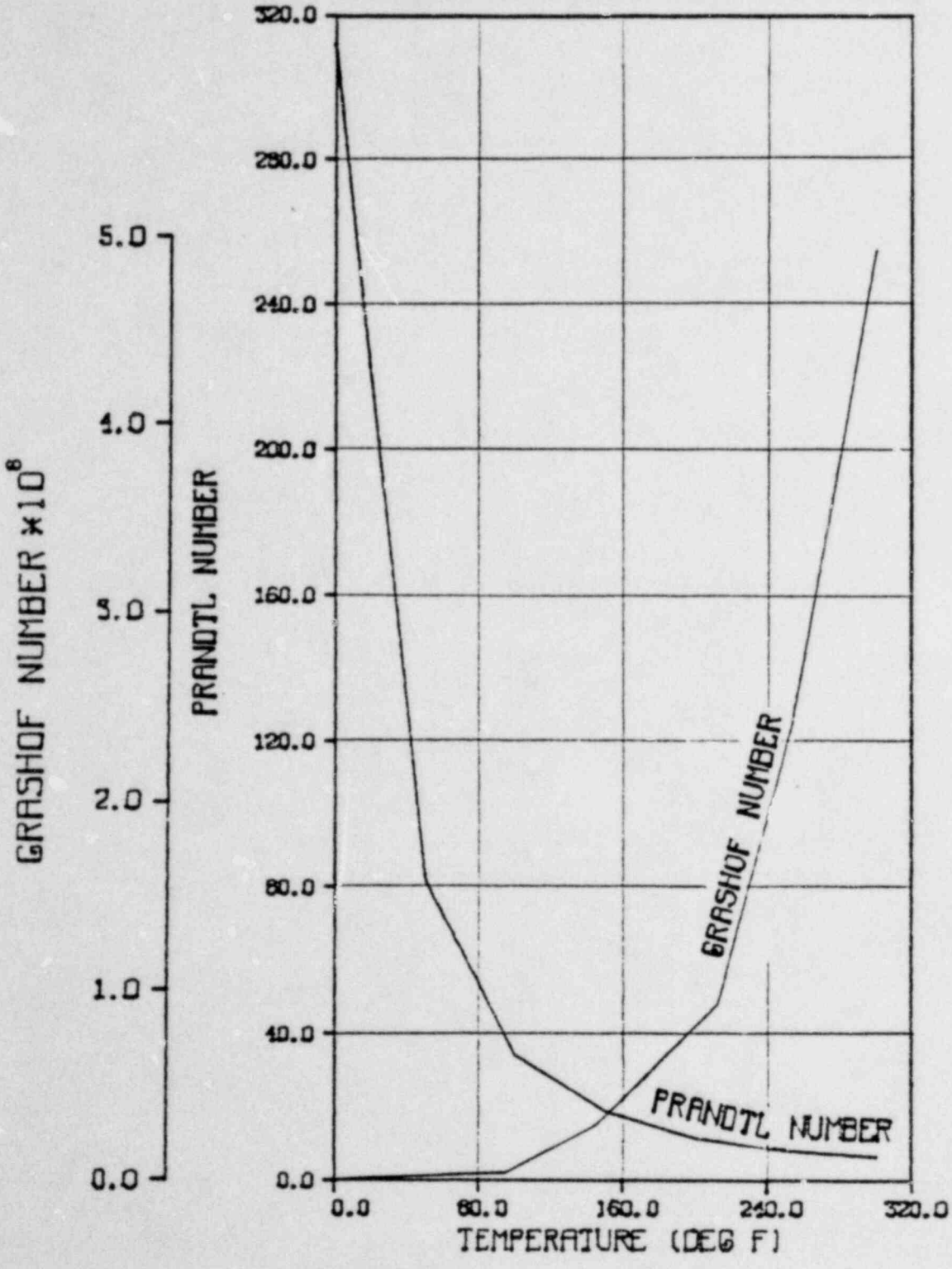

Figure 3-12. Grashof and Prandtl Numbers of Water and Ethylene Glycol Solution

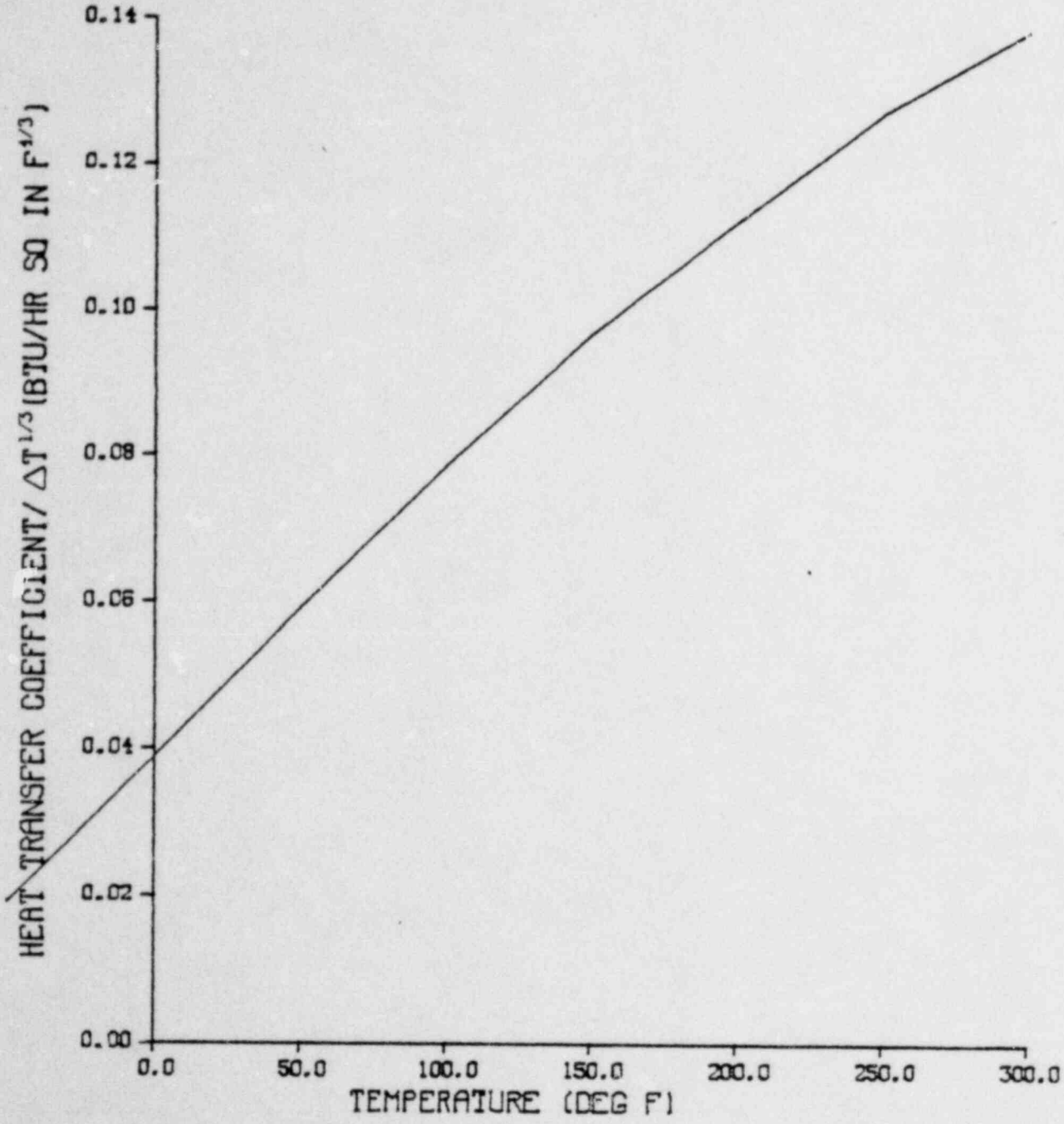

Figure 3-13. Heat Transfer Coefficient Representing Natural Circulation in Upper Shield Tank

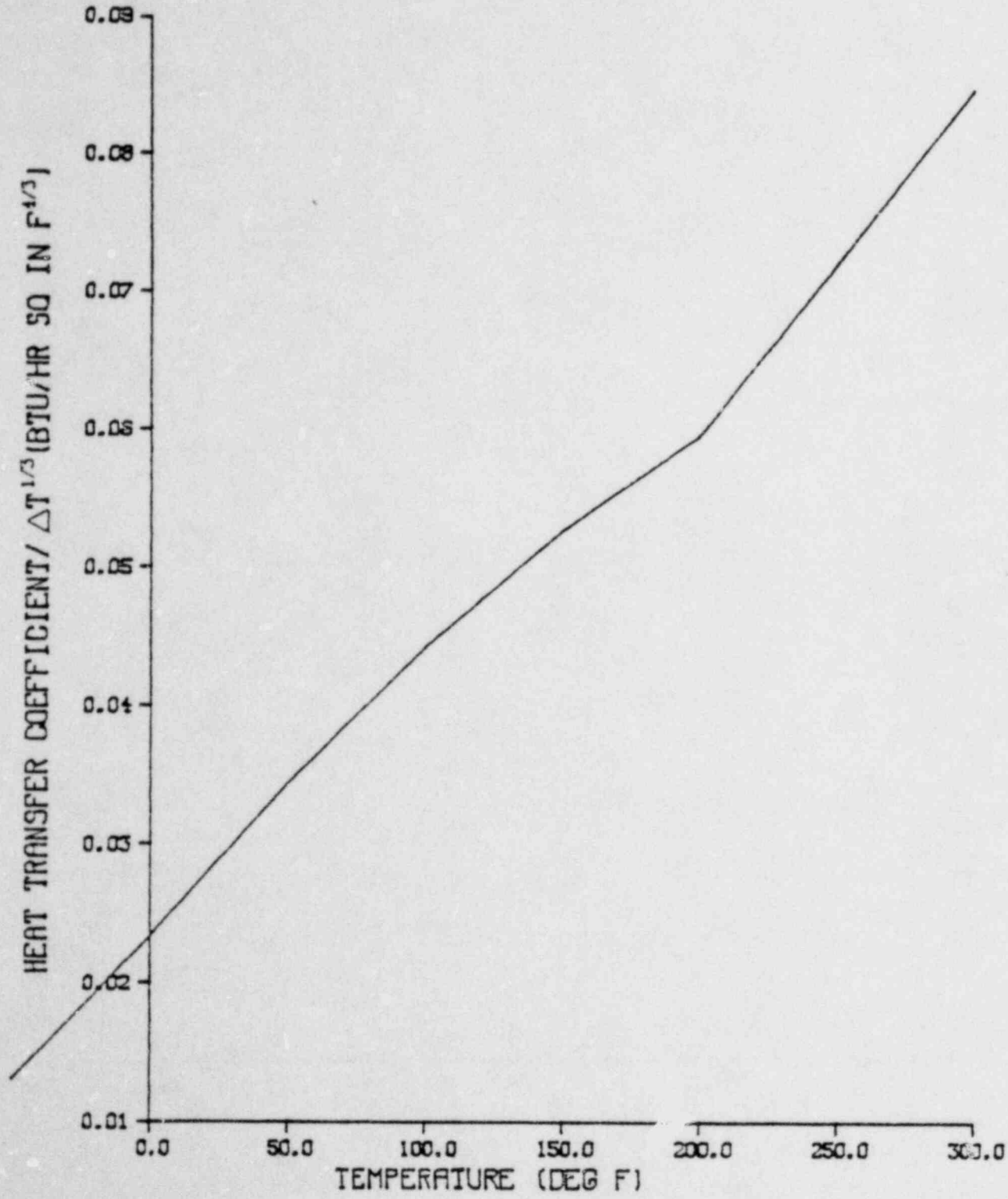

Figure 3-14. Heat Transfer Coefficient Representing Natural Circulation in Lower Shield Tank

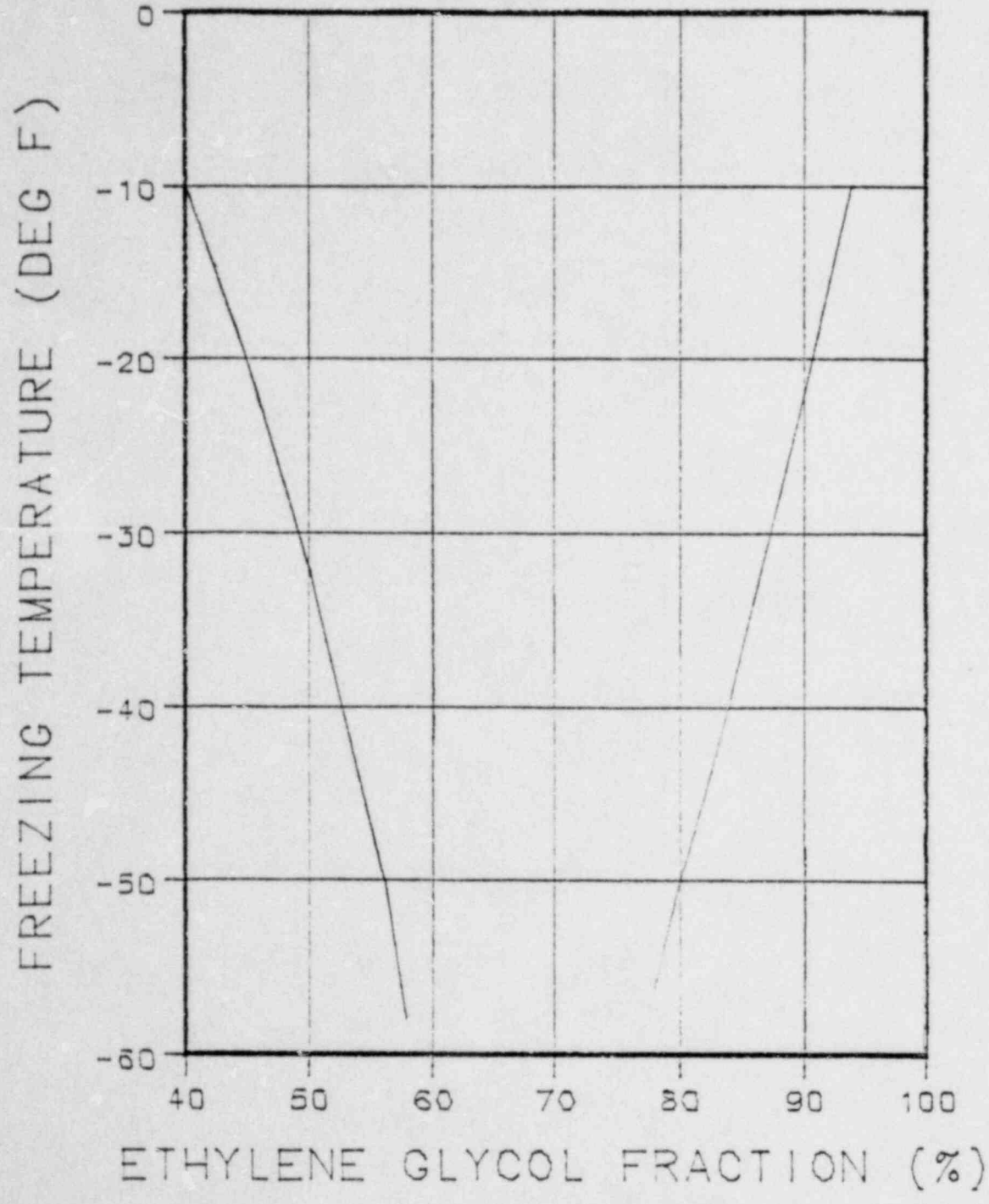

Figure 3-15. Freezing Point of an Ethylene Glycol Solution as a Function of Temperature

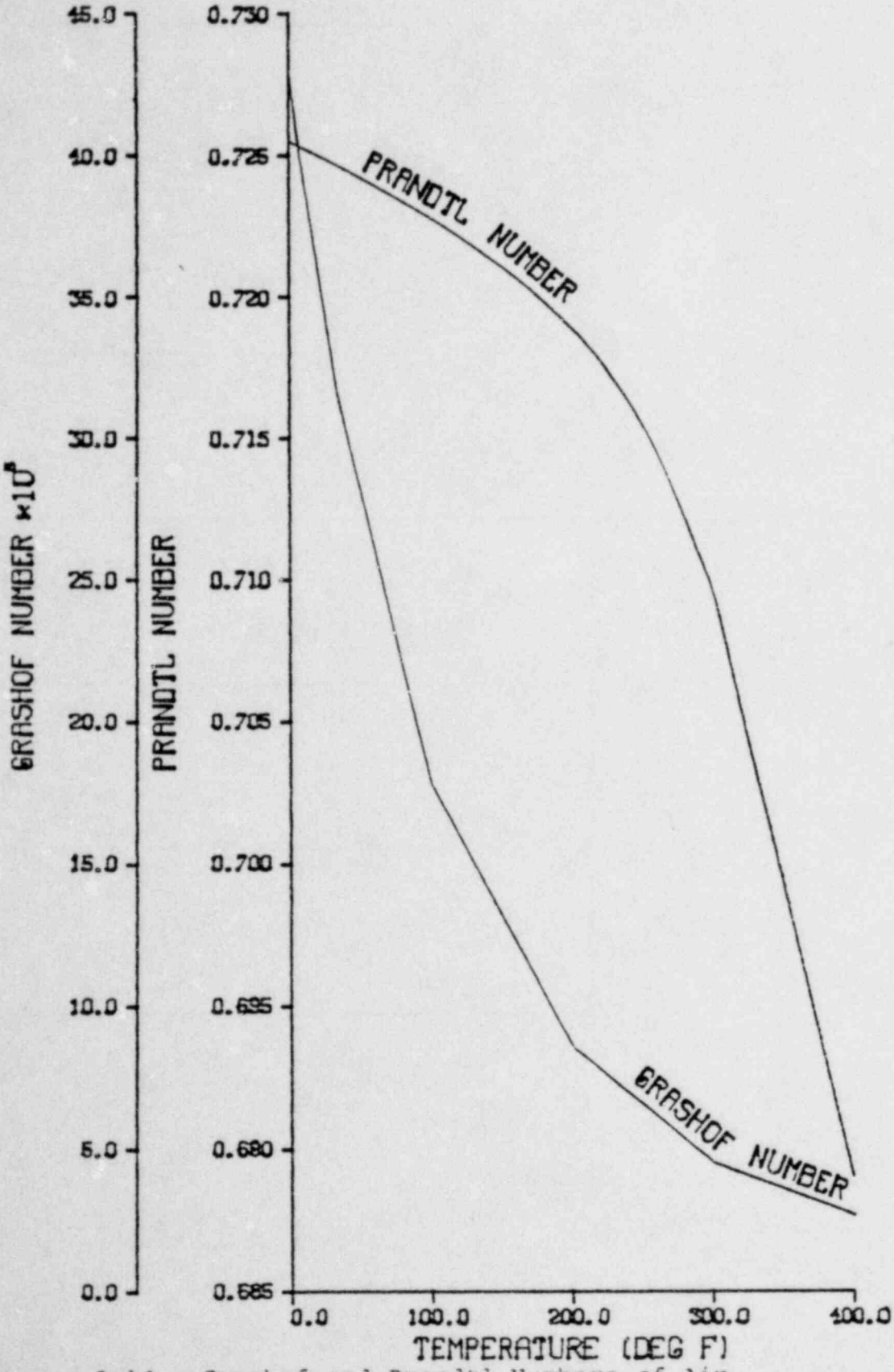

Figure 3-16. Grashof and Prandtl Numbers of Air

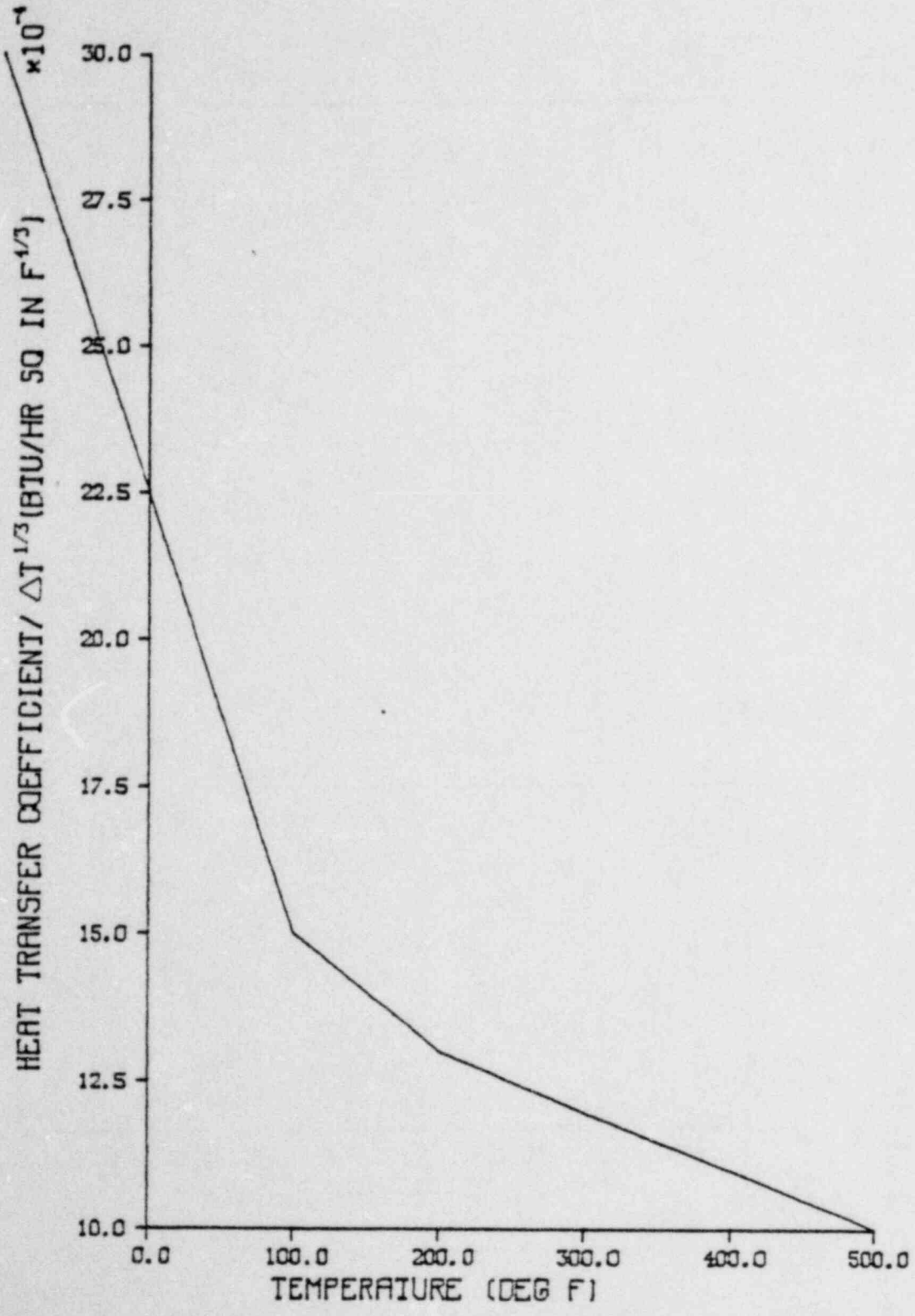

Figure 3-17. Heat Transfer Coefficient Representing Natural Circulation in Air

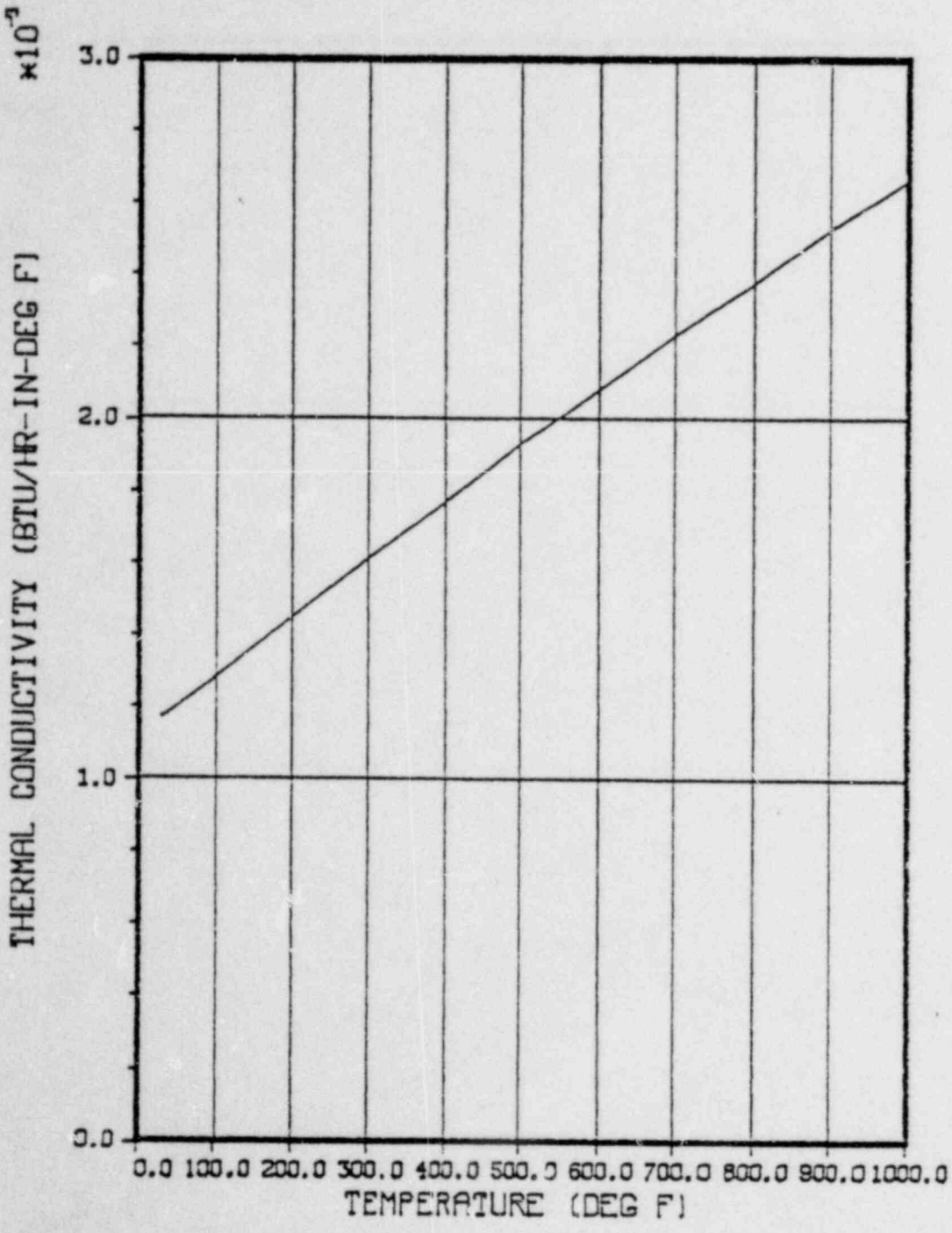

Figure 3-18. Thermal Conductivity of Stationary Air

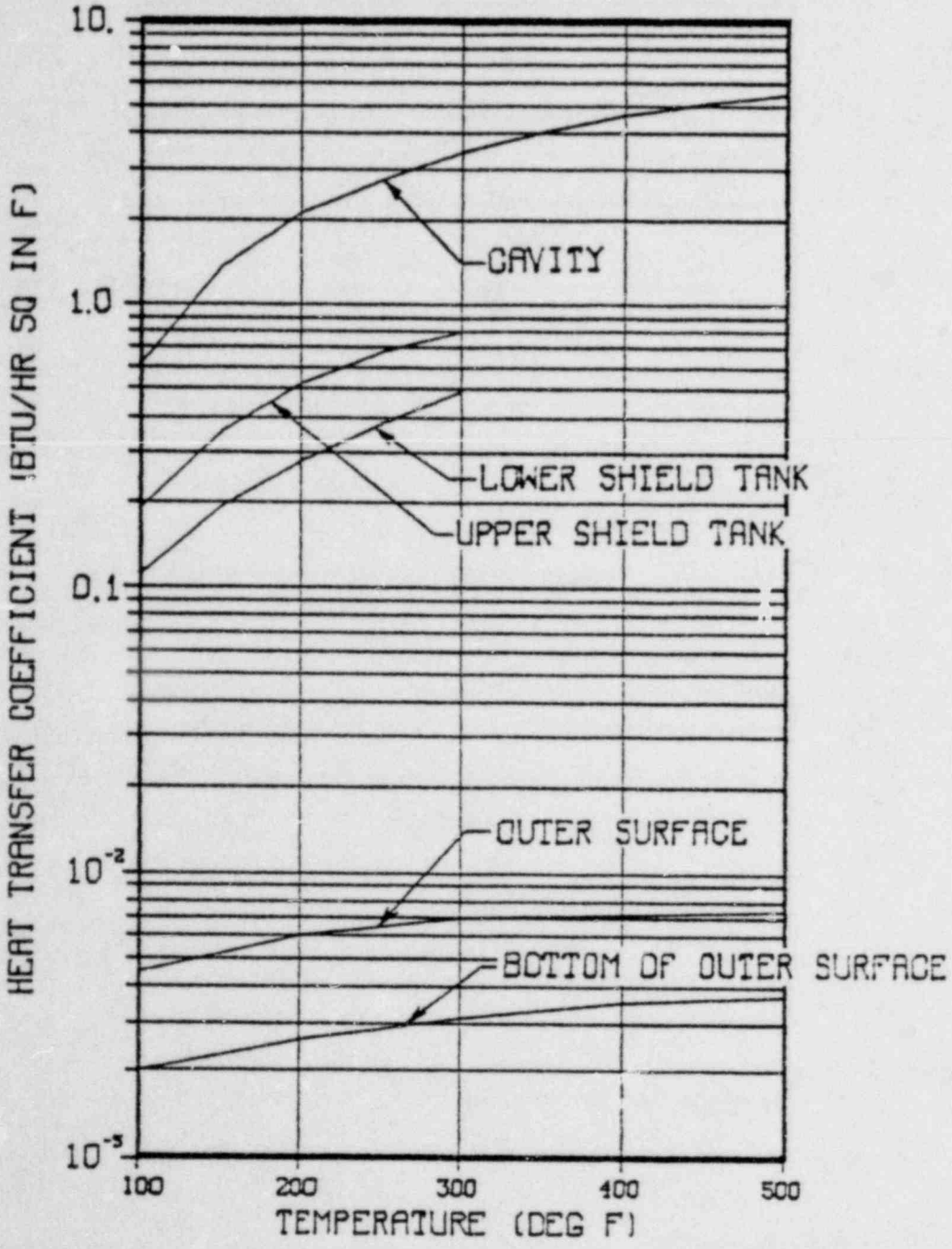

Figure 3-19. Comparison of Natural Circulation Heat Transfer Coefficients

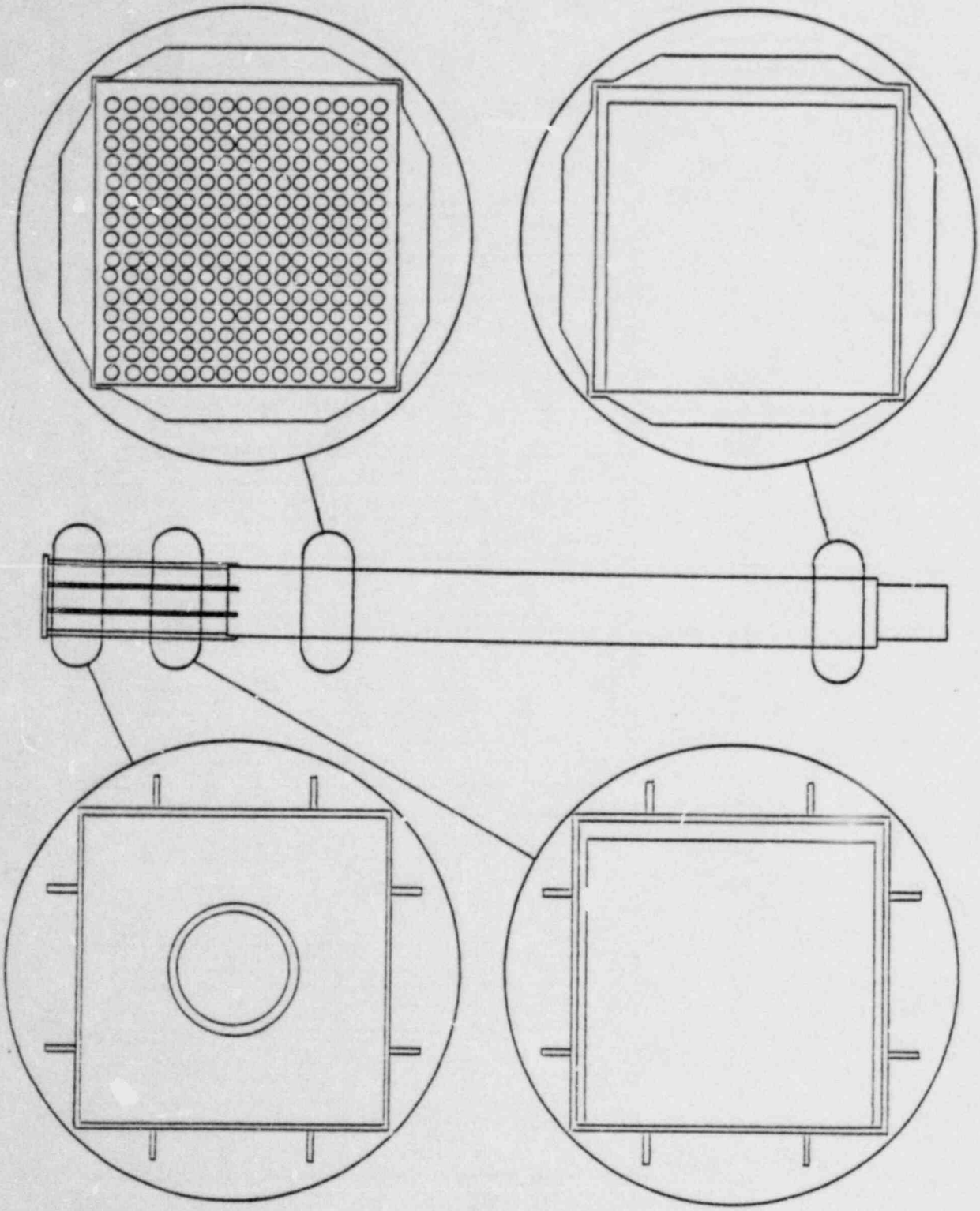

Figure 3-20. Fuel Assembly and Basket Configuration for Single PWR Fuel Assembly

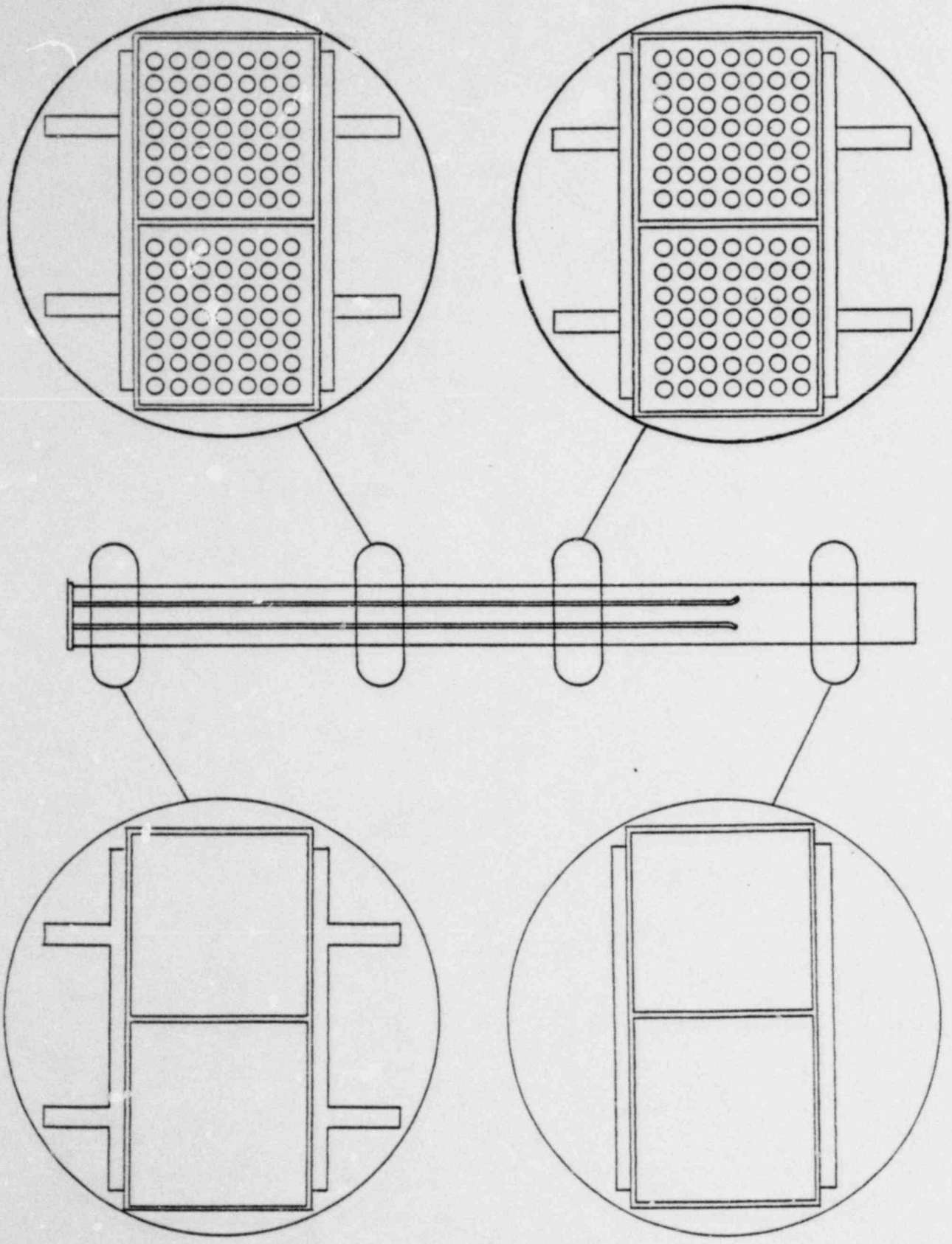

Figure 3-21. Fuel Assembly and Basket Configuration for Two BWR Fuel Assemblies

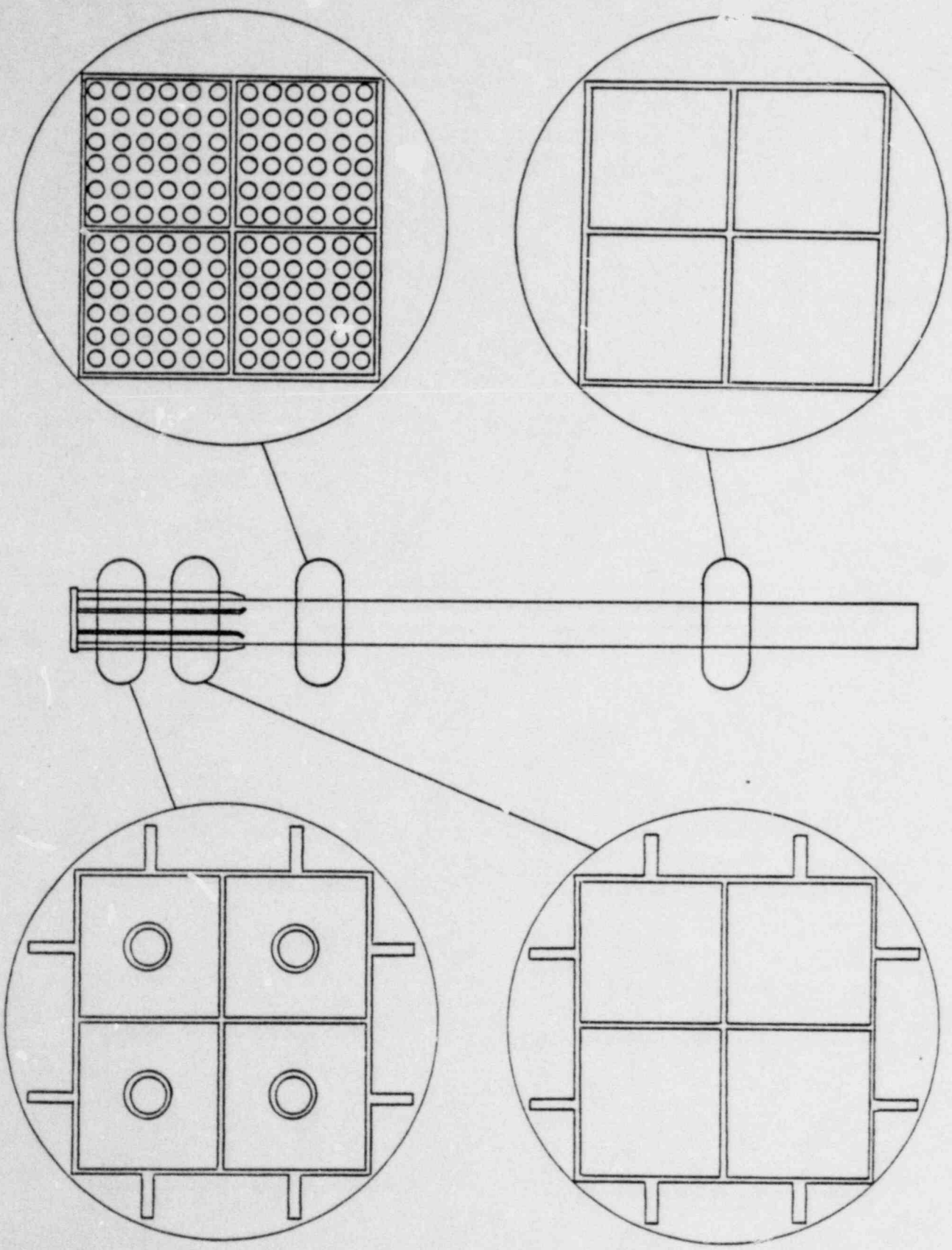

Figure 3-22. Fuel Assembly and Basket Configuration for Four BWR Fuel Assemblies

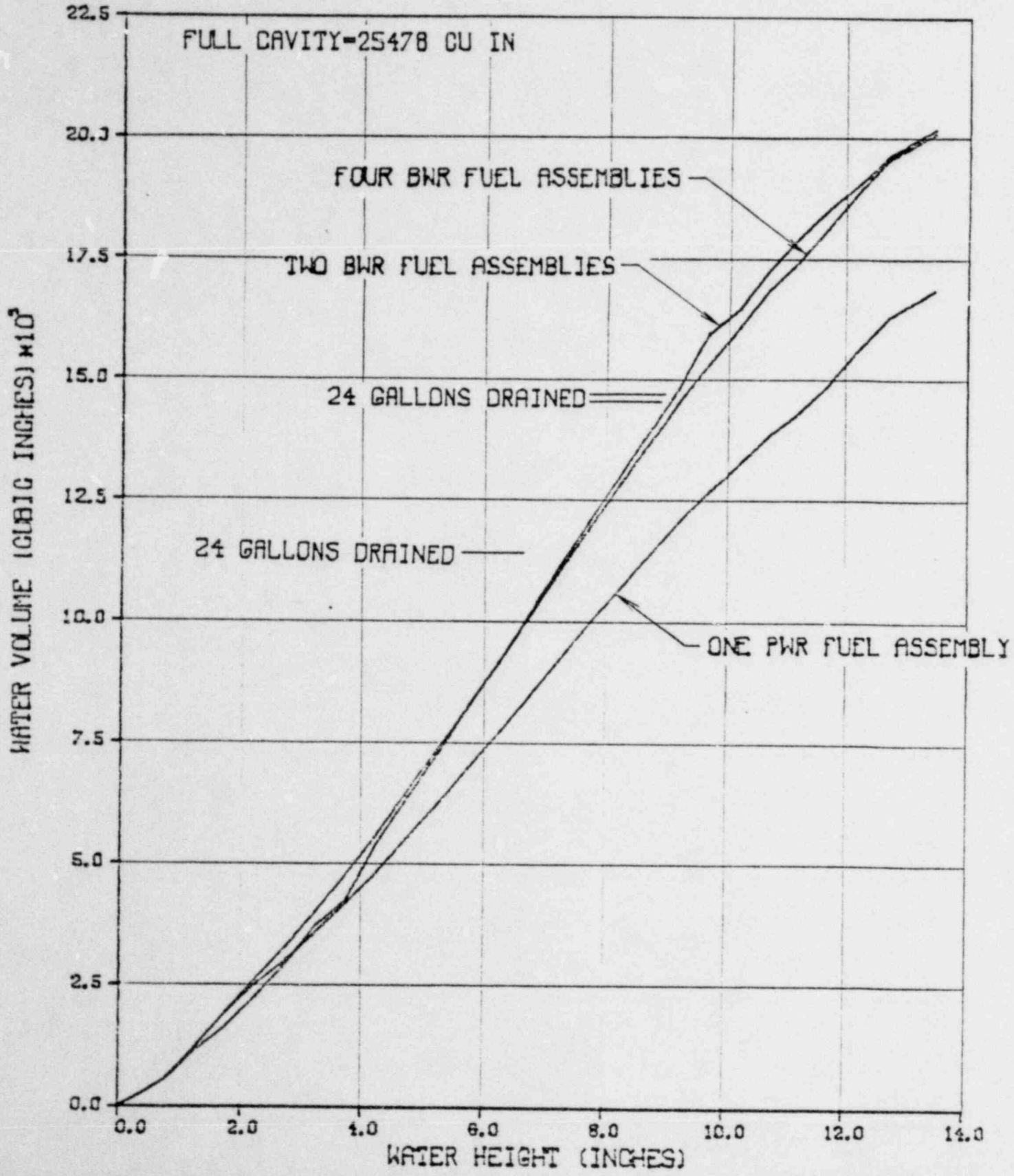

Figure 3-23. Cavity Water Volume to Height Relationship

3.3. Technical Specification of Components

The cask components that are significant to the thermal analysis are as follows:

- Vent valves
- Drain valves
- Cavity rupture disks
- Shield tank rupture disks
- O-ring seals

The temperatures of each component must not exceed the rated temperature of that component to assure that containment is not lost during normal transport or accident conditions.

The vent valves and drain valves are Miser Fire Valves, Part No. 1/2FG466TSW or equivalent with modified sealing balls. These valves are manufactured by Worcester Controls Corporation. This valve is fire rated which indicates that all components of the valve have been selected to maintain their seals in a high temperature environment.

The modification to the sealing balls consists of drilling a relief hole in the ball so that no water is trapped in the passage when the valve is in the closed position. This prevents damage to the valve under either freezing or high temperature conditions.

Three typical valves were subjected to leakage tests at 520°F and 985 psig using nitrogen as the working fluid. Typical leakage rates through the valves during these tests were between 2 and 3 x 10^{-7} SCFM with no leakage detected at the mountings of the

valves.

The test report is included in Reference 3.8.

The rupture disk that is intended to relieve cavity overpressure is designed to relieve at 1100 psig and 600°F. The rupture disk is manufactured by In-Val-Co and is certified by the ASME.

The fixture which supports the rupture disk is modified to accept a relief valve that is intended to seal the cavity when the pressure is 200 psig or less.

There are four rupture disks which protect the shield tanks from overpressurization. Each disk is designed to rupture at a pressure of 100 psig and 315°F.

All of the rupture disks are designed to operate at the saturation temperature that corresponds to the pressure that is to be relieved. Consequently, there are no temperature limitations on the rupture disks and only the pressures need be examined to assure that the rupture disks are not forced to release cavity contents or shield tank contents.

3.4. Thermal Evaluation for Normal Transport Conditions

Normal conditions of transport encompasses the maximum and minimum ambient temperatures and the maximum and minimum decay heat that will be encountered during the normal operation of the cask. Ambient temperatures of 130°F and -40°F represent the upper and lower bounds of all temperatures that are expected to be encountered in the continental United States within a 99% confidence level (Reference 3.8). The maximum decay heat is 11.5 kW and the minimum is the value which will prevent freezing of the cavity water when the cask is exposed to a -40°F environment. Lesser amounts of decay heat can be transported; however, the cavity must be drained if subfreezing temperatures are anticipated during transport.

All of the analyses of normal transport conditions are based upon a stationary cask with no wind or other air motion except for the air motion associated with natural convection. The cask is assumed to be experiencing maximum insolation in conjunction with the high ambient temperatures and no insolation when the ambient temperature is -40°F. Additionally, the transport vehicle is assumed to be a part of the environment and does not contribute to the heat rejection capability of the cask.

3.4.1. Thermal Model

Modelling of the thermal characteristics of the NAC-1 spent fuel shipping cask requires the physical properties of the cask materials, the computer program, the model geometry, and the boundary conditions. Material properties are described in Section 3.2 and the HEATING-5 computer program which was utilized for the analyses is described in Section 3.6. The geometrical representation of the cask is described beginning in Section

3.4.1.1.

3.4.1.1. Geometrical Representation

Evaluation of the heat flow within the NAC-1 cask is a three-dimensional problem. The radial direction, as opposed to the axial and azimuthal directions, is the most important dimension because heat is transferred primarily in this mode. The θ coordinate is also important because the shield tank has gusset plates which facilitate heat transfer to the outer surface of the cask. In addition, the source of heat is not uniform around the surface of the cask cavity. Likewise, the axial dimension is not as important as the radial direction. However, it cannot be neglected because the end impact limiters act as large heat rejection surfaces. The cask has been modelled by dividing it into seven different axial segments which were represented independently. These independent sections were coupled by the uniform boundary condition at the surface of the cavity. An effective thermal conductivity was calculated for each of the seven sections of the cask which combined the effects of the heat flowing through the various materials contained in that segment. These seven axial segments were then coupled using r-z geometry to create a model of the entire cask using the effective thermal conductivities for each of the seven axial pieces. This representation of the entire cask allows the heat which flows axially and radially through the cask to be modelled while it implicitly represents the heat flow in the azimuthal direction.

The water in the cavity will transfer heat from the fuel to the basket primarily by natural convection and from the basket to the cavity wall also by natural convection. When the cask is horizontal, the temperature change of the water as it flows from the top to the bottom of the cavity and transfers 11.5 kW to the cavity wall is less than $6^{o}F$. To approximate this condition, the

boundary condition on the cavity surface was taken as a linear (dependent) variation of the temperature over the portion of the cavity where the water is in contact with the cask wall and adiabatic over the remainder of the surface.

The seven segments that represent the entire cask are as follows:

- Upper impact limiter and closure plug
- Cask wall with upper cowl
- Expansion tank
- Cask wall with shield tank
- Cask wall with lower cowl
- Cask wall with lead void
- Lower impact limiter

The geometric relationship and relative size of each segment is shown in Figure 3-24. Each of these seven pieces was converted into a segment of the cask in r-z geometry only. This was accomplished by utilizing the effective thermal conductivities which were calculated for the various axial pieces. The individual r-z segments were coupled to form an r-z composite of the entire cask. The modelling focused on paths for heat flow to external surfaces to assure correct representation of the transmission of heat from the cavity to the environment.

3.4.1.1.1. Cask Wall with Shield Tank

The section of the cask that includes the shield tank is the most important portion of the modelling of the cask. Approximately 85% of the heat flows through this section. It is represented in only two dimensions (r, θ) because there is no significant variation in the axial direction in this segment of the cask. This model

of the wall was used for all cask model pieces which contained the wall of the NAC-1 cask. The geometry of this section is shown in Figure 3-25.

The shield tank in the NAC-1 cask is slightly different than it appears in the model. In the actual cask, the outer stainless steel shell near the expansion tank is twice as thick as the normal outer stainless steel shell thickness. This double thickness has not been considered in the model since it appears for only five inches along the 178 inch outer shell.

The shield tanks have been treated as an internal boundary condition with the heat transfer coefficient representing natural circulation of the water and ethylene glycol solution as described in Section 3.2.2. The upper shield tank was characterized by a correlation representing convection between parallel plates with the lower plate heated and the upper plate cooled. The lower shield tank was represented by a correlation for heat transfer from a cylinder to an infinite body and from an infinite body to a cylinder.

The water that is between the gusset plates and the gusset supports has been represented as stationary water with conduction as the only mechanism for heat transfer. The gusset supports have holes to allow movement of water into and out of a confined region. However, it has been assumed that such motion is restricted to temperature equilibrium and no natural circulation exists.

3.4.1.1.1.1. Copper Fins

The interfaces between the lead and stainless steel shells of the cask wall are subject to large dimensional changes due to the different thermal expansion rates of these two materials. To

provide good thermal communication across these surfaces, copper fins were welded to both shells. The fins penetrate into the lead region so that both mechanical and metallurgical bonds are formed as the lead is poured into the cask.

The modelling of the cask requires the definition of the effective conductivity of the fins and the surrounding lead. To determine this conductivity, HEATING-5 was used to represent the heat flow through a typical section of lead and stainless steel that included one copper fin. Since the spacing between the copper fins is similar on both shells, one representation of the typical cell is sufficient to determine all of the characteristics of the lead-steel interface.

The model which was employed is shown in Figure 3-26. The geometry was restricted to a two-dimensional representation and the legs of the fin were divided into segments as shown. The total contact area between the lead and copper, as well as the thickness of the fin, was preserved. The effective length was reduced slightly to achieve these desired similarities between the model and the fin. The material properties employed in this representation of the fin are presented in Sections 3.2.1 and 3.2.3.

The process of pouring the lead is not perfect. Therefore, bubbles of air can be trapped under the fin during the pour and shrinkage during the cooling period following the lead pour may also produce a gap between the lead and stainless steel. The geometries considered for air voids are shown in Figure 3-27. HEATING-5 cases were completed to represent the fin with varying widths and thicknesses of the air gap and at several different temperatures.

The temperature profiles in this section of the lead and steel shell are presented in Figures 3-28, 3-29, and 3-30 for cases with no air gap, air gap only under the fin, and complete air

gap, respectively. The temperature distributions provide the data that is necessary to determine an effective thermal conductivity for the lead region which includes the copper fin. The effective thermal conductivity is defined as the ratio of the heat flux to the temperature gradient across the fin region. In equation form this is expressed as:

$$k = \frac{q/A}{dT/dx} \quad \text{or} \quad k = \frac{q/A}{\Delta T/t}$$

where:

- k is the effective thermal conductivity in BTU/hr-in-^{o}F
- q/A is the heat flux passing through the lead in BTU/hr-in^2
- ΔT is the temperature difference across the lead containing the fin in ^{o}F
- t is the thickness of the lead containing the fin in inches

The effective thermal conductivity of the fin, lead, and any air gap is presented in Figures 3-31, 3-32, and 3-33 as functions of temperature, air gap thickness, and air gap width, respectively. The effective thermal conductivity representing the case where an air gap exists only under the fin will be used to represent the interface between the lead and the inner shell throughout this analysis. The cases with a complete air gap will be utilized to represent the interface at the outer shell. This conservative approach assumes that the separation of the lead and steel is complete where thermal expansion would cause the most separation and assumes the contraction could only induce lead-steel contact between the fins. The temperature dependence of the thermal conductivities for these two cases is presented in Figures 3-34 and 3-35 where the scales are expanded to illustrate the detail characteristics of these functions and straight line segments are

employed to duplicate the linear interpolation in HEATING-5.

3.4.1.1.2. Upper Impact Limiter and Closure Plug

The upper impact limiter is bolted directly to the closure plug which is bolted to the cask body. The joint between the plug and the cask body incorporates a double O-ring seal. The combination of the upper impact limiter and closure plug is the next section of the cask to be analyzed.

The geometry of the upper impact limiter and closure plug is shown in Figure 3-36. The wood that is contained in the upper impact limiter is not included in the model because of its low thermal conductivity. The epoxy and fiberglass cloth which are present between the wood were not modelled for the same reason. The elimination of these materials is conservative because any heat flowing through them will reduce the temperatures in the stainless steel shell. The tubes that accept the bolts that fasten the imact limiter to the closure plug have been represented by square channels in the r, θ, z coordinate system.

3.4.1.1.3. Cask Wall with Upper Cowl

The upper cowl was modelled two dimensionally. This piece is only five inches long and contains fiberglass cloth to prevent air from circulating in the region adjacent to the cask wall. The model includes a portion of the upper end casting and is adjacent to the impact limiter. In the actual cask, the upper cowling region contains gusset plates in the cowling. The fiberglass cloth is interspersed between these gussets and fills the entire air space of the region. Because of the fiberglass

cloth, very little heat flows through this section. A two dimensional model is sufficient to represent this segment of the cask since there is a negligible difference in the quantity of heat ejected by the cask if the gusset plates are eliminated from the model. The geometry of this section is shown in Figure 3-37.

3.4.1.1.4. Expansion Tank

The fourth section of the cask is the expansion tank and the adjacent portion of the cask wall. The geometry of this section is shown in Figure 3-38 where the tanks and cask wall are separated for clarity. The modelling included the antisplash baffles inside the expansion tank but excluded the contents of the tank. The tank will contain the air and the excess water and ethylene glycol solution that cannot be accommodated in the shield tank. This liquid will be resting on the lower surfaces of the tank between baffles. However, its position cannot be defined. Consequently the liquid was not included in the model to assure that the results are conservative by eliminating this indefinable path for heat flow to the outer surfaces of the cask.

3.4.1.1.5. Cask Wall with Lower Cowl

The fifth section of the cask is the portion where the lower cowl meets the shield tank. The geometry of this region is shown in Figure 3-39. The air region above the shell serves as an insulator so that heat cannot easily escape from this portion of the cask. Unlike the upper cowl region, there are no gusset plates present in this segment of the cask. The air space above the cask wall has again been filled with fiberglass cloth. Natural circulation of air will not occur due to the presence of the fiberglass cloth.

3.4.1.1.6. Cask Wall with Lead Void

A portion of the cask includes an air region in the lead. This void allows for the expansion of the lead during the fire and serves as an insulator which hampers the heat flow through these segments. This segment is modelled as the sixth axial piece of the cask. Its geometry is shown in Figure 3-40. The air region in the cowl portion is again filled with fiberglass cloth so that no air circulation takes place.

3.4.1.1.7. Lower Impact Limiter

The final section of the cask is the lower impact limiter including the lower end casting, trunion supports, and impact limiter shell. The geometry of this section is shown in Figure 3-41. It is quite complicated because of the configuration of the lower end casting. The truncated conical portion of the casting was represented as a cylinder with the diameter of the smallest portion of the truncated cone. The woods and air in the cavities of the impact limiter were not included in the model to assure conservatism by excluding these minor heat flow paths.

3.4.1.1.8. R-Z Cask Model

When each of these sections is joined, a complete model of the cask is created. Each of these sections has an effective thermal conductivity which was used in the creation of the r-z model of the cask.

The effective thermal conductivity of the various regions was calculated separately by assuming radial one dimensional heat flow

through each of the seven regions. The difference between the cavity and external surface temperatures were used to calculate an effective k. This thermal conductivity was changed until the inner and surface temperatures matched those which were calculated in the more realistic two and three dimensional models. The temperature distribution in the one dimensional segment was not compared with the more complex model since only the difference between the cavity and outer temperatures are important in calculating the effective thermal conductivity.

The assumption that is implicit in this modelling technique is the omission of the azimuthal heat transfer between modelled sections. This heat transfer has been included in the calculation of the effective thermal conductivities for each section and implicitly included in the entire model. Thus all three dimensional heat transfer possibilities have been included in the r-z model utilized to determine the heat transfer characteristics of the cask.

3.4.2. Maximum Temperature

The thermal model requires the bulk water temperature in the cavity to be the same in all seven segments of the cask and the sum of the heat transported to the environment in each segment to be 11.5 kW when the ambient temperature is 130°F. The calculation of the heat flow within each segment is based upon a cavity surface temperature that is constant over the contact surface between the cask wall and the water. The temperature difference between the cask wall and the bulk water temperature has been determined from the correlated heat transfer coefficient in natural circulation in water presented in Section 3.2.2 and Figure 3-10. The temperature difference between the cask wall and the bulk fluid temperature in the region adjacent to the shield tanks is 6°F when the decay heat load is 11.5 kW. Similarly, the

temperature difference adjacent to the expansion tank is only 3°F.

The temperature profiles in the cask when the ambient temperature is 130°F is presented in Figure 3-42. The radial and angular dependence of the temperatures at the center of the cask are presented in Figures 3-43 and 3-44, respectively, to provide increased definition of the temperature distribution. Radial temperature profiles are presented at the top, middle and bottom of the cask where gusset plates traverse the shield tanks. Profiles are also presented at the middle of the upper and lower shield tanks. The angular temperature profiles are depicted for the inside surface of the inner shell and the outer surfaces of the outer shell and shield tank.

The temperatures at the locations of each of the mechanical seals are presented in Table 3-6 for the 130°F ambient temperatures. Table 3-6 also includes the allowable temperatures for each of the components. The calculated temperatures are all below the allowable component temperatures so no component failures are anticipated due to overheating.

3.4.3. Minimum Temperatures

The minimum temperatures in the cask can occur during either of two modes of operation. If the cavity is completely drained prior to the initiation of the shipment, the minimum temperatures will approach the ambient temperature. However, if the cavity contains water during the shipment, the decay heat load must be limited to values which will prevent freezing of the water in the cavity. Freezing, in this instance, is defined as a wall temperature of 32°F which will preclude the formation of any ice film adjacent to the cask wall. The decay heat load that results in a cavity surface temperature of 32°F when the ambient

temperature is -40°F is 3.11 kW. The temperature profiles in the cask for this case is presented in Figure 3-45. The radial and angular dependence of the temperature distributions are presented in Figures 3-46 and 3-47, respectively. The temperatures at each of the mechanical seals are presented in Table 3-7.

3.4.4. Maximum Internal Pressure

The expansion of the water in the cavity as the temperatures increase will increase the pressure within the cavity. The relationship between the steady state pressure and temperature was developed in Section 3.2.6. The bulk water temperature is 318°F when the decay heat load is 11.5 kW and the ambient temperature is 130°F. The resulting cavity pressure is 118 psia. The rated pressures of each of the cavity seals is presented in Table 3-8 and this cavity pressure is substantially below any of the failure pressures.

3.4.5. Maximum Thermal Stresses

The maximum thermal stresses have been determined in section 2 (structural analysis) based on the temperatures derived from the model discussed in section 3.4.1. Table 3-9 and Figures 3-48 and 3-49 summarize the results of the anaylses.

3.4.6. Evaluation of Package Performance for Normal Conditions of Transport

The maximum and minimum temperatures of various cask components are shown in Tables 3-6 and 3-7. Temperature variations in the

cask are shown in Figures 3-42 through 3-47. These figures and tables show that the NAC-1 spent fuel shipping cask will safely transport fuel under normal conditions of operation. There will be no loss of containment from the cask during normal operation.

Table 3-6. Maximum Temperatures at Location of the Cavity Seals

Component	Temperature (deg F)
valves	
relief	300
upper vent	290
lower vent	289
upper drain	275
lower drain	271
O-rings	
inner	318
outer	319

Table 3-7. Minimum Temperatures at Location of the Cavity Seals

Component	Temperature (deg F)
valves	
relief	12
upper vent	1
lower vent	1
upper drain	-2
lower drain	-2
O-rings	
inner	32
outer	10

Table 3-8. Rated Pressure of Cavity Seals

Component	Rated Pressure (psig)	Rated Temperature (deg F)
Vent Valves	985	520
Drain Valves	985	520
Rupture Disk	1100	600
Shield Tank Burst Valve	100	316

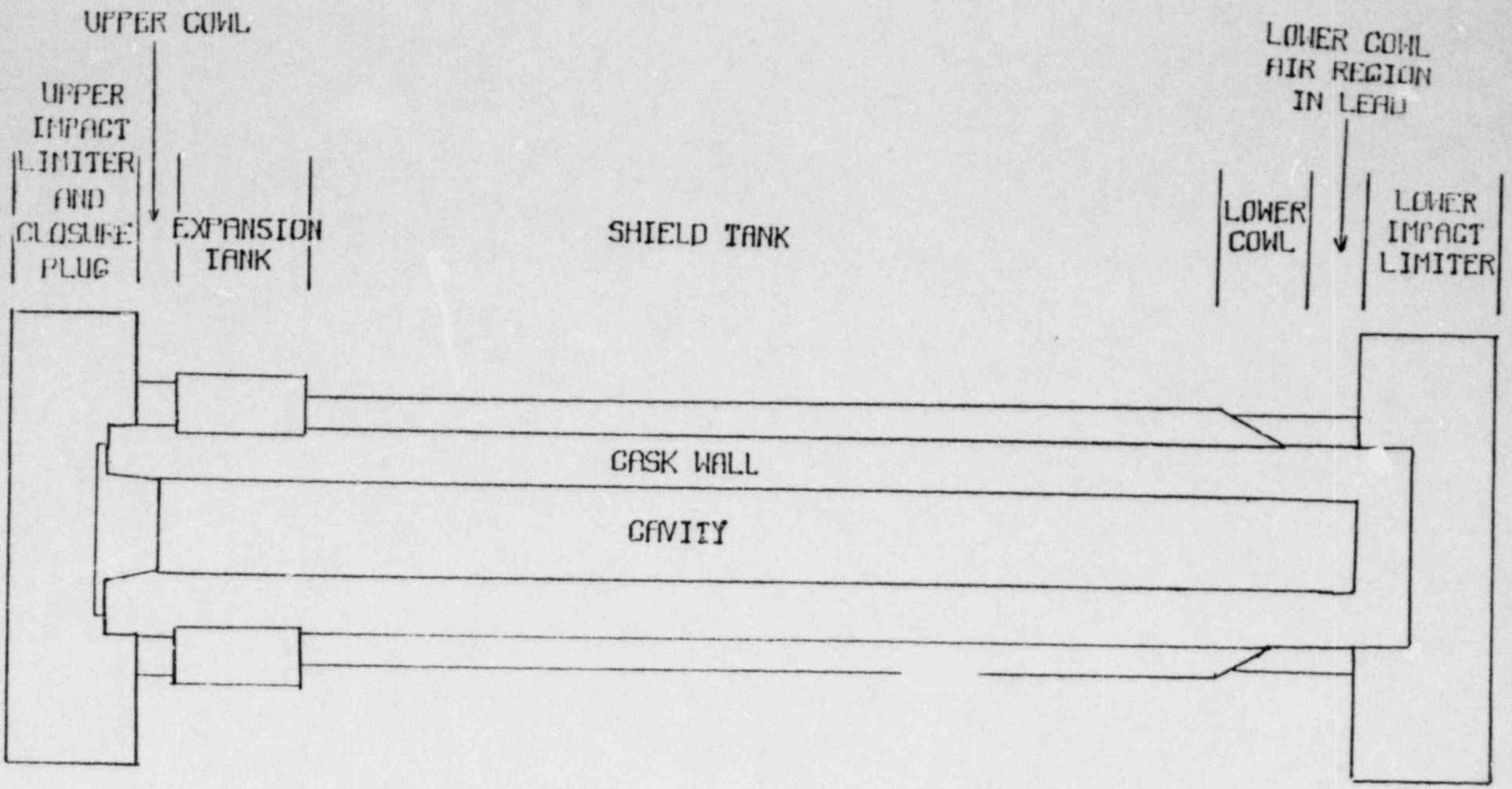

Figure 3-24. Schematic of Thermal Models of NAC-1 Cask

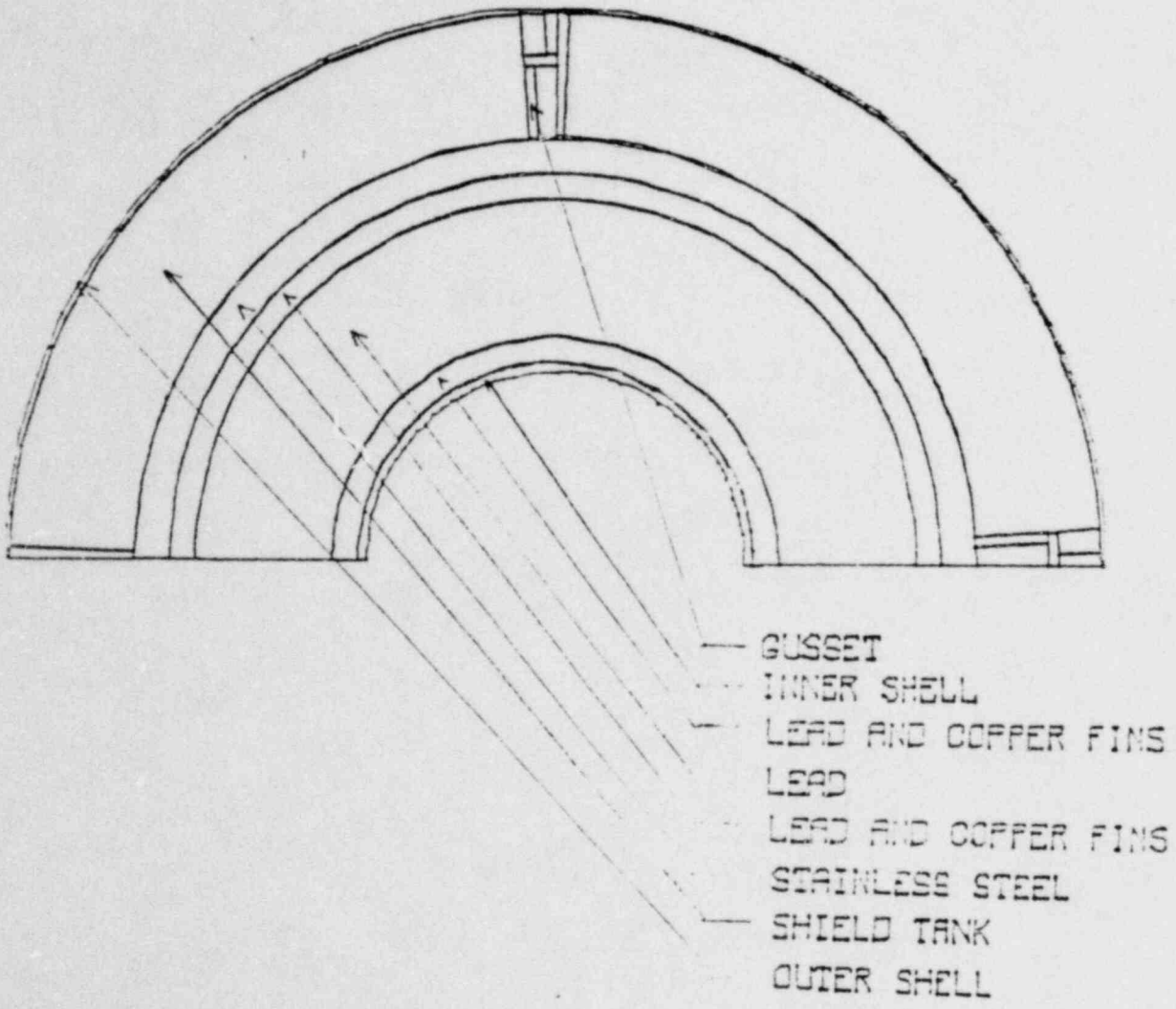

Figure 3-25. Model Geometry of Cask Wall Including Shield Tank

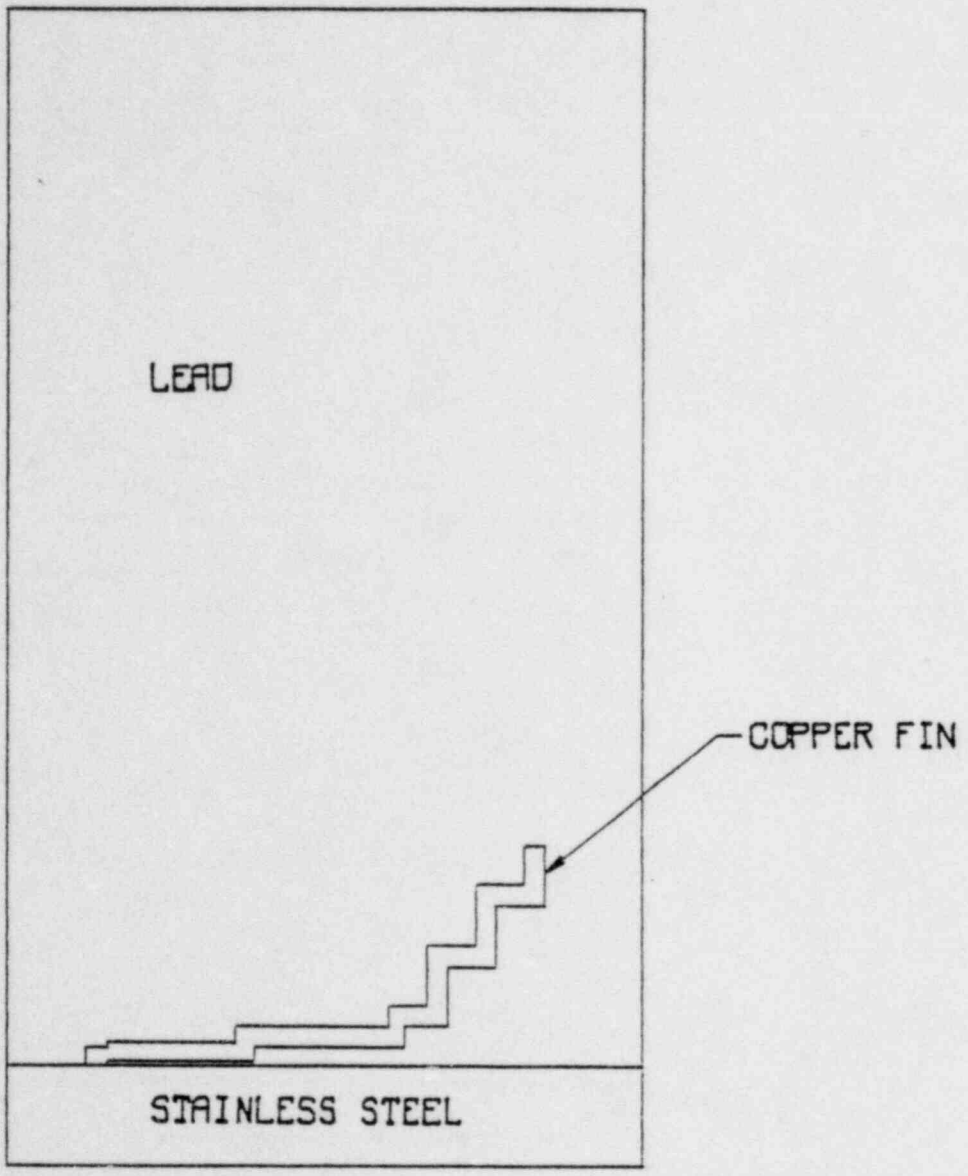

Figure 3-26. Two Dimension Model of Copper Fin

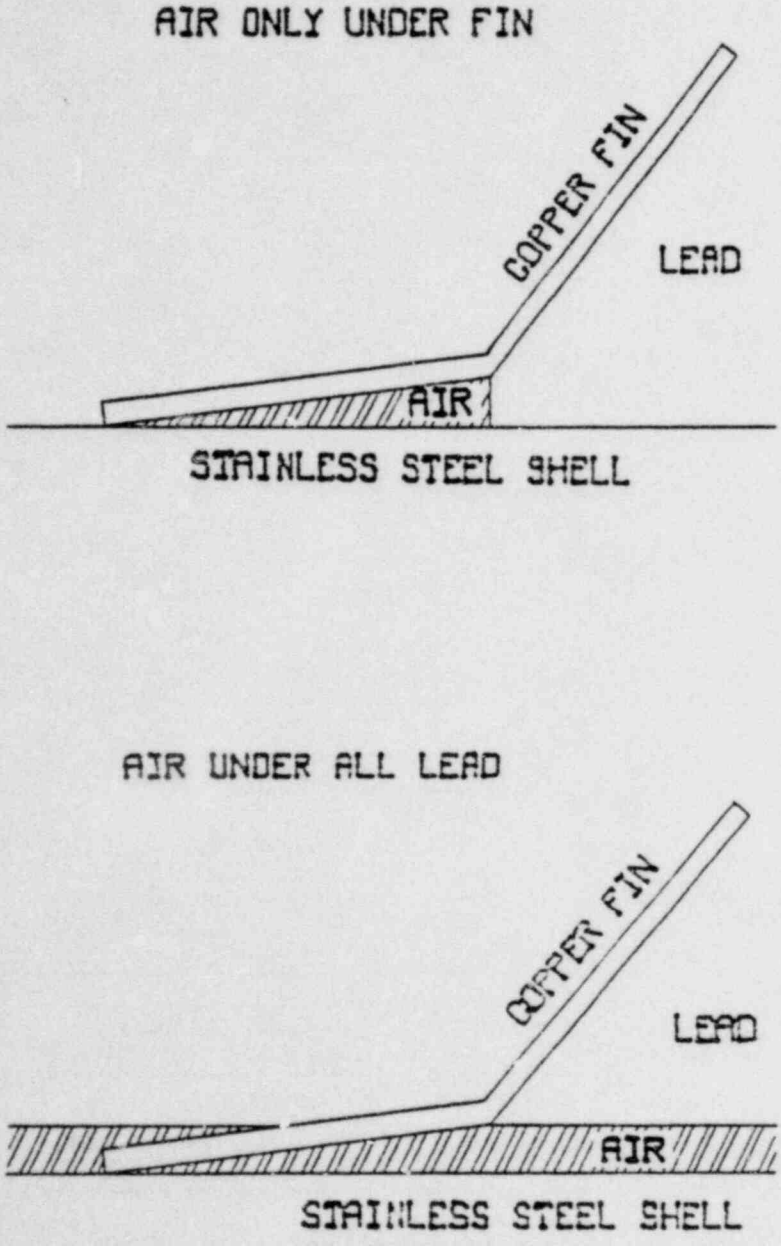

Figure 3-27. Void Geometries Modelled With Heating-5

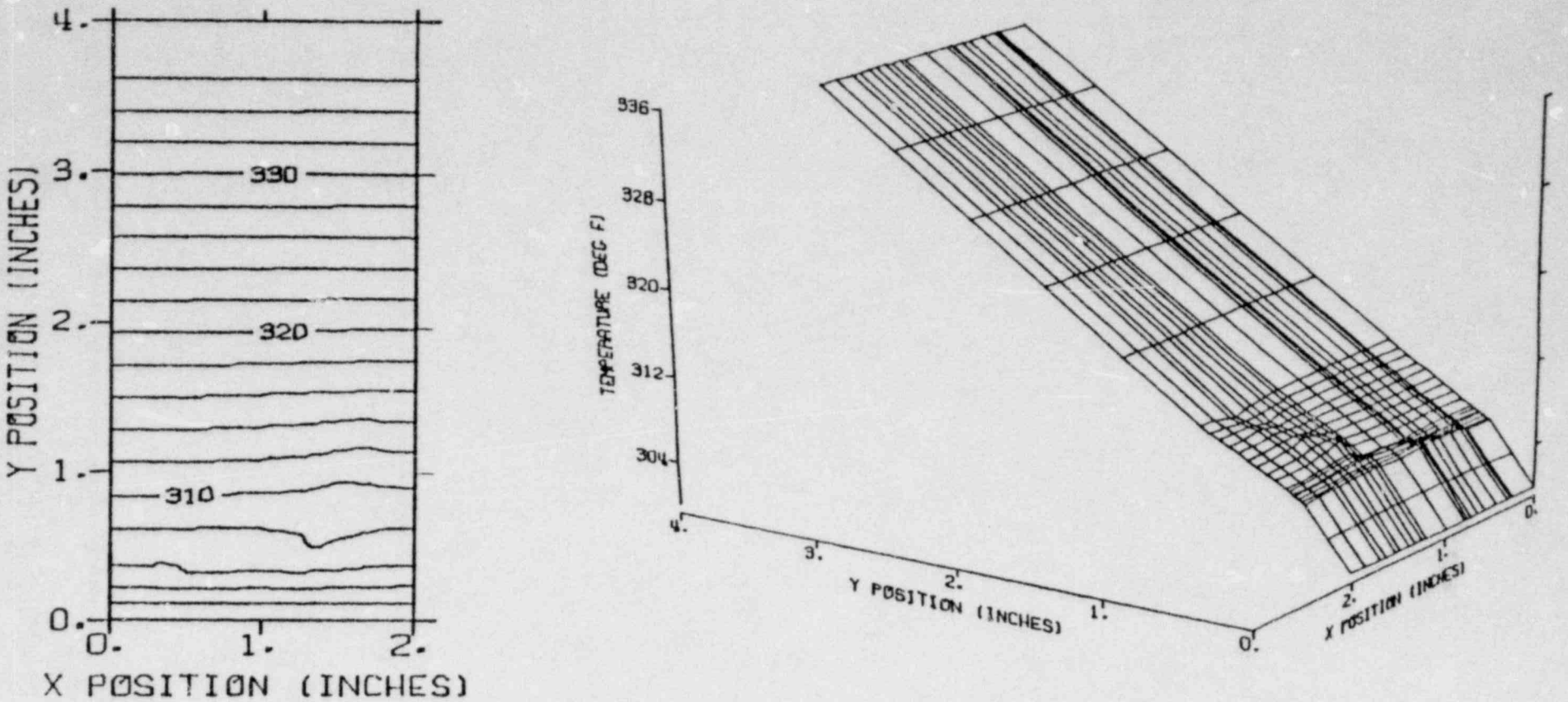

Figure 3-28. Temperature Profiles in Fin Unit Cell With No Air Gap

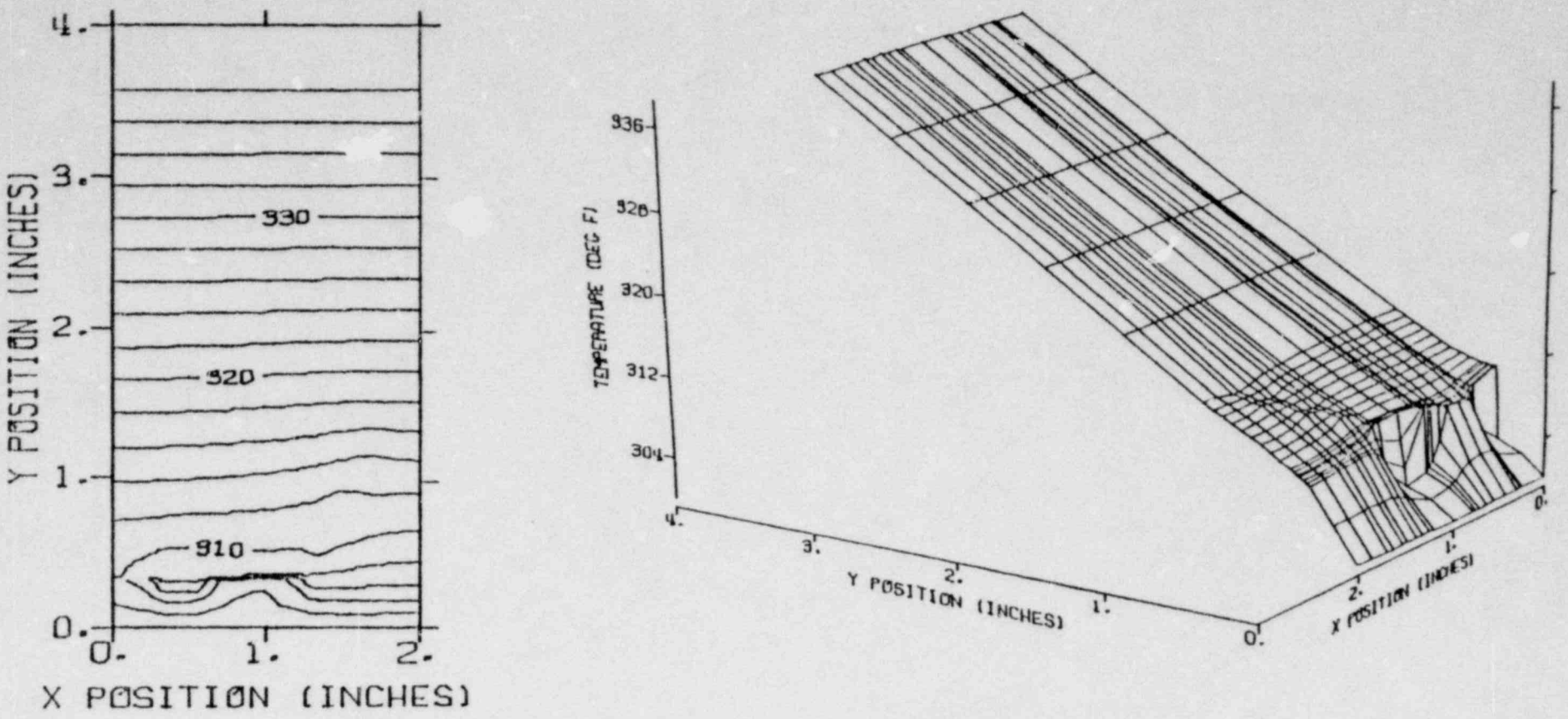

Figure 3-29. Temperature Profiles in Fin Unit Cell With Air Only Under the Fin

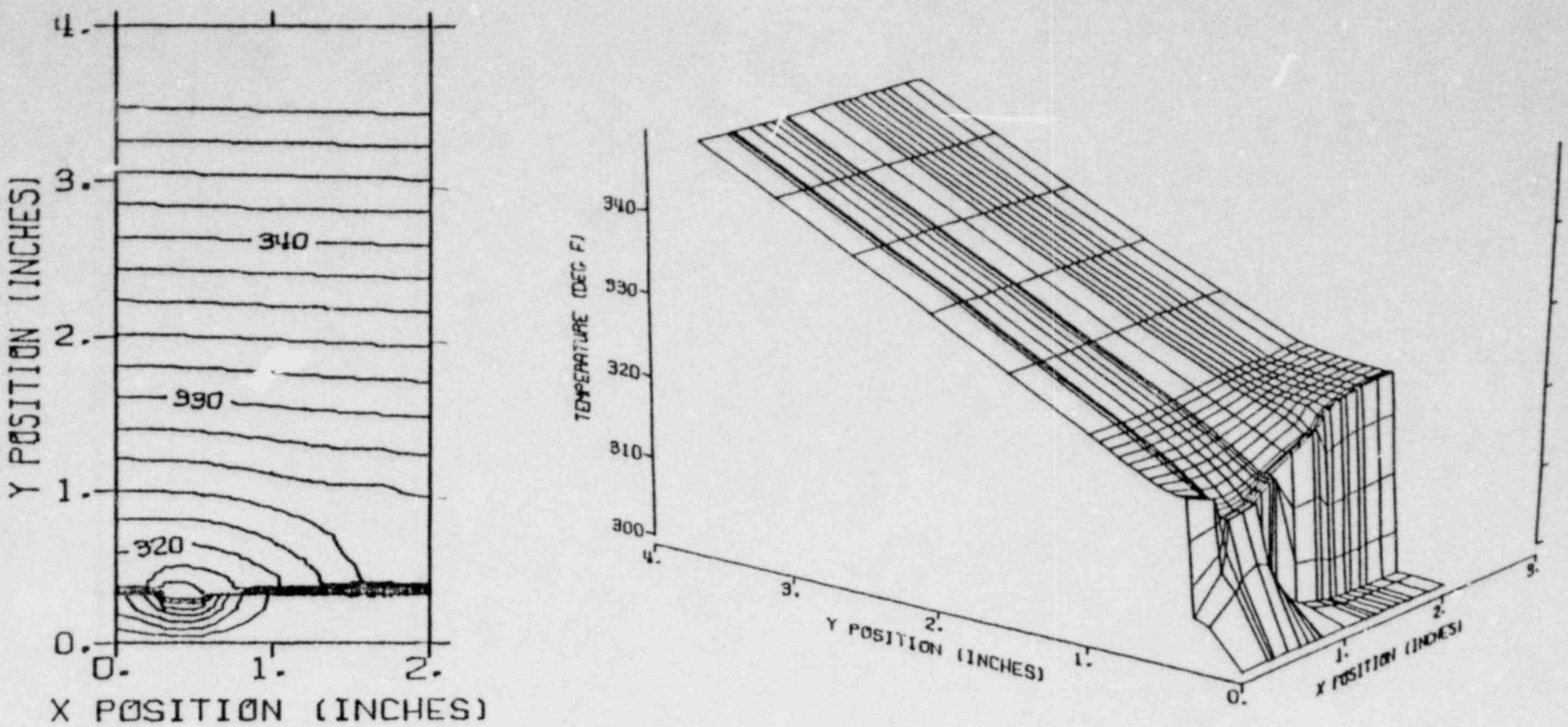

Figure 3-30. Temperature Profiles in Fin Unit Cell With Complete Air Gap

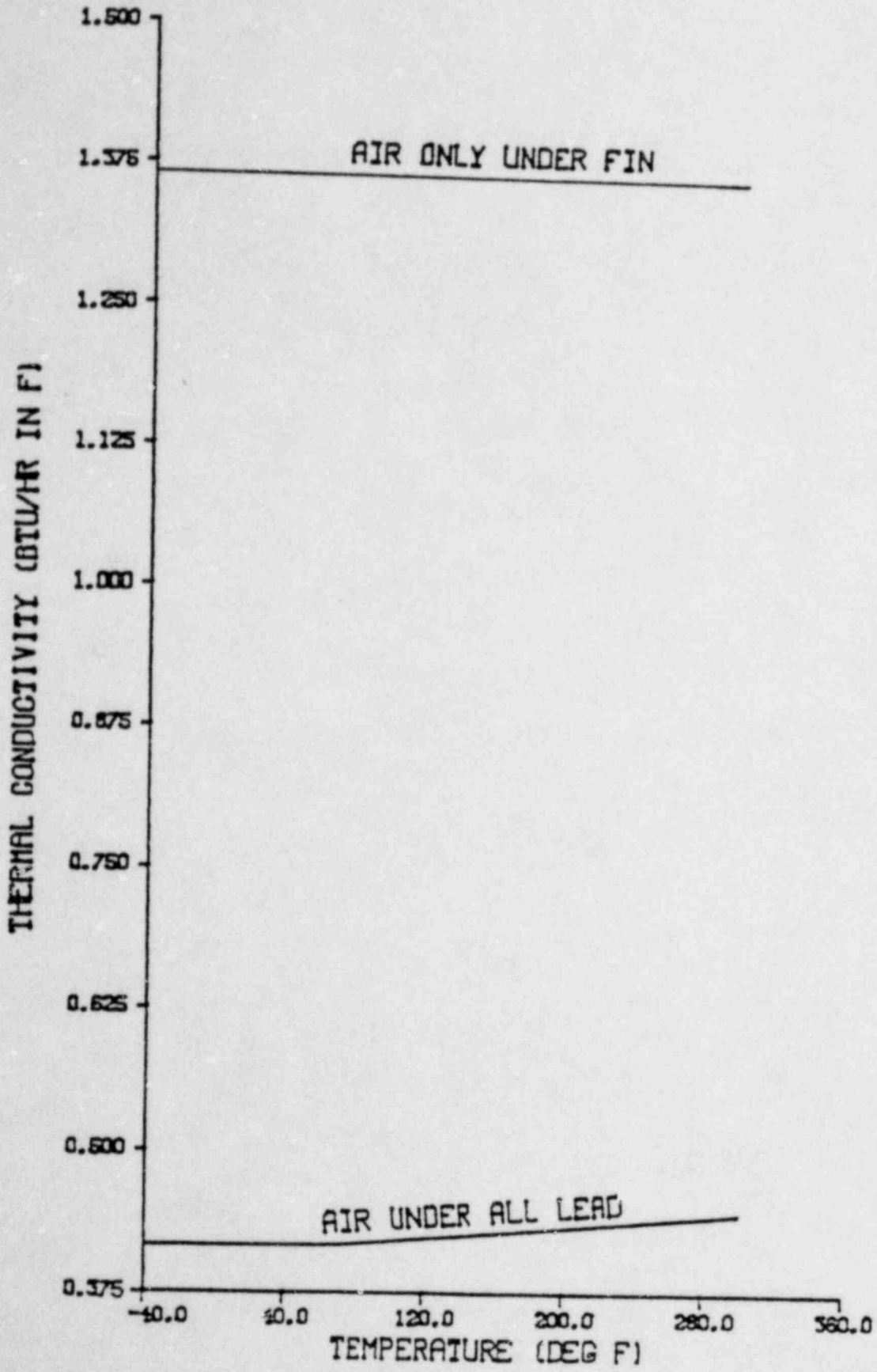

Figure 3-31. Thermal Conductivity of Fin Region as a Function of Temperature

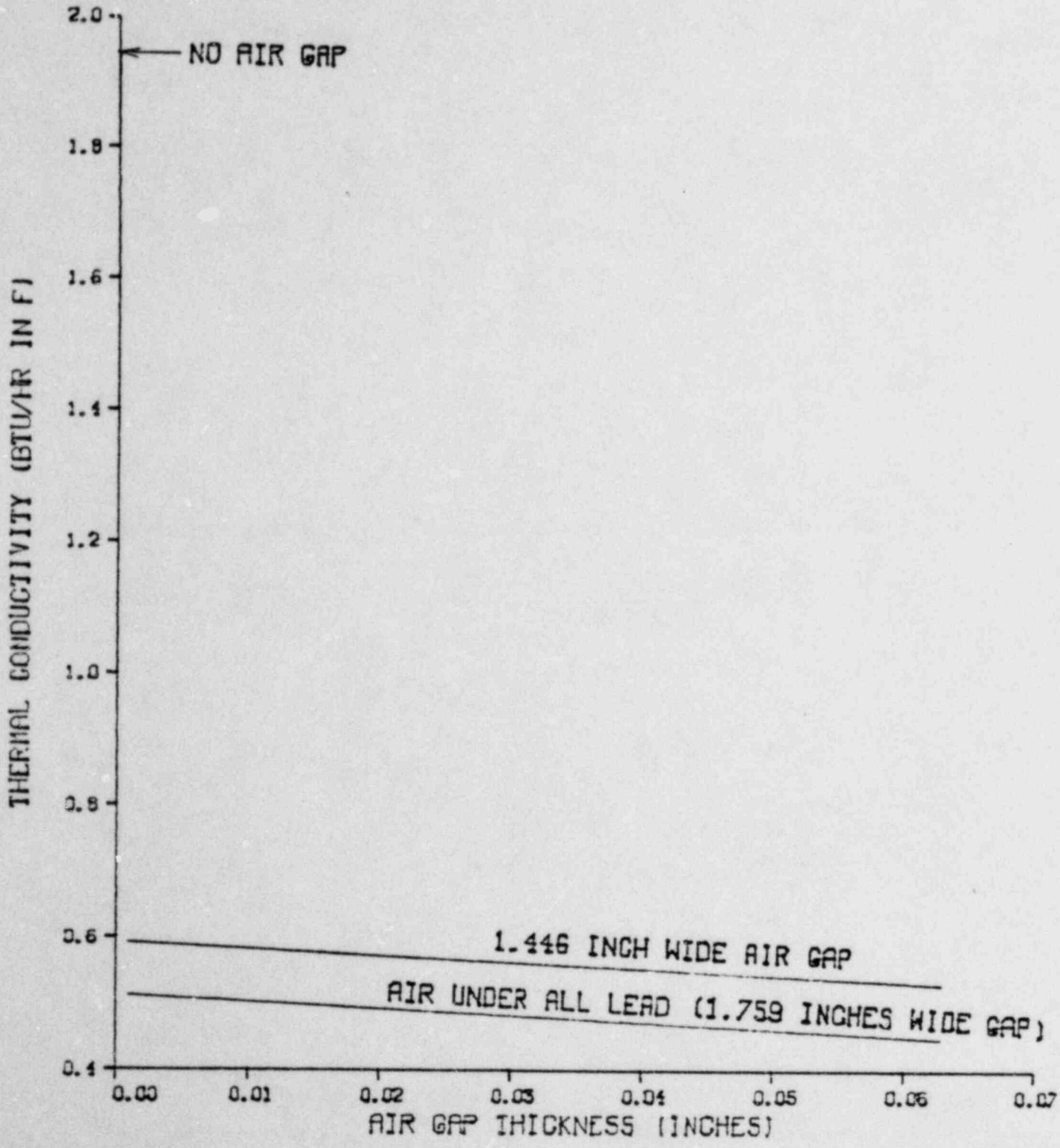

Figure 3-32. Thermal Conductivity of Fin Region as a Function of Air Gap Thickness

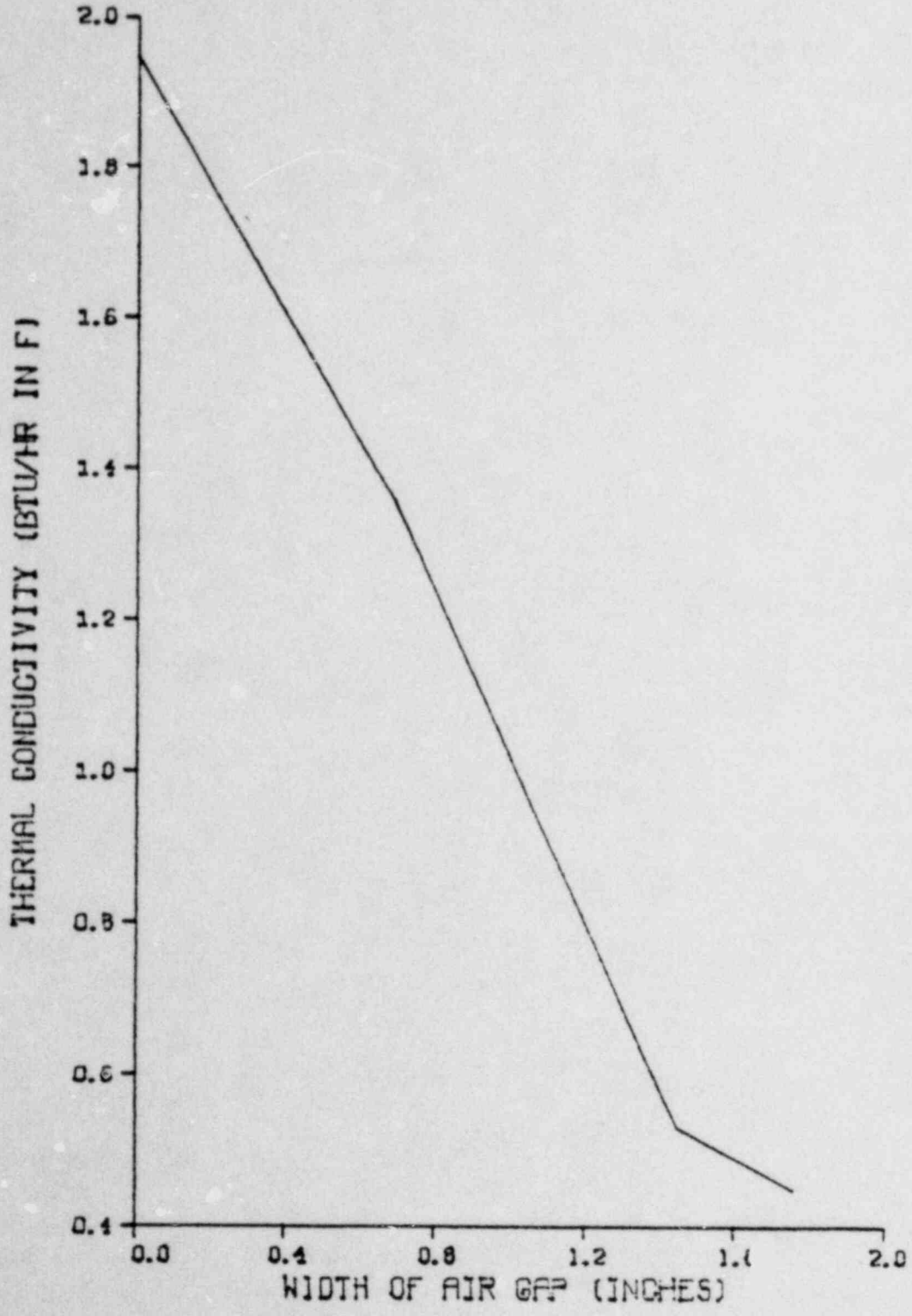

Figure 3-33. Thermal Conductivity of Fin Region as a Function of Width of the Air Gap

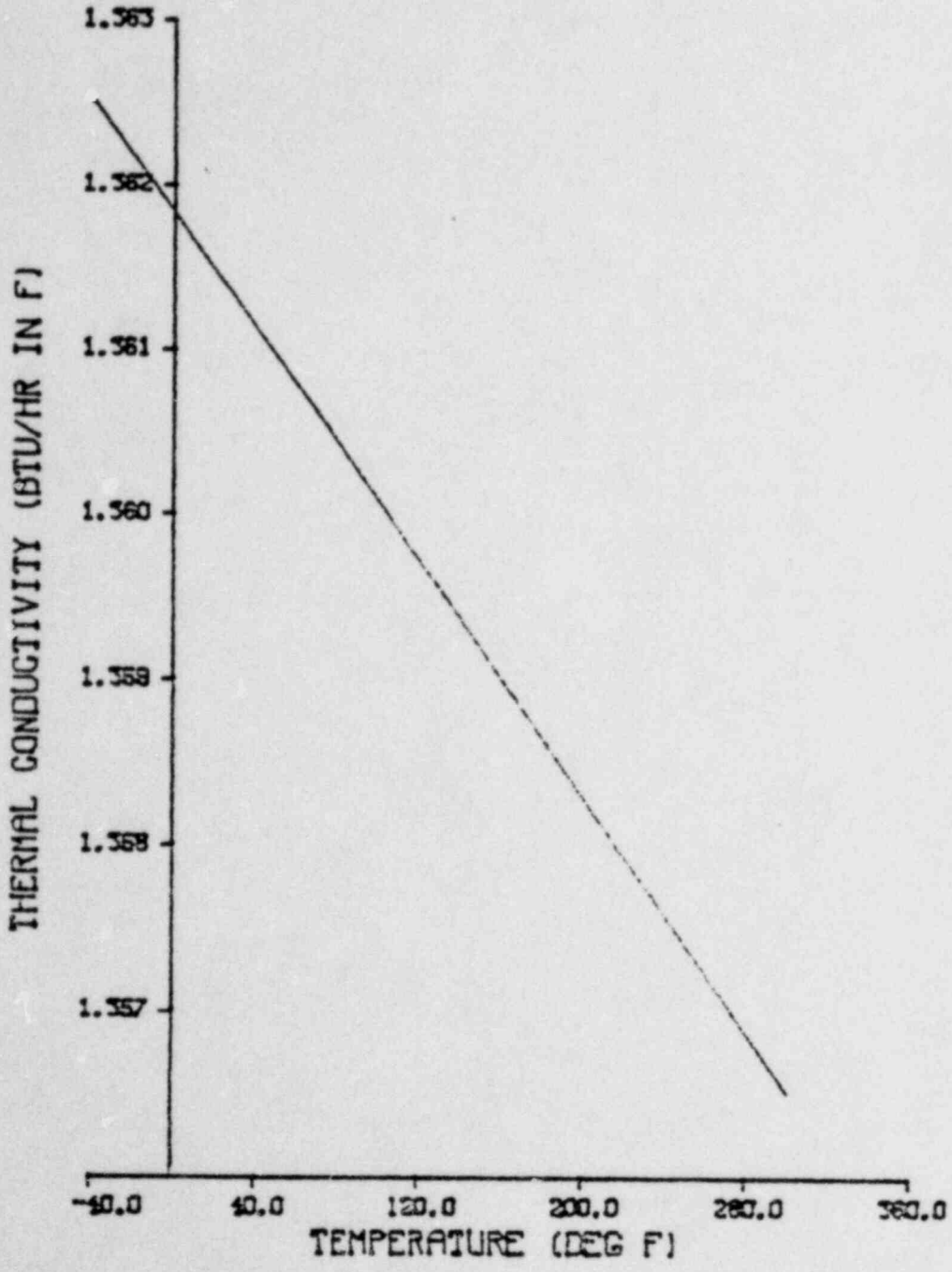

Figure 3-34. Thermal Conductivity of Fin Region at Inner Surface of Lead

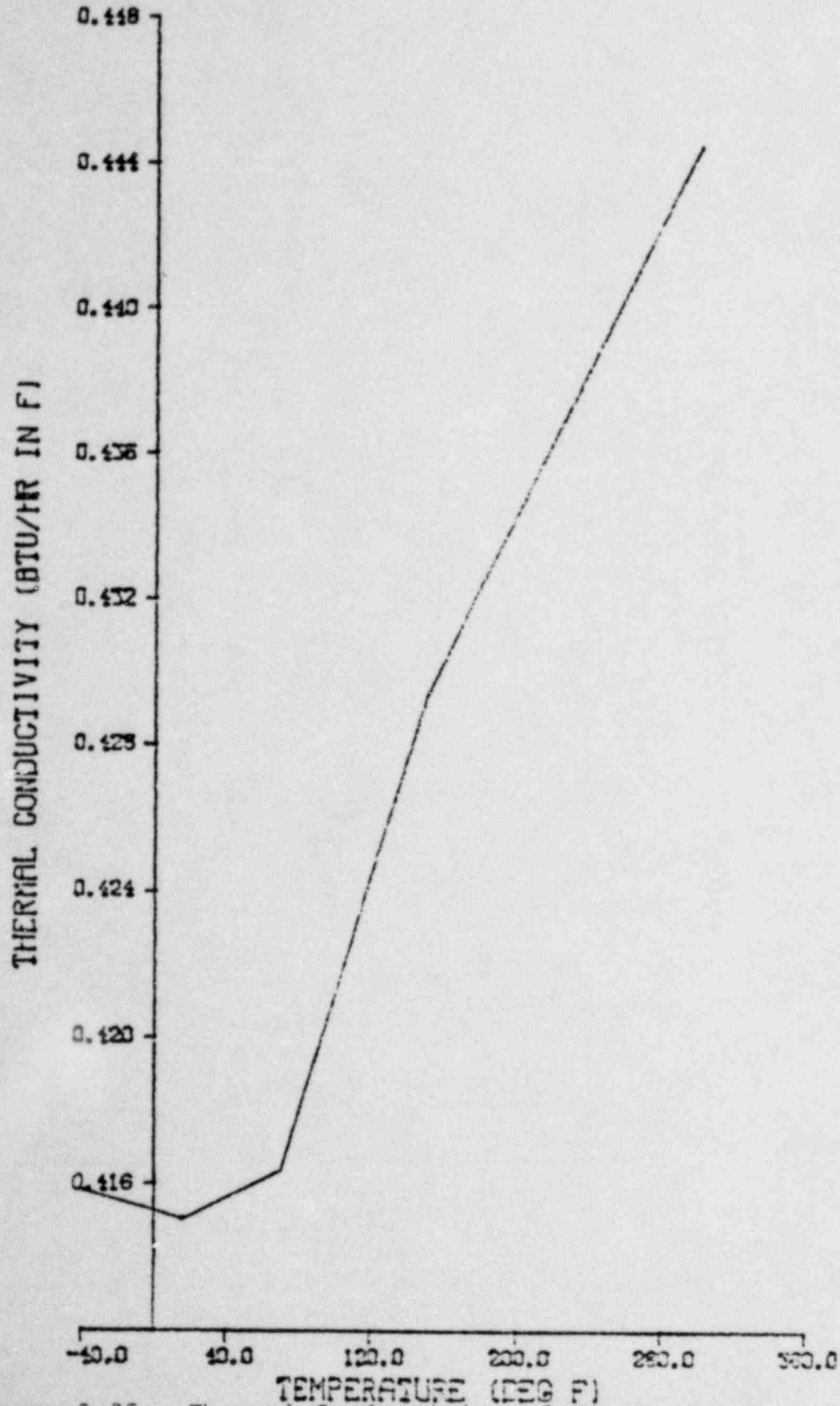

Figure 3-35. Thermal Conductivity of Fin Region at Outer Surface of Lead

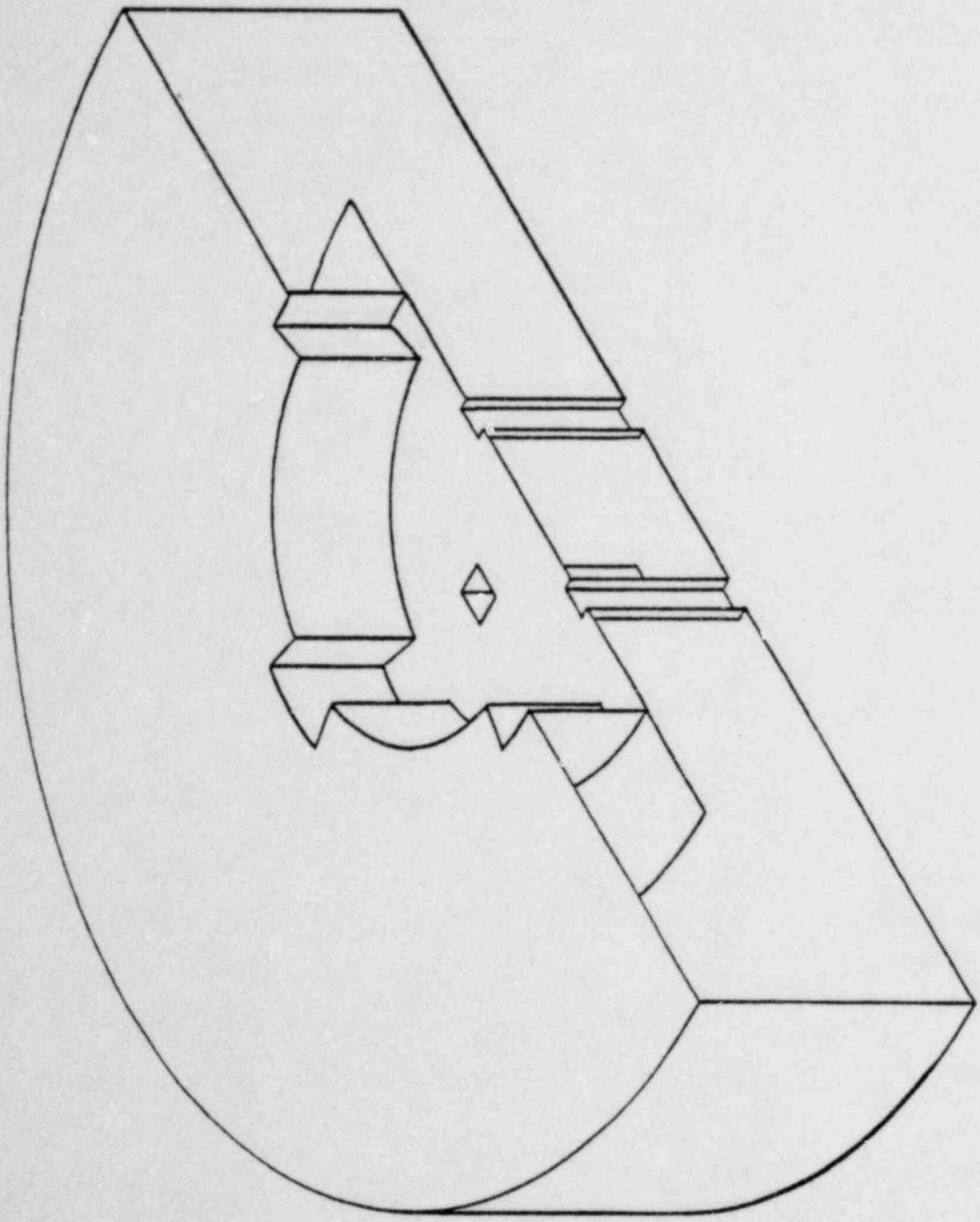

Figure 3-36. Upper Impact Limiter Model Geometry

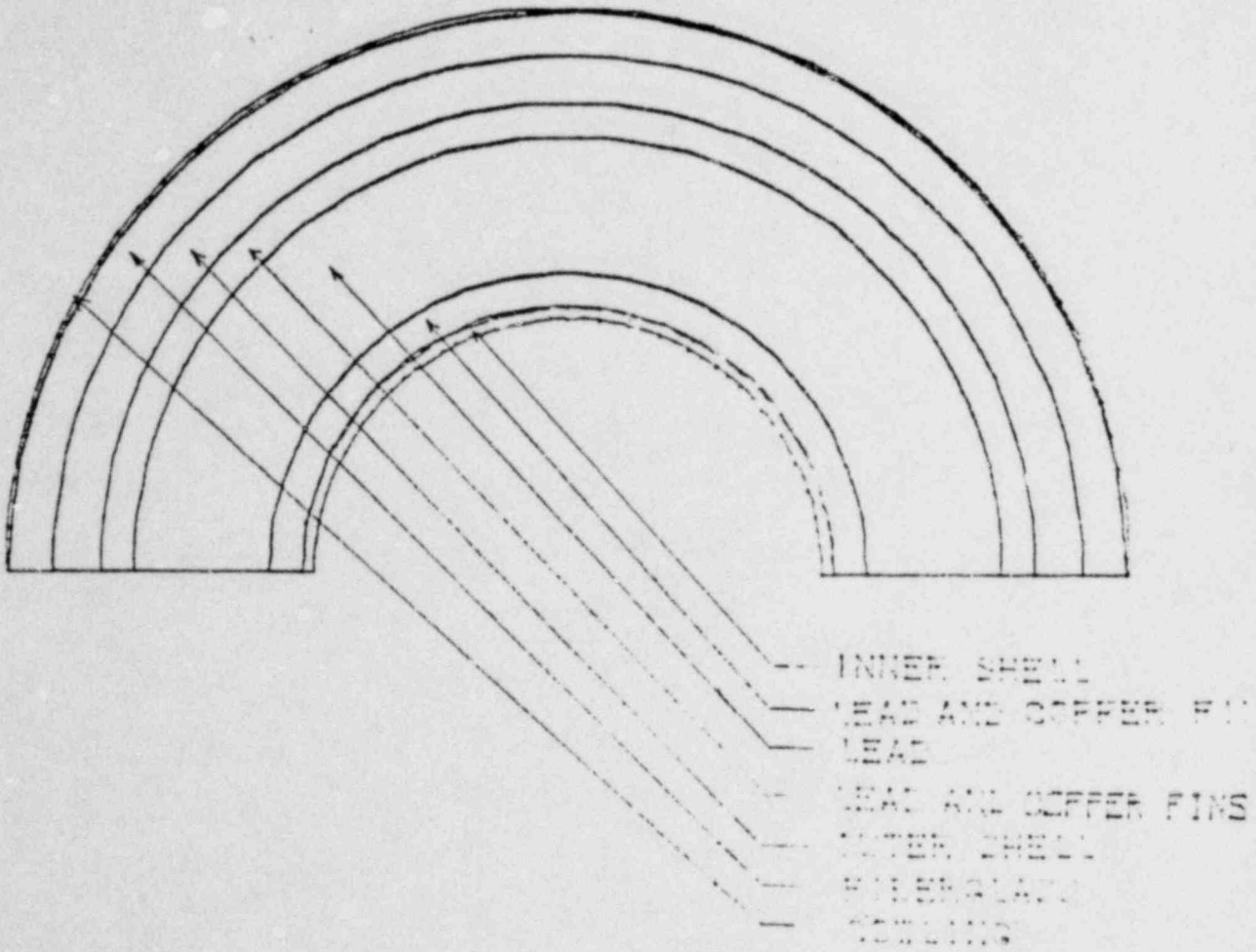

Figure 3-37. Upper Cowling Model Geometry

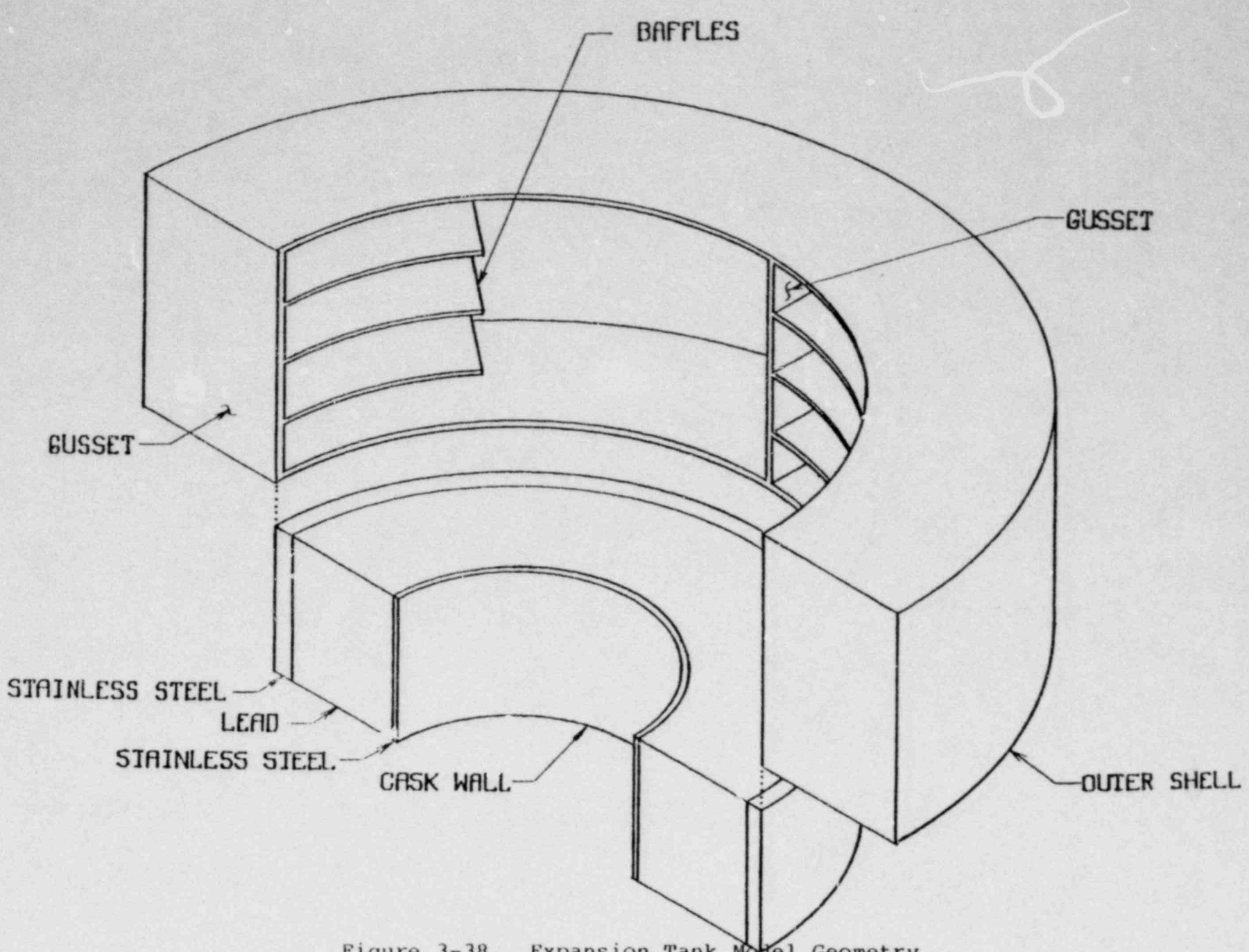

Figure 3-38. Expansion Tank Model Geometry

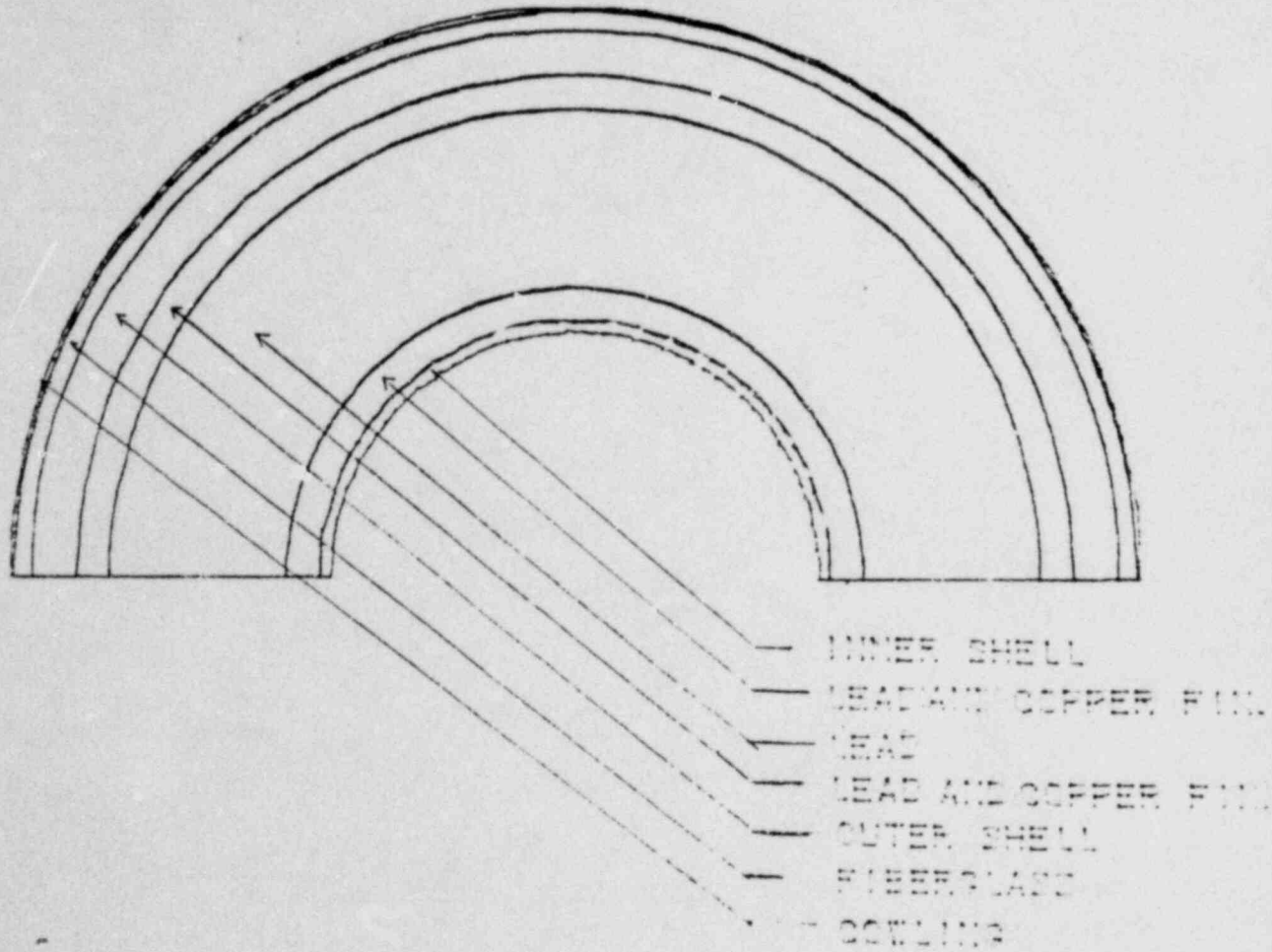

Figure 3-39. Lower Cowling Model Geometry

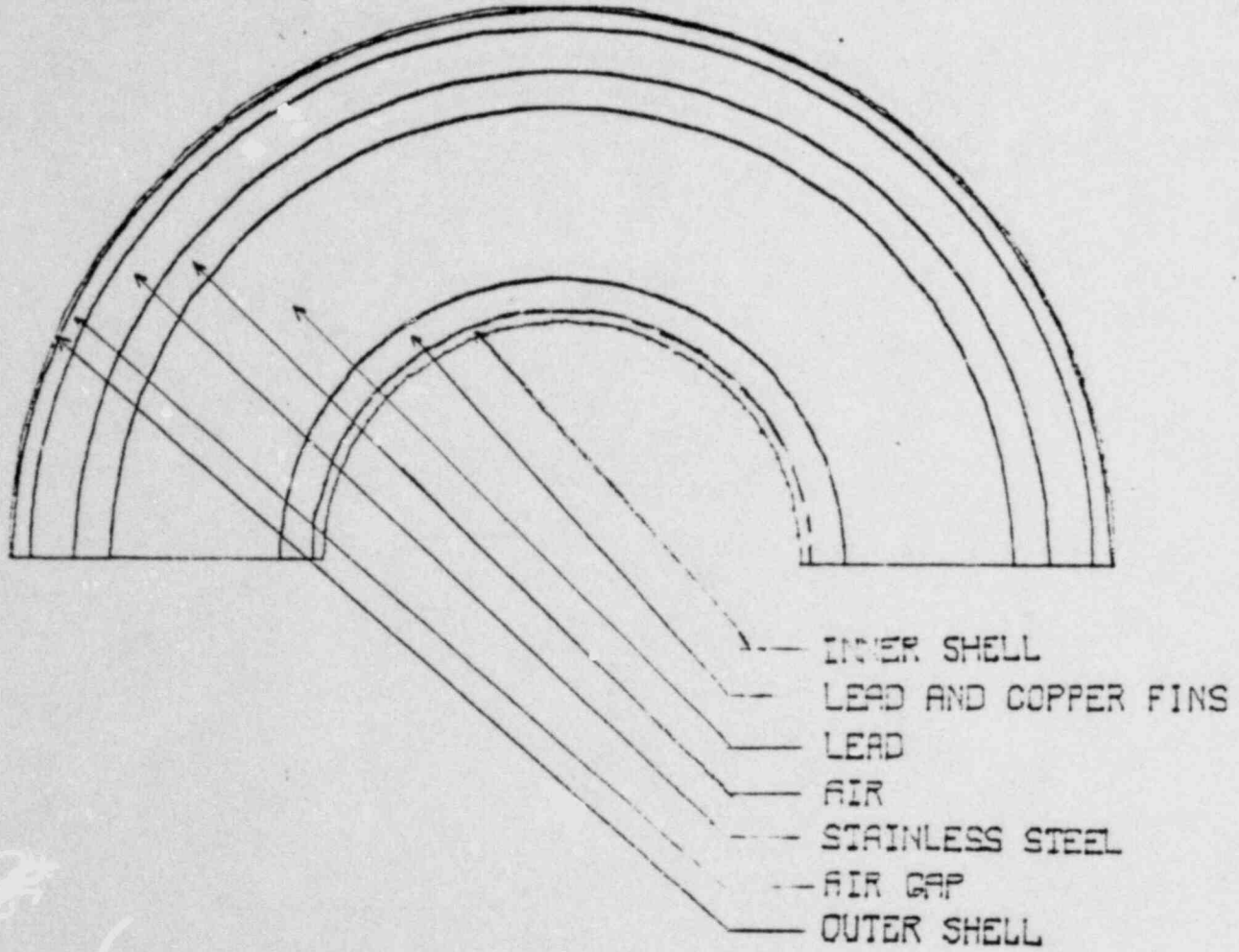

Figure 3-40. Model Geometry of Cask Wall With Air Gap In Lead

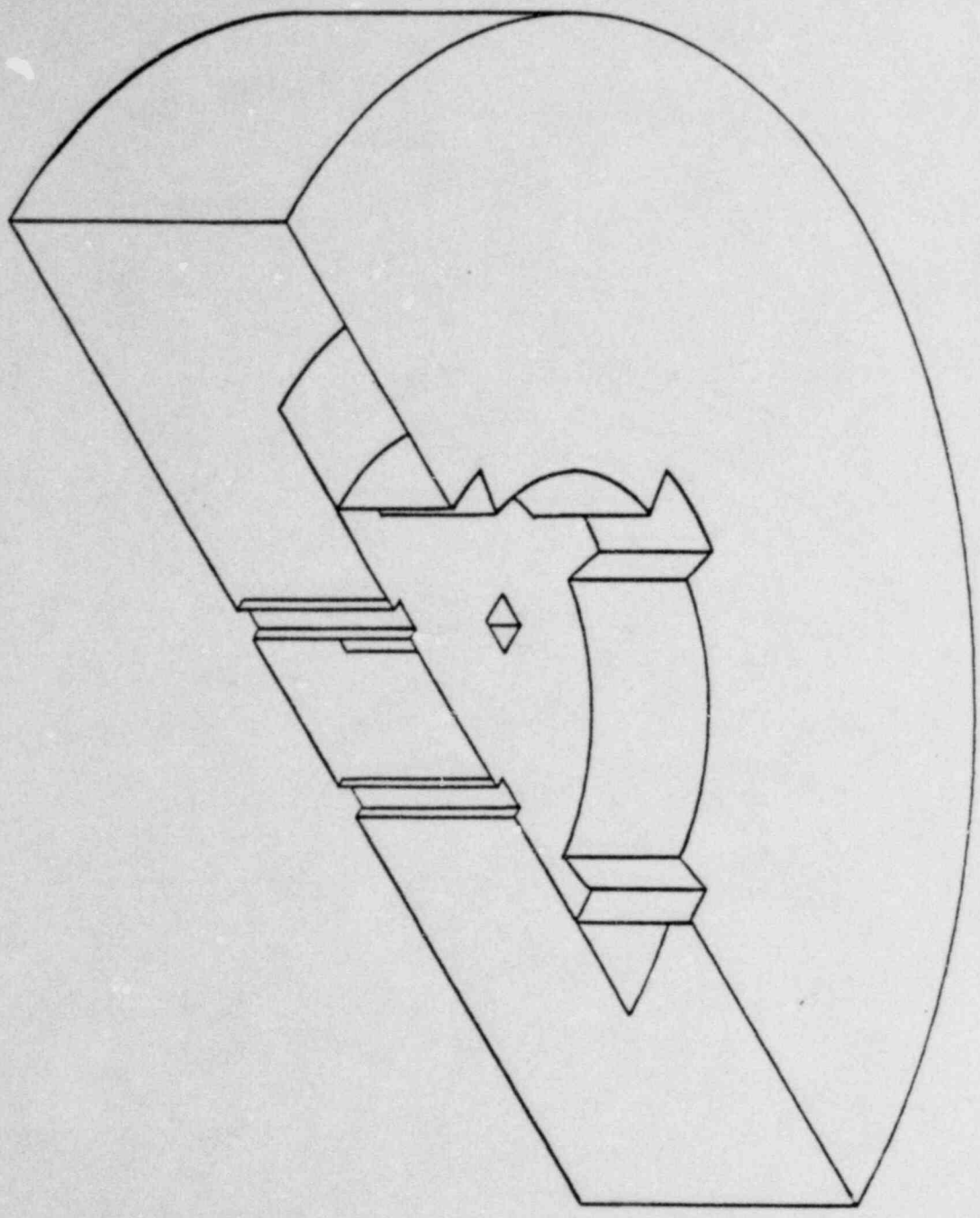

Figure 3-41. Lower Impact Limiter Model Geometry

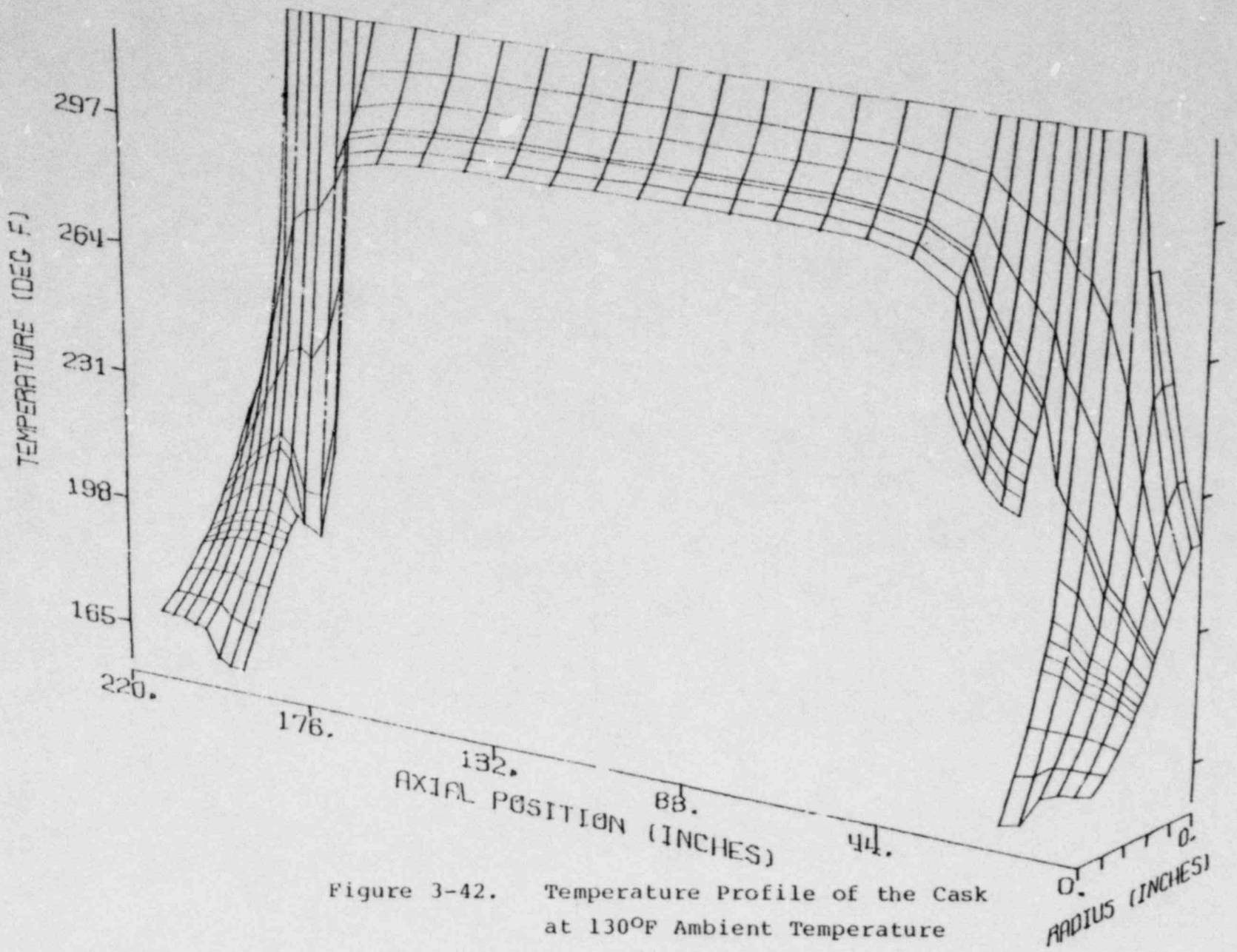

Figure 3-42. Temperature Profile of the Cask at 130°F Ambient Temperature

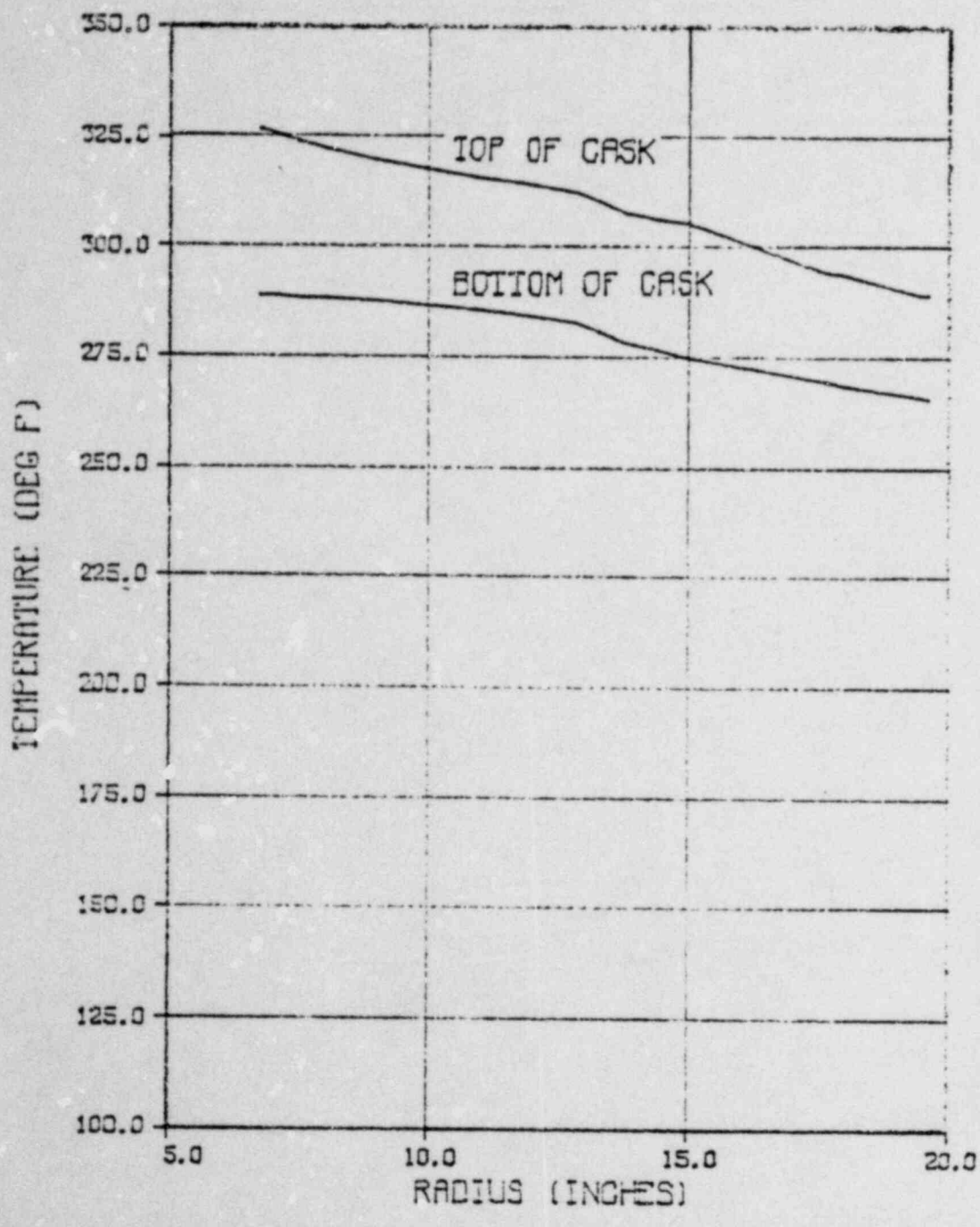

Figure 3-43. Radial Temperature Dependence at Cask Center for 130°F Ambient Temperature

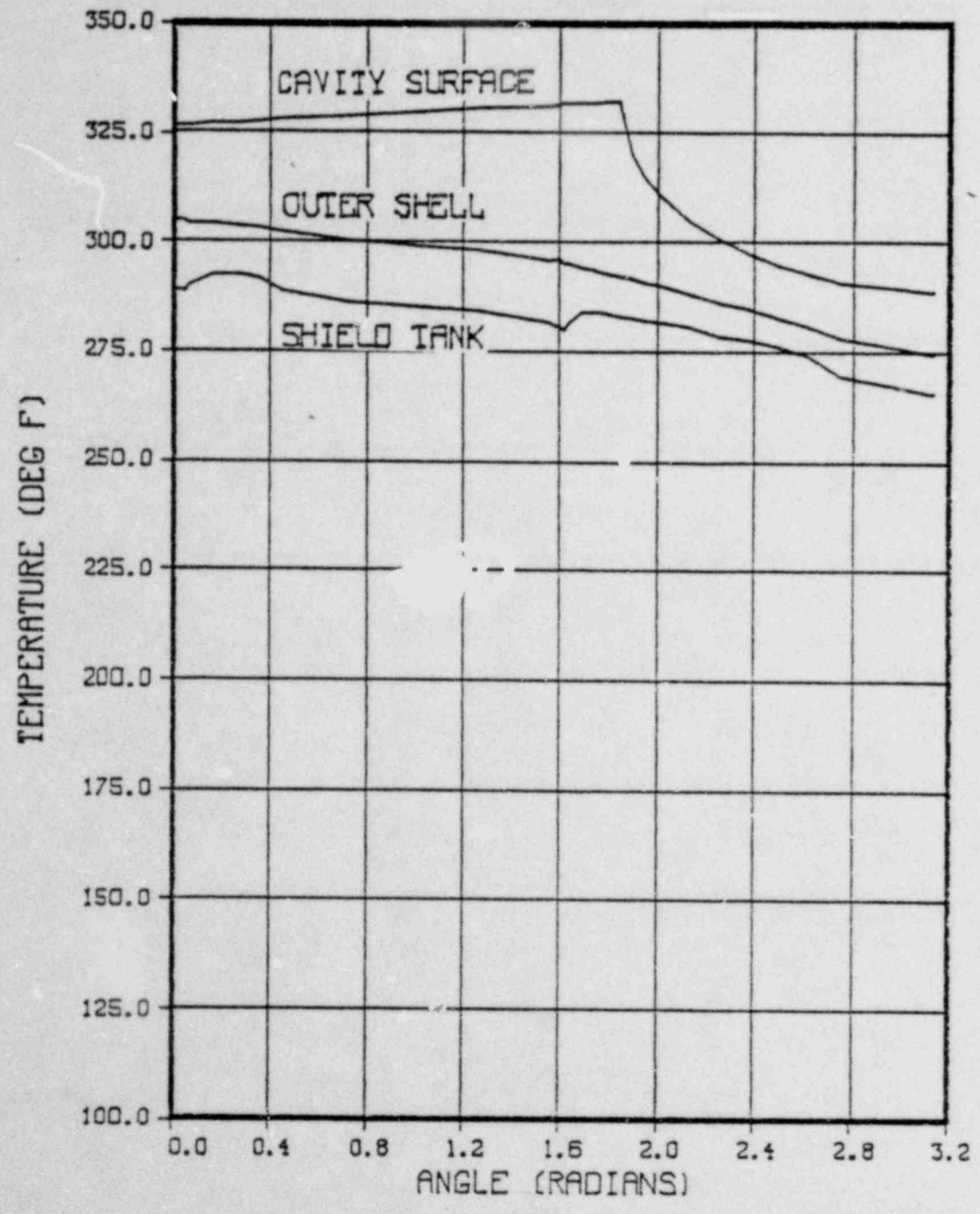

Figure 3-44. Angular Temperature Dependence at Cask Center For 130°F Temperature

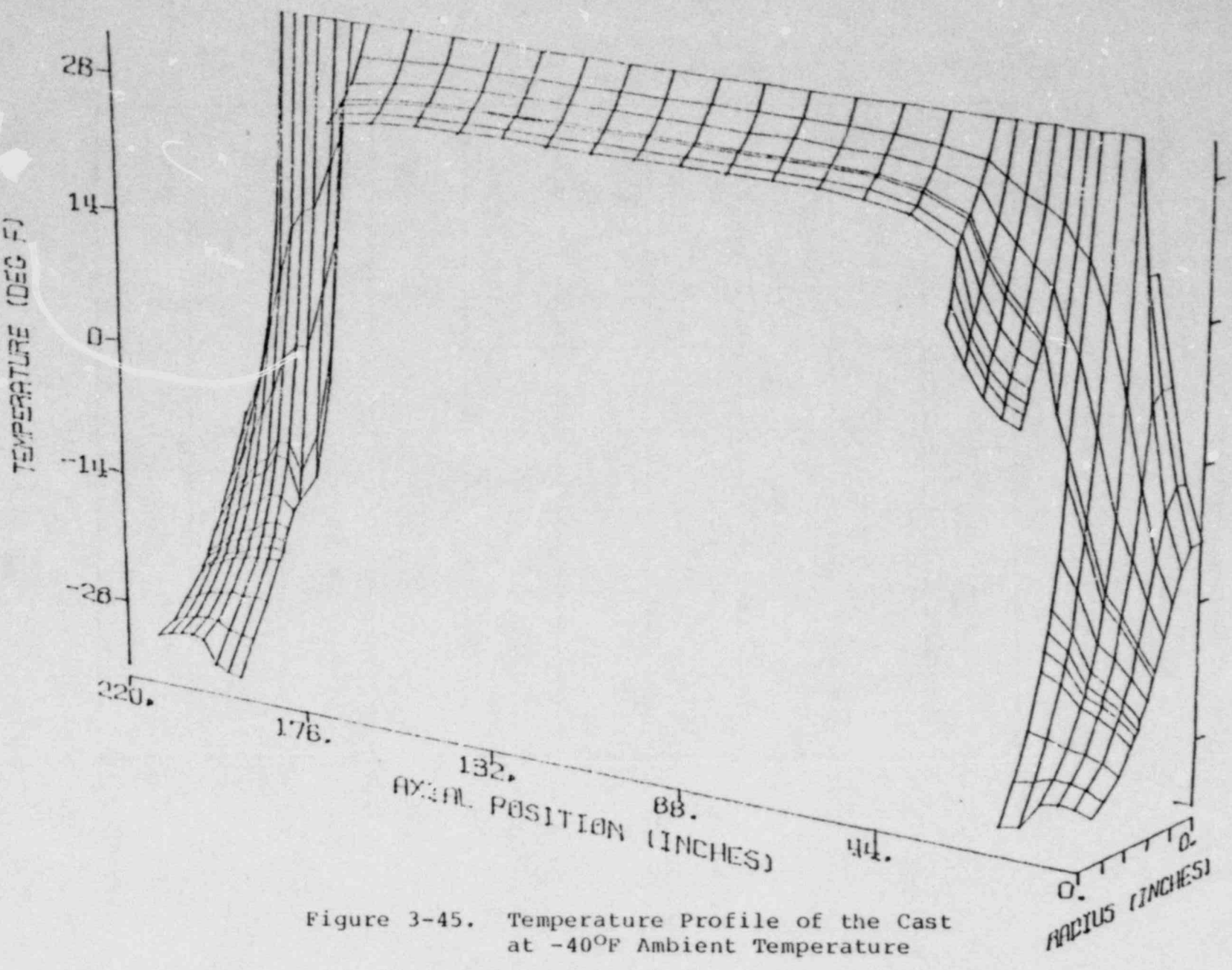

Figure 3-45. Temperature Profile of the Cast at -40°F Ambient Temperature

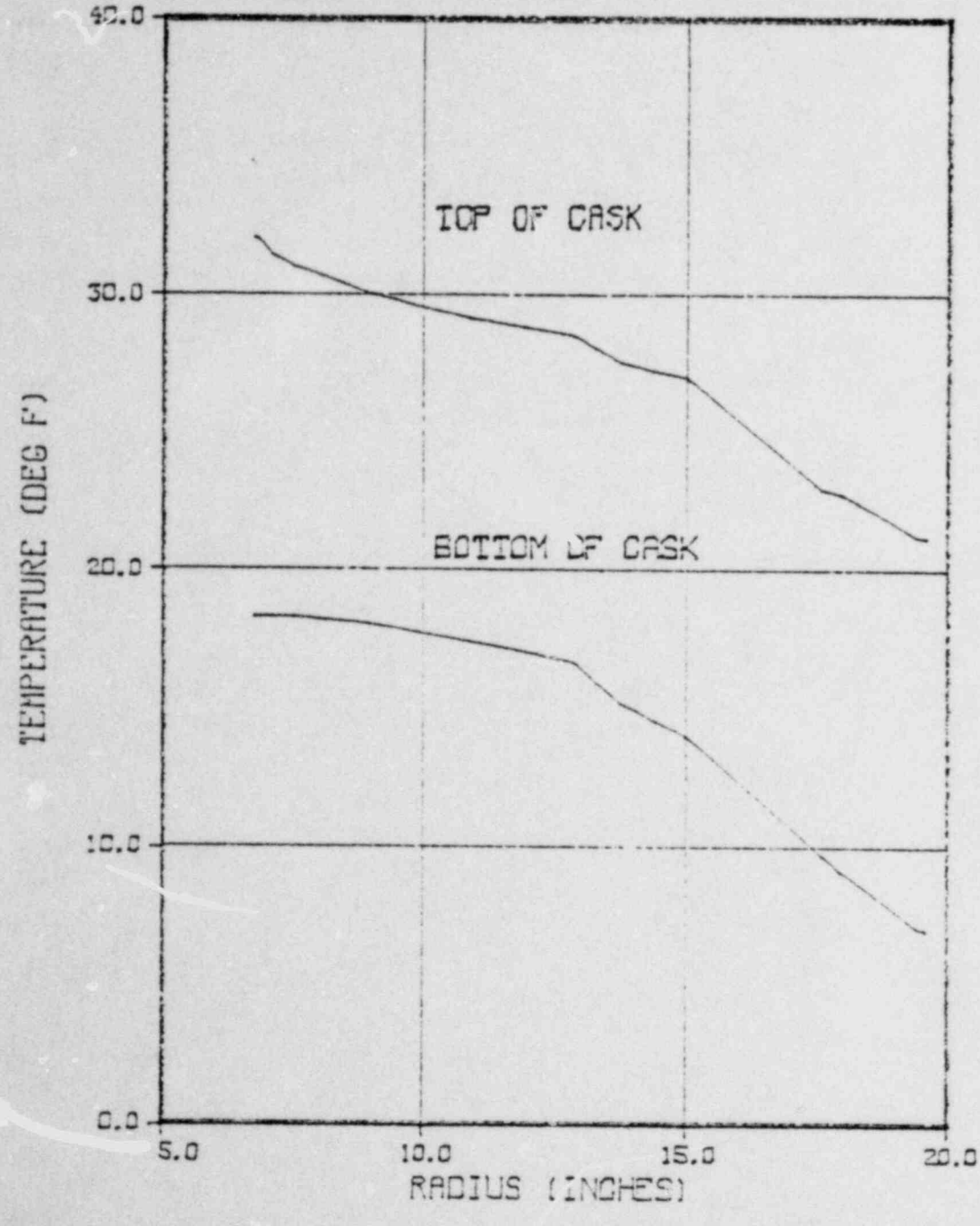

Figure 3-46. Radial Temperature Dependence at Cask Center for -40°F Ambient Temperature

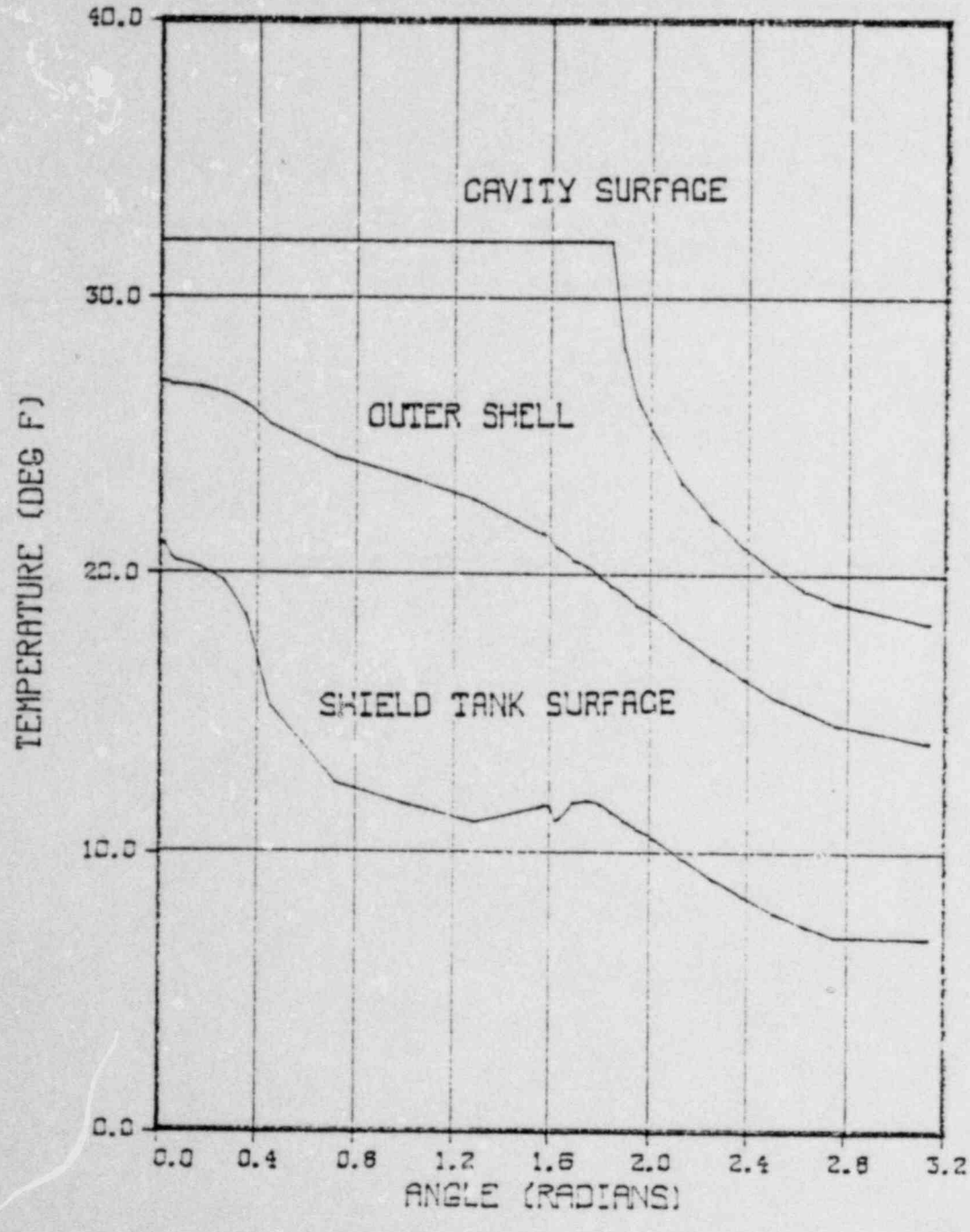

Figure 3-47. Angular Temperature Dependence at Cask Center for -40°F Ambient Temperature

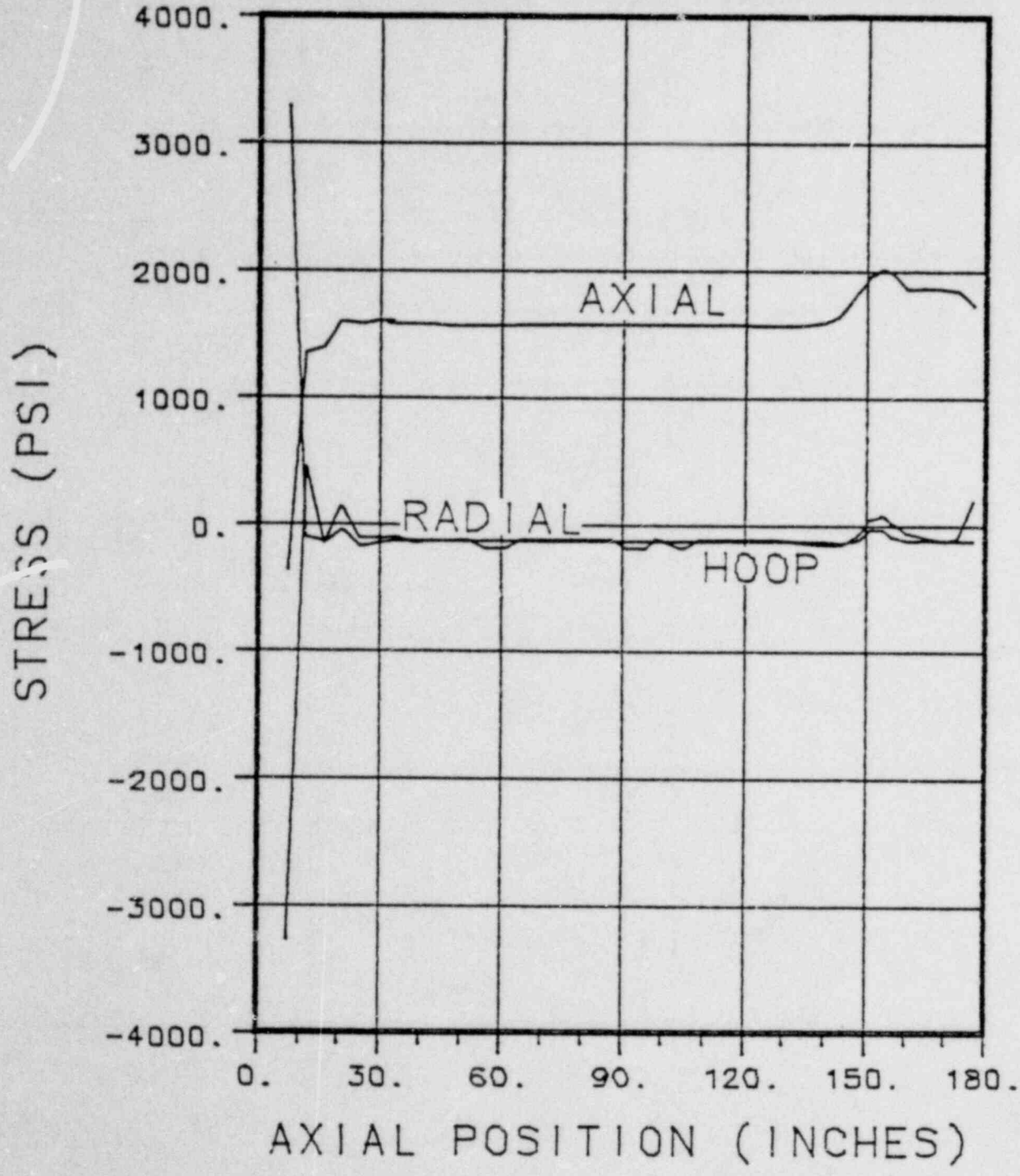

Figure 3-48. Thermal Stress Distribution When Ambient is 130°F

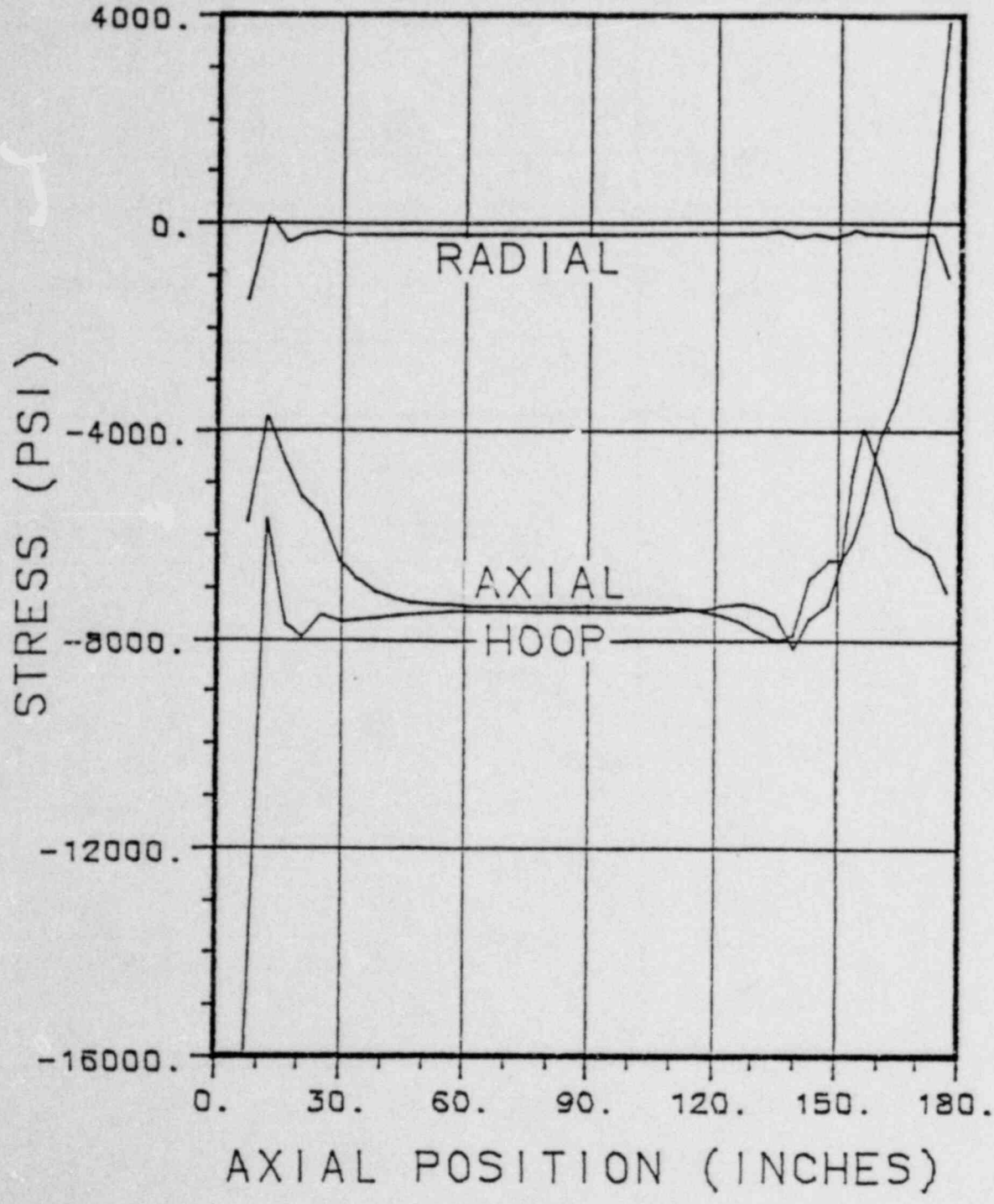

Figure 3-49. Thermal Stress Distribution When Ambient is -40°F

3.5. Hypothetical Accident

The hypothetical accident scenario encompasses four specific events which are:

1. 30 foot free fall onto unyielding surface
2. 40 inch free fall onto 6 inch diameter steel pin
3. one-half hour fire
4. immersion in large body of water.

By requiring each event to occur such that the maximum damage is inflicted on the cask, this hypothetical accident will be worse than any accident that the cask will reasonably experience.

The 30 foot free fall and 40 inch free falls are mechanical accidents that damage the cask structure but neither has any thermal impact. Likewise, the immersion in a large body of water will not induce any substantial thermal transients. The only consequence of either drop event is in the altering of the heat flow paths that are effective during the fire accident.

The analysis of the hypothetical accident will be restricted to the evaluation of the cask characteristics during the fire. In particular, the objective of the evaluation will be the determination of the maximum cavity temperature and pressure to assure that the cavity seals are not subject to conditions that will cause their failure. It has been assumed that the ambient temperature is 130°F at the start of the fire. This is a conservative analysis. If the cask safely survives the fire accident when the temperature at the commencement of the fire is 130°F it will not lose containment if the ambient temperature is 100°F before the fire begins.

3.5.1. Thermal Model

The thermal model for the analysis of the hypothetical accident is basically identical to the model for the analysis of normal transport conditions. There is one major change to the model to properly represent the conditions during the fire. The ambient conditions are changed to remove the insolation and increase the temperature of the surroundings to 1475°F to represent the fire. Simultaneously, the emissivity of the cask outer surface is increased to 0.8 to represent the blackening of the surface during the fire.

The mechanical damage to the shield tanks and impact limiters has the possibility of altering the heat flow paths that are important to the analysis of the consequences of the fire. The model depicts the unaltered cask geometry for consevatism because any damage will not reduce the length of the heat flow path between the cask body and the outer surfaces of the shield tank. Should the gussets or shield tank shell be deformed, the heat flow path would not be shortened. Consequently, the heat flow between the shield tank and the cask body would not be altered dramatically by the mechanical damage during either fall.

The boundary condition at the cavity surface is a constant temperature to represent the natural circulation within the cavity. The temperature of the wall was determined from an energy balance over the cavity contents with the necessary corrections for the temperature difference between the bulk fluid temperature and the wall temperature due to natural circulation. In equation form, this is expressed as:

$$\frac{dT_b}{dt} = M\,C_p\,(Q_d - Q_c)$$

and

$$T_b - T_w = h\,Q_c/A$$

where T_b is the bulk cavity coolant temperature in ^oF

T_w is the wall temperature in ^oF

t is time in hours

M is the total mass of the cavity coolant in pounds

C is the mass weighted average specific heat in BTU/lb^oF

Q_d is the decay heat generation rate in BTU/hr

Q_c is the heat conducted from the cavity to the cask wall in BTU/hr

h is the heat tansfer coefficient describing natural circulation in BTU/hr-in-^oF (See Figure 3-10)

A is the heat transfer area in square inches

The derivative in this expression was evaluated using temperature differences at time intervals of five minutes throughout the fire and post fire transients. The transient was followed until the maximum cavity temperature was reached as indicated by the heat conducted out of the cavity matching the decay heat produced by the fuel assembly.

3.5.2. Cask Temperatures

The temperature histories during the fire and post fire periods were calculated using the model described in Section 3.5.1. During the fire the insolation was set to zero while the post fire conditions included insolation. The emissivity of the cask surface was set to 0.8 during and after the fire to represent the blackening of the surface during the fire.

The temperature histories of the cask are presented in Figures 3-50 to 3-53. The temperature histories of the cavity water, lead, valves and rupture disk, and the O-rings are presented in Figures 3-54 to 3-57.

3.5.3. Maximum Internal Pressure

The relationship between the cavity pressure and coolant temperature was discussed in Section 3.2.6 for steady state conditions. This relationship has been employed to determine the cavity pressure during the fire accident because the variation of the cavity temperature is sufficiently slow that it can be considered to be a succession of steady state conditions. The history of the cavity pressure during this accident is presented as a function of temperature in Figure 3-58. A plot of the cavity pressure as a function of time of the accident appears in Figure 3-59. The cavity pressure at the end of the fire is 173 PSIA.

The cavity pressure will be increased if there are any fuel rods that have suffered clad penetration during transport or during the drop accidents that precede the fire. Clad failure will release the fission product gases to combine with the air and steam within the cavity.

The fuel rod internal pressure at the end of burnup is designed not to exceed the reactor coolant pressure. Assuming the fuel rods within the cask have reached this condition and the internal volume available to accommodate these gases is unchanged from beginning of irradiation, there is a total volume of 165 cubic inches of gases in a complete PWR fuel assembly. When this gas is released to the cavity, the pressure will be increased by about 11.5 psi which will increase the maximum pressure to 836 psia.

There will be no chemical reactions within the cavity that can release chemical products or energy that could increase the pressure beyond the value calculated above.

3.5.4. Maximum Thermal Stresses

The maximum thermal stresses for the hypothetical accident conditions have been evaluated in Section 2 based on the temperatures calculated in Section 3.5.1. Figures 3-60 through 3-63 summarize the results of the thermal stresses obtained in section 2.

3.5.5. Evaluation of Package Performance for the Hypothetical Accident Condition

Figures 3-50 through 3-57 and Table 3-8 show that the NAC-1 spent fuel shipping cask will not lose containment during the hypothetical accident. All temperatures and pressures of the valves and O-rings are below their respective rated failure temperatures and pressures.

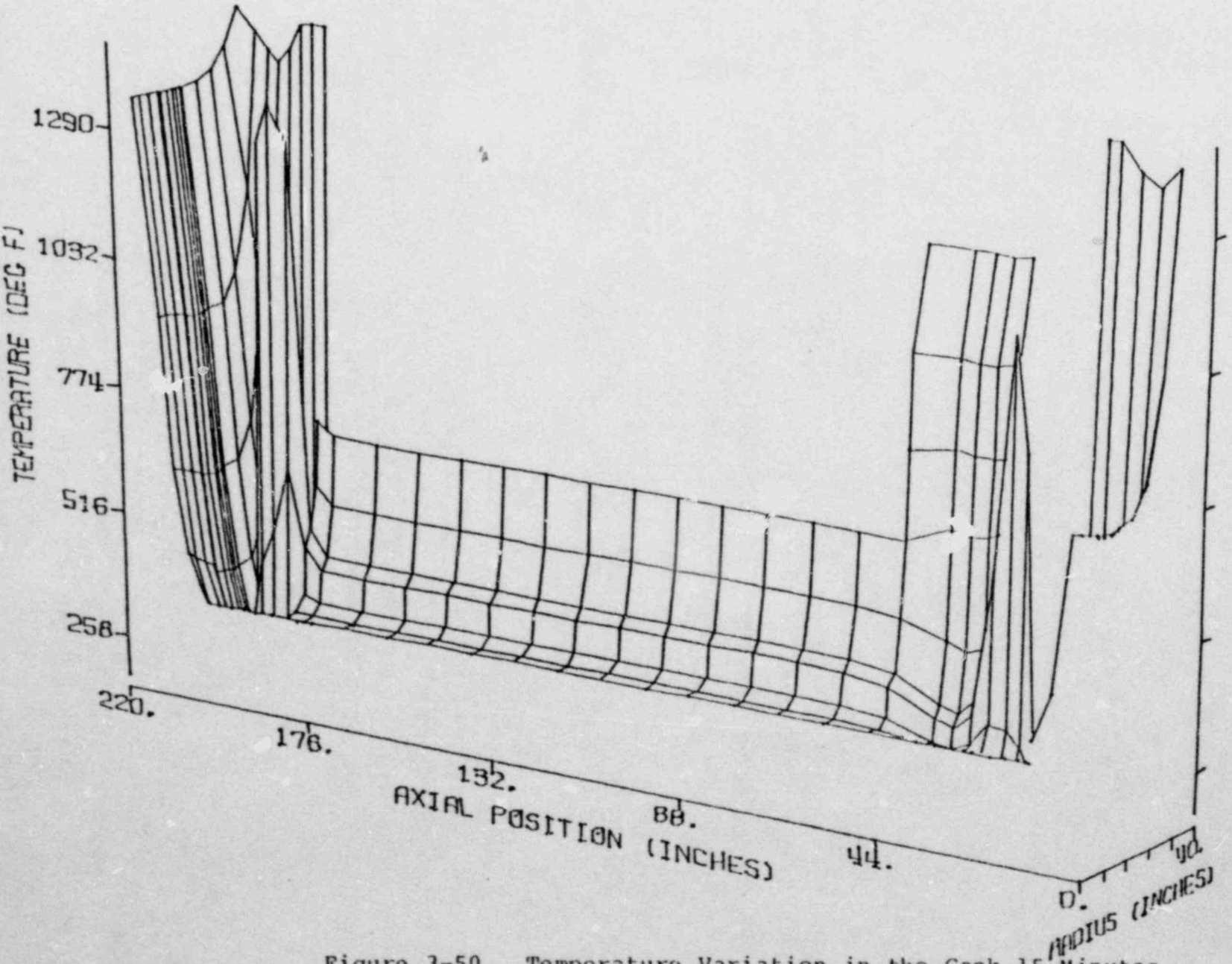

Figure 3-50. Temperature Variation in the Cask 15 Minutes After the Commencement of the Fire

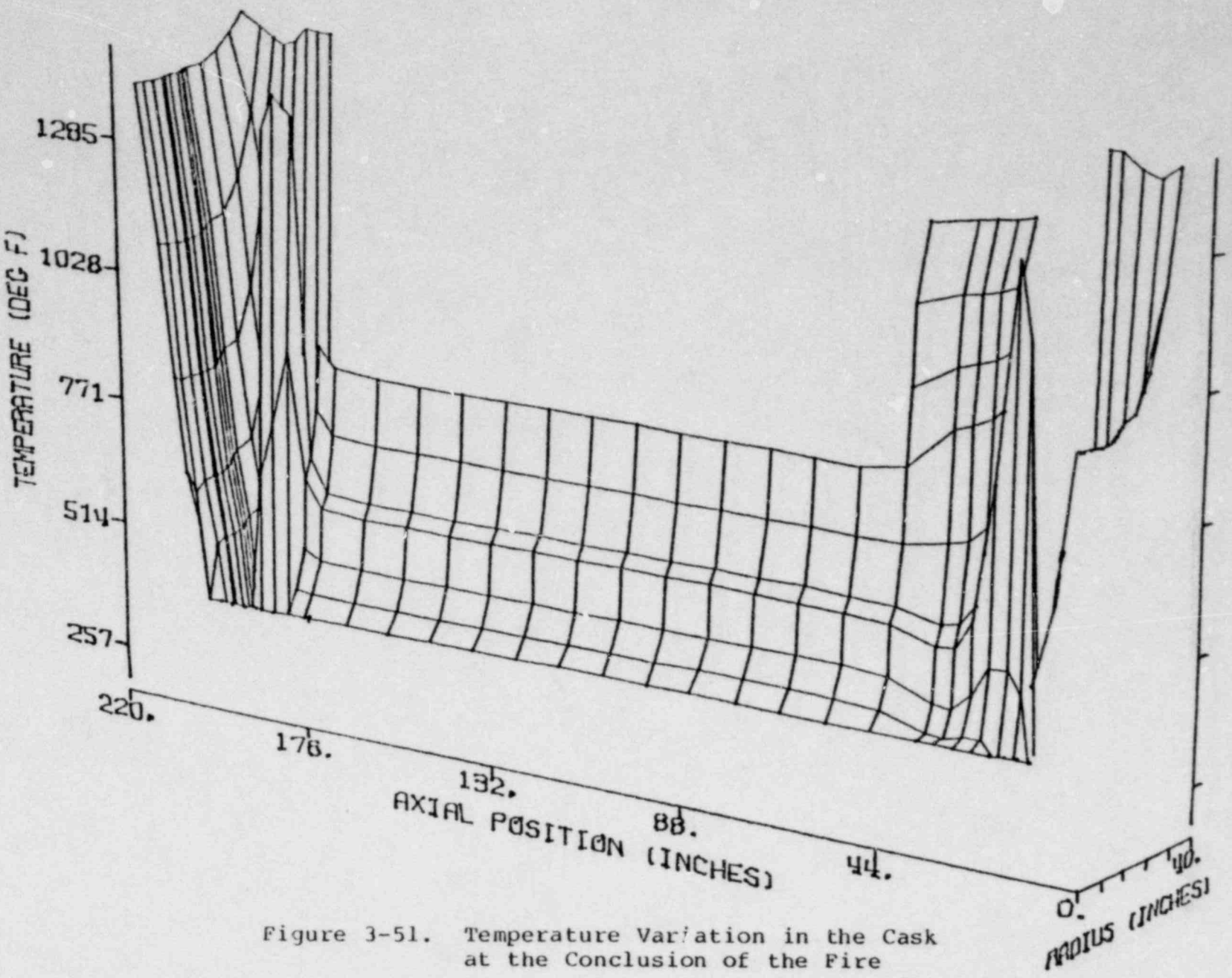

Figure 3-51. Temperature Variation in the Cask at the Conclusion of the Fire

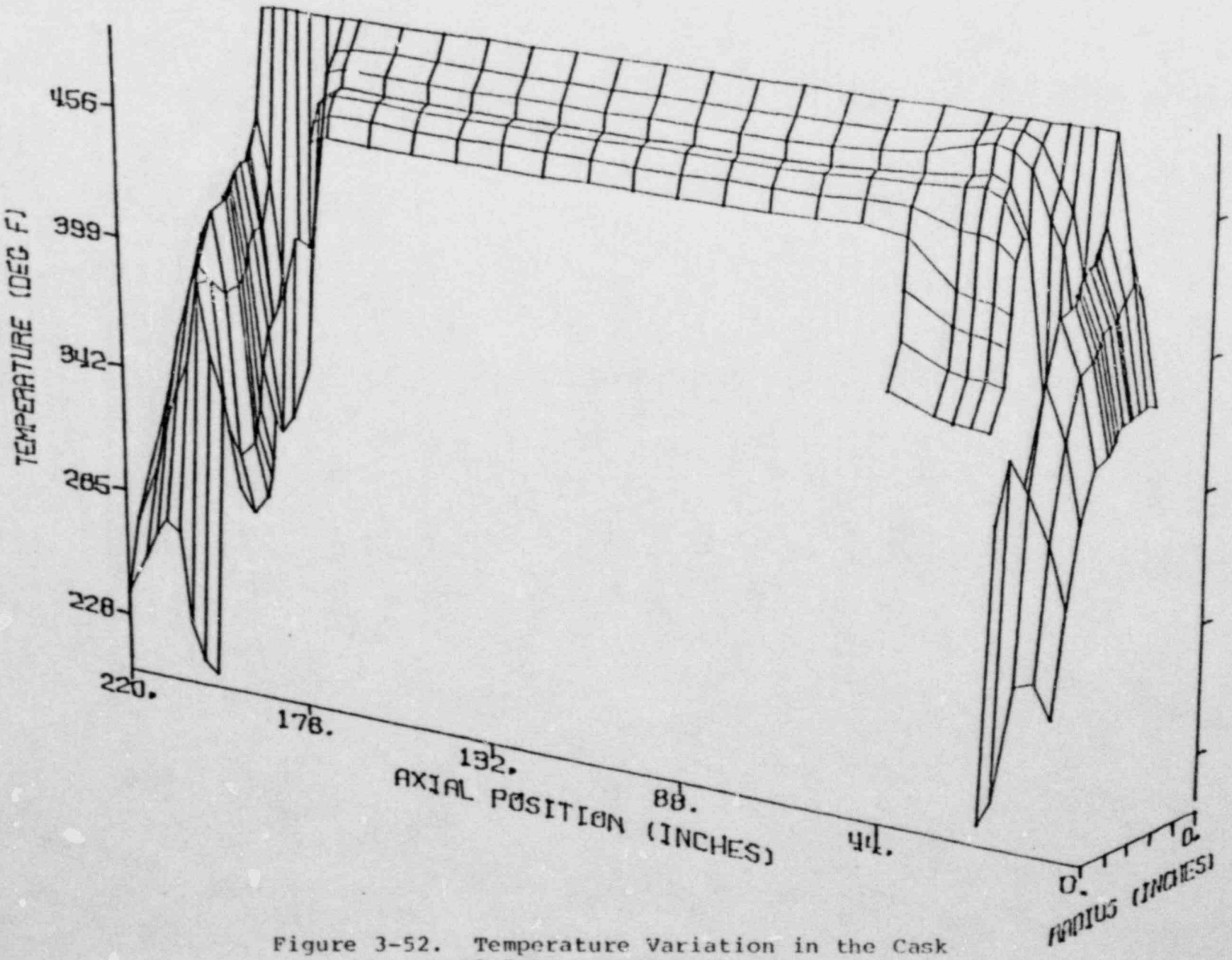

Figure 3-52. Temperature Variation in the Cask 1.5 Hours After the Fire

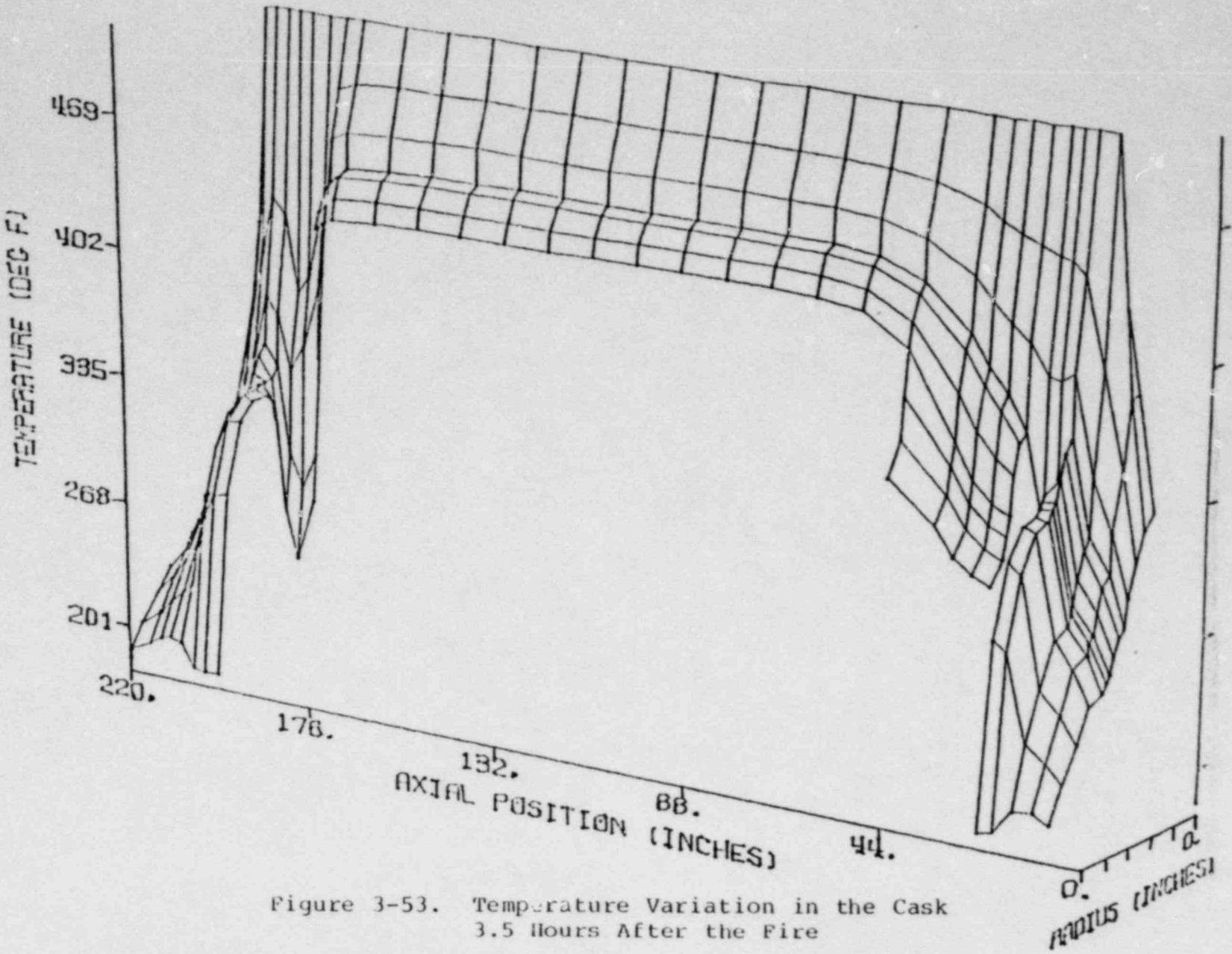

Figure 3-53. Temperature Variation in the Cask 3.5 Hours After the Fire

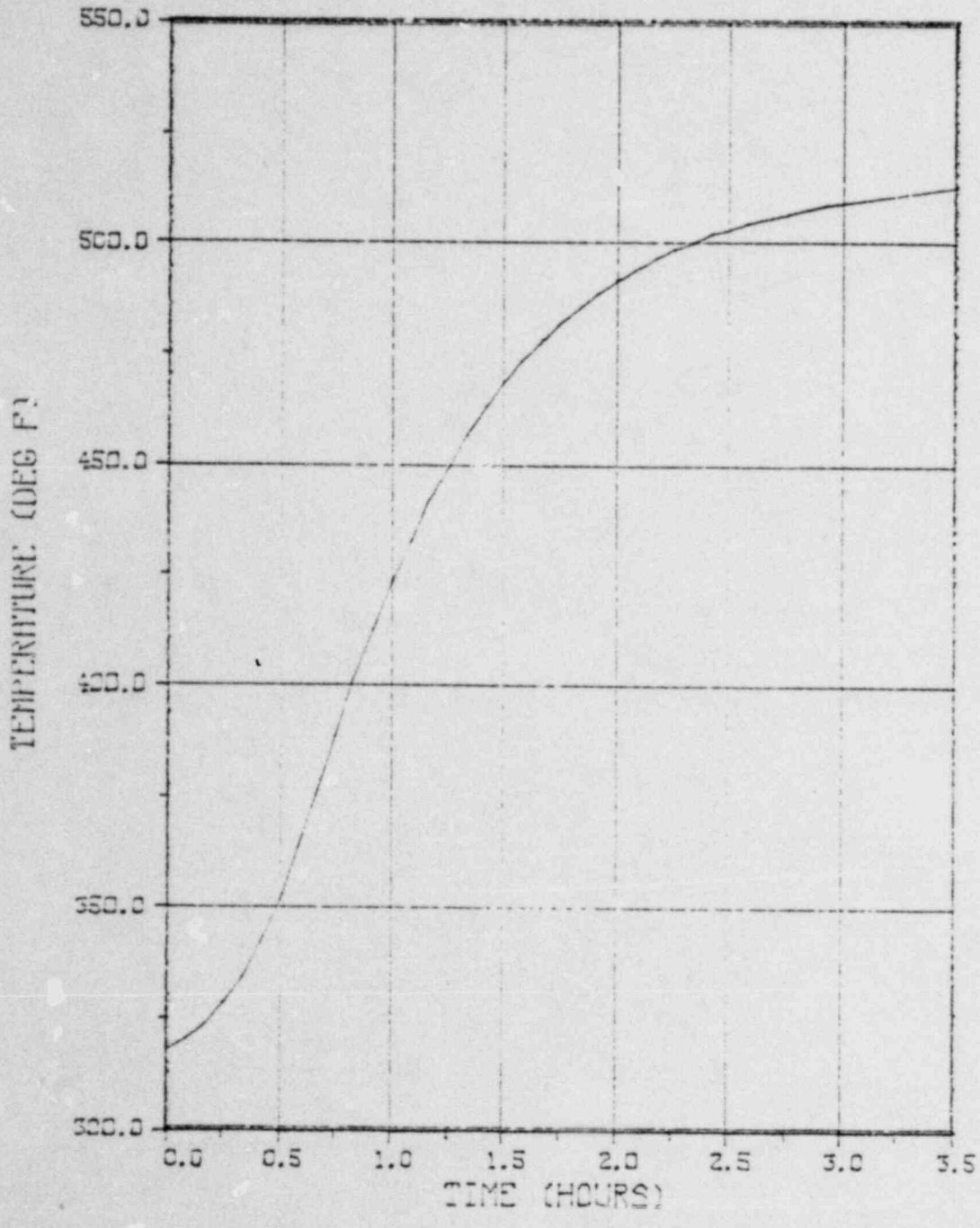

Figure 3-54. Temperature Profile of the Cavity Water During and After the Fire

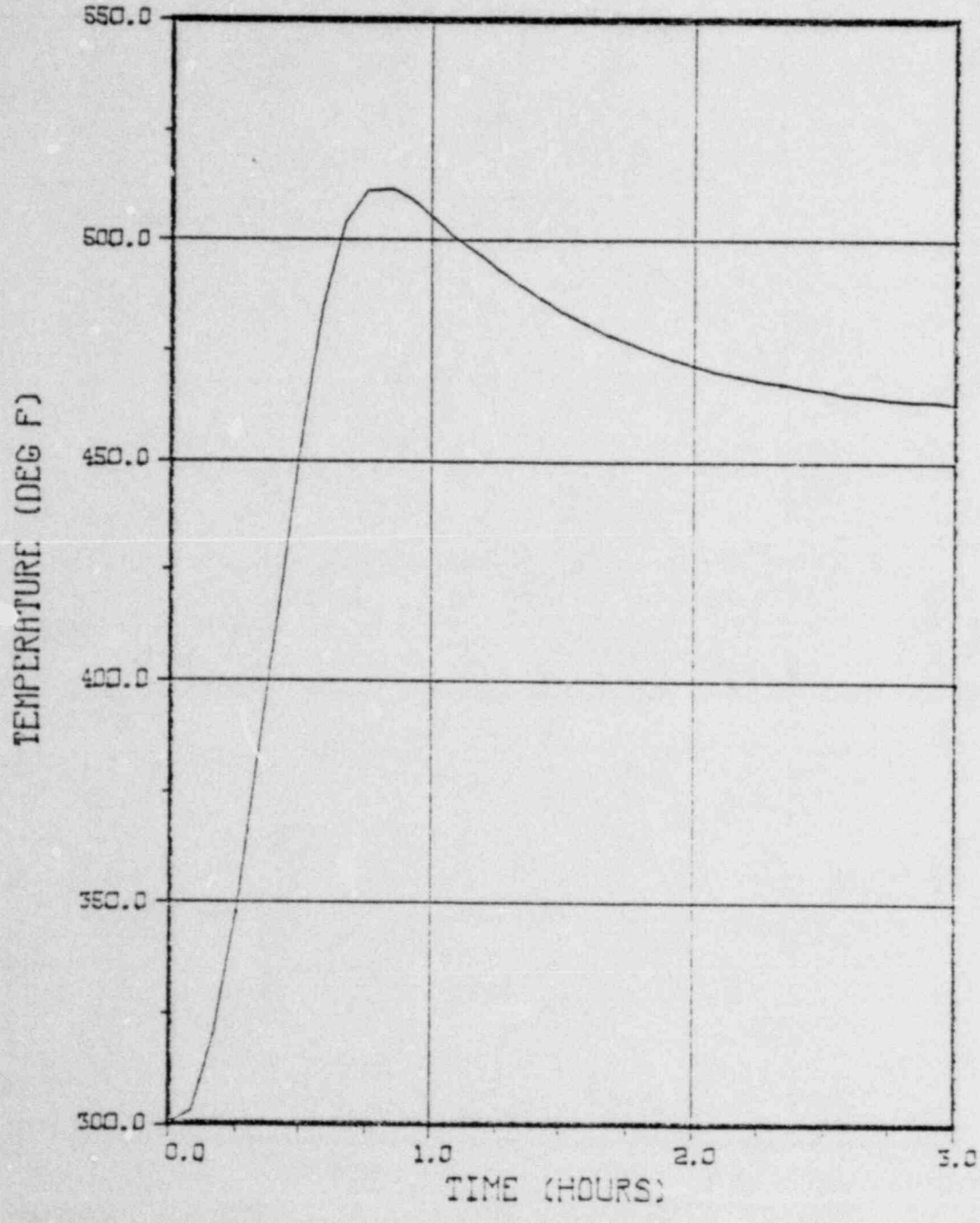

Figure 3-55. Temperature Profile of the Lead During and After the Fire

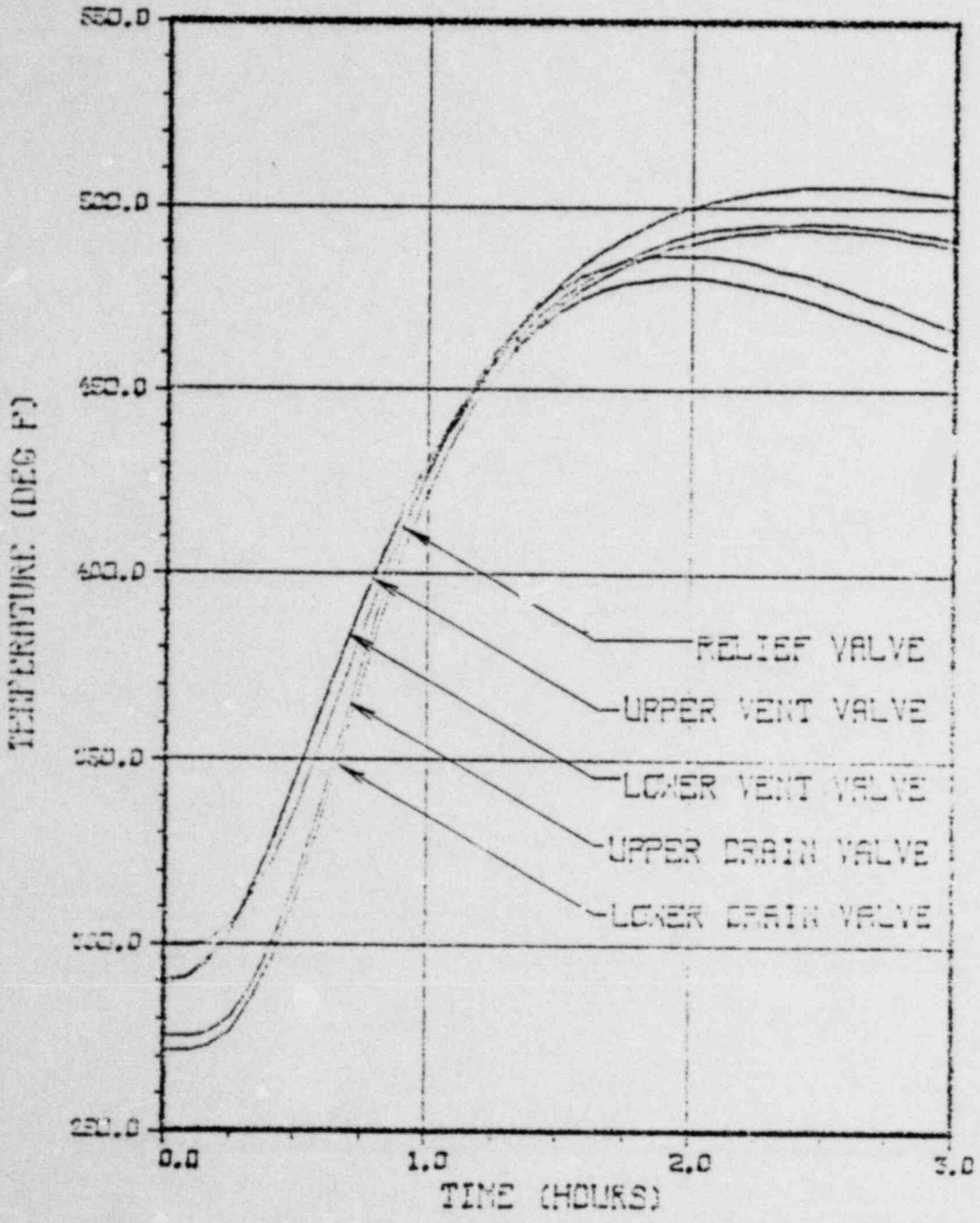

Figure 3-56. Temperature Profile of the Valves and Rupture Disk During and After the Fire

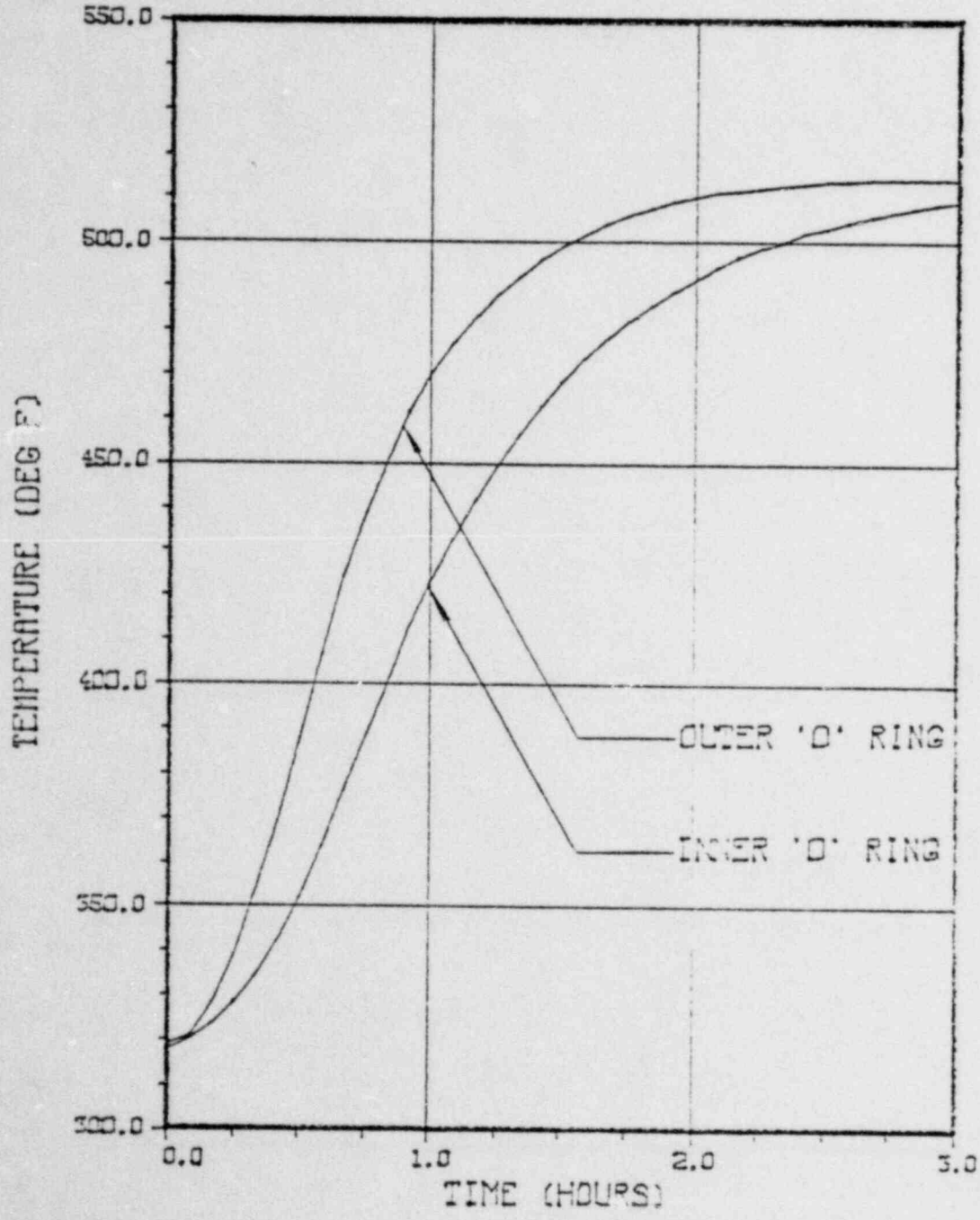

Figure 3-57. Temperature Profile of the O-Rings During and After the Fire

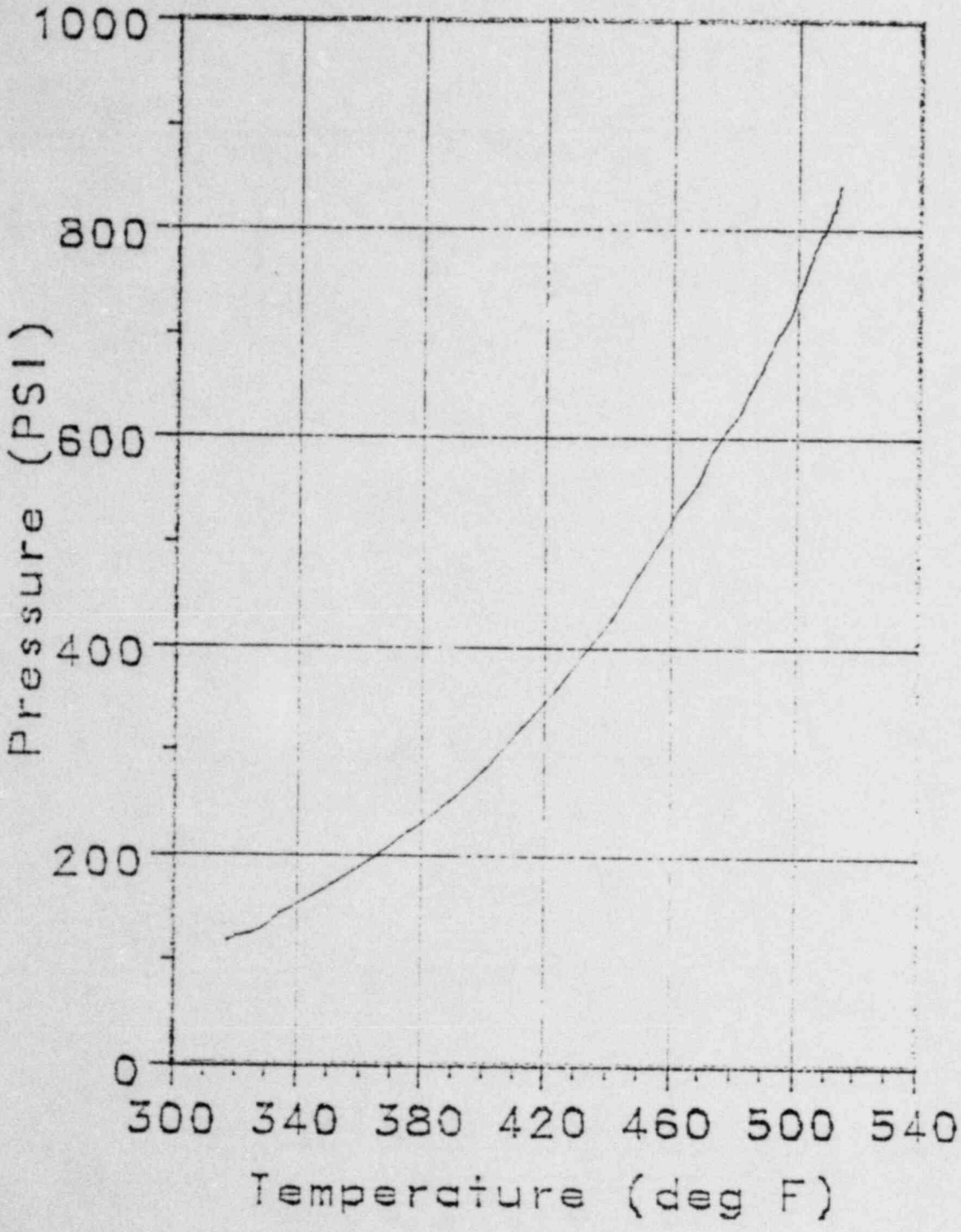

Figure 3-58. Cavity Pressure as a Function of Cavity Temperature

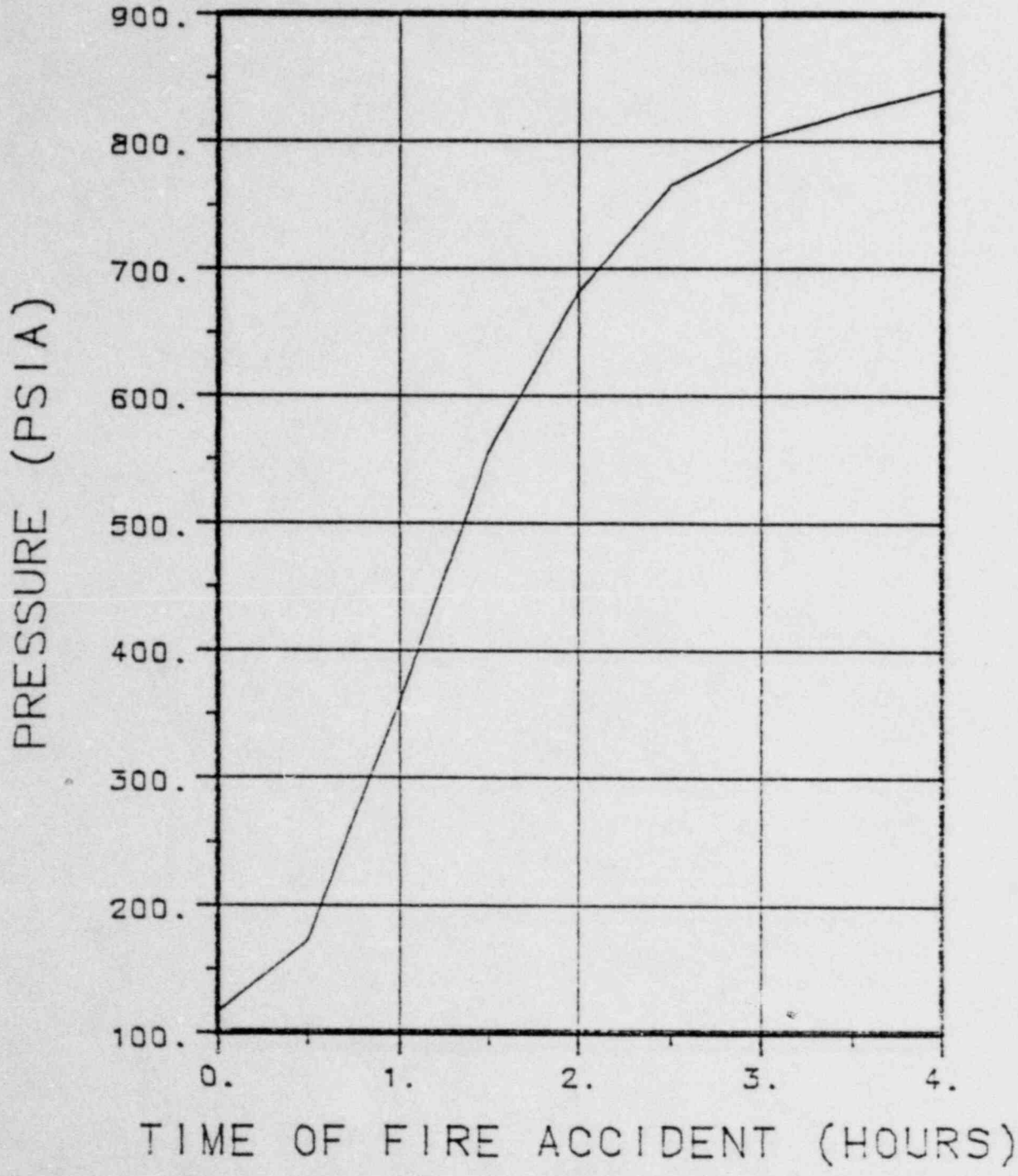

Figure 3-59. Cavity Pressure During the Fire Accident

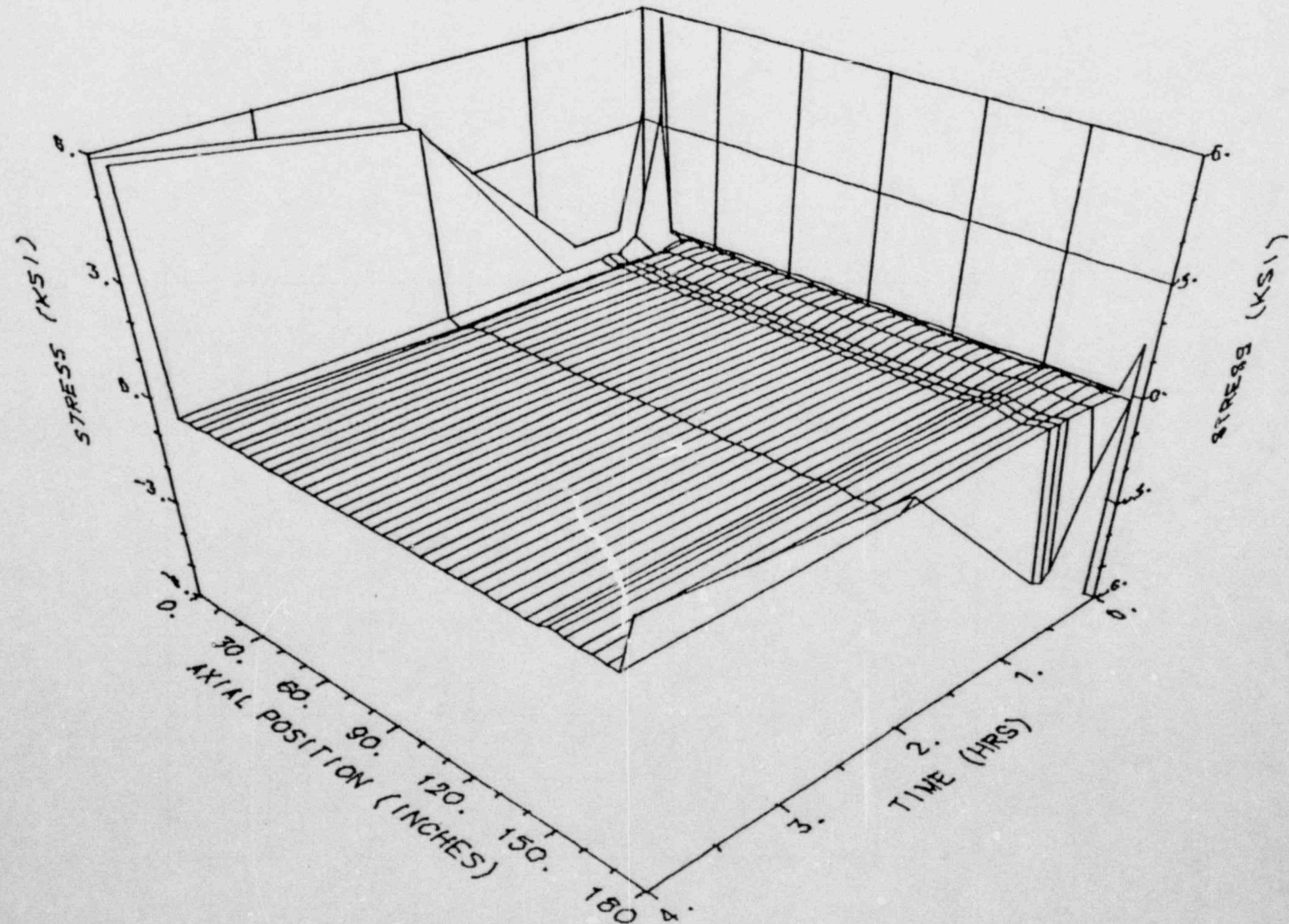

Figure 3-60. Summary of Radial Stresses During the Fire

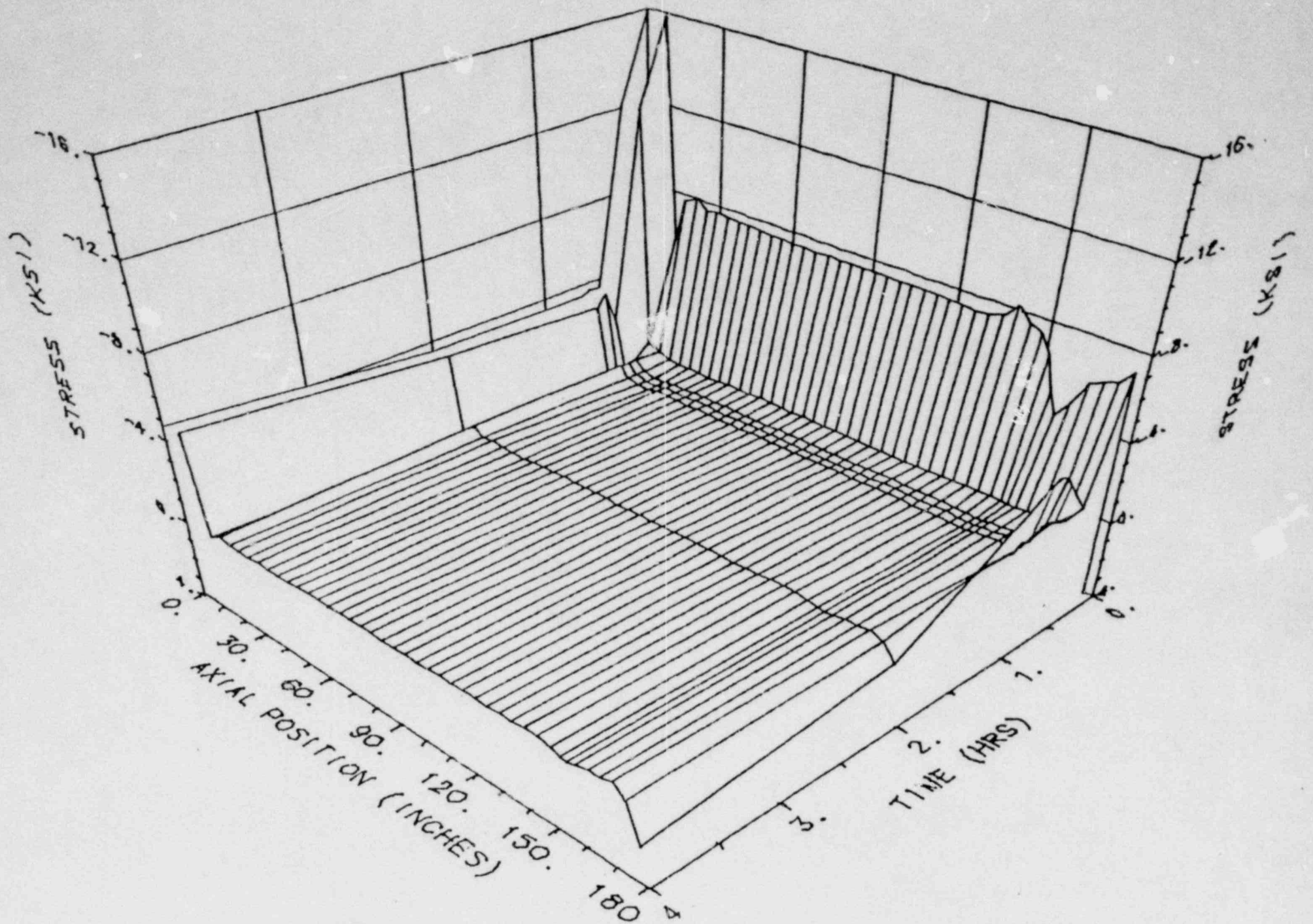

Figure 3-61. Summary of Hoop Stresses During the Fire

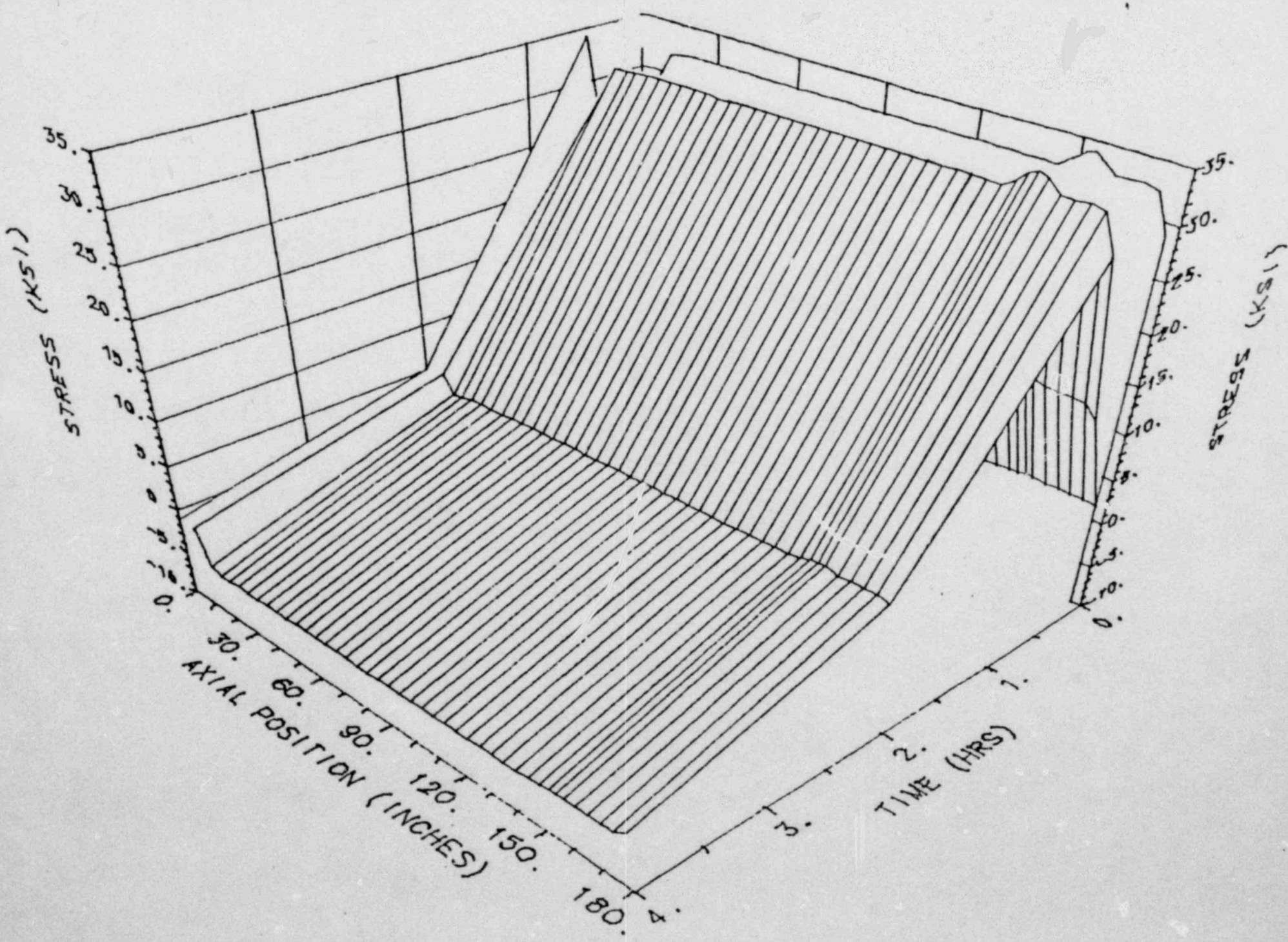

Figure 3-62. Summary of Axial Stresses During the Fire

3.6. Appendices to Thermal Analyses

The following sections contain material which is intended to supplement the information presented in the previous sections.

3.6.1. HEATING-5 Program Description

HEATING-5 solves steady-state and/or transient heat conduction problems in one-, two-, or three-dimensional Cartesian or cylindrical coordinates or one-dimensional spherical coordinates. The modelled geometrical shapes are divided into regions whose boundaries are parallel to the axes of the coordinate system. The thermal conductivity, density, and specific heat may be both spacial and temperature dependent. The thermal conductivity may also be anisotropic. Materials may undergo a change of phase. Heat generation rates may be dependent on time, temperature, or position and boundary conditions may be time dependent. The boundary conditions, which may be surface-to-surface, include fixed temperatures, prescribed heat fluxes, natural circulation, or radiation. The parameters describing the boundary conditions may be time- and/or temperature dependent. The mesh spacing can be varied along each axis. The code is designed to allow a maximum of 100 regions, 50 materials, and 50 boundary conditions.

A transient problem may be solved using any one of several finite difference schemes. These include an implicit technique based upon the Crank-Nicholson procedure, the classic implicit procedure, an explicit method which is stable for a time step of any size, and the classic explicit procedure which involves the first forward time difference. The solution of the system of equations arising from the implicit technique is accomplished by point successive overrelaxation iteration, and includes procedures to estimate the optimum acceleration parameter. The

time step size for implicit transient calculations may be varied as a function of the maximum temperature change at a node. Transient problems involving materials with change of phase capabilities cannot be solved using the implicit technique with this version of HEATING-5.

3.6.2. References

3.1 ASME Boiler and Pressure Vessel Code, Section III, Nuclear Vessels, The American Society of Mechanical Engineers, New York, New York, 1971.

3.2 Edwards, A. L., A Compilation of Thermal Property Data for Computer Heat Conduction Calculations, UCRL-50589, 1969.

3.3 Rosenhow, W. M. and Harry V. Choi, Heat, Mass, and Momentum Transfer, Prentice Hall, Inc., 1961.

3.4 Kreith, Frank, Principles of Heat Transfer, International Textbook Company, Third Edition, 1976.

3.5 Glycols, published by Union Carbide Corporation, 1971, and ASHRAE Handbook of Fundamentals, published by the American Society of Heating, Refrigerating, and Air Conditioning Engineers, Inc., New York.

3.6 Keenan, J. H. and Keyes, F. G., Thermodynamic Properties of Steam, John Wiley and Sons, 1959.

3.7 MacDonald, P. E., ed, MATPRO-Version 09, A Handbook of Material Properties for Use in the Analysis of Light Water Reactor Fuel Behavior, EG&G Idaho, Inc., 1976.

3.8 Safety Analysis Report for Nuclear Fuel Services, Inc. Spent

Fuel Shipping Cask Model No. NFS-4, Nuclear Fuel Services, Inc. USNRC Docket 6698, September, 1972.

3.9 McCabe, W. L. and Smith, J. C., Unit Operations of Chemical Engineering ,McGraw-Hill, Inc., Third Edition, 1976.

3.10 Hildebrand, F. B., Advanced Calculus for Applications, Prentice Hall, Inc., 1962.

3.6.3. Methods Verification

Solutions obtained with the computer program HEATING-5 were compared with analytical solutions to the identical heat transfer problems. The results of this analysis show that HEATING-5 is computer program which can readily be applied to the thermal analysis of the NAC-1 shipping cask and accurately describes the heat transfer which is occurring through the cask. This benchmarking also ensures that the computer program is working properly as well as shows the ability of the analyst to model and solve heat transfer problems correctly using HEATING-5. Four different problems were solved using both analytical and computer solution methodologies. The analytic solution is exact and the HEATING solution is considered to be an approximate answer to be compared with the exact solution. Problems were chosen to test the various types of situations that HEATING-5 can handle which were used in the thermal analysis of the NAC-1 cask. The chosen heat transfer problems are:

- One dimensional cylinder at steady state conditions
- Two dimensional slab at steady state conditions
- One dimensional slab with varying thermal conductivity at steady state conditions
- One dimensional slab at transient conditions

The error in the HEATING-5 solution was calculated and the results of the comparisons are shown in Table 3-10. This table shows that the error in the HEATING-5 solution is very small and that this computer program accurately calculated the heat transfer in each of these problems.

The one dimensional, cylindrical problem is as follows:

A tube 2.36 inches OD is lagged with a 1.97 inch layer of asbestos, for which the conductivity is 0.01 BTU/hr-in-^{o}F, followed by a 1.57 inch layer of cork with a conductivity of 0.0025 BTU/hr-in-^{o}F. If the temperature of the outside of the pipe is 302^{o}F and the temperature of the outer surface of the cork is 86^{o}F, calculate the heat loss in BTU per hour per inch of pipe. Figure 3-64 is a representation of the geometry of the problem (from Reference 3.9).

The analytical answer to this problem is 5.2199 BTU/hr-in whereas the answer calculated using HEATING-5 is 5.2605 BTU/hr-in. This represents an error of only 0.78%; a very slight error.

Figure 3-65 is a representation of the two dimensional steady state problem. The text accompanying the figure is as follows:

Three edges of a thin square plate are maintained at 0^{o}F. The fourth plate is maintained at 300^{o}F. Each side of the plate is 2 inches in length. Calculate the steady state temperature distribution in the plate (Reference 3.10).

The anayltical and HEATING solutions to this problem are shown in Figure 3-66. Since the maximum error in the HEATING-5 answer is only 0.24%, it is impossible to see a difference in the two solutions. Figure 3-67 presents the difference between the

temperatures calculated by HEATING-5 and by an analytical method. This graph shows that HEATING-5 correctly calculates the temperature distribution in a two dimensional geometrical figure.

The next problem considered is a 3 inch slab where the thermal conductivity varied as a function of temperature. The text of the problem is:

The conductivity of an insulating material is a function of temperature which can be represented by the equation $k(T) = 0.031(1 + 0.1T)$ which is valid in the temperature range from 100 to 300°F. If one side of the 3 inch slab is kept at 100°F and the other side is maintained at 300°F, calculate the heat flow per unit area for this slab (Reference 3.4).

The exact solution to this problem is 3.6200 BTU/hr-in^2 while the HEATING solution to the same problem is 3.6178 BTU/hr-in^2. This represents a very slight error of only 0.04%. The results of the variable thermal conductivity problem demonstrate that HEATING-5 precisely handles situations where the thermal conductivity of a material changes as the temperature in the material varies.

The final benchmark problem is a transient problem which demonstrates that HEATING-5 can treat time dependent situations. The problem is as follows:

A flat semi-infinite slab of plastic initially at 70°F is placed between two plates at 250°F. The slab is 1.0 inches thick. How long will it take to heat the slab to an average of 210°F? (from Reference 3.9).

The analytical answer to this problem is 16 minutes (0.2667 hours). HEATING produced a very similar answer of 15.87 minutes (0.2645 hours). This represents a small error of 0.83%.

The above four sample problems conclusively demonstrate that the computer program HEATING-5 can accurately solve a wide range of heat conduction problems which are applicable to the thermal analysis of the NAC-1 spent fuel shipping cask. Therefore, HEATING-5 is well suited for the calculations which must be performed in this analysis.

3.6.4. Sample Input for HEATING-5

The following pages present typical input for HEATING-5 calculations of the following sections of the cask:

- Lead-Fin-Stainless Steel Unit Cell
- Upper Impact Limiter and Closure Plug
- Cask Wall with Upper Cowl
- Expansion Tank
- Shield Tank Portion of Cask
- Cask Wall with Lower Cowl
- Cask Wall with Lead Void
- Lower Impact Limiter

The input shown here limits the number of iterations to 300. Each of the calculations described here was run repeatedly using the output from one case to form the input for the succeeding case. Thus, the number of iterations was considerably in excess of 300 in addition to permitting operator control of the progress of calculation.

3.6. APPENDICIES TO THERMAL ANALYSES

Table 3-10. HEATING-5 INPUT FOR THE ANALYSIS OF THE COPPER FIN

```
ANALYSIS OF COPPER FIN
10000     7      35      4      0      0      1      3
   15    14       0      1      4      0      0     20
                  7                    5
    1   300  1.0E-8    1.9
    1     2      0.   2.009  1.003 3.6275
    1                                  1
    2     2      0.   1.641  0.878  1.003
    1
    3     3   1.641   1.704  0.878  1.003
    1
    4     2   1.704   2.009  0.878  1.003
    1
    5     2      0.   1.484  0.815  0.878
    1
    6     3   1.484   1.704  0.815  0.878
    1
    7     2   1.704   2.009  0.815  0.878
    1
    8     2      0.   1.484  0.690  0.815
    1
    9     3   1.484   1.547  0.690  0.815
    1
   10     2   1.547   2.009  0.690  0.815
    1
   11     2      0.   1.328  0.627  0.690
    1
   12     3   1.328   1.547  0.627  0.690
    1
   13     2   1.547   2.009  0.627  0.690
    1
```

14	2	0.	1.328	0.502	0.627
1					
15	3	1.328	1.391	0.502	0.627
1					
16	2	1.391	2.009	0.502	0.627
1					
17	2	0.	1.203	0.439	0.502
1					
18	2	1.203	1.391	0.439	0.502
1					
19	2	1.391	2.009	0.439	0.502
1					
20	2	0.	0.719	0.392	0.439
1					
21	3	0.719	1.256	0.392	0.439
1					
22	2	1.256	2.009	0.392	0.439
1					
23	2	0.	0.563	0.376	0.392
1					
24	3	0.563	1.256	0.376	0.392
1					
25	4	1.256	2.009	0.376	0.392
1					
26	4	0.	0.250	0.329	0.376
1					
27	4	0.250	0.313	0.329	0.376
1					
28	3	0.313	0.782	0.329	0.376
1					
29	4	0.782	2.009	0.329	0.376
1					
30	4	0.	0.250	0.313	0.329
1					
31	4	0.250	0.313	0.313	0.329
1					

```
    32          3       0.313       0.563       0.313       0.329
     1
    33          4       0.563       2.009       0.313       0.329
     1
    34          1          0.       2.009       0.219       0.313
     1
    35          1          0.       2.009          0.       0.219
     1                                                2
     1      STEEL                                            -1
     2       LEAD                                            -2
     3     COPPER                                            -3
     4        AIR                                            -4
     1        15.
     1          1
                                                       15.         0
     2          2       15.
     3          1      100.
          5.346E-12
    0.      0.250      0.313      0.563      0.719      0.782      1.203      1.256
  1.328      1.391      1.484      1.547      1.641      1.704      2.009
     1          2          2          2          2          2          1          1
     1          1          1          1          1          2
    0.      0.219      0.313      0.329      0.376      0.392      0.439      0.502
  0.627      0.690      0.815      0.878      1.003     3.6275
     1          1          1          2          1          2          1          2
     1          2          1          2          5
     1          1
     1      300.
     1         12
   70.0      .7166      100.0      .7250      150.0      .7500      200.0      .7750
  250.0      .8000      300.0      .8166      350.0      .8416      400.0      .8666
  450.0      .8833      500.0      .9083      550.0      .9250      600.0      .9416
     2         10
   68.0      1.667      209.0      1.663      400.0      1.525      499.0      1.408
  581.0      1.208      630.0      1.008      717.0       .808      800.0       .750
```

```
   980.0      .725   1267.0      .725
       3         3
    -184.  21.5560     32.     19.34     1981   16.1166
       4        11
      32.  0.00117    100.  0.00128     200.  0.00145     300.  0.00161
     400.  0.00177    500.  0.00193     600.  0.00208     700.  0.00223
     800.  0.00238    900.  0.00253    1000.  0.00266
ANALYSIS OF COPPER FIN
 0.00000         0
```

Table 3-11. HEATING-5 INPUT FOR THE ANALYSIS OF THE UPPER IMPACT LIMITER AND PLUG

3D ANALYSIS OF IMPACT LIMITER AND PLUG

10000	1	28	3			1	9
14	19	11		5			50
		7			5		
1	300	1.E-8	1.9				
1	1	0.	35.891	.7854	3.92699	0.	.109
1						1	
2	1	35.891	36.	.7854	1.15632	0.	19.734
1							
3	1	35.891	36.	1.15632	1.23643	0.	19.734
1		2				1	1
4	1	35.891	36.	1.23643	2.35617	0.	19.734
1		3				1	1
5	1	35.891	36.	2.35617	2.42253	0.	19.734
1		4				1	1
6	1	35.891	36.	2.42253	2.79253	0.	19.734
1		5				1	1
7	1	35.891	36.	2.79253	3.16253	0.	19.734
1		6				1	1
8	1	35.891	36.	3.16253	3.53253	0.	19.734
1		7				1	1
9	1	35.891	36.	3.53253	3.92699	0.	19.734
1		8				1	1
10	1	15.125	35.891	.7854	3.92699	19.609	19.734
1							1
11	1	15.125	15.375	.7854	3.92699	10.609	10.859
1							
12	1	15.375	22.5	.7854	3.92699	10.609	10.734
1							
13	2	15.375	22.5	.7854	1.309	10.734	19.609
1							
14	2	15.375	22.5	1.83260	2.35617	10.734	19.609
1							
15	2	15.375	22.5	2.35617	2.8798	10.734	19.609

```
1
16          2   15.375      22.5    3.4034   3.92699   10.734   19.609
1
17          2   17.25       17.75   1.309    1.8326    10.734   19.734
1
18          1   17.25       17.75   2.8798   3.4034    10.734   19.734
1
19          3   6.33965     8.58965  .7854    .88954     .109    10.609
1
20          3   6.33965     8.58965 2.25205   2.46839    .109    10.609
1
21          3   6.33965     8.58965 3.82285   3.92699    .109    10.609
1
22          1   12.75       15.125   .7854    3.92699   10.609   10.859
1
23          1   0.          12.75    .7854    3.92699   10.609   10.859
1
24          1   0.          12.75    .7854    3.92699   10.859   12.859
1                9
25          1   0.          8.7375   .7854    3.92699   12.859   13.859
1                9
26          1   0.          8.2948   .7854    3.92699   13.859   16.109
1                9           9
27          1   0.          7.85205  .7854    2.6269    13.859   18.359
1                9           9                                    9
28          1   0.          7.85205  2.6269   3.92699   13.859   18.359
1                9           9
1     STEEL                 .28612                -3
2   GUSSETS                 .28612                -4
3   B HOLES                 .28612                -5
1     320.
1        1    130.
  5.346E-12                 .3333    .41680       2
                  -1
2        1    130.
  5.346E-12   .000833         .25
```

```
      3         1      130.
       5.346E-12                .3333                    2
                        -2
      4         1      130.
       5.346E-12                .3333    .028189         2
                        -2
      5         1      130.
       5.346E-12                .3333    .211396         2
                        -2
      6         1      130.
       5.346E-12                .3333    .494806         2
                        -2
      7         1      130.
       5.346E-12                .3333    .711246         2
                        -2
      8         1      130.
       5.346E-12                .3333                    2
                        -2
      9         2      320.

        0.   6.33965  7.85205   8.2948   8.58965   8.7375    12.75   15.125
    15.375     17.25    17.75     22.5    35.891      36.
         3         1        1        1         1         2         2         1
         1         1        1        3         1
     .7854     .85074   .88954  1.15632   1.23643     1.309    1.8326   2.25205
   2.35617   2.42253  2.46839   2.6269   2.79253    2.8798   3.16253    3.4034
   3.53253   3.82285  3.92699
         1         1        1        1         1         1         1         1
         1         1        1        1         1         1         1         1
         1         1
        0.      .109   10.609   10.734   10.859    12.859    13.859    16.109
    18.359    19.609   19.734
         1         3        1        1         1         1         1         1
         1         1
         1         5
     100.     .0015     200.     .0013     300.     .0012     400.     .0011
```

```
    500.    .0010
      2       5
    100.    .0015    200.    .0013    300.    .0012    400.    .0011
    500.    .0010
      3      12
    -40.    .6466    100.    .7250    150.    .7500    200.    .7750
    250.    .7977    300.    .8260    350.    .8425    400.    .8650
    450.    .8875    500.    .9083    550.    .9275    600.    .9442
      4      12
    -40.    .0368    100.    .0413    150.    .0427    200.    .0442
    250.    .0454    300.    .0471    350.    .0480    400.    .0493
    450.    .0506    500.    .0517    550.    .0528    600.    .0538
      5      12
    -40.    .6008    100.    .6736    150.    .6968    200.    .7201
    250.    .7411    300.    .7674    350.    .7828    400.    .8037
    450.    .8246    500.    .8439    550.    .8617    600.    .8773
3D ANALYSIS OF IMPACT LIMITER AND PLUG
      0.      0
```

Table 3-12. HEATING-5 INPUT FOR THE ANALYSIS OF UPPER COWLING

```
ANALYSIS OF UPPER COWLING

10000       2      29       5                          1      23
    8      21                        6                         50
                    7                          5
    1     500  1.0E-10     1.9
    1       1    6.75  7.0625 0.000000  .112757
    1                   1
    2       1    6.75  7.0625 1.843800 3.141590
    1
    3       2  7.0625  7.9625 0.000000 3.141590
    1
    4       3  7.9625    11.6 0.000000 3.141590
    1
    5       4    11.6    12.5 0.000000 3.141590
    1
    6       1    12.5   13.75 0.000000 3.141590
    1
    7       5   13.75  14.891        0. 3.141590
    1
    8       1  14.891     15.        0. 3.121590
    1                      3
    9       1  14.891     15.  .451027 1.570796
    1                      4
   10       1  14.891     15. 1.570796 1.637136
    1                      5
   11       1  14.891     15. 1.637136 2.007136
    1                      6
   12       1  14.891     15. 2.007136 2.377136
    1                      7
   13       1  14.891     15. 2.377136 2.747136
    1                      8
   14       1  14.891     15. 2.747136 3.141590
    1                      2
   15       1    6.75  7.0625  .112757  .225514
```

```
 1                9
16        1    6.75   7.0625  .225514  .338270
 1               10
17        1    6.75   7.0625  .338270  .451027
 1               11
18        1    6.75   7.0625  .451027  .575446
 1               12
19        1    6.75   7.0625  .575446  .699865
 1               13
20        1    6.75   7.0625  .699865  .824283
 1               14
21        1    6.75   7.0625  .824283  .948702
 1               15
22        1    6.75   7.0625  .948702 1.073121
 1               16
23        1    6.75   7.0625 1.073121 1.197540
 1               17
24        1    6.75   7.0625 1.197540 1.321958
 1               18
25        1    6.75   7.0625 1.321958 1.446377
 1               19
26        1    6.75   7.0625 1.446377 1.570796
 1               20
27        1    6.75   7.0625 1.570796 1.637136
 1               21
28        1    6.75   7.0625 1.637136 1.740468
 1               22
29        1    6.75   7.0625 1.740468 1.843800
 1               23
 1   STEEL                                  -1
 2   FIN I                                  -2
 3    LEAD                                  -3
 4   FIN O                                  -4
 5 FIBERGLAS  .00833
 1   320.0
 1       2  331.86
```

```
2         1    130.0
 5.346E-12              0.3333 0.833521        2
                   -5
3         1    130.0
 5.346E-12 0.000833     0.25
4         1    130.0
 5.346E-12              0.3333                 2
                   -5
5         1    130.0
 5.346E-12              0.3333 0.028189        2
                   -5
6         1    130.0
 5.346E-12              0.3333 0.211396        2
                   -5
7         1    130.0
 5.346E-12              0.3333 0.494806        2
                   -5
8         1    130.0
 5.346E-12              0.3333 0.711246        2
                   -5
9         2   332.03

10        2   332.20

11        2   332.36

12        2   332.71

13        2   332.89

14        2   333.08

15        2   333.26

16        2   333.44
```

```
      17        2   333.62

      18        2   333.81

      19        2   333.99

      20        2   334.17

      21        2   334.27

      22        2   334.42

      23        2   334.57

    6.75   7.0625   7.9625     11.6     12.5    13.75   14.891      15.
       1        3        5        3        2        1        1
0.000000  .112757  .225514  .338270  .451027  .575446  .699865  .824283
 .948702 1.073121 1.197540 1.321958 1.446377 1.570796 1.637136 1.740468
1.843800 2.007136 2.377136 2.747136 3.141590
       1        1        1        1        1        1        1        1
       1        1        1        1        1        1        1        1
       2        2        1        3
       1       12
   -40.0    .6466    100.0    .7250    150.0    .7500    200.0    .7750
   250.0    .7975    300.0    .8200    350.0    .8425    400.0    .8650
   450.0    .8875    500.0    .9083    550.0    .9275    600.0    .9442
       2        3
   -40.0   1.3625     70.0   1.3606    300.0   1.3565
       3       10
    68.0    1.667    209.0    1.663    400.0    1.525    499.0    1.408
   581.0    1.208    630.0    1.008    717.0     .808    800.0     .750
   980.0     .725   1267.0     .725
       4        5
   -40.0   0.4158     15.0  0.41506     70.0   0.4164    150.0  0.42934
   300.0   .4445
       5        5
```

```
  100.0    .0015    200.0    .0013    300.0    .0012    400.0    .0011
  500.0    .0010
    6        5
  100.0    .00075   200.0    .00065   300.0    .00060   400.0    .00055
  500.0    .00050
ANALYSIS OF UPPER COWLING
    0.0    0
```

Table 3-13. HEATING-5 INPUT FOR THE ANALYSIS OF THE CASK CROSS SECTION THROUGH THE EXPANSION TANK

CASK CROSS SECTION THROUGH EXPANSION TANK

10000	1				4	4	
11	15	18		6			50
		7			5		
1	300	1.0E-8	1.9				
1	1	6.75	7.0625	0.0	1.8438	0.0	16.4375
1		1					
2	1	6.75	7.0625	1.8438	3.141592	0.0	16.4375
1							
3	2	7.0625	7.9625	0.0	3.141592	0.0	16.4375
1							
4	3	7.9625	11.6	0.0	3.141592	0.0	16.4375
1							
5	4	11.6	12.5	0.0	3.141592	0.0	16.4375
1							
6	1	12.5	13.75	0.0	3.141592	0.0	16.4375
1							
7	1	22.25	22.5	0.0	0.451027	0.0	16.4375
1			3				
8	1	22.25	22.5	0.451027	1.570796	0.0	16.4375
1			4				
9	1	22.25	22.5	1.570796	1.637136	0.0	16.4375
1			5				
10	1	22.25	22.5	1.637136	2.007136	0.0	16.4375
1			6				
11	1	22.25	22.5	2.007136	2.377136	0.0	16.4375
1			7				
12	1	22.25	22.5	2.377136	2.747136	0.0	16.4375
1			8				
13	1	22.25	22.5	2.747136	3.141592	0.0	16.4375
1			9				
14	1	13.75	22.25	0.0	.141592	0.0	0.25
1							
15	1	13.75	22.25	0.0	0.008427	0.25	16.25
1							
16	1	13.75	22.25	1.562369	1.579223	0.25	16.25

```
 1
17       1    13.75    22.25 3.133166 3.141592     0.25    16.25
 1
18       1    13.75    22.25 0.008427 0.698132   4.1875     4.25
 1
19       1    13.75    22.25 1.579223 2.268928   4.1875     4.25
 1
20       1    13.75    22.25 0.008427 0.698132      8.5   8.5625
 1
21       1    13.75    22.25 1.579223 2.268928      8.5   8.5625
 1
22       1    13.75    22.25 0.008427 0.698132  12.8125  12.8750
 1
23       1    13.75    22.25 1.579223 2.268928  12.8125  12.8750
 1
24       0    13.75    22.25 0.698132 1.562369     0.25    16.25
 1            2        2
25       0    13.75    22.25 2.268928 3.133166     0.25    16.25
 1            2        2
26       0    13.75    22.25 0.008427 0.698132     0.25   4.1875
 1            2        2
27       0    13.75    22.25 1.579223 2.268928     0.25   4.1875
 1            2        2
28       0    13.75    22.25 0.008427 0.698132     4.25      8.5
 1            2        2
29       0    13.75    22.25 1.579223 2.268928     4.25      8.5
 1            2        2
30       0    13.75    22.25 0.008427 0.698132   8.5625  12.8125
 1            2        2
31       0    13.75    22.25 1.579223 2.268928   8.5625  12.8125
 1            2        2
32       0    13.75    22.25 0.008427 0.698132  12.8750    16.25
 1            2        2
33       0    13.75    22.25 1.579223 2.268928  12.8750    16.25
 1            2        2
34       1    13.75    22.25      0.0 3.141592    16.25  16.4375
```

```
1
1    STEEL                                    -1
2    FIN I                                    -2
3     LEAD                                    -3
4    FIN O                                    -4
1    506.5
1        2    506.5

2        3
 2.851E-11            0.3333                 2
                  -6
3        1    100.0
 2.851E-11 0.000833     0.25
4        1    100.0
 2.851E-11            0.3333                 2
                  -5
5        1    100.0
 2.851E-11            0.3333 0.028189        2
                  -5
6        1    100.0
 2.851E-11            0.3333 0.211396        2
                  -5
7        1    100.0
 2.851E-11            0.3333 0.494806        2
                  -5
8        1    100.0
 2.851E-11            0.3333 0.711246        2
                  -5
9        1    100.0
 2.851E-11            0.3333 0.833521        2
                  -5
6.75   7.0625   7.9625     9.5     11.6     12.5     13.    13.75
18.    22.25    22.5
 1        2        2       2        1        1        1        2
 1        1
 0.0 0.008427 0.451027 0.698132 1.562369 1.570796 1.579223 1.637136
```

```
1.8438 2.007136 2.268928 2.377136 2.747136 3.133166 3.141592
     1       1       1       1       1       1       1       1
     1       1       1       1       1       1
   0.0    0.25     1.5  3.6875  4.1875    4.25    4.75      8.
   8.5  8.5625  9.0625 12.3125 12.8125 12.8750  13.375     15.
 16.25 16.4375
     1       1       1       1       1       1       1       1
     1       1       1       1       1       1       1       1
     1
     1      12
 -40.0   .6466   100.0   .7250   150.0   .7500   200.0   .7750
 250.0   .7975   300.0   .8200   350.0   .8425   400.0   .8650
 450.0   .8875   500.0   .9083   550.0   .9275   600.0   .9442
     2       3
 -40.0  1.3625    70.0  1.3606   300.0  1.3565
     3      10
  68.0   1.667   209.0   1.663   400.0   1.525   499.0   1.408
 581.0   1.208   630.0   1.008   717.0    .808   800.0    .750
 980.0    .725  1267.0    .725
     4       5
 -40.0  0.4158    15.0 0.41506    70.0  0.4164   150.0 0.42934
 300.0  0.4445
     5       5
 100.0   .0015   200.0   .0013   300.0   .0012   400.0   .0011
 500.0   .0010
     6       5
 100.0  .00075   200.0  .00065   300.0  .00060   400.0  .00055
 500.0  .00050
CASK CROSS SECTION THROUGH EXPANSION TANK
   0.0    0
```

Table 3-14. HEATING-5 INPUT FOR THE ANALYSIS OF CASK CROSS SECTION THROUGH THE SHIELD TANK

ANALYSIS OF CASK CROSS SECTION

10000	2	45	5			1	28
10	25			7			50
		7			5		
1	500	1.0E-10	1.9				
1	1	6.75	7.0625	0.0	.021780		
1		1					
2	2	7.0625	7.9625	0.0	3.141592		
1							
3	3	7.9625	12.85	0.0	3.141592		
1							
4	4	12.85	13.75	0.0	3.141592		
1							
5	1	13.75	15.0	0.0	3.141592		
1							
6	1	17.956	19.435	0.0	0.021780		
1							
7	1	17.581	17.956	0.0	0.065340		
1							
8	1	15.0	17.581	0.043560	0.065340		
1							
9	5	15.0	17.581	0.0	0.043560		
1							
10	5	17.956	19.435	0.021780	0.065340		
1							
11	0	15.00	19.435	0.065340	1.549016		
1		10	10				
12	1	15.0	19.435	1.549016	1.570796		
1							
13	1	17.956	19.435	1.570796	1.592576		
1							
14	1	17.581	17.956	1.570796	1.637136		
1							
15	1	15.0	17.581	1.614345	1.637136		

```
 1
16        5     15.0    17.581 1.570796 1.614345
 1
17        5   17.956    19.435 1.592576 1.637136
 1
18        0     15.0    19.435 1.637136 3.119812
 1                 3         3
19        1     15.0    19.435 3.119812 3.141592
 1
20        1   19.435      19.6      0.0 0.451027
 1                             4
21        1   19.435      19.6 0.451027 1.570796
 1                             5
22        1   19.435      19.6 1.570796 1.637136
 1                             6
23        1   19.435      19.6 1.637136 2.007136
 1                             7
24        1   19.435      19.6 2.007136 2.377136
 1                             8
25        1   19.435      19.6 2.377136 2.747136
 1                             9
26        1   19.435      19.6 2.747136 3.141592
 1                             2
27        1     6.75    7.0625    1.8438 3.141592
 1
28        1     6.75    7.0625  .021780  .043560
 1                11
29        1     6.75    7.0625  .043560  .065340
 1                12
30        1     6.75    7.0625  .065340  .161762
 1                13
31        1     6.75    7.0625  .161762  .258184
 1                14
32        1     6.75    7.0625  .258184  .354605
 1                15
33        1     6.75    7.0625  .354605  .451027
```

```
 1                16
34        1    6.75   7.0625  .451027  .725524
 1                17
35        1    6.75   7.0625  .725524 1.000022
 1                18
36        1    6.75   7.0625 1.000022 1.274519
 1                19
37        1    6.75   7.0625 1.274519 1.549016
 1                20
38        1    6.75   7.0625 1.549016 1.570796
 1                21
39        1    6.75   7.0625 1.570796 1.592576
 1                22
40        1    6.75   7.0625 1.592576 1.614345
 1                23
41        1    6.75   7.0625 1.614345 1.637136
 1                24
42        1    6.75   7.0625 1.637136 1.688802
 1                25
43        1    6.75   7.0625 1.688802 1.740468
 1                26
44        1    6.75   7.0625 1.740468 1.792134
 1                27
45        1    6.75   7.0625 1.792134 1.843800
 1                28
 1   STEEL          .286128                -1
 2   FIN I                                 -2
 3    LEAD                                 -3
 4   FIN O                                 -4
 5   WATER  0.0329
 1   320.0
 1       2  326.68

 2       1  100.0
 5.346E-12          0.3333                 2
                -5
```

```
3       3
                              0.3333                  2
                    -6
4       1     100.0
  5.346E-12 0.000833     0.25
5       1     100.0
  5.346E-12              0.3333                  2
                    -5
6       1     100.0
  5.346E-12              0.3333 0.028189         2
                    -5
7       1     100.0
  5.346E-12              0.3333 0.211396         2
                    -5
8       1     100.0
  5.346E-12              0.3333 0.494806         2
                    -5
9       1     100.0
  5.346E-12              0.3333 0.711246         2
                    -5
10      3
                              0.3333                  2
                    -7
11      2     326.75

12      2     326.82

13      2     326.88

14      2     327.18

15      2     327.48

16      2     327.78

17      2     328.08
```

```
        18          2   328.93

        19          2   329.78

        20          2   330.63

        21          2   331.49

        22          2   331.55

        23          2   331.62

        24          2   331.69

        25          2   331.76

        26          2   331.92

        27          2   332.08

        28          2   332.24

      6.75    7.0625    7.9625     12.85     13.75      15.0    17.581    17.956
    19.435      19.6
         1         2         5         2         2         1         1         1
         1
       0.0  0.021780  0.043560  0.065340  0.161762  0.258184  0.354605  0.451027
  0.725524  1.000022  1.274519  1.549016  1.570796  1.592576  1.614345  1.637136
  1.688802  1.740468  1.792134  1.843800  2.007136  2.377136  2.747136  3.119812
  3.141592
         1         1         1         1         1         1         1         1
         1         1         1         1         1         1         1         1
         1         1         1         3         3         3         1         1
         1        12
     -40.0     .6466     100.0     .7250     150.0     .7500     200.0     .7750
     250.0     .7975     300.0     .8200     350.0     .8425     400.0     .8650
```

```
   450.0     .8875     500.0     .9083     550.0     .9275     600.0     .9442
       2         3
   -40.0    1.3625      70.0    1.3606     300.0    1.3565
       3        10
  -279.4     1.908      68.0     1.667     209.0     1.663     400.0     1.525
   581.0     1.208     630.0     1.008     717.0      .808     800.0      .750
   980.0      .725    1267.0      .725
       4         5
   -40.0    0.4158      15.0   0.41506      70.0    0.4164     150.0   0.42934
   300.0    0.4445
       5         5
  -100.0      .003     100.0     .0015     200.0     .0013     300.0     .0012
   500.0     .0010
       6         8
   -50.0     .0188       0.0     .0387      50.0     .0590     100.0     .0785
   150.0     .0965     200.0     .1121     250.0     .1269     300.0     .1382
       7         8
   -50.0    .01294       0.0    .02349      50.0    .03448     100.0    .04428
   150.0    .05270     200.0    .05969     250.0    .07207     300.0    .08473
ANALYSIS OF CASK CROSS SECTION
     0.0     0
```

Table 3-15. HEATING-5 INPUT FOR THE ANALYSIS OF THE CASK CROSS SECTION THROUGH THE LOWER COWLING

ANALYSIS OF LOWER COWLING

10000	2	29	5				23
8	21			7			50
		7			5		
1	500	1.0E-10	1.9				
1	1	6.75	7.0625	0.000000	.112757		
1		1					
2	1	6.75	7.0625	1.843800	3.141590		
1							
3	2	7.0625	7.9625	0.000000	3.141590		
1							
4	3	7.9625	12.85	0.000000	3.141590		
1							
5	4	12.85	13.75	0.000000	3.141590		
1							
6	1	13.75	15.0	0.000000	3.141590		
1							
7	5	15.	15.5	0.	3.141590		
1							
8	1	15.5	15.609	0.	3.121590		
1			3				
9	1	15.5	15.609	.451027	1.570796		
1			4				
10	1	15.5	15.609	1.570796	1.637136		
1			5				
11	1	15.5	15.609	1.637136	2.007136		
1			6				
12	1	15.5	15.609	2.007136	2.377136		
1			7				
13	1	15.5	15.609	2.377136	2.747136		
1			8				
14	1	15.5	15.609	2.747136	3.141590		
1			2				
15	1	6.75	7.0625	.112757	.225514		

```
  1                9
 16        1    6.75   7.0625  .225514  .338270
  1               10
 17        1    6.75   7.0625  .338270  .451027
  1               11
 18        1    6.75   7.0625  .451027  .575446
  1               12
 19        1    6.75   7.0625  .575446  .699865
  1               13
 20        1    6.75   7.0625  .699865  .824283
  1               14
 21        1    6.75   7.0625  .824283  .948702
  1               15
 22        1    6.75   7.0625  .948702 1.073121
  1               16
 23        1    6.75   7.0625 1.073121 1.197540
  1               17
 24        1    6.75   7.0625 1.197540 1.321958
  1               18
 25        1    6.75   7.0625 1.321958 1.446377
  1               19
 26        1    6.75   7.0625 1.446377 1.570796
  1               20
 27        1    6.75   7.0625 1.570796 1.637136
  1               21
 28        1    6.75   7.0625 1.637136 1.740468
  1               22
 29        1    6.75   7.0625 1.740468 1.843800
  1               23
  1   STEEL                                   -1
  2   FIN I                                   -2
  3    LEAD                                   -3
  4   FIN O                                   -4
  5     AIR                                   -7
  1   320.0
  1       2  331.86
```

```
2         1     130.0
 5.346E-12                0.3333 0.833521        2
                    -5
3         1     130.0
 5.346E-12 0.000833       0.25
4         1     130.0
 5.346E-12                0.3333                 2
                    -5
5         1     130.0
 5.346E-12                0.3333 0.028189        2
                    -5
6         1     130.0
 5.346E-12                0.3333 0.211396        2
                    -5
7         1     130.0
 5.346E-12                0.3333 0.494806        2
                    -5
8         1     130.0
 5.346E-12                0.3333 0.711246        2
                    -5
9         2   332.03

10        2   332.20

11        2   332.36

12        2   332.71

13        2   332.89

14        2   333.08

15        2   333.26

16        2   333.44
```

```
      17        2   333.62

      18        2   333.81

      19        2   333.99

      20        2   334.17

      21        2   334.27

      22        2   334.42

      23        2   334.57

    6.75   7.0625   7.9625    12.85    13.75     15.0     15.5   15.609
       1        3        5        3        2        1        1
0.000000  .112757  .225514  .338270  .451027  .575446  .699865  .824283
 .948702 1.073121 1.197540 1.321958 1.446377 1.570796 1.637136 1.740468
1.843800 2.007136 2.377136 2.747136 3.141590
       1        1        1        1        1        1        1        1
       1        1        1        1        1        1        1        1
       2        2        1        3
       1       12

   -40.0    .6466    100.0    .7250    150.0    .7500    200.0    .7750
   250.0    .7975    300.0    .8200    350.0    .8425    400.0    .8650
   450.0    .8875    500.0    .9083    550.0    .9275    600.0    .9442
       2        3
   -40.0   1.3625     70.0   1.3606    300.0   1.3565
       3       10
    68.0    1.667    209.0    1.663    400.0    1.525    499.0    1.408
   581.0    1.208    630.0    1.008    717.0     .808    800.0     .750
   980.0     .725   1267.0     .725
       4        5
   -40.0   0.4158     15.0  0.41506     70.0   0.4164    150.0  0.42934
   300.0   0.4445
       5        5
```

100.0	.0015	200.0	.0013	300.0	.0012	400.0	.0011
500.0	.0010						
6	5						
100.0	.00075	200.0	.00065	300.0	.00060	400.0	.00055
500.0	.00050						
7	11						
32.	.00117	100.0	.00128	200.	.00145	300.	.00161
400.	.00177	500.0	.00193	600.	.00208	700.	.00223
800.	.00238	900.0	.00253	1000.	.00266		

ANALYSIS OF LOWER COWLING

0.0 0

Table 3-16. HEATING-5 INPUT FOR THE ANALYSIS
OF THE LEAD VOID REGION

ANALYSIS OF AIR SECTION

10000	2	29	4			1	23
8	21			6			50
		7			5		
1	300	1.0E-8	1.9				
1	1	6.75	7.0625	0.000000	.112757		
1		1					
2	1	6.75	7.0625	1.843800	3.141590		
1							
3	2	7.0625	7.9625	0.000000	3.141590		
1							
4	3	7.9625	12.75	0.000000	3.141590		
1							
5	4	12.75	13.75	0.000000	3.141590		
1							
6	1	13.75	15.0	0.000000	3.141590		
1							
7	4	15.00	15.5	0.000000	3.141590		
1							
8	1	15.5	15.609	0.000000	.451027		
1			3				
9	1	15.5	15.609	.451027	1.570796		
1			4				
10	1	15.5	15.609	1.570796	1.637136		
1			5				
11	1	15.5	15.609	1.637136	2.007136		
1			6				
12	1	15.5	15.609	2.007136	2.377136		
1			7				
13	1	15.5	15.609	2.377136	2.747136		
1			8				
14	1	15.5	15.609	2.747136	3.141590		
1			2				
15	1	6.75	7.0625	.112757	.225514		

```
1                10
16       1    6.75   7.0625  .225514  .338270
1                11
17       1    6.75   7.0625  .338270  .451027
1                12
18       1    6.75   7.0625  .451027  .575446
1                13
19       1    6.75   7.0625  .575446  .699865
1                14
20       1    6.75   7.0625  .699865  .824283
1                15
21       1    6.75   7.0625  .824283  .948702
1                16
22       1    6.75   7.0625  .948702 1.073121
1                17
23       1    6.75   7.0625 1.073121 1.197540
1                18
24       1    6.75   7.0625 1.197540 1.321958
1                19
25       1    6.75   7.0625 1.321958 1.446377
1                20
26       1    6.75   7.0625 1.446377 1.570796
1                21
27       1    6.75   7.0625 1.570796 1.637136
1                22
28       1    6.75   7.0625 1.637136 1.740468
1                23
29       1    6.75   7.0625 1.740468 1.843800
1                 9
1    STEEL                                  -1
2    FIN I                                  -2
3     LEAD                                  -3
4      AIR                                  -4
1    320.0
1        2  331.86
```

```
2         1    130.0
 5.346E-12                0.3333 0.833521        2
                   -5
3         1    130.0
 5.346E-12 0.000833         0.25
4         1    130.0
 5.346E-12                0.3333                 2
                   -5
5         1    130.0
 5.346E-12                0.3333 0.028189        2
                   -5
6         1    130.0
 5.346E-12                0.3333 0.211396        2
                   -5
7         1    130.0
 5.346E-12                0.3333 0.494806        2
                   -5
8         1    130.0
 5.346E-12                0.3333 0.711246        2
                   -5
9         2   334.57

10        2   332.03

11        2   332.20

12        2   332.36

13        2   332.71

14        2   332.89

15        2   333.08

16        2   333.26
```

```
      17          2   333.44

      18          2   333.62

      19          2   333.81

      20          2   333.99

      21          2   334.17

      22          2   334.27

      23          2   334.42

    6.75     7.0625   7.9625   12.75   13.75    15.0    15.5  15.609
       1          3        5       3       2       1       1
0.000000    .112757  .225514  .338270 .451027  .575446 .699865 .824283
 .948702   1.073121 1.197540 1.321958 1.446377 1.570796 1.637136 1.740468
1.843800   2.007136 2.377136 2.747136 3.141590
       1          1        1       1       1       1       1       1
       1          1        1       1       1       1       1       1
       2          2        1       3
       1         12
   -40.0      .6466    100.0   .7250   150.0   .7500   200.0   .7750
   250.0      .7975    300.0   .8200   350.0   .8425   400.0   .8650
   450.0      .8875    500.0   .9083   550.0   .9275   600.0   .9442
       2          3
   -40.0     1.3625     70.0  1.3606   300.0  1.3565
       3         10
    68.0      1.667    209.0   1.663   400.0   1.525   499.0   1.408
   581.0      1.208    630.0   1.008   717.0    .808   800.0    .750
   980.0       .725   1267.0    .725
       4         11
    32.0    .00117      100.  .00128     200.  .00145   300.0  .00161
    400.    .00177      500.  .00193     600.  .00208     700. .00223
    800.    .00238      900.  .00253    1000.  .00266
```

```
    5       5
  100.0    .0015    200.0    .0013    300.0    .0012    400.0    .0011
  500.0    .0010
    6       5
  100.0   .00075    200.0   .00065    300.0   .00060    400.0   .00055
  500.0   .00050
ANALYSIS OF AIR SECTION
    0.0     0
```

Table 3-17. HEATING-5 INPUT FOR THE ANALYSIS OF THE LOWER IMPACT LIMITER

```
3D ANALYSIS OF IMPACT LIMITER

10000      1      38      3                                    1      22
   12     27       8                5                                50
                   7                                5
    1    300   1.E-8    1.9
    1      1      0.   35.891    .7854   3.92699      0.      .109
    1                                                   1
    2      1  35.891      36.    .7854   1.15632      0.    19.734
    1
    3      1  35.891      36.  1.15632   1.23643      0.    19.734
    1                        2                          1       1
    4      1  35.891      36.  1.23643   2.35617      0.    19.734
    1                        3                          1       1
    5      1  35.891      36.  2.35617   2.42253      0.    19.734
    1                        4                          1       1
    6      1  35.891      36.  2.42253   2.79253      0.    19.734
    1                        5                          1       1
    7      1  35.891      36.  2.79253   3.16253      0.    19.734
    1                        6                          1       1
    8      1  35.891      36.  3.16253   3.53253      0.    19.734
    1                        7                          1       1
    9      1  35.891      36.  3.53253   3.92699      0.    19.734
    1                        8                          1       1
   10      1  15.125  35.891    .7854   3.92699   19.609   19.734
    1                                                           1
   11      1  15.125  15.375    .7854   3.92699   10.609   10.859
    1
   12      1  15.375    22.5    .7854   3.92699   10.609   10.734
    1
   13      2  15.375    22.5    .7854     1.309   10.734   19.609
    1
   14      2  15.375    22.5  1.83260   2.35617   10.734   19.609
    1
   15      2  15.375    22.5  2.35617    2.8798   10.734   19.609
```

1							
16	2	15.375	22.5	3.4034	3.92699	10.734	19.609
1							
17	2	17.25	17.75	1.309	1.8326	10.734	19.734
1							
18	1	17.25	17.75	2.8798	3.4034	10.734	19.734
1							
19	3	6.33965	8.58965	.7854	.88954	.109	10.609
1							
20	3	6.33965	8.58965	2.25205	2.46839	.109	10.609
1							
21	3	6.33965	8.58965	3.82285	3.92699	.109	10.609
1							
22	1	12.75	15.125	.7854	3.92699	10.609	10.859
1							
23	1	0.	6.75	.7854	.81807	18.859	10.859
1			9				
24	1	0.	6.75	.81807	.85074	18.859	10.859
1			10				
25	1	0.	6.75	.85074	.97824	18.859	10.859
1			11				
26	1	0.	6.75	.97824	1.15632	18.859	10.859
1			12				
27	1	0.	6.75	1.15632	1.51092	18.859	10.859
1			13				
28	1	0.	6.75	1.51092	1.78542	18.859	10.859
1			14				
29	1	0.	6.75	1.78542	2.05992	18.859	10.859
1			15				
30	1	0.	6.75	2.05992	2.33441	18.859	10.859
1			16				
31	1	0.	6.75	2.33441	2.35617	18.859	10.859
1			17				
32	1	0.	6.75	2.35617	2.37797	18.859	10.859
1			18				
33	1	0.	6.75	2.37797	2.42253	18.859	10.859

```
 1                          19
34        1        0.     6.75  2.42253  2.46839  18.859   10.859
 1                          20
35        1        0.     6.75  2.46839  2.54880  18.859   10.859
 1                          21
36        1        0.     6.75  2.54880   2.6292  18.859   10.859
 1                          22
37        1        0.     6.75   2.6292  3.92699  18.859   10.859
 1
38        1        0.    12.75    .7854  3.92699  10.609   10.859
 1
 1    STEEL             .28612                   -3
 2  GUSSETS             .28612                   -4
 3  B HOLES             .28612                   -5
 1     320.
 1        1     130.
  5.346E-12              .3333   .41680        2
                  -1
 2        1     130.
  5.346E-12  .000833      .25
 3        1     130.
  5.346E-12              .3333                 2
                  -2
 4        1     130.
  5.346E-12              .3333  .028189        2
                  -2
 5        1     130.
  5.346E-12              .3333  .211396        2
                  -2
 6        1     130.
  5.346E-12              .3333  .494806        2
                  -2
 7        1     130.
  5.346E-12              .3333  .711246        2
                  -2
 8        1     130.
```

	5.346E-12		.3333		2		
		-2					
9	2	326.68					
10	2	326.82					
11	2	326.88					
12	2	327.48					
13	2	328.08					
14	2	328.93					
15	2	329.78					
16	2	330.63					
17	2	331.49					
18	2	331.55					
19	2	331.62					
20	2	331.76					
21	2	331.92					
22	2	332.24					
0.	6.33965	6.75	8.58965	12.75	15.125	15.375	17.25
17.75	22.5	35.891	36.				
3	1	1	2	1	1	1	1
2	3	1					
.7854	.81807	.85074	.88954	.97824	1.15632	1.23643	1.309
1.51092	1.78542	1.8326	2.05992	2.25205	2.33441	2.35617	2.37797

```
 2.42253  2.46839   2.5489   2.6292  2.79253  2.8798  3.16253  3.4034
 3.53253  3.82285  3.92699
       1        1        1        1        1       1        1       1
       1        1        1        1        1       1        1       1
       1        1        1        1        1       1        1       1
       1        1
      0.     .109   10.609   10.734   10.859  18.859   19.609  19.734
       1        3        1        1        2       1        1
       1        5
     100.   .0015     200.   .0013     300.  .0012     400.   .0011
     500.   .0010
       2        5
     100.   .0015     200.   .0013     300.  .0012     400.   .0011
     500.   .0010
       3       12
     -40.   .6466     100.   .7250     150.  .7500     200.   .7750
     250.   .7977     300.   .8260     350.  .8425     400.   .8650
     450.   .8875     500.   .9083     550.  .9275     600.   .9442
       4       12
     -40.   .0368     100.   .0413     150.  .0427     200.   .0442
     250.   .0454     300.   .0471     350.  .0480     400.   .0493
     450.   .0506     500.   .0517     550.  .0528     600.   .0538
       5       12
     -40.   .6008     100.   .6736     150.  .6968     200.   .7201
     250.   .7411     300.   .7674     350.  .7828     400.   .8037
     450.   .8246     500.   .8439     550.  .8617     600.   .8773
3D ANALYSIS OF IMPACT LIMITER
      0.       0
```

Table 3-18. Comparison Between HEATING-5 and Analytical Solutions to Sample Heat Transfer Problems

Problem	Analytical Solution	HEATING-5 Solution	% Error
1-D Cylinder at Steady State	5.2199 BTU/hr	5.2605 BTU/hr	0.78
2-D Slab at steady state	see Figure 3-66	see Figure 3-67	0.24 (maximum)
1-D Slab variable k	3.6200 BTU/hr-in2	3.6178 BTU/hr-in2	0.04
1-D Slab transient	16 min (0.2667 hrs)	15.87 min (0.2645 hrs)	0.83

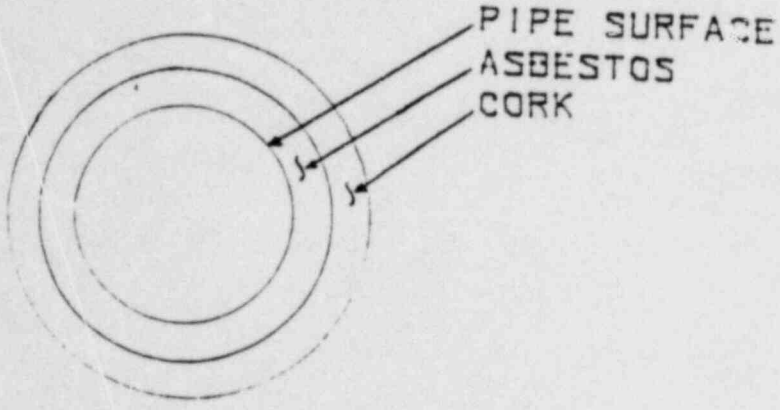

Figure 3-64 Geometry of One Dimensional Sample Problem

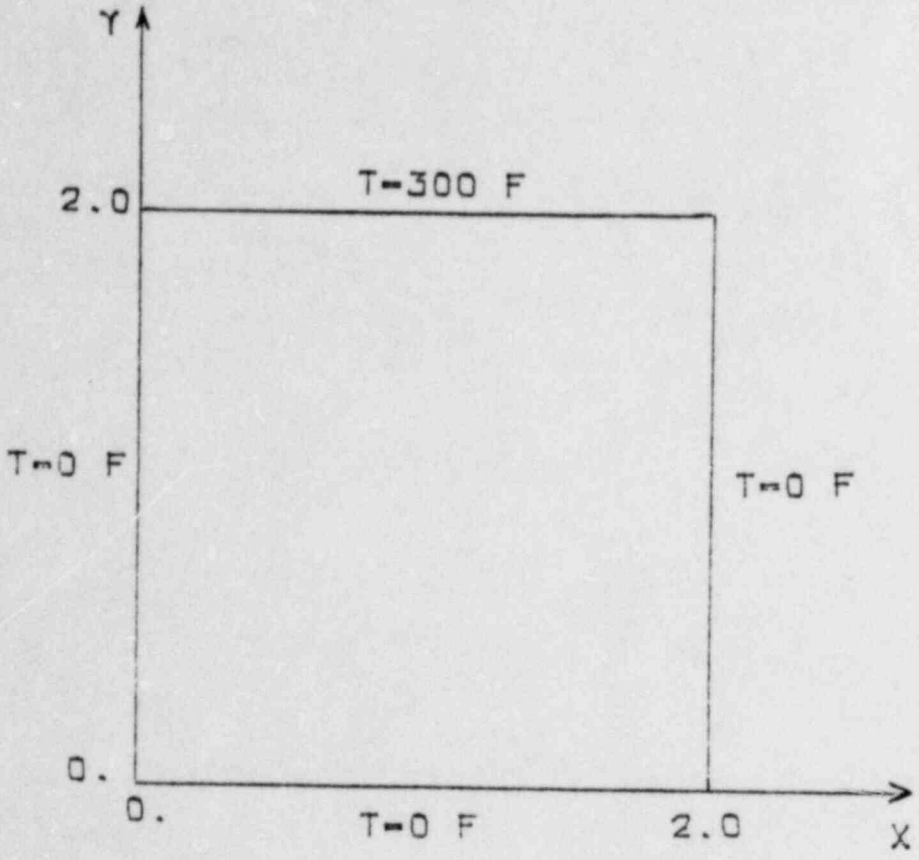

Figure 3-65 Geometry of Two Dimensional Sample Problem

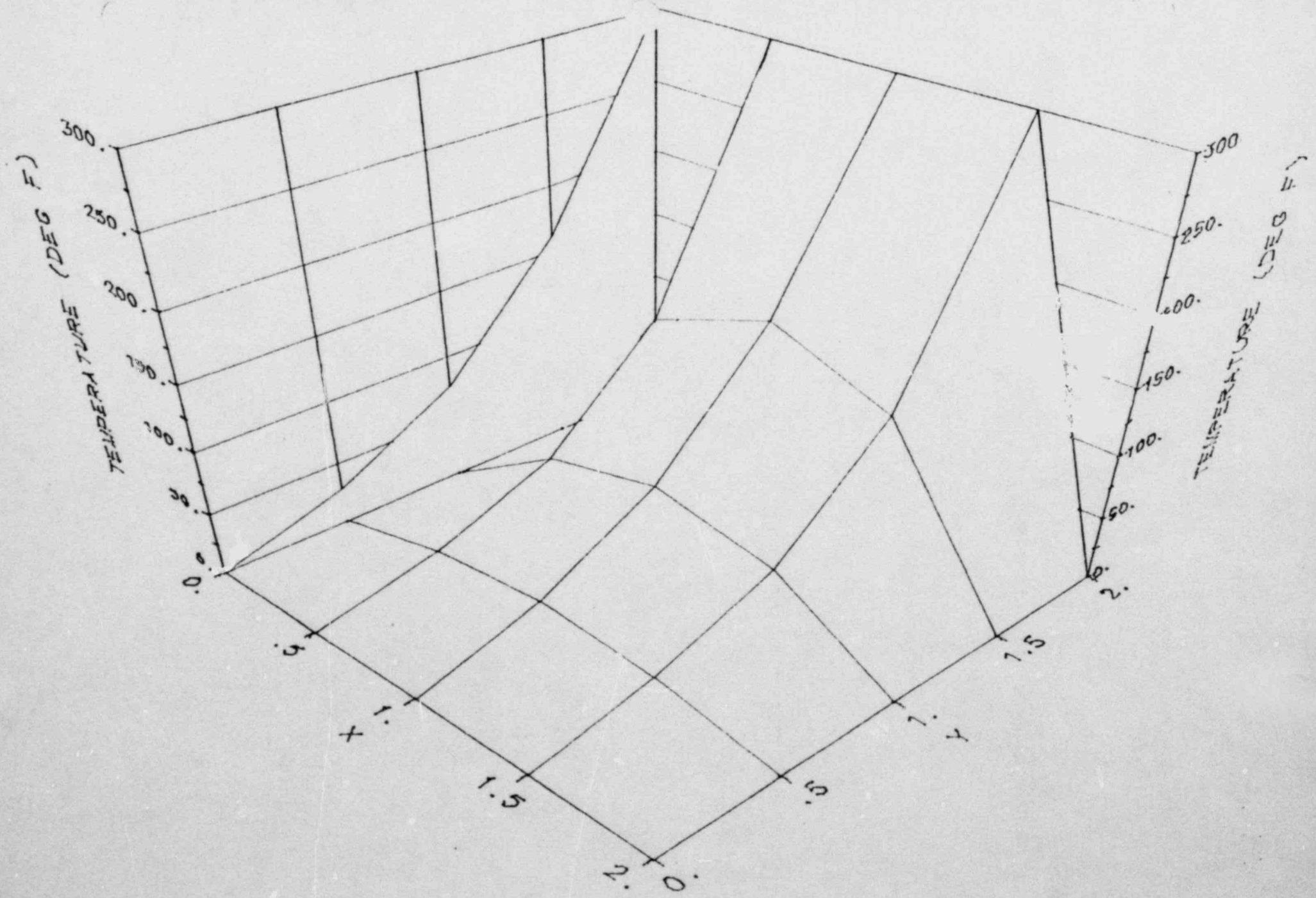

Figure 3-66 Analytical Solution of Two Dimensional Sample Problem

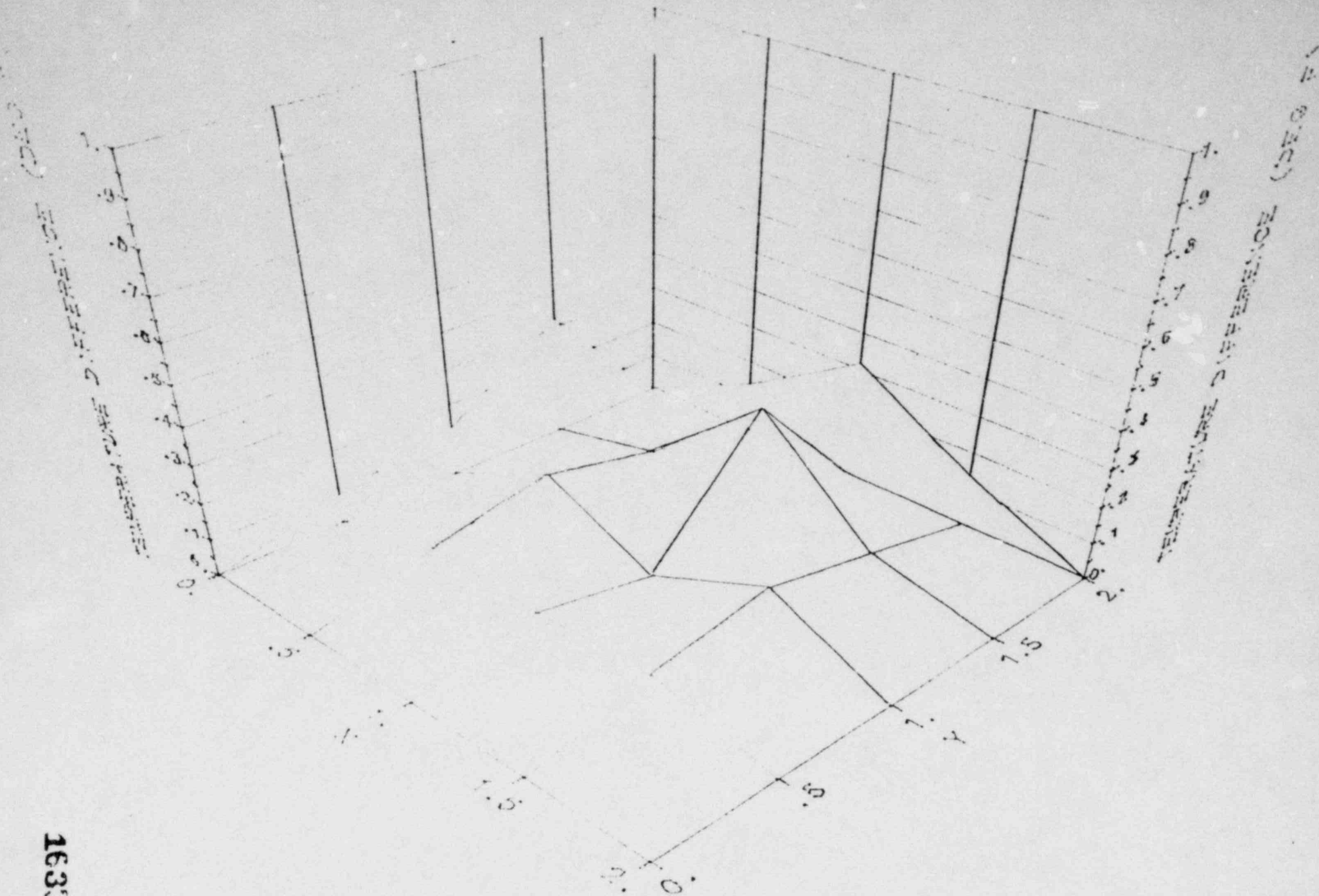

3-67 Temperature Differences Between the Analytical and the Computer Solutions of the 2-D Sample Problem